DTIC FILE COPY

(1)

AD-A204 239

UNITED STATES AIR FORCE

SUMMER FACULTY RESEARCH PROGRAM

1988

PROGRAM TECHNICAL REPORT

UNIVERSAL ENERGY SYSTEMS, INC.

VOLUME 1 OF 2

PROGRAM DIRECTOR, UES

RODNEY C. DARRAH

PROGRAM ADMINISTRATOR, UES

SUSAN K. ESPY

PROGRAM MANAGER, AFOSR

[illegible]

DISTRIBUTION STATEMENT A

Approved for public release;
Distribution Unlimited

SUBMITTED TO

AIR FORCE OFFICE OF SCIENTIFIC RESEARCH

BOLLING AIR FORCE BASE

WASHINGTON, DC

DECEMBER 1988

DTIC
ELECTE
FEB 2 8 1989
S
D

89 2 8 059

SECURITY CLASSIFICATION OF THIS PAGE

REPORT DOCUMENTATION PAGE

REPORT SECURITY CLASSIFICATION: UNCLASSIFIED	1b. RESTRICTIVE MARKINGS
2a. SECURITY CLASSIFICATION AUTHORITY	3. DISTRIBUTION/AVAILABILITY OF REPORT: APPROVED FOR PUBLIC RELEASE; Distribution Unlimited
2b. DECLASSIFICATION/DOWNGRADING SCHEDULE	
4. PERFORMING ORGANIZATION REPORT NUMBER(S)	5. MONITORING ORGANIZATION REPORT NUMBER(S): AFOSR-TR- 89-0036
6a. NAME OF PERFORMING ORGANIZATION: Universal Energy Systems, INc	6b. OFFICE SYMBOL (If applicable):
7a. NAME OF MONITORING ORGANIZATION: AFOSR/XOT	
6c. ADDRESS (City, State and ZIP Code): 4401 Dayton-Xenia Road, Dayton, OH 45432	7b. ADDRESS (City, State and ZIP Code): Building 410, Bolling AFB, DC 20332
8a. NAME OF FUNDING/SPONSORING ORGANIZATION: AFOSR	8b. OFFICE SYMBOL (If applicable): XOT
9. PROCUREMENT INSTRUMENT IDENTIFICATION NUMBER: F49620-85-C-0013	
8c. ADDRESS (City, State and ZIP Code): Building 410, Bolling AFB, DC 20332	10. SOURCE OF FUNDING NOS.

PROGRAM ELEMENT NO.	PROJECT NO.	TASK NO.	WORK UNIT NO.
61102F	3396	D5	

11. TITLE (Include Security Classification): USAF Summer Faculty Research Program - Management Report - 1988

12. PERSONAL AUTHOR(S): Rodney C. Darrah, Susan K. Espy

13a. TYPE OF REPORT	13b. TIME COVERED	14. DATE OF REPORT (Yr., Mo., Day)	15. PAGE COUNT
Annual	FROM _____ TO _____	December 1988	

16. SUPPLEMENTARY NOTATION

17. COSATI CODES			18. SUBJECT TERMS (Continue on reverse if necessary and identify by block number)
FIELD	GROUP	SUB. GR.	

19. ABSTRACT (Continue on reverse if necessary and identify by block number)

See Attached

20. DISTRIBUTION/AVAILABILITY OF ABSTRACT: LASSIFIED/UNLIMITED XX SAME AS RPT. ☐ DTIC USERS ☐	21. ABSTRACT SECURITY CLASSIFICATION: UNCLASSIFIED

22a. NAME OF RESPONSIBLE INDIVIDUAL	22b. TELEPHONE NUMBER (Include Area Code)	22c. OFFICE SYMBOL
Lt Col Claude Cavenaer	202-767-4970	XOT

AFOSR-TR- 89-0036

PREFACE

The United States Air Force Summer Faculty Research Program (USAF-SFRP) is designed to introduce university, college, and technical institute faculty members to Air Force research. This is accomplished by the faculty members being selected on a nationally advertised competitive basis for a ten-week assignment during the summer intersession period to perform research at Air Force laboratories/centers. Each assignment is in a subject area and at an Air Force facility mutually agreed upon by the faculty members and the Air Force. In addition to compensation, travel and cost of living allowances are also paid. The USAF-SFRP is sponsored by the Air Force Office of Scientific Research, Air Force Systems Command, United States Air Force, and is conducted by Universal Energy Systems, Inc.

The specific objectives of the 1988 USAF-SFRP are:

(1) To provide a productive means for U. S. Faculty Members to participate in research at Air Force Laboratories/Centers;

(2) To stimulate continuing professional association among the Faculty and their professional peers in the Air Force;

(3) To further the research objectives of the United States Air Force;

(4) To enhance the research productivity and capabilities of the Faculty especially as these relate to Air Force technical interests.

During the summer of 1988, 153-faculty members participated. These researchers were assigned to 23 USAF laboratories/centers across the country. This four volume document is a compilation of the final reports written by the assigned faculty members about their summer research efforts.

AFOSR-TR- 89-0036

(AFSC)

is
190-12.

Division

89 2 8 053

UNITED STATES AIR FORCE

SUMMER FACULTY RESEARCH PROGRAM

1988

PROGRAM TECHNICAL REPORT

UNIVERSAL ENERGY SYSTEMS, INC.

VOLUME I OF IV

Program Director, UES
Rodney C. Darrah

Program Administrator, UES
Susan K. Espy

Program Manager, AFOSR
Lt. Col. Claude Cavender

DTIC
COPY
INSPECTED
1

Submitted to

Air Force Office of Scientific Research

Bolling Air Force Base

Washington, DC

December 1988

Accession For
NTIS
DTIC
Unannounced
Justification
By
Distribution
Dist
A-1

TABLE OF CONTENTS

SECTION	PAGE
Preface	i
List Of Participants	ii
Participant Laboratory Assignment	xxviii
Research Reports	xxxii

PREFACE

The United States Air Force Summer Faculty Research Program (USAF-SFRP) is designed to introduce university, college, and technical institute faculty members to Air Force research. This is accomplished by the faculty members being selected on a nationally advertised competitive basis for a ten-week assignment during the summer intersession period to perform research at Air Force laboratories/centers. Each assignment is in a subject area and at an Air Force facility mutually agreed upon by the faculty members and the Air Force. In addition to compensation, travel and cost of living allowances are also paid. The USAF-SFRP is sponsored by the Air Force Office of Scientific Research, Air Force Systems Command, United States Air Force, and is conducted by Universal Energy Systems, Inc.

The specific objectives of the 1988 USAF-SFRP are:

(1) To provide a productive means for U. S. Faculty Members to participate in research at Air Force Laboratories/Centers;

(2) To stimulate continuing professional association among the Faculty and their professional peers in the Air Force;

(3) To further the research objectives of the United States Air Force;

(4) To enhance the research productivity and capabilities of the Faculty especially as these relate to Air Force technical interests.

During the summer of 1988, 153-faculty members participated. These researchers were assigned to 23 USAF laboratories/centers across the country. This four volume document is a compilation of the final reports written by the assigned faculty members about their summer research efforts.

LIST OF 1988 PARTICIPANTS

NAME/ADDRESS	DEGREE, SPECIALTY, LABORATORY ASSIGNED
Dr. Ibrahim A. Ahmad Professor and Director Division of Statistics Dept. of Math Sciences Northern Illinois University DeKalb, IL 60115 (815) 753-6739	Degree: Ph.D., Statistics, 1975 Specialty: Statistics and Operations Research Assigned: Armament Laboratory
Dr. Robert J. Arenz Professor Dept. of Mechanical Engineering Gonzaga University Spokane, WA 99258 (509) 328-4220	Degree: Ph.D., Aeronautical Eng., 1964 Specialty: Solid Mech. Assigned: Materials Laboratory
Dr. Lucia M. Babcock Assistant Professor Dept. of Chemistry Louisiana State University Choppin Hall Baton Rouge, LA 70803 (504) 388-3239	Degree: Ph.D., Chemistry, 1978 Specialty: Gas Phase Ion-Molecule Chem. Assigned: Air Force Geophysics Lab.
Dr. Praphulla K. Bajpai Professor Dept. of Biology University of Dayton 300 College Park Dayton, OH 45469 (513) 229-3029	Degree: Ph.D., Animal Physiology, 1965 Specialty: Physiology and Biomaterials Assigned: Harry G. Armstrong Aerospace Medical Research Laboratory
Dr. Stephen D. Baker Professor Dept. of Physics Rice University Houston, TX 77251-1892 (713) 527-8101	Degree: Ph.D., Physics, 1963 Specialty: Nuclear Physics Assigned: Air Force Geophysics Lab.
Dr. Pradip M. Bakshi Research Professor Dept. of Physics Boston College Chestnut Hill, MA 02167 (617) 552-3585	Degree: Ph.D., Theoretical Physics, 1962 Specialty: Quantum Theory Assigned: Air Force Geophysics Lab.

NAME/ADDRESS	DEGREE, SPECIALTY, LABORATORY ASSIGNED
Dr. Shankar S. Bale Professor Dept. of Science and Math Saint Paul's University Lawrenceville, VA 23868 (804) 848-3111	Degree: Ph.D., Genetics, 1971 Specialty: Toxicology-Cytogenetics Assigned: Harry G. Armstrong Aerospace Medical Research Laboratory
Mr. Beryl L. Barber Assistant Professor Dept. of Electronics Eng. Oregon Institute of Technology 3201 Campus Drive Klamath Falls, OR 97601-8801 (503) 882-6890	Degree: MSEE, Electrical Eng., 1961 Specialty: RF/Microwave Components Assigned: Rome Air Development Center
Dr. Bryan R. Becker Assistant Professor Dept. of Aerospace Engineering University of Missouri 600 West Mechanic Independence, MO 64050-1799 (816) 276-1279	Degree: Ph.D., Eng. Science, 1979 Specialty: Computational Fluid Dynamics Assigned: Aero Propulsion Laboratory
Dr. Reuben Benumof Professor Dept. of Applied Sciences College of Staten Island 130 Stuyvesant Pl. Staten Island, NY 10301 (718) 390-7973	Degree: Ph.D., Physics, 1945 Specialty: Semiconductor Physics Assigned: Air Force Geophysics Lab.
Mr. George N. Bratton Associate Professor Dept. of Math and Comp. Science Austin State Peay State Univ. P O Box 8343 Clarksville, TN 37044 (615) 648-7834	Degree: Ed.D., Mathematics Ed., 1977 Specialty: Statistics Assigned: Electronics Systems Division
Dr. Dan R. Bruss Assistant Professor Dept. of Physical Sciences Albany College of Pharmacy 106 New Scotland Avenue Albany, NY 12208 (518) 445-7225	Degree: Ph.D., Chemistry, 1985 Specialty: Physical Organic Chemistry Assigned: Frank J. Seiler Research Lab.

NAME/ADDRESS	DEGREE, SPECIALTY, LABORATORY ASSIGNED
Dr. Ronald Bulbulian Associate Professor Dept. of Health, Physical Education and Recreation University of Kentucky Seaton 100 Lexington, KY 40506 (606) 257-7904	Degree: Ph.D., Physiology, 1980 Specialty: Exercise Physiology Assigned: School of Aerospace Medicine
Dr. Charles M. Bump Assistant Professor Dept. of Chemistry Hampton University P O Box 6483 Hampton, VA 23668 (804) 727-5330	Degree: Ph.D. Organic Chemistry, 1979 Specialty: Organic Synthesis Assigned: Frank J. Seiler Research Lab.
Dr. John A. Burke, Jr. Professor Dept. of Chemistry Trinity University 715 Stadium Drive San Antonio, TX 78284 (512) 736-7316	Degree: Ph.D., Chemistry, 1963 Specialty: Inorganic Compounds Assigned: School of Aerospace Medicine
Mr. Mike Burlakoff Assistant Professor Dept. of Computer Science Southwest Missouri State Univ. 901 S. National Springfield, MO 65804 (417) 836-5930	Degree: MS., Math, Computer Sci., 1965 Specialty: Computer Science Assigned: Avionics Laboratory
Dr. Larry W. Byrd Assistant Professor Dept. of Mechanical Engineering Arkansas State University P O Box 1080 State University, AR 72467-1080 (501) 972-3421	Degree: Ph.D., Mechanical Eng., 1984 Specialty: Mechanical Engineering Assigned: Flight Dynamics Laboratory
Dr. Clarence Calder Associate Professor Dept. of Mechanical Engineering Oregon State University Corvallis, OR 97331 (503) 754-2427	Degree: Ph.D., Mechanical Eng., 1969 Specialty: Stress Wave Propagation Assigned: Astronautics Laboratory

NAME/ADDRESS	DEGREE, SPECIALTY, LABORATORY ASSIGNED
Dr. Richard T. Carlin Assistant Professor Dept. of Chemistry Polytechnic University 333 Jay St. Brooklyn, NY 11201 (718) 260-3339	Degree: Ph.D., Chemistry, 1983 Specialty: Inorganic Chemistry Assigned: Frank J. Seiler Research Lab.
Dr. Gene O. Carlisle Professor Dept. of Chemistry and Physics West Texas State University Canyon, TX 79016 (806) 656-2282	Degree: Ph.D., Inorganic Chem., 1969 Specialty: Coordination Chemistry Assigned: Materials Laboratory
Dr. Patricia Carlson Professor Dept. of Humanities Rose-Hulman Institute of Tech. 5500 Wabash Terre Haute, IN 47803 (812) 877-1511	Degree: Ph.D., Language & Lit., 1973 Specialty: Document Design Assigned: Human Resources Laboratory: Logistics & Human Factors Div.
Dr. David R. Cecil Professor Dept. of Mathematics Texas A&I University Campus Box 172 Kingsville, TX 78363 (512) 592-1839	Degree: Ph.D., Mathematics, 1962 Specialty: Algebra (Finite Fields) Assigned: Wilford Hall Medical Center
Dr. Wayne A. Charlie Associate Professor Dept. of Civil Engineering Colorado State University Fort Collins, CO 80523 (303) 491-8584	Degree: Ph.D., Civil Engineering, 1975 Specialty: Geotechnical Engineering Assigned: Engineering & Services Center
Dr. Steven C. Chiesa Assistant Professor Dept. of Civil Engineering Santa Clara University Santa Clara, CA 95053 (408) 554-4697	Degree: Ph.D., Civil Eng., 1982 Specialty: Biological Waste Treatment Assigned: Occupational and Environment Health Laboratory

NAME/ADDRESS	DEGREE, SPECIALTY, LABORATORY ASSIGNED
Dr. Karen C. Chou Associate Professor Dept. of Civil Engineering Syracuse University Syracuse, NY 13244-1190 (315) 423-3314	Degree: Ph.D., Structural Eng., 1983 Specialty: Structural Engineering Assigned: Flight Dynamics Laboratory
Dr. Phillip A. Christiansen Associate Professor Dept. of Chemistry Clarkson University Potsdam, NY 13676 (315) 268-4099	Degree: Ph.D., Physical Chem., 1978 Specialty: Physical Chemistry Assigned: Astronautics Laboratory
Dr. Keith A. Christianson Assistant Professor Dept. of Electrical Engineering University of Maine Orono, ME 04469 (207) 581-2244	Degree: Ph.D., Materials Science and Engineering, 1985 Specialty: Electronic Materials Assigned: Rome Air Development Center
Dr. Mingking K. Chyu Assistant Professor Dept. of Mechanical Eng. Carnegie Mellon University Pittsburgh, PA 15213 (412) 268-3658	Degree: Ph.D., Heat Transfer, 1986 Specialty: Heat Transfer Assigned: Aero Propulsion Laboratory
Dr. Jerry D. Clark Assistant Professor Dept. of Physics Wright State University 248 Fawcett Hall Dayton, OH 45435 (513) 426-3917	Degree: Ph.D., Physics, 1982 Specialty: Atomic Physics Assigned: Aero Propulsion Laboratory
Dr. Lane Clark Assistant Professor Dept. of Mathematics University of New Mexico Albuquerque, NM 87106 (505) 277-2104	Degree: Ph.D., Mathematics, 1980 Specialty: Graph Theory Assigned: Weapons Laboratory

NAME/ADDRESS	DEGREE, SPECIALTY, LABORATORY ASSIGNED
Dr. Donald F. Collins Faculty in Physics Dept. of Physics Warren Wilson College Swannanoa, NC 28778 (704) 298-3325	Degree: Ph.D., Physics, 1970 Specialty: Optics, Image Processing Assigned: Air Force Geophysics Lab.
Dr. Susan T. Collins Assistant Professor Dept. of Chemistry California State University 18111 Nordhoff Street Northridge, CA 91330 (818) 885-3367	Degree: Ph.D., Physical Chem., 1981 Specialty: Matrix Isolation Spectroscopy Assigned: Astronautics Laboratory
Dr. Charles D. Covington Assistant Professor Dept. of Electrical Engineering University of Arkansas Bell Engineering Center 3217 Fayetteville, AR 72701 (501) 575-6583	Degree: Ph.D., Electrical Eng., 1984 Specialty: Digital Signal Processing Assigned: Harry G. Armstrong Aerospace Medical Research Laboratory
Dr. Parvis Dadras Professor Dept. of Mech. Systems Eng. Wright State University Dayton, OH 45435 (513) 873-2944	Degree: Ph.D., Mechanical Eng., 1972 Specialty: Mechanics of Materials Assigned: Materials Laboratory
Dr. John F. Dalphin Professor Dept. of Computer Science Towson State University Baltimore, MD 21204 (301) 321-3701	Degree: Ph.D., Mathematics, 1973 Specialty: Computer Science Assigned: Electronics Systems Division
Mr. Darin S. DeForest Research Associate Dept. of Computer Science Arizona State University Tempe, AZ 85287 (602) 965-3664	Degree: B.Sc., Computer Science, 1984 Specialty: Programming Language Design Assigned: Rome Air Development Center

NAME/ADDRESS	DEGREE, SPECIALTY, LABORATORY ASSIGNED
Dr. David H. DeHeer Associate Professor Dept. of Biology Calvin College 3201 Burton Street, S.E. Grand Rapids, MI 49506 (616) 957-6083	Degree: Ph.D., Molecular Biology, 1972 Specialty: Molecular Biology Assigned: Engineering & Services Center
Dr. Eustace L. Dereniak Associate Professor Dept. of Optical Science University of Arizona 528 N. Martin Tucson, AZ 85719 (602) 621-1019	Degree: Ph.D., Optics, 1976 Specialty: Infrared Physics Assigned: Arnold Engineering Development Center
Prof. Paul T. Dingman Assistant Professor Dept. of Electronics Eng. Tech. Oregon Institute of Technology 3201 Campus Drive Klamath Falls, OR 97601-8801 (503) 882-6890	Degree: MSEE., Electrical Eng., 1974 Specialty: Digital, Microprocessors Assigned: Rome Air Development Center
Dr. David A. Dolson Assistant Professor Dept. of Chemistry Murray State University Murray, KY 42071 (502) 762-4490	Degree: Ph.D., Physical Chem., 1981 Specialty: Laser Spectroscopy Assigned: Weapons Laboratory
Dr. Hugh K. Donaghy Assistant Professor Dept. of Computer Science Rochester Inst. of Technology 1 Lomb-Memorial Drive Rochester, NY 14623 (716) 475-2994	Degree: Ph.D., Philosophy, 1972 Specialty: Natural Language Processing Assigned: Rome Air Development Center
Dr. Stephen J. Dow Assistant Professor Dept. of Math and Statistics Univ. of Alabama in Huntsville Huntsville, AL 35899 (205) 895-6252	Degree: Ph.D., Mathematics, 1982 Specialty: Discrete Mathematics Assigned: Armament Laboratory

NAME/ADDRESS	DEGREE, SPECIALTY, LABORATORY ASSIGNED
Dr. Derek Dunn-Rankin Assistant Professor Dept. of Mechanical Engineering University of California 616 Engineering Irvine, CA 92717 (714) 854-0460	Degree: Ph.D., Mechanical Eng., 1985 Specialty: Laser Diagnostics (combustion) Assigned: Aero Propulsion Laboratory
Dr. Deanna S. Durnford Assistant Professor Dept. of Agric. & Chem. Eng. Colorado State University Ft. Collins, CO 80523 (303) 491-5252	Degree: Ph.D., Civil Eng., 1982 Specialty: Groundwater Assigned: Engineering & Services Center
Dr. Suren N. Dwivedi Associate Professor Dept. of Mechanical Eng. University of North Carolina Charlotte, NC 28223 (704) 547-2303	Degree: Ph.D., Engineering, 1976 Specialty: Material Processing Assigned: Materials Laboratory
Dr. Wayne A. Eckerle Associate Professor Dept. of Mech. & Ind. Eng. Clarkson University Potsdam, NY 13676 (315) 268-2203	Degree: Ph.D., Fluid Mech., 1985 Specialty: Experimental Fluid Mechanics Assigned: Aero Propulsion Laboratory
Dr. J. Kevin Ford Assistant Professor Dept. of Psychology Michigan State University East Lansing, MI 48824 (517) 353-5006	Degree: Ph.D., Philosophy, 1983 Specialty: Industrial/Organ. Psychology Assigned: Human Resources Laboratory: Training Systems
Prof. Michael E. Frantz Assistant Professor Dept. of Math and Physics University of LaVerne 1950 Third Street LaVerne, CA 91750 (714) 593-3511	Degree: M.S., Mathematics, 1978 Specialty: Partial Differential Equations Assigned: Air Force Geophysics Lab.

NAME/ADDRESS	DEGREE, SPECIALTY, LABORATORY ASSIGNED
Dr. Barry K. Fussell Assistant Professor Dept. of Mechanical Engineering University of New Hampshire Kingsbury Hall Durham, NH 03824 (603) 862-1352	Degree: Ph.D., Mechanical Eng., 1987 Specialty: Systems Modeling & Controls Assigned: Materials Laboratory
Dr. Hugh. P. Garraway, III Associate Professor Dept. of Computer Science Univ. of Southern Mississippi Box 5106 Hattiesburg, MS 39406 (601) 266-4949	Degree: Ph.D., Instruc. Tech., 1980 Specialty: Computer Based Learning Assigned: Human Resources Laboratory: Training Systems
Dr. Christopher P. Godfrey Assistant Professor Dept. of Computer Science Missouri Western State College 4525 Downs Drive St. Joseph, MO 64507 (816) 271-4372	Degree: Ph.D., Physics, 1982 Specialty: High Energy Astrophysics Assigned: Air Force Geophysics Lab.
Dr. Barry P. Goettl Assistant Professor Dept. of Psychology Clemson University 108 Brackett Hall Clemson, SC 29634-1511 (803) 656-2831	Degree: Ph.D., Psychology, 1987 Specialty: Engineering Psychology Assigned: Harry G. Armstrong Aerospace Medical Research Laboratory
Dr. Gerald W. Grams Professor School of Geophysical Sciences Georgia Tech. Atlanta, GA 30332 (404) 894-3628	Degree: Ph.D., Meteorology, 1966 Specialty: Atmospheric Physics Assigned: Avionics Laboratory
Dr. Edward K. Greenwald Assistant Professor Engineering Professional Dev. Univ. of Wisconsin-Madison 432 N. Lake Street Madison, WI 53706 (608) 262-0573	Degree: Ph.D., Physics, 1967 Specialty: Electrical Engineering Assigned: Engineering & Services Center

NAME/ADDRESS	DEGREE, SPECIALTY, LABORATORY ASSIGNED
Prof. William M. Grissom Assistant Professor Dept. of Physics Morehouse College 830 Westview Dr., S.W. Atlanta, GA 30314 (404) 681-2800	Degree: M.S.E., Mechanical Eng., 1978 Specialty: Combustion Diagnostics Assigned: Arnold Engineering Development Center
Dr. David A. Grossie Assistant Professor Dept. of Chemistry Wright State University Dayton, OH 45435 (513) 873-2210	Degree: Ph.D., Chemistry, 1982 Specialty: X-ray Crystallography Assigned: Materials Laboratory
Dr. Vijay K. Gupta Professor Dept. of Chemistry Central State University Wilberforce, OH 45384 (513) 376-6423	Degree: Ph.D., Chemistry, 1969 Specialty: Physical Chemistry Assigned: Materials Laboratory
Dr. Awatef Hamed Dept. of Aerospace Eng. University of Cincinnati Mail Location 70 Cincinnati, OH 45221 (513) 475-5630	Degree: Ph.D., Engineering, 1972 Specialty: Engineering Assigned: Flight Dynamics Laboratory
Dr. Albert A. Heaney Professor Dept. of Electrical Eng. California State University Shaw & Cedar Avenues Fresno, CA 93740-0094 (209) 294-4823	Degree: Ph.D., Electrical Eng., 1972 Specialty: Computer Engineering Assigned: Eastern Space Missile Center
Dr. David Hemmendinger Assistant Professor Dept. of Compt. Sci. & Eng. Wright State University Research Bldg. 317 Research Blvd. Kettering, OH 45420 (513) 259-1345	Degree: Ph.D., Philosophy, 1973 Specialty: Logic Programming Assigned: Avionics Laboratory

NAME/ADDRESS	DEGREE, SPECIALTY, LABORATORY ASSIGNED
Dr. Bennye S. Henderson Associate Professor Dept. of Biology Jackson State University 1325 Lynch Street Jackson, MS 39217 (601) 968-2586	Degree: Ph.D., Physiology, 1979 Specialty: Physiology Assigned: School of Aerospace Medicine
Dr. Darrell E.P. Hoy Assistant Professor Dept. of Mechanical Eng. Tennessee Technological Univ. Box 5014 Cookeville, TN 38505 (615) 372-3732	Degree: M.S.E., Mechanical Eng., 1985 Specialty: Ballistic Impact Shocks Assigned: Arnold Engineering Development Center
Dr. Manuel A. Huerta Professor Dept. of Physics University of Miami P O Box 248046 Coral Gables, FL 33124 (305) 284-2323	Degree: Ph.D., Physics, 1970 Specialty: Plasma Physics Assigned: Armament Laboratory
Dr. Randolph B. Huff Professor Dept. of Chemistry Presbyterian College Clinton, SC 29325 (803) 833-2820	Degree: Ph.D., Inorganic Chem., 1969 Specialty: Physical-Inorganic Chemistry Assigned: Occupational and Environment Health Laboratory
Dr. Neil J. Hutzler Associate Professor Dept. of Civil Engineering Michigan Tech. University Houghton, MI 49931 (906) 487-2194	Degree: Ph.D., Environmental Eng., 1978 Specialty: Environmental Engineering Assigned: Engineering & Services Center
Dr. Douglas E. Jackson Professor Dept. of Math Sciences Eastern New Mexico University Portales, NM 88130 (505) 562-2367	Degree: Ph.D., Mathematics, 1969 Specialty: Math/Statistical Information Assigned: Human Resources Laboratory: Manpower & Personnel Division

NAME/ADDRESS	DEGREE, SPECIALTY, LABORATORY ASSIGNED
Dr. Oleg G. Jakubowicz Assistant Professor Dept. of Elect. & Compt. Eng. State University of New York 238 Bell Hall Buffalo, NY 14260 (716) 636-2406	Degree: Ph.D., Physics, 1984 Specialty: Neural Nets Assigned: Rome Air Development Center
Dr. Manjit S. Jawa Professor Dept. of Mathematics Fayetteville State University Fayetteville, NC 28301 (919) 486-1675	Degree: Ph.D., Applied Math., 1967 Specialty: Applied Mathematics Assigned: Arnold Engineering Development Center
Dr. David W. Jensen Assistant Professor Dept. of Aerospace Eng. Pennsylvania State University 233N Hammond Bldg. University Park, PA 16802 (814) 863-1077	Degree: Ph.D., Structures Tech., 1986 Specialty: Advanced Composite Materials Assigned: Astronautics Laboratory
Dr. Eric R. Johnson Associate Professor Dept. of Chemistry Ball State University Muncie, IN 47306 (317) 285-8078	Degree: Ph.D., Biochemistry, 1974 Specialty: Protein Biochemistry Assigned: School of Aerospace Medicine
Dr. William M. Jordan Assistant Professor Dept. of Mech. & Indus. Eng. Lousiana Tech. University P O Box 10348 Ruston, LA 71272 (318) 257-4304	Degree: Ph.D., Intersiciplinary Eng., 1985 Specialty: Composite Materials Assigned: Weapons Laboratory
Dr. Mohammad A. Karim Assistant Professor Dept. of Electrical Eng. University of Dayton KL-241D Dayton, OH 45469 (513) 229-3611	Degree: Ph.D., Electrical Eng., 1982 Specialty: Electro-Optics Assigned: Avionics Laboratory

NAME/ADDRESS	DEGREE, SPECIALTY, LABORATORY ASSIGNED
Dr. Arkady Kheyfets Assistant Professor Dept. of Mathematics North Carolina State Univ. Box 8205 Raleigh, NC 27695-8205 (919) 737-3265	Degree: Ph.D., Physics, 1986 Specialty: Mathematical Physics Assigned: Weapons Laboratory
Prof. Daisy W. Kimble Assistant Professor Dept. of Chemistry Southern University P O Box 11487 Baton Rouge, LA 70813 (504) 771-3734	Degree: M.S., Analytical Chem., 1986 Specialty: Analytical Chemistry Assigned: School of Aerospace Medicine
Dr. Yulian B. Kin Associate Professor Dept. of Engineering Purdue University Calumet Potter Building Hammond, IN 46323 (219) 989-2684	Degree: Ph.D., Fatigue Stress Analysis 1971 Specialty: Stress Analysis Assigned: Flight Dynamics Laboratory
Dr. Samuel P. Kozaitis Assistant Professor Dept. of Electrical Eng. Florida Institute of Tech. Melbourne, FL 32901-6988 (305) 768-8000	Degree: Ph.D., Electrical Eng, 1986 Specialty: Optics, Computer Architecture Assigned: Rome Air Development Center
Dr. Janet U. Kozyra Assistant Research Scientist University of Michigan Space Physics Research Lab. 2455 Hayward Ann Arbor, MI 48109-2143 (313) 747-3550	Degree: Ph.D., Atmospheric Sci., 1986 Specialty: Space Physics Assigned: Air Force Geophysics Lab.
Dr. Charles E. Lance Assistant Professor Dept. of Psychology University of Georgia Athens, GA 30602 (404) 542-3053	Degree: Ph.D., Psychology, 1985 Specialty: Industrial/Organizational Psy. Assigned: Human Resources Laboratory: Manpower & Personnel Division

NAME/ADDRESS	DEGREE, SPECIALTY, LABORATORY ASSIGNED
Dr. Thomas L. Landers Assistant Professor Dept. of Industrial Engineering University of Arkansas 4176 Bell Engineering Ctr. Fayetteville, AR 72703 (501) 575-6042	Degree: Ph.D., Industrial Eng., 1985 Specialty: Reliability & Maintainability Assigned: Human Resources Laboratory: Logistics & Human Factors Div.
Prof. Anastas Lazaridis Assistant Professor Dept. of Mechanical Eng. Widener University Chester, PA 19013 (215) 499-4487	Degree: Sc.D., Thermal Fluids, 1969 Specialty: Ablation, Solar Energy Assigned: Armament Laboratory
Dr. L. James Lee Associate Professor Dept. of Chemical Eng. The Ohio State University 140 W. 19th Avenue Columbus, OH 43210 (614) 292-2408	Degree: Ph.D., Chemical Eng., 1979 Specialty: Polymer & Composite Processing Assigned: Materials Laboratory
Dr. Robert Y. Li Assistant Professor Dept. of Electrical Eng. University of Nebraska Lincoln, NE 68588 (402) 472-5892	Degree: Ph.D., Electrical Eng., 1981 Specialty: Image Processing Assigned: Avionics Laboratory
Dr. Irving Lipschitz Associate Professor Dept. of Chemistry University of Lowell 1 University Lane Lowell, MA 01854 (617) 452-5000	Degree: Ph.D., Physical Chem., 1965 Specialty: Vibrational Spectroscopy Assigned: Air Force Geophysics Lab.
Dr. Harold G. Longbotham Visiting Assistant Professor Dept. of Electrical Eng. Univ. of Texas - San Antonio San Antonio, TX 78285 (512) 691-5518	Degree: Ph.D., Electrical Eng., 1985 Specialty: Nonlinear Digital Filtering Assigned: School of Aerospace Medicine

NAME/ADDRESS	DEGREE, SPECIALTY, LABORATORY ASSIGNED
Dr. David A. Ludwig Assistant Professor Dept. of Mathematics Univ. of North Carolina at Greensboro Greensboro, NC 27412 (919) 334-5836	Degree: Ph.D., Biostatistics, 1982 Specialty: Biostatistics, Exp. Design Assigned: School of Aerospace Medicine
Dr. Douglas A. Mandra Associate Professor Dept. of Psychology Francis Marion College P O Box 7500 Florence, SC 29501 (803) 661-1378	Degree: Ph.D., Psychology, 1974 Specialty: Experimental Psychology Assigned: Human Resources Laboratory: Operations Training Division
Dr. Robert E. Masingale, Sr. Professor Dept. of Chemistry Jarvis Christian College Hawkins, TX 75765 (214) 769-2174	Degree: Ph.D., Organic Chemistry, 1968 Specialty: Organic & Analytical Chemistry Assigned: Harry G. Armstrong Aerospace Medical Research Laboratory
Dr. John P. McHugh Assistant Professor Dept. of Mechanical Eng. University of New Hampshire 133 Kingsbury Durham, NH 03824 (603) 862-1899	Degree: Ph.D., Applied Mechanics, 1986 Specialty: Fluid Mechanics Assigned: Air Force Geophysics Lab.
Dr. Michael L. McKee Associate Professor Dept. of Chemistry Auburn University Auburn, AL 36849-5312 (205) 826-4043	Degree: Ph.D., Chemical Physics, 1977 Specialty: Molecular Orbital Theory Assigned: Frank J. Seiler Research Lab.
Dr. Thomas T. Meek Associate Professor Dept. of Materials Sci. & Eng. University of Tennessee 434 Dougherty Engineering Bldg. Knoxville, TN 37966-2200 (615) 970-0940	Degree: Ph.D., Ceramic Eng., 1977 Specialty: Ceramic Processing Assigned: Materials Laboratory

NAME/ADDRESS	DEGREE, SPECIALTY, LABORATORY ASSIGNED
Dr. Tammy J. Melton Assistant Professor Dept. of Chemistry St. Norbert College DePere, WI 54115 (414) 337-3206	Degree: Ph.D., Inorganic Chem., 1986 Specialty: Inorganic Synthesis Assigned: Frank J. Seiler Research Lab.
Dr. Carolyn W. Meyers Assistant Professor Dept. of Mechanical Eng. Georgia Inst. of Technology School of Mechanical Eng. Atlanta, GA 30332 (404) 894-3264	Degree: Ph.D., Physical Metallurgy, 1984 Specialty: Microstructure Assigned: Engineering & Services Center
Dr. David W. Mikolaitis Assistant Professor Dept. of Engineering Sciences University of Florida 231 Aero Gainesville, FL 32611 (904) 392-0961	Degree: Ph.D., Theoretical & Applied Mechanics, 1981 Specialty: Applied Math Assigned: Armament Laboratory
Dr. Kwang S. Min Professor Dept. of Physics East Texas State University Commerce, TX 75428 (214) 885-5483	Degree: Ph.D., Physics, 1962 Specialty: Signal Processing Assigned: Armament Laboratory
Dr. Joseph J. Molitoris Professor Dept. of Physics Muhlenberg College Allentown, PA 18104 (215) 821-3413	Degree: Ph.D., Physics, 1985 Specialty: Nuclear Physics Assigned: Armament Laboratory
Mr. Augustus Morris Instructor Dept. of Manufacturing Eng. Central State University Wilberforce, OH 45384 (513) 376-6435	Degree: B.S., Biomedical Eng., 1981 Specialty: Biomedical Engineering Assigned: Flight Dynamics Laboratory

NAME/ADDRESS	DEGREE, SPECIALTY, LABORATORY ASSIGNED
Dr. William P. Mounfield Assistant Professor Dept. of Mechanical Eng. Louisiana State University R2513-A CEBA Bldg. Baton Rouge, LA 70803-6413 (504) 388-6488	Degree: Ph.D., Mechanical Eng., 1985 Specialty: Automatic Controls Assigned: Engineering & Services Center
Dr. Nanda L. Mukherjee Associate Professor Dept. of Chemical Eng. Tuskegee University Tuskegee, AL 36088 (205) 727-8050	Degree: Ph.D., Chemical Eng., 1967 Specialty: Kinetics Assigned: Flight Dynamics Laboratory
Dr. Richard S. Myers Professor Dept. of Physical Sciences Delta State University P O Box 3255 Cleveland, OH 38733 (601) 846-4482	Degree: Ph.D., Physical Chem., 1968 Specialty: Experimental Physical Chem. Assigned: Engineering & Services Center
Dr. Himanshoo V. Navangul Professor Dept. of Chemistry and Physical Science North Carolina Wesleyan College Wesleyan Station Rocky Mount, NC 27804 (919) 977-7171	Degree: Ph.D., Physical Chem., 1967 Specialty: Molecular Spectroscopy Assigned: Air Force Geophysics Lab.
Dr. Mark A. Norris Assistant Professor Dept. of Mechanics Virginia Polytechnic Inst. and State University 227 Norris Hall Blacksburg, VA 24061 (703) 961-4576	Degree: Ph.D., Eng. Mechanics, 1986 Specialty: Structural Dynamics & Controls Assigned: Astronautics Laboratory
Dr. Mufit H. Ozden Associate Professor Dept. of Systems Analysis Miami University 2303 Kreger Hall Oxford, OH 45056 (513) 529-5937	Degree: Ph.D. Eng. Systems, 1975 Specialty: Operations Research Assigned: Human Resources Laboratory: Logistics & Human Factors Div.

NAME/ADDRESS	DEGREE, SPECIALTY, LABORATORY ASSIGNED
Prof. Martin A. Patt Associate Professor Dept. of Electrical Eng. University of Lowell 1 University Ave. Lowell, MA 01854 (617) 452-5000	Degree: M.S., Electrical Eng., 1964 Specialty: Computer Applications Assigned: Air Force Geophysics Lab.
Dr. David G. Payne Assistant Professor Dept. of Psychology SUNY Binghamton Binghamton, NY 13901 (607) 777-4610	Degree: Ph.D., Cognitive Psy., 1984 Specialty: Human Memory Assigned: Harry G. Armstrong Aerospace Medical Research Laboratory
Dr. William Z. Plachy Professor Dept. of Chemistry & Biochem. San Francisco State University San Francisco, CA 94132 (415) 338-1436	Degree: Ph.D., Physical Chem., 1967 Specialty: Physical Chemistry Assigned: School of Aerospace Medicine
Dr. Patricia L. Plummer Professor Dept. of Physics & Chemistry Columbia Univ. of Missouri Columbia, NC 65211 (314) 882-3053	Degree: Ph.D., Chemical Physics, 1964 Specialty: Quantum Chemistry Assigned: Frank J. Seiler Research Lab.
Dr. Leonard E. Porter Professor Dept. of Physics & Astronomy University of Montana Missoula, MT 59812 (406) 243-6223	Degree: Ph.D., Nuclear Physics, 1965 Specialty: Nuclear Physics Assigned: Weapons Laboratory
Dr. Ramalingam Radhakrishnan Assistant Professor Dept. of Civil Engineering Prairie View A&M University Prairie View, TX 77084 (409) 857-2418	Degree: Ph.D, Structure Eng., 1974 Specialty: Structures Assigned: Engineering & Services Center

NAME/ADDRESS	DEGREE, SPECIALTY, LABORATORY ASSIGNED
Dr. Periasamy K. Rajan Professor Dept. of Electrical Eng. Tennessee Tech. University Box 5004 Cookeville, TN 38505 (615) 372-3308	Degree: Ph.D., Electrical Eng., 1975 Specialty: Digital Signal Processing Assigned: Avionics Laboratory
Dr. Panapakkam A. Ramamoorthy Associate Professor Dept. of Elect. & Computer Eng. University of Cincinnati M.L. #30 Cincinnati, OH 45220 (513) 475-4247	Degree: Ph.D., Digital Signal Processing, 1977 Specialty: Optical Memory Assigned: Avionics Laboratory
Dr. Dharam S. Rana Associate Professor Dept. of Management & Marketing Jackson State University 1400 J.R. Lynch Jackson, MS 39217 (601) 968-2534	Degree: Ph.D., Statistics, 1976 Specialty: Quantitative Techniques Assigned: Human Resources Laboratory: Manpower & Personnel Division
Dr. Sunita S. Rana Instructor Dept. of Computer Science Jackson State University 1400 Lynch Street Jackson, MS 39217 (601) 968-2105	Degree: Ph.D., Biology, 1969 Specialty: Computer Science Assigned: Human Resources Laboratory: Training Systems
Dr. Hal C. Reed Associate Professor Dept. of Biology Oral Roberts University 7777 S. Lewis Tulsa, OK 74171 (918) 495-6945	Degree: Ph.D., Entomology, 1982 Specialty: Insect Behavior Assigned: School of Aerospace Medicine
Dr. Michael D. Rice Associate Professor Dept. of Computer Science George Mason University 4400 University Dr. Fairfax, VA 22030 (703) 323-3884	Degree: Ph.D., Mathematics, 1973 Specialty: Computer Science/Math Assigned: Weapons Laboratory

NAME/ADDRESS	DEGREE, SPECIALTY, LABORATORY ASSIGNED
Dr. Mateen M. Rizki Assistant Professor Dept. of Computer Science Wright State University 410 Fawcett Hall Dayton, OH 45435 (513) 873-2394	Degree: Ph.D., Computer Science, 1985 Specialty: Modeling and Simulation Assigned: Avionics Laboratory
Dr. Thomas R. Rogge Professor Dept. of Eng. Science & Math Iowa State University 3015 Black Eng. Ames, IA 50010 (515) 294-2956	Degree: Ph.D., Applied Math, 1964 Specialty: Finite Element Analysis Assigned: School of Aerospace Medicine
Dr. Joe M. Ross Assistant Professor Dept. of Chemistry Central State University Wilberforce, OH 45384 (513) 376-6214	Degree: Ph.D., Molecular Bio., 1977 Specialty: Biochemistry of Macromolecules Assigned: School of Aerospace Medicine
Dr. Joseph E. Saliba Assistant Professor Dept. of Civil & Engr. Mechanics University of Dayton 300 College Park Dayton, OH 45469 (513) 229-3847	Degree: Ph.D., Solid Mechanics, 1983 Specialty: Engineering Mechanics Assigned: Harry G. Armstrong Aerospace Medical Research Laboratory
Dr. Dhiraj K. Sardar Assistant Professor Dept. of Physics University of Texas Div. of Earth & Physical Sci. San Antonio, TX 78285-0663 (512) 691-5462	Degree: Ph.D., Physics, 1980 Specialty: Materials Science & Lasers Assigned: School of Aerospace Medicine
Prof. Sonia H. Sawtelle Teaching Associate Dept. of Education Univ. of Texas - San Antonio San Antonio, TX 78285 (512) 691-4412	Degree: MS., Exercise Physiology, 1975 Specialty: Exercise Physiology Assigned: School of Aerospace Medicine

NAME/ADDRESS	DEGREE, SPECIALTY, LABORATORY ASSIGNED
Dr. Paul O. Scheie Professor Dept. of Physics Texas Lutheran College 1000 West Court Seguin, TX 78155 (512) 379-4161	Degree: Ph.D., Biophysics, 1965 Specialty: Electrophysiology Assigned: School of Aerospace Medicine
Dr. James L. Schmutz Professor Dept. of Chemistry Central Wesleyan College 1 Wesleyan Drive Central, SC 29630 (803) 639-2453	Degree: Ph.D., Chemistry, 1976 Specialty: Inorganic Polymers Assigned: Frank J. Seiler Research Lab.
Dr. Jodye I. Selco Assistant Professor Dept. of Chemistry University of Redlands P O Box 3080 Redlands, CA 92373-0999 (714) 793-2121	Degree: Ph.D., Chemical Physics, 1983 Specialty: Spectroscopy, Kinetics Assigned: Astronautics Laboratory
Dr. Shawky E. Shamma Professor Dept. of Math/Statistics University of West Florida Pensacola, FL 32514 (904) 474-2281	Degree: Ph.D., Applied Math, 1969 Specialty: Applied Mathematics Assigned: Armament Laboratory
Dr. Rameshwar P. Sharma Associate Professor Dept. of Mechanical Engineering Western Michigan University 2065 Kohrman Hall Kalamazoo, MI 49008 (616) 383-1408	Degree: Ph.D., Mechanical Eng., 1978 Specialty: Fluid Mechanics Assigned: Astronautics Laboratory
Dr. Larry R. Sherman Professor Dept. of Chemistry University of Akron Akron, OH 44325-0001 (216) 375-7333	Degree: Ph.D., Analytical Chem., 1969 Specialty: Organotin Chemistry Assigned: Occupational and Environment Health Laboratory

NAME/ADDRESS	DEGREE, SPECIALTY, LABORATORY ASSIGNED
Dr. James A. Sherwood Assistant Professor Dept. of Mechanical Eng. University of New Hampshire Kingsbury Hall Durham, NH 03824 (603) 862-2624	Degree: Ph.D., Aerospace Eng., 1987 Specialty: Solid Mechanics Assigned: Flight Dynamics Laboratory
Dr. Sanford S. Singer Professor Dept. of Chemistry University of Dayton 300 College Park Dayton, OH 45469 (513) 229-2833	Degree: Ph.D., Biological Chem., 1967 Specialty: Enzymology Assigned: Harry G. Armstrong Aerospace Medical Research Laboratory
Dr. Trilochan Singh Professor Dept. of Mechanical Eng. Wayne State University Detroit, MI 48202 (313) 577-3845	Degree: Ph.D., Mechanical Eng., 1970 Specialty: Chemical Combustion Assigned: Astronautics Laboratory
Dr. Jorge L. Sintes Chairman Dept. of Preventive Dentistry and Community Health Meharry Medical College 1005 D.B. Todd Blvd. Nashville, TN 37208 (615) 327-6185	Degree: Ph.D., Nutrition, 1978 Specialty: Dentistry Assigned: Wilford Hall Medical Center
Dr. Kenneth M. Sobel Associate Professor Dept. of Electrical Engineering The City College of New York 138th St. & Convent Ave. New York, NY 10031 (212) 690-4241	Degree: Ph.D., Electrical Eng., 1980 Specialty: Eigenstructure Assigned: Flight Dynamics Laboratory
Dr. Jonathan M. Spector Assistant Professor CSIS Jacksonville State University Pelham Road Jacksonville, AL 36265 (205) 231-5718	Degree: Ph.D., Philosophy, 1978 Specialty: Logic Assigned: Human Resources Laboratory: Training Systems Division

NAME/ADDRESS	DEGREE, SPECIALTY, LABORATORY ASSIGNED
Dr. Gary R. Stevens Assistant Professor Dept. of Statistics Oklahoma State University 301 MS Stillwater, OK 74078 (405) 624-5684	Degree: Ph.D., Statistics, 1986 Specialty: Stochastic Processes Assigned: Occupational and Environment Health Laboratory
Dr. Patrick J. Sweeney Asst. Dean of Engineering University of Dayton 300 College Park, KL201 Dayton, OH 45469 (513) 229-2736	Degree: Ph.D., Mechanical Eng., 1977 Specialty: Computer Modeling Assigned: Flight Dynamics Laboratory
Dr. Michael Sydor Professor Dept. of Physics University of Minnesota Duluth, MN 55812 (218) 726-7205	Degree: Ph.D., Physics, 1965 Specialty: Optics, Material Science Assigned: Materials Laboratory
Dr. Douglas G. Talley Assistant Professor Dept. of Mechanical Eng. University of Michigan 313 Automotive Lab Ann Arbor, MI 48109-2121 (313) 936-0429	Degree: Pn.D., Mechanical Eng., 1978 Specialty: Combustion Assigned: Aero Propulsion Laboratory
Dr. David J. Townsend Associate Professor Dept. of Psychology Montclair State College Upper Montclair, NJ 07042 (201) 893-7222	Degree: Ph.D., Cognitive Psy., 1982 Specialty: Cognitive Science Assigned: Rome Air Development Center
Dr. Donald R. Ucci Associate Professor Dept. of Elect. & Computer Eng. Illinois Inst. of Technology 3300 S. Federal Chicago, IL 60616 (312) 567-3405	Degree: Ph.D., Electrical Eng., 1986 Specialty: Adaptive Arrays Assigned: Rome Air Development Center

NAME/ADDRESS	DEGREE, SPECIALTY, LABORATORY ASSIGNED
Dr. Ahmad D. Vakili Associate Professor Dept. of AE/ME Univ. of Tennessee Space Inst. Tullahoma, TN 37388 (615) 455-0631	Degree: Ph.D., Aerospace Eng., 1978 Specialty: Unsteady Flows Assigned: Arnold Engineering Development Center
Dr. Richard S. Valpey Assistant Professor Dept. of Chemistry Wilberforce University Wilberforce, OH 45384 (513) 376-2911	Degree: Ph.D., Organic Chemistry, 1983 Specialty: Organic Synthesis Assigned: Materials Laboratory
Dr. Peter J. Walsh Professor Dept. of Physics Fairleigh Dickinson University Teaneck, NJ 07666 (201) 692-2493	Degree: Ph.D., Physics, 1960 Specialty: Superconductivity Assigned: Rome Air Development Center
Dr. Kenneth L. Walter Associate Professor Dept. of Chemical Engineering Prairie View A&M University Prairie View, TX 77446 (409) 857-2827	Degree: Ph.D., Chemical Eng., 1972 Specialty: Chemical Engineering Process Assigned: Rome Air Development Center
Dr. Gwo-Ching Wang Associate Professor Dept. of Physics Rensselaer Polytechnic Inst. Troy, NY 12180-3590 (518) 276-8387	Degree: Ph.D., Materials Science, 1978 Specialty: Surface Sciences Assigned: Rome Air Development Center
Dr. Andrew P. Whipple Associate Professor Dept. of Biology Taylor University Upland, IN 46989 (317) 998-5333	Degree: Ph.D., Biology, 1979 Specialty: Cell Biology Assigned: Harry G. Armstrong Aerospace Medical Research Laboratory

NAME/ADDRESS	DEGREE, SPECIALTY, LABORATORY ASSIGNED
Prof. Sharon T. Williams Instructor Dept. of Chemistry Southern University Baton Rouge, LA 70813-2074 (504) 771-3990	Degree: M.S., Biochemistry, 1981 Specialty: General Chemistry Assigned: School of Aerospace Medicine
Dr. Lawrence A. Witt Assistant Professor Dept. of Psychology Western Illinois University Macomb, IL 61455 (309) 298-1593	Degree: Ph.D., Psychology, 1985 Specialty: Industrial/Organ. Psychology Assigned: Human Resources Laboratory: Operations Training Division
Dr. Frank A. Witzmann Assistant Professor Dept. of Biology IUPUI - Columbus 4601 Central Avenue Columbus, IN 47203 (812) 372-8266	Degree: Ph.D., Biology, 1981 Specialty: Protein Analysis Assigned: Harry G. Armstrong Aerospace Medical Research Laboratory
Dr. William E. Wolfe Associate Professor Dept. of Civil Engineering Ohio State University 2070 Neil Avenue Columbus, OH 43210 (614) 292-0790	Degree: Ph.D., Engineering, 1979 Specialty: Geotechnical Engineering Assigned: Flight Dynamics Laboratory
Dr. John R. Wright Professor Dept. of Chem., Physical Sci. Southeast Oklahoma State Univ. Box 4181, Station A, SEOSU Durant, OK 74701 (405) 924-0121	Degree: Ph.D., Chemistry, 1971 Specialty: Biochemistry Assigned: School of Aerospace Medicine
Prof. Wafa E. Yazigi Instructor Dept. of Mathematics Columbia Basin College 2600 N. 20th Pasco, WA 99301 (509) 547-0511	Degree: M.S., Aeronautical Eng., 1986 Specialty: Solid Mechanics Assigned: Armament Laboratory

NAME/ADDRESS	DEGREE, SPECIALTY, LABORATORY ASSIGNED
Dr. Lawrence F. Young Associate Professor Dept. of QA/IS, CBA University of Cincinnati ML 30 Cincinnati, OH 45220 (513) 475-7169	Degree: D.Sc., Industrial Eng., 1978 Specialty: Industrial Engineering Assigned: Human Resources Laboratory: Logistics & Human Factors Div.
Dr. Robert K. Young Professor Dept. of Psychology University of Texas Mezes 330, Psychology Dept. Austin, TX 78713 (512) 471-9228	Degree: Ph.D., Exp. Psychology, 1954 Specialty: Experimental Psychology Assigned: Human Resources Laboratory: Manpower & Personnel Division
Dr. Juin S. Yu Professor Dept. of Mechanical Eng. West Virginia Tech. Montgomery, WV 25136 (304) 442-3248	Degree: Ph.D., Mechanical Eng., 1964 Specialty: Thermofluid Transport Assigned: Aero Propulsion Laboratory

PARTICIPANT LABORATORY ASSIGNMENT

C. PARTICIPANT LABORATORY ASSIGNMENT (Page 1)

1988 USAF/UES SUMMER FACULTY RESEARCH PROGRAM

AERO PROPULSION LABORATORY (AFWAL/APL)
(Wright-Patterson Air Force Base)

1. Bryan Becker
2. Mingking Chyu
3. Jerry Clark
4. Derek Dunn-Rankin
5. Wayne Eckerle
6. David Mikolaitis
7. Douglas Talley
8. Juin Yu

ARMAMENT LABORATORY (AD)
(Eglin Air Force Base)

1. Ibrahim Ahmad
2. Stephen Dow
3. Manuel Huerta
4. Anastas Lazaridis
5. Kwang Min
6. Joseph Molitoris
7. Shawky Shamma
8. Wafa Yazigi

HARRY G. ARMSTRONG AEROSPACE MEDICAL RESEARCH LABORATORY (AAMRL)
(Wright-Patterson AFB)

1. Praphulla Bajpai
2. Shankar Bale
3. Charles Covington
4. Barry Goettl
5. Robert Masingale
6. David Payne
7. Joseph Saliba
8. Sanford Singer
9. Andrew Whipple
10. Frank Witzmann

ARNOLD ENGINEERING DEVELOPMENT CENTER (AEDC)
(Arnold Air Force Base)

1. Eustace Dereniak
2. William Grissom
3. Darrell Hoy
4. Manjit Jawa
5. Ahmad Vakili

ASTRONAUTICS LABORATORY (AL)
Edwards Air Force Base)

1. Clarence Calder
2. Phillip Christiansen
3. Susan Collins
4. David Jensen
5. Mark Norris
6. Jodye Selco
7. Rameshwar Sharma
8. Trilochan Singh

AVIONICS LABORATORY (AFWAL/AL)
(Wright-Patterson Air Force Base)

1. Mike Burlakoff
2. Gerald Grams
3. David Hemmendinger
4. Mohammad Karim
5. Robert Li
6. Periasamy Rajan
7. Panapakkam Ramamoorthy
8. Mateen Rizki

EASTERN SPACE AND MISSILE CENTER (ESMC)
(Patrick Air Force Base)

1. Albert Heaney

C. PARTICIPANT LABORATORY ASSIGNMENT (Page 2)

ELECTRONIC SYSTEMS DIVISION (ESD)
(Hanscom Air Force Base)

1. George Bratton
2. John Dalphin

ENGINEERING AND SERVICES CENTER (ESC)
(Tyndall Air Force Base)

1. Wayne Charlie
2. David DeHeer
3. Deanna Durnford
4. Edward Greenwald
5. Neil Hutzler
6. William Mounfield
7. Richard Myers
8. Ramalingam Radhakrishnan

FLIGHT DYNAMICS LABORATORY (FDL)
(Wright-Patterson Air Force Base)

1. Larry Byrd
2. Karen Chou
3. Awatef Hamed
4. Yulian Kin
5. Augustus Morris
6. Nanda Mukherjee
7. James Sherwood
8. Kenneth Sobel
9. Patrick Sweeney
10. William Wolfe

FRANK J. SEILER RESEARCH LABORATORY (FJSRL)
(USAF Academy)

1. Dan Bruss
2. Charles Bump
3. Richard Carlin
4. Michael McKee
5. Tammy Melton
6. Patricia Plummer
7. James Schmutz

GEOPHYSICS LABORATORY (AFGL)
(Hanscom Air Force Base)

1. Lucia Babcock
2. Stephen Baker
3. Pradip Bakshi
4. Reuben Benumof
5. Donald Collins
6. Michael Frantz
7. Christopher Godfrey
8. Janet Kozyra
9. Irving Lipschitz
10. John McHugh
11. Himanshoo Navangul
12. Martin Patt

HUMAN RESOURCES LABORATORY (HRL)
(Brooks, Williams, and Wright-Patterson Air Force Bases)

1. Patricia Carlson
2. Kevin Ford
3. Hugh Garraway
4. Douglas Jackson
5. Charles Lance
6. Thomas Landers
7. Douglas Mandra
8. Mufit Ozden
9. Dharam Rana
10. Sunita Rana
11. Jonathan Spector
12. Lawrence Witt
13. Lawrence Young
14. Robert Young

C. PARTICIPANT LABORATORY ASSIGNMENT (Page 3)

MATERIALS LABORATORY (ML)
(Wright-Patterson Air Force Base)

1. Robert Arenz
2. Gene Carlisle
3. Parvis Dadras
4. Suren Dwivedi
5. Barry Fussell
6. David Grossie
7. Vijay Gupta
8. L. James Lee
9. Thomas Meek
10. Carolyn Meyers
11. Michael Sydor
12. Richard Valpey

OCCUPATIONAL AND ENVIRONMENTAL HEALTH LABORATORY (OEHL)
(Brooks Air Force Base)

1. Steven Chiesa
2. Randolph Huff
3. Larry Sherman
4. Gary Stevens

ROME AIR DEVELOPMENT CENTER (RADC)
(Griffiss Air Force Base)

1. Beryl Barber
2. Keith Christianson
3. Darin DeForest
4. Paul Dingman
5. Hugh Donaghy
6. Oleg Jakubowicz
7. Samuel Kozaitis
8. David Townsend
9. Donald Ucci
10. Peter Walsh
11. Kenneth Walter
12. Gwo-Ching Wang

SCHOOL OF AEROSPACE MEDICINE (SAM)
(Brooks Air Force Base)

1. Ronald Bulbulian
2. John Burke
3. Bennye Henderson
4. Eric Johnson
5. Daisy Kimble
6. Harold Longbotham
7. David Ludwig
8. William Plachy
9. Hal Reed
10. Thomas Rogge
11. Joe Ross
12. Dhiraj Sardar
13. Sonia Sawtelle
14. Paul Scheie
15. Sharon Williams
16. John Wright

WEAPONS LABORATORY (WL)
(Kirtland Air Force Base)

1. Lane Clark
2. David Dolson
3. William Jordan
4. Arkady Kheyfets
5. Leonard Porter
6. Michael Rice

WILFORD HALL MEDICAL CENTER (WHMC)
(Lackland Air Force Base)

1. David Cecil
2. Jorge Sintes

RESEARCH REPORTS

RESEARCH REPORTS

1988 SUMMER FACULTY RESEARCH PROGRAM

Technical Report Number	Title	Professor
Volume I		
Armament Laboratory		
1	Measuring Systems Effectiveness and Systems Availability of Hardened Targets Subject to a Variety of Weapons	Dr. Ibrahim Ahmad
2	Model Drawing Algorithms for a Matching Problem	Dr. Stephen Dow
3	Two Dimensional Simulation of Railgun Plasma Armatures	Dr. Manuel Huerta
4	Modeling Reactive Fragments	Dr. Anastas Lazaridis
5	Target-Aerosol Discrimination Techniques for Active Optical Proximity Sensors	Dr. Kwang Min
6	The Dynamics of Projectile Impact	Dr. Joseph Molitoris
7	ARIMA Modeling of Residuals in AD/KR TDOP Models	Dr. Shawky Shamma
8	Stress Analysis for a Fin Stabilized Projectile	Dr. Wafa Yazigi
Arnold Engineering Development Center		
9	Infrared Charge Transfer Device Characterization	Dr. Eustace Dereniak
10	Liquid Film Cooling In Rocket Engines	Dr. William Grissom
11	Diffuser Failure Investigation/Non-Interference Stress Measurement System Algorithms Study	Dr. Darrell Hoy
12	Solid Rocket Motor Plume Analysis Through Emission Computerized Tomography	Dr. Manjit Jawa
13	Skin Friction Measurement Using Surface Mounted Hot Films	Dr. Ahmad Vakili

Astronautics Laboratory		
14	Study of Embedded Sensors in Graphite-Epoxy Composites	Dr. Clarence Calder
15	Core Polarization in Lithium and Aluminum	Dr. Phillip Christiansen
16	The Photochemistry of μ3-(η-Diethylacetylene)-Decacarbonyltriosmium in Solid Argon	Dr. Susan Collins
17	Composite-Embedded Fiber-Optic Strain Sensors	Dr. David Jensen
18	Observer Design for the AFAL Grid Structure Using Low-frequency Accelerometer Data	Dr. Mark Norris
19	Photochemistry of Azulene Solutions and a Novel Photochemical Nitration Process	Dr. Jodye Selco
20	Injection System and Spray Characteristics	Dr. Rameshwar Sharma
21	Chemical Kinetic Mechanisms for $CH_4/NO_2/O_2$ Flames	Dr. Trilochan Singh
Eastern Space and Missile Center		
22	Generic Requirements for a CAE/CAD/CAM System	Dr. Albert Heaney
Electronics Systems Division		
23	Alaskan HF Test Data Analysis	Dr. George Bratton
24	Stage 1 Analysis of Alaskan High Frequency Radio Network	Dr. John Dalphin
Engineering and Services Center		
25	High Intensity Stress Wave Propagation in Partially Saturated Sand	Dr. Wayne Charlie
26	Individualization of Human Tissue by the Serologic Identification of Erythrocyte Antigens	Dr. David DeHeer
27	Estimation of Jet Fuel Contamination in Soils	Dr. Deanna Durnford
28	Cogeneration Assessment on Military Bases	Dr. Edward Greenwald

29	Soil Vapor Extraction of Volatile Organic Chemicals	Dr. Neil Hutzler
30	A Preliminary Investigation of Neural Networks for the Air Force Engineering and Services Center	Dr. William Mounfield
31	Rapid Measurements of Adsorption and Desorption of Volatile Organic Compounds	Dr. Richard Myers
32	Prefabricated Hypar Structural System Cost Comparison with Box and Arch Structures	Dr. Ramalingam Radhakrishnan

Volume II
Frank J. Seiler Research Laboratory

33	Thermal Decomposition Kinetic Studies of NTO by High Performance Liquid Chromatography	Dr. Dan Bruss
34	Preparation and Properties of Nitronium Tetrachloroaluminate	Dr. Charles Bump
35	Homogeneous Ziegler-Natta Catalysis in Lewis Acid Molten Salts	Dr. Richard Carlin
36	A MCSCF Study of the Rearrangement of Nitromethane to Methyl Nitrite	Dr. Michael McKee
37	The Effects of Sodium Chloride on Room Temperature Molten Salts	Dr. Tammy Melton
38	AB Initio and Chemical Dynamics Study of Energetic Materials	Dr. Patricia Plummer
39	Separators for Molten Salt Batteries	Dr. James Schmutz

Geophysics Laboratory

40	Radiative Association In Ion-Molecule Reactions: Reactions of Some Carbon Cations	Dr. Lucia Babcock
41	Upward Continuation of Gravity Data With Error Estimates	Dr. Stephen Baker
42	Impulse Approximation Formalism for Atom Molecule Collisions	Dr. Pradip Bakshi
43	Total Dose Effect on Soft Error Rate for Dynamic MOS Memory Cells	Dr. Reuben Benumof

44	Digital Photometric Calibration of and Analysis with Video Imagers in the Ultraviolet	Dr. Donald Collins
45	A Model for Intensified Frontogenesis Over a Modified Mountain Ridge	Dr. Michael Frantz
46	Gamma and X Radiation from Solar Flares	Dr. Christopher Godfrey
47	Theoretical and Observational Studies of Geomagnetic Storm-Related Ion and Electron Heating in the Subauroral Region	Dr. Janet Kozyra
48	Update of the Hitran Database	Dr. Irving Lipschitz
49	Spectral Domain Decomposition	Dr. John McHugh
50	On the Possible Inclusion of "Heavy" Molecules in the HITRAN Database	Dr. Himanshoo Navangul
51	Software Tools for Processing Large Lidar Data Streams	Dr. Martin Patt

Rome Air Development Center

52	Noise Calculations in a RADAR Receiver	Dr. Beryl Barber
53	Stability of Au/W/GaAs and Au/Pt/Ti/GaAs Schottky Barrier Height: A Preliminary Study	Dr. Keith Christianson
54	Parallel Runtime System For Lucid	Dr. Darin DeForest
55	Pre-Sort Processor Phase Distortion Evaluation	Dr. Paul Dingman
56	A PROLOG Natural Language Front End to an ERIC Object Oriented Database	Dr. Hugh Donaghy
57	No Report Submitted at this Time	Dr. Oleg Jakubowicz
58	Design of an Optical Correlator Testbed and Optical Co-Processor	Dr. Samuel Kozaitis
59	Characteristics of Dialog in a Noisy Channel for Performing a Time-Oriented Task	Dr. David Townsend
60	The Effects of Nonlinearities of High Speed Analog-to-Digital Converters on Digital Beamforming Arrays	Dr. Donald Ucci

61	Studies in Microwave Superconductors	Dr. Peter Walsh
62	Chemical Vapor Deposition of Titanium Compounds with an Atomic Layer Epitaxy System	Dr. Kenneth Walter
63	Surface Effects on the High Temperature Superconducting YBaCuO Thin Films grown by RF Sputtering	Dr. Gwo-Ching Wang

Weapons Laboratory

64	Realization of Sublayer Relative Shielding Order in Electromagnetic Topology	Dr. Lane Clark
65	Diode Laser Probe of Vibrational Energy Transfer Kinetics in Sulfur Monoxide	Dr. David Dolson
66	Evaluating How Laser Irradiation Damages Loaded Composite Materials	Dr. William Jordan
67	Relativistic Effects in GPS Time Transfer	Dr. Arkady Kheyfets
68	Stopping Power and Penetration Physics	Dr. Leonard Porter
69	Performance Models for Parallel Algorithms	Dr. Michael Rice

Volume III
Air Force Wright Aeronautical Laboratories
Aero Propulsion Laboratory

70	Computation of the Flow Field and Heat Transfer in a Rectangular Passage with a Turbulator	Dr. Bryan Becker
71	Use of Laser Light Visualization Techniques on Studies of Film Cooling Flow And Flow Over Cavities	Dr. Mingking Chyu
72	Experimental Study of Electronic Excitation of Xenon by Electon Impact	Dr. Jerry Clark
73	Cars Thermometry in Droplet-Laden Flows	Dr. Derek Dunn-Rankin

74	Measurement of the Velocity Field and Heat Transfer Coefficients Associated with a Rectangular Wall Jet	Dr. Wayne Eckerle
75	Lifted Jet Diffusion Flames	Dr. David Mikolaitis
76	Interpretation of a Lifted Turbulent Diffusion Flame as a Problem in Stratified Combustion	Dr. Douglas Talley
77	Diffusion and Convection in the Condenser of a Gas-Loaded Heat Pipe	Dr. Juin Yu
Avionics Laboratory		
78	Ada Compiler Evaluation Capability	Dr. Mike Burlakoff
79	A Study of Sky Backgrounds and Sub-Visual Cirrus at the Megalidar Site and a Proposed Turbulence Monitoring Facility for Wright-Patterson AFB	Dr. Gerald Grams
80	Formal Verification of VHDL Specifications	Dr. David Hemmendinger
81	Low Voltage Broadband Beam Steering Devices Using Liquid Crystals	Dr. Mohammad Karim
82	Model-based Target Recognition Using Laser Radar Imagery	Dr. Robert Li
83	Signal Processing for ESM Receivers	Dr. Periasamy Rajan
84	Neural Networks and their Applications in Digital Receiver Design	Dr. Panapakkam Ramamoorthy
85	Applications of Evolutionary Learning Strategies to Pattern Recognition Tasks	Dr. Mateen Rizki
Flight Dynamics Laboratory		
86	Heat Flux Prediction for Nucleate Boiling in Liquid Metal Heat Pipes	Dr. Larry Byrd
87	Reliability Study of Nonlinear Structural Response under Reversible Cyclic Loading Processes	Dr. Karen Chou
88	Survey and Assessment of Validation Data Base for Shockwave Boundary Layer Interaction in Supersonic Inlets	Dr. Awatef Hamed

89	Failures of F-16 Transparencies Analysis and Failure Prevention Recommendations	Dr. Yulian Kin
90	Visual Capabilities on a Robot Aided Aircraft Refueler Prototype	Mr. Augustus Morris
91	Reaction Kinetic of Halon 1301 Suppression of Fire Explosion in an Aircraft Fuel Tank	Dr. Nanda Mukherjee
92	Development of an Aircraft Tire-Wheel Interface Model for Flange/Beadseat Contact Loads	Dr. James Sherwood
93	Robust Eigenstructure Assignment for Flight Control Design	Dr. Kenneth Sobel
94	A Computer Model for Air-to-Air Combat (Force on Force) Assessment	Dr. Patrick Sweeney
95	Damage in Graphite/Epoxy Plates Subjected to Low Velocity Impact	Dr. William Wolfe
Materials Laboratory		
96	Analysis Methods for Nonlinear Mechanical Behavior of Glassy Polymers	Dr. Robert Arenz
97	Laser Hardened Materials Via Magnetically Aligned Polypeptide-Phthalocyanines	Dr. Gene Carlisle
98	Joining of Carbon-Carbon Composite Materials	Dr. Parviz Dadras
99	Rapid Simulation for Experimental Validation of H Section Forging Using Finisher Punch	Dr. Suren Dwivedi
100	QPA Control of the End Milling Process	Dr. Barry Fussell
101	Single-Crystal Diffraction Analysis of Compounds with Potential Nonlinear Optical Properties	Dr. David Grossie
102	Effect of Various Metals on the Thermal Degradation of a Chlorotrifluorethylene Based Fluid	Dr. Vijay Gupta

103	Characterization of Heat Transfer and Reaction in the Autoclave Curing of Graphite/Epoxy Composites by Scaling Analysis	Dr. L. James Lee
104	A Study of the Melting of the Plagioclase Feldspars in a Microwave Field	Dr. Thomas Meek
105	Reaction Zone Characeristics of Titanium Aluminide Composites	Dr. Carolyn Meyers
106	Photoreflectance Measurements of Unintentional Impurities in Undoped Galium Arsinide	Dr. Michael Sydor
107	The Synthesis of 2-Formyl Pyridoimidazoles	Dr. Richard Valpey

Volume IV
Human Systems Division Laboratories
Harry G. Armstrong Aerospace Medical Research Laboratory

108	Ceramic Composites for Studying Bone Ingrowth and Remodeling	Dr. Praphulla Bajpai
109	In Vitro Cytotoxic Effects of Perfluorodecanoic Acid on Human Peripheral Blood Lymphocytes	Dr. Shankar Bale
110	Auditory Modeling	Dr. Charles Covington
111	Cognitive Demands of Tracking Strategies as Assessed by the Optimum-Maximum Procedure	Dr. Barry Goettl
112	Evaluation of an Extraction Procedure for the Analysis of Serum Steroids	Dr. Robert Masingale
113	Performance in a Visual Monitoring Task with Serial and Simultaneous Display Formats	Dr. David Payne
114	A Nonlinear Lumped Parameter Model for the Seated Humans	Dr. Joseph Saliba
115	In Vitro Modeling of Perfluoro-N-Decanoate Effects on Enzymes of Fatty Acid Metabolism	Dr. Sanford Singer
116	Perfluorodecanoic Acid Efflux from Cultured Primary Rat Hepatocytes	Dr. Andrew Whipple

117	Determination of Perfluoro-N-Decanoic Acid Toxicity in Vitro and in Vivo Via Two-Dimensional Polyacrylamide Gel Electrophoresis	Dr. Frank Witzmann
Human Resources Laboratory		
118	Hypertext and Intelligent Interfaces for Text Retrieval	Dr. Patricia Carlson
119	Linking Training Evaluation to Training Needs Assessment: Development of a Conceptual Model	Dr. J. Kevin Ford
120	A Concept for an Intelligent Tool to Facilitate the Development of Qualitative Process Models in Novice Programmers	Dr. Hugh Garraway
121	A Tool for Studying the Effect of Range Restriction on Correlation Coefficient Estimation	Dr. Douglas Jackson
122	Evaluation of a Methodology for Estimating Cross-AFS Transferability of Skills	Dr. Charles Lance
123	An Expert System Approach for Reliability Data Analysis	Dr. Thomas Landers
124	No Report Submitted at this Time	Dr. Douglas Mandra
125	Graphical Programming of Simulation Models in an Object-Oriented Environment	Dr. Mufit Ozden
126	A Study of Interaction Between Job Properties and Personal Characteristics in the New PACE System	Dr. Dharam Rana
127	An Intelligent Tutor for the IBM System/360 Assembly Language: BIGBLUE	Dr. Sunita Rana
128	Preliminary Design Considerations for an Advanced Instructional Design Advisor	Dr. Jonathan Spector
129	Effectiveness of Contract Monitors In An Air Force Human Resources Laboratory: Prediction and Measurement	Dr. Lawrence Witt

130	Computer Support of Creativity in Unified Life Cycle Engineering	Dr. Lawrence Young
131	The Relationship Between Inspection Time and Intelligence	Dr. Robert Young
Occupational and Environmental Health Laboratory		
132	Solvent Extraction of Boron From Wastewater	Dr. Steven Chiesa
133	Extention of the Detection Limits of Arsenic and Selenium in Solid Samples by ICP/AES Utilizing Preconcentration Techniques	Dr. Randolph Huff
134	Determination of Asbestos Fibers in Environmental Samples Using Scanning Electron Microscopy and Energy Dispersive X-ray Analyses (SEM-EDXA)	Dr. Larry Sherman
135	Analysis of Contaminated Ground Water Using Kriging Methods	Dr. Gary Stevens
School of Aerospace Medicine		
136	Blood Flow Distribution In The Non-Working Forearm During Exercise	Dr. Ronald Bulbulian
137	Photophysics and Photochemistry of Transition Metal Complexes of 8-Quinolinamine Schiff Bases	Dr. John Burke
138	Immunocytochemical Localization of Vasoactive Intestinal Peptide, Neuropeptide Y and Arginine Vasopressin within the Supra-chiasmatic Nuclei of the Rat	Dr. Bennye Henderson
139	Development of Improved Assays for Cholesterol and Major Lipoprotein Fractions	Dr. Eric Johnson
140	Plasma Catecholamine Assays by High Performance Liquid Chromatography	Dr. Daisy Kimble
141	Application of Nonlinear Filters to VEP Data	Dr. Harold Longbotham
142	Extensions of Several Difference Score Approaches for the Analysis of Time Ordered Repeated Measures	Dr. David Ludwig

143	Spin Label Studies of Oxygen in Biological Systems	Dr. William Plachy
144	The Stinging Wasps (Hymenopter: Vespidae) of South Texas	Dr. Hal Reed
145	Modeling of Blood Flow in the Systemic Human Arterial Tree	Dr. Thomas Rogge
146	The Separation of HDL2 and HDL3 Using the Technique of Ultra-centrifugation	Dr. Joe Ross
147	An Experimental Design to Demonstrate the Dispersion Effects of Salt Water on OPTICAL PULSES	Dr. Dhiraj Sardar
148	Literature Search on Nutrition and the Relation to Tactical Air Command Pilots, G-Tolerance and Energy Output	Dr. Sonia Sawtelle
149	A Small Inert-Gas Generator	Dr. Paul Scheie
150	High Performance Liquid Chromatography (HPLC) Determination of High Energy Phosphate Pool	Dr. Sharon Williams
151	Chemiluminescent Probes Based on Luminol and Luminol Derivatives	Dr. John Wright

Wilford Hall Medical Center

152	PC - Mainframe Interface for Data Entry	Dr. David Cecil
153	Oral Health	Dr. Jorge Sintes

1889s

1988 - USAF - UES SUMMER FACULTY RESEARCH PROGRAM

Sponsored by the
Air Force Office of Scientific Research
Conducted by the
Universal Energy Systems, Inc.

Final Report

Measuring Systems Effectiveness and Systems Availability of Hardened Targets Subject to a Variety of Weapons

Prepared by:	Ibrahim A. Ahmad
Academic Rank:	Professor
Department:	Statistics Division
University:	Northern Illinois University
Research Location:	The Armament Laboratory Eglin AFB, FL
USAF Researcher:	George C. Crews
Date:	August 10, 1988
Contact No:	F 49620-87-R-0004



Measuring Systems' Effectiveness and Systems' Availability of Hardened Targets Subject to a Variety of Weapons

By
Ibrahim A. Ahmad

ABSTRACT

This report is a trial to conceptualize two aspects of systems effectiveness and systems availability when these systems are embodied in hardened targets that are subject to a variety of weapons. The emphasis is on statistical analysis of the developed concepts and particularly as on estimation of systems availability and systems effectiveness under a variety of different data schemes.

Several computer programs are currently in use that attempt to evaluate systems effectiveness but suffer from some limitations in the scope of systems that they apply to. Also, they are simple simulations and may require very complex procedures.

This report is in two parts dealing with the effectiveness and availability of systems respectively. The intention is to lay the foundation for a coherent theory of systems effectiveness and availability that is applicable to hardened target and to bring its statistical inference to reality.

Acknowledgments

The author is in debted to the Air Force Systems Command and the Air Force Office of Scientific Research for their sponsorship of this research. Special thanks are due to the Air Force Armament Laboratory for making it all possible, in particular, I am grateful to Dr. Sam Lambert and Mr. George Crews for making my stay at Eglin AFB most pleasant and for providing an environment of intellectual challenge. A word of appreciation is due Mr. John Collins for stimulating discussions on topics discussed in this report and Mr. Gus Gesselman for his assistance. The support and hospitality of the entire staff of the Technology Assessment Branch was inmeasurable and is deeply appreciated.

I. INTRODUCTION.

The research reported here is an attempt to lay probabilistic and statistical foundations to some of the main elements involved in the ongoing research on "vulnerability assessments of hardened targets to a variety of conventional weapons". A massive program, the WETV, is now in use at the Armament Laboratory at Eglin AFB which does give a frequency (probability) value of "residual target performance" of targets after being hit by weapons. In WETV, two main concepts that are assessed on empirical basis are "system performance" and "system (partial) availability" after impact. Thus the research reported here will center on these two concepts, offering concise definitions, basic properties, and statistical inference for each of them. This approach (which is probabilistic in nature) should allow for modification and most likely improvement on the WETV program.

The concept of "system's performance" is a refinement of the usual reliability concepts, see Barlow and Proschan (1981). In WETV, a notion of system's performance is used which does not allow differently structured systems to have different performances (an unrealistic situation) and also it uses an averaging process that is not time dependent (yet another unrealistic case). Hence we try to remedy these shortcomings in the definition we propose and study here, so when adopted to WETV, the new definition improves the program's output.

The availability of systems (targets) subject to weapons' impact is the other concept that we develop in this report. Systems are operational for a random period of time and they fall idle after impact and go into repair, again for a random period of time. We ask about the probability that the system will be available (operational) at a time t_0 or a set of points of time $t_1,\ldots,t_k$ or during a period $[t_0,t_0 + x_0]$ or during a set of periods $[t_1,t_1+x_1], \ldots, [t_k,t_k+x_k]$ that are nonoverlapping. We develop all these concepts and device ways to use test data to estimate the availability measures. Another measure that is addressed in the WETV is partial availability, where, after impact (and thus during repair), the system is partially performing (at a degraded level). This notion need to be developed from a statistical viewpoint.

As pointed out by Scott (1986 and 1988), military systems can share common set of components. Therefore, the subsystems that share a set of components (subsystem) are not independent. Often the common subsystem is very essential and/or expensive, and it is also likely to be well protected. Thus, when a system fails, it is probably because of its non shared set fails. We use a newly develped way to assess the performance of the shared subsystem even if only data about the whole system's performance is available. We thus address a crucial shortcoming in WETV identified in Scott (1986 and 1988).

II. OBJECTIVES OF THE RESEARCH.

The overall objectives of this research are to lay statistical and probabilistic foundations to the concepts of "performance" and "availability" of systems (targets) that are subject to weapons destruction. The goal is to provide ways and means to use test results to obtain estimates of systems performance and systems availability after weapons impact. This would allow for developing the same output that is now obtained via simulation methods in the computer program "Weapons Effects/Targets Vulnerability" (WETV).

The specific objectives of the research can be outlined as follows:

Objectives of Part One - Study of Systems Performance.

(1) Define the concept of system performance in terms of component performance. This is done when all components (subsystems) of the system are independent and also when components share a "core" component(s).

(2) Based on test data of individual components (subsystems), we will develop statistical ways to estimate the systems performance and give confidence bounds for such functions.

(3) Develop computer programs to carry out the necessary computations in (2).

(4) Study the statistical properties of the proposed estimates.

(5) When subsystems share a core component (or subsystem) and the data can only be obtained

for the whole subsystem, we develop a way to use it to estimate the performance of the core subsystem.

Objectives of Part Two - Study of Systems Availability.

(1) Define several notions of availability measures for the case of operational repair. We provide definitions for: single point availability, interval availability, joint point availability and also joint interval availability.

(2) For each of the above notions and based on data about operational times and repair times, we give estimates of the availability and provide their plausible statistical properties.

(3) The concept of partial availability is discussed and suggestions for its possible definitions are given.

Note that in the above three objective we deal with single component systems (i.e., the data is collected about the whole system). The extension of these concepts to multicomponent (with possible dependence between components) systems will be part of the follow up study designed for the Research Initiative Program.

(4) Computer programming to carry out the calculation in (2) and (3) will also be developed and tested on simulated data.

III. PART ONE - SYSTEMS' PERFORMANCE FUNCTION.

Using a geometrical model of target components including breach plates obtained from the FASTGEN computer program, the WETV program simulates the residual target performance is, however, after weapon impact on the target along one shotline. The residual target performance is a function of the damage to each individual subsystem as expressed through the probabilities of survival for each subsystem. It is also a function of how each subsystem is connected with the rest. Thus to define systems performance in a better way than in WETV we proceed as follows:

Case One - All Independent Subsystems (Phases): Let X_i denote the performance or

effectiveness of component (subsystem or phase) $i, i=1,2,...,M$. X_i 's are considered to be random variables which may themselves be functions of random variables, i.e, $X_i = X_i(T_{i1}, \ldots, T_{iL_i})$, where $T_{i1}, \ldots, T_{iL_i}$ are independent random variables. Let $\rho(X_1, \ldots, X_M)$ be an increasing function in each argument that represents the overall system's performance. Further let ρ_0 denote the minimum successful performance level of the system, i.e, we say that the system is successfully performing if and only if $\rho(X_1, \ldots, X_M) \geq \rho_0$. Otherwise the system fails. Hence the probability of successful system performance is given by:

$$P(\rho_0) = P[\rho(X_1,...X_M) \geq \rho_0] = E\ I(\rho_0, X_1, \ldots, X_M)$$
$$= \int \cdots \int I(\rho_0, x_1, ...x_M)\ dF_1(x_1) \cdots dF_m(x_M), \qquad (1)$$

where $I(\rho_0, x_1, \ldots, x_M) = 1$ if $\rho(x_1, \ldots, x_M) \geq \rho_0$ and is 0 otherwise and the symbol E is the expected value. If one wants the average (mean) system's performance we define it by

$$\bar{P} = \int_0^\infty P(\rho) dL(\rho), \qquad (2)$$

where $L(\rho)$ is some suitably chosen weight function such that $\bar{P} < \infty$.

Note that in WETV $\rho(X_1, \ldots, X_M) = \prod_{i=1}^{M} X_i$. regardless of how the system is connected. Thus (1) corrects this by incorporating the formation of the system into $\rho(X_1, \ldots, X_M)$. Also, WETV evaluates $E\rho(X_1, \ldots, X_M) = \prod_{i=1}^{M} E\ X_i$ (the expexted value is denoted by E) as the "system performance". This is actually the average system's performance in (2) for the above choice of $\rho(X_1, \ldots, X_M)$.

Estimating $P(\rho_0)$: Let $X_{i1}, \ldots, X_{iN_i}$ denote a random sample from of size N_i from subsystem i , where $i=1, \ldots, M$. We propose to estimate $P(\rho_0)$ by:

$$\hat{P}_N(\rho_0) = \left(\prod_{i=1}^{M} N_i\right)^{-1} \sum_{j_1=1}^{N_1} \cdots \sum_{j_m=1}^{N_M} I\ (\rho_0, X_{1j_1}, \ldots, X_{Mj_M}). \qquad (3)$$

Hence to estimate the average performance we take

$$\hat{P}_{\underset{\sim}{N}} = \int_0^\infty \hat{P}_{\underset{\sim}{N}}(\rho) dL(\rho). \tag{4}$$

If we need to construct a confidence interval for $P(\rho_0)$, we need first to evaluate the large sample variance of $\hat{P}_{\underset{\sim}{N}}(\rho_0)$. In order to do so we need some notations: Let $(1_i, \underset{\sim}{0})$ denote the vector of size M with zero everywhere except at the i-th position, there is one there. Write

$$E[I(\rho_0, X_1, \ldots, X_M) \,|X_i = x_i] = I_{(1_i, \underset{\sim}{0})}(\rho_0, x_i), i = 1, \ldots, M. \tag{5}$$

Write

$$\varsigma_i^2 = Var\, I_{(1_i, \underset{\sim}{0})}(\rho_0, X_i) \quad , i = 1, \ldots, M. \tag{6}$$

Then, see Ahmad (1981),

$$Var\, \hat{P}_{\underset{\sim}{N}}(\rho_0) = \sum_{i=1}^{M} \frac{1}{N_i} \varsigma_i^2 + 0(N^{-2}), \tag{7}$$

where $N = min\,(N_1, \ldots, N_M)$. To estimate $Var\, \hat{P}_{\underset{\sim}{N}}(\rho_0)$ we need to estimate $\varsigma_i^2 \quad , i = 1, \ldots, M$.

Let

$$V_{j_i}^{(i)} = \Big(\prod_{h \neq i} N_h^{-1}\Big) \Sigma_{(i)}\, I(\rho_0, X_{1\alpha_1}, \ldots X_{(i-1)\alpha_{(i-1)}}, X_{ij_i}, X_{(i+1)\alpha_{(i+1)}}, \ldots, X_{M\alpha_M}), \tag{8}$$

where $\Sigma_{(i)}$ is the sum over all indexes $1 \leq \alpha_h \leq N_h, h \neq i$. Thus

$$\hat{P}_{\underset{\sim}{N}}(\rho_0) = N_i^{-1} \sum_{j_i=1}^{N_i} V_{j_i}^{(i)}. \tag{3*}$$

We estimate ς_i^2 by :

$$\hat{\varsigma}_i^2 = (N_i - 1)^{-1} \sum_{j_i=1}^{N_i} (V_{j_i}^{(i)} - \hat{P}_{\underset{\sim}{N}}(\rho_0))^2. \tag{9}$$

Hence we estimate $\sigma_{\underset{\sim}{N}}^2 = Var\, \hat{P}_{\underset{\sim}{N}}(\rho_0)$ by:

$$\hat{\sigma}_{\underset{\sim}{N}}^2 = \sum_{i=1}^{M} N_i^{-1} \hat{\varsigma}_i^2. \tag{10}$$

Now, since $(\hat{P}_{\underset{\sim}{N}}(\rho_0) - P(\rho_0))$ is asymptotically normal with zero mean and variance $\sigma_{\underset{\sim}{N}}^2$, we can

construct an aproximately normal confidence interval for $P(\rho_0)$ as follows:

$$\hat{P}_{N}(\rho_0) \pm z_{\alpha/2}\sqrt{\hat{\sigma}_{N}}. \tag{11}$$

where $z_{\alpha/2}$ is such that $\Phi(z_{\alpha/2}) = 1 - \alpha/2$ and $\Phi(\cdot)$ is the distribution function of the standard normal variable.

In the above, of course, a crucial question is how do we choose the function ρ ? . One suggestion dealt with previously (see Barlow and Proschan (1981) or Ahmad (1981)) is to take ρ to reflect the structure of the system. Thus if the system is connected in series then $\rho(X_1, \ldots, X_M) = min(X_1, \ldots, X_M)$ and if the system is connected in parallel then $\rho(X_1, \ldots, X_M) = max(X_1, \ldots, X_M)$. In the WETV program they take $\rho(X_1, \ldots, X_M) = \prod_{i=1}^{M} X_i$ regardless of the system's configuration. None of the above choices is entirely satisfactory and we will work more to resolve this issue in the immediate future.

Case Two - All subsystems Share a Core Subsystem. Here we shall assume that $X_i = Y_i Y_c$ where $Y_1, \ldots, Y_M, Y_c$ are independent random variables. In this case

$$P(\rho_0) = \int \cdots \int I(\rho_0, x_1, \ldots, x_M) dH(x_1, \ldots, x_M), \tag{12}$$

where $H(x_1, \ldots, x_M)$ is the joint distribution function of $X_1, \ldots, X_M$. Note that

$$H(x_1, \ldots, x_M) = \int_0^{\infty} \prod_{i=1}^{M} F_i(x_i/y_c) dF_c(y_c). \tag{13}$$

where $F_i(\cdot)$ is the distribution function of Y_i ,$i=1,...,M$, $i=c$ Hence

$$P(\rho_0) = \int \cdots \int \int I(\rho_0, u_1 y_c, \ldots, u_M y_c)) dF_1(u_1) \cdots dF_M(u_M) dF_c(y_c). \tag{14}$$

Estimating $P(\rho_0)$: If the data is collected is on all independent components $Y_1, \ldots, Y_M, Y_c$, then one can use the argument of Case One as applied to formula (14). This leads to the estimator:

$$P_{N,N_c}(\rho_0) = [(\Pi_i\ N_i)N_c]^{-1} \sum_{j=1}^{N_1} \cdots \sum_{j_m=1}^{N_M} \sum_{j_c=1}^{N_c} I(\rho_0, Y_{1j_1} Y_{cj_c}, \ldots, Y_{Mj_M} Y_{cj_c}). \tag{15}$$

Thus we can carry out the procedures of Case One here. If, on the other hand, the data is collected on $X_1, \ldots, X_M$ dependent subsystems where all of them share subsystems Y_c as above, then we need to estimate $H(x_1, \ldots, x_M)$ first:

$$\hat{H}_N(x_1, \ldots, x_m) = (\prod_{i=1}^{M} N_i)^{-1} \Sigma_C \; I(X_{1j_1} \leq x_1 \ldots, X_{Mj_M} \leq Y_M), \tag{16}$$

where the sum is over all $1 \leq j_i \leq N_i, i=1,\ldots,M$. Thus we estimate $P(\rho_0)$ by (3). Let us now obtain the asymptotic variance of $\hat{P}_N(\rho_0)$ in this case and show that it is not estimable based on $X_1, \ldots, X_M$ only. Again using the argument of Hoeffding (see Serfling (1980)) we get that

$$\hat{P}_N(\rho_0) = \sum_{i=1}^{M} N_i^{-1} \sum_{j_i=1}^{N_i} I_{(1,\ldots,0)}(\rho_0, X_{ij_i}) + 0_p\,(N^{-2}). \tag{17}$$

But noting that $X_i = Y_i Y_c$ and using the fact that for any two random variables X and Y,

$$Var(X) = E\,(Var(X \mid Y)) + Var(E(X \mid Y)), \tag{18}$$

we get that

$$Var\,\hat{P}_N(\rho_0) = \sum_{i=1}^{M} N_i^{-1}\, E\,\varsigma_i^2(Y_c) + \sum_{i=1}^{M} N_i^{-1}\, Var\,\mu_i(Y_c) + 0(N^{-2}), \tag{19}$$

where

$$\mu_i(Y_c) = E\,[I_{(1,\ldots,0)}(\rho_0, Y_{ij_i} Y_c) \mid Y_c], and$$

$$\varsigma^{i2}(Y_c) = Var\,[I_{(1,\ldots,0)}(\rho_0, Y_{ij_c} Y_c) \mid Y_c].$$

As easily seen from (19), in order to estimate $Var\,(P_N(\rho_0))$ one needs a good guess about Y_c without which it is not possible to estimate $Var\,\hat{P}_N(\rho_0)$. Whether $\hat{P}_N(\rho_0)$ is approximately normal remains to be studied as it does not follow from case one.

A situation may arise where the data is collected on $X_1, \ldots, X_M$ yet it is desirable to estimate, say, the distribution function of $Y_c, F_c(\cdot)$. This can be accomplished if there are ways to guess the distribution functions of $Y_1, \ldots, Y_M$. To make things precise we let M = 2. Assume that for $i=1,2$, $0 \leq Y_i \leq T_i$, $F_i(u) = \frac{K_i}{u} f_i(u)$ where $f_i(u)$ is the first derivative of $F_i(u)$.

Also assume that $F_i(x_i/y_c) = \phi_i(x_i,x_2)F_i(x_{i^*}/y_c)$ where $x_i \neq x_i$ and $\phi_i(\cdot,\cdot)$ is a known function. Then for all u ,

$$F_c(u) = H(T_1u, T_2u) - \frac{1}{2}\{K_1uh_1(u)[1 - \phi_1(T_1u, T_2u)\phi_1(1,\frac{T_2}{T_1})] + K_2uh_2(u)$$

$$[1 - \phi_2(T_1u, T_2u)\phi_2(1,\frac{T_1}{T_2})]\} - K_1K_2u^2T_1T_2h(T_1u, T_2u), \tag{20}$$

where $H(\cdot,\cdot)$ and $h(.,.)$ denote respectively the joint distribution function and probability density function of (X_1,X_2) , $h_i(\cdot)$ denotes the marginal probability density of X_i, i=1,2, K_i is some positive constant i=1,2. If for example $F_i(u) = (\frac{u}{T_i})^{\alpha_i+1}$, i=1,2, $0 \leq Y_i \leq T_i$ then

$$F_c(u) = H(T_1u, T_2u) - \frac{T_1T_2u^2}{(\alpha_1+1)(\alpha_2+1)}h(T_1u, T_2u). \tag{21}$$

The technical proofs of (20) and (21) will be published elsewhere. Now to estimate $F_c(u)$ suppose that $X_{i1}, \ldots, X_{iN_1}$ denote a random sample from the i-th subsystem , i=1,2. Let $N = min\,(N_1,N_2)$ and define a known sequence of joint distribution functions $\Delta_N\,(x_1,x_2)$ with known joint probability density $\delta_n(x_1,x_2)$. To estimate $F_c(u)$ we need to estimate both $H(\cdot,\cdot)$ and $h(\cdot,\cdot)$. To estimate $H(x_i,x_2)$ we take the estimate

$$H_N(x_1,x_2) = (N_1N_2)^{-1}\sum_{j_1=1}^{N_1}\sum_{j_2=1}^{N_2}\Delta_N\,(X_{1j_1} - x_1, X_{2j_2} - x_2), \tag{22}$$

and we estimate $h(x_1,x_2)$ by taking

$$h_N(x_1,x_2) = \frac{\partial^2}{\partial x_1\partial x_2}H_N(x_1,x_2) = (N_1N_2)^{-1}\sum_{j_1=1}^{N_1}\sum_{j_2=1}^{N_2}\delta_N(X_{ij_1} - x_1, X_{2j_2} - x_2). \tag{23}$$

Thus plugging (22) and (23) into (21) we get an estimate of $F_c(u)$ say $F_{cN}(u)$. If we want to estimate the marginals $h_i(u)$ we take

$$h_N(x_i) = \int h_N(x_1,x_2)dx_{i^*},\ i \neq i^*. \tag{24}$$

Thus plugging (22) - (24) into (20) we get an estimate of $F_c(u)$ in this case as well.

The estimate of $F_c(u)$ presented above need be studied fully and if a confidence interval for $F_c(u)$ is desired then we need to evaluate the variance of the estimate $F_{cN}(u)$ and also demonstrate that it is approximately normal. After this is done, then an algorithm to calculate $F_{cN}(u)$ and $Var(F_{cN}(u))$ will be developed to give the basis to construct confidence interval for $F_c(u)$.

The two assumptions needed to derive (20) are not very restrictive since they are satisfied by, for example, distributions of the form $F_i(u) = (\frac{u}{T_i})^{\alpha_i+1}$, $i=1,2$, $0 \leq u \leq T_i$ which is a distribution with positive aging property, precisely it is a distribution with increasing failure rate (IFR) (see Barlow and Proschan (1981) for details).

IV. PART TWO - SYSTEM'S AVAILABILITY MEASURES.

First we shall develop concepts of system availability when the whole system is considered as one component. Then we shall indicate how the development to multi- components case may be handled.

Consider a system which is either in functional or failing states. Let F and G denote the distribution functions of the failure times and repair times respectively with (finite) means μ_F and μ_G. Let $I_k(t) = 1$ if the system is operational at time t when it was originally (at time t = 0) in state k, k = 0,1 with 0 failed state and 1 = functional state.

Definition (1). The point availability of the system is $A_k(t) = P(I_k(t) = 1)$. The interval availability of the system is $R_k(x,t) = P\{I_k(u) = 1, \textit{ for all } u \in [t,t+x]\}$. The joint availability of the system is $A_k(x,t) = P\{I_k(t) = 1, I(t+x) = 1\}$. Finally, the joint interval availability of the system is $R_k((x_1,t_1),(x_2,t_2)) = P[I_k(u) = 1$ for all $u \in [x_1,x_1+t_1]$ *and* $I_k(v) = 1$ *for all* $v \in [x_2,x_2+t_2]]$. The extension of joint and joint interval availability to more than two points or intervals can also be defined.

We shall now give probabilistic form of all the above notions in terms of the distributions F and G. To do so, let us define the n-fold convolution of a distribution function:

$$F^{(N)}(t) = \int_0^t F^{(N-1)}(t-u)dF(u). \tag{1}$$

Similarly we define $G^{(N)}(t)$. Then $F^{(N)}(t)$ is the distribution function of $X_1 + \cdots + X_N$ where $X_i's$ are independent with distribution F. Define the renewal distribution function:

$$H(u) = \sum_{N=0}^{\infty} \int_0^u F^{(N)}(u-v)dG^{(N)}(v). \tag{2}$$

Using renewal theory argument (see Cox (1962) and Barlow and Hunter (1961)) we see that:

$$A_1(t) = \bar{F}(t) + \int_o^t \bar{F}(t-u)dH(u) = \bar{F}(t) + H(t) - \int_0^t H(t-w)dF(w). \tag{3}$$

$A_2(t)$ is obtained from (3) by putting G in place of F, thus

$$A_0(t) = G(t) - \int_0^t \bar{G}(t-u)dH(u) = G(t) - H(t) + \int_0^t H(t-w)dG(w), \tag{4}$$

where $\bar{F} = 1 - F(\bar{G} = 1 - G)$. Next, let us obtain expressions for $R_k(x,t)$. Again by renewal theory argument:

$$\begin{aligned} R_1(x,t) &= \bar{F}(x+t) + \int_0^{x+t} \bar{F}(x+t-u)dH(u) \\ &= \bar{F}(x+t) + \bar{F}(x)H(t) + \int_x^{x+t} H(x+t-w)dF(w). \end{aligned} \tag{5}$$

Similarly,

$$R_0(x,t) = \int_0^t \bar{F}(x+t-u)dH^*(u) = \bar{F}(x)H^*(t) - \int_x^{x+t} H^*(x+t-w)dF(w), \tag{6}$$

where $H^*(u) = \sum_{N=0}^{\infty} \int_0^u F^{(N)}(u-w)dG^{(N+1)}(w)$. Note that

$$\begin{aligned} A_k(x,t) &= P[I_k(t) = 1, I_k(x+t) = 1] = P[I_k(x+t) = 1 \,|\, I_k(t) = 1]P[I_k(t) = 1] \\ &= P[I_k(x+t) = 1 \,|\, I_k(t) = 1]A_k(t). \end{aligned} \tag{7}$$

Thus all we need is to evaluate $P[I_k(x+t) = 1 \,|\, I_k(t) = 1]$. Using the concept of forward recurrance times to breakdown and coupling it with renewal theory we get that

$$P[I_k(x+t) = 1 \,|\, I_k(t) = 1] = \frac{R_k(x,t)}{A_k(t)} + \int_0^x \Psi_k(u,t)A_0(x-u)du, \tag{8}$$

where

$$\Psi_1(x,t) = \frac{1}{A_1(t)} [f(x+t) + \int_0^t f(x+t-u)h(u)du] \tag{9}$$

and

$$\Psi_0(x,t) = \frac{1}{A_0(t)} [\int_0^t f(x+t-u)h^*(u)du], \tag{10}$$

with f and h (also h^*) the probability density functions corresponding to F, H, (also H^*), respectively. Hence

$$A_k(x,t) = R_k(x,t) + A_k(t) \int_0^x \Psi_k(u,t)A_0(x-u)du. \tag{11}$$

Finally, if $[x_1,x_1+t_1]$ and $[x_2,x_2+t_2]$ are two nonoverlapping intervals i.e. $x_1+t_1 \leq t_2$, then

$$R_1(x_1,t_1),(x_2,t_2)) = R_1(x_2+t_2-t_1,t_1) + A_1(t_1) \int_0^{t_2-x_1-t_1} \Psi_1(x_2+t_2-t_1+u,t_1)$$

$$R_0(x_2,t_2-t_1-x_1-u)du \tag{12}$$

The expression for $R_0((x_1,t_1),(x_2,t_2))$ can be derived analogously.

Let us now look at the limiting behavior of the above measures (as time increases).

$$\lim_{t \to \infty} A_1(t) = \lim_{t \to \infty} A_0(t) = \mu_F/(\mu_F + \mu_G) = A, \; say. \tag{13}$$

Also note that if $F(t)=1-e^{-t\mu_F}$ *and* $G(t)=1-e^{-t\mu_G}$, then,

$$A_1(t) = [\mu_F/(\mu_F + \mu_G)] + \{[\mu_G/(\mu_F + \mu_G)] \; exp \; [-(\mu_F + \mu_G)t]\}, \tag{14}$$

and

$$A_2(t) = [\mu_G/(\mu_F + \mu_G)] - \{[\mu_F/(\mu_F + \mu_G)] \; exp \; [-(\mu_F + \mu_G)t]\}. \tag{14a}$$

Next,

$$\lim_{t \to \infty} R_1(x,t) = \lim_{t \to \infty} R_0(x,t) = (\mu_F + \mu_G)^{-1} \int_x^\infty \bar{F}(u)du = R(x), \; say \tag{15}$$

Also, we have,

$$\lim_{x \to \infty} A_k(x,t) = A_k(t) \frac{\mu_F}{\mu_F+\mu_G}, \; k=0,1, \tag{16}$$

$$\lim_{x \to \infty} \lim_{t \to \infty} A_k(x,t) = \mu_F^2/(\mu_F + \mu_G)^2 \ , k=0,1, \tag{17}$$

and

$$\lim_{t \to \infty} A_k(x,t) = A(x) = R(x) + \frac{1}{\mu_F + \mu_G} \int_0^x \bar{F}(u) A_0(x-u)du. \tag{18}$$

Note also that

$$cov\,(I_k(x+t), I_k(t)) = A_k(x,t) - A_k(x+t)A_k(t). \tag{20}$$

So that,

$$\lim_{t \to \infty} cov\,(I_k(x+t), I_k(t)) = A_k(x) - (\frac{\mu_F}{\mu_F + \mu_G})^2.$$

Thus the limiting autocorrelation is:

$$\rho_k(x) = \{A_k(x) - (\mu_F/(\mu_F + \mu_G))^2\}/\mu_F \mu_G (\mu_F + \mu_G)^2. \tag{21}$$

Now, we move to show how we can estimate the above measures of availability. Let $X_1, \ldots, X_m$ denote a random sample for F, i.e. X_1 is the duration of failure times, i = 1,2 .., m , and let $Y_1, \ldots, Y_n$ denote the operational times, i.e. X_j is drawn from G. To estimate $A_1(t)$, we need to estimate F and H. Let $\{\Delta_m\}$ be a sequence of distribution function such that $\Delta_m(x) \to I(x)$ as $m \to \infty$. Write $\bar{\Delta}_m = 1 - \Delta_m$. Thus to estimate $\bar{F}(t)$ we take:

$$\bar{F}_m(t) = m^{-1} \sum_{i=1}^{m} \bar{\Delta}_m(X_i - t). \tag{22}$$

Next, we need to estimate $H(t) = \sum_{N=0}^{\infty} \int_0^t F^{(N)}(t-w)dG^{(N)}(w)$. We propose the estimate:

$$H_{m,n}(t) = \sum_{N=0}^{Q(m,n)} \int_0^t F_m^{(N)}(i-w)dG_n^{(N)}(w) = \sum_{N=0}^{Q(m,n)} U_{m,n}^{(N)}, \tag{23}$$

where $Q(m,n)$ is an integer function of m and n, and

$$U_{m,n}^{(N)} = [\binom{m}{N}\binom{m}{N}]^{-1} \Sigma_{c_1} \Sigma_{c_2} \Delta_{m,n}\,(X_{i_1} + \cdots + X_{i_N} + Y_{j_1} + \cdots + Y_{j_n} - t), \tag{24}$$

with

$$\Delta_{m,n}(t) = \int_0^t \Delta_m(t-u)d\Delta_n(u),$$

and Σ_{c_1} extends over all $1 \le i_1 < \cdots < i_N \le m$ and Σ_{c_2} extends over all $1 \le j_1 < \cdots < j_N \le n$. Hence $A_1(t)$ is estimated by:

$$\begin{aligned} A_1^{m,n}(t) &= \bar{F}_m(t) + H_{m,n}(t) - \int_0^t H_{m,n}(t-w)dF_m(w) \\ &= \bar{F}_m(t) + H_{m,n}(t) - \phi_{m,n}(t). \end{aligned} \tag{25}$$

where

$$\phi_{m,n}(t) = \sum_{N=0}^{Q(m,n)} \left[\binom{m}{N+1} \binom{n}{N} \right]^{-1} \Sigma_{C_1} \Sigma_{C_2} \Delta_{m,n}(X_{i_1} + \cdots + X_{i_{N+1}} + Y_{j_1} + \cdots + Y_{j_N} - t), \tag{26}$$

where Σ_{c_1} extends over all $1 \le i_1 < \cdots < i_{N+1} \le m$. Similarly,

$$A_0^{(m,n)}(t) = G_n(t) - H_{m,n}(t) + \eta_{m,n}(t), \tag{27}$$

where

$$G_n(t) = n^{-1} \sum_{j=1}^{n} \Delta_n(Y_j - t),$$

and

$$\eta_{m,n}(t) = \sum_{N=0}^{Q(m,n)} \left[\binom{m}{N} \binom{n}{N+1} \right]^{-1} \Sigma_{c_1} \Sigma_{c_2} \Delta_{m,n}(X_{i_1} + \cdots + X_{i_N} + Y_{j_1} + \cdots + Y_{j_{N+1}} - t). \tag{28}$$

When $t \to \infty$, we estimate $A = \mu_F/(\mu_F + \mu_G)$ by $\hat{A} = \bar{X}/(\bar{X} + \bar{Y})$ where $\bar{X}$ and $\bar{Y}$ are the sample means of $X' s_i$ and $Y' s_j$ respectively. To estimate $R_1(x,t) = \bar{F}(x+t) + \bar{F}(x)H(t) + \int_x^{x+t} H(x+t-w)dF(w)$ we use $\bar{F}_m(x+t), \bar{F}_m(x)$, and $H_{m,n}(t)$ and estimate the last term by:

$$\varsigma_{m,n}(x,t) = m^{-1} \sum_{i=1}^{m} H_{m,n}(x+t-X_i) I(x \le X_i \le x+t). \tag{28}$$

Hence we get the estimate

$$R_1^{(m,n)}(x,t) = \bar{F}^m(x+t) + \bar{F}_m(x)H_{m,n}(t) + \varsigma_{m,n}(x,t). \tag{29}$$

To estimate $R_0(x,t) = \bar{F}(x)H^*(t) - \int_x^{x+t} H^k(x+t-w)df(w)$, we define

$$H^*_{m,n}(t) = \sum_{N=0}^{Q(m,n)} [\binom{m}{N}\binom{N}{N+1}]^{-1} \Sigma_{c_1} \Sigma_{c_2} \Delta_{m,n}(X_{i_1} + \cdots + X_{i_N} + Y_{j_1} + \cdots + Y_{j_{N+1}} - t),$$

and

$$\varsigma_{m,n}(x,t) = m^{-1} \sum_{i=1}^{m} H^*_{m,n}(x+t-X_i)I(x \leq X_i \leq x+t).$$

To estimate $\lim_{t \to \infty} R_k(x,t) = R(x) = \frac{1}{\mu_F + \mu_G} \int_x^{\infty} \bar{F}(u)du$ we take

$\hat{R}(x) = \frac{1}{\bar{x} + \bar{Y}} \int_x^{\infty} \bar{F}_m(u)du$. As for the joint availability

$A_1(x,t) = R_1(x,t) + A_1(t)\int^x \Psi_1(u,t)\, A_0(x-u)du$, all the terms are estimated above in (29), (25), and (27) except for $\Psi_1(x,t)$ which is $\frac{1}{A_{1(t)}} [f(x+t) + \int_0^t f(x+t-u)h(u)du]$ and to estimate it we need to estimate $f(t)$ and $h(t)$ but these are easily done by taking $F_m(t) = \frac{d}{dt}F_m(t)$ and $h_{m,n}(t) = \frac{d}{dt}H_{m,n}(t)$.

Joint interval availability is estimated in the same fashion. Note that the statistical properties of the above estimators need be investigated and we shall do so in the follow up. Programs to carry these calculations need also be developed and the first is now being done at the Armament Laboratory to estimate $A_k(t)$.

Before we close this section let us say a few words about the concept of Partial Availability. One such approach is as follows: Suppose that an α portion of the failed items exhibit partial availability of random duration Z. Assume that Z has distribution function Q(z) and is independent of X (failure time) and Y operational time. Define $I_k(t) = 1$ if the system is fully operational at time t if it were in state k = 0,1 initially, =Z if the system is partially operational at time t at level $Z \epsilon (0,1)$, and = 0 if the system failed at t. Thus

$$E\ (I_1(t)) = A_1(t) + \alpha\ E(Z)(1 - A_1(t))\ and$$

$$E\ (I_0(t)) = A_0 + \alpha\ E(z)(1 - A_0(t)).$$

We can take the above quantities as measures of partial availability. A lot more research is needed to develop this, and may be other, concepts of partial availability.

Another area that needs exploration is how to define availability concepts of systems of multicomponents. One primitive way to do that is to define a system availability function $A(A_{1k}(t), \ldots, A_{pk}(t))$ of each component availability, e.g. if we have a series system then its availability function would be $\prod_{i=1}^{P} A_{i_k}(t), k = 0,1$. This concept needs further study.

V. RECOMMENDATIONS.

The computer program WETV obtains via simulation and deterministic functions the residual target performance (RTP) in a way that disregards the structure of the target and the relative importance of its components. It is thus recommended that such a program obtains the individual components (phases) RTP's and that this data is used according to our Part One in obtaining systems RTP. This of course requires the development of the function $\rho(X_1,X_2,\ldots,X_M)$. If X_i represent the life of phase i, then $\rho(\cdot, \ldots, \cdot)$ can be taken the life function, see Esary and Marshall (1970) . If X_i represents another performance phenomenon such as resistance to bombing, then mechanisms to develop ρ are needed. This research we intended to carry in the follow up of this summer research.

In case where subsystems or phases share a basic subsystem(s), then we require testing to be done on all components separately, but if only testing can be done on the phases that share common component(s) then we must at least know the kind of distributions the independent (unshared) components have in order to do inference. If this is not possible, then we face a very serious problem. The programing of the achieved research need be done and incorporated into the existing WETV program.

The concept of partial availability of hardened targets need be fully developed and its estimation procedures implemented onto a new computer program. When we have single

component targets, further researach developed here is nearly complete, but when we have multi-component systems of targets, the research need be developed. When this is done, we would be able to evaluate the (partial) availability of hardened targets after hits and estimate the level of performance of the target. This can be done for either a point in time, set of points in time, an interval in time, or a set of non overlapping time intervals.

In conclusion we started an attempt here to lay the mathematical and statistical foundations for measuring residual performance of targets after weapons impact and also to measure the availability of those targets at future time points or interval when perhaps other raids are likely to happen again.

The technical achievements of this research reported here will be published in specialized probability and statistical journals and the effort will continue till all remaining issues are resolved and results are implemented. The final product should be a more concise evaluation of systems RTP and availability.

REFERENCES

AHMAD, I.A. (1981), "*Asymptotic properties of system reliability estimators*", SIAM J. Applied Math., 41, 413-422.

BARLOW, R.E. and F. PROSCHAN (1981), "*Statistical Theory of Reliability and Life Testing*". To Begin With, Silver Spring, MD.

BARLOW, R.E. and L.C. HUNTER (1961), "*Reliability Analysis on one-unit system*", *Operations Res.*, 9, 200-208.

COX, D.R. (1962), "*Renewal Theory*", Methun, London, UK.

ESARY, J.D. and A.W. MARSHALL (1970). *Coherent life Functions.* SIAM J. Applied Math., 18, 810-814.

SCOTT, M. (1986), "*Systems effectiveness concerning vulnerability of hardened targets to a variety of weapons*", Final Report, USAF - UES SFRP, Eglin AFB, FL.

SCOTT, M. (1988), "*Systems effectiveness for targets with repair or replacement facilities of damaged components*", USAF - UES RIP, Final Report.

SERFLING, R.J. (1980), "*Approximation Theory of Mathematical Statistics*", Wiley & Sons, New York, NY.

1988 USAF-UES SUMMER FACULTY RESEARCH PROGRAM

GRADUATE STUDENT RESEARCH PROGRAM

Sponsored by the

AIR FORCE OFFICE OF SCIENTIFIC RESEARCH

Conducted by the

Universal Energy Systems, Inc.

FINAL REPORT

Model Drawing Algorithms for a Matching Problem

Prepared by :	Stephen J. Dow, Ph.D.
Academic Rank:	Assistant Professor
Department and	Dept. of Mathematics and Statistics
University:	The University of Alabama in Huntsville
Research Location:	AFSC AD/KRTA Eglin AFB, FL 32542
USAF Researcher:	John Lindegren
Date:	August 1988
Contract No:	F49620-87-R-0004

Model Drawing Algorithms for a Matching Problem

by

Dr. Stephen J. Dow

ABSTRACT

A matching problem for obtaining motion parameters requires rapid generation of a 2D graphics image of a 3D model undergoing a 6 degree of freedom motion and perspective projection. The nontrivial part of the 3D model is a solid of revolution modeled as a series of truncated cones on a common axis, from which a sihouette must be extracted. Methods using a boundary tracking algorithm or morphological operators to extract the silhouette from a binary digital line drawn images are described. Then an algebraic approach is presented using homogeneous coordinates to reduce the motion and perspective projection to an invertible projective transformation followed by a simple orthographic projection. This made it possible to derive equations of the boundary curves forming the silhouette.

Acknowledgements

I would like to thank the Air Force Systems Command and the Air Force Office of Scientific Research for sponsoring this research and Universal Energy Systems for managing the program so well. I also thank John Lindegren, George Weekly, and Al Smith for the technical assistance they provided throughout my visit and the valuable discussions we had.

I. Introduction

One of the functions of the Computer Science Directorate of the AFSC Armament Division at Eglin AFB is the extraction of motion parameters (position and orientation) of objects contained in film or video images. This research addresses mathematical and algorithmic issues involved in a model matching approach to this problem. This approach uses the known imaging geometry of the camera and known dimensions of the object to synthesize graphical images of the object for arbitrary choices of the motion parameters; the motion parameters are varied until the graphical and film images match. In the manual matching system the graphical and camera images are overlayed and a human operator adjusts the motion parameters by joystick until the two images line up with one another. The motion parameters yielding the best match are recorded. Research is underway to automate or partially automate this matching process. The algorithms currently being considered for automated matching would use a graphical image similar to that used in the manual system. The author's previous work in developing image processing algorithms for Army applications and his knowledge of the mathematics of computer graphics contributed to his selection for this effort.

II. Objectives of the Research Effort

The research objectives as set out prior to the period of

performance were to investigate image processing algorithms applicable to the automation of the attitude determination system. This broad problem involves several major subproblems, namely model drawing (generating a 2D graphical image of a 3D model of the object of interest), feature extraction from the digitized film image, and matching algorithms relating the features and the graphical image. Both the manual system and the proposed automated system depend on accurate model generation. The model drawing software in the current manual system is not well documented and the algorithm contains inaccuracies which become apparent at certain viewing angles; i.e. the model becomes obviously distorted. For these reasons this research effort has focused on the model drawing subproblem.

III. Coordinate Transformations

This section discusses algebraic methods for performing the necessary coordinate transformations. Homogeneous coordinates are used to allow all the transformations to be represented in a consistent way using matrix multiplication and scaling. The use of homogeneous coordinates for representing computer graphics transformations can be found in Sutherland (1974) and the textbook by Foley and Dam (1982). For completeness a brief explanation is included here. Ordinary 3-dimensional coordinates (x,y,z) of a point in space are called Euclidean coordinates. Homogeneous coordinates have four components; any scalar multiple (xt,yt,zt,t)

of the vector (x,y,z,1) is called a set of homogeneous coordinates for the point with Euclidean coordinates (x,y,z). To retrieve the Euclidean coordinates of a point with homogeneous coordinates (x,y,z,w) with w nonzero one simply divides through by w and takes the first three components. Points with w = 0 are termed points at infinity and will be avoided here. The usefulness of this system here is based on the representation of transformations by a 4x4 matrix A, using the equations [x',y',z',w'] = [x,y,z,1]A, x" = x'/w', y" = y'/w', z" = z'/w'.

We denote this transformation by T_A. That is,

$T_A(x,y,z) = (x",y",z")$.

If $A = \begin{bmatrix} a & b & c & 0 \\ d & e & f & 0 \\ g & h & i & 0 \\ 0 & 0 & 0 & 1 \end{bmatrix}$ then T_A has the same effect as multiplication of the 3 component vector (x,y,z) by the 3x3 upper left submatrix of A. In particular, if this upper left submatrix is a rotation matrix, then T_A is a rotation.

If $A = \begin{bmatrix} 1 & 0 & 0 & 0 \\ 0 & 1 & 0 & 0 \\ 0 & 0 & 1 & 0 \\ a & b & c & 1 \end{bmatrix}$ then [x,y,z,1]A = [x+a,y+b,z+c,1] so that T_A is a translation by (a,b,c). These two transformations can be combined to perform any rigid motion of a 3D object.

The imaging process is modeled as a perspective projection. This transformation sends points in space to a plane called the projection plane or view plane, using a special point called the center of projection. Geometrically, the projection of a given

point p is defined to be the point where the line joining p and the center of projection intersects the projection plane. The equations of the projection are simplified by the use of a coordinate system defined in terms of the camera called the viewing coordinate system, or v.c.s. The z-axis of the v.c.s. is the center line of sight of the camera, with negative z in front of the camera. The origin is placed so that the film lies in the plane is z = f, where f is the focal length of the camera. (It is assumed that the film plane is perpendicular to the line of sight of the camera.) The x and y axes of the v.c.s. are oriented following the standard conventions (positive x right, positive y up) relative to the camera. Within this coordinate system, the imaging process is well approximated by a perspective projection with projection plane z = -f and center of projection at the origin. It is easily seen using similar triangles that the image of a point (x,y,z) under this projection is (-xf/z, -yf/z, -f).

This transformation may be represented as T_A, where

$$A = \begin{bmatrix} -f & 0 & 0 & 0 \\ 0 & -f & 0 & 0 \\ 0 & 0 & -f & 1 \\ 0 & 0 & 0 & 0 \end{bmatrix}.$$

Using these transformations we can now describe the sequence of operations involved in converting the coordinates of an individual point on the object of interest to the display screen coordinates where that point will appear in the final image. Essentially three coordinate systems are involved: the object coordinate system,

viewing coordinate system, and screen coordinate system.

The object coordinate system is set up in a convenient way relative to the objects of interest in the images, which in the application at hand are munitions dropped from aircraft. The main body of such objects is approximately a solid of revolution about a central nose to tail axis. This provides a convention for the object coordinate system: the x-axis runs along this central axis, with the tail at x = 0 and the nose on the positive x-axis. The y-axis is oriented up in the aircraft's frame of reference and the z-axis is then determined by the requirements of a right-handed, orthogonal coordinate system. In this coordinate system roll, pitch, and yaw refer to rotations about the x, z, and y axes respectively.

The viewing coordinate system, as discussed earlier, is set up in a convenient way relative to the camera. The conversion from object to viewing coordinates is called the viewing transformation. If the camera position and orientation relative to the object coordinate system are known a priori, a change of coordinates matrix performing the viewing transformation can be constructed using these parameters. When these parameters are unknown the procedure calls for the the computations to be performed using an identity viewing transformation; i.e. the v.c.s. and object coordinate system are treated as one and the same. In this case, the matching process determines motion parameters relative to the camera for each frame. Subtracting parameters determined for the first frame from those of

later frames effectively determines parameters in the object coordinate system determined by the first frame position and orientation.

The complete transformation from initial postion object coordinates to final position screen coordinates is T_A, where

$$A = A_{roll}A_{pitch}A_{yaw}A_{trans}A_{view}A_{proj}A_{scr}$$

$$A_{roll} = \begin{bmatrix} 1 & 0 & 0 & 0 \\ 0 & c & -s & 0 \\ 0 & s & c & 0 \\ 0 & 0 & 0 & 1 \end{bmatrix} \qquad A_{pitch} = \begin{bmatrix} c & s & 0 & 0 \\ -s & c & 0 & 0 \\ 0 & 0 & 1 & 0 \\ 0 & 0 & 0 & 1 \end{bmatrix}$$

$$A_{yaw} = \begin{bmatrix} c & 0 & s & 0 \\ 0 & 1 & 0 & 0 \\ -s & 0 & c & 0 \\ 0 & 0 & 0 & 1 \end{bmatrix} \qquad A_{trans} = \begin{bmatrix} 1 & 0 & 0 & 0 \\ 0 & 1 & 0 & 0 \\ 0 & 0 & 1 & 0 \\ x & y & z & 1 \end{bmatrix}$$

A_{view} = viewing transformation matrix

$$A_{proj} = \begin{bmatrix} -f & 0 & 0 & 0 \\ 0 & -f & 0 & 0 \\ 0 & 0 & -f & 1 \\ 0 & 0 & 0 & 0 \end{bmatrix} \qquad A_{scr} = \begin{bmatrix} a & 0 & 0 & 0 \\ 0 & b & 0 & 0 \\ 0 & 0 & 0 & 0 \\ d & e & 0 & 1 \end{bmatrix}.$$

For convenience we have used the same symbols c and s in the three rotation matrices; of course, they actually denote the cosine and sine of 3 different angles. As discussed above the view transformation matrix may be an identity matrix, in which case it is not needed. As stated earlier f is the camera focal length. Parameters a, b, d, and e control the final scaling and translation to device dependent screen coordinates; using the terminology of the current calibration system they are

a = rasters/inch in x direction, b = rasters/inch in y direction,

d = raster x coordinate of center of projection,

e = raster y coordinate of center of projection.

IV. Model Representation and Silhouette Extraction

Having constructed the matrix A as defined in the previous section, any given point can be transformed from its initial position object coordinates to final screen coordinates by the operations $[u,v,0,w] = [x,y,z,1]A$, $x_{screen} = u/w$, $y_{screen} = v/w$. The next problem is to decide which points to transform in this way and plot on the screen to obtain the desired graphical image of the object. Normally, the two endpoints of a line segment on the object are transformed, and a command to draw a line is sent to the graphics screen. The graphics hardware takes care of the scan conversion of the line; i.e. given the endpoint coordinates it determines the individual pixels making up the line on the screen.

As mentioned in the previous section the main body of the objects of interest is a solid of revolution, with the x-axis as the axis of revolution. This part of the object is specified by giving a sequence of pairs (x,r), where r is the radius of the body at the given x-coordinate. If (x_1,r_1) and (x_2,r_2) are two consecutive such pairs, then in effect the section of the body between planes $x = x_1$ and $x = x_2$ is being approximated by a truncated cone. The remaining parts of the object are represented as polygons.

If hidden line elimination is not required, the polygonal parts can be drawn by simply transforming the vertex coordinates and drawing the edges; pairs of vertices forming edges are stored as a list of pairs of indices into the vertex coordinate table. The

first approach to drawing the main body consists of generating a grid of line segments densely covering the body. The grid points are obtained by parametizing each cross-sectional circle. If the (x,r) pairs are (x_i,r_i), i = 1,2,...,n and the number of points on each circle is m, then the grid points are $p_{ij} = (x_{ij},y_{ij},z_{ij})$, i = 1,2,...,n, j = 1,2,...,m, where

$x_{ij} = x_i$,

$y_{ij} = r_i\cos(360(j-1)/m)$,

$z_{ij} = r_i\sin(360(j-1)/m)$. The grid lines are the line segments

$p_{ij}p_{i+1,j}$, i = 1,2,...,n-1, j = 1,2,...,m,

$p_{ij}p_{i,j+1}$, i = 1,2,...,n, j = 1,2,...,m-1, and

$p_{im}p_{i1}$, i = 1,2,...,n.

The dense grid of lines produced may be undesireable compared to a drawing in which only the edges along the boundary of the main body are generated. This boundary will be called the silhouette. We now consider methods of extracting this silhouette. In this section digital approaches are described. These use a binary digital image, an array of zeros and ones, each entry of which corresponds to a pixel. Such an array in graphics memory is manipulated by the graphics line drawing calls. An equivalent array can be accessed directly by declaring it in the program and replacing the calls to the graphics screen with calls to a subroutine which scan-converts lines into the array. A version of Bresenham's algorithm for scan-converting lines was used here; see Foley and Dam (1982). The array is initialized to all zeros and the pixels on the scan-converted lines are set to one.

The following discussion assumes knowledge of connectivity concepts which can be found in Rosenfeld and Kak (1982). The scan conversion produces 8-connected digital line segments. Since any grid point can be reached from any other grid point by a sequence of grid lines, it follows that the set of one-valued pixels in the array is 8-connected. Here we need the assumption that the pixels on the image boundary (first and last rows and columns of the array) are all zeros; i.e. the object being drawn does not run off the edge of the image. The 4-connected components of zeros (i.e. the background components) consist of one surrounding component which contains all the pixels on the image boundary together with a number of interior components between the grid lines. The pixels forming the silhouette may be defined as the one-valued pixels having at least one 4-neighbor in the surrounding background component. There are a number of methods for identifying this set of pixels, that is, producing a new binary image in which only these pixels have value one. One method is boundary tracking, a method commonly used to obtain the chain code representation of the boundary of an object. A boundary tracking algorithm starts at some pixel on the boundary of an object, then steps from one pixel to the next along the boundary, at each step moving to an 8-neighbor of the current pixel and recording the direction taken at that step as one entry in the chain code. A clockwise (or counterclockwise) search of the 8-neighbors of the current pixel is used to find the next boundary pixel. This approach has been implemented on a VAX workstation, with the silhouette being

drawn as a sequence of individual pixel plotting commands once the boundary track is complete.

Another digital method of silhouette extraction may be more efficient in the presence of special purpose hardware for performing morphological operations. Assume that the binary digital image has been produced as before. Set the pixels on the image boundary equal to some value other than 0 or 1, say 2. Now perform the following neighborhood operation recursively until no pixel changes value: $A_{out}(i,j) = 2$ if $A_{in}(i,j) = 0$ and at least one of the 4-neighbors of $A_{in}(i,j)$ is a 2, otherwise $A_{out}(i,j) = A_{in}(i,j)$.
This sequence of operations stops when all pixels in the surrounding background component have been labeled 2; intuitively, the 2's on the image boundary expand out until they run into the 1's of the object. Now perform one more neighborhood operation to label the silhouette: $A_{out}(i,j) = 1$ if $A_{in}(i,j) = 1$ and at least one of the 4-neighbors of $A_{in}(i,j)$ is a 2, otherwise $A_{out}(i,j) = 0$.

V. Algebraic Methods for Computing Boundary Curves

As mentioned earlier the main body of our object is modeled as a series of solid truncated cones. The solid truncated cone is bounded by three surfaces (a cone and two planes) which fall into the category of quadric surfaces. General techniques for drawing quadric surfaces have appeared, for example Levin (1976). In the special case of a solid truncated cone, the boundary of the projected solid (the silhouette) is a single ellipse or consists of portions of

two ellipses and two line segments. We present a computational method for distinguishing the cases and computing the applicable equations needed to draw the boundary curve.

Let T_{op} denote the orthographic projection defined by $T_{op}(x,y,z) = (x,y)$. Because the method discussed below uses this rather than the perspective projection to get from 3D to 2D we need to express the transformation T_A of section 3 (which includes the perspective projection) as the composition of an invertible transformation followed by the orthographic projection. Note that

$$A_{proj}A_{scr} = \begin{bmatrix} -af & 0 & 0 & 0 \\ 0 & -bf & 0 & 0 \\ d & e & 0 & 1 \\ 0 & 0 & 0 & 0 \end{bmatrix} = \begin{bmatrix} -af & 0 & 0 & 0 \\ 0 & -bf & 0 & 0 \\ d & e & 0 & 1 \\ 0 & 0 & 1 & 0 \end{bmatrix} \begin{bmatrix} 1 & 0 & 0 & 0 \\ 0 & 1 & 0 & 0 \\ 0 & 0 & 0 & 0 \\ 0 & 0 & 0 & 1 \end{bmatrix} = A_1A_2$$

The matrix A_1 is invertible, while the matrix A_2 represents the orthographic projection. Let $B = A_{roll}A_{pitch}A_{yaw}A_{trans}A_{view}A_1$. Then $A = BA_2$, and B is invertible.

A quadric surface is the set S_Q of points (x,y,z) satisfying an equation of the form

(1) $$Q(x,y,z) = q_1x^2 + q_2y^2 + q_3z^2 + q_4xy + q_5xz + q_6yz + q_7x + q_8y + q_9z + q_0 = 0.$$

This equation may be written in matrix form as

(2) $$[x\ y\ z\ 1]A_Q[x\ y\ z\ 1]^t = 0,$$

where $$A_Q = \begin{bmatrix} q_1 & q_4/2 & q_5/2 & q_7/2 \\ q_4/2 & q_2 & q_6/2 & q_8/2 \\ q_5/2 & q_6/2 & q_3 & q_9/2 \\ q_7/2 & q_8/2 & q_9/2 & q_0 \end{bmatrix}$$

Conversely, given a 4x4 matrix A there is a corresponding quadratic form $Q(x,y,z)$. The matrix A need not be symmetric; in general corresponding off-diagonal entries are added to obtain coefficients q_4 through q_9.

The quadric surface of interest here is a circular cone having equation $y^2 + z^2 = (mx + b)^2$. (Note : the term cone as used here includes the case of a cylinder.) In matrix form the equation is

(3) $$[\ x\ y\ z\ 1\ ]\ A_{cone}\ [\ x\ y\ z\ 1\ ]^t = 0,$$

where $A_{cone} = \begin{bmatrix} m*m & 0 & 0 & mb \\ 0 & -1 & 0 & 0 \\ 0 & 0 & -1 & 0 \\ mb & 0 & 0 & b*b \end{bmatrix}$.

This surface undergoes the transformation T_B defined above and then is orthographically projected to obtain its image in screen coordinates. Applying the transformation T_B to the cone gives the quadric surface S_Q with matrix $A_Q = B^{-1}A_{cone}(B^{-1})^t$.
To see this suppose (x,y,z) is on the cone and (x",y",z") = $T_B(x,y,z)$. Then [x y z 1] satisfies equation (3), and
[x" y" z" 1] = (1/w')[x' y' z' w'],
where [x' y' z' w'] = [x y z 1]B. Hence
$w'[\ x"\ y"\ z"\ 1]B^{-1} = [\ x'\ y'\ z'\ w']B^{-1} = [\ x\ y\ z\ 1\ ]$. Substituting this expression into (3) and dividing through by w'^2 gives
$[\ x"\ y"\ z"\ 1\ ]\ B^{-1}A_{cone}(B^{-1})^t\ [\ x"\ y"\ z"\ 1\ ]^t = 0$, which shows that (x",y",z") satisfies (2) with $A_Q = B^{-1}A_{cone}(B^{-1})^t$.
This matrix A_Q is symmetric, so we may use the notation given earlier for the entries of A_Q. The equation of the transformed surface S_Q is then given by (1).

When $Q(x,y,z)$ is written as a polynomial $a_0z^2 + b_0(x,y)z + c_0(x,y)$, the discriminant $D_Q = b_0^2 - 4a_0c_0$ is found to be

$$D_Q = (q_5^2 - 4q_1q_3)x^2 + (2q_5q_6 - 4q_3q_4)xy + (q_6^2 - 4q_2q_3)y^2 + (2q_5q_9 - 4q_3q_7)x + (2q_6q_9 - 4q_3q_8)y + q_9^2 - 4q_3q_0$$

The orthographic projection of the surface S_Q is

$T_{op}(S_Q) = \{ (x,y) :$ there exists z with (x,y,z) on $S_Q \}$

$= \{ (x,y) : D_Q >= 0 \}$. The boundary of this set is determined by examining the solution set of the equation $D_Q = 0$. The boundary consists of two lines if and only if D_Q can be factored as $D_Q = (d_0x + d_1y + d_2)(d_3x + d_4y + d_5)$ and the two factors are unequal. In this case setting the two factors equal to 0 gives equations of the two lines. See Bloom (1979), p. 449, for more justification and explanation.

Next we derive equations (in screen coordinates x, y) for the ellipses which are the projections of the circular cross sections of our model. In initial position each such circle may be described as the intersection of a cone with a plane having equation $x = c$. It was shown above that applying the transformation T_B gives a transformed cone having equation (1) with the coefficients q_i from the matrix $A_Q = B^{-1}A_{cone}(B^{-1})^t$. When the same is done for the plane $x = c$, the coefficients of the equation of the transformed plane are easily computed from the matrix B giving

(4) $(b_{11} - b_{14}c)x + (b_{21} - b_{24}c)y + (b_{31} - b_{34}c)z + b_{41} - b_{44}c = 0.$

where b_{ij} is the ij entry of B^{-1}. If the coefficient of z in (4) is zero, the cross section is oriented along the line of sight so that

the projection of the cross section degenerates to a line segment. Disregard this case for the moment so that equation (4) can be rewritten as

(5) $$z = a_p x + b_p + c_p.$$

Now the equation of the ellipse which is the image of the given cross section is obtained by substituting the expression for z in (5) into equation (1). The result is an equation of the form

(6) $$ax^2 + bxy + cy^2 + dx + ey + f = 0,$$

where the coefficients are expressions in $q_0,\ldots,q_9,a_p,b_p,c_p$. Following this procedure for two successive x coordinates gives the equations of two ellipses. Either one of these ellipses falls inside the other and the boundary of the projected truncated cone is the larger ellipse or this truncated cone gives rise to bounding lines whose equations were computed above. In the latter case, each of the bounding lines is tangent to the two ellipses, and the line segment joining the two points of tangency is part of the boundary. To compute the endpoints of each line segment, we solve simultaneously the equation of the boundary line found above, say $d_0x + d_1y + d_2 = 0$, and equation (6) above of the ellipse. In the case where the coefficient of z in (4) is zero (and the ellipse collapses to a line segment), we replace (6) in this procedure with (4). In other words, this case reduces to finding the intersection of two lines with known equations.

The silhouette of the entire solid of revolution consists of portions of the line segments and ellipses computed for each of the

component truncated cones. It can be obtained by scan-converting these ellipses and line segments and then applying one of the digital silhouette extraction techniques discussed in section 4.

We conclude this section with some remarks comparing the methods. The model drawing software in current use apparently identifies two extreme points on each projected cross-section and connects these with two series of line segments to form an approximate silhouette. It is possible to produce a reasonably accurate silhouette by this method when each section has linear boundaries, which is generally the case in side views or near side views, but the method produces a false silhouette otherwise. The situation worsens as one approaches an end view and the nose "folds" (changes from convex to concave). At this point it becomes obvious that the silhouette is incorrect; however it should be noted that the silhouette may be significantly inaccurate prior to this event. Whether the grid lines of section 4 or the algeraically derived lines and ellipses are used, this problem is eliminated by the methods discussed here as a result of the fact that both the linear and elliptical boundaries are included. The algebraic method improves on the grid line approach in that the linear boundaries are computed exactly up to machine round off, rather than relying on one of the m longitudinal grid lines of a given section approximating each linear boundary.

VI. Recommendations

The software implementation of the methods discussed here was hurried and needs further testing; the principles of the methods have been demonstrated though. The models generated by previous methods should be compared with those generated by the methods developed here; this may be particularly useful in determining accuracy as a function of orientation for those methods which have problems with end views. The algorithms presented here deal with all views in a consistent manner. Further research should concentrate on the feature extraction and matching algorithms needed for automated matching.

References

Bloom, D M., Linear Algebra and Geometry, Cambridge University Press, 1979.

Foley, J.D. and Dam, A.v., Fundamentals of Interactive Computer Graphics, Addison-Wesley, 1982.

Levin, J., A Parametric Algorithm for Drawing Pictures of Solid Objects Composed of Quadric Surfaces, Comm. of the ACM 19, pp. 555-563, 1976.

Rosenfeld, A. and Kak, A.C., Digital Picture Processing, Academic Press, 1982.

Sutherland, I.E., Sproull, R.F., and Schumacker, R.A., A Characterization of Ten Hidden Surface Algorithms, ACM Computing Surveys 6, pp. 1-55, 1974.

1988 USAF - UES SUMMER FACULTY RESEARCH PROGRAM

Sponsored by the

AIR FORCE OFFICE OF SCIENTIFIC RESEARCH

Conducted by the

Universal Energy Systems, Inc.

FINAL REPORT

Two Dimensional Simulation of Railgun Plasma Armatures

Prepared by:	Manuel A. Huerta, Ph. D.
Academic Rank:	Professor
Department and :	Physics Department
University:	University of Miami
Research Location:	AFATL/SAH
	Eglin AFB, FL 32542-5000
USAF Researcher:	Mr. Kenneth K. Cobb

Date:	26 Aug 1988
Contract No:	F49620-87-R-0004

Two Dimensional Simulation of Railgun Plasma Armatures

by

Manuel A. Huerta

ABSTRACT

We report on our development of a two dimensional MHD code to simulate the internal dynamics of a railgun plasma armature. We use the equations of resistive MHD, with Ohmic heating, and radiation heat transport. We use an explicit Flux Corrected Transport code to advance all quantities in time. Preliminary runs show the growth and shedding of plasma structures in response to a small perturbation upon an initial equilibrium. We completed a run of an isothermal plasma armature that reached the end of a 1 m barrel. We have done many debugging runs of a full radiation heat transport model. At this point we are completing the revised code for this model. We expect to run it in a Cray-2 in the near future.

Acknowledgements

I would like to thank the Air Force Systems Command and the Air Force Office of Scientific Research for sponsorship of this research. I would also like to thank Universal Energy Systems for the efficient way in which they administered the USAF - UES Summer Faculty and Graduate Student Research Program.

I spent the summer at AFATL together with my graduate student, Mr. G. C. Boynton. Our experience was productive and enjoyable thanks to the cooperation we received from many people at AFATL. First we would like to thank Dr. Sam Lambert for making it possible for us to use the excellent computer resources at AFATL as well as the Cray-2 at the AFWL, Kirtland AFB. Next we would like to thank Mr. Kenneth K. Cobb who helped us so many times in actually getting access to the resources that we needed. We also thank him for interesting discussions of work in rail guns, specially his own B dot coil analysis. We thank Capt. E. Cottle for setting us up with abundant disk space and other resources on the VAX 8650 at site A15, and Mr. Andy Marino for his system assistance on that machine. We also thank the staff of the RSPL at AFATL, specially Mr. Mike Wallace, Capt. Mike Mets, and Mr. Phil Destin, for setting us up on their VAX 785, and for their assistance in getting postscript output from the Printserver 40. We also used the Vax 8650 at the IPL at AFATL and we thank the staff, specially Mr. Lee Prestwood, Mr. Larry Neal, and Matt Shannon. These two machines were valuable in themselves for debugging purposes, but they were essential to let us connect to the UV2 machine at AFATL through which we networked via TELNET to the Cray at AFWL. Last, but not least, we thank Mr. Ron Hunt of AFATL for his help in setting up our accounts at the AFWL and other assistance.

I. INTRODUCTION

I have had contacts with the AFATL/SAH branch since the beginning of their heavy involvement with research on electromagnetic railguns with a plasma armature. An impressive railgun facility has been built on Okaloosa Island at site A15 and there is quite a bit of experimental activity on diagnostics of the arc plasma armature. There are also people there working on developing one dimensional computer simulations of the plasma armature.

My graduate student, Mr. G. Christopher Boynton, and I have been working under a recently expired AFOSR grant on a two dimensional simulation of armature plasmas but we still have not completed the work. One of our principal needs was access to a supercomputer to run our programs. We also could profit from abundant access to a VAX 8650 such as is available at the site A15 railgun facility for debugging purposes. These common interests made it appear that spending a summer of intensive research work would be valuable.

II. OBJECTIVES OF THE RESEARCH EFFORT

Our work centers on continuing the development of a two dimensional time dependent simulation of plasma armatures. We model the plasma with the equations of resistive MHD and we use a two dimensional fully explicit FCT code to advance all quantities in time. The physical effects that we include in our model are the same as in the steady, one dimensional model of Powell and Batteh[1]. Therefore we leave out viscosity, and other effects that can be important in a boundary layer. A good deal of effort has also been expended on developing graphical methods that allow convenient display of the results.

We have done several runs in the University of Miami's VAX 8650, which does about 1,000 steps per hour of CPU time for a plasma with an adiabatic energy equation

and a calculational grid with 20 by 240 cells. Mr. Boynton and I presented a paper[2] with the equations and some of the results of this work for the adiabatic case. We continued the calculation after that paper and in Figure 1 we show the pressure plotted vertically over the rectangular grid that covers the 2-dimensional plasma. Here the pressure distribution is shown after 200,000 time steps that represent an elapsed time of 89.87 μsec. By this point the VAX 8650 has accumulated about 200 hours of CPU time and we have to keep reducing the time step size to avoid numerical instabilities.

Clearly this problem is one that requires a supercomputer. Our objective during the summer of 1988 was to run isothermal and fully heat conducting models at the VAX 8650 available at site A15. We also intended to submit runs at the Cray located at the Air Force Super Computer Center (AFSCC) at the Air Force Weapons Laboratory (AFWL) at Kirtland AFB.

III. COMPUTER FACILITIES UTILIZED IN THE WORK

From the start we enjoyed excellent cooperation from everyone we were connected with. Mr. Kenneth K. Cobb always got us in touch with the right person to get what we needed. We were soon running and debugging in the site A15 VAX 8650 thanks to the assistance of Capt. E. Cottle and Mr. Andy Marino. The early work was delayed because the brand new VAX 8650 would crash often. Another problem was the need to bring down the 8650 because it is not protected against lightning. This was specially bothersome because thunderstorms are common here in the summer. These problems will be remedied when the 8650 is moved to the new building being constructed at site A15 where it will have the proper lightning protection and power conditioning equipment.

We invested some time in learning to use the Cyber 176 at the Math Lab at Eglin

AFB. We gave this up, however, because it was clear that this machine would not be much faster than the 8650 at site A15 because of the many competing users. In order to network to the Cyber, and later on to the Cray, we had to go to the main base, which is about 20 miles away from site A15 because the site is not yet in the network. That is another thing that will be improved when the new building is completed.

We did our networking and computing at the main base using two computer facilities. First the Radar Signal Processing Laboratory (RSPL) where there is a VAX 785. Here we were assisted by Mr. Mike Wallace, and others. We also used the Image Processing Laboratory (IPL) where there is a VAX 8650. From either of these labs we connected to the Math Lab's VAX 8650, called node UV2. From this node we could connect to the Cyber, or via TELNET, later on, to the Cray at the AFSCC. Clearly there were a lot of machines involved and it took time to get accounts in all of them. We encountered crashing problems at these labs too. The IPL's 8650 was brand new and crashed often for its own reasons. A faulty air conditioning system also brought both machines down several times.

We obtained our account numbers in the CRAY-2 at the AFSCC around the beginning of our 7th week. Up until that moment we had been spending most of our time working with the VAX 8650 at site A15. From that moment on we spent most of our time at the main base networking to the Cray and debugging at the IPL computer.

IV. WORK ACCOMPLISHED

We did many runs of a fully heat conducting model, although with fixed ionization fractions. Even with that simplification we found many bugs in the program. The bugs sometimes took time to show themselves and for us to understand what was

happening. Sometimes we thought we were getting a numerical instability and we started to develop an implicit code to advance the temperature in time. Then it turned out that we simply had a programming error. Even now, at the end of the summer research period, we have not had a completely successful run of the fully heat conducting program. We believe that we are close to that goal, however, and that the explicit FCT method will run successfully with a time step size that is not unreasonably small.

We have developed a successful program to calculate the ionization fractions from the Saha equations and include them in our main program. To save CPU time, however, we have developed a lookup table of true temperature and ionization fractions in terms of pressure and density. The main program will interpolate in the table instead of using the Saha equations at each grid point, at each time step.

Rather than continue running the full program we decided it would be wise to use the last few weeks learning to use the Cray and running an isothermal model. We have also been learning the use of the DISSPLA graphics system that is available in the Cray. This seems very powerful but is different from the NCAR system that we have been using.

V. ISOTHERMAL PLASMA

We show some of the results obtained for the isothermal run at the site A15 VAX 8650. Figure 2 shows the progress of the run. It was first submitted on 11 August, 1988 at 10:51. By 11:41 it had done 1000 time steps. By 12:24 it was up to 2000 time steps, and so on. However, it can be seen that in other days it might not run at all, depending on the weather, and whether the system manager could restart it when we were physically not there but working at the main base. The table shows that it would run at a rate of about 1500 time steps per hour of CPU time in the

8650. The run ends when the armature has advanced one meter. We know that this takes about 120000 time steps. Even as this report is being written it has done some 62000 time steps. We will take it down on the last day and finish it at the University of Miami's VX 8650. It is fortunate for us that we have been working with fully compatible machines.

We use a computational grid that has 20 cells in the short direction from rail to rail. The long direction of the grid begins at the rear of the projectile at cell 1 and extends toward the breech for a length of 200 cells. The conducting plasma ends at cell 100. Beyond that there are 100 cells of low density, nonconducting plasma that extends to the end of the computational region. The boundary condition at the 200th cell is very passive so as to have no effect. Essentially any plasma that gets to the end of the computational region with nonzero velocity simply leaves. The nonconducting region is made large so that as the conducting plasma expands toward the rear it will not reach the end of the computational region by the time the run ends. This way we can follow the phenomena that may occur back there.

Figure 3 shows the density profile over the entire grid of 20 by 200 cells after 37,000 time steps. The highest density shown is some 15 kg/m^3. The lowest density is at the rear, with a value of about 0.1 kg/m^3, but plotted with zero height. Figure 4 shows the pressure profile magnified near the region where the plasma density is very low and the the plasma is taken to be nonconducting. Here the equilibrium is showing some strong disturbances building up. Figure 5 shows the vector field for the current density vector J. It shows a deformation of the boundary between the conducting and the nonconducting plasmas, and a buildup of current density right at the interface.

From the above figures it can be seen that at least in the isothermal case, where

the initial equilibrium is 1 dimensional, the plasma seems pretty sturdy. The deformations at the rear boundary grow but do not seem to have a terribly disruptive effect upon the plasma.

VI. RECOMMENDATIONS

We believe it is not self serving to recommend that this work be continued. We have spent about two years working on this difficult problem and we are close to the point where we will have a successful code. This sort of two dimensional simulation will do a lot to obtain further insights into the behavior of plasma armatures. The principal insights so far have been provided by the one dimensional models. Most of the 1 dimensional models have been steady, along the lines of Ref. 1. Recently Batteh and Rolader[3] have reported on a time dependent 1 dimensional simulation.

Our work encompasses all that 1 dimensional work and extends it to 2 dimensions where there are profound differences. For example, not only would the ussal one dimensional equilibrium develop instabilities of various sorts, but a 2 dimensional equilibrium does not even exist. We are hopeful to continue this work and develop impressive displays of the armature simulation. We are excited that the AFSCC provides output to 16mm film. It would really be nice to have movies of the armature simulation in a variety of conditions.

We expect that our accounts at the A15 and the UV2 Vaxes 8650, and at the AFSCC Cray will continue for a while longer so we can conclude this stage of our work.

REFERENCES

1. Powell, J. D., and Batteh, J. H., "Plasma Dynamics of an Arc-Driven Electromagnetic Projectile Accelerator," J. Appl. Phys., **52**, 2717 (1981)

2. Huerta, M. A., and Boynton, G. C.,"Two Dimensional Time Dependent MHD Simulation of Plasma Armatures", Proceedings of the 4th Symposium on Electromagnetic Launch Tecchnology", Austin, Texas, April 1988.

3. Batteh, J. H., and Rolader, G. E., "Modeling of Transient Effects in Railgun Plasma Armatures," U. S. Army Ballistic Research Laboratory, Contract Report No. BRL-CR-567, March 1987.

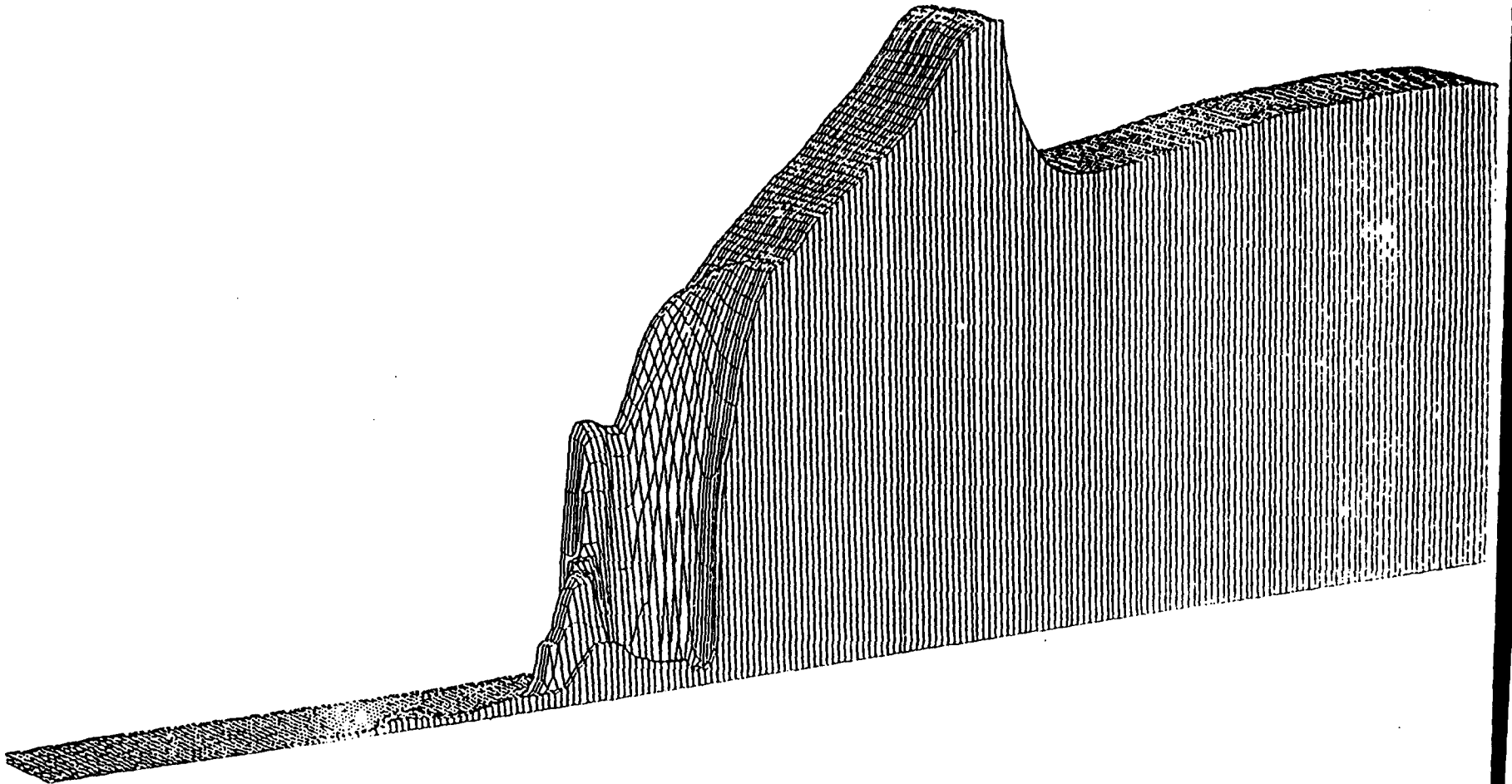


Figure 1

Time = 8.9873E-05 s, SFRM = 4.9E-02 m, VFRM = 1.1E+03 m/s, AFRM = 1.22E+07 m/s^2
Projectile toward right
1_240_rho_200000.psc

```
Directory DJA2:[CHRISTPF.ISO_BIG]

M_JX_000000.OUT;2     11-AUG-1988 10:51
M_JX_000000.OUT;1     11-AUG-1988 10:48
M_JX_001000.OUT;1     11-AUG-1988 11:41
M_JX_002000.OUT;1     11-AUG-1988 12:24
M_JX_003000.OUT;1     11-AUG-1988 13:08
M_JX_004000.OUT;1     11-AUG-1988 13:56
M_JX_005000.OUT;1     17-AUG-1988 14:22
M_JX_006000.OUT;1     17-AUG-1988 15:04
M_JX_007000.OUT;1     17-AUG-1988 15:47
M_JX_008000.OUT;1     17-AUG-1988 16:29
M_JX_009000.OUT;1     17-AUG-1988 17:12
M_JX_010000.OUT;1     17-AUG-1988 17:56
M_JX_011000.OUT;1     18-AUG-1988 07:04
M_JX_012000.OUT;1     18-AUG-1988 07:47
M_JX_013000.OUT;1     18-AUG-1988 08:30
M_JX_014000.OUT;1     18-AUG-1988 09:13
M_JX_015000.OUT;1     18-AUG-1988 10:01
M_JX_016000.OUT;1     18-AUG-1988 10:47
M_JX_017000.OUT;1     18-AUG-1988 11:29
M_JX_018000.OUT;1     18-AUG-1988 12:11
M_JX_019000.OUT;1     18-AUG-1988 13:15
M_JX_020000.OUT;1     18-AUG-1988 14:03
M_JX_021000.OUT;1     18-AUG-1988 14:50
M_JX_022000.OUT;1     18-AUG-1988 15:51
M_JX_023000.OUT;1     19-AUG-1988 08:28
M_JX_024000.OUT;1     19-AUG-1988 09:10
M_JX_025000.OUT;1     19-AUG-1988 09:53
M_JX_026000.OUT;1     19-AUG-1988 10:35
M_JX_027000.OUT;1     19-AUG-1988 11:18
M_JX_028000.OUT;1     19-AUG-1988 12:00
M_JX_029000.OUT;1     19-AUG-1988 12:42
M_JX_030000.OUT;1     19-AUG-1988 13:25
M_JX_031000.OUT;1     19-AUG-1988 14:07
M_JX_032000.OUT;1     19-AUG-1988 14:49
M_JX_033000.OUT;1     19-AUG-1988 17:16
M_JX_034000.OUT;1     23-AUG-1988 14:37
M_JX_035000.OUT;1     23-AUG-1988 15:20
M_JX_036000.OUT;1     23-AUG-1988 16:06
M_JX_037000.OUT;1     23-AUG-1988 16:49
M_JX_038000.OUT;1     23-AUG-1988 18:20

Total of 40 files.
```

Figure 2. The file M_JX_001000.out;1 was produced on 11-August-1988, at 11:41. The figure shows the progress of the calculation up to 38,000 time steps.

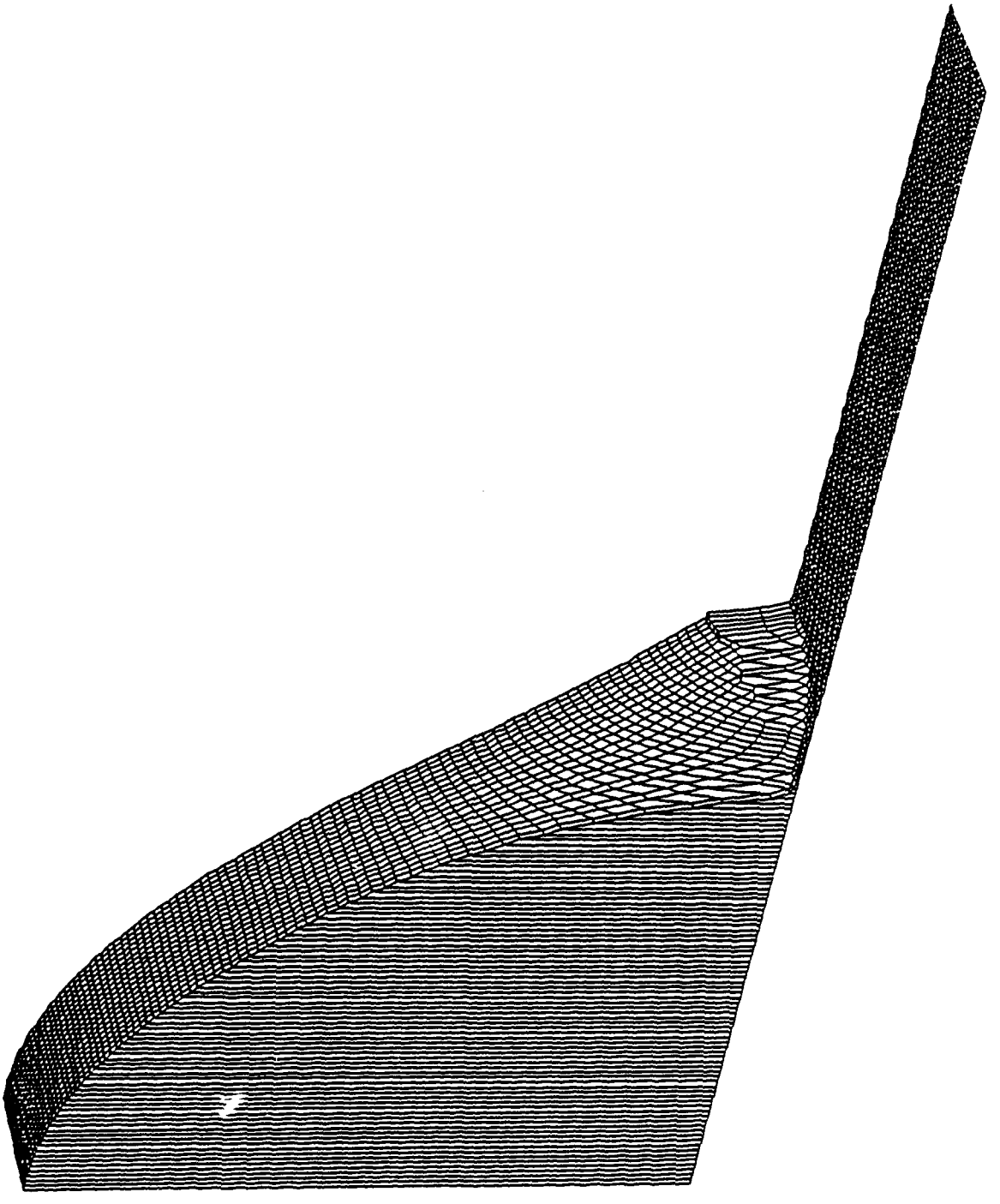


Figure 3. Plasma density profile after 37,000 time steps. The time step size is about 3.7 nanoseconds, and the elapsed time is 1.38E-4 sec.in this as well as in all the figures that follow.

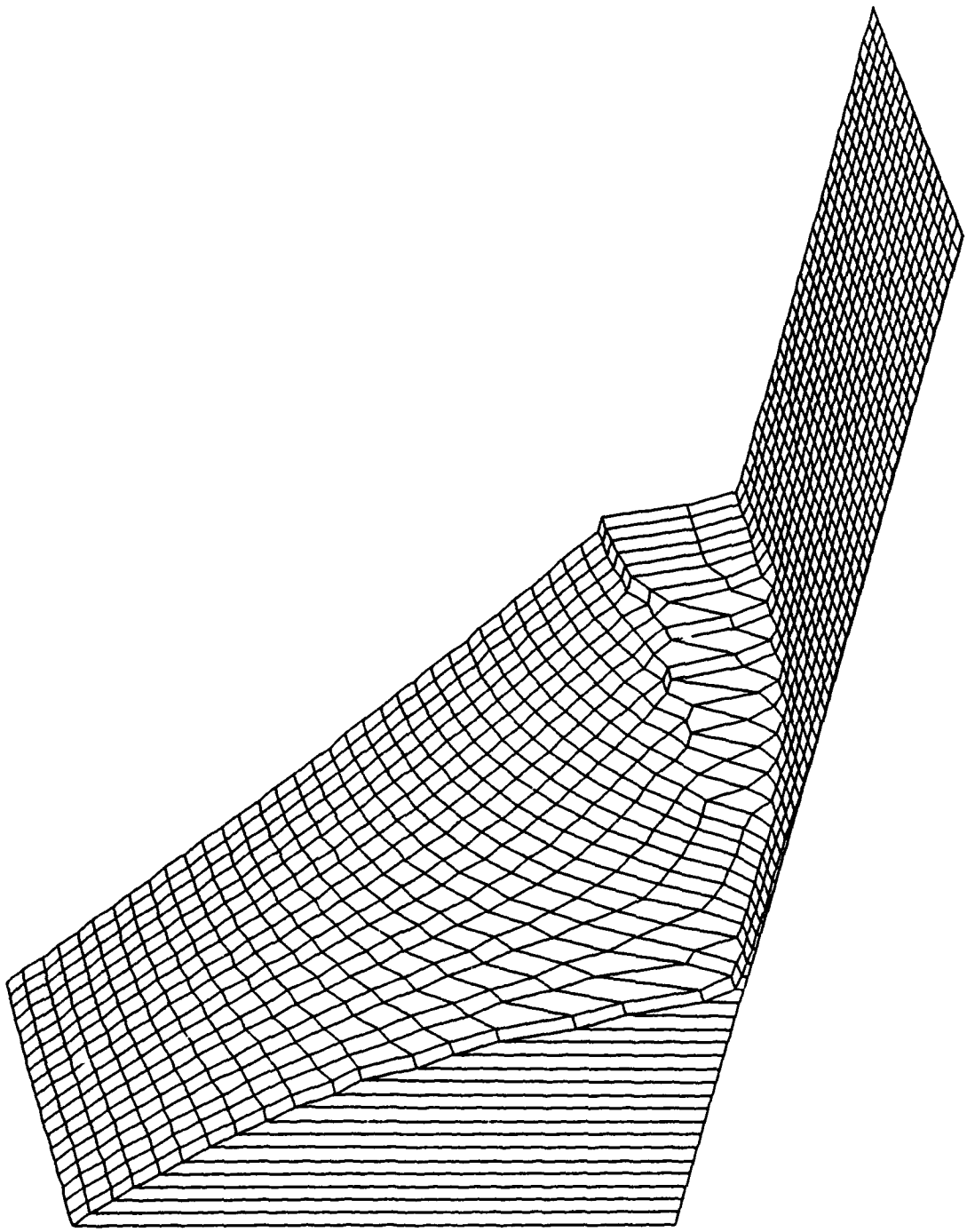


Figure 4. Magnified view of the density profile near the end of the conducting plasma region.

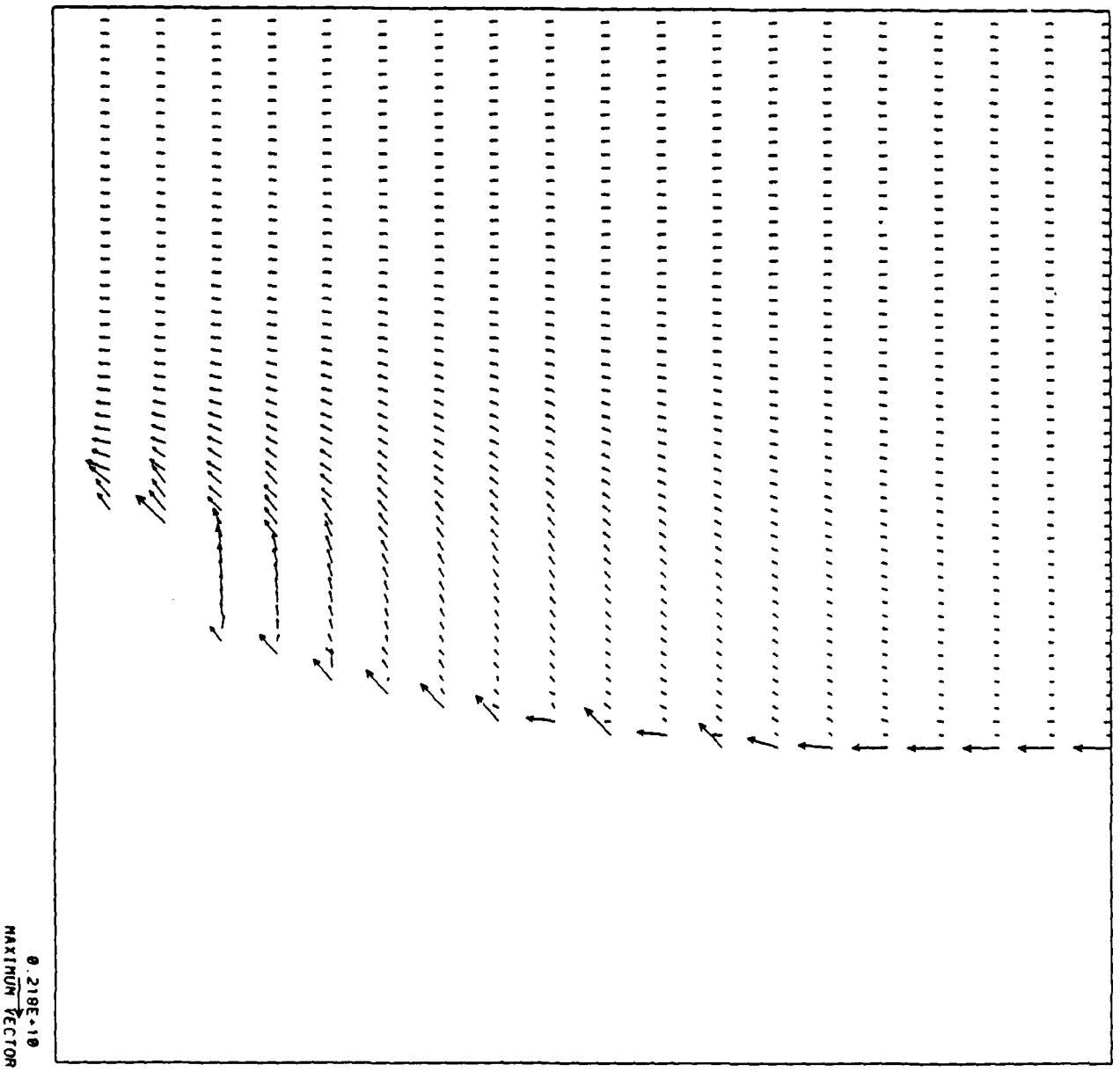


Figure 5. The current density vector field J. It shows a concentration at the end of the conducting region.

1988 USAF-UES SUMMER FACULTY RESEARCH PROGRAM/
GRADUATE STUDENT RESEARCH PROGRAM

Sponsored by the
AIR FORCE OFFICE OF SCIENTIFIC RESEARCH
Conducted by the
Universal Energy Systems, Inc.

FINAL REPORT

MODELING REACTIVE FRAGMENTS

Prepared by:	Anastas Lazaridis
Academic Rank:	Assistant Professor
Department:	Mechanical Engineering
University:	Widener University
Research Location:	AFATL/MNW Eglin AFB, FL 32542-5000
USAF Researcher:	Albert L. Weimorts, Jr.
Date:	August 19, 1988
Contract No:	F49620-87-R-0004

MODELING REACTIVE FRAGMENT WARHEADS

by

Anastas Lazaridis

ABSTRACT

The interaction of a reactive fragment with its target is a complicated process in which several physical phenomena occur simultaneously. In general, impact and penetration through the skin of the target are associated with shock waves that produce spall and vaporific effects. The latter result from chemical reactions and secondary combustion in and around an expanding turbulent jet. The effectiveness of the reactive fragment is commensurate with the target materials it encounters, the geometry after impact, particle size, velocity, and temperature of spall, environmental pressure and temperature, dispersion and mixing characteristics of the reactants, and reaction kinetics. For modeling purposes, all targets are grouped in two classes. The first consists of several layers of solid materials, such as plates of metals or organic composites, while the second is a fluid confined behind one or two layers of solid materials.

This work presents an evaluation of the literature obtained from a computer search and in-house sources, identifies gaps in the available information, defines areas of further research, and makes recommendations for future experimental and theoretical work.

ACKNOWLEDGMENTS

I wish to thank the Air Force System Command and the Air Force Office of Scientific Research for sponsoring this investigation. My appreciation also goes to the Air Force Armament Laboratory and its management for exposure to many aspects of the work conducted there and the opportunity to perform this study. Special thanks go to Mr. Albert L. Weimorts, Jr. for his constant interest in the success of this work, Dr. Samuel C. Lambert for his assistance in administrative matters, Mr. Ronald B. Boulet for his encouragement and interest in the early part of this work, Mr. Edward C. Poston, Jr. and Dr. Joseph C. Foster, Jr. for sharing their knowledge and technical expertise with me, Cpt. Otmar (Nick) Yakaboski for his help in the office, and to the members of the secretarial pool, Mrs. Elva Lovering, Mrs. Kathy Fuszner, Mrs. Joan Thielan, and Mrs. Donna Welle. I am especially grateful to Mr. Andrew G. Bilek for his friendship, warmth, and continued support during my stay at Eglin Air Force Base.

I. INTRODUCTION

Reactive fragments are projectiles that contain a small quantity of a highly reactive material and are designed to break up from a warhead in similar fashion as the standard rod fragments. Upon impact, the reactive material is released and the potential for a fast chemical reaction with behind-the-target debris becomes a possibility. If the proper conditions are present, such a reaction can generate enough energy to destroy the target.

The concept of the reactive fragment kill mechanism was demonstrated with large scale tests in which single projectiles filled with a hypergolic oxidizer were shot at normal incidence onto different types of targets, and damage was assessed compared to results obtained with inert projectiles. This comparative experimentation technique indicated that fuel tanks can be made to explode catastrophically[1], and radar antennae and airplane sections can be damaged extensively[2-7]. It was also reported that the energy release payoff of reactive projectiles can be as high as 4:1 compared to conventional explosives[8] and total impulse delivered can be twice as much as the same weight of a high explosive[2].

The Bombs and Warheads Section of the Armament Laboratory at Eglin Air Force Base is obviously interested in the reactive fragment kill mechanism and has supported a major part of the ongoing research. It is currently involved in a program to generate the necessary scientific information for the development of an appropriate vulnerability model, which can be used to assess the efficacy of this energy enhancement technique vis-a-vis other more conventional methods.

My field of expertise is the fluid-thermal sciences with research interests in energy engineering and consequently combustion. Prior to this assignment I performed a study on the thermal characteristics of spall behind aluminum and steel targets attacked by shaped charge warheads. Although the reactive fragment problem is different than that of the shaped charge jet, it exhibits many similarities with it.

Examples include the generation of shock waves, perforation, spall, and the important phenomenon known as vaporifics.

II. OBJECTIVES OF THE RESEARCH EFFORT

The interaction of a reactive fragment with its target is a complicated process that is associated with several physical phenomena. In general, impact and penetration through the skin of a target are associated with shock waves that produce spall and vaporific effects. The latter occur as a result of simultaneous chemical reactions of metal and oxidizer, and secondary combustion of materials in the spall. Other phenomena include melting, ablation, air entrainment, and particle dispersion in and around an expanding turbulent jet.

The intent of the overall program is to isolate the phenomena associated with the interaction of a reactive fragment and its target, assess the relative contribution of all pertinent parameters, and establish a quantitative cause and effect relationship between them. The objectives of this work were to conduct a literature search and obtain pertinent bibliography, identify areas of further research, and develop a plan for the definition of future experimental and/or theoretical work in the pursuit of a predictive model.

III. DISCUSSION OF RESEARCH FINDINGS

To reach the goals of the overall program, the project was broken into several tasks. This phase consisted of a) familiarization with ongoing research on the topic, b) isolating individual physical phenomena that occur simultaneously as the reactive fragment interacts with its target and conducting a literature search, c) evaluating the material obtained from the literature search and procuring the appropriate bibliography, d) examining the available information and

identifying any gaps that require further research, and e) developing a plan for future work.

Reports on relevant work supported directly by the laboratory became the first source of information. One of these projects investigated potential reactive materials and concluded that some highly reactive oxidizing agents were the most attractive candidates [3]. Based on this result, all subsequent experimentation focused on one or two of these reactive oxidizers.

Current interest in the reactive fragment concept stems from the success of field tests with either simulated potential targets or components of real targets. These tests demonstrated the ability of the reactive fragment to cause catastrophic failure of tanks containing hydrocarbon fuel and to incapacitate solid components of air or land targets, such as an airplane wing or a radar antenna[1-4]. When the oxidizer dispersed in the vapor region, partially filled fuel tanks were reported to suffer less damage than those that were completely filled[4]. A hypervelocity application in an oxygen-starved atmosphere also showed promising results[5-7]. In an attempt to estimate the peak pressure behind a target, the Fluid Dynamics of Hydraulic Ram IV computer program was used with an additional routine for thermochemical calculations. Since chemical kinetic information was not available, predictions were based on some arbitrary assumptions for the start and finish of the reaction. With those assumptions, the peak pressure behind the target was shown to correlate with experimental measurements[4]. These studies demonstrated the effectiveness of the reactive fragment, but failed to develop data that can be used to model it.

In an effort to understand how the reactive fragment interacts with the target, an attempt was made to isolate the individual physical phenomena that take place simultaneously. The most important of these were judged to be a) projectile-to-target impact, penetration, and spall formation, b) simultaneous dispersion of particles, mixing, and chemical

reaction in an expanding turbulent jet, c) air entrainment behind this jet, and d) secondary combustion. The term vaporifics is used for the net combined effect of all these factors. Other less important, but still pertinent phenomena include aerodynamic heating, wind effects, and ablation. These were not considered in this work.

A literature search was conducted using the DTIC/DROLS, DIALOG, BRS, and COMPUSERVE's Energy and Chemical Abstracts Databases. The basic areas of interest in this first search were spallation, reactive turbulent jet characteristics, combustion, metal and fuel oxidation kinetics, and the particular oxidizers used. Approximately one-third of the more than two-hundred sources identified was selected for further study. A little more than half of this has been received to date.

An excellent account of the state-of-the-art of enhanced energy coupling techniques was given by Beckofen, et al.[9] This report reviewed two-hundred-twenty-one references, summarized relevant Soviet literature with a bibliography of two-hundred-ninety items, and gave an additional list of two-hundred-ten references on chemical oxidation reactions and reaction kinetics. The latter was a mere collection of literature, which was deemed to be pertinent, but was not discussed. The need to develop a detailed quantitative model for vulnerability analyses was stressed throughout this report. Emphasis was also placed on the lack of information involving the effects of target altitude and velocity. Conclusions related to the reactive fragment program were: a) Vaporific effects result from combined contributions of mechanical and chemical processes and include rapid combustion of metals; b) Oxidation or oxidation-like processes are greatly enhanced by pure oxygen, but they also occur in nitrogen, carbon dioxide, and exhaust gas atmospheres; c) Vaporific combustion is commensurate with the mixing of reactants, shock heating of the mixture, and particle size of solids in the mixture; d) Soviet research has generated extensive information on metal combustion and explosion.

The lack of a verifiable vulnerability model for reactive fragments was also stated by Cunningham[4]. His tests with reactive projectiles showed evidence of improved lethality[3,4,8], which is consistent with known chemical reaction data. Brown, et al. discussed vaporific effects behind aluminum, steel, and titanium targets after impact with solid reactive projectiles[10]. They also gave a detailed description of the butterfly blast impulse gauge they used along with a procedure for its calibration. Similar attempts were made with aluminum and jet fuel targets by Williams[11] and Wittrock, et al.[12] Their results were reported to be marginally better than steel pellets. Waggener conducted experiments using reactive projectiles filled with an explosive and reported that the peak pressure behind the target was two to three times that obtained from the same amount of explosive placed in steel projectiles[13]. An explanation was offered based on heats of formation in some of the reactions that could occur. To improve explosion efficiency, Tulis, et al. placed an oxidizer and a fuel in different compartments of the same container, and attempted to mix them by a combination of simultaneous implosion and explosion. The expected outcome did not materialize as the reaction turned to a deflagration. The cause of the failure to achieve detonation was attributed to the establishment of a buffer zone of reaction products at the interface between the two reactants, which tended to expand and push the reactants apart[14]. The rapid oxidation of diesel fuel was studied by Von Elbe and McHale. They reported the occurence of high blast pressures that were larger when the ambient atmosphere was air instead of nitrogen and even more so when it was oxygen[15,16].

A good account of spallation and metal ignition was given by Piechocki, et al. in a closely related study to reactive fragments[17]. In recent publications, Grady used an "energy balance" theory to describe spall characteristics of metals and obtain an estimate of spall particle sizes[18,19].

The oxidation of nonvolatile metals leads to the formation of metal

oxides that cover the exposed surfaces of the metal and prevent its direct contact with oxygen. Oxidation can continue further only by diffusion of gas through the oxide protective layer. For most metals, if the oxide film remains compact, the diffusion kinetics of the process are given by the solution $x = (2At)^{1/2}$, where x is the oxide film thickness, t is the reaction time, and A is a constant proportional to the product of the diffusion coefficient and the reaction rate[20]. The amount of gas diffusing through the oxide film and the reaction rate are inversely proportional to the film thickness and consequently to the square root of the time. This result, however, is valid only after some time from the onset of the process when a steady distribution of the concentrations of the diffusing substances is established in the film. In the initial stages of the process, the reaction rate has a more complex time dependence. In some cases, the growth of the film decreases almost exponentially with time and virtually ceases after a while. When there is a large difference between the physical properties of the metal and its oxide, the film disintegrates as the temperature of the oxidation process is increased and the access of oxygen to the surface of the metal is facilitated. When the combustion temperature reaches the melting point of the oxide, the liquid oxide is blown by the gas current. This enhances the oxidation process by exposing fresh metal. The combustion temperature of iron in air, for example, is below the melting point of the oxides formed. Therefore, the oxide film blocks the surface from exposure to oxygen and minimizes its rate of combustion. This condition between the combustion temperature and the melting point of the oxides formed can be reversed if the ambient air temperature is increased. In that case, iron can burn freely in air. When iron is burned in an oxygen atmosphere, its combustion temperature exceeds the melting point of the oxides, which are blown off to expose the metal surface and allow it to continue its combustion[21,22]. Finely particulated aluminum is combustible. Its presence in an explosive mixture can enhance the effects of detonation resulting in higher quasistatic pressure levels compared to similar conditions exclusive of the aluminum particles[23]. When aluminum burns, various oxides form, but eventually all the oxides

turn to the most stable compound Al_2O_3, which condenses out[24]. Ar important feature of the evaporation and combustion of condensed phases is the thermal inertia of the condensed phase caused by its high heat capacity. Pressure fluctuations ensure penetration of the combustion gases into the pores of the solid. With a change in the pressure, the conditions in the gas phase change rapidly, but the thickness of the heating zone in the condensed phase can not adjust to the change as quickly, and the pulsating combustion mechanism of condensed phases confined in closed spaces may occur[21].

In the area of metal ignition and combustion, Tulis presented experimental results for unconfined dispersions of aluminum particles in air that produced detonation velocities to 1.9 km/s. The surface area for such detonations was estimated at 3-4 sq.m./g while finely atomized particles were stated to be less potent[25]. An experimental apparatus for the study of dust fires and explosions, and experiments involving sulfur dust dispersions were discussed by McKown[26]. An empirical formula was used by Gurevich, et al. to calculate the limiting ignition temperature of aluminum particles in the range of 1-50 microns. Experimental data were shown to correlate with the predictions, which indicated that the ignition limit can be below the melting point of the metal oxide as long as the particles are small[27]. The experiments of Gal'chenko, et al. indicated that the oxidation of aluminum in a carbon dioxide environment proceeds in the same way as in an oxygen atmosphere except that the critical ignition temperature can be higher than the melting point of the metal oxide. This temperature depends on the rate of heat transfer from the medium surrounding the metal and the amount of energy entering directly to it[28]. Smelkov, et al. presented experimental evidence indicating that aluminum particles in the range of 0.5-3 mm burn in two distinct periods. In the first period, the particles are at the vapor temperature of the metal while the second period is characterized by the combustion of metal particles behind an oxide protective film at a temperature near the melting point of the oxide[29]. In the work of Belyaev, et al., aluminum powder with particle sizes to 300 microns was

imbedded in fuel-oxidizer mixtures at initial concentrations of up to 20%. It was found that the ignition time of smaller particles was shorter than that of the larger particles, the ignition time decreased as particle concentration increased, and burning time increased with aluminum particles[30].

Metal combustion has also been modeled mathematically. Grigor'ev and Grigor'eva investigated radiation effects in metal combustion. Their development of the model was based on the assumption that metal particles were heated by the flow of hot oxidizer that diffuses in the metal[31]. A mathematical model for conglomerates of metallic particles neglecting radiation was discussed by Bondarev, et al. An asymptotic solution gave ignition limits for highly porous conglomerates. It is stated that the integro-differential equations governing the problem need to be solved numerically when the conglomerates have high enough densities. An example is given for boron particles[32]. The flammability limit of a conglomerate of metallic particles was studied by Gurevich, et al.[33] Another model was developed by Grachukho, et al. to treat the combustion of metallic particles introduced into a fuel as an additive. Experimental results for magnesium were found to agree with the mathematical predictions[34]. Gremyachkin, et al. considered a model of the combustion of a metal droplet in which a condensed oxide is formed both in the gas and on the surface of the burning metal droplet. For small droplets the oxide around the droplet does not affect the combustion rate appreciably. The dependence of the time of combustion of aluminum droplets on the parameters of their environment was obtained[35]. A very basic model of pyrophoricity/hypergolicity of metals as a function of their particle size was generated by Beltran. Boron was used as an example to verify the accuracy of this model[36].

Of the seven references obtained on the characteristics of reactive flows, only one considered the reaction of condensed phases[37-44]. The analysis of Al Fakir and Houlain led to the determination of the total reaction rate in terms of the so called diffusional and kinetic speeds

under the assumption that decomposition in either the condensed or gaseous phase results in the same final products[37].

IV. FUTURE RESEARCH NEEDS

Although much information is currently available, there is need for further research in some fundamental areas of the reactive fragment problem. Tests to date demonstrated its potential lethality, but generated very little data that can be used in a vulnerability model. Important questions that are still unanswered include the chemical reaction kinetics of the reactants, the dispersion and mixing characteristics of fuel and oxidizer at different impact velocities and angles of obliquity, the spall sizes behind the target and their compatibility with metal ignition/oxidation requirements, the effect of moisture in the air, and what happens in oxygen-starved atmospheres especially if the target moves at relatively high speeds. In addition, most of the information involving the reaction of potential target materials with candidate reactive substances is known at low to moderate temperatures. New data must be generated to provide reaction characteristics at environmental conditions compatible with the reactive fragment application.

The first two questions are somewhat interrelated even though they are different in nature. In fast reactions, the dispersion and mixing of the reactants is the controlling mechanism while chemical kinetics takes a secondary role. Nevertheless, reaction kinetics determine when the reaction starts and whether it can be sustained. If the reaction is too rapid, interfacial forces may split the reactants apart and the reaction may cease to continue unless a mechanism is present for mixing the reactants. The latter could be provided by the target.

Existing hydrodynamic codes are capable of monitoring the internal energy of striker and target as functions of their geometry, relative

impact velocity, and materials involved, and can indicate the state and phase of these materials, but not their particle size.[9] To model the reactive fragment quantitatively, these computer codes need to be expanded to include the effects of the parameters that control the processes behind the target. The latter are particle size, transient pressure and temperature, dispersion and mixing of the reactants, and reaction kinetics. The last two of these are dependent on flow and molecular diffusion characteristics. For modeling purposes, targets may be grouped in two classes with the first consisting of various layers of solid materials, such as plates of aluminum, steel, or organic composites, while the second may comprise several solid, typically metallic, layers followed by a fluid confined behind them. It is to be noted that under proper conditions most materials are potential fuels.

V. RECOMMENDATIONS

This survey has uncovered information from the literature, which is applicable to the reactive fragment problem. Since this work is not completed, it is advisable to continue the literature search in the areas of reactive flows, high temperature metal and hydrocarbon oxidation reactions, their kinetics, and mathematical modeling.

Using the results of Grady's work [19], average particle sizes behind aluminum targets were calculated to be in the range from less than one millimeter to about ten millimeters. A few controlled impact experiments can determine the validity of this estimate.

Based on the findings of this investigation, a parallel effort of both experimental and theoretical nature is recommended. The experimental work consists of three different groups of tests.

1. Controlled Impact Tests - Using inert and oxidizer filled projectiles on single and multiple layer targets in controlled environments, obtain behind the target particle sizes and temperatures, environmental

temperature and pressure histories, dispersion/mixing behavior, physical characteristics and chemical composition of the debris for normal and oblique impacts at different velocities and initial environmental conditions, ranging from those at sea level with various amounts of moisture content to those at high altitude. These tests will produce direct data on impact and vaporific effects behind the target. Special instrumentation needed inludes high-speed photography and pyrometry.

2. Static Tests - Mixing hydrocarbon fuels or metallic particles at different conditions with a reactive oxidizer in a closed container, obtain temperature and pressure histories, heats of reaction, and time needed for reaction initiation and completion with or without the presence of air and moisture. Both stoichiometric and non-stoichiometric amounts should be tested. These tests can provide reactivity data of the oxidizer with potential target materials.

3. Dynamic Tests - In a shock tube equipped with high speed photographic equipment and necessary sensors, measure reaction characteristics of fuel and oxidizer at various inlet velocities and initial conditions. Application of spectroscopy, high-speed photography, and laser technology may be in order for these tests.

In addition to generating important data, these tests will provide answers to whether vaporific effects are as pronounced in oxygen-starved atmospheres as they are at sea level and if atmospheric moisture affects the hypergolicity of materials.

On the theoretical side, determining the hypergolic limits of some metals of interest to this program, mathematical methods in oxidation, theories on the kinetics of reactions involved, and developing computer algorithms of metal oxidation are some areas that come to mind.

This investigator plans to propose a continuation of effort to include a) expanding and completing the literature survey, b) obtaining hypergolic limits for metals of interest to this program, c) researching mathematical techniques toward developing a computer algorithm for metal oxidation, and d) analyzing data from the proposed tests.

REFERENCES

1. Tulis, A. J., "Liquid Filled Pellets", Report No. AFATL-TR-78-70, Air Force Armament Laboratory, Eglin AFB, FL 32542 (July 1978).

2. Martin Marietta Aerospace, "Reactive Fragment Tests Against Radar Antenna Targets", Report No. OR 18,268, AFATL, Eglin AFB, FL 32542 (Mar. 1985).

3. Cunningham, J. E., "Reactive Fragment Investigation", Report No. AFATL-TR-82-52, Air Force Armament Laboratory, Eglin AFB, FL 32542 (Aug. 1982).

4. Cunningham, J. E., "Reactive Fragment Warhead", Report No. AFATL-TR-85-47, Air Force Armament Laboratory, Eglin AFB, FL 32542 (Oct. 1985).

5. Remar, J. and Gagliano, J., "Reactive Projectile Study for SDI Application", Report No. AFATL-TR-87-09, Air Force Armament Laboratory, Eglin AFB, FL 32542 (Apr.1987).

6. Watt, R. M., "Hypervelocity Impact Tests of Reactive Projectiles", Report No. AEDC-TSR-86-V24, Arnold Engineering Development Center, Tullahoma, TN (Sept. 1986).

7. Watt, R. M., "Reactive Projectile Test", Data Package for Report No. AEDC-TSR-86-V24, Arnold Engineering Development Center, Tullahoma, TN (Aug. 1986).

8. Cunningham, J. E., "Reactive Warhead Handling Technology and Application Assessment", Report No. AFATL-TR-86-12, Air Force Armament Laboratory, Eglin AFB, FL 32542 (June 1986).

9. Backofen, J. E., Jr., Kennedy, D. R., and Golovin, M. N., "Enhanced Energy Coupling Phenomena: A State-of-the-Art Survey and Assessment", Air Force Armament Laboratory, Eglin AFB, FL 32542 (Apr. 1980).

10. Brown, R. E., Kato, K. G., and Zernow, L., "Quantitative Evaluation of Pyrophoric Impact Effects - Phase II", Report No. AFATL-TR-74-36, Air Force Armament Laboratory, Eglin AFB, FL 32542 (Jan. 1974).

11. Williams, R. W., "Hypergolic Fragments", Report No. AFATL-TR-82-69, Air Force Armament Laboratory, Eglin AFB, FL 32542 (Sept. 1982).

12. Wittrock, E. P. and Williams, R. E., "An Investigation of Composite Hypergolic Fragments", Report No. AFATL-TR-83-76, Air Force Armament Laboratory, Eglin AFB, FL 32542 (Oct. 1983).

13. Waggener, S. S., "Combustion of Reactive Cased Explosively Filled Cylinders", Report No. NSWC-TR-82-279, Naval Surface Weapons Center, Dahlgren, VA 22448 (Aug. 1982).

14. Tulis, A. J., Austing J. L., Foster, J. C., Jr., and Forbes, K., "Blast Enhancement Using Fuel/Oxidizer Explosive Detonation", Report No. G06051H055-14, Air Force Armament Laboratory, Eglin AFB, FL 32542 (June 1986).

15. Von Elbe, G. and McHale, E. T., "Chemical Initiation of FAE Clouds", Report No. AFOSR-TR-78-1479, Air Force Office of Scientific Research, Bolling AFB, Washington, D.C. 20332 (Oct. 1978).

16. Von Elbe, G. and McHale, E. T., "Chemical Initiation of FAE Clouds", Report No. AFOSR-TR-81-0255, Air Force Office of Scientific Research, Bolling AFB, Washington, D.C. 20332 (Nov. 1980).

17. Piechocki, J. J., Burchfield, J.A., and Kennedy, D. R., "Active Warhead Exploitation - Phase I", Air Force Armament Laboratory, Eglin AFB, FL 32542 (May 1976).

18. Grady, D. E., Bull. Am. Phys. Soc. 30, 8, 1305 (1985).

19. Grady, D. E., "A Strain-Rate-Dependent Spall Mechanism Transition in Metals", Report No. SAND-87-0741C, Sandia National Laboratory, Albuquerque, N. M. 87185 (1987).

20. Kofstad, P., High-Temperature Oxidation of Metals, J. Wiley & Sons, Inc., New York, N.Y. (1966).

21. Frank-Kamenetskii, D. A., Diffusion and Heat Transfer in Chemical Kinetics, Plenum Press, New York, N.Y. (1969).

22. Robertson, D. G. C. and Jenkins, A. E., " The Reaction of Liquid Iron and Its Alloys in Pure Oxygen", Heterogeneous Kinetics at Elevated Temperatures, G. R. Belton and W. L. Worrell, Editors, Plenum Press, New York, N.Y. (1970), pp 393-408.

23. Veyssiere, B., Bouriannes, R., and Manson, N., "Detonation Characteristics of Two Ethylene-Oxygen-Nitrogen Mixtures Containing Aluminum Particles in Suspension", Gas Dynamics of Detonations and Explosions, J. R. Bowen, et al., Editors, Progress in Astronautics and Aeronautics, Vol 75, AIAA, New York, N.Y. (1981).

24. Mann, D. M. and Weaver, D. P., "An Optical and Mass Spectrometric Study of the Aluminum-Oxygen Flames", AFPRL-TR-84-053, Air Force Rocket Propulsion Laboratory, Air Force Space Technology Center, Edwards AFB, CA (1984).

25. Tulis, A. J., "Detonation of Unconfined Solid Fuel Particles Dispersed in Air", Proc. Sixth Int'l Pyrotechnics Seminar, pp. 615-633 (1978).

26. McKown, G. L., "Investigation of Methods for Detection and Control of Pyrotechnic Dust Fires and Explosions", Proc. Sixth Int'l Pyrotechnics Seminar, pp. 402-409 (1978).

27. Gurevich, M. A., Lapkina, K. I., and Ozerov, E. S., "Ignition Limits of Aluminum Particles", Fizika Goreniya i Vzryva 6, 2, pp. 172-175 (Apr.-Jun. 1970) - Combustion, Explosion, and Shock Waves, pp. 154-157 (1972).

28. Gal'chenko, Yu. A., Grigor'ev, Yu. M., and Merzhanov, A. G., "Ignition of Aluminum in Carbon Dioxide", Fizika Goreniya i Vzryva 9, 1, pp. 115-119 (Jan.-Feb. 1973) - Combustion, Explosion, and Shock Waves, pp.96-98.

29. Smelkov, G. I., Aleksandrov, A. A., Pekhotikov, V. A., and Grishin, E. V., "Combustion of Large Aluminum Particles in an Air Flow", Fizika Goreniya i Vzryva 14, 5, pp. 33-37 (Sep.-Oct. 1978) - Combustion, Explosion, and Shock Waves, pp. 581-584 (1979).

30. Belyaev, A. F., Ermolaev, B. S., Korotkov, A. I., and Frolov, Yu. V., "Combustion Characteristics of Powdered Aluminum", Fizika Goreniya i Vzryva, 5, 2, pp.207-217 (1969) - Combustion, Explosion, and Shock Waves, pp. 142-148.

31. Grigor'ev, A. I. and Grigor'eva, I. D., "Ignition of Metal Particles", Fizika Goreniya i Vzryva, 12, 2, pp. 208-211 (Mar.-Apr. 1976) - Combustion, Explosion, and Shock Waves, pp.182-184.

32. Bondarev, V. N., Zolotko, A. N., Klyachko, L. A., Polishchuk, D. I., Shevchuk, V. G., and Yakovleva, T. A., "Ignition of Conglomerates of Metallic Particles", Fizika Goreniya i Vzryva, 13, 2, pp. 164-168 (Mar.-Apr. 1977) - Combustion, Explosion, and Shock Waves, pp. 136-139.

33. Gurevich, M. A., Ozerov, E. S., and Chivilikhin, S. A., "Flammability Limit of a Conglomerate of Metallic Particles", Fizika Goreniya i Vzryva, 8, 4, pp. 526-532 (Oct.-Dec. 1972) - Combustion, Explosion, and Shock Waves, pp. 432-436.

34. Grachukho, V. P., Stepanov, A. M., and Khvattsev, A. A., "Estimate of the Dispersion of Products of Combustion of a Metal Particle", Fizika Goreniya i Vzryva, 12, 4, pp. 519-530 (Jul.-Aug. 1976) - Combustion, Explosion, and Shock Waves, pp. 470-480.

35. Gremyachkin, V. M., Istratov, A. G., and Leipunskii, O. I, "Mechanism of Combustion of an Aluminum Droplet in a Gaseous Oxidizer", Arch. Termodyn. Spalania, 8, 1, pp. 13-26 (1977).

36. Beltran, M. R., "Pyrophoric and Hypergolic Properties [illegible]on", Report No. AD-B089 774L, JANNAF 21st Combustion Me[illegible], pp. 65-99 (Oct. 1984).

37. Al Fakir, M. S. and Houlain, P., "Kinetic Pa[illegible]ers of Solid Propergol Combustion in Flammable Flows", C[illegible] Int'l Berthelot - Vieille - Mallard - Le Chatelier 1, pp. 31[illegible] (1981).

38. Strahle, W. C., "Stagnating Turbulent Reac[illegible]g Flows", Report No. ARO-20658.5-EG, U.S. Army Research Office, [illegible]. O. Box 12211, Research Triangle Park, NC 27709 (Jan. 1988).

39. Pope, S. B., "PDF Methods for Turbulent Reactive Flows", Prog. Energy Combust. Sci. 11, pp. 119-192 (1985).

40. Varma, A. K., Mansfield, P. I., and Sandri, G., "Second-Order Closure Modeling of Variable Density Turbulent Flows", Report No. ARAP-2-PU, Purdue University, West Lafayette, IN 47907 (1979).

41. Dupoirieux, F., "Numerical Calculations of Turbulent Reactive Flows and Comparison with Experimental Results", Workshop on the Gas Flame Structure, Novosibirsk (Jul. 1986).

42. Pospelov, V. A. and Fedotov, A. V., "Estimate of the Influence of Chemical Kinetics on the Parameters of a Turbulent Layer During the Mixing of Hydrogen and Fluorine", Trudy Leningradskiy Politekhnicheskiy Institut imeni, M. I. Kabinina, Leningrad, Nr. 352, pp. 51-54 (1976).

43. Sirignano, W. A., "Molecular Mixing in a Turbulent Flow: Some Fundamental Considerations", Combust. Sci. and Tech. 51, pp. 307-322 (1987).

44. Smith, G. D. and Giel, T. V., "An Experimental Investigation of Reactive Turbulent Recirculating Jet Mixing", Report No. AFDC-TR-79-79, Arnold Eng'g Dev't Center, Tullahoma, TN (May 1980).

1988 USAF-UES SUMMER FACULTY RESEARCH PROGRAM

Sponsored by the

AIR FORCE OFFICE OF SCIENTIFIC RESEARCH

Conducted by the

Universal Energy Systems, Inc.

FINAL REPORT

Prepared by:	Kwang S. Min, Ph.D.
Academic Rank:	Professor
Department and University:	Physics Department East Texas State University
Research Location:	AFATL/MNF Eglin AFB Ft. Walton Beach Fl. 32542
USAF Researcher:	Capt. James Hawkins
Date:	16 Aug. 1988
Contract No.	F49620-87-R-0004

Target-Aerosol Discrimination Techniques for Active Optical Proximity Sensors

by

Kwang S. Min

ABSTRACT

Development of all-weather Active Optical Proximity Sensors have been of vital interests to USAF for the applications in armament systems. False signals caused by cloud, fog, and snow interfere with proper response of the sensors, and efforts to discriminate the target signals from those of aerosol have been in progress for nearly two decades [1-18].

Upon examination of recent efforts by the Air Force [5-10] and by the Army [11-15], developments of three new methods for the aerosol discrimination were initiated. They utilize signal processing techniques to separate the Ladar returns. Their preliminary simulation results are encouraging. In the process, a new aerosol model has been introduced.

Some considerations for the realistic system implementation of these methods are given, and possible uses of parallel computing archtecture, optical signal processing, and ASIC technology are discussed. Prospective utilizations of signal processing on artificial neural nets and Kalman or adaptive filtering are also included.

Acknowledgements

I would like to thank the Air Force Systems Command and the Air Force Office of Scientific Research for sponsorship of this reasearch. Deep appreciation goes to Universal Energy Systems for their kind concern and all administrative arrangement of the program.

My research experience at AFATL was rewarding and enlightening. Dr. Sam Lambert, Chief Scientist of the Laboratory, gave warm guidance and everlasting encouragement. Capt. James Hawkins and Mr. Robert Orgusaar whom I collaborated with closely furnished a great deal of help during the course of this research. I am indebted to present and former branch chiefs of MNF, Ron Boulet and Lanny Burdge for their hospitality. Numerous helps of Capt. Mike Caraway in C-language programming and his encouragement in every aspect of the research were of great value.

Interactions with Mr. Roy Stables and Dr. E. Friday of TEAS, and Messers Bob Erhart, Dennis Goldstein, Dick Mabry, Bob Erdman, Harris Barker, and Dr. Duane Finello of the laboratory were productive. Discussion with Mr. Walter Smith, who initiated the alternate sector subtraction algorithm, was delightful. Various help in VAX computations were provided by Major David A. Gaitros, Mr. Brian Brazil, and Airman Daniel Joey of AD/KR and are deeply appreciated. Mr. Thad Wallace's kind cooperation in the use of HP300 for the Motorola software examination activity is acknowledged.

I. INTRODUCTION

1. Statement of problem

The effectiveness of a missile warhead against air targets can be significantly improved if detonation takes place at a desired distance from the target toward an optimum direction. To maximize effectiveness a proximity sensor shoud provide a detonation signal at an optimum range based upon the encounter kinematics (optimum burst point). Active optical proximity sensors are considered to be advantageous over radio frequency sensors for proximity fuzing in terms of: (1) its range and azimuthal resolution, and (2) susceptibility to countermeasures. However, numerous earlier efforts to develop a robust optical sensor for this application have not been fully successful [1-18]. Presence of dense clouds, fog, or snow will create false signals and will obscure the proper detection of the target.

2. Background and Existing Work

Development of an all-weather active optical sensor, which provides proximity fuzing capability highly resistant to aerosol interference and electronic countermeasures, has been one of goals of AFATL/MNF for some time. Typical contracual activities in recent years include work by Santa Barbara Research Center [5], Delco Electronics [6], Honeywell [7] and McDonnell Douglas [8] (Self Detecting Optical Proximity Sensor, or SDOPS) and Motorola (Near Infrared Fuze Technology, or NIFT) [9]. These efforts as well as Independent Research and Development programs have been addressing the issue.

Some earlier programs [3,4] deal with discrimination of cloud return and target signal by means of detecting the polarization differences. The Santa Barbara Research Center approach utilizes innovative optical design to discriminate the false signal from the target. Delco Electronics employed analog filtering techniques to discriminate the shape of the return signals. The SDOPS efforts by Honeywell and McDonnell Douglas which spans from 1979 through 1984 deals with various optical system designs to facilitate an alternate sector subtraction algorithm. This effort has been extended further in the NIFT program to refine algorithm and sensor design and was carried out form 1985 thru 1988 by Motorola.

Harry Diamond Laboratory (US Army) has been actively engaged in characterizing aerosol signatures, devising signal deconvolution techniques, and developing effective discrimination methodology [11-15]. Their efforts are analytical and well formulated. Recent work by Sztankay [15] summarizes most of their activities in aerosol-target discrimination in 0.9 um IR range. A few documents from the Navy Weapons Center describe their activities in this area. However, those on hand date from the 1970's.

My research interests have been in the area of digital signal/image processing and their applications to various systems. Recent work include the introduction of a new transform [19] and a separation of signals [20] utilizing orthogonal transforms and filtering. This contributed to my assignment to study of this problem during 1988 Summer Faculty Research Program at the AFATL/MNF on Eglin AFB.

II. OBJECTIVES OF THE RESEARCH:

Currently, there is no robust all-weather active optical proximity sensor available. Numerous efforts to develop a fuze which is capable of discriminating the target and aerosol returns have been in progress for nearly two decades. For the SFRP assignment, the writer was assigned to this problem and charged to do the followng:

(1) study the algorithms currently in use for the aerosol discrimination

(2) develop an alternate technique or techniques if possible.

Studies of most of efforts by all three branches of services on the subject are carried out including recent programs. Some considerations for the refinement of current techniques are given.

On the other hand, development of alternate techniques to allow discrimination of real target signals from false alarms produced by aerosols were initiated and preliminary results obtained. These techniques are based on signal processing principles, and the initial simulation results are studied. A limited study of hardware implementations of the proposed algorithms to realistic systems is also carried out.

Most of the software for the development of the techniques and their simulations are to be developed by the Summer Graduate Student Research Fellow (HSM), and to be written in C-language or pascal for a convenient modular approach. Use of graphics is fully emphasized throughout. Some considerations will be given for future applications of signal processing in the fuze program.

III. POSSIBLE REFINEMENT OF EXISTING WORK

At the onset of the summer research program a reasonable amount of time was invested in learning encounter kinematics through fly-out and end-game programs to deal with air-to-air encounter and fuzing problems. It provided a general understanding of the field. A draft copy of the final report of the NIFT project (Motorola) was studied along with reports on a few preceeding programs. Also examined is the Active Optical Fuze Model software written by Motorola for the HP300 computer. The report covers the work spanning the last two and a half year, and the software included some simulations and illustrations for the NIFT project. The copy of the software version on hand required a little alteration to run the entire program.

After the study of several technical reports on the optical proximity sensors and related aerosol-target discrimination techniques, fair comprehension of the assignment was achieved. Some of the thoughts given to the possible refinement of the existing effort are listed below.

[a] Possible Refinement of SDOPS

Improved optical and electronic designs currently available may be able to remedy most of the limitatations and shortcomings reported in the final report.

[b] Possible Modification of NIFT

Lack of normalization of intensity of pencil beams to achieve effective alternate sector subtraction was one of difficulties in the proper implemention of the algorithm. Use of star

couplers and some difficulties encountered in tooling the optical fibers may have caused this hardship. Instead of using a limited number of laser diodes and spliting the beams, it may be more effective to use individual diode for each pencil beam, and normal the return signal digitally. Diodes and signal processing VLSIs are becoming more affordable and the clock speed of the ICs is steadily increasing.

[c] Further Considerations on Alternate Sector Subtraction Algorithms:

The alternate sector subtraction algorithm is primarily for aerosol rejection and aimed at fuzing action under adverse weather conditions; therefore, it may be possible to achieve similar results using signal processing techniques.

This may not have been practical several years ago when the high speed signal processor was not cost effective for a fuze. New developments in microelectronics and the computing architecture currently available make them possible to implement. Three alternate approaches to this problem have been considered. The first one involves multiple sensor array and is applicable to seekers as well as to fuzes. The second and the third method can be implemented with one sensor only or a multiple sensor arrangement. To secure a more dependable system, these techniques may be implemented in parallel for the purpose of double checking. These proposed methods are described briefly in the next section.

IV. DEVELOPMENT OF NEW TECHNIQUES

Three new techniques proposed for the target-cloud signal separation will be discussed here and their implementations and preliminary results obtained are presented in the next section. Prior to doing that a new cloud model utilized throughout the simulation will be introduced.

[a] Aerosol Models

Harry Diamond Labortory of the Army has been engaged in the study of effects of aerosol in near infrared Ladar devices for over a decade and published numerous reports on the subject. To study algorithm for the aerosol rejection, it is essential to examine suitable and realistic aerosol models. After utilizing HDL expressions for a simple model, a new aerosol model has been initiated. This proposes a simpler expression for the cloud, and is based on more realistic physical basis than ones commonly used by many researchers. Detailed discription of this model is given in a separate report submitted to the AFATL. Three alternate method initiated for the target-aerosol separation are listed below.

[b] Correlation Method

This method employes sensor arrays. Arrays can be two dimension, or one dimension. Original implementation was carried out for an array of 4x8 sensors in two dimensions. It should be noted that the array size can be extended to any number. However, processing time increases dratically with array size.

Assume that every sensor receives a time sequence of signals simultaneously. Signal averaging will take place first, then normalization of the data vector follows. Then correlations (inner product for this case) of each data vector with all other data vectors are taken. Mapping these correlation values by using imaging technique, it is easy to discriminate the type of signals sensed by each detector and classify the regions of the sensor array according to characteristics of the signals received. In the initial configuration, a 32 sensors two dimensional array was considered, and then a 8 sensors one-dimensional case has been considered also. Details and illustrations of this effort are given in the report to the laboratory.

Initial simulation results are encouraging, and further investigation for various types of data and sensor array configurations is recommended.

[c] Spectral Extraction Method

The second method of discrimination is based on the spectral selection (or filtering) technique similar to the method used by the PI for some other applications [20]. Noting that the target signature and the returns from the aerosol have different characteristic features, several orthogonal transforms were investigated in search of the most suitable basis function sets. Fourier, Hartley, Cosine, and Triangular transforms were attempted. The results using each of the above transforms are compared and effectiveness evaluated. Preliminary results indicate that the method successfully

separate mixed target-aerosol returns. Of course, the filter design and the window shaping to optimize the effect are extremely important and detailed experimentaions and analysis are desirable to improve the effectiveness of this method in the future. Most part of this effort was delegated to the GSRP fellow (HSM), and details and illustrations are given in her report and report to the laboratory.

[d] Waveform Extraction Method

The third method of separation is based on the monitoring of the time behavior of the signal waveform. After the noise reduction filtering (neighhood averaging), the derivative and the second order derivative are taken to facilitate the examination of the signal time behavior. Identifying the point of inflection and the bending edge of the potentialtarget signal peak, interpolation between these two points will be taken. By subtracting the estimated cloud signature from the mixed signal, the target signal can be extracted. Another version of this wave extraction method is also devised. In this version, noise is put in from the beginning, and the tracking of the waveform is carried out to find peaks and vallies. Again, detail is given in the report to the laboratory.

V. CONCLUSIONS

It appears to be possible to achieve the separation of mixed target-cloud signals by utilizing signal processing

techniques. All three techniques proposed are showing encouraging results in their preliminary simulations. Implementation of these algorithms to realistic systems needs to be studied with caution. In view of stringent requirements on the fuzing functions: (1) extremely short response time, and (2) miniature size processing elements, systematic studies shuld be carried out to implement these methods sucessfully. With currently available technology, it should be feasible to iimplement these algorithms.

1. Hardware Considerations

Several companies including Texas Instruments, Motorola, and AT & T have been active in advancing the signal processing VLSI technologies. For example, TI will be marketting their newest 32 bit floating point high speed DSP chip, TMS320C30, this fall. Their internal applications with FFT and other processing have been reported in the ICASSP-88 already. AT & T ccounter part, DSP-32, is also reporting its progress. recently E-Systems, with collaboration of Harris, claims they have produced chips utilizing ASIC tchnology which performs a 256 point FFT in 20 microseconds. The prices of these IC's are decreasing drastically, and implementation of a specific algorithm can be easily achieved. For a bread board application, it is possible to down load programs written in C-language to avoid expensive and time consuming assembly language coding during the algorithm implementation process.

2. Feasibility Studies

For the implementation of the correlation method, it may be necessary to depend on a parallel computing achitecture, utilizing ssystolic arrays, or an alternate optical processing aarchitecture. Many efforts toward the development of miniature systolic arrays are in progress [22], and a solid state optical correlator chip is presently available from Litton [23].

Systematic studies of appropriate implementations of proposed techniques and testing should be carried out with the full utilizations of all the resouces currently available or under development.

VI. RECOMMENDATIONS

With a limited exposure during the summer, the writer perceived a premature feeling which may be in error. This tentative peception is as follows:

Until recently, most Air Force efforts in the development of fuzes has been in the direction of minimizing the signal processing of the sensor signal. Perhaps, it is prompted by stringent requirement of extremely short decision times and the non-availability of fast,inexpensive, and small signal processing devices. With recent developments in microelectronics and computing technology, a new approach to fuzing may be possible. For examples a DOE/DOD joint effort undertaken by Los Alamos, the Predictive Fuze Program, and the signal processing of sensor outputs.

This summer's effort focused on looking into an alternate algorithm for target-aerosol separation from a signal processing point of view. In the process, several other related processes of target detection, identification, localization, direction finding, and motion estimation are considered in terms of signal processing. Some possible applications are listed below.

1. Near Term Applications

1.1 Aimable or Directional Fuze

For the purpose of constructing a target detecting device for an aimable warhead fuze, use of two dimensional array of sensors, either active or passive may be helpful. It will detect a target or targets, find the direction, and estimate the size. It may be possible to provide data on motion and identity. If it is implemented with optical correlators currently available in solid state form, the optical processor will provide fast processing of the lengthy algorithms required for the proposed correlation method or its variations for the passive case.

Dual mode target detection devices (passive/active) in which an active sensor is used for ranging and a passive array is used for azimuthal and high value spot sensing may be viable. Again, the optical processor will play an important role in this sscheme.

1.2 Future Threat (Stealth Target)

Some realistic targets may be equipped with countermeasures

like electronic jamming, or other concealing schemes such as using special absorbing or reflecting substances to reduce the target signature. Scattering or diffusing materiel (chaff) in addition to the natural aerosols may add difficulty in target detection.

To cope with the above mentioned situations, extensive study including sophisticated signal processing is required to design an "intelligent fuze" or "sensor". It may require incorporation of an adaptive system, Artificial Neural Nets (ANN), or a conventional AI expert system or combination of them.

1.3 Development of Advanced Filters

Development of several robust filtering techniques seems to be helpful in the development of fuze/seeker programs. Possible candidates are listed below.

(1) Matching Filter Techniques

One of the most powerful techniques in pattern recognition and classification is the use of cross correlation measures utilizing known templates. Our proposed correlation method in signal separation has some similarity in the basic concepts except that it does not require a prestored template.

If we want to be effective in identification of the target, and localization of a high value spot in the target, this method is one of the better solutions.

A continued study in this approach, especially aiming at high speed processing, should be considered.

(2) Adaptive and Kalman Filtering

Inherently the Ladar returns or radar signals are noisy. And some of them interfere and inhibit proper target detection. Before processing any signals obtained for a specific purpose, it is desirable to reduce the noise level. Effective utilization of adaptive filtering or Kalman filtering may enhance the efficiency of subsequent processing.

(3) Filter Design and Window Shaping

For signal separation or target identification, it is desirable to design digital filters for those specific tasks. Design of digital filters is possible by continued examination of signature data and trial. Also important is the selection of the optimum window shape.

If an algorithm to automate the selection of optimum set of filter coefficients for digital filters according to the input signal characters and predetermined function, it will have wide range of applications in fuze/seeker programs.

2. Long Term Development

2.1 Image Based Fuze

Recent development in high speed scanning and imaging technology may make it possible to develop a fuze based on the video images. RF as well as IR imagings can be accomplished, and matching filters may be utilized for the target recognition using prestored templates. Motion of the target can be estimated by observing the time sequence of the target images, and the optimum burst point may be estimated easily from this data.

Acquisition and construction of a high speed digitizer and efficient (posssibly optical or any other form of parallel processing) image and logic processing devices are essential to accomplish this goal.

2.2 Neural Nets Applications

Artificial neural nets has been considered to be a good classifier. Recently Castelaz presented a paper on its applications in defense [22]. His work was mainly with the Army. The Naval Weapons Center has a program applying neural nets for fuzes. Of course, the technology is yet to be developed to meet the demanding requirements for air target fuzing, but it certainly is a possible avenue for the Air Force to look into for the future utilization in the area of fuze and seeker.

2.3 Superconducting Long Wave Infrared Passive Sensor

A small scale program to develop a long wave passive optical sensor using high temerature superconductors is in progress at AFATL. By masking the wafer, it is possible to make it a two dimensional thin film sensor array. Associating appropriate optics and processing electronics, a high speed sensing and imaging device can be constructed. By using a few of them (possibly two for each quadrant), it may be possible to construct a seeker-fuze combination.

REFERENCES

1. J. E. Manz: A Ladar Cloud/Target Polarization Discrimination Technique, AFWL-TR-70-76, Air Force Weapons Laboratory, 1970.
2. C. Brenner and F. Gremmell:Experimental Cloud Backscatter Measurement at 0.9 Micron, AFATL-TR-71-145, Air Force Armament Laboratory (Motorola), 1971
3. P.C. Anderson and T.G. McRae: Performance of Optical Proximity Fuze in Degraded Atmospheres., AFATL-TR-72-180, Air Force Armament Laboratory (University of Florida), 1972.
4. R.H. Kohl et al.: Feasibility Investigation of Polarization Techniques for Surface-Cloud Descrimination with an Optical System, AFATL-TR-73-242, Air Force Armament Laboratory (University of Tennessee), 1973.
5. Larry C. Falberg : Active Optical Air Target Detection Device, AFATL-TR-73-180, Air Forece Armament Laboratory (Santa Barbara Research), 1973
6. D.E. Ruch and L.H. Koski: Target Descrimination Techniques for Optical Proximity Sensors, AFATL-TR-76-82, Air Force Armament Laboratory (Delco Electronics), 1976
7. Motorola: Scanning Optical Proximity Techniques(Dual mode sensors), Unpublished AFATL effort (Keene,MNF), 1976
8. G. Benjamin Hocker & Paul Nachman: Self-Detecting Sensors for Fuzes, AFATL-TR-80-64, Air Force Armament Laboratory (Honeywell), 1980

9. J. E. Gallagher and S.M. Borowko: Self-Detecting Optical Proximity Sensor (SDOPS), AFATL-TR-85-58, Air Force Armament Laboratory (McDonnell Douglas), 1985.

10. Missile Fuze Section Engineering Staff: Near Infrared Fuze Technology (NIFT), AFATL-TR-88-99, Air Force Armament Laboratory (Motorola), 1988

11. Dennis W. McGuire, Michael Conner, and Theodore H. Hopp: Aerosol Discrimination by Electronic High- and Low-pass Filtering, HDL-TR-1939, Harry Diamond Laboratories, 1981.

12. Dennis W. McGuire and Michael Conner:The Deconvolution of Aerosol Backscattered Optical Pulses to Obtain System-Independent Aerosol Signatures, HDL-TR-1944, Harry Diamond Laboratories, 1981.

*13. Zoltan G. Sztankay, Dennis W. McGuire, Robert W. Tucker, and Nealman Gupta: "Target/Aerosol Discrimination Technique for Active Optical Fuzes(U)", Proceedings of 21st IRIS Symposium on Infrared Countermeasures, 1983. (confidential)

14. Neelam Gupta: Simulation and Analysis of Wide-Angle Active Optical Sensor Returns Using Measured Pencil-Beam Target Signatures, HDL-TR-2043, Harry Diamond Laboratories, 1984.

15. Zoltan G. Sztankay: Backscatter From Clouds and Aerosols at 0.9 um and its Effects on Active Sensors, HDL-TR-2114, 1987

16. R. E. Bird: Aerosol Discrimination for Active Optical Fuzes, NWC TP 5586, 1974.

17. R. E. Bird: Active Optical Aerosol Discrimination Design Techniques, NWC TP 5826, 1976.

18. R. E. Bird:Extinction and Backscattering by Fog and Smoke in the 0.33 to 12.0 micrometer Wave Length Region, NWC TP 5850 ,1976.

19. K. Min et al., "A Fast Triangular Transform and Its Applications," Proc. IEEE International Conference on Acoustics, Speech, and Signal Processing, 1987 pp. 1811-1814. 1987.

20. K. Min et al., " Automated Two Speaker Separation System", Proc. IEEE International Conference on Acoustics, Speech, and Signal Processing, 1988 pp. 537-540, 1988.

21. P. F. Castelaz :"Neural Networks in Defense Application", Proc. IEEE International Conference on Neural Networks, 1988 pp.II-473-480, 1988.

22. K. S. Kung :VLSI Array Processing, Prentice Hall, 1988.

23. W. E. Ross, D. Psaltis, and R. H. Anderson:Two-dimensional Magneto-Optic Spatial Light Modulator for Signal Processing, SPIE Vol.341 Real Time Signal Processing V, pp. 191-198, 1982.

1988 USAF-UES SUMMER FACULTY RESEARCH PROGRAM

Sponsored by the

AIR FORCE OFFICE OF SCIENTIFIC RESEARCH

Conducted by the

Universal Energy Systems, Inc.

FINAL REPORT

Prepared by:	Dr. Joseph J. Molitoris
Academic Rank:	Professor
Department and College:	Physics Muhlenberg
Research Location:	USAFATL/MNW Eglin AFB Eglin AFB, FL 32542
USAF Researcher:	Joseph C. Foster, Jr.
Date:	19 August 1988
Contract No:	F49620-87-R-0004

The Dynamics of Projectile Impact

by

Joseph J. Molitoris

ABSTRACT

The physics of impact and penetration is relevant to both the development of armor and armor penetrators. This dynamic process was studied through the use and development of one-dimensional physics models and a two-dimensional hydrodynamic code. The appropriateness of the physics assumptions in these models was verified by comparison with both final state and time resolved data.

ACKNOWLEDGEMENTS

The hospitality of the Munitions and Warheads branch is gratefully acknowledged. I express my appreciation to Joe Foster, without whom this research would not have been possible. The support of Leo Wilson, Don Lorey, and Dave Lambert was also much appreciated. In particular, I am grateful for the data provided by Leo and the Hull simulations run by Don. Useful discussions with Stan Jones are acknowledged.

I am indebted to Sam Lambert for his support and an overview plus a tour of the base. I thank the Air Force Systems Command, the Air Force Office of Scientific Research, and Universal Energy Systems for the sponsorship and administration of this program.

I. INTRODUCTION

The mechanism of the deformation of metals at high velocities is of both practical and fundamental interest. The basic question is: What is it that happens when a projectile interacts with a target? The entire event has a duration of only 100 μs with much that is essential occurring during the first 10 μs. The answer to this question is dependent on the velocity of the projectile, the geometry of the interaction, and the material properties of both the projectile and the target.

The Anti-Armor group of the Munitions and Warheads branch at the Armament Laboratory of Eglin Air Force Base has many years of experience with the dynamics of impact and penetration. My research background is in theoretical nuclear physics where (surprisingly) the physics models and terminology are similar. In both fields of physics, one speaks of the projectile impacting the target. Shock waves are formed and propagate in the projectile and target material. Through studying collisions at different velocities and with different elements, one hopes to learn about the material equation of state.

II. OBJECTIVES OF THE RESEARCH EFFORT

My goal for the summer was to become acquainted with the state of the art techniques of the Munitions and Warheads

branch. The Anti-Armor group is interested in simple engineering models of the impact and penetration of a target by a rod. These include the Taylor theory for the impact of a specimen against an anvil[1] and the Tate theory (which makes use of the Bernoulli equation) for the penetration of a rod into a target.[2]

Several open problems which were investigated include: the velocity dependence of the yield strength of the impactor; the formation of a mushroom at the tip of the penetrator; the loss of mass from the penetrator; the limitations of one or two dimensional models; and how to model the impact using energy principles.

The approach followed in researching these goals was both analytical and computational. Analytical methods were employed wherever possible. But I also became familiar with the FORTRAN code Hull. During my summer research I became acquainted with the various experimental facilities including the high frame rate camera, the X-ray examination of metal samples, and the 50 and 120 mm gun ballistics experiments.

The major items of work performed as part of the research were:

1. Search the literature and maintain a bibliography.
2. Set up and utilize the 80286 computer hardware and

software.

3. Study and modify the one dimensional models of impact and penetration.

4. Develop FORTRAN programs for simulation and data analysis.

5. Analyze time resolved impact data as obtained by Leo Wilson and the AFATL-MNW Anti-Armor group.

6. Document results in this final report.

III. SHOCK PHYSICS

One dimensional models[1-5] have their place in understanding the complicated process of impact and penetration. The practical goal is to predict as well as possible the results of a particular penetrator-armor combination with a model that is either analytic or at least solvable with small computer programs. These simple physics or engineering models are hence useful in the design process.

For a rod impacting an anvil at $t = 0$, the initial conditions are those of a shock. In the reference frame where the shock is at rest, the particle velocity of the unshocked matter is $u_o = u_s$ and that of the matter through which the shock wave has passed is $u = u_s - u_p$. Conservation of mass across the shock front gives

$$\rho_o u_o = \rho u \qquad (1)$$

and conservation of momentum implies

$$\rho_o u_o^2 - \rho u^2 = p - p_o \qquad (2)$$

whereas the statement of conservation of energy is

$$1/2\ u_o^2 + p_o/\rho_o + e_o = 1/2\ u^2 + p/\rho + e \quad . \qquad (3)$$

The Rankine-Hugoniot energy equation gives the locus of end states reachable by shock transition from the initial state at pressure p_o and specific volum $\nu_o = 1/\rho_o$.

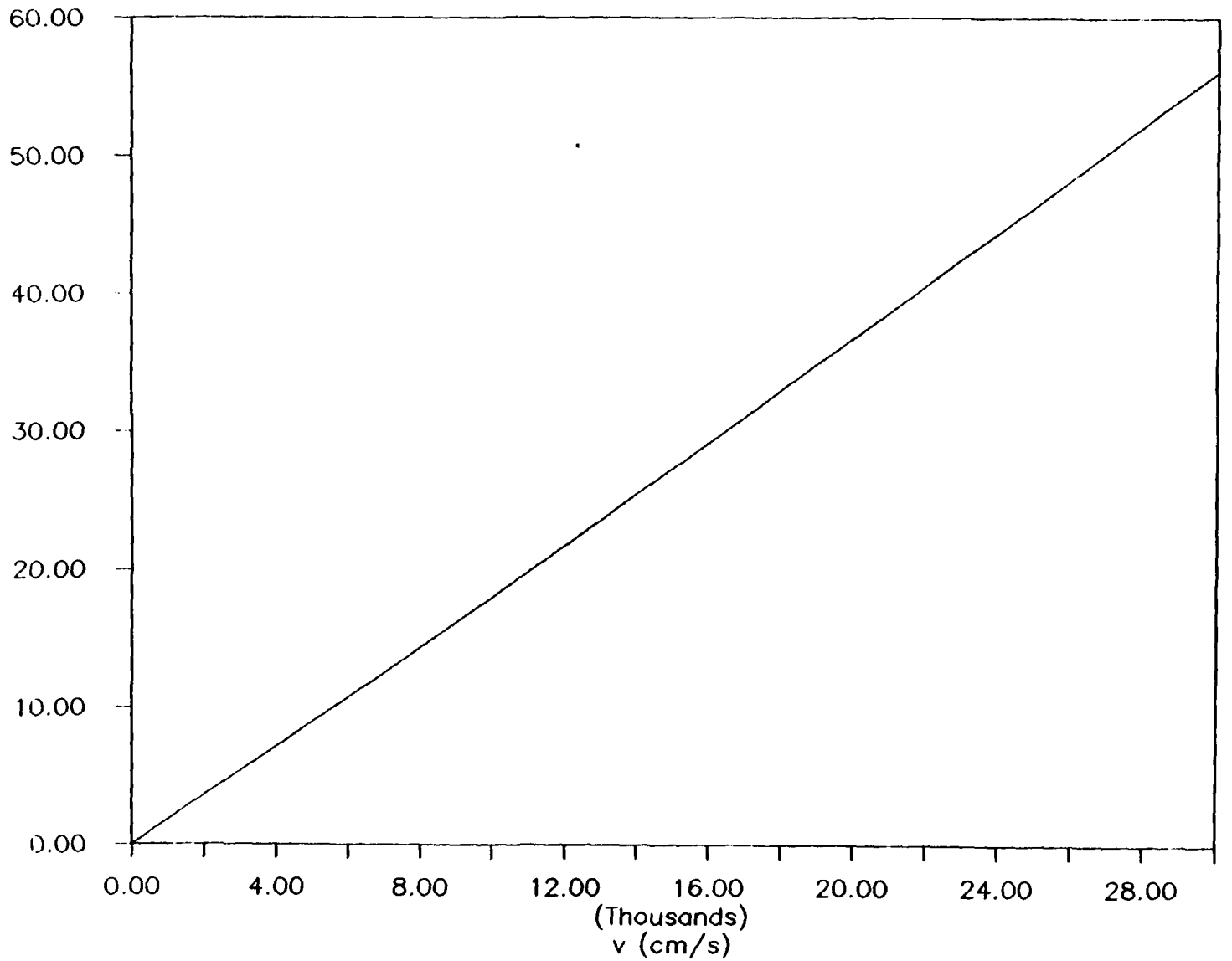
A simple application of these ideas equates the pressure in the target to that in the projectile

$$\rho_p\ u_p\ u_{sp} = \rho_t\ u_t\ u_{st} \qquad (4)$$

Together with the fact that $u_p + u_t = v$ and a linear parameterization for the dependence of shock velocity on particle velocity, this allows one to calculate the velocity dependence of the variables by solving a quadratic equation. For definiteness, consider Cu impacting steel.[6] As the impact velocity ranges from 100 to 300 m/s, the particle velocity in the copper varies from 50.8 to 152 m/s and the shock velocity in the copper ranges from 3.99 to 4.14 km/s. In Figure 1 is shown the pressure at the interface over this velocity range. Note that the pressure is quite high, going from 18.1 kbar at 100 m/s to 56.1 kbar at 300 m/s.

Since this shock pressure only exists for a very short time $\tau < 10\ \mu s$, the dynamic strength properties of the solid at high strain rate are probed. Indeed, at the higher velocities, the effect resembles a small explosion: most solids are damaged by plastic flow and fracture.

Figure 1


60.00
50.00
40.00
30.00
20.00
10.00
0.00
p (d/cm²)
(Times 1E9)
0.00
4.00
8.00
12.00
16.00
20.00
24.00
28.00
(Thousands)
v (cm/s)

IV. TAYLOR MODEL

The classic theory of impact is the Taylor model.[1] Consider the impact of a rod of initial length l_o and area $A_o = \pi r_o^2$ onto a semi-infinite rigid boundary. Let the front end of the rod be just at the boundary at t = 0. Denote the instantaneous length of the rod by l, the location of the back end by s, and the distance from the boundary to the plastic interface by h. The back end velocity of the rod is then

$$v = ds/dt = \dot{s} \tag{5}$$

and the velocity of the plastic front is

$$\lambda = dh/dt = \dot{h} \ . \tag{6}$$

The geometry of the model then requires that $l_o = h + l + s$, from which we find

$$dl/dt = \dot{l} = - (\lambda + v) \ . \tag{7}$$

Thus the rod decreases in length due to the motion of both the back end and the plastic front.

Now consider the balance of mass in the dynamic plastic deformation of the front end of the rod. The amount of mass lost during an infinitesimal time step dt is just ρ ds A_o and the amount of matter eroded is ρ dh $(A - A_o)$. Hence we obtain the fluid dynamic continuity equation:

$$(\lambda + v) = \gamma \lambda \tag{8}$$

where $\gamma = A/A_o$.

The momentum of the plastically deformed wafer is changed by a force gradient. The Taylor model assumes that the pressure Y is constant across the plastic interface. The material properties are thus idealized by hypothesizing perfect plasticity: there is a constant stress exerted by the material when it deforms plastically. The impulse-momentum theorem then implies

$$0 - \rho\ (dh + ds)\ A_o\ v = (Y\ A_o - Y\ A)\ dt\ .$$

or

$$\rho\ (\lambda + v)\ v = Y\ (\gamma - 1)\ . \qquad (9)$$

In the context of the Taylor model, this momentum equation and the continuity equation uniquely determine the parameters λ and γ. The final physics ingredient is the equation which governs the deceleration of the undeformed length of rod. This follows from Newton's second law:

$$dv/dt = \dot{v} = -Y/\rho l\ . \qquad (10)$$

Equations (9) and (10) may be combined to give

$$\dot{l}\ v + l\ \dot{v} = -Y\gamma/\rho\ . \qquad (11)$$

Note that this last equation has elements of both mass and momentum loss. One may obtain the approximate Taylor yield strength of a material by assuming that λ is constant and the average velocity is $v_o/2$. This value is given in terms of the final length l_1 and undeformed length l_f:

$$Y_T = \rho\ v^2\ (l_o - l_f)\ /\ [2\ (l_o - l_1)\ \ln(l_o/l_f)]\ . \qquad (12)$$

Other one-dimensional models tend to amount to a different relationship between λ and v. In the Taylor model, λ

decreases slightly with velocity or grows with time during the impact. In an energy based approach,[3] the value of λ is smaller than in the Taylor model at high velocities and strains. Hawkyard's statement of conservation of energy gives

$$\gamma\rho v^2/2Y + \gamma - 1 = \gamma \ln \gamma \qquad (13)$$

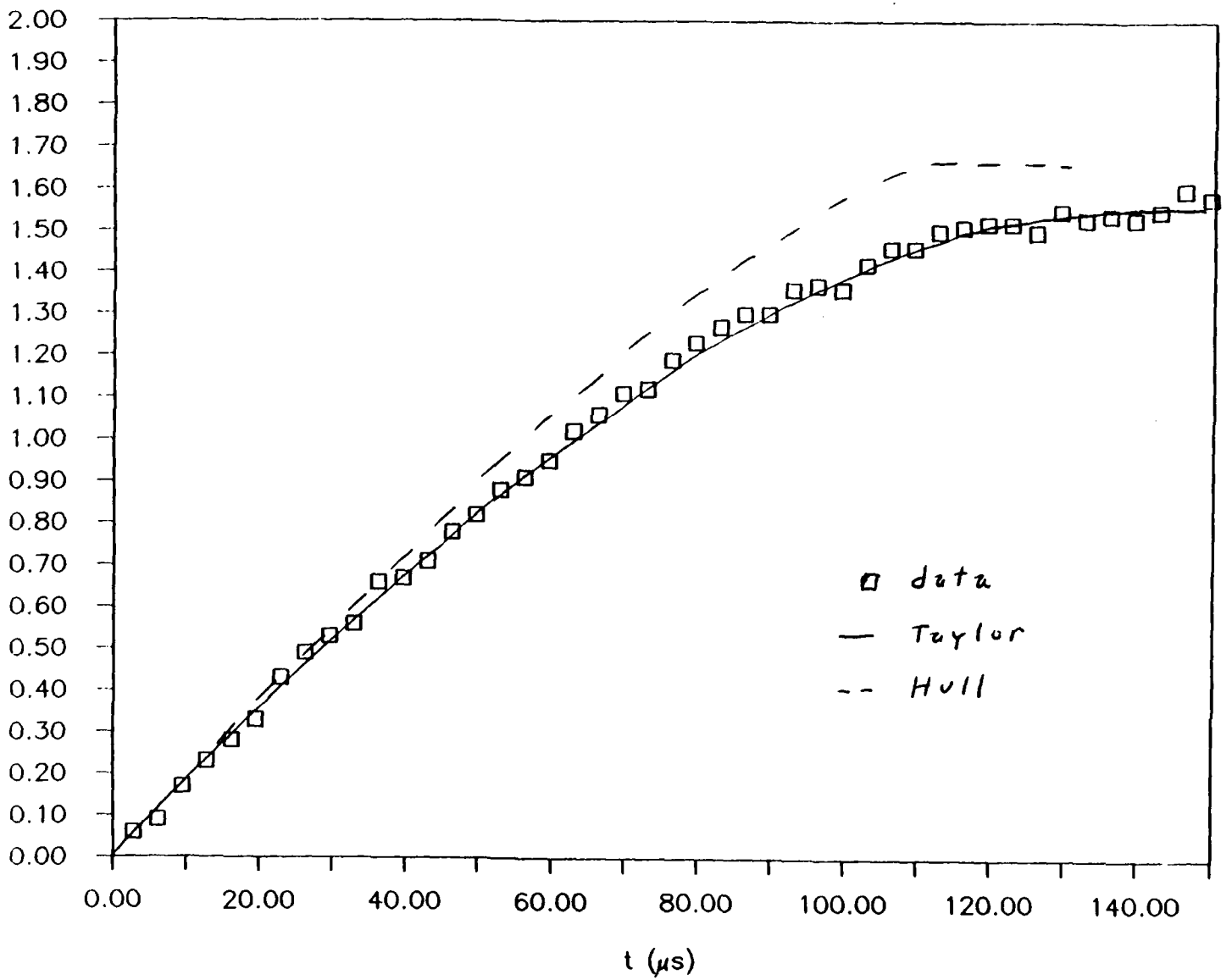
which may be solved numerically for $\gamma = \gamma(v)$. In the Jones-Foster model[4], the value of λ is assumed to be a constant which can be extracted from experiment.

These models were examined in a time dependent way using simple FORTRAN programs. The results were compared to time resolved Taylor anvil data. Word processing, data analysis, and programming were all be done on an 80286 personal computer.

V. EXPERIMENT

The Taylor anvil setup consisted of a 30 caliber barrel, through which rods were fired using 1-5 grains of red dot propellant and a polypropolux obturator. Data collected by Leo Wilson from a high speed camera with a frame rate of 300,000 - 500,000 frames per second was available for analysis. This enables time resolution at the 2 μs level. The camera is a Cordin 330A streak and framing camera, which uses a nitrogen driven rotating mirror. Standard 35 mm Tri-X ASA 400 film was used.

Figure 2

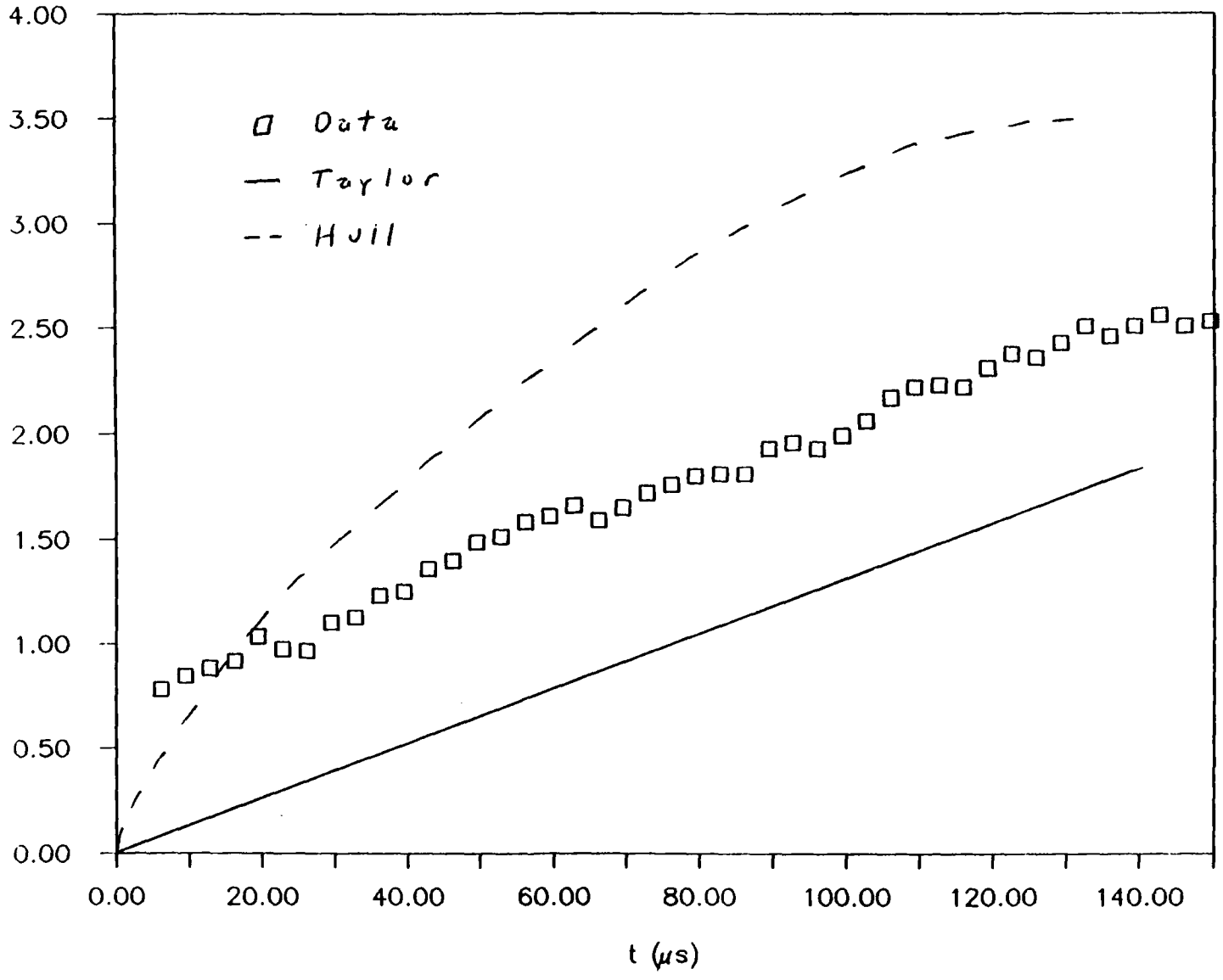

2.00
1.90
1.80
1.70
1.60
1.50
1.40
1.30
1.20
1.10
1.00
0.90
0.80
0.70
0.60
0.50
0.40
0.30
0.20
0.10
0.00
s (cm)
0.00
20.00
40.00
60.00
80.00
100.00
120.00
140.00
t (μs)
data
Taylor
Hull

The shot UK-145 was chosen for a detailed analysis. This shot consisted of an OFHC Cu rod impacting a 4340 steel anvil. The rod had dimensions l_o = 5.72 cm and r_o = .380 cm (30 caliber). The camera was set at a frame rate of 300,000 frames per second. The velocity as determined from the pressure transducers was 18,900 cm/s. From the pre-impact pictures, a least squares velocity of 18,800 cm/s was determined. In Figure 2, this is the slope at t = 0.

The final dimensions of the specimen were total length l_1 = 4.17 cm and undeformed length l_f = 1.65 cm. In dimensionless form, these are $p_1 = l_1/l_o$ = .729 and $p_2 = l_f/l_o$ = .288 . The approximate Taylor yield from equaton (12) is 3.3 kbar. Solving equations (5) to (10) numerically, one can fit p_1 with Y = 4.0 kbar or p_2 with Y = 3.4 kbar in the full Taylor model. The Jones-Foster model has the same ambiguity, giving yields of 3.7 and 3.1 kbar, respectively, taking the value of λ from the experiment. In the Hawkyard model, these values are 4.1 and 3.5 kbar.

In Figure 2, the deceleration function for the back end of the rod is shown. All measurements were made using a vernier caliper from 8×10 viewgraphs blown up from the 35 mm negatives. The Taylor model with Y = 4.0 kbar fits the deceleration function perfectly! However, the modified Taylor model and the Jones-Foster model provide equally good agreement with the data. As seen in the figure, a calculation with the fluid dynamic code Hull also comes very

Figure 3


4.00
3.50
3.00
2.50
2.00
1.50
1.00
0.50
0.00
Data
Taylor
Hill
0.00
20.00
40.00
60.00
80.00
100.00
120.00
140.00
t (μs)
h (cm)

close.

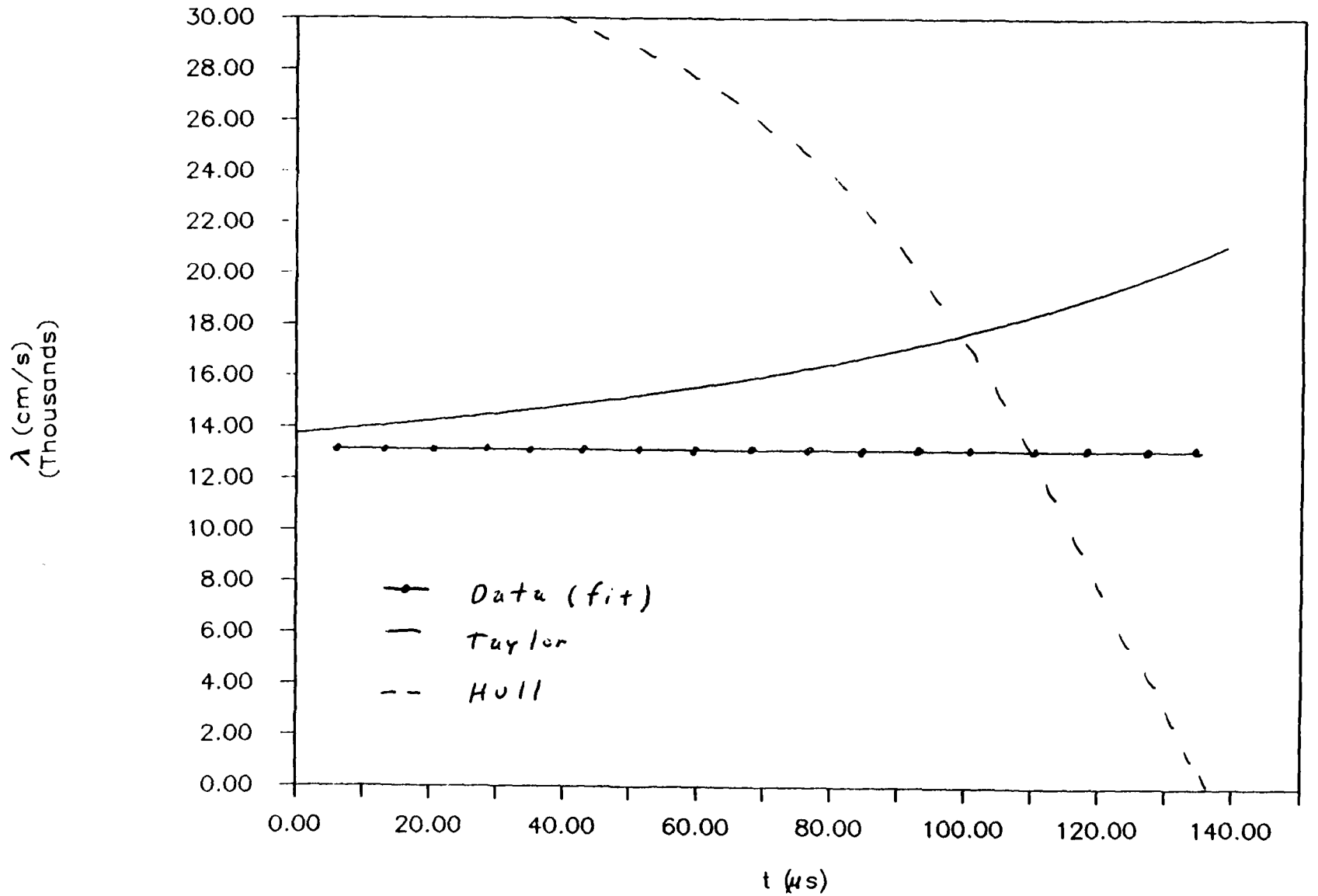
The point where the rod first undergoes deformation may be located from the time resolved data and in the fluid dynamic simulations. In the Taylor model, this quantity is

$$h = \int_0^t \lambda \, dt.$$

The full Taylor model given by solving equations (5) to (10) gives a value of h which is not linear with time. Refer to Figures 3 and 4. This is because λ is an increasing function of time or a decreasing function of velocity in the full Taylor model. Note that the experimental data does not support this. At t = 0, the data gives $\lambda \geq 1.28$ km/s. For later times $5 < t < 135$ μs, the data is linear with least squares slope 13,140 cm/s. The Hull simulations support a large value for the plastic front velocity initially, but disagree with the constant late time behaviour. The Taylor model may be modified to have λ = 13,140 cm/s by rejecting equation (9). This is shown by the line labeled Taylor in Figure 3.

The last question to be addressed is that of radial growth. According to the Taylor model, the radius of each wafer is fixed as it is plastically formed. Hence, the radius at the anvil interface is a constant r = .585 cm in the full Taylor model and r = .593 cm in the modified Taylor model. Refer to Figure 5. Both the Jones-Foster and the Hawkyard models also lack radial growth. The data shows this growth at the anvil interface up to about 50 μs. The experimental value

Figure 4


30.00
28.00
26.00
24.00
22.00
20.00
18.00
16.00
14.00
12.00
10.00
8.00
6.00
4.00
2.00
0.00
λ (cm/s)
(Thousands)
Data (fit)
Taylor
Hull
0.00
20.00
40.00
60.00
80.00
100.00
120.00
140.00
t (μs)

for the final radius is .737 cm, much in excess of any of the model predictions. The occurrence of radial growth as well as the freeze-out time is predicted by the fluid dynamic simulation. However, the final radius is not predicted correctly.

VI. PENETRATION

In the physics of penetration, there is a unique symmetry: both target and projectile are influenced by each other being shocked, deforming, undergoing stress, and changing motion. In this penetration process,[2] first there is a surface impact followed by steady driving and final stopping periods. This amounts to replacing equation (6) by the velocity of the front end

$$u = dz/dt = \dot{z} \tag{14}$$

thereby changing the rod erosion equation (7) to

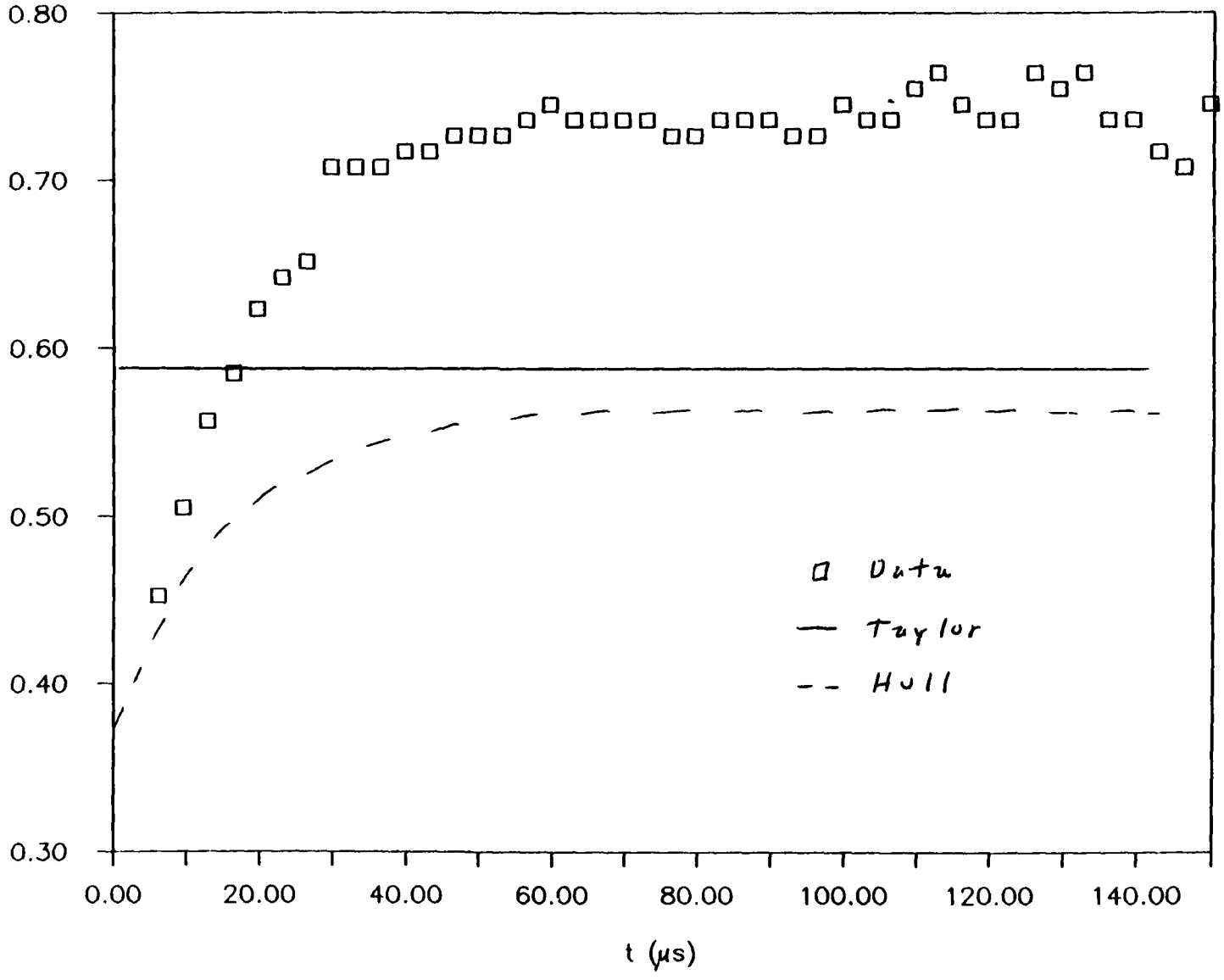
$$\dot{l} = - (v - u) \ . \tag{15}$$

The relationship between u and v is then taken from the Bernoulli or modified Bernoulli equation. The equation of motion is still (10). This approach has recently been shown to have some problems[5] and requires further study.

VII. RECOMMENDATIONS

Time resolved Taylor anvil data at 300,000 frames per second over a range of velocities - v = 100, 200, and 300 m/s -

Figure 5


0.80
0.70
0.60
0.50
0.40
0.30
r (cm)
0.00
20.00
40.00
60.00
80.00
100.00
120.00
140.00
t (μs)
Data
Taylor
Hull

would be most useful for the same material (e.g., OFHC Cu) and fixed l_o/d_o. It is essential to have 5 to 10 frames before impact and the other 65 to 70 after impact, if possible including some of the rebound. A laser could be used to backlight the interaction region and thus improve the sharpness of the images. This is essential to precisely extract the radial growth function and the deformation front velocity.

I propose to continue this analysis and extend it with higher frame rate (up to 2,000,000 frames per second) data which will be available in Fall 1988. Helium would need to be used to drive the rotating mirror at these greater speeds. This higher frame rate data will provide insight into the dynamics of the first 10 μs of impact, where the physics of the shock process must be included.

Hydrodynamic simulations can continue to provide insight into the effects of the material equation of state. Improvements in the hydrodynamic codes might be suggested by comparison to experiment and the one dimensional models.

I propose to also investigate in future work the validity of the physics assumptions of one dimensional penetration models.

REFERENCES

1. G. Taylor, Proc. Roy. Soc. A194 (1948) 289.

2. A. Tate, J. Mech. Phys. Sol. 15 (1967) 387.

3. G. Hawkyard, Int. J. Mech. Sci. 11 (1969) 313.

4. S. Jones, P. Gillis, J. Foster, J. Appl. Phys. 61 (1987) 499.

5. S. Jones, P. Gillis, J. Foster, J. Mech. Phys. Sol. 35 (1987) 121.

6. LASL Shock Hugoniot Data, ed. S. Marsh, Berkeley: UC Press, 1980.

1988 USAF-UES SUMMER FACULTY RESEARCH PROGRAM
GRADUATE STUDENT RESEARCH PROGRAM

Sponsored by the

AIR FORCE OFFICE OF SCIENTIFIC RESEARCH

Conducted by the

Universal Energy Systems, Inc.

FINAL REPORT

ARIMA MODELING OF RESIDUALS IN AD/KR TDOP MODELS

Prepared by:	Shawky E. Shamma	and	Anne L. Siegman
Academic Rank:	Professor		Student
Department and University:	Department of Mathematics University of West FLorida		Department of Mathematics University of Miami

Research Location: Directorate of Computer Science
Armament Laboratory
Eglin Air Force Base

USAF Researcher: John Lindegren

Date: 1 August, 1988

Contract No: F49620-88-C-0053

ARIMA MODELING OF RESIDUALS IN AD/KR TDOP MODELS

by

Shawky E. Shamma and Anne L. Siegman

ABSTRACT

The measurement residuals generated by AD/KR Test Data Optimal Processor (TDOP) for extracting optimal vehicle trajectory depend on the error model used in the software for the measurement processing. These residuals are found often to be correlated, not white noise as assumed by TDOP. A set of software and algorithms for time series analysis which makes use of ARIMA (autoregressive integrated moving average) has been used to analyze some of the measurement residuals obtained from TDOP output and obtain the ARIMA model coefficients that fit the measurement residuals and that can be used in turn to correct the raw measurements for a rerun of TDOP software or in a "renovation" processing of TDOP.

The advantage of this approach is that one can achieve an improved accuracy in applying TDOP in tracking, weapon scoring, and system accuracy evaluations.

ACKNOWLEDGEMENTS

We would like to thank the Air Force Systems Command, Air Force Office of Scientific Research, and Universal Energy Systems, Inc. for providing a worthy research program for University faculty and their students.

We would like to acknowledge Dr. Sam Lambert, Chief Scientist, Armament Laboratory; Dr. Massey Valentine, Director of Computer Science Directorate, and Ralph Duncan, Chief Test Support Division, for providing us with the opportunity to spend a very interesting summer at Freeman Mathematical Laboratory, Eglin AFB. We would also like to express our appreciation to George Weekly, Chlotia Posey, John Lindegren, Stanley Moore, Jean Carter, Judy Stapleton, Henry Jones, Arvy Wang, and Odelia Keaton for providing a stimulating working atmosphere. To all these people, we are grateful and especially to John Lindegren for his encouragement and invaluable assistance.

I. INTRODUCTION

In a previsit to Eglin Air Force Base, the participants and the sponsor agreed on an SFRP effort consisting of basic goals and objectives. These goals and objectives are summarized in Section II of this report. Sections III - VI contain the approaches taken in realizing each of the objectives of the effort and the results of each approach. Section VII contains suggestions for follow-on work for completion and continuation of the research effort.

II. OBJECTIVES OF THE EFFORT

1. Examination of AD/KR TDOP Test Data Optimal Processor (TDOP) Square Root Information/Smoother (SRIF/S) which is used for extractin vehicle trajectory estimates, and making recommendations about any changes for achieving improved accuracy of the results.

2. Using the INU measurements' residuals for identification and diagnostic checking of Autoregressive-Integrated-Moving-Average (ARIMA) modeling of Inertial Navigation Unit measurements.

III. EXAMINATION OF TEST DATA OPTIMAL PROCESSOR--TDOP:

This section contains an introduction about TDOP.

i. TDOP Overview

The AD/KR TDOP is a computational algorithm that processes measurements to deduce a minimum error estimate of the state of a system by utilizing knowledge of system and measurement dynamics, assumed statistics of system noises and measurement errors, and available information. This information includes time-space-positon

information, inertial navigation measurement, statistical error models of these measurement sources, and a dynamical model of the tracked vehicle (adaptable to any vehicle). By combining this information in an optimum manner via a two-pass processing technique (optimal filtering, optimal smoothing) major accuracy improvement, compared to less powerful processing techniques, is realized. TDOP has been applied to a variety of tracking, weapon scoring, and systems accuracy evaluation.

ii. Model and Problem Definitions

The following linear (linearized) state and measurement models are adopted in TDOP:

$$\underline{x}_{k+1} = \Phi_k \underline{x}_k + \underline{w}_k \quad (1)$$

$$\underline{y}_k = H_k \underline{x}_k + \underline{v}_k \quad (2)$$

in which both $\underline{w}_k$ and $\underline{v}_k$ are zero-mean, uncorrelated white random sequences of covariance $E\,\underline{w}_k \underline{w}_k^t = \Sigma_k^w$ and $E\,\underline{v}_k \underline{v}_k^t = \Sigma_k^w$

The vector $\underline{x}_k$ is the state, and has 15 state components, consisting of vehicle kinematic and INU variables, as well as instrument error parameters (e.g. biases). The vector, y_k, is the observation vector and may include inertial as well as external measurements. Φ_k, H_k, Σ_k^w and Σ_k^v may all be time-varying and the relationships among the elements of $\underline{x}$ and $\underline{y}$ may be relaxed to be nonlinear.

The estimation problem is to obtain estimates of the states $\{\underline{x}_k\}$ from the measurements $\{\underline{y}_k\}$.

The details of algorithms implemented in AD/KR TDOP processor software are obtained in references [3] and [4]. Topics discussed

include the special structure of the state model and the consequent simplifications of the general SRIF/S procedure, measurement synchronization logic developed for TDOP, and the specific measurement models and measurement sensitivity matrices implemented in the filter

IV. MODELING TDOP RESIDUALS

The residuals generated by TDOP are:

i) Filter and Smoother residuals

ii) Measurement residuals

The residuals are often correlated, not white noise as assumed by TDOP or any other filter/smoother based on the approach originated by R. H. Kalman.

Since an examination of some residuals in TDOP (see section VI) indicated that the residuals for typical data are highly correlated, it became necessary to consider in what way the model ought to be modified in order to extract any structural components from these residuals.

In section VI, we show how the autocorrelations of the residuals may be used to suggest a suitable model.

Using the autocorrelation function of the residuals, $\underline{R}_t$, the ARMA modeling, [1], (after extracting nonlinearity components) may be applied to identify a model

$$\hat{\Phi}(B)\underline{R}_t = \hat{H}(B)\underline{a}_t \qquad (3)$$

where B is the backward shift operator and $\underline{a}_t$ is white noise.

Equation (3) may be solved for $\underline{R}_t$, obtaining a model for the residuals $\underline{R}$ in terms of white noise $\underline{a}$, i.e.

$$\underline{R}_t = \Phi^{-1}(B)H(B)\underline{a}_t \qquad (4)$$

In particular, we show here how the ARIMA modeling can be used in a vector form (ARMAV) for three componenets of the state vector which are mutually dependent (i.e. DELV,PSI INU attitude residuals, VELM):

The TDOP software uses, [3] and [4], inertial velocity measurements in the XYZ local level coordinate system as measured by a vehicle navigation unit (INU). The XYZ coordinate axes correspond to a NED (North, East, Down) system rotated clockwise about the vertical axis by an angle termed the "wander angle".

Within TDOP, the state model adopted include terms within the state dynamic equations that describe the attitude error PSI, and the velocity error DELV, and the measurement error model include the inertial velocity measurements. These relations are given by:

$$\underline{DELV}(t + Dt) = \underline{DELV}(t) + VXPMAT(t) * \underline{PSI}(t) + \underline{WDELV}(t), \quad (5)$$

$$\underline{PSI}(t + Dt) = PHIMAT(t) * \underline{PSI}(t) + \underline{WPSI}(t), \quad (6)$$

$$\underline{VELM}(t) = ROTMAT_{RG}^{P} * (\underline{VEL}(t) + \underline{DELV}(T)) + \underline{N}, \quad (7)$$

where:

$$VXPMAT(T) = \begin{bmatrix} 0 & -DVU & DVN \\ DVU & 0 & -DVE \\ -DVN & DVE & 0 \end{bmatrix}$$

$$\begin{bmatrix} DVE \\ DVN \\ DVU \end{bmatrix} = \left(\begin{bmatrix} AE \\ AN \\ AU \end{bmatrix} - ROTMAT * \begin{bmatrix} 0 \\ 0 \\ G \end{bmatrix} \right) * DT$$

$$PHIMAT(t) = \begin{bmatrix} EPSI & 0 & 0 \\ 0 & EPSI & 0 \\ 0 & 0 & EPSI \end{bmatrix},$$

$$PSI = \exp(-DT / TAU) \qquad (8)$$

TAU = First order Markov time constant (currently set to infinity, corresponding to random walk process; 1/TAU --> 0 --> EPSI--> 1).

(AN,AE,AU) = Vehicle acceleration state vector in earth-fixed Cartesian coordinates.

$ROTMAT_{LL}^{RG}$ = Rotation matrix from vehicle local level coordinates to test range coordinates.

$ROTMAT_{RG}^{P}$ = Rotation matrix from test range coordinates to INU platform coordinates (includes wander angle rotation from local level north to platform north).

DT = Measurement update interval.

G = Magnitude of gravitational acceleration.

Equations (5), (6) and (7) can be arranged in one matrix equation as follows:

$$\underline{C}(t + DT) = M * \underline{C}(t) + \underline{R}_t + K\underline{v}_t \qquad (9)$$

where

$$C = \begin{bmatrix} DELV \\ PSI \\ VELM \end{bmatrix}, \qquad M = \begin{bmatrix} I & VXPMAT & 0 \\ 0 & PHIMAT & 0 \\ ROTMAT & 0 & 0 \end{bmatrix}$$

$$K = \begin{bmatrix} 0 & 0 & 0 \\ 0 & 0 & 0 \\ 0 & 0 & \text{ROTMAT} \end{bmatrix}, \quad \underline{v} = \begin{bmatrix} 0 \\ 0 \\ \underline{\text{VEL}} \end{bmatrix}, \quad \underline{R} = \begin{bmatrix} \underline{\text{WDELV}}(t) \\ \underline{\text{WPSI}}(t) \\ \underline{N} \end{bmatrix}$$

If we model $\underline{R}_t$, using ARIMA, as

$$\hat{\Phi}(B) * \underline{R}_t = \hat{H}(B) * \underline{a}_t. \tag{10}$$

Using equation (9) and (10), we get

$$\underline{C}(t + Dt) = M * C(t) + \hat{\Phi}^{-1}(B) * \hat{H}(B) * \underline{a}_t + K\underline{v} \tag{11}$$

Reference [11] has software packages for modeling ARMAV, however these software packages are not available at the sponsor's site.

V. RELATION OF ARIMA AND STATESPACE FORMS FOR THE RESIDUALS

The model, equation (10), for the residuals $\underline{R}_t$ can be converted to a state space model and thus can be analyzed using state space techniques. Following ref. [5], [6], and [11], suppose we write equation (10) in more detail as follows

$$\underline{R}_t - \hat{\Phi}_1 \underline{R}_{t-1} - \cdots \hat{\Phi}_p \underline{R}_{t-p} = \underline{a}_t + \hat{H}_1 \underline{a}_{t-1} + \cdots + \hat{H}_q \underline{a}_{t-q} \tag{12}$$

where $\underline{a}_t$ is a sequence of independent mutlivariate normal vectors with variance Σ and mean zero; $\hat{\Phi}(B)$ and $\hat{H}(B)$ are matrix polynomials in B with $\Phi(0) = H(0) = I$.

The model may also be written as

$$\underline{R}_t = \hat{\Phi}^{-1}(B) \hat{H}(B) \underline{a}_t = \sum_{s=1}^{\infty} \Psi_i \underline{a}_{t-s}. \tag{13}$$

The Ψ_s matrices are known as the impulse response matrices and may be computed as $\hat{\Phi}^{-1}(B) \hat{H}(B)$.

To write (12) in a state space form, we proceed as follows: Denoting conditional expectation by symbol $|$, we have

$$\underline{R}_t = \sum_{s=i}^{\infty} \Psi_s \underline{a}_{t+i-s} \tag{14}$$

and

$$\underline{R}_{t+i} = R_{t+i}\Big|_t + \Psi_{i-1}\underline{a}_{t+1} \tag{15}$$

However, from equation (12), we have

$$\underline{R}_{t+p}\Big|_t = \hat{\Phi}_1 \underline{R}_{t+p-1}\Big|_t + \ldots + \hat{\Phi}_p \underline{R}_t. \tag{16}$$

Hence we may substitute for $\underline{R}_{t+p\ t}$ into the right-hand side of equation (15) when i=p to close the system of equations. This results in a state space form of the model as

$$\begin{bmatrix} \underline{R}_{t+1} \\ \underline{R}_{t+2}|_{t+1} \\ \vdots \\ \underline{R}_{t+p}|_{t+1} \end{bmatrix} = \begin{bmatrix} 0 & I & \cdots & 0 & 0 \\ 0 & 0 & \cdots & I & 0 \\ \vdots & \vdots & & \vdots & \vdots \\ \hat{\Phi}_p & \hat{\Phi}_{p-1} & \cdots & \cdots & \hat{\Phi}_1 \end{bmatrix}$$

$$* \begin{bmatrix} \underline{R}_t \\ \underline{R}_{t+1}|_t \\ \vdots \\ R_{t+p-1}|_t \end{bmatrix} + \begin{bmatrix} I \\ \Psi_1 \\ \vdots \\ \Psi_{p-1} \end{bmatrix} \underline{a}_{t+1}$$

Or in a more compact form

$$\underline{Z}_{t+1} = F\underline{Z}_t + G\underline{a}_{t+1}. \tag{17}$$

It should be noted that the state vector $\underline{Z}_t$ is comprised of conditional expectations of $\underline{R}_t$ and that the first r components of $\underline{Z}_t$ are equal to $\underline{R}_t$.

VI. RESIDUAL ANALYSIS

This section displays plots of some residuals and identification of a class of ARIMA models capable of representing the individual residuals as a time series with errors as white noise a_t. In identifying such models, examination of several statistical tests were made, including examination of data, autocorrelation and partial autocorrelation functions, power spectrum and remaining residuals from ARIMA representation of residuals from TDOP as a time series. We will call these residuals from ARIMA representation, RR_t, as compared with residuals from TDOP, which are denoted R_t.

Although we made a thorough investigation of the INU measurements, attention in this report is directed to representative cases which display particularly interesting or critical aspects of the data structures.

The TDOP state $\underline{x}$ consists of three types of variables: vehicle kinenmatics, systematic INU errors and related parameters, and bias errors. The measured INU velocity vector $\underline{v}$ differs from the true vehicle velocity $\underline{v}$ by two types of errors, systematic and random. Thus, $\underline{v}_{INU}$ is modeled as

$$\underline{v}_{INU} = \underline{v} + \underline{DELV}_{INU} + \underline{n}, \tag{18}$$

in which $\underline{n}$ is assumed to be white noise and $\underline{DELV}_{INU}$ represents the systematic error expressed by (5), in which $\underline{WDELV}(t)$ is assumed to be white noise.

We examined $\underline{WDELV}(t)$ (x,y,z components) from TDOP processing of one pass (389.1 seconds) of a real flight mission. There are 3891 data points for each component of $\underline{WDELV}$. It was noted that there

are jump discontinuities in the data at the rate of ~ 10.2 seconds. These discontinuities are apparently due to synchronization of time clocks, time tagging and recording of the data. The sponsor feels that such a problem can be corrected and it is not a reflection of existing physical structure of the data. Therefore, there is no need to model these discontinuities by "intervention models", [2].

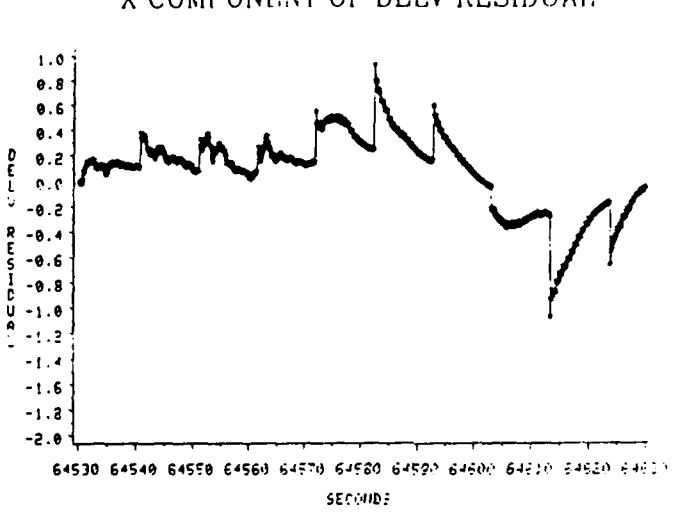
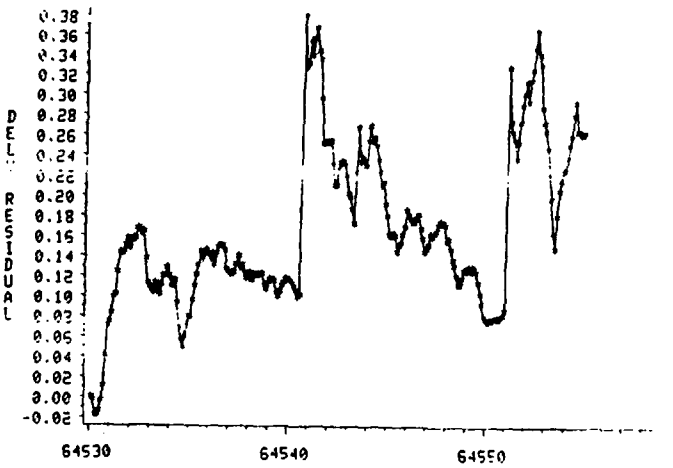


Figure (1)

The data was divided in sixteen subdata sets of 250 points. The data in Figure 1 are the first 1000 data residuals of x component of DELV. It shows the jump discontinuities in the data. Figures (2) and (4) show selected detailed data from some typical subsets of length 250 points. Strong variations in these graphs can be intuitively observed from the smoothers' predicted trajectory of the whole pass in Figures (5) and (6) at strong variations in accelerationsince the acceleration was modeled as a random walk in TDOP and therefore a structured component of acceleration would result in strong variation (errors) in the residuals.

X COMPONENT OF DELV RESIDUAL



Y COMPONENT OF DELV RESIDUAL

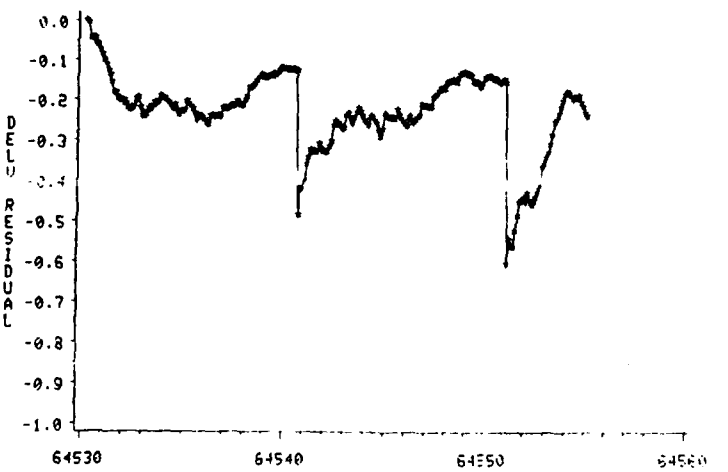
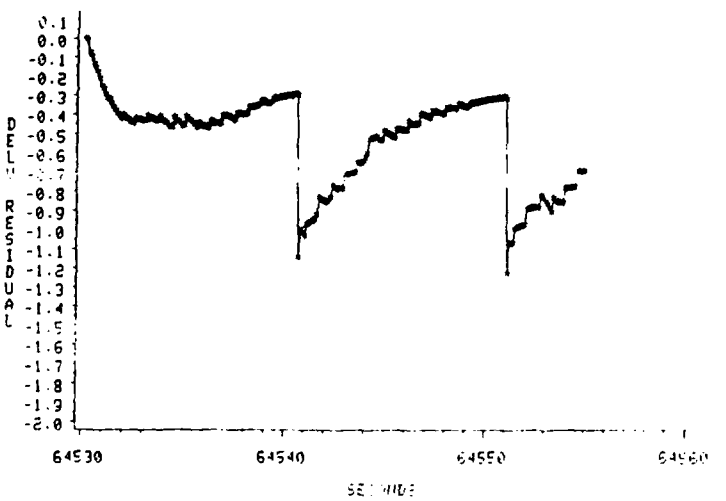
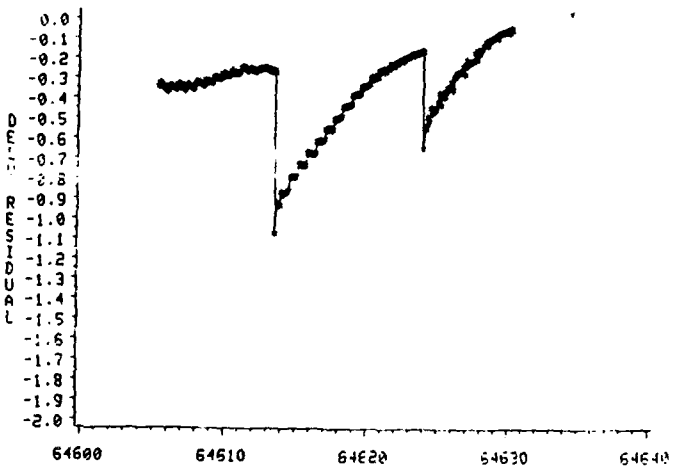


Figure (2)

Z COMPONENT OF DELV RESIDUAL



X COMPONENT OF DELV RESIDUAL



Y COMPONENT OF DELV RESIDUAL

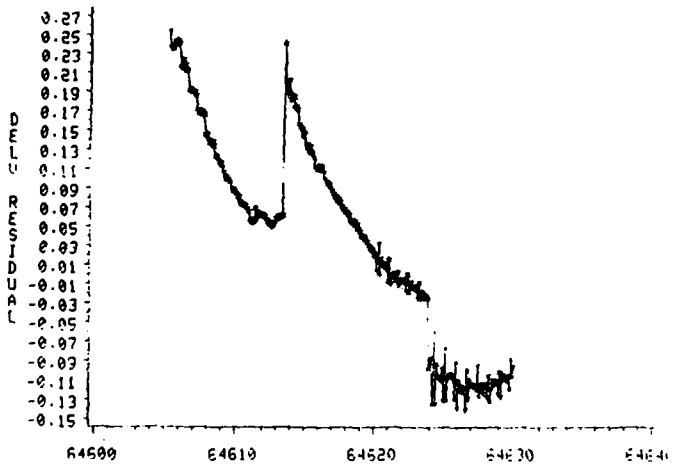
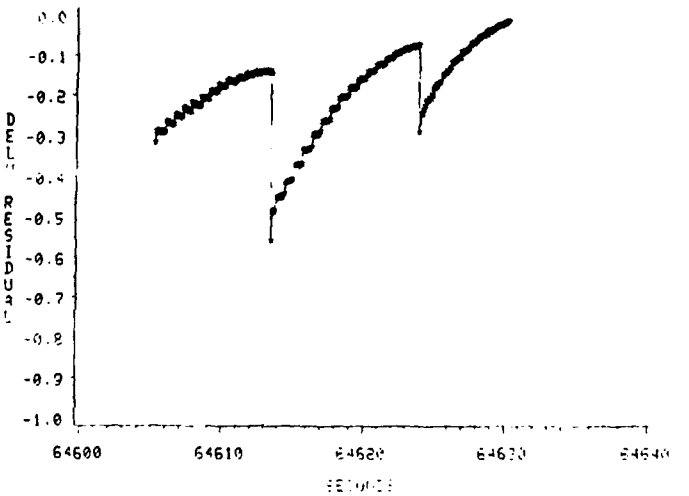
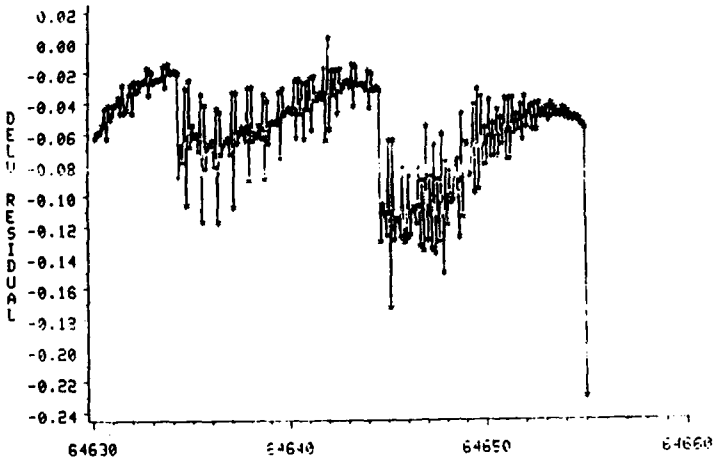


Figure (3)

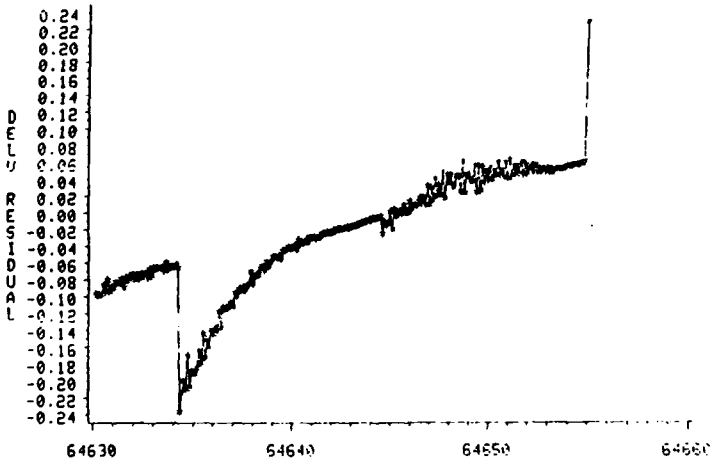
Z COMPONENT OF DELV RESIDUAL



X COMPONENT OF DELV RESIDUAL



Y COMPONENT OF DELV RESIDUAL



Z COMPONENT OF DELV RESIDUAL

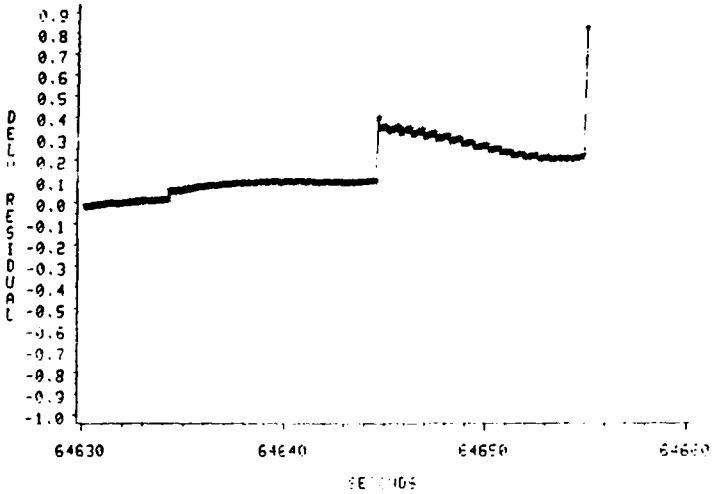


Figure (4)

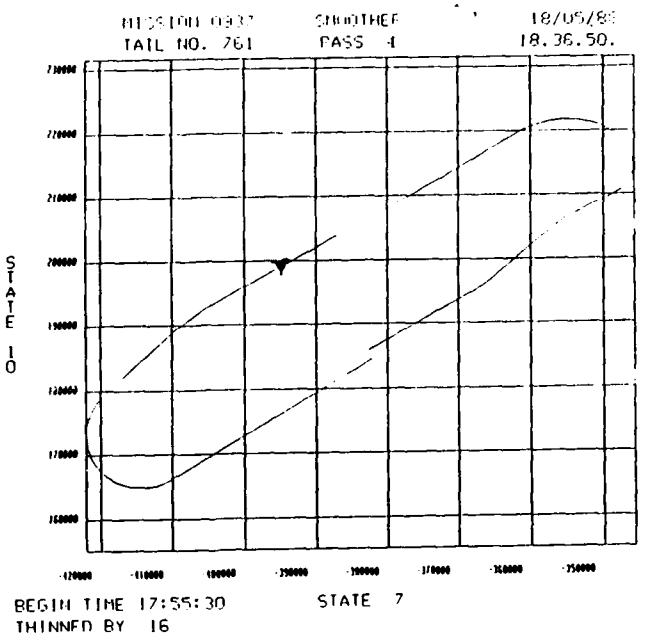


Figure (5). Position Trajectory

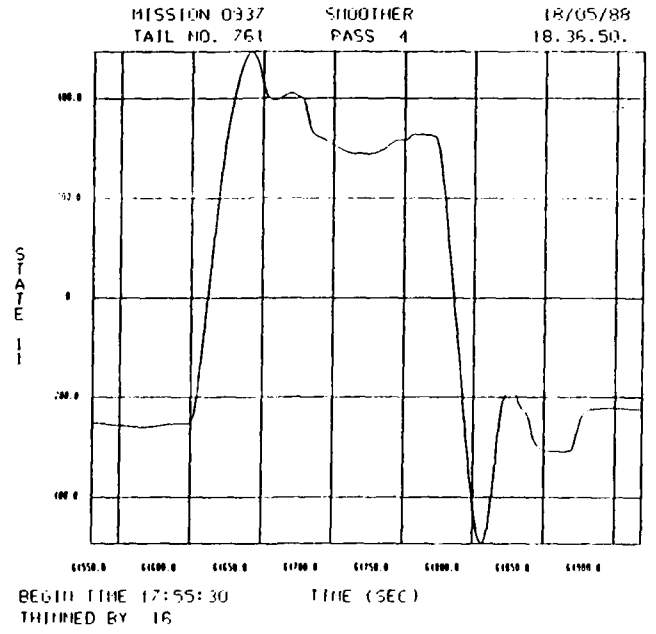


Figure (6). Velocity Trajectory

PLOT OF AUTOCORRELATIONS

LAG	CORR	-1.0 -.8 -.6 -.4 -.2 0 .2 .4 .6 .8 1.0
1	931	
2	868	
3	803	
4	731	
5	670	
6	604	
7	530	
8	463	
9	401	
10	347	
11	312	
12	281	
13	254	
14	229	
15	203	
16	186	
17	171	
18	160	
19	149	
20	137	
21	125	
22	119	
23	113	
24	114	

Figure (7)

PLOT OF PARTIAL AUTOCORRELATIONS

LAG	CORR	-1.0 -.8 -.6 -.4 -.2 0 .2 .4 .6 .8 1.0
1	931	
2	013	
3	- 051	
4	- 084	
5	031	
6	- 063	
7	- 104	
8	012	
9	012	
10	019	
11	099	
12	012	
13	005	
14	- 025	
15	- 025	
16	031	
17	- 016	
18	022	
19	- 011	
20	- 009	
21	008	
22	035	
23	003	
24	041	

Figure (7) shows the autocorrelation and partial autocorrelation functions for the first 250 data points of residuals in x-component of DELV. It indicates that these residuals are not white noise as assumed in TDOP. Figure (8) shows the same results for the differenced data. Figures (7) and (8) suggest an ARIMA model of order (1,0,0) i.e. $\hat{R}x_{t+1} - \hat{\phi}_1 \hat{R}x_t = a_{t+1}$, $\hat{R} = R - \mu$ where a_{t+1} is white noise. Applying Box-Jenkins method as described in the software [9], [10], it was found that $\hat{\phi}_1$=0.9362. Figure (9) shows the correlation of the residuals RRx_t of the residuals DELVx (i.e. Rx) and it reflects the white noise behavior.

PLOT OF AUTOCORRELATIONS

LAG	CORR	-1.0 -.8 -.6 -.4 -.2 0 .2 .4 .6 .8 1.0
1	-.060	
2	.007	
3	.051	
4	-.088	
5	.032	
6	.087	
7	-.016	
8	-.020	
9	-.058	
10	-.154	
11	-.017	
12	-.030	
13	.012	
14	.036	
15	-.065	
16	-.018	
17	-.055	
18	-.004	
19	-.006	
20	-.014	
21	-.050	
22	-.014	
23	-.075	
24	-.055	

PLOT OF PARTIAL AUTOCORRELATIONS

LAG	CORR	-1.0 -.8 -.6 -.4 -.2 0 .2 .4 .6 .8 1.0
1	-.060	
2	.003	
3	.052	
4	-.082	
5	.022	
6	.090	
7	.001	
8	-.033	
9	-.066	
10	-.149	
11	-.040	
12	-.038	
13	.016	
14	.028	
15	-.044	
16	-.007	
17	-.059	
18	-.011	
19	-.041	
20	-.047	
21	-.068	
22	-.025	
23	-.071	
24	-.068	

Figure (8a)

PLOT OF AUTOCORRELATIONS

LAG	CORR	-1.0 -.8 -.6 -.4 -.2 0 .2 .4 .6 .8 1.0
1	-.031	
2	.030	
3	.071	
4	-.066	
5	.050	
6	.100	
7	-.001	
8	-.005	
9	-.045	
10	-.140	
11	-.007	
12	-.022	
13	.020	
14	.042	
15	-.058	
16	-.012	
17	-.048	
18	.003	
19	.001	
20	-.006	
21	-.041	
22	-.006	
23	-.063	
24	-.043	

Figure (8b)

PLOT OF PARTIAL AUTOCORPELATIONS

LAG	CORR	-1.0 -.8 -.6 -.4 -.2 0 .2 .4 .6 .8 1.0
1	-.031	
2	.029	
3	.073	
4	-.063	
5	.042	
6	.103	
7	.011	
8	-.023	
9	-.055	
10	-.135	
11	-.021	
12	-.020	
13	.033	
14	.041	
15	-.032	
16	.006	
17	-.044	
18	.006	
19	-.024	
20	-.028	
21	-.046	
22	.001	
23	-.044	
24	-.037	

Figure (9a)

Figure (9b)

An examination of the autocorrelation and partial autocorrelation functions of all other subsets of the data revealed that the ARIMA model of order (1,0,0) is a satisfactory model for all cases, where $\hat{\phi}_1$ varied from 0.9048 to 0.9847, except for the fourth and fifth subsets of 250 data points. It was found that such a model was not adequate for the residuals of DELVy for the fourth and fifth data sets, and not adequate for the residuals of DELVx in the fifthdata set. Of course,this result is clear from examination of Figure (10) for the correlations of RRx, for such a model. Figure (10) shows these residuals after fitting an ARIMA (1,0,0) model.

PLOT OF AUTOCORRELATIONS

LAG	CORR.	-1.0 -.8 -.6 -.4 -.2 .0 .2 .4 .6 .8 1.0
1	-.287	XXXX+XXI +
2	.583	I +XXXXXXXXXXXX
3	-.017	+ I +
4	.388	+ I +XXXXXX
5	.038	+ IX +
6	.400	+ IXXXX+XXXXX
7	-.102	+ XXXI +
8	.529	+ IXXXX+XXXXXXXX
9	-.142	+XXXXI +
10	.387	+ IXXXX+XXXXX
11	-.007	+ I +
12	.273	+ IXXXXX+X
13	.021	+ IX +
14	.260	+ IXXXXX+X
15	-.067	+ XXI +
16	.309	+ IXXXXX+XX
17	-.068	+ XXI +
18	.187	+ IXXXXX+
19	.004	+ I +
20	.153	+ IXXXX +
21	-.036	+ XI +
22	.178	+ IXXXX +
23	-.134	+ XXXI +
24	.219	+ IXXXXX+

Figure (10)

PLOT OF PARTIAL AUTOCORRELATIONS

LAG	CORR.	-1.0 -.8 -.6 -.4 -.2 .0 .2 .4 .6 .8 1.0
1	-.287	XXXX+XXI +
2	.546	+ IXX+XXXXXXXXXX
3	.334	+ IXX+XXXXX
4	.235	+ IXX+XXX
5	.050	+ IX +
6	.223	+ IXX+XXX
7	-.158	X+XXI +
8	.213	+ IXX+XX
9	.033	+ IX +
10	-.090	+XXI +
11	.005	+ I +
12	.026	+ IX +
13	-.019	+ I +
14	-.011	+ I +
15	-.070	+XXI +
16	-.036	+ XI +
17	.038	+ IX +
18	-.092	+XXI +
19	-.051	+ XI +
20	.052	+ IX +
21	-.052	+ XI +
22	.004	+ I +
23	-.092	+XXI +
24	-.005	+ I +

Several other models were attempted to model x and y components but the residuals from each model failed to be white noise. For example, fitting a model

$(1 - \Phi_2 B^2)\ \hat{Rx}_t = a_t$,

produced residuals RRx_t having correltations as shown in Figure (11). It indicates the presence of low and high frequency components in the data which suggests the need for sinusoidal fitting. This result is evidenced also from Figure (12) for the specturm of the residuals Rx_t.

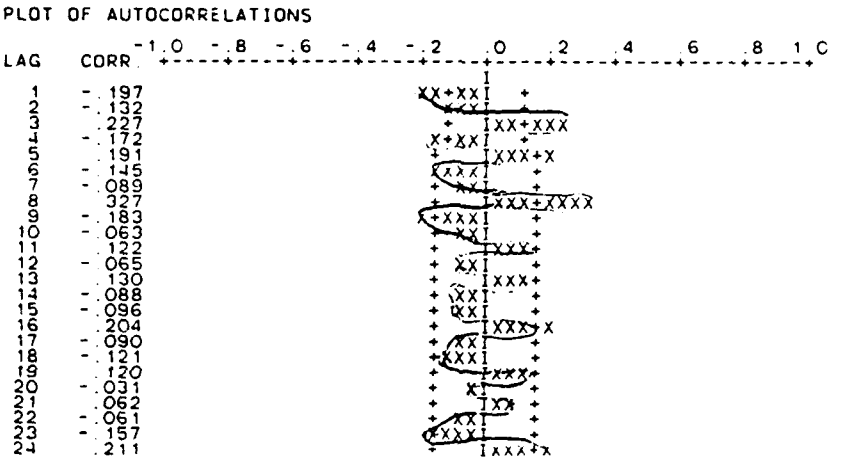
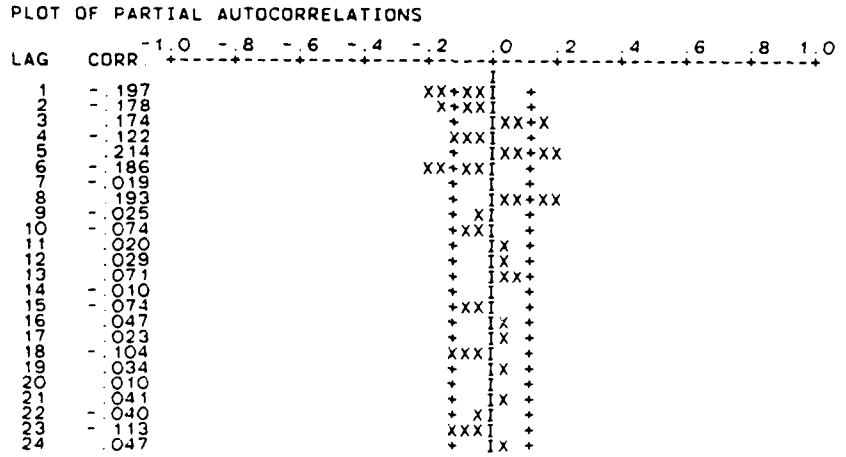


Figure (11)



SPECTRUM OF X-COMPONENT OF DELV RESIDUAL

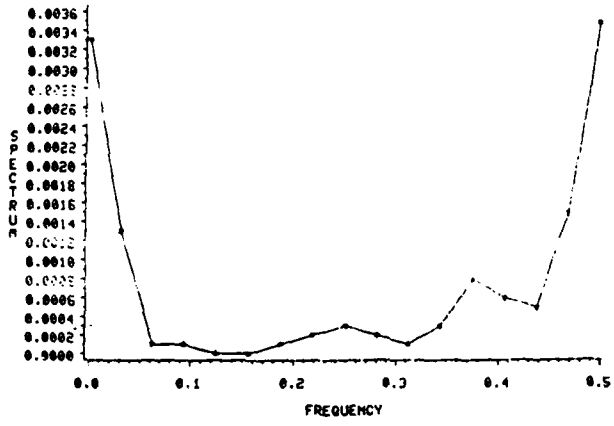


Figure (12)

The last subset of data which contains 192 data points, was also modeled satisfactorily by $(1 - 0.9419\ B)\ \hat{Rx}_t = (1 - 0.9419B^2)a_t$ with autocorrelation and partial autocorrelation functions of RRx as shown in Figures (13 a) and (13 b).

As a means of promoting efficiency in the processing of measurement data, we considered two ways of data compression through decimation and direct reduction by dividing the data into

PLOT OF AUTOCORRELATIONS

LAG	CORR.	-1.0 -.8 -.6 -.4 -.2 0 .2 .4 .6 .8 1.0
1	.006	
2	-.004	
3	-.003	
4	.005	
5	-.006	
6	.002	
7	-.008	
8	.008	
9	-.007	
10	.004	
11	-.009	
12	.005	
13	-.007	
14	.004	
15	-.010	
16	.007	
17	-.005	
18	-.002	
19	-.005	
20	.003	
21	-.003	
22	.001	
23	-.006	
24	-.001	

Figure (13a)

PLOT OF PARTIAL AUTOCORRELATIONS

LAG	CORR.	-1.0 -.8 -.6 -.4 -.2 0 .2 .4 .6 .8 1.0
1	.006	I
2	-.004	I
3	-.003	I
4	.005	I
5	-.006	I
6	.002	I
7	-.008	I
8	.008	I
9	-.008	I
10	.004	I
11	-.009	I
12	.005	I
13	-.007	I
14	.004	I
15	-.010	I
16	.007	I
17	-.004	I
18	-.002	I
19	-.004	I
20	.003	I
21	-.003	I
22	.001	I
23	-.006	I
24	-.001	I

Figure (13b)

subdata sets consisting of 500 points each. The work on decimation is still in progress . The work on piecewise modeling of 500 points each indicated that the best model that fits such piecewise modeling is of ARIMA (0,1,2) type.

i.e. $(1 - B)\,\hat{Rx}_t = (1 - \theta_2 B^2)a_t$.

Figure (14) shows plots for the correlations of the residuals RRx of the eighth 500 data points for computed $\theta_2 = 0.9205$.

PLOT OF AUTOCORRELATIONS

LAG	CORR.	-1.0 -.8 -.6 -.4 -.2 0 .2 .4 .6 .8 1.0
1	.009	I
2	-.016	I
3	.007	I
4	-.005	I
5	.013	I
6	-.011	I
7	.001	I
8	-.003	I
9	.007	I
10	-.003	I
11	-.002	I
12	-.003	I
13	.008	I
14	.000	I
15	-.012	I
16	.008	I
17	.005	I
18	-.006	I
19	-.001	I
20	-.004	I
21	.004	I
22	.002	I
23	.003	I
24	-.012	I

Figure (14a)

PLOT OF PARTIAL AUTOCORRELATIONS

LAG	CORR	-1.0 -.8 -.6 -.4 -.2 0 .2 .4 .6 .8 1.0
1	009	
2	- 016	
3	008	
4	- 005	
5	013	
6	- 011	
7	002	
8	- 004	
9	007	
10	- 003	
11	- 001	
12	- 003	
13	008	
14	- 001	
15	- 012	
16	008	
17	005	
18	- 006	
19	000	
20	- 004	
21	004	
22	002	
23	003	
24	- 012	

Figure (14b)

It should be noted that one can find, in some cases, more than one model that would fit a given set of data.

The above modeling efforts were limited to modeling individual residuals because the sponsor did not have a software for modeling multi-variate time series data. Equations (5), (6) and (7) show the dependence and relation between some variables of the state.

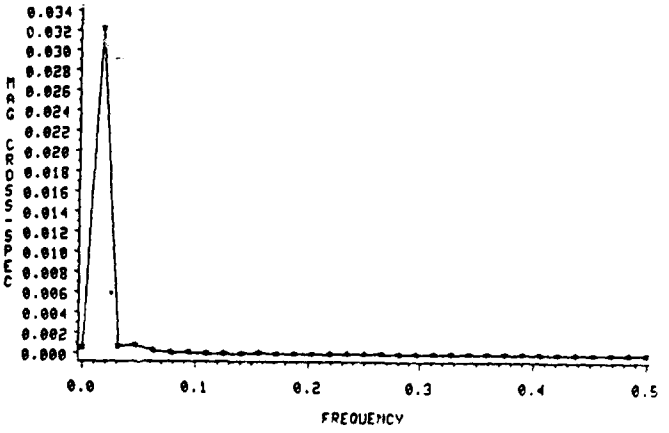


Figure (15)

Figure (15) shows the cross-spectrum between x and y components of DELV for one of the data sets. These results indicate a need for using a software for modeling multivariate time series data for the vector residual $\underline{R}_t$ as indicated in section V. This software is available at the University of West Florida.

Finally, residuals from the filter processing in TDOP are currently being studied. It is anticipated that improvements in modeling the filter residuals would result in improvements in the smoother's results since the smoother is made of forward and backward filters.

VII. RECOMMENDATIONS

1. Complete the work in progress about modeling the filter residuals.
2. Develop ARMAV models, using [11], for the vector residuals $\underline{R}_t$.
3. Implement the deterministic model developed by the sponsor [15] for the Schuler sinusoidal cycle error terms in a data reconstruction or "renovation" processing.
4. Examine methods for extracting the currently unmodeled terms in TDOP from the raw measurements in a pre-process and then input the corrected measurements data directly into TDOP.
5. Develop a method for computing the first order Markov time constant (currently set to infinity in TDOP, corresponding to random walk process).
6. Modify TDOP to account for developed procedures that would enhance accuracy of the results.

REFERENCES:

1. Box, C.E.P. and G.M. Jenkins. (1970). "Time Series Analysis, Forecastin, and Control". Holden Day Inc., 1976

2. Shumway, Robert H., "Applied Statistical Time Series Analysis", Prentice-Hall, 1988.

3. Rozelle, K.D., "AD/KR TDOP Models and Algorithms: Volume 2", VERAC Report R-054087, May 1987.

4. O'Conner, C.L., C.P. Rizzo, and K.D. Rozelle, "AD/KR TDOP Models and Algorithms: Volume 1", VERAC Report R-053-87, May 1987

5. Akaike, H., "Markovian Representation of Stochastic Processes and its Application to the Analysis of Autoregressive Moving Average Processes", Annals of the Institute of Statistical Mathematics, 26, 1974, 363-387

6. Akaike, H., "Canonical Correlations Analysis of Time Series and the Use of an Information Criterion", in Mehra, R. and Lainiotis, D.G. (eds), Advances and Case Studies in System Identification, Academic Press, 1976

7. Pham-Dinh-Tuan, "on the Fitting of Multivariate Processes of the Autoregressive-Moving Average Type", Biometrike 65, 1978, 99-107

8. Priestley, M.D., "System Identification, Kalman Filtering, and Stochastic Control", in Brillinger, D.R. and Tiao, G.C., eds, Directions in Time Series, Institute of Mathematical Statistics, 1980

9. BMDP Statistical Software, University of California Press, 1981 edition.

10. IMSL Library, 1984 edition

11. SAS Library: Econometrics and Time Series Library, 1982 edition

12. Gelb, Arthur, "Applied Optimal Estimation", The M.I.T. Press, 1984

13. Kaminski, Paul G. and Arhtur E. Bryson, Jr., "Discrete Square Root Smoothing", proc. of AIAA conference on Guidance and Control, 1972

14. Parvin, Richard H., "Principles of Guided Missile Design", Van Nostrand Co., Inc., 1962

15. Lindegren, John, "A Model for Schuler Sinusoidal Cycle Dynamics of a Vehicle Trajectory", Private Communication, July, 1988

1988 USAF-UES SUMMER FACULTY RESEARCH PROGRAM

GRADUATE STUDENT RESEARCH PROGRAM

Sponsored by the

AIR FORCE OFFICE OF SCIENTIFIC RESEARCH

Conducted by the

Universal Energy Systems, Inc.

FINAL REPORT

Prepared by: Wafa E. Yazigi

Academic Rank: Instructor

Department: Mathematics Department

University: Columbia Basin College

Research Location: AFATL/FXA
Eglin Air Force Base, Florida

USAF Researcher: Kurt Gothe

Date: 18 Aug 88

Contract No.: F49620-87-R-0004

STRESS ANALYSIS FOR A FIN STABILIZED PROJECTILE

ABSTRACT

A stress analysis was done on a projectile where the stresses at the critical sections in the structure were evaluated and compared to the maximum allowable stresses that the structure can withhold before any deformation occurs. As a result structural failure criteria were established which in turn would be a basis for the design of the projectile. Similar analysis was also done for the sabot.

ACKNOWLEDGEMENTS

I wish to thank the Air Force Systems Command and the Air Force Office of Scientific Research for sponsorship of this research. Universal Energy Systems must be mentioned for their concern and help to me in all administrative and directional aspects of this program.

My experience was rewarding and enriching because of many different influences. Mr Gerald Winchenbach provided me with support, encouragement, and a truly enjoyable working atmosphere. I want to thank all the staff at the Laboratory for all their help and support.

I. INTRODUCTION

My background in structural dynamics and stress analysis is a result of both academic and practical experience. I have a bachelors degree in mechanical engineering and a masters degree in aeronautics and astronautics with concentration in structural analysis and finite elements and also a masters degree in applied mathematics. I have worked on projects involving theoretical as well as finite element analysis of structures. My background in mathematics has been very helpful in researching the different engineering problems.

II. OBJECTIVES OF THE PROPOSED RESEARCH EFFORT:

My assignment this summer of 1988 was to do a theoretical stress analysis on a fin stabilized projectile launched with a sabot. I did the analysis and I have achieved a satisfactory result. I would like to further investigate the problem by doing a finite element analysis of the projectile and sabot, and compare my results to the experimental results which would lead to fewer iterations in the design and testing.

III. THEORETICAL ANALYSIS:

This analysis was accomplished using the classical techniques as outlined in References 2-6.

ρ_1 = density of material for $L_5 < x < L_T$

ρ_2 = density of material for $L_0 < x < L_5$

D_0 = outside diameter of the cylinder. $L_0 < x < L_3$

D_1 = diameter of the first drill

D_2 = diameter of the second drill

D_h = diameter of the connection between the two materials

D_i = outer diameter of the cross section at $x = L_i$, $i = 3, 4, 5, 6, 7$

$L_8 = (D_0 L_7 - D_7 L_3) / (D_0 - D_7)$

L_T = total length of the projectile

a = acceleration (the maximum value of the acceleration obtained from interior ballistics)

E = modulus of elasticity of the material

M_i = mass of the projectile from $x = L_i$ to $x = L_T$, $i = o, 1, \ldots, 7$

V_i = volume of the projectile from $x = L_i$ to $x = L_T$, $i = o, \ldots, 7$

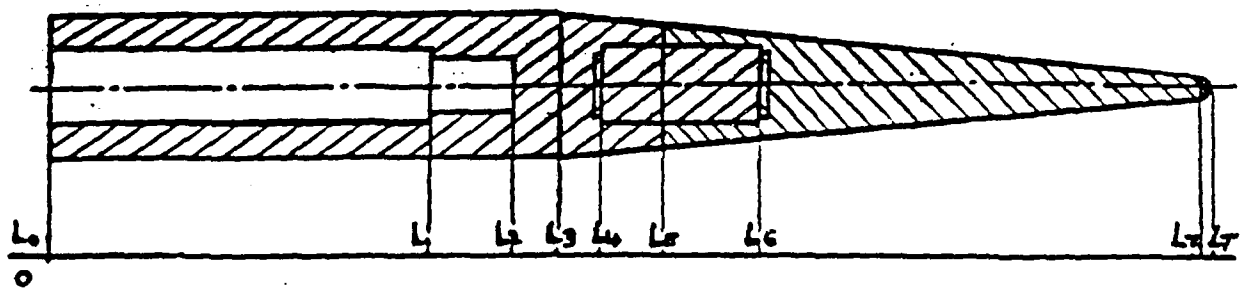
A_i = the cross sectional area at $X = L_i$, $i = o, \ldots, 7$

R = radius of gyration of the cylinder $\sqrt{\frac{I}{A}}$

I = moment of inertia of the cylinder

σ_i = compressive stress at $x = L_i$. The stress at any cross section is

$$\sigma_i = \frac{M_i a}{A_i}, \text{ where } M_i = \rho V_i$$



The critical sections are at x = o, x = L_4 and x = L_6

1. The stress at x = o is $\sigma_o = \frac{M_o\, a}{A_o}$

$$\sigma_o = a\left[\rho_2\left[(D_o^2 - D_1^2)\frac{L_1}{4} + (D_o^2 - D_2^2)\frac{(L_2 - L_1)}{4} + \frac{D_o^2}{4}(L_3 - L_2) + D_o^2\frac{(L_8 - L_3)}{12} - D_5^2\frac{(L_8 - L_5)}{12}\right] + \rho_1\left[\frac{D_5^2}{12}(L_8 - L_5) - \frac{D_7^2}{12}(L_8 - L_7) + \frac{D_7^3}{6}\right] + W\right] \Big/ \frac{(D_o^2 - D_1^2)}{4}$$

where W = $\frac{D_h^2}{4}(L_6 - L_5)(\rho_2 - \rho_1)$ if the material with density ρ_1, is drilled at the connection.

$\frac{D_h^2}{4}(L_5 - L_4)(\rho_1 - \rho_2)$ if the material with density ρ_2 is drilled at the connection.

The maximum allowable static stress σ_{yo} at x = o is obtained from the equations in table 1. Where $\frac{L}{R}$ is specified.

$$\frac{L}{R} = \frac{4\, L_3}{\sqrt{D_o^2 + D_1^2}}$$

The dynamic stress (σ_{y_o}) dyn. is (σ_{y_o}) dyn. = m . σ_{y_o}, get m from table 2.

2. The stress at $x = L_6$ is σ_6

$$\sigma_6 = \frac{a\left[\frac{1}{\quad}\left[\frac{D_6^2\,(L_8 - L_6)}{12} - \frac{D_7^2\,(L_8 - L_7)}{12} + \frac{D_T^3}{6}\right]\right]}{\frac{D_o^2}{4}\,\frac{(L_8 - L_6)}{(L_8 - L_3)}}$$

The maximum dynamic stress $\sigma_{y_6} = \frac{K\,E\,I_6}{A\,L_7^2}\,\eta$

where K is determined from Table 3. Specify $\frac{Io}{I_3}$ and $\frac{n}{L_T}$

where $I_6 = I_3\left[\frac{L_8 - L_6}{L_7 - L_3}\right]^4$ and $I_3 = \frac{\pi}{64}\,(D_3^4 - D_h^4)$

$$A_6 = \frac{\pi}{4}\,(D_6^2 - D_h^2)\quad,\quad I_o = \frac{\pi}{64}\,D_7^4$$

and $n = \left|2\,L_3 - L_7\right|$

if $\sigma_6 > \sigma_{y_6}$ material deforms

3. Max. dynamic stress at $x = L_4$ is $\sigma_{y_4} = \frac{K\,E\,I_4}{A_4\,L_7^2}\,\eta$

where $A_4 = \frac{\pi}{4}\,(D_4^2 - D_h^2)$

$$I_4 = I_3\left[\frac{L_8 - L_4}{L_7 - L_3}\right]^4$$

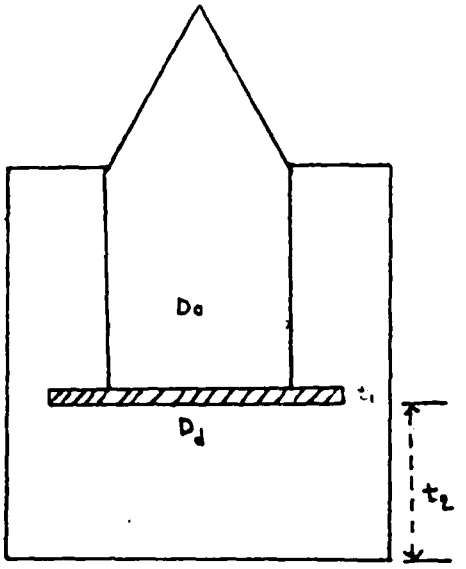
K is determined from Table 3. As in Case 2.

if $\sigma_4 > y_4$ the material deforms.

$$\text{where } \sigma_4 = a\left[\sigma_2\left[\frac{D_4^2}{12}(L_8 - L_4) - \frac{D_5^2}{12}(L_8 - L_5)\right] + (\sigma_1 - \sigma_2)\, D_h^2\,(L_5 - L_4)\right.$$

$$\left. + \sigma_1\left[\frac{D_5^2}{12}(L_8 - L_5) - \frac{D_7^2}{12}(L_8 - L_7) + \frac{D_T^3}{6}\right]\right] \Big/ \frac{(D_4^2 - D_h^2)}{4}$$

Analysis for the sabot



The force exerted by the projectile on the sabot is $F = m_o a$ where
m_o = mass of the projectile
a = max. acceleration of the projectile

Case 1: Without the metal bar the shear stress τ on the sabot

$$\tau = \frac{F}{\pi D_o t_2}$$

if $\tau > \tau_U$ (ultimate shear strength of the sabot material), then the sabot fails.

Case 2: If $\tau > \tau_U$, then add a metal disk as in the figure /let t_1, and D_d be the thickness and diameter of the disk.

Then $D_d \geq \frac{F}{\pi \tau (t_2 - t_1)}$ such that $D_o < D_d < D_s$

where D_s = diameter of the sabot

and $t_1 = .75 \left[\frac{3}{8} q \left(\frac{D_d}{2}\right) \frac{(3+\nu)}{\sigma_{y\ disk}} \right]^{1/2}$, ν = Poisson's Ratio

where $q = \frac{4F}{\pi D_d^2}$

If $\frac{F}{\pi D_d (t_2 - t_1)} > \tau_{u\ sabot}$ then sabot fails

TABLE 1.

Material	$\frac{L}{R}$	$\sigma = \frac{Q}{A}$ = allowable unit load $\frac{Lb}{in^2}$
Structural Steel	$\frac{L}{R} < C_c$	$\frac{Q}{A} = \frac{1 - \frac{\left(\frac{L}{R}\right)^2}{2C_c^2}}{m} \cdot \sigma_y$
	$C_c < \frac{L}{R} < 200$	$\frac{Q}{A} = \frac{149{,}000{,}000}{\left(\frac{L}{R}\right)^2}$
		where $C_c = \sqrt{\frac{2\pi^2 E}{y}}$
		$m = \frac{5}{3} + \frac{3(L/r)}{8C_c} - \frac{\left(\frac{L}{R}\right)^3}{8C_c^3}$
		for σ_y = 33K 36K 42K 46K 50K
		C_c = 131.7 126.1 116.7 111.6 107.0
Carbon Steel	$\frac{L}{R} \leq 140$	$\frac{Q}{A} = 15{,}000 - \frac{1}{4}\left(\frac{L}{R}\right)^2$
	$\frac{L}{R} > 140$	$\frac{Q}{A} = \frac{18{,}750}{1 + .25 \sec\left(\frac{.75L}{2R}\sqrt{\frac{1.76Q}{EA}}\right)}$
Silicon Steel	$\frac{L}{R} \leq 130$	$\frac{Q}{A} = 20{,}000 - .46\left(\frac{L}{R}\right)^2$
	$\frac{L}{R} > 130$	$\frac{Q}{A} = \frac{25{,}000}{1 + .25 \sec\left(\frac{.75L}{2R}\sqrt{\frac{1.8Q}{EA}}\right)}$
	$\frac{L}{R} \leq 120$	$\frac{Q}{A} = 24{,}000 - .66\left(\frac{L}{R}\right)^2$

TABLE 1. (continued)

Nickel Steel	$\frac{L}{R} > 120$	$\frac{Q}{A} = \frac{30,000}{1 + .25 \sec\left(\frac{.75L}{2r}\sqrt{\frac{1.83Q}{EA}}\right)}$	
High-Strength Steel	$0 < \frac{L}{R} < 140$	$\frac{Q}{A} = 15,000 - .325\left(\frac{L}{R}\right)^2$	for $\sigma_y = 33K$
	$140 < \frac{L}{R} < 200$	$\frac{Q}{A} = \frac{15,000}{.5 + \frac{1}{15,860}\left(\frac{L}{R}\right)^2}$	for $\sigma_y = 33K$
	$0 < \frac{L}{R} < 120$	$\frac{Q}{A} = 20,500 - .605\left(\frac{L}{R}\right)^2$	$\sigma_y = 45K$
	$120 < \frac{L}{R} < 200$	$\frac{Q}{A} = \frac{20,500}{.5 + \frac{1}{11,630}\left(\frac{L}{R}\right)^2}$	$\sigma_y = 45K$
	$0 < \frac{L}{R} < 110$	$\frac{Q}{A} = 22,500 - .738\left(\frac{L}{R}\right)^2$	$\sigma_y = 50K$
	$110 < \frac{L}{R} < 200$	$\frac{Q}{A} = \frac{22,500}{.5 + \frac{1}{10,460}\left(\frac{L}{R}\right)^2}$	$\sigma_y = 50K$

TABLE 1. (continued)

	$0 < \frac{L}{R} < 105$	$\frac{Q}{A} = 25{,}000 - .902\left(\frac{L}{R}\right)^2$	$\sigma_y = 55K$
	$105 < \frac{L}{R} < 200$	$\frac{Q}{A} = \frac{25{,}000}{.5 + \frac{1}{9{,}510}\left(\frac{L}{R}\right)^2}$	$\sigma_y = 55K$
Low Carbon & Low Alloy Steel	$\frac{L}{R} < 181$	$\frac{Q}{A} = 36{,}000 - 1.172\left(\frac{L}{1.5R}\right)^2$	for $\sigma_y = 36K$
	$\frac{L}{R} < 135$	$\frac{Q}{A} = 79{,}500 - 51.9\left(\frac{L}{1.5R}\right)^{1.5}$	for $\sigma_y = 75K$
	$\frac{L}{R} < 110$	$\frac{Q}{A} = 113{,}000 - 11.15\left(\frac{L}{1.5R}\right)^2$	for $\sigma_y = 103K$
	$\frac{L}{R} < 95$	$\frac{Q}{A} = 145{,}000 - 18.36\left(\frac{L}{1.5R}\right)^2$	for $\sigma_y = 132K$
	$\frac{L}{R} < 90$	$\frac{Q}{A} = 179{,}000 - 27.95\left(\frac{L}{1.5R}\right)^2$	for $\sigma_y = 163K$

TABLE 1. (continued)

Cast Iron	$\frac{L}{R} < 100$	$\frac{Q}{A} = 12{,}000 - 60\ \frac{L}{R}$
	$\frac{L}{R} < 70$	$\frac{Q}{A} = 9{,}000 - 40\ \frac{L}{R}$
Structural Aluminum 6061-T6 6062-T6	$\frac{L}{R} < 10$	$\frac{Q}{A} = 19{,}000$
	$10 < \frac{L}{R} < 67$	$\frac{Q}{A} = 20{,}400 - 135\ \frac{L}{R}$
	$\frac{L}{R} > 67$	$\frac{Q}{A} = \frac{51{,}000{,}000}{\left(\frac{L}{R}\right)^2}$
Structural Aluminum 2014-T4	$\frac{L}{R} < 1.732\pi\sqrt{\frac{1.5E}{F_{co}}}$	$\frac{Q}{A} = F_{co}\ \frac{1 - .385\left(\frac{L}{R}\right)}{\pi\sqrt{\frac{1.5E}{F_{co}}}}$
	$\frac{L}{R} > 1.732\pi\sqrt{\frac{1.5E}{F_{co}}}$	$\frac{Q}{A} = \frac{\pi^2 E(1.5)}{\left(\frac{L}{R}\right)^2}$

where $F_{co} = F_{cy}\left(1 + \frac{F_{cy}}{200{,}000}\right)$

TABLE 1. (continued)

and

F_{cy} = 35,000 for 2014-T4

F_{cy} = 42,000 for 2024-T3

F_{cy} = 40,000 for 2024-T4

F_{cy} = 35,000 for 6061-T6

Structured Aluminum

$$\frac{L}{R} < 1.414\pi\sqrt{\frac{1.5E}{F_{co}}} \qquad \frac{Q}{A} = F_{co}\left[1 - \frac{F_{co}\left(\frac{L}{R}\right)^2}{6\pi^2 E}\right]$$

where $F_{co} = 1.075\ F_{cy}$ and F_{cy} = 66,000 for 7075-T6

Structured Magnesium Alloy

$$\frac{Q}{A} = \frac{\sigma}{1 + f K_1^2 \cdot \frac{L^2}{R^2}} \quad \text{not to exceed } \sigma^1$$

where:

ALLOY	σ	f	σ^1
AMC585-T51	160,900	.00249	36,000
AMC585	46,000	.00072	22,000
AMC575	34,300	.00053	19,000
AMC525	25,500	.00040	16,000
AM35	16,750	.00026	11,000

K_1 = .5

TABLE 1. (continued)

For other material use the following:

a. $\frac{L}{R} < 30$ Then the max. allowable stress is equal to the yield-point stress of material, f_y,

b. $30 < \frac{L}{R} < 100$ Then max. allowable stress is given by:

$$(\sigma_{c_o})_{static} = \frac{f_y}{1 + .25 \sec\left(.75\frac{L}{2R}\sqrt{\frac{\sigma_{co}}{AE}}\right)}$$

where σ_{c_o} = critical buckling load, lb.

I = least moment of inertia of cross sectional area, in^4

A = cross sectional area, in^2

R = least radius of gyration of cross sectional area $= \sqrt{\frac{I}{A}}$, in

f_y = yield-point stress of material, PSI

L = length of column, in

E = modulus of elasticity, PSI

c. if $\frac{L}{R} > 100$ then $(\sigma_{c_o})_{static} = \frac{\pi^2 E}{\left(\frac{L}{R}\right)^2}$

TABLE 2.

Dynamic stress = η · static stress, where η is a constant which depends on the material as in the following table.

Material	η
2024 AL (anneated)	1
2024 AL	1.2
ARMCO iron	2.1
SAE 1020 steel	2.2
SAE 1020 steel	2.5
Mild steel	2.9
SAE 1040 steel	1.8
VIBRAC steel	1.5
SAE 4140 steel	1.1
SAE 4130 steel	4.0
SAE 4340 steel	1.3
Magnesium alloy	1.15
Anneated copper	1.2
302 stainless steel	1.18
Brass	6.0
Otherwise	1.0

TABLE 3.

Values of K for values of $\frac{Io}{I}$ and $\frac{n}{LT}$

Io/I	0.01	0.1	0.2	0.4	0.6	0.8
n/L_T						
0	2.15	4.81	6.02	7.48	8.47	9.23
0.2	3.13	6.11	7.20	8.33	9.01	9.49
0.4	4.84	7.68	8.42	9.10	9.45	9.49
0.6	7.53	9.08	9.38	9.62	9.74	9.81
0.8	9.56	9.77	9.80	9.84	9.85	9.86

IV. RECOMMENDATIONS:

A. The results of my research should be used in the design and testing of fin stabilized projectiles.

B. A finite element analysis should be done in order to have more accurate results which in turn will enhance the design process and cut down on testing.

REFERENCES

1. Alexander Blake, "Practical Stress Analysis in Engineering Design," Mariel Dekker, Inc., New York, 1982.

2. Kornhauser, M., "Structural Effects of Impact," Sparta Books, Inc. Cleaner-Hume Press, London, 1964.

3. Shewmo, N.P.G. and Zackay, V.F., "Response of Metals to High Velocity Deformation," Interscience Publishers, New York, 1960.

4. Roark, R.J. and Young W.C., "Formulas for Stress and Strain 5th Edition," McGraw-Hill, 1975.

5. Rinehart, J.S. and Pearson, J., "Behavior of Metals Under Impulsive Loads," American Society for Metals, Cincinnati, Ohio, 1949.

1988 USAF-UES SUMMER FACULTY RESEARCH PROGRAM/

GRADUATE STUDENT RESEARCH PROGRAM

sponsored by the

AIR FORCE OFFICE OF SCIENTIFIC RESEARCH

conducted by the

Universal Energy Systems, Inc.

FINAL REPORT

Infrared Charge Transfer Device Characterization

Prepared by:	Eustace L. Dereniak
Academic Rank:	Associate Professor
Department and	Optical Sciences Center
University:	University of Arizona
Research Location:	Arnold Engineering Development Center Arnold AFB Tullahoma, TN 37389
USAF Researcher:	Marshall Kingery
Date:	15 August 1988
Contract No.:	F49620-87-R-0004

ABSTRACT

Infrared Charge Transfer Device Characterization

by

Eustace L. Dereniak

This report summarizes the test methodology necessary to characterize an advanced infrared focal plane array. These arrays were characterized in a low background flux in order to measure their read noise, noise equivalent input (NEI), responsivity, dynamic range, and spatial crosstalk. The focal planes had arsenic-doped silicon detectors in a hybrid-charge transfer readout and were cryogenically cooled by liquid helium.

ACKNOWLEDGMENTS

This Summer's appointment was interesting, educational and rewarding. I feel that I not only learned some new technology, but I made some new friends. I would like to thank the people from Calspan Corp. who were friendly and helpful during my visit: Marshall Kingery, who helped me through some awkward political situations as well as helping me find living accommodations; Lavelle Whitehead, who provided me with support encouragement and an enjoyable working atmosphere, even when the air conditioning didn't work; and especially Neil Fry, who really made me feel as part of the team in the laboratory.

I would like to thank the Air Force Systems Command and the Air Force Office of Scientific Research for giving me the faculty research position. I would also like to thank AEDC of Arnold AFB, Tennessee for accepting me for whatever reason.

I. INTRODUCTION

My research interests are in the area of infrared sensor systems, including infrared optical components, analog/digital electronics, cryogenics, and radiometric analysis. More recently, I have been involved in evaluating infrared detector materials and two-dimensional arrays of infrared detectors (i.e., PtSi, Ext. Silicon and hi-temperature superconductors). My background in measuring and understanding two-dimensional arrays were of particular interest to this work. The possibility to help characterize infrared focal planes for the Air Force and learn new technology for myself was available. This Air Force facility (AEDC) has been chartered to radiometric characterize the advanced focal plane of the future IR sensors; therefore, AEDC was the obvious place to work on this technology. However, I believe there was a mutual benefit working in this high technology research facility.

II. OBJECTIVES OF THE RESEARCH EFFORT

The objectives of this research were to measure the performance of a state-of-the-art infrared charge transfer readout focal plane arrays at low-background flux levels. The arrays were two-dimensional arrays used for staring infrared sensors. The performance in this context is array's responsivity, conversion gain, dynamic range, noise, noise equivalent input (NEI-photons), and spatial crosstalk. The background photon levels were sufficiently low to measure the

read noise limit of the device, provided the dark current was low.

Since several focal plane arrays were evaluated, this report will specifically be written about the data analysis procedure and findings on the single planar hybrid, 20 x 64, switched fet array using blocked impurity band (Stetson, 1986) arsenic-doped silicon (Si:As) detectors. The most critical parameter to measure was noise. A great deal of time was spend on building hardware and analyzing different ways to properly measure noise. The process, called correlated double sampling (CDS) (Dereniak, 1984; Barbe, 1975) in noise measurements, was evaluated for these arrays, but a good way to implement CDS was not found. Several measurement approaches, both analog and digital, were evaluated in software and hardware.

III. DATA ANALYSIS APPROACH/FORMULATION

This analysis presents the formulas and approach to evaluating the parameters of interest for a FPA in the Focal Plane Characterization Chamber (Whitehead,1988). The data presently is only to exemplify the use of the equations and not to be an interpretation of any performance characteristics. The parameters or figures of merit measured were:

- Conversion Gain
- Effective Capacitance
- Responsivity
- Noise
- Noise Equivalent Input
- Crosstalk

A. Conversion Gain (Effective Capacitance)

The conversion gain (volt/electron) gives a relation between electrons collected on the detector and output voltage from the focal plane. The conversion gain is dependent on both the detector/storage capacitance and the gain from the on-chip source follower amplifier. Both are lumped together in an effective capacitance.

Generally, one wants to know the amount of charge which produced a signal voltage and ultimately the photon flux level, related by the quantum efficiency, which produced that charge. The charge integrated by the detector during an integration time is measured by the detector current in the detector bias lead. This current corresponds to all (20 x 64 = 1280) detectors. The single pixel current and the corresponding video output voltage for a fixed integration time (Ti) is needed for this analysis. A plot of detector current vs signal voltage is shown in Figure 1. The slope is used in calculating conversion or effective capacitance.

$$C_{eff} = \frac{\Delta Id}{\Delta Vo} \bullet \frac{Ti}{N}$$

where

$\Delta Id/\Delta Vo$ = slope from Id vs Vd curve

Ti=integration time

N=number of detectors

The reason for N in the equation is that the detector current is the total current of all detectors. Substituting in the values measured gives:

$$C_{eff} = 0.4_{pf}$$

The conversion gain is the voltage reflected to the output for one electron of charge collected by the detector.

$$C.G. = \frac{q}{C_{eff}}$$

$$= 0.4\ \mu v/electron$$

B. Responsivity

The peak spectral responsivity for a pixel is calculated using the following equation:

$$R_i\left(\lambda p,f\right) = \frac{V_o\, C_{eff}}{E_e\, A_d\, T_i}$$

where

V_o = signal voltage due to irradiance, E_e

E_e = irradiance on FPA

C_{eff} = effective Capacitance of pixel/readout

A_d = detector active area

T_i = integration time

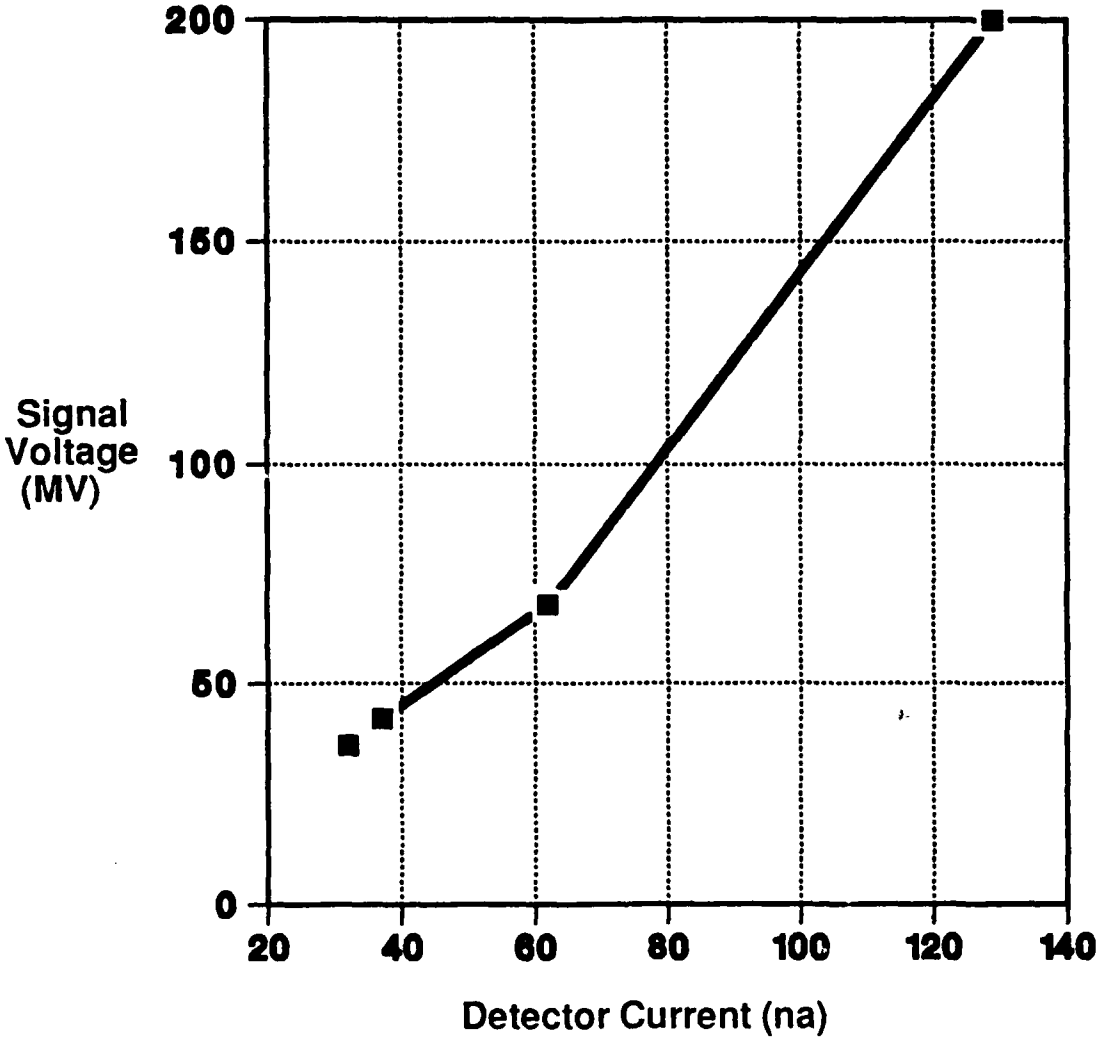


Fig. 1 Signal Voltage vs Detector Current for 1ms Integration Time

The irradiance on the FPA is defined as the blackbody radiation normalized by the detector normalized responsivity.

$$Ee = \frac{A_{bb}}{R^2}\int_o^{\lambda} R_n(\lambda) L_e(\lambda, T)\, d\lambda$$

A_{bb} = blackbody area

R = range array to blackbody

$R_n(\lambda)$=normalized responsivity

$L_e(\lambda,T)$=blackbody radiance

$$L_e(\lambda, T) = \frac{2c^2 h}{\lambda^5\left(e^{hc/K\lambda T} - 1\right)}$$

Substituting into responsivity expression.

$$R_i(\lambda_p, f) = 32\, amp/watt$$

Solving for the photoconductive gain * quantum efficiency product one gets 1.8, from:

$$R_i(\lambda, f) = \frac{\eta\lambda q}{hc} \bullet G$$

$$\eta G = 1.8$$

From this data, it appears that the photoconductive gain is high. This conclusion is reconfirmed by time-constant data as well as responsivity vs integration time data.

C. Dynamic Range

The dynamic range was measured; however, the high voltages were limited by an external amplifier not the array. The maximum signal level was 800 mv with a minimum tare of 1.8 mv. The noise was about 358 microvolts, which gives a dynamic range of 2228 for 1 ms integration time. The tare "does" vary with integration time, indicating an array temperature problem.

D. Optimum Bias vs Signal-to-Noise Ratio

The signal/noise measurements were made using a two-point difference technique between reset and signal level as shown in Figure 2.

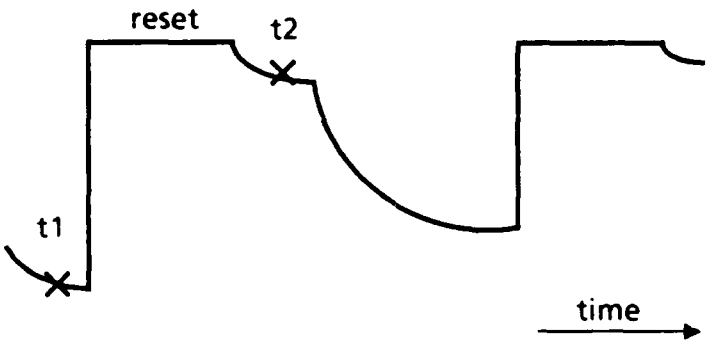


Figure 2 Video Waveform

This technique measures the voltages pre and post to resetting the detector to a reference voltage. This is sometimes called substracted double samples (SDS), (Fugerer,1988). It is not the classical correlated double-sampling often referred to in the literature (Barbe, 1975). The voltage levels at t1 and t2 were sampled and held, A/D converted and stored in computer memory. This was done for 1000 frames.

The noise was defined as the temporal noise associated with a pixel over several frames (i.e., 100).

For n frames of data, the noise of a single pixel is expressed as:

$$T_i = \left| \frac{\sum_{i=1}^{n} \Delta V_i^2 - \frac{1}{n} \left| \sum_{i=1}^{n} \Delta V_i \right|^2}{n-1} \right|^{1/2}$$

$$\Delta V_i = V_i(t2) - V_i(t1)$$

This is the temporal noise for one pixel over 100 frames if n=100.

A plot of signal/noise vs detector bias voltage is shown in Fig. 3, showing a peak at 3.0 volts. This follows the predicted values by Szmulowicz (1988). However, due to other considerations, a 2.8 volt bias was used for measurements. This is only 10% less than peak. The noise was measured to be 358 microvolts. It seems that the reset noise was large for this device, because making a CDS measurement improved the noise significantly.

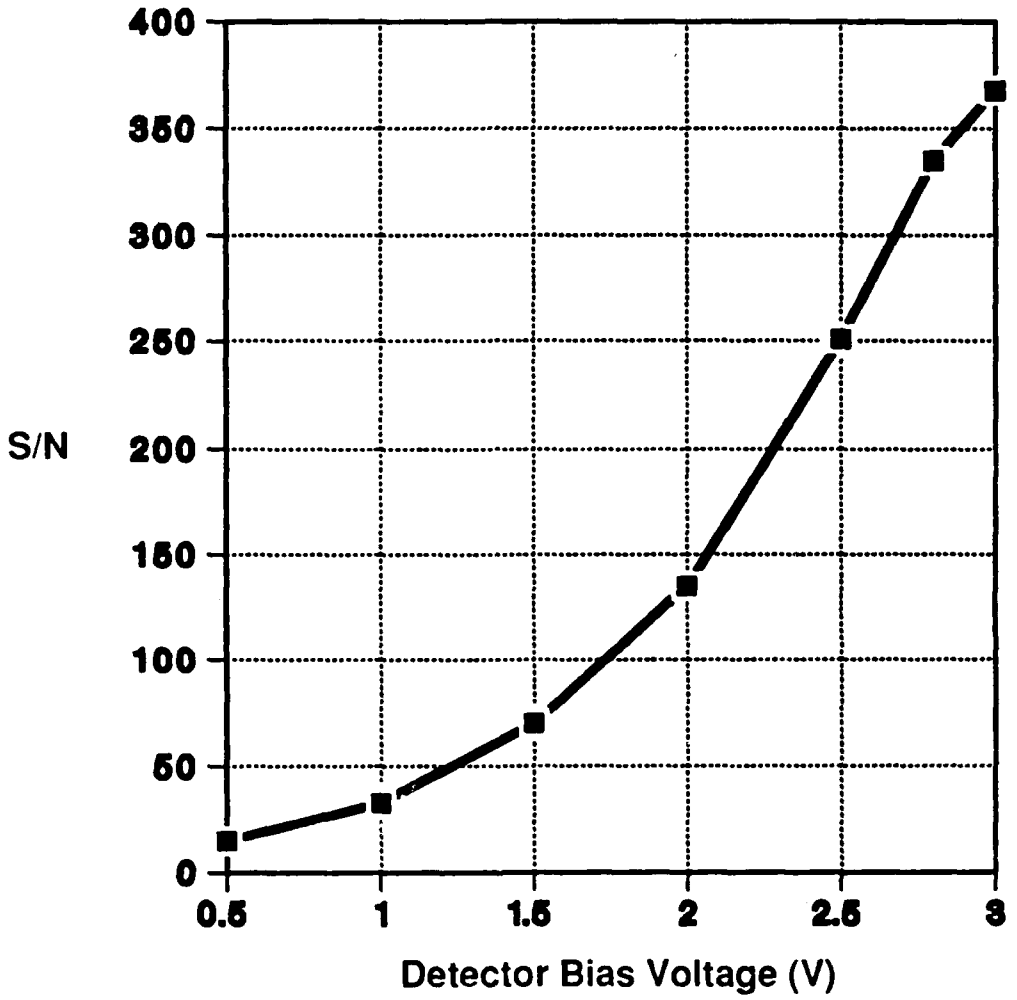


Fig. 3 Signal-To-Noise Ratio vs Detector Bias At 10K

E. Noise Equivalent Input (NEI)

This is the number of photons at maximum wavelength that is incident on the detector to get a signal to noise ratio of one (1). It is independent of the integration time; so strictly speaking, one must be read noise limited.

$$NEI = \frac{Noise}{<\eta G> G_p C.G.}$$

where

Noise = read noise voltage

$<\eta G>$ = quantum efficiency*photoconductive gain

G_p = post amplifier gain

C.G. = conversion gain

NEI = 5000 photons

An alternative equation for calculating NEI is to use a measure s/n ratio method and the following expression:

$$NEI = \frac{E_p A_d T_i}{S/N}$$

where

E_p = photon irradiance on array

A_d= area of pixel

T_i = integration time

This is only if the signal measured is a low value and the noise remains the read noise.

IV. RECOMMENDATIONS

Infrared focal plane arrays using charge transfer techniques as readout are being tested in low-background flux levels. These high-performance arrays are very difficult to evaluate, especially noise measurements--as was experienced this Summer. Wide dynamic range requirements and conventional voltage levels dictate lower noise devices, thus more difficult measurements. Both analog and digital noise measurements were made and gave correct noise results in a benign environment of the laboratory. The issue of whether CDS is required in addition to SDS is a guess at this point without further data. A low-noise CDS capability would surely make AEDC a unique place to test arrays.

There are several improvements which would enhance the focal plane array test facility.

1) Lag - The percentage of the signal left after a pixel irradiance has goes to zero, measuring the temporal crosstalk similar to the spatial crosstalk presently being done. This could be done very cheaply with an x-ray source (fe-55) to excite a pixel.

2) Timing Diagram Generation - The present means of changing the time waveforms are cumbersome via the timing generator and word generator. Using a commercially available pattern generator to set up the timing and word generation would make the system easier to operate and accessible to all personnel (i.e., Pulse Instruments-P5800 or Interface Technology -4000).

3) Data Collection - The data for evaluation should be done while the arrays are running continuously.

4) Mean Variance Curve - Data should be taken to make a plot of temporal noise as a function of the photon irradiance level. If the array is BLIP, the slope should be constant.

5) Spatial Variance vs Signal Level - (Mooney and Dereniak,1987)

Further research is needed in the characterization of FPA with respect to modulation transfer function (MTF). This relates to number five above and a mini-proposal planned to be submitted. The key parameter in the output video display is MTF. A means to measuring this is similar to IR scene generator, but only much simpler.

The approach is to use interference fringes of known spatial frequency and intensity projected onto the FPA. Such a sinsusoidal fringe pattern would be capable of having its frequency and orientation changed in a simple predictable way.

REFERENCES

Barbe, D. IEEE, 63, 38, 1975.

Dereniak, E. L. and D. G. Crowe, Optical Radiation Detectors, John Wiley and Sons, 1984.

Fugerer, B. Private Communicate, AEDC, (615) 454-6889, 1988.

Mooney, J. and E. Dereniak, Optical Eng. Mar. 1987.

Stetson, S. et al SPIE 686, 9 1986.

Szmulowicz, F., F. Madarasz, and J. Diller, "Temperature dependence of the figures of merit for blocked impurity band detectors," J. Appl. Phy, 63, 11 June, 1988.

Whitehead, G. V., P. D. Elrod, K. B. Jarrett, and R. P. Young, Development of a Focal Plane Array Test Capability, AEDC-TR-87-41, May, 1988

1988 USAF-UES SUMMER FACULTY RESEARCH PROGRAM

GRADUATE STUDENT RESEARCH PROGRAM

Sponsored by the

AIR FORCE OFFICE OF SCIENTIFIC RESEARCH

Conducted by the

Universal Energy Systems, Inc.

FINAL REPORT

LIQUID FILM COOLING IN ROCKET ENGINES

Prepared by: William M. Grissom

Academic Rank: Assistant Professor

Department and University: Physics Department, Morehouse College

Research Location: AEDC, SVT/900
Arnold AFS, Tenn 37389

USAF Researcher: Chad Limbaugh

Date: August 18, 1988

Contract No: F49620-87-R-0004

LIQUID FILM COOLING IN ROCKET ENGINES

by
William M. Grissom

ABSTRACT

A simple analysis based upon proven heat transfer correlations can be used to accurately calculate the liquid evaporation rate and vapor mixing in liquid film-cooled rocket engine combustion chambers. The vapor transpired from the liquid film greatly decreases the normal convective heat transfer rate so that radiation becomes significant. The radiative heat flux is absorbed at the walls and transmitted to the liquid film by boiling heat transfer. Under certain conditions the radiative heat flux can cause burnout of the liquid film. If too high of a coolant flow rate is used, large waves form on the liquid film and droplets are mechanically sheared off of the liquid film without evaporation, making ineffective use of the liquid for cooling. The gaseous mixing of the vapor downstream of the liquid film can be analyzed by using existing integral correlations in a differential form to account for free-stream acceleration in the throat. The analysis provides excellent correlation of the existing experimental data and fair comparison in an absolute sense.

I. INTRODUCTION

Many liquid rocket engines employ a film of liquid fuel as thermal protection for the combustion chamber walls. This process was experimentally studied in the 1950's and 1960's, however no general analysis procedure was established at that time. Since then a number of fundamental heat transfer studies have been performed which allow the liquid film cooling problem to be broken into discrete mechanisms for a more fundamental analysis.

Heat is transferred to the liquid film by both radiation and convection from the hot combustion gases. The vapor transpired from the film tends to decrease the convective heat transfer rate below what it would be for a dry wall. This vapor then mixes with the hot gases entrained in the boundary layer and lowers the boundary layer temperature by calorimetric mixing. This provides thermal protection downstream of the liquid film.

I have a background in heat transfer and fluid flow, with academic training in mechanical and aerospace engineering, and have performed previous research in the liquid spray cooling of a heated surface, which initially appeared related to the present problem. I have performed previous studies of liquid rocket combustion diagnostics and have current research interests in rocket injector droplet sizing.

II. OBJECTIVES OF THE RESEARCH EFFORT

The present summer's work is a continuation of an analysis begun and reported last summer on the same AFOSR/UES program. To avoid repetition the results from last summer are only briefly mentioned, reference to the Summer 1987 report will provide the details. All of the work is being prepared as an AEDC technical report.

The focus of the present research was to develop a computer code to automate the calculations and eliminate many of the approximations necessary in the hand calculations performed last summer. To allow this, significant effort was required to develop analytical expressions for the radiative emittance plots given in heat transfer texts. Additional effort was necessary to adapt existing gaseous film cooling correlations to an accelerating flow.

III. LIQUID FILM EVAPORATION

A. Convective Heat Transfer

The skin friction factor (non-dimensional wall shear stress) and Stanton number (non-dimensional heat transfer coefficient) are calculated by standard correlations for a flat-plate, (properties evaluated at the mean temperature):

$$C_f = 0.0592\ Rx^{-0.2}$$

$$St = \tfrac{1}{2}\ C_f\ Pr^{-0.6} \qquad \text{(Eq. III.1)}$$

For fully-developed flow (Ref. 1):

$$St = 0.023\ ReD^{-0.2}\ Pr^{-0.6}$$

The flat-plate and fully-developed flow correlations can be patched together by defining an effective x_e for use in Eq. III.1. The function suggested last summer was found to have singularity problems and is replaced by the following:

$$x_e = 3.53\ D \left[1 + \left(\frac{x}{3.53\ D}\right)^{-4}\right]^{-1/4}$$

The convective heat flux vaporizes a mass flux (per surface area) of liquid:

$$\dot{m}_{conv} = \frac{h\ \Delta T}{\lambda^*} = \frac{G\ C_{pg} St\ \Delta T}{\lambda^*}$$

The total vapor generated by both convective and radiative heat transfer is "blown" into the boundary layer. This blown mass decreases the normal wall shear stress and convective heat flux by a factor (Ref. 2):

$$\frac{h}{h_o} = \frac{\ln(1+H)}{H} \quad ; \text{ where } \quad H = C_{pg}\left[\frac{\Delta T}{\lambda^*} + \frac{\dot{m}_{rad}}{h}\right]\left[\frac{Mg}{Mv}\right]^a$$

$$a = 0.6 \text{ if } Mv<Mg \text{ or } 0.35 \text{ if } Mv>Mg$$

Knuth's correlation (Ref. 3) determines the maximum coolant flow rate to avoid the

transition to large waves, and the corresponding liquid loss by droplet shearing:

$$\Gamma_{cr} = 1.01\ 10^5\ \mu_v^2/\mu_\ell$$

B. Radiative Heat Transfer

The simplest and most effective approach in determining the radiation from high density gases is to use the total emittance, E, which is the ratio of the radiant intensity of the gas to that of a blackbody at the same temperature, averaged over the entire spectrum.

The most recent emittance data is compiled by Siegel and Howell (Ref. 4). This data is replotted as a function of the optical density, ρ_{opt}, which is the gas partial pressure times the path length through the gas. At very high optical densities the emittances reach limiting values, E_f, of 0.825 for H_2O and 0.231 for CO_2. These curves may be analytically fit to a function:

$$E = E_f \left[1 + \left[\frac{\rho_{opt}}{c}\right]^{-n}\right]^{-1/n}$$

with coefficients:

H_2O			CO_2		
T(°K)	c	n	T (°K)	c	n
1000	0.165	0.45	1000	0.05	0.6
2000	0.90	0.65	1500	0.075	0.6
3000	2.05	0.61	2000	0.15	0.6

A correction must be made for a total pressure different than 1 atm by multiplying a correction factor, K_p, to each emittance. The curves for these pressure corrections can be fit analytically by:

H_2O: $$K_p = 1 + C_1\{1 - \exp[(1-P[1+\rho_{H_2O}])/C_2]\ \}$$

where: $$C_1 = 0.26 + 0.74\ \exp(-2.5\ \rho_{H_2O})$$
$$C_2 = 0.75 + 0.31\ \exp(-10\ \rho_{H_2O}) \quad \text{atm}$$
$$\rho_{H_2O} <> \text{atm}\cdot\text{m}$$

$$CO_2: \quad \log_{10} K_p = 0.036\, \rho_{CO_2}^{-0.483} \left[1 + (2 \log_{10} P)^{-m}\right]^{-1/m}$$

where: $m = 100\, \rho_{CO_2}$
$P <> atm$
$\rho_{CO_2} <> atm \cdot m$

An additional correction factor is necessary to account for overlaps in the two spectra. This correction can be expressed analytically for T > 1200K as:

$$\Delta E = 0.0551\, Kx \left[1-\exp(-4\, \rho_{opt})\right] \left[1-\exp(-12.5\, \rho_{opt})\right]$$

where: $Kx = 1 - \left| \frac{2\, Nw}{Nw+Nc} - 1 \right|^n$

$$n = 5.5 \left[1 + (1.09\, \rho_{opt})^{-3.86} \right]^{-1/3.88}$$

$\rho_{opt} <> atm \cdot m$
Nw = mole fraction of water in mixture
Nc = mole fraction of CO_2 in mixture

The total gas emittance is then:

$$Eg = Ew + Ec - \Delta E$$

In evaluating these terms it is necessary to input the optical path length through the gas. Since this generally varies over the sight angle, the most direct method would be to calculate the emittance at a number of sight angles and to average them, weighted by the projected area at each angle. However, a simpler approach is to use an overall effective length. A very simple expression is quite accurate in determining the effective length (Ref. 4):

$$Leff = 0.95\, (4V/A)$$

where V is the chamber volume and A is the surrounding surface area.

In applying this formula, the downstream section of the chamber will be assumed to be an infinite cylinder, for which Leff = 0.95 D. If the cloud of droplets coming out of the injector is assumed to be perfectly reflective, then the upstream direction can

also be considered an infinite cylinder. Since the droplets have numerous partially reflecting surfaces compared with the volume of absorbing liquid, this is probably the best assumption.

It is also necessary to consider the possibility of reflective walls. In this case the effective sight paths will be longer. The simplest correction, due to Egleti (Ref. 15), is to multiply the above effective length by a factor of Aw to the power -0.85 ; where Aw is the wall absorptivity.

With the gas emittance so determined the radiant heat flux is calculated as:

$$\dot{Q}_{rad} = \sigma \, Aw \, Eg \, [Tg^4 - Tv^4]$$

where: $\sigma = 5.67\ 10^{-8}\ W/m^2 \bullet {}^\circ K^4$

which vaporizes a mass flux, $\dot{m}_{rad} = \dot{Q}_{rad} / \lambda^*$

The fraction of radiation transmitted through the liquid film is: $\exp(-\alpha t)$; where α is the absorptivity of the liquid, weighted over the spectrum of the radiation, and the liquid film thickness, t, can be calculated from the wall shear stress. Assuming viscous flow:

$$t = \sqrt{\frac{2 \nu \Gamma}{\tau_w}}$$

where Γ is the local coolant mass flow (per circumference).

This heat is then conducted into the liquid film by boiling heat transfer. With a high enough heat flux the surface can become covered by poorly conducting vapor, causing the surface temperature to rapidly rise, usually with catastrophic results. This rather abrupt transition is termed "burnout". The correlation of Katto, et al (Ref. 5, 6) can be used to predict the burnout heat flux:

$$\dot{Q}_{bo} = 0.0164 \, \lambda \, \rho_\ell^{0.534} \, \rho_v^{0.133} \left[\frac{U_\ell \, \sigma_\ell}{\ell} \right]^{0.333}$$

IV. VAPOR FILM COOLING

After the liquid film has vaporized it continues to provide thermal protection to the wall by calorimetric mixing with the hot gases in the boundary layer. Numerous correlations have been presented for this process, termed "gaseous film cooling". They are normally expressed in terms of a "cooling effectiveness":

$$\eta \equiv \frac{Tg - Taw}{Tg - Tv}$$

where Tg is the free-stream gas temperature, Tv is the saturation temperature of the vapor, and Taw is the "adiabatic wall temperature" which is the "mixing-cup" temperature of the gases in the boundary layer.

The cooling effectiveness is usually plotted against a dimensionless distance along the wall:

$$X = K\,x \;; \quad \text{where:} \quad K \equiv G\,\mu_g^{0.25} \cdot M_v^{-1.25}$$

where: M_v = coolant vapor mass flow (per circumference)

$G \equiv \rho_g U_g$ = freestream gas mass flow rate per chamber cross-sectional area

x = distance downstream from injection point

The most successful of the flat-plate integral solutions is that due to Kutateladze, et al (Ref. 7). Re-deriving their results for the case of vapor injection a distance x_i downstream of the leading edge gives:

$$\eta = \left[1 + \frac{Cpg}{Cpv} \left(0.325\,[X+X_o]^{0.8} - 1\right) \right]^{-1} \qquad \text{(Eq. IV.1)}$$

X_o is a fictional, non-dimensional upstream position given by:

$$X_o = (3.08 + X_i^{0.8})^{1.25} - X_i$$

$$\text{where:} \quad X_i = K\,x_i$$

A number of corrections are necessary to account for non-uniform free-stream flow:

- To correct for freestream turbulence of rms fluctuation, e, the non-dimensional distance, X, above can be multiplied by a factor, $K_t = 1 + 10.2\ e$, based upon the data of Carlson and Talmor (Ref. 8) and Marek (Ref. 9).

- To correct for different freestream and coolant gases the Cpg/Cpv ratio above can be multiplied by a factor $K_M = (Mv/Mg)^{0.14}$, based upon the data of Goldstein, et al (Ref. 10), where Mv and Mg are the molecular weights of the vapor and coolant, respectively.

- To conduct the thermal radiation absorbed at the wall back into the freestream gas requires the actual wall temperature to be higher than the boundary layer gases, Taw, by Q_{rad} / h, where h can be calculated from Eq. III.1.

- The radiant heat will also go into the heat balance of the boundary layer gases. Assuming that it is spread evenly over the entire boundary layer mass, the temperature increase with distance will be:

$$\frac{\Delta T_{aw}}{\Delta x} = \frac{\dot{Q}_{rad}}{\dot{M}_{bl}\ C_{pg}} = \frac{3.08\ \dot{Q}_{rad}}{\dot{M}_v\ C_{pg}\ (X+Xo)^{0.8}}$$

- To correct for high-speed free-stream flow velocities the "recovery temperature" should be used in place of the free-stream stagnation temperature:

$$Tg|_r = Tg - (1-r)\frac{V^2}{2Cpg}$$

where: r = "recovery factor" = $Pr^{1/3}$ for a turbulent boundary layer.

A final concern in applying Kutateladze correlation to a rocket engine is with free-stream gas acceleration. In this case the correlation in the form of Eq. IV.1 cannot be applied directly, since it was derived for the case of constant free-stream conditions. However, the correlation can be used to express the differential change in the effectiveness at every free-stream condition, in effect reconstructing the governing ordinary differential equation governing the gaseous cooling. Integrating from the injection point, the effectiveness at every position can be determined.

Since the free-stream gas temperature can change, the cooling effectiveness must be discarded in favor of the absolute boundary layer temperature, T_{aw}, to avoid

confusion:

$$T_{aw} = T_g - \eta(T_g - T_v)$$

The rate of change with position of T_{aw} is:

$$dT_{aw}/dx = -(T_g - T_v)\, d\eta/dx$$

where:

$$\eta = \left[1 + K_M \left[\frac{Cpg}{Cpv}\right] \left[0.325\ (K_t X + Xo)^{0.8} - 1 \right] \right]^{-1}$$

$$d\eta/dx = -0.26K\ K_t K_M \left[\frac{Cpg}{Cpv}\right] (K_t X + Xo)^{-0.2}\ \eta^2$$

expressing X in terms of η:

$$d\eta/dx = -0.1963\ K\ K_t K_M \left[\frac{Cpg}{Cpv}\right] \eta^2 \left[1 + \frac{Cpv}{K_M Cpg} \left[\frac{1}{\eta} - 1\right] \right]^{-\frac{1}{4}}$$

T_{aw} at the next downstream position is then found:

$$T_{aw}(x+\Delta x) = T_{aw}(x) + dT_{aw}/dx|_x\ \Delta x$$

From this new value the local value of η is calculated, using the local value of T_g, for evaluation of $d\eta/dx$ at the new position.

The parameters which will vary in the nozzle of a rocket are the free-stream mass flow-rate per area, G, and the free-stream recovery temperature, Tg_r. The first is found simply from the area change, since the mass flow is conserved:

$$G = G_{ch}\,(A_{ch}/A)\,; \qquad \text{ch - values in the combustion chamber}$$

In order to calculate the recovery temperature above, the local free-stream gas velocity can be estimated using the isentropic relations for compressible flow:

$$V = G/\rho$$

where:

$$\rho = \rho_{ch}\, b^{-[1/(\gamma-1)]}$$

$$b \equiv 1 + \tfrac{1}{2}(\gamma-1)M^2$$

with M found implicitly from:

$$\frac{A}{A_t} = \frac{1}{M}\left[2b/(\gamma+1)\right]^{\left[(\gamma+1)/2(\gamma-1)\right]}$$

where A_t is the area of the nozzle throat.

There is also some indication that "centrifugal force" effects may be important in the throat turns, however, the data is inconclusive. The results of Carlson and Talmor (Ref. 8) in a rectangular duct were somewhat anomalous since they don't reduce correctly for the case of zero turning angle. Rousar and Ewen's data (Ref. 11), shows a turning correction, based upon their empirical mixing model. Their data is being reanalyzed, as of this writing, in terms of the differential method described above to determine if such turning correction factors are required.

V. COMPARISON WITH EXPERIMENTS

Space limitations require only a brief description of comparisons of the analysis with liquid film cooling experiments.

- Kinney et al (Ref. 12)
These tests were conducted at low temperatures (700-1150° K) in a fully-developed flow with water coolant. The measured evaporation rates are an average of 40% higher than calculated and well correlated with the calculations.

- Knuth (Ref. 3)
Similar conditions to Kinney, et al. The measured evaporation rate is 11% and 60% lower than calculated in two tests and 20% higher than calculated in one case.

- Morrell (Ref. 13)
These were conducted in a LOx/ammonia rocket at various O/F ratios. The data is well correlated by the analysis. The measured liquid film lengths are 35% shorter than calculated with water coolant. With ethanol coolant Knuth's limit for transition to "large waves" was exceeded and the measured liquid film lengths are 3 times shorter than calculated.

- Warner and Emmons (Ref. 14)
These tests were at a temperature of 2222° K in fully-developed flow. The measured evaporation rates were 77% larger than calculated with water and ammonia coolants

and 105% higher than calculated with ethanol coolant.

- Kesselring, et al (Ref. 15)
These tests were in a OF_2/B_2H_6 rocket (3900° K) with B_2H_6 as coolant. In this case radiation was dominant. The calculations agree best with the data if a gas emittance of 0.77 is assumed.

VI. BOUNDARY CONDITIONS FOR A 3-D TURBULENCE MODEL

The liquid film evaporation results can be used as boundary conditions to a 3-D turbulence model, such as the KIVA code (κ-ϵ model) presently used at AEDC. This necessitates changes to the conservation equations at the grid points next to the liquid film.

The continuity equation is simply changed by the imposed mass flux of vapor transpired from the film. Likewise, the energy equation is simply changed by including the specific heat of the transpired vapor.

The momentum equation is the most difficult to modify. In principle the turbulence model can be carried all the way to the wall, however this necessitates an unusually large number of grid points in order to follow the steep velocity profile close to the wall. In practice the grid is usually extended into a region close to the wall where a universal, logarithmic profile is known to exists, allowing extrapolation to the wall. For the case of transpiration from the wall, a similar logarithmic "law of the wall" is known (Ref. 18):

$$\frac{2\,U_*}{V_W}\left[\left(1+\frac{U\,V_W}{U_*^2}\right)^{\frac{1}{2}}-1\right] = 2.5\,\ln\left(\frac{y\,U_*}{\nu}\right)+C$$

where:

$$C = 5.0 + \frac{2\,U_*}{V_W}\left[\left(1+10.8\,\frac{V_W}{U_*}\right)^{\frac{1}{2}}-1\right] - 10.8$$

V_W = "blowing velocity" of vapor off liquid film
y = distance from wall
U = axial velocity at position y

Given an axial velocity, U, at the last grid point a distance y from the wall the "shear

velocity", U_*, is found implicitly using the Newton-Raphson method. From this the wall shear stress is found:

$$\tau_w = \rho \; U_*^2$$

The shear stress at the last grid point is then:

$$\tau = \tau_w + \rho \; V_w \; U$$

After many iterations through the turbulence model the program should converge to appropriate values of U and τ.

Indeed, the flat-plate correlations used in this study could be entirely eliminated by calculating the evaporation rate using the wall shear stress determined above. From Reynold's analogy (with Pr correction):

$$St = \tfrac{1}{2} \; C_f \; Pr^{-0.6}$$

This approach would be necessary for a case in which the free-stream flow conditions are not known a priori. However, in most rocket engines all indications are that the flow is straight downstream, with no recirculations, and that the flat-plate approximation is valid. To eliminate the use of the correlations would place an unnecessary burden on the 3-D simulation, requiring a fine axial spacing to reproduce the initial velocity profile development at the leading edge.

VII. CONCLUSIONS

It is possible to correlate the existing liquid film data from rocket engine tests using a model based on simple heat transfer correlations. In rockets with moderate combustion temperatures (2000-3500 K), both convective and radiant heat transfer must be considered, with radiation dominating at the upper end. Knuth's criterion is useful for estimating the critical coolant flow rate to avoid droplet shearing from the liquid film. Radiant burnout of the liquid film before complete evaporation is likely. Downstream of the liquid film standard gaseous film cooling correlations can be applied in a differential form to calculate the wall temperature and concentration as the vapor mixes with the freestream gas. Significant corrections to these correlations are required for freestream turbulence and turning effects at the throat.

VIII. RECOMMENDATIONS

A FORTRAN computer program which implements all of the liquid film evaporation calculations of Sec. IV has been delivered to AEDC. It has been thoroughly checked against experimental data and is ready to be implemented. It is suggested that the calculated evaporation rates be multiplied by a factor of 1.5 to account for various effects not considered in the analysis, such as liquid film "roughness", droplet shearing, etc.

A computer code to implement the gaseous film cooling calculations is under development. It will be used to compare the analysis to existing data in three Aerojet reports (Ref. 11, 16, 17) to determine the effects of throat turns. This is being continued as a present minigrant project. The 3-D turbulence model used at AEDC can be used to calculate the vapor mixing downstream of the liquid film directly. The analysis presented here can be used as a check upon the 3-D model in the gaseous film cooling region.

ACKNOWLEDGEMENTS

The research reported herein was sponsored by the Air Force Office of Scientific Research/AFSC under Contract F49620-85-C-0013 of the Universal Energy Systems Summer Faculty Research Program. The study was conducted at Arnold Engineering Development Center, Arnold AFS, Tennessee. Appreciation is due Chad Limbaugh and William McGregor (Sverdrup Technology) for suggesting the topic and supervising the work. Marshall Kingery (Air Force) supervised the faculty program and arranged several enjoyable outside activities.

REFERENCES

1. Humble, L.V., et. al. NACA Report 1020, 1951.
2. Hartnett, J.P. et. al. Heat and Mass Transfer in Boundary Layers. Vol.1 N. Afgan, editor, Pergamon, 1972.
3. Knuth, E.L. "The Mechanics of Film Cooling". JPL Memo 20-85, September 1953.
4. Siegel, R. and Howell, J.R. Thermal Radiation Heat Transfer, second edition, Hemisphere, (1981), Section 17.5 - 17.6 .
5. Monde, M. and Katto, Y. Int. Journal of Heat and Mass Transfer, Vol.21, 1978.
6. Katto, Y. and Ishii, K. 7th Int. Heat Transfer Conf., Vol.4, Toronto, 1978, p.435.
7. Kutateladze,S.S. et al. High Temperature (Soviet),Vol.1, Sept-Oct 1963.
8. Carlson, L.W. and Talmor, E. Int. Journal of Heat and Mass Transfer, Vol.11, 1968, p. 1695.
9. Marek, C.J. et al. NASA TN D-7958, June 1975.
10. Goldstein, R.J. et al. Int. J. of Heat and Mass Transfer, Vol. 9, 1966, p.1341.
11. Rousar, D.C. and Ewen, R.L. "Hydrogen Film Cooling Investigation", NASA CR-121235, August 1973 (Aerojet).
12. Kinney, G.R. et al. NACA Report 1087, 1952.
13. Morrell,G. NACA RM E51E04, July 1951.
14. Warner, C.F. and Emmons, D.L. Trans. ASME Journal of Heat Transfer, May 1964, p. 271.
15. Kesselring,R.C. et al. "Boundary Cooled Rocket Engines for Space Storable Propellants". NAS7-767, NASA-CR-129260, June 1972, (Rocketdyne).
16. Ewen, R.L. "Hydrogen Film/Conductive Cooling", NASA CR-120926, November 1972 (Aerojet).
17. Rousar, D.C. and Ewen, R.L. "Combustion Effects on Film Cooling", NASA CR-135052, February 1977 (Aerojet).
18. Cebeci, T. and Bradshaw, P. Momentum Transfer in Boundary Layers, 1977.

NOMENCLATURE

Aw = absorptivity of chamber walls

Cf = skin friction factor $\equiv 2\tau_w/\rho_g U_g^2$

Cp = specific heat per mass

C_t = correction constant for turbulence

D = diameter of combustion chamber at position x

e = freestream turbulence intensity

E = emittance of combustion products

G = free-stream mass flow per area = $\rho_g U_g$

h = convective heat transfer coeff.

K = $G \mu g^{0.25} / Mv^{1.25}$

L_{eff} = average optical path length

m_v = total coolant evaporation rate per surface area

M = molecular weight

Pr = Prandtl no of gas $\equiv \mu_g C_{pg}/Kg$

P = absolute pressure

Pg = partial pressure of species

Q = heat flux

ReD = Reynold's no based on diameter $\equiv G D/\mu_g$

Rex = " " " " position $\equiv G x/\mu_g$

St = Stanton no $\equiv h/(G Cpg)$

T = absolute temperature

Tv = saturation temperature of coolant

ΔT = Tg-Tv

U = axial velocity

U* = "shear velocity" = $(\tau_w / \rho)^{1/2}$

x = axial distance from injector

X = dimensionless distance = K x

y = distance from chamber wall

Greek Symbols:.

λ = latent heat of vaporization of coolant

λ^* = λ + Cpl(Tv-Tc)

Γ = liquid coolant mass flow rate per circumference

η = film cooling effectiveness

ρ = mass density

ρ_{opt} = optical density $\equiv$ PgL

σ = surface tension of coolant or Stephan's const.

μ_g = dynamic viscosity

ν = kinematic viscosity $\equiv \mu/\rho$

1988 USAF-UES SUMMER FACULTY RESEARCH PROGRAM/

GRADUATE STUDENT RESEARCH PROGRAM

Sponsored by the

AIR FORCE OFFICE OF SCIENTIFIC RESEARCH

Conducted by the

Universal Energy Systems, Inc.

FINAL REPORT

DIFFUSER FAILURE INVESTIGATION/ NONINTERFERENCE STRESS MEASUREMENT SYSTEM ALGORITHMS STUDY

Prepared by:	Darrell E.P. Hoy, Ph.D.
Academic Rank:	Assistant Professor
Department and University:	Mechanical Engineering Department Tennessee Technological University
Research Location:	Arnold Engineering Development Center Arnold AFB Tullahoma, TN 37389-5000
USAF Researcher:	Dr. Louis Deken Mr. Henry Jones
Date:	23 Aug 1988
Contract No:	F49620-87-R-0004

DIFFUSER FAILURE INVESTIGATION/

NONINTERFERENCE STRESS MEASUREMENT SYSTEM ALGORITHMS STUDY

by

Darrell E.P. Hoy

ABSTRACT

Investigation of repeated cracking occurring in turbine engine diffusers was undertaken. Past histories of diffusers used in jet engine test cells at AEDC were examined and evaluated. The most likely critical load parameters in the cracking process were found to be: geometric stress concentration effects, residual stress effects, acoustic loads, and vibrational response. An investigative plan was formulated to quantify these parameters and to generate an improved diffuser model.

Investigation of the algorithms used in the Noninterference Stress Measurement System for determining turbine-blade vibratory deflections and stresses was also made. Examination of the techniques used for measurement of integral-order vibrations (4 sensor technique and SDOF technique) led to the proposal of a "combined" technique for measuring integral-order resonant vibrations. Advantages of the combined technique include multiple determination of resonant amplitudes and frequencies using only off-resonance measurements, elimination of the need to establish "DC trends" in the data. The deflection-to-stress conversion procedures were also evaluated and found to be appropriate. A summary of the requirements for interfacing with the finite element model was written.

ACKNOWLEDGEMENTS

I wish to thank the Air Force Systems Command, the Air Force Office of Scientific Research, Arnold Engineering Development Center, and Sverdrup Technologies, Inc. for their support of this research.

In addition, I would particularly like to thank both Mr. Henry Jones and Dr. Louis Deken for their help and concern for this research and for myself personally. Mr. Marshall Kingery is also to be commended fully for his help, advice, and personal attention throughout this program.

I. INTRODUCTION

The research efforts of this investigator were directed along two independent areas in the field of jet engine testing. These were:

(1) The investigation and evaluation of the factors involved in the failure of turbine engine diffusers by cracking.

Turbine engine diffusers are located in the jet engine test cells for purposes of exhaust containment and flow regulation. As such, they are exposed to the severe and complex load environment generated in the proximity of the jet engine exhaust plume. Repeated failures by fracture (both brittle and fatigue) have been observed in the diffusers and supporting structures. Such failures are very costly both in terms of man-hours and repair/replacement costs.

(2) The study of processing algorithms used in the testing of turbine engine blades by the Noninterference Stress Measurement System (NSMS) under development at AEDC.

The NSMS system is designed to measure turbine-blade vibratory deflections and stresses by use of noncontacting optical probes. Measurements of the vibrations are taken during actual engine operation. Processing algorithms are then utilized to convert the NSMS data (blade arrival times) to the corresponding deflections and stresses. Areas of concern include the

processing of vibrations which are integral multiples of engine speed and the interfacing with the finite element model for purposes of stress computation.

The primary research interests of this investigator are in the field of experimental stress analysis with a particular interest in optical measurement methods, digital imaging, and stress-wave measurements. As such my assignment to the aforementioned tasks this summer was a very suitable extension of my research interests.

II. OBJECTIVES OF THE RESEARCH EFFORT

A. Diffuser Failure Investigation (In Conjunction with Dr. Louis Deken):

(1) Evaluate previous studies and failure histories of the turbine engine diffusers at AEDC to identify the current state of knowledge with regard to each of the major design parameters.

(2) Formulate a suitable plan for the development of an appropriate diffuser model which can be used to relate the applied loads to the onset of diffuser crack formation.

B. Noninterference Stress Measurement System (NSMS) Processing Algorithms (In Conjunction with Mr. Henry Jones):

(1) Investigate the techniques currently employed in the determination of integral-order turbine blade vibrations (SDOF and 4 sensor techniques). Examine the effects of static deflections, nonintegral vibrations, etc. Suggest methods for improvement of current integral-order processing algorithms.

(2) Examine the deflection-to-stress conversion procedures employed by NSMS. Identify interface requirements, potential problems, and sources of error.

(3) Suggest and try various test cases as appropriate.

III. DIFFUSER FAILURE INVESTIGATION

At AEDC, a number of diffusers are employed in the J-series and T-series turbine engine test cells. Several of these diffusers, particularly those employed in the J1 and J2 test cells, have had a repeated history of failure by crack formation in the diffuser walls, supports, and/or supply piping. Repair and replacement costs of these diffusers are quite high; hence, the motivation for a permanent solution to this problem is strong.

To date, diffuser design in the J-cells has employed only basic design calculations together with estimated values of the load parameters. Detailed models combined with measurements of the actual load conditions have not been utilized. Hence, the first objective of this work was to determine the current state of knowledge and failure histories in each of the major design/test areas. This is summarized as follows:

(1) Mechanical Analyses - Determination of mechanical stresses in the J-cells has been primarily in the form of basic design calculations (thin-walled pressure vessels, simple bending formulas, etc). Stress concentration factors, residual stresses, and fatigue stresses have not been accounted for in previous studies.

(2) Thermal Analyses - Both finite element modeling and thermocouple measurements were previously used in determining the temperatures within the "panel coil" walls of the diffuser (see Figure 1). Maximum temperatures on the order of 400-500 ^{o}F were indicated. No

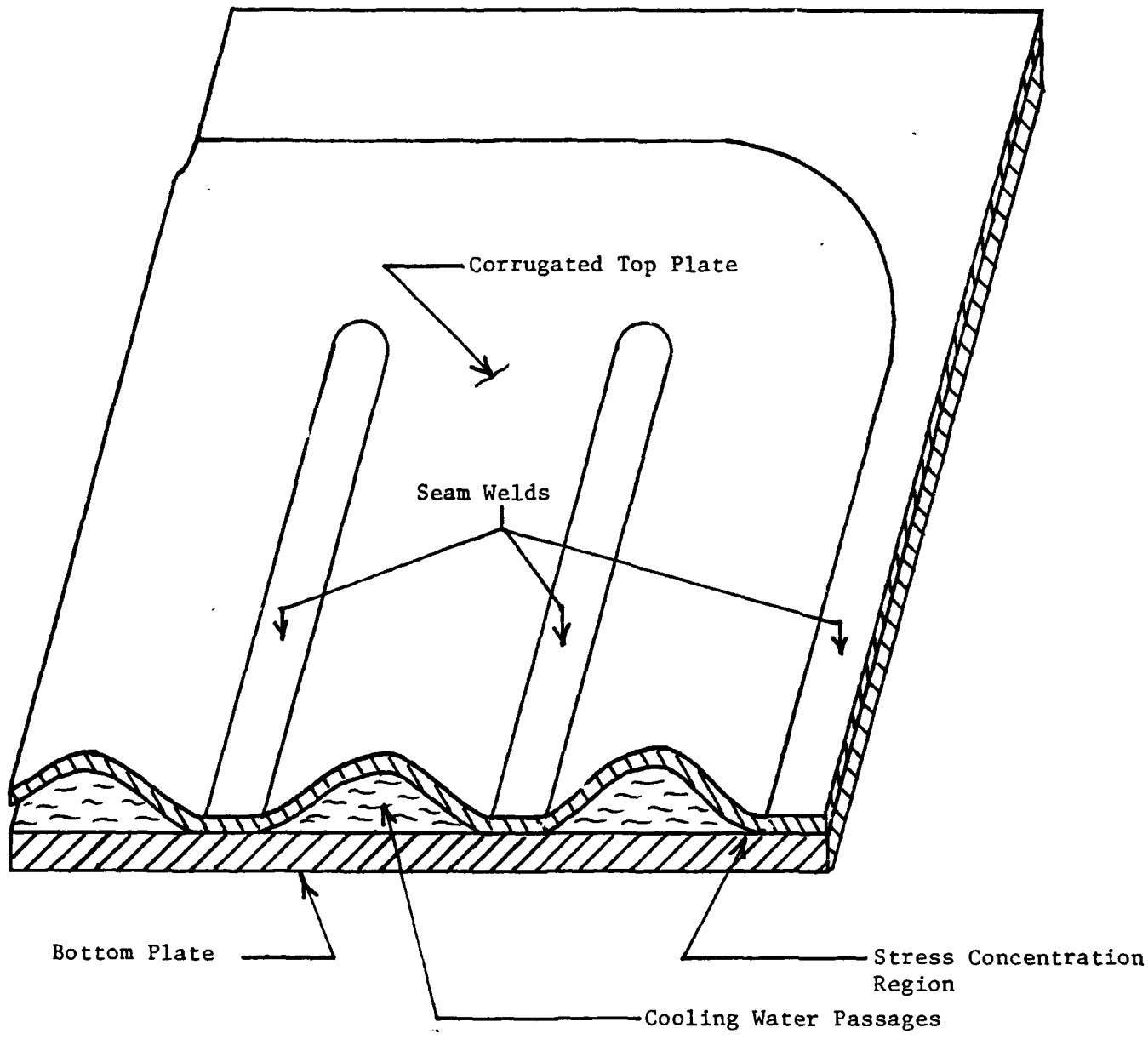


Figure 1: "Panelcoil" section used in diffuser wall construction.

direct measurements of inner surface (near exhaust plume) temperatures have been made.

(3) Vibration Analyses - A limited number of accelerometer measurements were made. These indicate a strong axial vibrational displacement in the panel coil walls in the frequency range of 30-100 Hz with a peak of 57 Hz.

(4) Acoustic Loads - The diffusers are subject to large acoustical loads; however, little data is available on the nature of these loads. The limited data available indicates the presence of high acoustic levels in the frequency range below 100 Hz.

(5) Metallurgical Examination - Metallurgical examination of the diffuser indicated that both fatigue and brittle-fracture cracks were present. Stress concentration areas present at the root of the the water passages in the panel coil served as the origin of a number of the cracks (Figure 1) Corrosion in the water passage is also thought to be an important factor.

Subsequent analysis of the design/test histories described above served to identify those parameters which appear to be most critical, and furthermore, indicated those areas in which further investigation is warranted. These are now discussed.

Examination of the panel coil itself reveals that the geometry of the panel coil construction leads to a region of high geometrical stress concentration at the "roots" of the water passages (Figure 1). This occurs due to the method of panel coil fabrication, i.e., the welding of the top corrugated panel to the bottom plate using seam and spot welds.

In addition, the fabrication procedure (welding and rolling) leads to areas very likely to contain high levels of residual stress. These factors surely affect the stress distribution within the panel coil significantly; hence, they should be accounted for in a realistic diffuser model.

The available accelerometer data indicates the presence of large axial vibration deflections in the center of the panel coil sections. The frequency of these vibrations is in the region of 30-100 Hz. There are no apparent sources of mechanical excitation which can be transmitted through the support structure. Hence, the vibrations are thought to be the result of acoustical excitation generated by the turbine engine during testing. This is further confirmed by noting that the measured frequency range is <100 Hz, i.e., the same as the observed vibrations. Again, the effects of acoustical loading, vibrational response, and their correlation have not been included in previous design studies.

The second objective was to formulate an investigative proposal to develop an appropriate diffuser model which, when combined with actual load measurements, would lead to the eventual solution of the diffuser failure problem. The following approach in solving the diffuser cracking problem was proposed:

(1) Construct an improved finite-element model of the diffuser by including both the effects of geometric stress concentration and residual stresses. The stress concentration factors existing in the panel coil should be determined experimentally using either 2-D or

frozen stress photoelasticity. These experimentally-determined concentration factors can then be included directly in the finite element model at the appropriate locations. Similarly, the residual stresses present due to the fabrication of the panel coil should be determined by the nondestructive, hole-drilling technique of residual stress determination. If any of these are found to be significant they can then be included in the model.

(2) Once a complete finite element model has been constructed, the correct external loads to be applied must be determined. Some data indicating both the thermal and pressure loads is available; these should be sufficient at least for the initial modeling. However, little data exists which indicates the acoustic excitation levels and the corresponding vibrational response of the diffuser. Hence, this data should be acquired by both measurement and theoretical modeling if possible. It should be noted that knowledge of both the acoustic and vibration environments would be very useful in another problem be encountered in the test cells, i.e., the rapid failure of some of the expansion joints in the exhaust ducting.

(3) Integration of the above experimental data and the finite element model would then enable determination of the stress levels associated with the crack formation process. With this information, appropriate design modifications could be made to eliminate the cracking problem.

IV. NONINTERFERENCE STRESS MEASUREMENT SYSTEM ALGORITHMS STUDY

The Noninterference Stress Measurement System (NSMS), under development at Arnold Engineering Development Center, is used to measure vibratory deflections and stresses in rotating turbine blades.[1-4] In this system, fixed optical probes are utilized to measure the blade vibratory deflections by recording the time-of-arrival of each blade as it intercepts the optical light plane of each probe (Figure 2). These recorded times are then processed to yield the blade deflections. Then, by relating to a finite element model, the corresponding stresses can be found. The processing algorithms used for the data reduction can be grouped into four major sections:

NSMS Data Processing Main Procedures (IPO Chart A)

Nonintegral Order Analysis (IPO Chart B)

Integral Order Analysis (IPO Chart C)

Stress Calculations (IPO Chart D)

The investigations of the Integral Order Analysis and Stress Calculation algorithms were the main focus of the NSMS portion of my work. These are now discussed.

The Integral Order Analysis algorithm is used to determine the deflections associated with vibrations whose frequency is an integral multiple of the engine speed. Unlike nonintegral vibrations, turbine blades undergoing integral-order vibrations appear to be nonmoving (standing waves) when viewed from a sensor in a stationary reference frame. Consequently, using two sensors in conjunction with an F.F.T. of the time series data (as is done in nonintegral analysis) will yield only

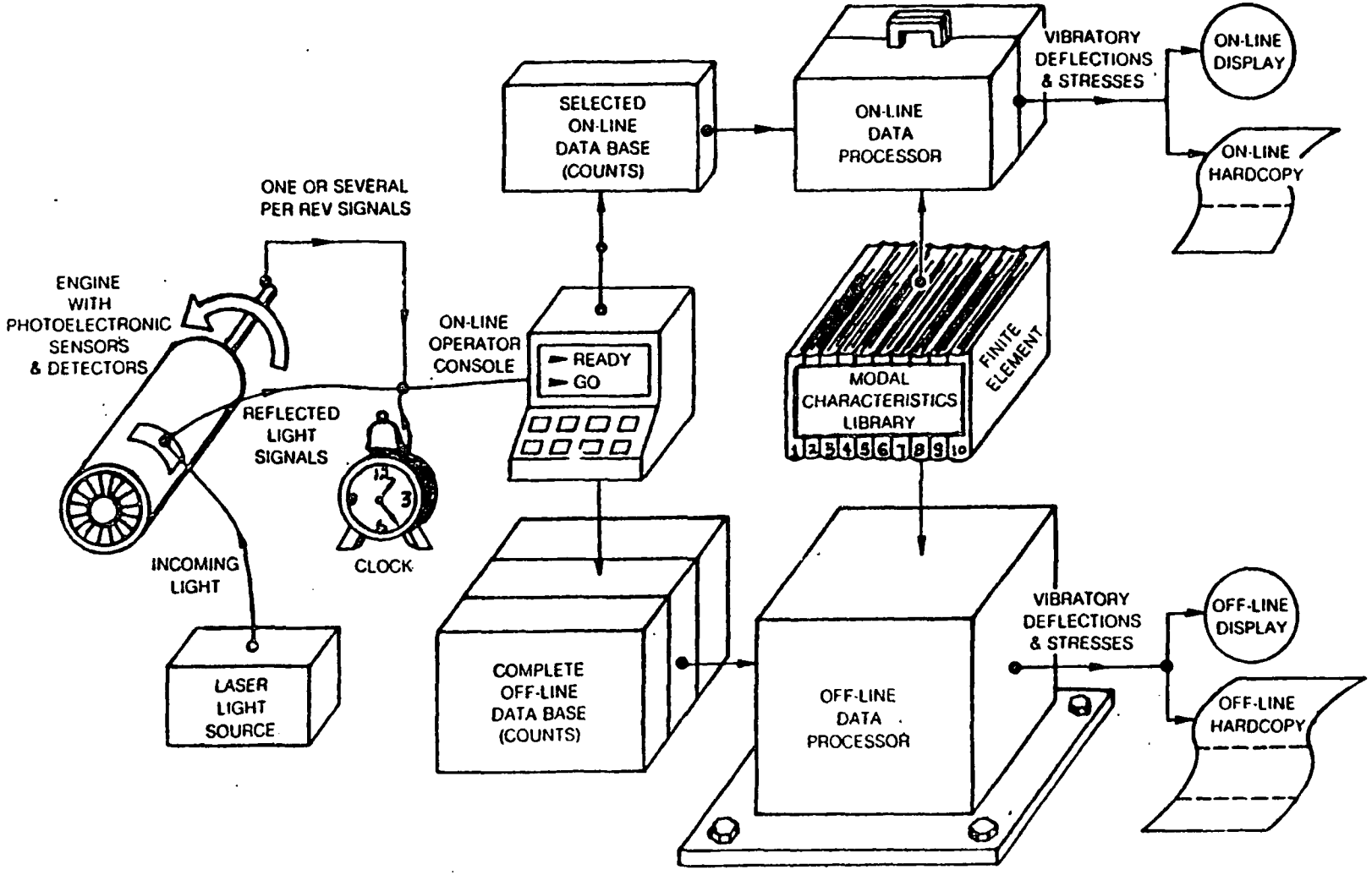


Figure 2: Noninterference Stress Measurement System (NSMS) for measurement of turbine blade vibrations.

a static deflection at each sensor instead of the desired vibratory deflection measurement. To overcome this problem, two different approaches have been utilized:

Four Sensor Technique - Four sensors located at four different circumferential locations around the turbine are used to record the wave profile of the integral-order standing wave which is present.

Single-Degree-of-Freedom Technique - Two sensors are employed to monitor the deflections of a single blade as engine speed is increased such that a transition through resonance occurs. By modeling the blade as a SDOF system, the resonant amplitude and phase can be determined.

Previous attempts to utilize these two techniques during an actual blade test have been inconclusive.[1] The lack of success during these tests was attributed to several factors including the presence of noise in the system, low blade excitation level, close sensor spacing, and data scatter.

As such, both methods were examined by this investigator, and their methodology was verified. In addition, a new "combined" technique was proposed by this investigator in order to overcome some of the shortcomings of the two previously mentioned techniques of integral-order analysis.

In the proposed "combined" technique, four sensors are used to measure the integral-order wave profiles occurring at several discrete engine speeds during transition through resonance. The amplitude, phase, engine order, and D.C. offset of the vibration can then be determined at each

discrete engine speed. The measurements made at each speed are then used to predict the resonant amplitude and frequency of the integral vibration. This "combined" approach has several advantages over the Four Sensor and SDOF techniques used individually. Among these are:

(1) Multiple determinations of resonant amplitude and frequency are possible allowing for rejection of errors.

(2) Determination of resonant amplitude and frequency can be made from near-resonance measurements.

(3) Extrapolation of "D.C. trends" from other frequencies below and above resonance is not necessary.

(4) Sensor spacing is less critical, since measurements are made at several different discrete frequencies and phases.

Appropriate test cases to verify the proposed "combined" technique were formulated; however, they could not be implemented at the time of writing due to a malfunction in the NSMS hardware simulator system. Future verification is pending.

The deflection-to-stress conversion methodology and algorithms were also examined in detail by this investigator. A summary of interface requirements between the finite element model and the NSMS algorithms was written. Upon examination, the stress conversion procedures were found to be appropriate. However, no test cases could be tried since a finite element model was not available.

V. SUMMARY OF RESULTS

A. DIFFUSER FAILURE INVESTIGATION

(1) The first objective was to evaluate the previous design studies and failure histories of diffusers to identify the critical design parameters. As a result, areas deemed to be critical and requiring further investigation were found to be:

(a) Stress concentration and residual stress effects in the "panel coil" diffuser wall itself.

(b) Acoustic loading and vibration response of the diffuser.

(2) The second objective was to formulate a plan for the development of an appropriate diffuser model. The resulting plan consists of the following main steps:

(a) Construction of a "hybrid" finite element model using experimentally determined stress concentration and residual stress effects.

(b) Measurement of the acoustic loads and vibration response.

(c) Combination of (a) & (b) to predict the load-crack formation relationship in the diffusers.

B. NONINTERFERENCE STRESS MEASUREMENT SYSTEM (NSMS) PROCESSING ALGORITHMS

The objectives of the NSMS study were to investigate the techniques currently employed in the determination of integral-order blade vibrations, to examine the deflection-to-stress conversion procedures, and to try various test cases as appropriate. The results of this work were:

(1) In the measurement of integral-order blade vibrations, a new "combined" technique of resonant vibration determination was proposed by this investigator. This technique allows for the multiple determinations (at off-resonant frequencies) of both resonant frequency and amplitude, without relying on knowledge of off-resonant "DC" trends.

(2) The deflection-to-stress conversion procedures were found to be appropriate.

(3) Test cases for the integral-order vibration measurement techniques were proposed; however, they could not be tried due to the unavailability of the NSMS simulator.

VI. RECOMMENDATIONS

As part of the Diffuser Failure Investigation, a research plan was formulated to develop an appropriate diffuser system model which, when combined with measured load quantities, would enable the determination of the exact causes of crack formation within the diffuser assembly. The first portion of this proposal will be submitted to the Research Initiation Program for a "Mini-Grant" award. Later proposals submitted by AEDC/Tenn Tech will then serve to complete the studies.

The basic recommendations outlined in the research plan for determination of and solution of the diffuser cracking problem are:

(1) Two-dimensional or frozen-stress photoelasticity should be employed for determination of the geometric stress concentration factors present in the panel coil design.

(2) The nondestructive, hole-drilling technique for residual stress determination is recommended for measurement of residual stresses existing in the fabricated panel coil sections.

(3) Using the experimentally-determined stress concentration factors and residual stress measurements, an improved finite element model can be constructed.

(4) Having constructed a complete finite element model, the acoustic, thermal, and pressure loadings must be determined experimentally and/or theoretically. Some data already exists for inputting thermal and pressure loads.

(5) Vibrational response of the diffuser to determine natural modes should be obtained both experimentally and from the finite element model.

(6) Combination of the finite element model and the experimental data will then allow determination of the stress states associated with crack formation. The appropriate design modifications can then be made to eliminate the cracking problem.

With regards to the Noninterference Stress Measurement System, the following recommendations are made:

(1) Further investigation of the techniques used for integral-order vibration measurement (4 sensor, SDOF, and the proposed "combined" technique) should be made using the NSMS hardware simulator. In particular, the effects of noise, DC offset, etc. should be noted and compared for these techniques.

(2) A detailed investigation of the proposed "combined" technique should be made including an error analysis and algorithm formulation.

REFERENCES

1. Private Communication with H.T. Jones, Sverdrup Technology, Inc., Arnold Engineering Development Center, Tullahoma, Tennessee, Summer 1988.

2. Chi, R.M. M.D. Page, L.G. Puffer, and J.H.T. Shu, "Further Study of NSMS Theory and Data Processing Algorithms," Report # R85-956905-R1, United Technologies Research Center, East Hartford, Connecticut, July, 1985.

3. Chi, R.M., et al. "Demonstration Testing of a Noninterference Stress Measurement System," Report # R87-957037-14F, United Technologies Research Center, East Hartford, Connecticut, July, 1987.

4. Shu, J. H. S.F. Labrecque, and R.M. chi, "Software Documentation for Demonstration Testing of a Noninterference Stress Measurement System," Report # R87-957037-15S, United Technologies Research Center, East Hartford, Connecticut, July, 1987.

1988 USAF-UES SUMMER FACULTY RESEARCH PROGRAM

Sponsored by the

AIR FORCE OFFICE OF SCIENTIFIC RESEARCH

Conducted by the

Universal Energy Systems, Inc

FINAL REPORT

Prepared by:	Manjit S. Jawa, Ph.D.
Academic Rank:	Professor
Department and University:	Mathematics Department Fayetteville State University Fayetteville NC 28303
Research Location:	Arnold Engineering Development Center Arnold AFB TN 37389
USAF Researcher:	Ron A. Belz, Ph.D.
Date:	6 August 1988
Contract No:	F49620-87-R-0004

SOLID ROCKET MOTOR PLUME ANALYSIS THROUGH EMISSION COMPUTERIZED TOMOGRAPHY

By

Manjit S. Jawa

ABSTRACT

ABEL Inversion Techniques are used to reconstruct the axial symmetric distribution of light emitting gases and particles in the plumes of solid rocket motors. The analysis of the plumes with asymmetrical distribution of the gases and particles is more complex. Emission computerized tomography will be further studied and researched to determine its effectiveness in reconstructing asymmetrical distributions.

ACKNOWLEDGEMENTS

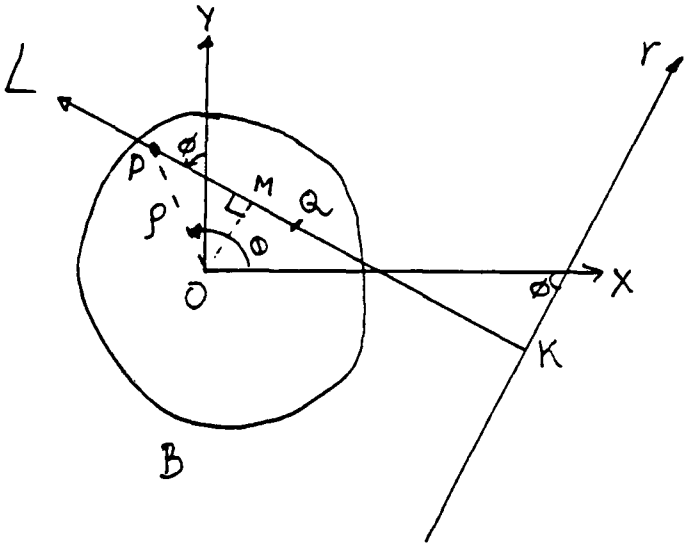
Historically, an important aspect of the Summer Research Faculty Program has been to help senior faculty members return to active scholarly research -- a long and ardous process. It required me to be associated with different researchers at Arnold Engineering Development Center to find a suitable research problem of mutual interest. Dr. Tim W. Swafford helped me in this symbiotic search. Initially I worked with Dr. Kyle G. Cooper and Dr. Dennis W. Lankford on the PARC 2D code for solving Navier-Stokes equation governing hypersonic chemically reacting flows. The objective was to strengthen the code. Subsequently, I worked with Mr Mike D. McClure and Mr. Jim R. Sirbaugh on Grid Generation Techniques in Computational Fluid Dynamics. Presently, I am working with Dr. Ron A. Belz on Solid Rocket Motor Plume Diagnosis through Computerized Emission Tomography. Ms. Rita Y. Walker also helped. I am thankful to each one of the aforementioned persons for their professional support in my research work.

I admire the seintillating support my Effort Focal Point, Mr. Marshall Kingery, gave me in my personal and professional activities. I am thankful to Universal Energy Systems, Inc for offering me the Summer Fellowship and to Air Force Office of Scientific Research for sponsoring this program and my research effort.

I. PROBLEM

Emission computerized tomography is mainly concerned with determination of an emission function, describing the distribution of emitting sources contained in an absorbing medium from a set of projections. The projections $p(r\phi)$ for single photon emission tomography (SPET) is defined by the integral equation

$$p(r,\phi) = \int_L f(\rho,\theta)\, e^{-\left[\int_{L(P)} \mu(\rho',\theta')\, dl'\right]}\, dl \qquad (1)$$



Where

B: is the body contour

OX,OY: are the axes of reference

P: any point (ρ,θ) on L

L: a line through P along which projection $p(r,\phi)$ is measured by the detector at K.

r : OM

ϕ : angle which line L makes with Y-axis

$f(r,\phi)$: emitting intensity at P

Q: any point (ρ',θ') on L(P)

$\mu(\rho',\theta')$: attenuation or absorption at Q

dl: an infinitesimal length at P along L

dl': an infinitesimal length at Q along L.

L(P): PK.

The related literature has been studied and researched in order to grasp and explain derivation and implications of (1) with regard to the problem under consideration - Solid Rocket Plume Analysis.

When the light emitting gases and particles in the plume are axially symmetric, (Figure 2) their distribution can be determined byABEL Inversion Techniques.

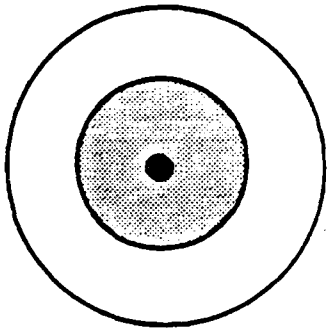


Figure 2

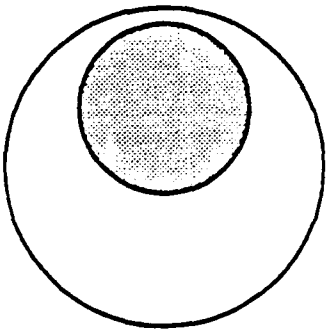


Figure 3

However, the analysis of more realistic phenomenon of asymmetrical distribution (Figure 3) is more difficult. The complexity is further compounded by the absorption of the containing medium.

II. CONCLUSION

I have studied and researched the problem in conjunction with my AEDC colleague, Dr. Ron A. Belz. C.T. reconstruction algorithms solves for $\mu(\rho,\theta)$ - the absorption coefficient using $p(\gamma,\phi) = \int_L \mu(\rho,\theta)\, dl$ (2) the standard format of the projection equation. Emission tomography must solve equation (1). The concern is under what consumption will equation (1) fall into equation (2) format? And how realistic are these assumptions?

The problem needs to be analyzed under assumptions such as zero absorption, uniform absorption, and variable absorption, with various forms of asymmetrical distribution of the light emitting gases and particles. Back-projection techniques,

possibly using the Donner Algorithms for Reconstruction Tomograpny produced by Lawrence Berkely Laboratory, University of California, Berkely seems promising. In order to carry out error analysis, phantom data will be generated using equation (1).

Presently, I am in the process of writing a Research Initiation Proposal to diagnose plumes from solid rocket motors under various synthetic and actual conditions.

1988 USAF-UES SUMMER FACULTY RESEARCH PROGRAM/
GRADUATE STUDENT RESEARCH PROGRAM

Sponsored by the

AIR FORCE OFFICE OF SCIENTIFIC RESEARCH

Conducted by the

Universal Energy Systems, Inc.

FINAL REPORT

Prepared by:	Ahmad D. Vakili
Academic Rank:	Associate Professor
Department and University:	Aerospace and University of Tennessee Space Institute
Research Location:	Arnold Engineering and Development Center Tullahoma, TN 37389
USAF Researcher:	Mr. W. T. Strike
Date:	September 15, 1988
Contract No.:	F49620-87-R-0004

SKIN FRICTION MEASUREMENT USING SURFACE MOUNTED HOT FILMS

by

A. D. Vakili

Abstract

Skin friction measurements using surface mounted hot film probes have been successfully made by many authors. In order to apply this measurement technique to high enthalpy high Mach number facilities, a probe capable of withstanding such test environments has been developed at AEDC by Mr. W. Strike and Mr. Joe Donaldson for prediction of skin friction forces on models in flow regimes noted. Measurement results, however, indicated significant levels of scatter among the data obtained as well as a lack of self-similar calibration behavior.

As a result of this summer's program, these discrepancies have been mainly explained and recommendations made to modify the probe and remedy the problem.

Acknowledgements

I wish to thank the Air Force Systems Command and the Air Force Office of Scientific Research for sponsorship of this research. Universal Energy Systems must be mentioned for their concern and help to Administrative aspects of this program.

Working at AEDC, during the Summer, was rewarding in many respects. I had a chance to become familiar with their operational procedure and friendships were made. I would like to thank all involved, especially the following. Mr. William T. Strike provided me with support, encouragement, an enjoyable working atmosphere, and stimulating discussions. Mr. Richard Matthews was helpful in being available for technical discussions. Mr. Joe Donaldson was helpful in giving technical details and discussions. I would like to thank Mr. A. Davenport for his helpful discussions on the arc heater.

Constant encouragement and support by Mr. Marshall Kingery who was the effort focal point was also of great significance to the success of this effort.

I. INTRODUCTION:

The importance of viscous effects in aerodynamics has motivated a large number of both theoretical and experimental investigation on boundary layer flows. Frictional forces introduced by viscous effects are of particular importance for high speed flows with heat transfer and in the presence of pressure gradients. In many cases, there are no prediction techniques, which are universally accepted, to calculate the skin friction drag under these conditions. Therefore, emphasis is placed on measurements. Considering that the skin friction drag is two to three orders of magnitude smaller than (any) other forces normally measured, direct and accurate measurement of skin friction is formidably difficult.

There are, however, indirect techniques to measure the skin friction. For example, indirect methods such as: boundary layer velocity profile, Preston tube, oil drop and surface hot film are commonly used. In practice, there are many difficulties associated with their application. Moreover, the indirect techniques are approximate approaches. There are, however, situations where approximate measurements would be of value, for example, at very high speeds and in regions of significant pressure gradient and heat transfer.

II. OBJECTIVES OF THE RESEARCH EFFORT:

A surface mounted hot-film probe had been previously developed for measuring skin friction on models in the high enthalpy and high Mach number facilities. Measurements results, however, indicated high levels of scatter in the data, as well as a lack of self-similar calibration. I was tasked to identify the source of discrepancies in calibration and the scatter in the measurements data.

I was also tasked to assist Mr. Andrew Davenport in preparation and analysis related to the Air Flow calibration facility tests of the Arc–Heater.

The fundamental reasons for discrepancies (in the calibration and measurements

by the hot-film) noted above, were identified. But new measurements could not be readily made until funding, facility and equipment were available.

III. TECHNICAL DISCUSSION:

The surface hot film techniques has been under development for the past thirty years. It has been successfully used by many authors (references) to make skin friction measurements. However, this technique is not routine or off-the-shelf and requires quite careful and complete care during calibration as well as measurements.

The principle for using hot film for skin friction measurements is based on, "Reynolds analogy", the analogy between momentum and heat transfer in the boundary layers. For Laminar incompressible flow at zero pressure gradient, Bellhouse showed that for a small heated wire Nusselt number is related to the wall shear in the following form $Nu \sim \left(\frac{\rho}{\mu}\tau_\omega\right)^{1/3}$. Later Liepman and Skinner assumed that thermal boundary layer due to the heated film was contained entirely within the laminar sublayer. Therefore, they extended the skin friction measurements, based on incompressible laminar flow, to the turbulent boundary layers. Further assumptions that the thermal boundary layer produced by the film is very close to the wall and therefore it is at the average wall properties and assuming constant local properties result in:

$$Nu = \left(\frac{q_\omega L}{k\Delta T}\right) \qquad \propto \qquad \left(\frac{\rho_\omega \tau_\omega}{\mu_\omega}\right)^{1/3} L^{2/3} \tag{2}$$

Heat balance for a heated film, flush mounted with the surface is:

Total Heat = Heat transferred to air + Heat transferred to substrate

$$i^2 R = q_{\text{wire-air}} + B$$

$$i^2 R = Nukw\Delta T + B$$

where:

$$\Delta T = T_w - T_{\text{air}}, w = \text{film width}$$

$$B = \text{heat transferred to substrate}$$

The substrate material has a major influence on the total heat transfer from the wire. Inaccurate accounting for the heat transferred to the substrate can result in a significant error in the shear stresses predicted in this manner. Watson's analysis indicated that a substrate temperature error of one degree Fahrenheit can result in a 27% error in the skin friction. Of course, the error depends on the substrate material as noted above.

There are two steps which must be followed to minimize or eliminate this problem. First, a substrate material must be used with very low thermal conductivity. Second, during calibration and measurements the substrate temperature must be accurately determined. The choice of substrate is limited from structural testing and manufacturing points. Measurements of substrate temperature can be accomplished by incorporating an additional thermocouple in the substrate at a proper location. A less accurate approach of determining the heat transfer to the substrate is to operate the film with no-flow at constant temperature during the calibration process. This, however, assumes that heat transfer from the film to the substrate is only a function of the temperature difference between the film and the substrate and is independent of the flow properties, which is not completely accurate. This process can be improved by measuring the no-flow heat transfer at several substrate temperatures and for several overheat ratios. A value corresponding to the measurement conditions can be identified using interpolation or extrapolation of the no-flow data, during calibration.

In reviewing the calibration data and the measurements results which were available, no-flow heat transfer data was only recorded for one overheat setting during the calibration. This data was used to find the no-flow Nusselt number, which agreed with the calibration results relatively well. Following this process, had the (no-flow) data been available, it would have led to a single calibration line (consistent with the literature) independent of overheat as it should be.

IV. CONCLUSIONS AND RECOMMENDATIONS:

A review was made of the constant temperature surface hot-film technique for the prediction of wall shear stresses. The calibration procedure was reviewed in order to determine why a shift in calibration curves had been observed for different overheat temperatures. The following conclusions are drawn:

1. The substrate material used for the effected probes must have a high thermal conductivity.
2. Heat transfer to the substrate is not accurately accounted for. (No–flow heat transfer from the probe should be recorded during calibration.)

In order to reduce and/or eliminate these problems, new probes must be made from materials with low thermal conductivity. It is also recommended that an additional thermocouple be incorporated in the substrate to identify the substrate heat transfer during test conditions. During calibration, the no-flow parameters must be recorded for proper identification of the heat transfer due to conduction.

REFERENCES

Bellhouse, B. J. and Schultz, D. L. "Determination of Mean and Dynamic Skin Friction, Separation and Transition in Low Speed Flow With a Thin Film Heated Element." J. F. M. Vol. 24, Pt 2., 1966, p. 379.

Brown, G. L., "Theory and Application of Heated Film for Skin Friction Measurement" Proc. 1967. Heat Transfer & Fluid Mech. Institute, Stanford Univ. Press. (1967).

Gadd, G. E. "A Note on the Theory of the Stanton Tube," Aeronautical Research Council R & M 3147, 1960.

Hayashi, M., Sakurai, A. and Aso, S., "A Study of a Multi-Layered Thin Film Heat Transfer Gauge and a New Method of Measuring Heat Transfer Rate with It," Trans. Japan Soc. Aero. Space Sci., Vol. 30, No. 88, Aug. 1987.

Hayashi, M. Sakurai, A. and Aso, S., "Measurements of Heat-Transfer Coefficients in the Interaction Regions Between Oblique Shock Waves and Turbulent Boundary Layers with a Multi-Layered Thin Film Heat Transfer Gauge," Trans. Japan Soc. Aero. Space Sci., Vol. 30, No. 88, Aug. 1987.

Menendez, A. N. and B. R. Ramaprian, "On the Measurement of Skin Friction In Unsteady Boundary Layers Using a Flush-Mounted Hot-Film Gauge," 1984, Iowa Institute of Hydraulic Research.

Watson, R. D., "Private Communications," at NASA Langley.

1988 USAF-UES SUMMER FACULTY RESEARCH PROGRAM/

GRADUATE STUDENT RESEARCH PROGRAM

Sponsored by the

AIR FORCE OFFICE OF SCIENTIFIC RESEARCH

Conducted by the

Universal Energy Systems, Inc.

FINAL REPORT

Study of Embedded Sensors in Graphite-Epoxy Composites

Prepared by:	Clarence A. Calder, Ph.D.
Academic Rank:	Associate Professor
Department and	Mechanical Engineering
University:	Oregon State University
Assisted by:	Gregory J. Price
	Undergraduate
	California Polytechnic
Research Location:	AFAL/VSSC Composite Structures Laboratory Edwards AFB, CA 93523
USAF Researcher:	James L. Koury

Date:	30 Sept 88
Contract No.:	F49620-87-R-0004

Study of Embedded Sensors in Graphite-Epoxy Composites

by

Clarence A. Calder

and

Gregory J. Price

ABSTRACT

The winding or layup fabrication process for composites lends itself to the development of "smart" structures which could sense load, vibration, or material degradation conditions using embedded sensors. Such embedded sensors would provide continuous information on the static and dynamic strain or displacement state of the structure (health monitoring) while being protected from the environment and severe surface conditions through the embedment.

In this study various strain and stress sensors were embedded in graphite-epoxy composite specimens to evaluate their potential for application in real structures. Conventional strain gages, strain wire, piezoelectric crystals, and the graphite tow itself were considered. Other possibilities such as various optical and acoustic techniques were beyond the scope of the project. The sensors were embedded in twelve-laminate panels which were cut into specimens suitable for cantilever loading and vibration tests.

While some difficulties were encountered with the delicate leads shorting out or breaking during the fabrication process, the strain gage, strain wire, and piezoelectric crystal all showed promise for use in "smart" structure applications. The graphite tow application presented several difficulties and was judged to require longer term development.

Acknowledgements

I would like to express gratitude to the Air Force Systems Command, the Air Force Office of Scientific Research, the Astronautics Lab, and Universal Energy Systems for sponsorship of this project. It has been a true opportunity to spend a delightful summer on an exciting and personally rewarding research study at the Astronautics Lab. The chance to associate with colleagues at AFAL, work in a modern composites structures lab, and be involved in research of current interest to the Air Force has been very beneficial and enlightening to me professionally.

I especially want to thank Mr. Jim Koury for his continued assistance and discussions regarding the project and future directions. My coauthor and fellow UES appointee, Greg Price, has been a joy to work with and one who learns quickly and is self-motivated. Dr. Frank Fair willingly provided much advice and direction, often in areas in which I have minimal training. MSgt Tim Carpenter assisted many times in the purchase of materials and location of needed instrumentation. Sgt Dave Lemley helped with the fabrication of panels and Jolaine Lamb provided kind and competent assistance with computerized literature surveys and obtaining copies of publications. I have appreciated the opportunity to become acquainted with other professionals in the Composites Lab, Lt. Doug DeHart, Dr. Peter Pollock, and Jim Wanchek, who have been supportive and always willing to help when needed.

The courteous assistance of Wayne Roe, Dick Clark and the staff at UES on matters pertaining to the administrative details of the appointment is gratefully acknowledged.

I. INTRODUCTION:

Engineered advanced composite materials are ideal for structural applications where high strength-to-weight and stiffness-to-weight ratios are especially advantageous as in the aircraft, spacecraft, and, more recently, automotive industries. The high specific stiffness translates into very high resonant frequencies for moving structures which minimizes vibration amplitudes and stresses, and consequently, the potential for fatigue damage. Very high interest in composite materials for the last thirty years has resulted in considerable research leading to a good understanding of the mechanics of fiber reinforced composites (1-4) as well as many experimental techniques which can be used to characterize the anisotropic behavior and provide material constants(5-11).

The winding or layup procedure for fiber reinforced composites lends itself to convenient installation of embedded sensors during fabrication. These permanently installed and protected sensors could be used during the service lifetime of the structure to monitor real time conditions and determine when loading or vibration is excessive, and when damage has occurred. Such instrumented "smart or intelligent" structures could use feedback circuitry for active vibration control in space applications requiring extreme stability and otherwise provide continuous "health monitoring" of the structure. Specifically, current program directives at AFAL deal with the development of smart structures to be used in space applications by incorporating embedded sensors, actuators, and microprocessors which can work interactively to provide active motion control.

In the present project conducted at the Air Force Astronautics Lab, current sensor technology was reviewed for potential application as embedded sensors in highly conductive graphite-epoxy fiber composites. In particular, conventional strain gages, constantan strain wire, piezoelectric crystals, and the graphite tow itself were considered.

Of these, the strain gages and piezoelectric crystals give localized measurements of stress or strain while the strain wire and graphite tow give an averaged strain measurement over the relatively long length of the sensor. Of these sensors, the piezoelectric transducer is limited to dynamic measurements due to its relatively short time constant. Associated with embedded sensor application, techniques for the electrical insulation of the sensor-lead wire package and means for convenient lead-wire exit and external electrical connection were evaluated. The technology was then adapted to embedment in composite beam specimens and tested statically and dynamically using a simple cantilever beam configuration.

My research interests have been in the general area of experimental stress analysis, transducer development, and associated instrumentation. Much of this work over the years has included the use of various type of strain gages and piezoelectric crystals as stress transducers. In fact, some of my research in the seventies dealt directly with embedded piezoelectric crystals as stress transducers in metals.(12,13) This background and research interest has fit nicely with my assigned project which I have especially enjoyed because it has given me the opportunity to apply this knowledge to modern advanced composites.

II. OBJECTIVES OF THE RESEARCH EFFORT:

The potential for future application of embedded sensors in "smart" structures depends on many factors among which include the parameter measured, its accuracy, reliability, durability, ease of installation, expected life, and influence by other variables. The primary objective of this study was to explore the feasibility of embedding various sensors in graphite-epoxy composites to provide continuous information on the stress-strain state and the condition of the composite during its service lifetime. My AFAL

research colleague, Mr. Jim Koury, and I decided to evaluate the feasibility of at least the following four transducers: conventional strain gages, constantan strain wire, piezoelectric crystals, and the graphite tow as a strain conductor.

This main objective was to be accomplished by the fabrication and testing of beam specimens with the various embedded transducers. These specimens would then be tested in simple cantilever bending with end loading in the static case, and in its first mode vibration in dynamic tests. The expected magnitude of strain and frequency of vibration could be determined analytically and compared with experimental results. With time permitting, additional tests in four point bending and tensile loading could be conducted on the specimens with a final test to fracture to evaluate degradation in stiffness and strength due to the embedded transducer and exiting leads.

Secondary objectives were to evaluate various means to electrically isolate the transducer package and associated lead wires from the conductive graphite tows, and to determine effective means to conveniently exit the leads from the tranducer lami ate. The latter should be done in a manner which would not severely hamper the winding process in order to have potential application in the real world.

III. EMBEDDED TRANSDUCERS CONSIDERED:

The basic characteristics including advantages and disadvantages for the embedded application will now be discussed for each sensor to be studied.

a. Conventional Foil Strain Gages - Strain gages are based on the principal that the resistance of an electrical conductor changes slightly when it elongates and shortens. This is represented by the fundamental relationship given by eq. 1,

$$\frac{\Delta R}{R} = F \epsilon \qquad (1)$$

where R is the gage resistance, ϵ is the normal strain, and F is the gage factor. Strain gages were invented in 1938 and have been developed into by far the most widely used means of strain measurement. Foil strain gages are extremely thin and can be packaged in rosettes which can determine strain in any direction at a point. They can be used to measure static or dynamic strains with extremely high frequency response. External signal conditioning, usually a form of a Wheatstone bridge, is required to provide a direct reading of strain magnitude and sign or a voltage output proportional to strain.

The technology is now firmly established with some information available for the application of embedded strain gages in purely research situations from Measurements Group, Inc.(7) They were used in a number of research studies in the early seventies (14-16) in boron and graphite-epoxy composites with reasonable success but installation and lead exit design was extremely inconvenient and fragile. Regardless, the strain gage is well established with some embedment experience and should be closely considered for "smart" structure applications. There are a number of sources of strain gages. Those used in this study were obtained from Measurements Group, P.O. Box 27777, Raleigh, NC 27611. Phone (919) 365-3800.

b. Long Wire Strain Sensor - Using the same principle as the conventional strain gage, an averaging type strain sensor can be fabricated from constantan wire and output measured with the usual strain indicators based on eq. 1. Constantan wire is available in very small diameters and with a tough polyimide coating for electrical insulation. Thus, it could be installed with the only connection needed at the exit surface of the composite. The wire could be conveniently positioned either parallel or perpendicular

with the fiber to provide an average strain measurement over the length of the conductor. The only reference found in the literature using this technique in an embedded mode was for very short (1/2") gage lengths (14) but the application was said to be successful. In the present study, an averaging gage over relatively long lengths would be of interest. Constantan strain wire with a thin polyimide insulation layer can be obtained from California Fine Wire Products, 338 S. fourth St., Grover City, CA 93433. Phone (805) 489-5144.

c. Long Strand Graphite Tow Sensor - As the graphite tow is electrically conductive (resistance about 17 χ/ft), it could conceivable be used as a strain sensor in the same manner as the long wire sensor. The appealing part is that the embedded sensor would be identical to the winding fiber and should not produce a degradation of the stiffness or strength. The possible use of a graphite fiber as a strain sensor in a nonconductive composite has been considered previously (4) but permanent changes in resistance was found after unloading. The highly brittle nature of the graphite filaments and the need to fully insulate the entire tow length used as a sensor tends to make this approach more of a long term development.

d. Piezoelectric Crystal Sensor - Piezoelectric crystals, natural and synthetic, have been used for years in transient measuring transducers such as accelerometers, seismometers, and ultrasonic transducers. Their use in transducers is described in elementary terms in Ref. 17 and 18 with more rigorous coverage in Ref. 19 and 20. The most commonly used piezoelectric materials are quartz and lead-zirconate-titanate (PZT), a ceramic. In the direct mode of operation, piezoelectric materials produce an electrical output when they are subjected to a stress/strain state. Thus, they are self-exciting and, in addition, are highly sensitive, simple to use, and can be made very thin (a few mils).

In a general state of stress, the voltage output of a piezoelectric crystal across the "i" crystal faces can be written in tensorial form as

$$V_i = K\, g_{ij}\, \sigma_j \qquad (2)$$

where i can take on 1,2 or 3 and summation over the j index is from 1 to 6, σ_j is the stress matrix, g_{ij} is the piezoelectric voltage coefficient, and K is a constant depending on crystal dimensions, the dielectric constant, and the total capacitance of the measuring circuit.

If the transducer is of the form of a thin rectangle aligned with the fibers (1-direction) and the stress is one-dimensional in the fiber direction, the voltage output across the faces (3 direction) would be given by

$$V_3 = K\, g_{31}\, \sigma_1 \qquad (3)$$

The writer has had previous experience with the embedment of quartz crystals for internal dynamic stress measurement in metals.(12,13) Recent work using large PZT ceramic crystals as actuators has been conducted but rather large degradation of the specimen was noted.(21) It should be noted that applications where low frequencies are encountered must have sufficient circuit capacitance to obtain low frequency response.(e.g. see Ref. 22)

For this study, quartz piezoelectric crystals were obtained from Valpey-Fisher Corp, 75 South St., Hopkinton MA 01748 (phone (508) 435-6831) and PZT ceramic crystals from Vernitron Piezoelectric Div., 232 Forbes Rd, Bedford, OH 44146 (ph. (216) 232-8600).

IV. TEST SPECIMEN FABRICATION

Embedded sensors were first studied in an epoxy molded beam to be able to check out functional operation without the difficulties associated with electrically isolating the transducers and lead wires, and installing them in a winding or layup fabrication. Then various means were used to electrically insulate the sensor-lead wire packages which were then installed into graphite-epoxy panels during the winding process.

Epoxy Beam - A beam mold was first fabricated from an aluminum plate with dimensions of 13" long by 1" wide by 0.5" thick. Sensors prepared for embedment were a 1/8" diam. by 0.008" thick quartz crystal, a 1/2" diam. by 0.017" thick PZT crystal, a strain gage two-element rosette (WA-06-120WT-120, GF 2.07) and a grid formed from 35 AWG constantan strain wire to give approximately 60 ohms of resistance. A release agent was sprayed on the mold surface and the sensors put in position as a 55A Ceibaggeigy epoxy resin was poured into the mold. The two crystals and rosette were located about 0.1" from the top and the strain wire grid about 0.10" from the bottom of the beam as schematically shown in Fig. 1.

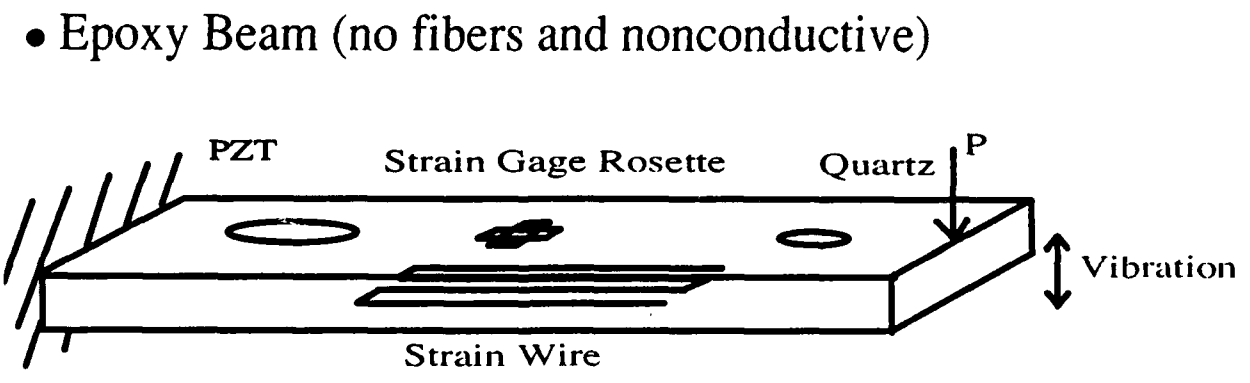


Fig. 1. Epoxy beam embedded sensor arrangement

Graphite-Epoxy Panels - Two graphite-epoxy panels were fabricated with embedded sensors using a model T-36-42 EN-TEC, Inc. tumble winder and a 14" square mandrel. They were wound with Fiberite prepreg roving, compound FX-13M37A for the first panel and FX-13F76 for the second. Each roving consisted of AS4 fiber and 976 resin with fiber content about 62%. Tabulated properties include a flexural modulus of 19.5 msi and specific gravity of 1.57. Prepreg roving was obtained from Fiberite Corp., 501 West 3rd St., Winona, MN 55987, Phone (507) 454-3611.

Each panel was 12 laminates thick with sensors embedded between the 9th and 10th laminate and positioned approximately at the center of the 14" length and spaced about 1.1" apart. This layout resulted in beams cut to be about 1.1" by 14". The panels were cured in a large autoclave evacuated to -26 in. Hg. Temperature and pressure were programmed to provide two-hour cure at 350 deg. F. and 85 psig using one hour to reach cure conditions and one hour to return to the ambiant state. The off-axis location, Fig. 2, was chosen so beams could be tested in bending or tension/compression.

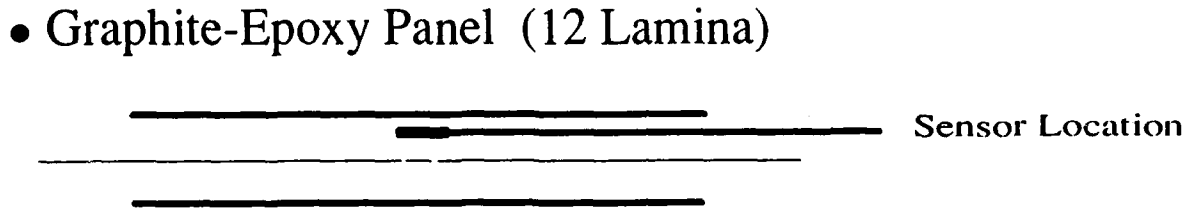


Fig. 2. 12-laminate Graphite-epoxy panel with off-axis sensor

The first panel contained embedded 1/8" and 1/2" piezoelectric crystals as in the epoxy beam, single strain gages of type CEA-03-250UN-350 and rectangular rosettes of type WA-06-250WT-350, 20" loops of constantan strain wire, and 20" loops of graphite tows. A total of fourteen embedded sensor beams resulted. Various means of insulating the sensors and leads included acryllic laquer spray, teflon tape, two types of epoxy adhesive

brushed on, and an RTV coating. All lead wires were tediously exited by feeding them through each wind, either near the mid panel or at one end.

Major changes in the second panel included use of 35 AWG lead wire with polyimide insulation, installation of much smaller (0.25" by 0.20" by 0.007") PZT crystals, cutting the corner fibers down each side to prevent post-cure curvature, and new attempts to provide durable and convenient lead wire exit by protecting the lead inside "staked" hypodermic needles. These were then removed and the leads attached to surface bonded terminals before the cure. Sixteen sensors were embedded in this panel. A lead stake is schematically shown in Fig. 3.

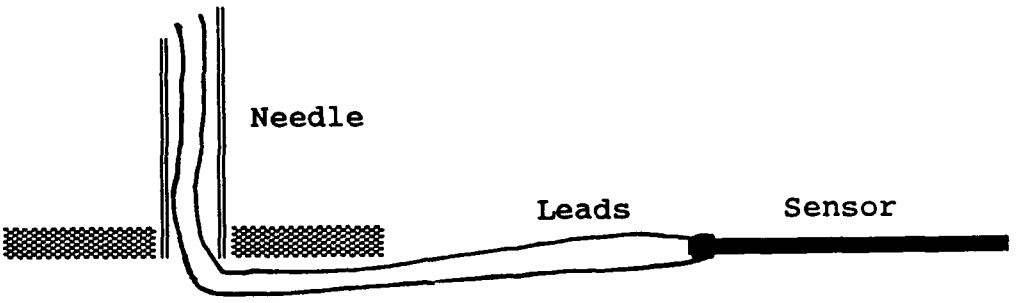


Fig. 3. Lead exit stake using hypodermic needle.

V. EMBEDDED SENSOR TEST RESULTS AND DISCUSSION

All sensors embedded in the non-conductive epoxy beam, two piezoelectric crystals, a rectangular rosette strain gage, and a strain wire grid, were found to be functional when tested as a cantilever beam with end loading and when excited in first mode vibration. End loading with a dial indicator for displacement was used to experimentally determine the EI value for the epoxy beam as 2925 lb-in^2. This resulted in an E for the epoxy of about 408 ksi which was reasonable.

From elementary beam theory, the strain at an interior point y units from the neutral

axis is given by eq. 4,

$$\epsilon = \frac{M y}{I E} \tag{4}$$

where M is the moment at the cross-section of the sensor location, I is the area moment of inertia, and E the Young's modulus. The first mode vibration frequency, f, of a cantilever beam of length L is given by

$$f = \frac{a}{2\pi}\left(\frac{1.875}{L}\right)^2 \quad \text{where } a = \sqrt{\frac{E I}{\rho A}} \tag{5}$$

where ρ is mass density and A is cross sectional area.

Conventional strain gage instrumentation was used for the rosette and strain wire gages. This included a Measurement Group digital strain indicator model P-3500 with an SB-10 switch and balance unit and a V/E 40 strain gage simulator for balancing a half-bridge circuit for the strain wire. Experimental measurements were found to be within 10% of theory for the two strain gages, and within about 22% for the strain wire assuming output will be an average over the wire length. This was recorded over a range of loads from 0.22 lb to 2.2 lb. Frequency measurements using a memory oscilloscope gave a frequency of about 28 Hz while eq. 5 for this beam predicts 29.5 Hz. Initial test with the crystals showed a phase lag with the strain gages but this low frequency response was corrected by the addition of 0.1 μF capacitance in parallel to the circuit.

At the time of fabrication of the first panel, no small diameter (a few mils) wire with enamel insulation was available so various attempts were tried to conveniently electrically insulate the lead wire and transducer package from the conductive tows. Of the 14 embedded sensors, only six were usable. The remainder either shorted out to the the companion lead or the graphite panel, or the lead broke at the surface or a lead

discontinuity occurred internal during the cure cycle. Of the usable gages, some had quite low resistance to the panel. Three embedded tows were attempted but none survived due to the very brittle nature of the exiting leads and to the difficulty in insulating the tow from the tows making up the composite. Also, considerable curvature, about 0.5 in. over a span of about 14 in. resulted from not cutting the tows at each end of the panel.

Beam test specimens were cut from the panel resulting in beams about 0.12" thick, 1.2" wide, and 14" long. Six specimens had no sensor and were to be used as a control to check material degradation caused by the embedded sensor. Operable sensors included a single strain gage, a rectangular rosette, two strain wire sensors, and two piezoelectric crystals. The beams were cantilevered (curvature up) by clamping to a semi-rigid surface and subjected to end loading and first-mode vibration. Tabulated results for the 2.20 lb end loading and vibration frequency are shown in Table 1 with comparison to theoretical values obtained from eqs. 4 and 5.

Table 1. Embedded sensor test results for end loading and vibration.

Specimen	Sensor	Exp. μStrain	Theor. μStrain	Exp. Freq., Hz	Theor. Freq., Hz
2-1	SG, single 0°	-121	-142	43.0	45.8
3-2	SGR, 0°	-90	-113	41.0	47.2
4-1	Strain wire	-135	-134	49.0	51.9
6-1	Strain Wire	-100	-99	47.5	49.4
5-2	PZT 1/2"	N.A.	N.A.	42.5	47.8
6-2	Quartz, 1/8"	N.A.	N.A.	41.5	46.4

The effect of low resistance for the strain wire, about 20 ohms, was corrected for in the calculations where a "dead" resistance of about 40 ohms was added in series to get the resistance to a level where the strain indicator would be operational. Results agree reasonable well with theory. The low experimental value for the piezoelectric sensors was probably due to the low lead resistance found after cure. This resulted in a low value of RC which could affect the low frequency response of the sensor (22). Cantilever beam deflection over four loads was used to evaluate the Young's modulus as 19.2 msi which was in good agreement to the predicted value by the program GENLAM (2). A Rockland frequency analyzer was used to get accurate natural frequency measurements. In some cases 60 Hz noise pickup was high but the analyzer allowed easy interpretation.

The second graphite-epoxy panel, completed near the end of the project, resolved some of the problems with the first panel. Of the 16 embedded sensors, 13 were at least partially operational. Several had resistances to ground which were lower than desirable. The enameled lead wire seemed to work well. The lead exit design with the "staked" hypodermic needles for protection with bonded and soldered terminals resulted in much easier winding of the panel and a much cleaner surface for preparation for cure. The tows were cut at the edges of the panel before cure which resulted in very straight specimens. After curing, the two panels were cut into specimens using the milling machine with final dimensions about 0.10" thick, 1.0" wide, and 14" long with no noticeable curvature. Four specimens without sensors were also obtained. Young's modulus was calculated from specimen 1-3 in cantilever deflection as before and found to be about 20.2 msi. Strain gage rosette data for this specimen gave Poisson's ratio to be 0.27. Tabulated results for two specimens with strain gage rosettes are given in Table 2 for 2.20 lb (1000 g) loading.

Table 2. Embedded sensor test results for end loading and vibration, panel 2.

Specimen	Sensor	Exp. μStrain	Theor. μStrain	Exp. Freq., Hz	Theor. Freq., Hz
2-1	SGR, 0°	180	181	42.1	44.7
1-3	SGR, 0°	192	206	41.7	45.7

While the approach here has been one of feasibility rather than accuracy, the results are reasonable and within limits expected. Further tests on these specimens will be conducted as a student project at Oregon State University.

VI. RECOMMENDATIONS

In this feasibility study, conventional foil strain gage rosettes and constantan strain wire were shown to be promising candidates for sensor embedment in graphite-epoxy smart structures for purposes of "health" monitoring and providing static and dynamic stress/strain information throughout the life of the structure. The strain gage gives a "point" measurement whereas the strain wire gives an average strain throughout its length. Both can be configured in minimum thickness - a few mils or less. In a manner similar to the strain wire, the graphite tow was considered as a strain sensor but found to be very fragile and difficult to electrically insulate from the tows in the composite.

Embedded piezoelectric crystals were shown to provide reliable dynamic/vibratory data at a point in the laminate with the advantage of being highly sensitive and requiring minimal circuitry. These crystals are generally sensitive to stress in all directions and can also be used as actuators although they have to be quite large for this purpose. An

interesting dual role is possible: first as a sensor only and second as an ultrasonic transducer for probing through the skin thickness.

For sensor distribution throughout a structure, the strain wire is appealing due to a minimum of electrical connections and exits from the structure. Strain gages and piezoelectric crystals would require a pair of leads from each sensor unless some means were devised for series or parallel embedded connections.

Applications in real structures will require embedded sensor techniques which do not require excessive installation effort and time during the winding process, and which do not significantly degrade the composite properties from a strength, stiffness, and fatigue strength point of view. The "staked" needle approach for lead exit and subsequent connection to bonded surface terminals was found to be highly promising but requires further development.

Future efforts should be directed at continued development of the strain gage, strain wire, and piezoelectric sensor with more emphasis on sensor accuracy, more development of lead wire exit techniques, improved insulation of embedded gage and leads from the graphite epoxy, and studies on the degradation of the composite specimens due to the embedded sensors. This should initially be done with the simplest of composites and specimen configurations - i.e. 0° laminate with tensile, compression, and four-point bending tests. This work would then be followed by similar studies with more complicated layups including non-flat surfaces such as tubular specimens, and more complicated loadings - biaxial, pressure, and torsion.

Each sensor should be developed to emphasize its particular advantages. The strain gage as a very accurate, extremely thin sensor for point measurements at relatively low cost.

Its inherent flexibility is well suited to non-flat surfaces and it has low sensitivity to strain perpendicular to the sensing direction. The strain wire should be developed to provide an average measurement over a long distance with a minimum of lead exits required. It should be very insensitive to strains perpendicular to the wire direction and should give an accurate reading of the average strain with a minimum of degradation to the structure. Piezoelectric crystals need to be developed for their sensitivity and potential to be used in an ultrasonics sense to detect delaminations and general material degradation through the thickness. Generally these crystals are sensitive to stresses in all directions so their output may not clearly delineate the true stress state. They are necessarily thicker than the strain gage and strain wire so may cause greater degradation in properties.

The embedded graphite tow approach is appealing in that the sensor is not a dramatically different material so reduction in composite properties should be minimal. However, the difficulty in effectively insulating the tow from the remainder of the composite along with the very brittle nature of the graphite filaments themselves would require a longer term development than the sensors previously mentioned.

A key to effective application of embedded sensors in composite structures is the development of techniques for the convenient embedding of the sensor package and lead exits without severely hampering the production process. The staked needle approach developed here shows promise and should be further developed.

REFERENCES

1. Ashton, J. E., et. al., Primer on Composite Materials:Analysis, Technomic, Westport, CT, 1969.

2. Tsai, S. W., Composite Design, Think Composites, Inc., Dayton, Ohio, 1987.

3. Delmonte, J., Technology of Carbon and Graphite Fiber Composites, Van Nostrand and Reinhold, 1981.

4. Lees, J. K., "Advanced Composites are Earning Their Wings", Mechanical Engineering, April 1988, pp. 50-53

5. Whitney, J. M., et. al., Experimental Mechanics of Fiber-Reinforced Composite Materials, Soc. for Experimental Mechanics, Prentice Hall, 1984.

6. Kobayashi, A. S. (ed.), Handbook on Experimental Mechanics, Prentice Hall, 1987.

   Ch. 2. Dally, J. W. and W. F. Riley, "Strain Gages."

   Ch. 3. McConnell, K. G. and W. F. Riley, "Strain Gage Instrumentation and Data Analysis."

   Ch. 19. Daniel, I.M., "Composite Materials."

7. Measurements Group, Inc., Strain Gage Applications on Composites, Part 3: Interlaminar Gaging of Composites, Application Note, 1988.

8. Halpin, J. C., et. al., "Characteristics of Anisotropic Composite Materials," Composite Materials: Testing and Design, ASTM STP 460, 1969, pp. 37-47.

9. Hoggett, J. T., "Test Methods for High-Modulus Carbon Yarn and Composites," Composite Materials: Testing and Design, ASTM STP 460, 1969.

10. Douglas, F. C., "Material Testing for Research: Challenge to the Imagination," TEST, Aug/Sept 1988, pp. 12-14.

11. Lucas, G. F., "Testing Advanced Materials", TEST, Aug-Sept 1988, pp.8-10.

12. Calder, C. A. and R. G. Dragnich, "Internal Dynamic Stress Measurement with an Embedded Quartz Crystal Transducer," Rev. Sci. Instrum., Vol. 43, No. 6, June 1972, pp. 883-886.

13. Dragnich, R. G. and C. A. Calder, "A Sandwich-Transducer Technique for Measurement of Internal Dynamic Stress," Exp. Mechanics, Vol. 13, No. 5, May 1973, pp. 199-203.

14. Egger, R. L., "Strain Gage Technology for Internal Strain Measurement In Boron-Epoxy Composites," AFFDL-TR-72-151, Boeing Aerospace, April 1973.

15. Daniels, I.M., et. al., "The Embedded Strain Gage Technique for Testing Boron/Epoxy Composites," Composite Materials: Testing and Design, ASTM STP 497, 1972, pp 257-272.

16. Akimany, F. J., et. al, "Development of Technology for Determination of Relationship Between Surface and Subsurface Strains in Boron-Epoxy Composites," AFFDL-TR-69-86, Aug 1970.

17. Valpey-Fisher Corp., "An Introduction to Piezoelectric Transducers", 1967.

18. Vernitron Piezoelectric Division, "Modern Piezoelectric Ceramics," Bedford, Ohio.

19. Cady, W. G., Piezoelectricity, Dover Pub., Inc., 1964.

20. Nye, J. F., Physical Properties of Crystals, Oxford University Press, 1957.

21. Crawley, E. F. and J. de Luis, "Use of Piezoelectric Actuators as Elements of Intelligent Structures," AIAA J., Vol. 25, No. 10, 1987, pp. 1373-1385.

22. Gurtin, M. E., "The Effect of Accelerometer Low-Frequency Response on Transient Measurements," Experimental Mechanics, Vol. 1, No. 6, 1961, pp. 206-208.

1988 USAF-UES SUMMER FACULTY RESEARCH PROGRAM/

GRADUATE STUDENT RESEARCH PROGRAM

Sponsored by the

AIR FORCE OFFICE OF SCIENTIFIC RESEARCH

Conducted by the

Universal Energy Systems, Inc

FINAL REPORT

CORE POLARIZATION IN LITHIUM AND ALUMINUM

Prepared by: Phillip A. Christiansen

Academic Rank: Associate Professor

Department and University: Chemistry Department, Clarkson University

Research Location: AFAL/LSX, Edwards AFB, CA 93523-5000

USAF researcher: Dr. Stephen L. Rodgers

Date: 14 Sept. 1988

Contract No. F49620-87-R-0004

CORE POLARIZATION IN LITHIUM AND ALUMINUM

by

Phillip A. Christiansen

ABSTRACT

Core-valence correlation potentials were computed for Li and Al using two and ten-electron core wavefunctions respectively. The potentials included dipole, quadrapole and higher order corrections within the constraints of the respective (s p d) and (s p d f) basis sets. With core polarization included, relativistic quantum Monte Carlo simulations were used to compute the first three Al ionization potentials which were found to be within 0.03 eV of experimental values. Modifications to include core polarization corrections in the MESA electronic structure codes used at AFAL were begun.

ACKNOWLEDGEMENTS

The support of this work by the Air Force Systems Command, the Air Force Office of Scientific Research, the Air Force Astronautics Laboratory and Universal Energy Systems is gratefully appreciated. I also wish to thank the members of the ARIES group at AFAL, especially Drs. D. D. Konowalow, S. L. Rodgers, M. E. Rosenkrantz and Capt. W. Lauderdale for many useful comments and technical support. The assistance of Dr. Rosenkrantz was particularly critical to this work.

I. INTRODUCTION:

It has been noted within the ARIES group at the Air Force Astronautics Laboratory that there are potential advantages in the use of lighter metals (Li, Be, Al, etc.) as reducing agents in conjunction with liquid hydrogen-oxygen rocket fuels. However to be practical the metals must be stabilized in atomic (or at most very small cluster) form. It has been speculated[1] that the large dipole polarizabilities of some of these metals might make it possible to form at least marginally stable van der Waals complexes involving single metal atoms (or perhaps diatomic molecules) surrounded by H_2 molecules. Liquid hydrogen temperatures would presumably make it possible to keep such complexes intact for sufficiently long time spans for it to be practical.

Relatively little is known about van der Waals complexes in general and almost nothing about these in particular. Only in the last few months have computational electronic structure studies been initiated to determine the stability of various $Li-H_2$ complexes. Due to the rather small magnitudes of the expected binding energies it is imperative that such studies be as precise as possible. Unfortunately the accuracy of alkali and alkaline-earth electronic structure predictions is greatly complicated by the large

core polarizabilities which can cause substantial core-valence correlation errors.[2] Furthermore such complications may not be limited to the left most columns of the periodic table. In recent relativistic effective potential quantum Monte Carlo (REP-QMC) simulations we noted a 0.1 eV error in the Al ionization potential. Although the error could be due to an inadequate trial wavefunction used in the simulation, considering the large core-valence correlation corrections in Mg, neglect of core polarization might also be a culprit.

If accurate predictions of van der Waals complex stabilities are to be made, whether for the alkalis, the alkali-earths or aluminum, the problem of core-valence correlation will have to be resolved. The most economical approach to the problem would probably involve algorithms such as those developed by Meyer and co-workers[2] and also by ourselves.[3]

II. OBJECTIVES OF THE RESEARCH EFFORT:

In REP-QMC calculations the local potential used in the QMC simulations is to some extent a function of the trial wavefunction employed.[4] The trial wavefunction is typically obtained from a conventional SCF (or SCF with small CI) calculation. The s and p potentials in the Al REP are quite repulsive whereas the d and higher potentials are

attractive. As a result it may be important to include "d" excitations in the Al ground state trial wavefunction for the QMC simulation to yield accurate energy values. One objective of this work has been to carryout accurate REP-QMC simulations for the Al ground state and positive ion. This required the generation of an appropriate spd basis set as well as small CI wavefunctions for both states. It was also necessary to adapt QMC simulation programs developed at Clarkson University to run on the AFWL Cray 2 supercomputer.

Regardless of whether core polarization shifts the Al ground state, there exists a 0.3 to 0.4 eV error in Al^{+2} REP calculations which is almost certainly due to neglect of core-valence correlation. A second goal of this work has been to determine the Al core polarizability and to generate a core polarization potential and effective field operator using the method described in reference 3.

Finally, to facilitate Li-H_2 studies in progress at AFAL it was imperative that polarization potentials and fields also be computed for Li. In addition it was also essential to modify the MESA electronic structure codes at AFAL to make full use of core polarization information.

III. ALUMINUM CORE POLARIZATION:

Recomputing the Al ionization potential using REPs[5] and a trial wavefunction for the ground state that included the important "d" configurations gave a value of 5.93(2) eV as compared to the experimental value of 5.99 eV. This discrepancy is of about the magnitude one would expect from the expansion used to fit the REP. We therefore refit the REP using a slightly larger expansion (see Table I.) and repeated the QMC simulations. The resulting ionization energy was 5.98(3) eV.

Although there are apparently no differential core polarization corrections between the Al ground state and ion, there is unqestionably a significant correction in the third ionization potential if not in the second. We therefore went ahead with the generation of the Al core polarization potential using the method described in reference 3. We assumed that the polarization was due primarily to the 2s and 2p filled shells and generated an REP based on Al^{+3} ion Dirac-Fock wavefunctions which included only the 1s shell in the core. The polarization potential was computed from SCF energies for the Al^{+3} ion in the presence of a negative point charge positioned a distance r from the nucleus. The point charge of course polarizes the normally spherical wavefunction and the difference between

the polarized and unpolarized energies gives a good approximation to an electron-ion scattering potential (at least for large values of r). The potential will include dipole, quadrapole and higher order corrections if the basis set allows. For small r the potential must be corrected for adiabatic effects. This was accomplished in a manner analogous to reference 3, by multiplying the potential by a cutoff function, C(r), defined as the square of the fraction of the 2s and 2p electron density inside the radius, r.

The above potential was then used in conjunction with the REP of Table I to compute the third ionization potential for aluminum. The resulting value was 28.49 as compared to the experimental value of 28.45 eV. Furthermore, by scaling r in the cutoff function by a factor of 0.82 ($r'=0.82r$) we reproduce the experimental ionization energy to five significant figures. The resulting polarization potential and corresponding effective field operator (as defined in references 1 and 2) are listed as gaussian expansions in Table II.

The REP of Table I and the polarization potential of Table II were then used in REP-QMC simulations to determine the Al ground state and Al^+ ion energies. These are listed in Table III along with the Al^{+2} values. With core polarization in REP-QMC simulations one can reproduce the first three

Table I. Aluminum three valence-electron relativistic effective potential including spin-orbit corrections.

	N	Expn.	Coef.	S.O.
s-d	2	1.089000	31.906618	
	2	1.233300	-97.472571	
	2	1.521900	149.016139	
	2	1.838800	-82.200975	
	1	2.397500	3.252523	
	0	1.935000	3.108370	
p-d	2	1.266800	-45.155702	0.008698
	2	1.445100	138.265253	0.034283
	2	1.805700	-178.155051	-0.037334
	2	2.229400	102.256751	0.002107
	1	6.139300	2.353166	0.002376
	0	5.455800	5.086351	-0.000032
d	2	1.337100	-0.741711	-0.000989
	2	3.799200	-6.666957	-0.003548
	2	11.329000	-18.373723	0.055210
	2	41.639900	-43.599284	-0.182633
	1	147.699700	-7.988923	0.287603

Table II. Aluminum core polarization potential and effective field operator both scaled using $r'=0.82r$. The computed core polarizability was 0.254 au.

Core Polarization Potential

N	Expn.	Coef.
0	0.005700	-0.002048
0	0.043000	-0.008804
0	0.178000	-0.033590
0	0.613900	-0.122936
0	3.182200	1.322514
0	4.808700	-24.633084
0	4.870000	23.478060

Effective Field Operator

N	Expn.	Coef.
2	0.004600	0.012316
2	0.028800	0.039264
2	0.092100	0.098090
2	0.242300	0.232045
2	0.503300	0.348912
2	0.951700	0.802436
2	2.950800	-1.837657

Table III. Comparison of computed aluminum ionization potentials (with and without core polarization) with experimental values. All energies are in eV. The numbers in square brackets include a 0.01 eV correction for spin-orbit coupling.

Species	IP	Method
Al^{++}		
	28.45	Expt.
	28.06	REP
	28.49	REP, V_{cpp} (no scaling)
	28.45	REP, V_{cpp}
Al^{+}		
	18.82	Expt.
	18.67(1)	REP-QMC
	18.81(1)	REP-QMC, V_{cpp}
Al		
	5.99	Expt.
	5.98(3)	REP-QMC
	[5.99(3)]	
	5.95(2)	REP-QMC, V_{cpp}
	[5.96(2)]	

ionization energies of aluminum to within 0.03 eV. This accuracy would be essentially impossible with more conventional electronic structure formulations.

IV. CORE POLARIZATION IN LITHIUM:

The lithium core includes only the 1s electrons and the core polarization potential was therefore computed using all-electron wavefunctions rather than with REPs. As with aluminum the cutoff function was again scaled, but using a value of 0.5. The lithium polarization potential and effective field operator are listed in Table IV. Using the potential in Table IV along with the Li REP from reference 5 and an energy optimized basis set we were able to reproduce the Li ionization potential to within four significant figures.

V. RECOMMENDATIONS:

Core polarization potentials of the type listed in Tables II and IV can be readily included in conventional electronic structure codes by simply adding the expansion to the residual (highest angular momentum) potential in a standard shape-consistent effective potential. However in order to include the criti al core-other-core or electron-other-core corrections, modifications to the code must be made.

Table IV. Lithium core polarization potential and effective field operator both scaled using $r'=0.5r$.

Core Polarization Potential

N	Expn.	Coef.
0	0.0072	-0.001920
0	0.0592	-0.009676
0	2.5296	-0.039715
0	11.4534	0.000094
0	4.7934	-0.004525
0	1.3799	0.083685
0	0.2485	-0.028873

Effective Field Operator

N	Expn.	Coef.
2	0.003000	-0.033771
2	0.026000	0.051340
2	0.002300	0.038903
2	0.116000	0.140688
2	0.295600	0.170258
2	0.471000	0.234780
2	2.366300	-0.516449

Modifications to the MESA code used at the Air Force Astronautics Laboratory have already been made to include the above two corrections in an approximate form. However these approximations have only limited applicability. It is therefore important that modifications to the codes be made to allow the computation of the effective field integrals necessary to reliably include the electron-other-core corrections. Furthermore, once these integrals have been computed, two-electron corrections can also be included.

Core polarization corrections must be included in electronic structure studies involving the alkali, alkaline-earth and similar elements if accurate predictions are to be made. With the modifications discussed above the Air Force Astronautics Laboratory would have access to one of the most advanced computer packages available for the study of molecules containing these elements.

In exploratory studies involving light-metal-H_2 van der Waals complexes, lithium is an obvious candidate due to its very large dipole polarizability. However because of its free radical nature, Li-H_2 complexes might be relatively unstable with regard to the formation of larger metallic clusters. This might also be true of related Al, B, etc. complexes. Unfortunately the metal-metal binding energies are sufficiently large that the energy required to break the

clusters during combustion might cancel out any advantage the van der Waals complexes would have in a rocket fuel. For this reason it might also be important to carry out studies involving hydrogen complexes of Be or Mg. The Mg polarizability is of roughly the same magnitude as that of Li. Be has obvious health risks but this might not be a serious constraint for propulsion systems operating outside the earths atmosphere. As with Li, the inclusion of core polarization corrections would be absolutely essential to make accurate predictions. Polarization potentials and effective field operators should probably be computed for all the Group IA, IIA and lighter Group IIIA elements.

Finally, the REP-QMC formalism employed in the Al calculations of Section III provides one of the most accurate methods for making molecular predictions for systems in which the electron pairing is radically varying. At the present time however there are no general computing packages available for molecular structure predictions using QMC with REPs, core polarization corrections, multiconfiguration trial wavefunctions, etc. The development of such a program package would compliment the MESA package currently in use and greatly enhance the Astronautics Laboratory's efforts.

REFERENCES

1. Konowalow, D.D., private communication.

2. Muller, W., Flesch, J., Meyer, W., "Treatment of intershell correlation effects in ab initio calculations by use of core polarization potentials. Method and application to alkali and alkaline earth atoms", J. Chem. Phys. 1984, 80, 3297.

3. Christiansen, P.A., "Core-valence correlation in relativistic effective potentials", Chem. Phys. Lett. 1986, 127, 50.

4. Christiansen, P.A., "Effective potentials and multiconfiguration wavefunctions in quantum Monte Carlo calculations", J. Chem. Phys. 1988, 88, 4867.

5. Pacios, L.F., Christiansen, P.A., "Ab initio relativistic effective potentials with spin-orbit operators. I. Li through Ar", J. Chem. Phys. 1985, 82, 2664.

1988 USAF-UES SUMMER FACULTY RESEARCH PROGRAM/

GRADUATE STUDENT RESEARCH PROGRAM

Sponsored by the

AIR FORCE OFFICE OF SCIENTIFIC RESEARCH

Conducted by the

Universal Energy Systems, Inc.

FINAL REPORT

THE PHOTOCHEMISTRY OF μ_3-(η-DIETHYLACETYLENE)-DECACARBONYLTRIOSMIUM IN SOLID ARGON

Prepared by:	Susan Collins and William Moran
Academic Rank:	Assistant Professor and Master's Degree Candidate
Department and University:	Department of Chemistry California State University, Northridge Northridge, California 91330
Research Location:	Air Force Astronautics Laboratory Astronautical Sciences Division Applied Research in Energy Storage Office High Energy Density Matter Group
USAF Researcher:	Steve Rodgers/Pat Carrick
Date:	August 17, 1988
Contract No:	F49620-88-R-0004 and F49620-88-C-0053

THE PHOTOCHEMISTRY OF μ_3-(η-DIETHYLACETYLENE)-DECACARBONYLTRIOSMIUM IN SOLID ARGON

by

Susan Collins and Will Moran

ABSTRACT

The photochemistry of μ_3-(η-diethylacetylene)-decacarbonyl-triosmium (compound I) was studied by FTIR at 10K in argon matrices. Upon irradiation at 470 nm, compound I readily converted to a nonacarbonyl intermediate (compound II), accompanied by the elimination of carbon monoxide. The isomer of compound II, (compound III), is obtained at higher temperatures (>300 K) (1). This isomer is obtained when the methylene-hydrogen migrates along the molecule to form an Os-H-Os hydride bond. Compound III was not produced upon warming to 50 K. However, a 10 K matrix of this was prepared from a stable, room temperature sample. Compound III was found to form a new photoproduct (compound IV) at 10 K which has a spectrum similar to compound I. The photochromic properties and IR spectra of compounds I, II, and III are discussed. A structure for compound IV is postulated.

ACKNOWLEDGMENTS

We would like to acknowledge the sponsorship of our work this summer by the Air Force Systems Command, the Air Force Office of Scientific Research and the Air Force Astronautics Laboratory. We also would like to acknowledge several individuals: Wayne Roe, Director of UES/AFAL relations, Steve Rodgers, Chief of AFAL/LSX division whose cheerfulness, relaxed manner and love of science provides an excellent atmosphere for research, Captain Walter Lauderdale, who introduced us to the Air Force Programs, Pat Carrick who taught us much about his new equipment and tolerated our use of it for ten weeks, Jodye Selco, and Dan Konowalow, for their helpful discussions.

We also would like to acknowledge persons from California State University, Northridge: Prof. Ed Rosenberg, whose ten years of work on osmium cluster compounds precedes us, Sharad Hajela and Bill Freeman who provided us with the compounds, and Gene Johnson who performed the first matrix experiments.

I. INTRODUCTION:

The AFAL/LSX invited us to participate in the UES summer program in order to strengthen relations between California State University, Northridge and LSX and so that we could participate in the buildup of the laser spectroscopy - matrix isolation laboratory. Our expertise in the area of matrix isolation and our desire to use the Air Force lasers for an ongoing project made our collaboration ideal. After more than half of our time was devoted to setting up the laboratory, we proceeded with our study of osmium cluster compounds.

Cluster compounds are an important link between individual metal atom chemistry and bulk metals. They serve as model catalytic compounds, in which hydrogen and other small molecules can add, break, and undergo a variety of unusual transformations. μ-(η-diethylacetylene)-decacarbonyltriosmium, compound I, exhibits rather unusual thermal and photo-chemical transformations. Hydrogen migrates from the capping ligand to the osmium ring (1). Furthermore, compound I can take up hydrogen molecules from the environment and store them in the osmium ring.

Our interest has been to study these reactions at 10 K, with the prospect of isolating intermediates and elucidating the reaction mechanisms. We observed two reactions related to compound I. The reversibility of one reaction is suggested by our data, an important observation related to storage and release of hydrogen.

II. OBJECTIVES OF THE RESEARCH EFFORT:

a. The bulk of our time was spent setting up the laser spectroscopy - matrix isolation laboratory. Here we were concerned with effectively coupling a Leybold Heraeus - ROK 10 cryostat, a Mattson Cygnus 100 FTIR, and a Lambda Physik FL 3002 dye laser-EMG 202 MSC excimer laser combination. Further work was to be done to also couple UV-VIS and luminescence apparatus.

b. With the remaining time, we were able to study the photochemistry of compounds I and III. It was known previously by us that compound I photolyses rapidly at 10 K in solid argon, resulting in the formation of a CO-9 intermediate species (compound II), and the elimination of carbon monoxide. It has been one of our goals this summer to determine the exact wavelength necessary to produce compound II using laser irradiation. Another goal has been to determine the FTIR spectrum of an isomer of compound II (compound III) at 10 K for comparison of its spectrum to compounds I and II. Compound III is known to be the photoproduct of compound I at higher temperatures (E_a = 71 kJ/mol) (1). We found that compound III readily converts to a compound IV at 10 K in argon. Another goal has been to analyze this.

c. Finally, a very important goal for us was to correlate the IR data of compounds I-IV to known spectra of other osmium cluster compounds. We wanted to explain the relative numbers of IR bands corresponding to the carbonyl stretching frequencies in terms of a) the mass and bonding properties of atoms in the positions, trans to the carbonyl group, and/or b) the Cotton-Kraihanzel treatment of metal-CO-ligand octahedral complexes (2).

III. ACCOMPLISHMENTS: APPROACH, RESULTS, AND DISCUSSION

a. Approach: The experimental apparatus was set up as shown in figure 1. This allowed for sample deposition from two jets, useful for simultaneous deposition of two compounds. In one position of the substrate we could deposit, irradiate with the laser or D_2 lamp, or take spectra.

Results and Discussion: With the apparatus as described we were able to cool the cryostat to about 10 K in 1 hour. The power output for the excimer laser was about 8 watts while the power output for the dye laser was 1 to 2 watts. During the experiments the pressure was about 10^{-6} torr.

b. Approach: In order to study the photochemistry of compounds I and III, the molecules were isolated in argon matrices at 10 K. The compounds have very low vapor pressures ($< 10^{-3}$torr), so conventional deposition methods were not employed. Rather, the solid was placed in the metal tubing of the deposition line, as close as possible to the cryostat chamber. This section of the metal tubing was heated to approximately 40°C by a heating tape, and argon was passed over this at a flow rate of approximately 3-4 mmole per hour. After approximately 90 min. the matrix was ready for UV-vis photochemical and FTIR investigation. The 30 watt-D_2 lamp and the excimer-pumped dye laser were used as photochemical light sources.

Results and Discussion: Our first study was to reconfirm that photolysis of compound I indeed produces a new species II with the same FTIR spectrum as had been previously obtained, (see Fig.4). Figure 3 is the spectrum of compound I before photolysis. In figure 4, the new product bands are observed as positive bands and the disappearing starting material bands as negative bands in the difference spectrum. Carbon monoxide also is seen as a product at 2138 cm^{-1}. Compounds I and II band frequencies are listed in Table I. Four main bands observed were 2090, 2051, 2019, and 1995 cm^{-1}.

These compare favorably to the reported spectrum of $Os_3(CO)_9(C_6H_5C{=}CC_6H_5)$ with bands at 2091, 2048, 2005, and 1992 (3). Thus a simple elimination of the bridging CO without any further arrangement is ascribed to compound II. This reaction is illustrated in figure 2.

We then tried to produce the same results with laser irradiation. Photolysis of compound I resulted from 470 nm irradiation (20 Hz, 1-2W, 20 min.). This is believed to be very close to the O-O transition of the lowest energy absorption band. This result implies that there is a small or zero barrier to carbon monoxide elimination.

Our second study was to obtain the FTIR spectrum of compound III and to investigate its photochemistry at 10 K. We discovered that irradiation of compound III with the deuterium lamp readily resulted in a new species, compound IV. Figure 6 illustrates the spectrum of compound III. Figure 7 illustrates the production of compound IV as a difference spectrum. The carbonyl stretching frequencies for compounds III and IV also are listed in Table I. Comparison of the bands in Table I for compounds I and IV reveal a striking result. With the exception of the bands at 2055 and 1839 cm^{-1} for compound I and the band at 2233 cm^{-1} for compound IV the remaining frequencies compare identically within ~ 5 cm^{-1}. This implies that compounds I and IV are nearly identical in structure. The band at 2233 cm^{-1} for compound IV is at very high frequency relative to the other CO bonds. This bond correlates well with known N_2 ligand frequencies. Possibly the photoproduct contains an nitrogen ligand, which formed due to its presence as an impurity during deposition. An example of this type of structure is provided by $Cr(CO)_nN_{n-6}$, in which the CO stretch frequencies range from 2086 to 1974 cm^{-1} and the N_2 stretch frequency is at 2237 cm^{-1} (4). Assuming that the structure of compound IV is as is illustrated in Fig. 5, then compound IV also must exhibit the bridging carbonyl frequency at around 1840 cm^{-1}. While we are able to detect those frequencies with our mercury-cadmium detector at Northridge, we were

unable to obtain this information with the indium-antinimide detector at Edwards.

With the possibility that Fig. 5 depicts the structure of compound IV, we postulate that in the presence of carbon monoxide, compound IV will photochemically convert to compound I. This implies that a 2 dimensional photochromism is possible at a certain temperature, where wavelength 1 would convert compound I to compound III and wavelength 3 would reverse the process. An intruiging possibility is that at another temperature a three dimensional photochromic process might occur, readily interconverting between compounds I, II, and III with three different wavelengths.

c. Approach: The IR carbonyl stretching frequencies of compounds I-IV are listed in Table I. The assignment of the individual bands is not obvious at the outset. As a first postulate we argue the mass of osmium is so large that the Os-C stretching frequency is quite low (a few hundred cm^{-1}). The Os-C vibration would have a very small coupling effect to the C-O stretch, and thus would serve to isolate the carbonyl group from other vibrations in the molecule. A local mode picture is appropriate. According to the theory of Cotton and Kraihanzel, as a carbonyl group stretches, d orbital density on the metal overlaps with the pi* carbonyl orbital. This weakens the CO bond and lowers the vibrational frequency. The method includes a symmetry effect on the carbonyl electron density due to the other carbonyls of the same metal vibrating in concert. The vibrational phase of the the other ligands will affect the d orbital density. A justification for using the symmetry argument for cluster compounds is that the parent $Os_3(CO)_{12}$ exhibits four bands, exactly what is predicted from a $M(CO)_4(L)_2$ species (5).

Results and Discussion: For a trans-$M(CO)_3(L)_3$ compound, two bands of A_1 and E symmetry are predicted. We start with the simplest of our four cluster compounds, compound II. Figure 2 illustrates its probable structure. Os(2) and Os(3) are structurally equivalent, but not equivalent to Os(1). Thus we would

expect four bands. In fact, we observe four major sets of bands, which are resolved further into a singlet at 2090 cm^{-1}, a doublet at 2051 and 2048 cm^{-1}, a doublet at 2019 and 2013 cm^{-1}, and a broad singlet at 1995 cm^{-1}. Presumably, the two doublets arise from symmetry breaking of the E modes, most probably due to angular distortion from pure octahedral symmetry. The most intense doublet pair is at 2051 and 2048 cm^{-1}. This would correspond to the perturbed E modes of Os(2) and Os(3). The set at 2019 and 2013 cm^{-1} is less intense and would correspond to the perturbed E mode of Os(1). The remaining bands at 2090 and 1995 cm^{-1} are assigned as the A_1 modes. We note in table I that the band at 2090 cm^{-1} retains a fairly constant frequency when comparing compounds I-IV, and that the band does not separate into two components. However the band at 1995 cm^{-1} does separate into two components for compounds I, III, and IV. On this basis, we assign the A_1 mode of Os(1) to the 2090 cm^{-1} band and the A_1 modes of Os(2) and Os(3) to the 1995 cm^{-1} band.

For compounds I, III, and IV, the presence of nine bands in the region between 2101 and 1977 cm^{-1} can be explained if we assume that the three degenerate E modes are split, and that the three osmiums are structurally inequivalent. The E modes are split because the octahedral geometry is not perfect. The split E modes of Os(2) and Os(3) separate into different frequencies because for compound I, the X-ray crystallographic data indicates that the bridging carbonyl is assymetrical (6). The Os(2)-C bond is 1.3 A and the Os(3)-C bond is 1.6 A. Presumably, this provides a substantially different contribution to the electron density at each osmium. For compound III, the inequivalence of Os(2) and Os(3) arises from the assymetrically bonded capping ligand. For compound IV the assymetry arises due to the presence of N_2. Thus the two bands that were assigned as E motions for compound II at 2051 and 2048 cm^{-1} now are separated into four bands at 2066, 2055, 2049, and 2025 cm^{-1} for compound I, at 2071, 2045, 2025, and 2014 cm^{-1} for compound III, and at 2233, 2068, 2049, and 2022 cm^{-1} for compound IV.

IV. RECOMMENDATIONS

Within the next six months to one year the AFAL will obtain a MCT detector, a helium cooled bolometer and a blue sensiter diode array detector. We are planning several trips back to the laboratory. The following experiments at Northridge are planned:

1) repeat the study of compound III with CO and N_2 experiments with our MCT detector.
2) repeat 1) with isotopically labeled CO and N_2.
3) measure the photoproduction wavelength for compound III with filters.

The following experiments at the AFAL are planned:

1) observe the time resolved photolysis by UV-vis absorption of compounds I and III using the blue sensitive diode array/ optical multichannel analyser.
2) measure the exact photoproduction wavelength for compound III with laser irradiation.

With these experiments completed, final conclusions can be made and the results will be submitted for publication.

TABLE I

I	IV	II	III
	2233		
2101	2096	2090	2099
2066	2068		2071
2055		2051	2045
2049	2049	2048	2025
2025	2022	2019	2014
2011	2009	2013	2000
1991	1997	1995	1993
1985	1988		1985
1979	1981		1977
1839			

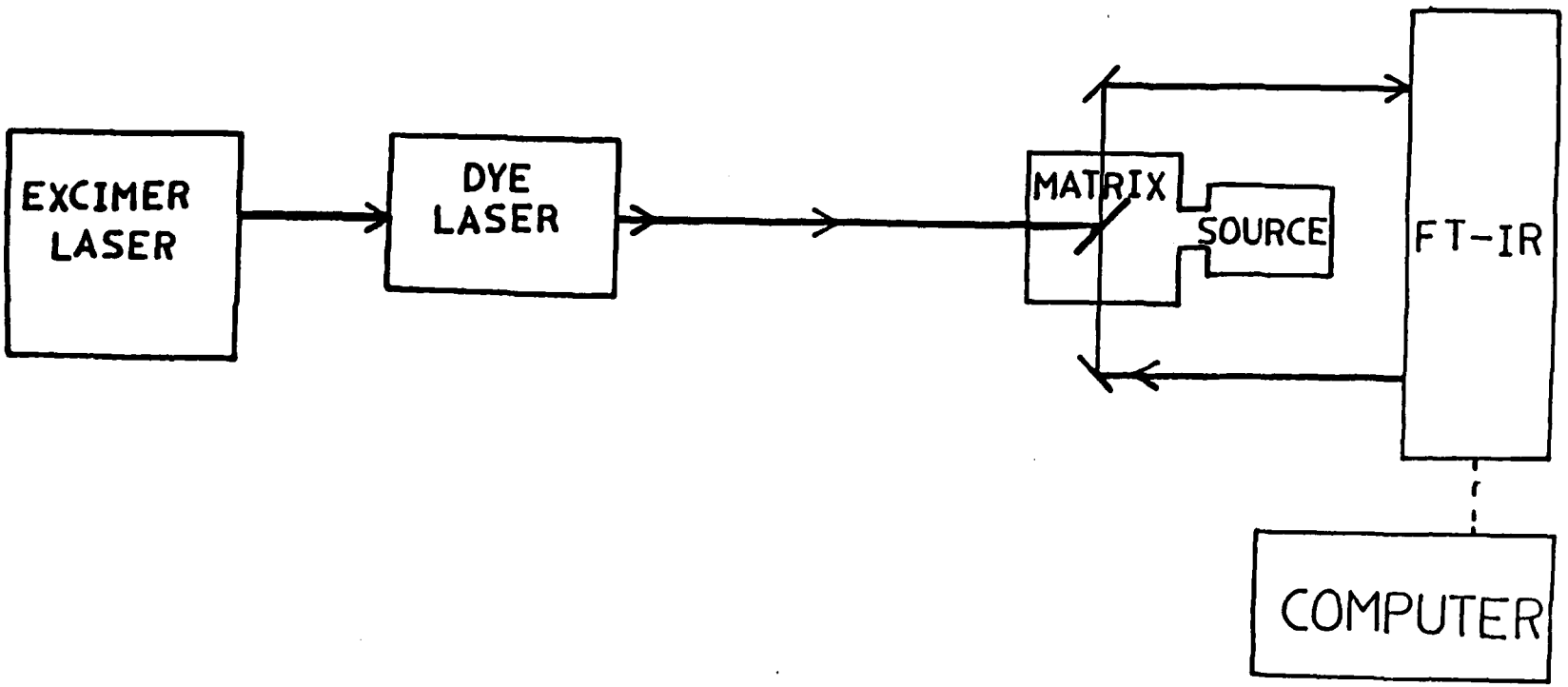
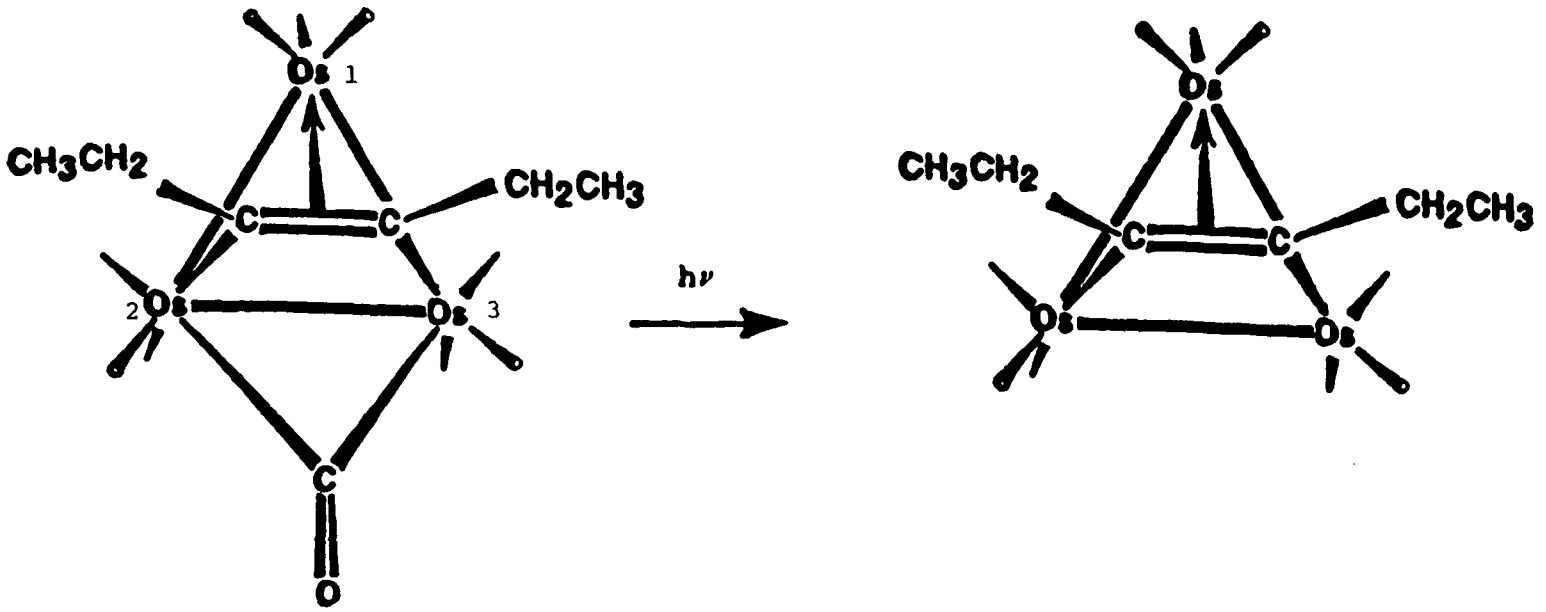


FIGURE 1

EXPERIMENTAL APPARATUS



I II

FIGURE 2

PROPOSED REACTION SCHEME OF COMPOUND I

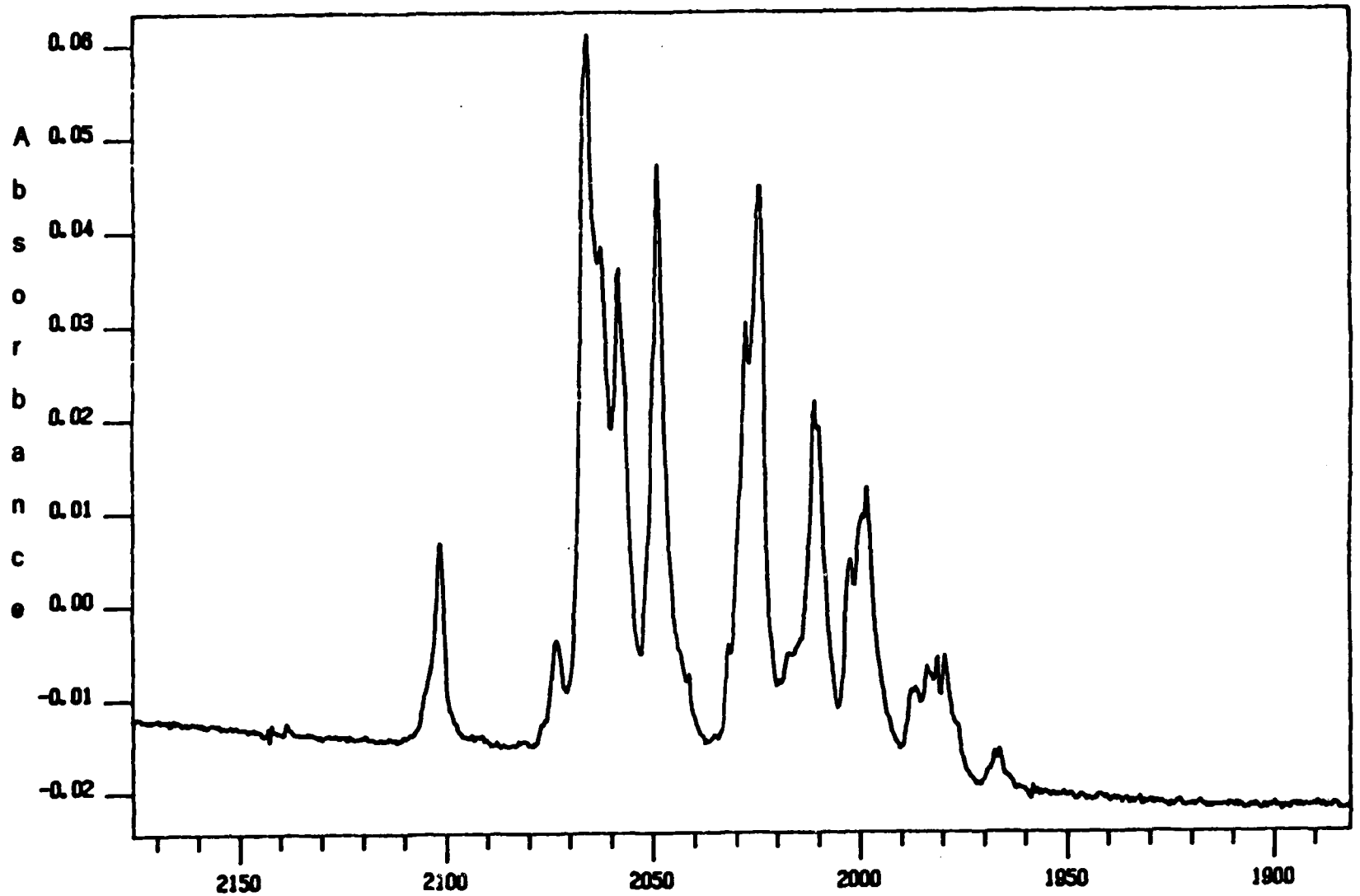


FIGURE 3

IR SPECTRUM OF COMPOUND I

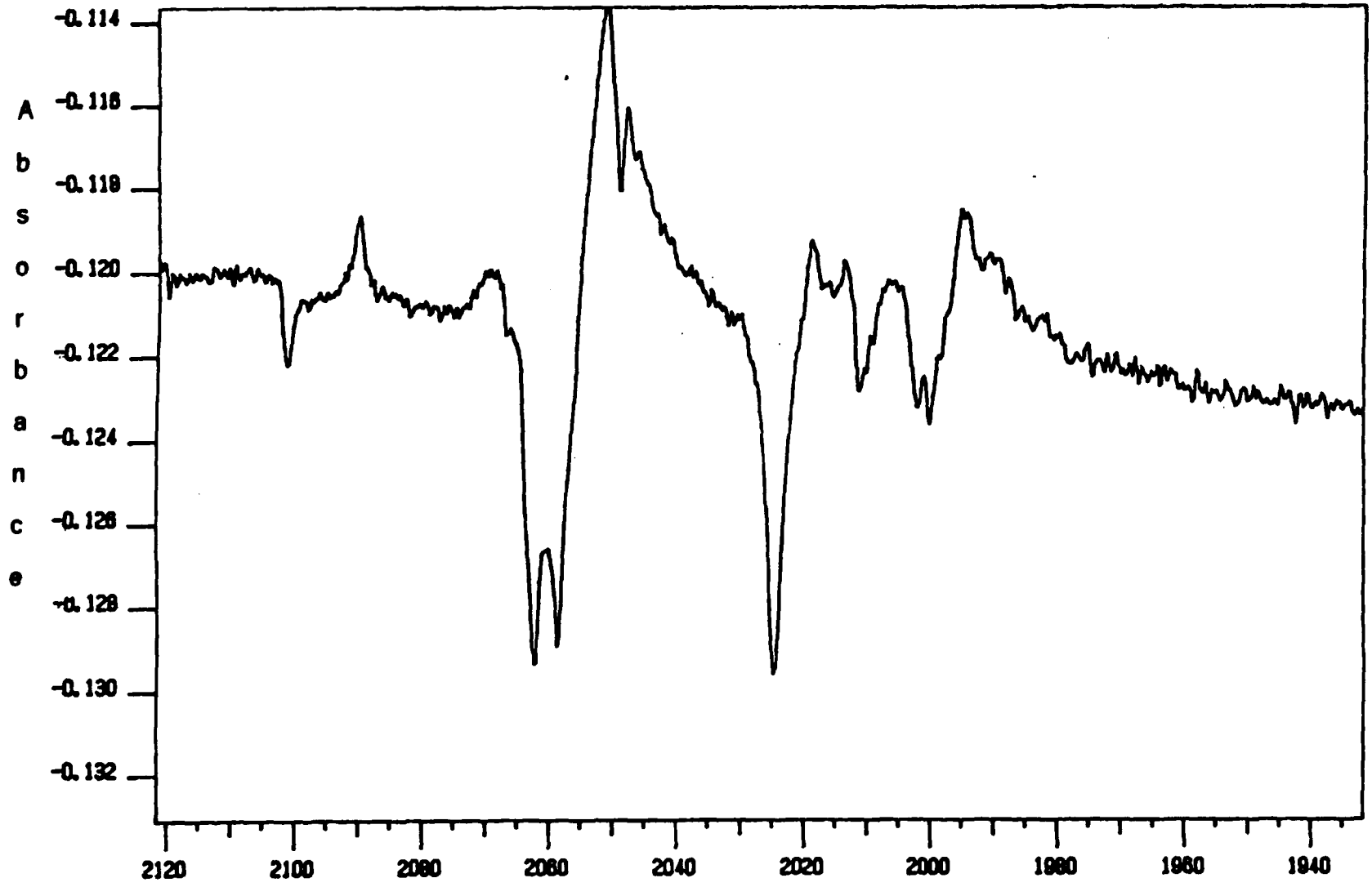
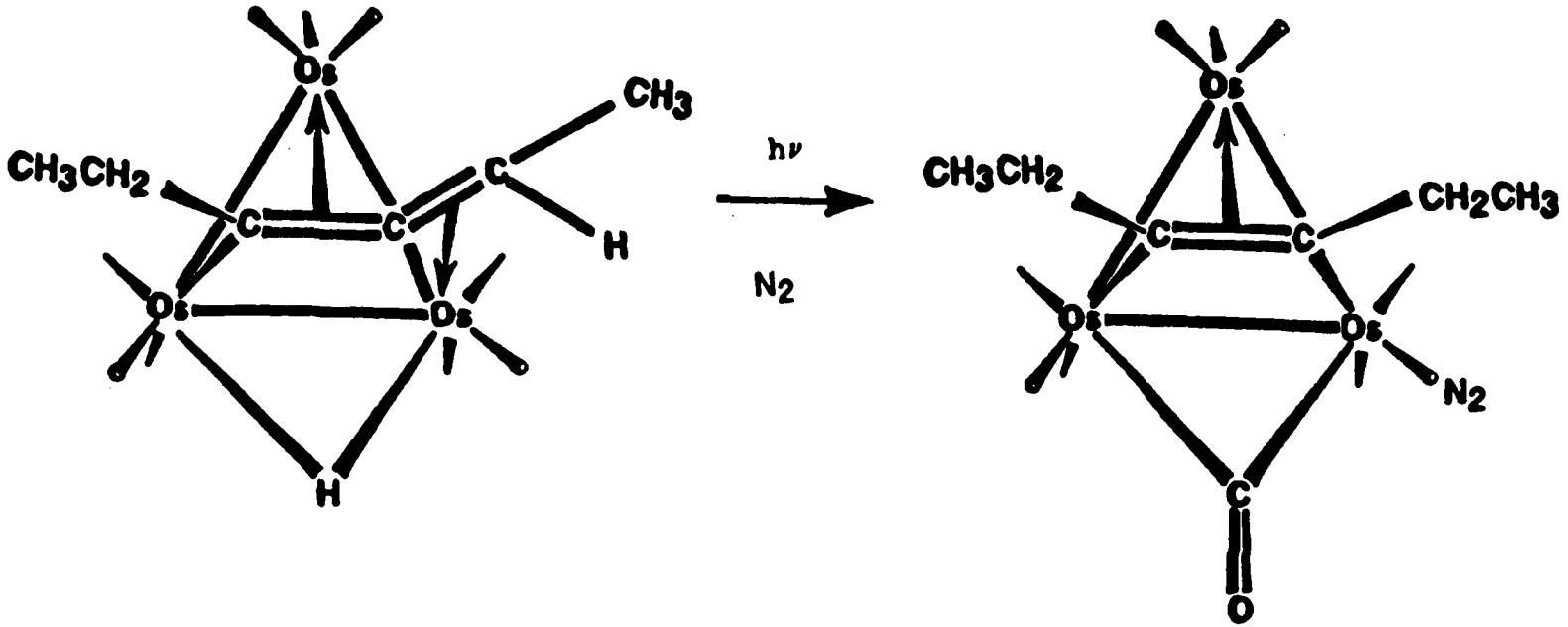


FIGURE 4

DIFFERENCE SPECTRUM OF COMPOUND I PHOTOLYZED TO GIVE COMPOUND II



III IV

FIGURE 5

PROPOSED REACTION SCHEME OF COMPOUND III

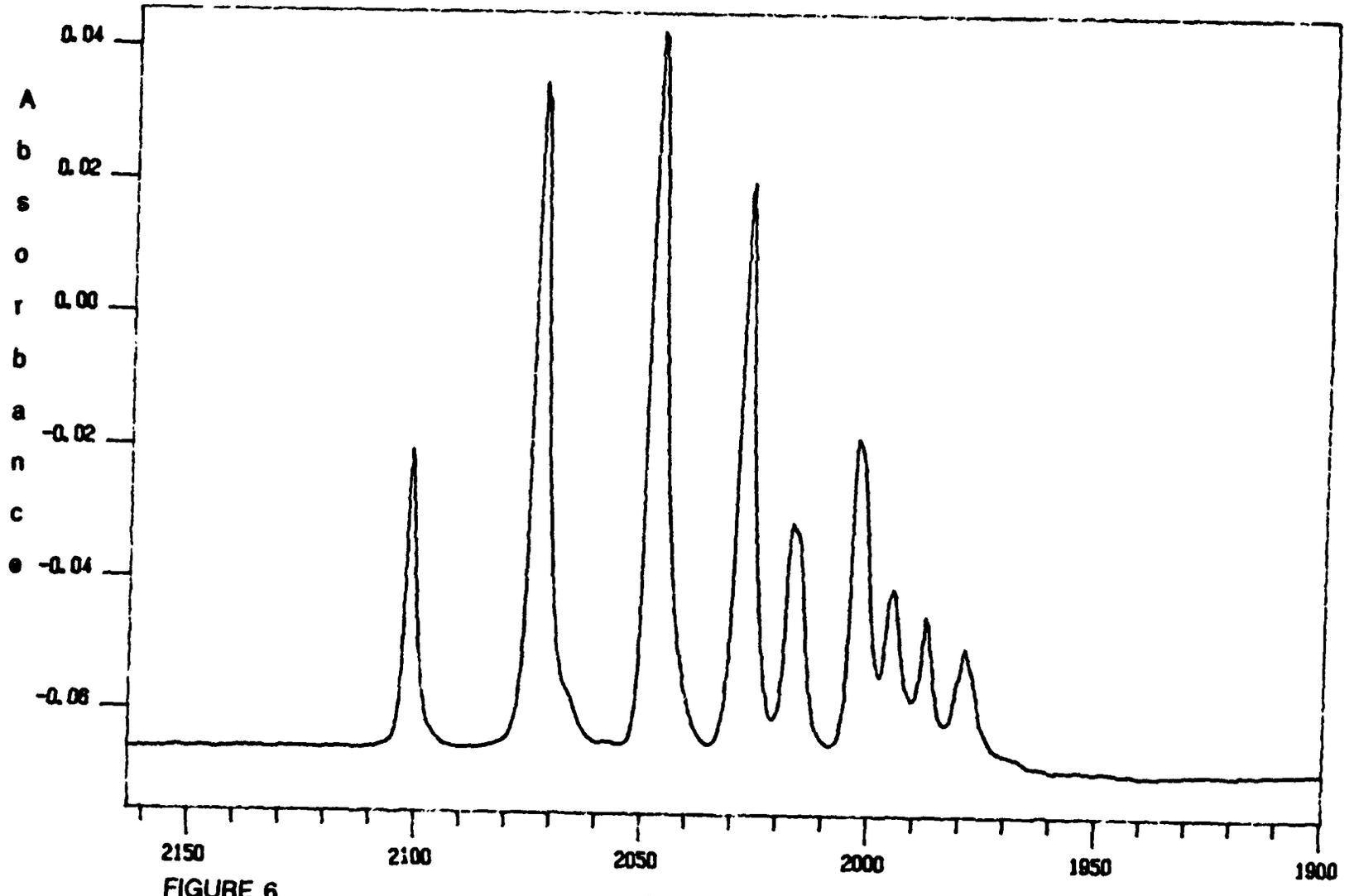


FIGURE 6

IR SPECTRUM OF COMPOUND #

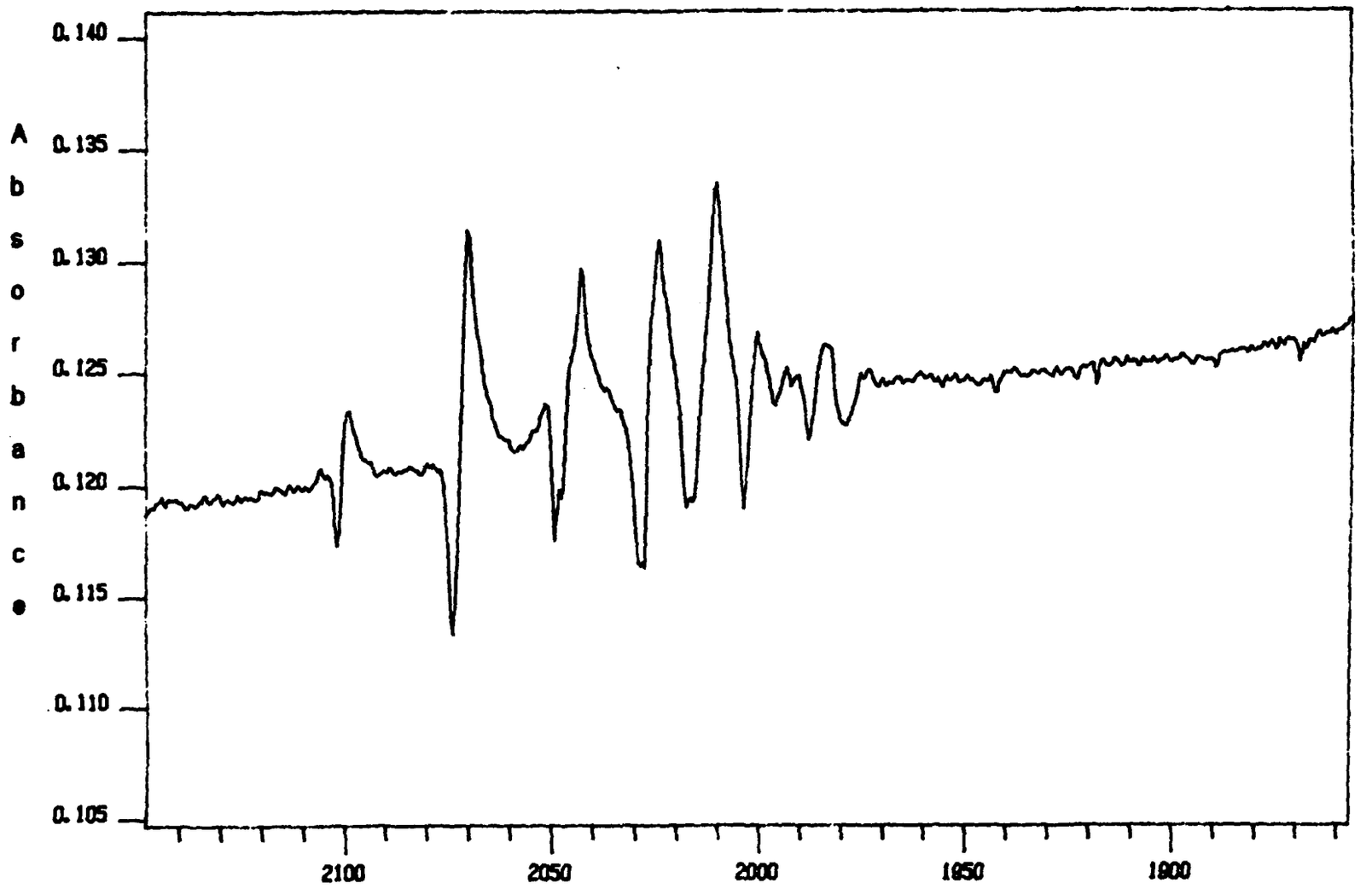


FIGURE 7

DIFFERENCE SPECTRUM OF COMPOUND II PHOTOLYZED TO GIVE COMPOUND IV

V. REFERENCES

1. Zhang, M., Master's Thesis, California State University, Northridge, 1987.

2. Cotton, F. and Kraihanzel, C.S., J. Am. Chem. Soc., 1962, 84, 4432.

3. Tachikawa, M., Shapeley, J.R., and Pierpont, C.G., J. Am. Chem. Soc., 1975, 97, 7172.

4. Turner, J. J., Simpson, M. B., Poliakoff, M., Maier, W.B., and Graham, M., Inorg. Chem., 1983,22,911.

5. Hardcastle, K., California State University, Northridge, private communication.

6. Rosenberg, E. and Bracker-Novack, J., California State University, Northridge, private communication.

1988 USAF-UES SUMMER FACULTY RESEARCH PROGRAM/

GRADUATE STUDENT RESEARCH PROGRAM

Sponsored by the

AIR FORCE OFFICE OF SCIENTIFIC RESEARCH

Conducted by the

Universal Energy Systems, Inc.

FINAL REPORT

COMPOSITE-EMBEDDED FIBER-OPTIC STRAIN SENSORS

Prepared by:	David W. Jensen, Ph.D., Assistant Professor/ Michael J. Koharchik, Graduate Student
Departments:	Aerospace Engineering/ Engineering Science and Mechanics
University:	The Pennsylvania State University University Park, PA 16802
Research Location:	USAF Astronautics Laboratory AFAL/VSSC Edwards AFB, CA 93523-5000
USAF Researcher:	Capt. Ted Doederlein
Date:	Sept. 21, 1988
Contract No:	F49620-88-C-0053

Composite-Embedded Fiber-Optic Strain Sensors

by
David W. Jensen, Ph.D.
and
Michael J. Koharchik

ABSTRACT

An experimental investigation was conducted on advanced composite structures with embedded fiber-optic strain sensors for smart structures applications. The fabrication procedure for embedding the sensors into advanced composite components was refined and the effects of the fiber optic inclusion on the tensile properties of composite laminates were examined. Difficulties encountered during fabrication involved maintaining the integrity and alignment of the optical fibers and protecting them during the filament winding and curing processes. Several 1.5 inch diameter composite tubes with embedded fiber-optic sensors were successfully fabricated. Preliminary results obtained from three independent optical systems, including an RF interferometer (NASA Langley Research Center), a Mach-Zehnder interferometer (Penn State University), and an optical time-domain reflectometer (G2 Corporation) indicate that further research is warranted, particularly in the area of interferometry. Additionally, two flat graphite/epoxy plates were filament wound and cut into one-inch wide specimens. Ten of these 22 specimens contained three embedded optical fibers each. Tensile tests conducted on these specimens indicated no discernible degradation in stiffness due to the embedded fiber-optic sensors.

I. INTRODUCTION:

Recent progress in the development of critical technologies has enabled the realistic consideration of smart structures (i.e., those capable of sensing conditions within the structure and responding accordingly). Successful implementation of such smart structures technology could significantly enhance the dynamic response of large flexible structures in space. One essential aspect of smart structures technology is the need to accurately sense structural deformations and vibrations in real time [Reference 1].

The application of embedded optical fibers as internal deformation sensors in large space structures is attractive for several reasons, particularly when employed in concert with advanced composite structures. Fiber-optic sensors - which are otherwise extremely fragile - can be embedded in advanced composite structures, protecting them from potentially hostile environments. These sensors are light-weight, geometrically flexible, compatible with the microstructure of advanced composites, immune to electro-magnetic interference, and relatively low cost. On the other hand, embedded fiber-optic strain sensors can provide continuous, in-service, distributed strain sensing for active health monitoring of structural components from "cradle-to-grave" [References 2 and 3]. Furthermore, judicious placement of these fibers in the structure can lead to the equivalent of an active neurological sensory network in an otherwise dormant structure.

In an effort to advance the state-of-the-art in composite-embedded fiber-optic strain sensor technology, a research program in this area has been initiated in the Department of Aerospace Engineering at The Pennsylvania State University [References 4 and 5]. Considerable energy has been expended over the past two years on research ranging from evaluating the state of the art to developing fabrication techniques for embedding the sensors. Most of this research has centered around the application of a Mach-Zehnder interferometer. The initial objective of this continuing research is to evaluate the range of performance of composite-embedded fiber-optic strain sensors and to calibrate their response to different combinations of stress fields and geometric configurations.

The College of Engineering at Penn State has extensive resources available for research in the field of advanced composite materials, including several faculty with considerable experience in composites and modern facilities in which to conduct meaningful research. For example, the embryonic Center for Composites has extensive manufacturing and testing facilities, including a numerically-controlled 3-axis McClean-Anderson W70SP filament winder capable of winding parts 24-inches in diameter by

84-inches long, a Creative Pultrusions pultruder, a 24-ton programmable Tetrahedron MTP-14 hot-press (850 degrees Fahrenheit) with mini-clave, a high temperature (850 degrees Fahrenheit) and pressure (200 psi) 36-inch by 84-inch Baron-Blakeslee BAC-37 autoclave, a 20,000 lb. tension-compression Instron 1350 servohydraulic tester with hydraulic grips, a 10-lb Bruel & Kjaer vibration exciter, a 1000-lb. Bruel & Kiaer impact hammer, a Nicolet 4094A digital storage oscilloscope with a 2-MHz sampling rate, a Mach-Zehnder interferometer, and a Systolics PC-1000 controller - to mention just a few.

The Mach-Zehnder interferometer, in particular, is an important piece of equipment for understanding and developing fiber-optic strain sensor technology [Reference 6]. This instrument utilizes a helium-neon optical signal split between two paths: (1) a sensor arm (composite part) and (2) a reference arm. Elongation of the sensor arm results in an increased optical path length, which causes a phase shift relative to the reference arm. The magnitude of this phase shift is proportional to the integrated elongation of the optical fiber. Electronic circuitry feeds back a voltage proportional to the magnitude of this phase shift to piezoelectric transducers (PZTs) in the reference arm in order to maintain a state of zero phase shift. This feedback voltage is proportional to the strain in the PZTs, which, in turn, is equal to the strain in the sensor.

The nature of the research performed at Penn State and under this summer research program ties in directly to AFAL's Smart Structures project directive [Reference 7]. The particular scientific area of interest in this project is the development of composite space structures which are capable of actively controlling structural vibrations by integrating sensors, microprocessors, and actuators into the structural material. This technology could be applied to a platform supporting a space-based laser, for example, which requires a great degree of stability in order to quickly and accurately lock on to hostile targets, yet is susceptible to self-induced vibrations forced by rapid aiming and firing maneuvers. A thorough understanding of the response and performance of these sensing, processing, and actuating componenets is essential to the eventual successful deployment of smart structures in space.

II. OBJECTIVES OF THE RESEARCH EFFORT:

This research effort focused on the sensing aspect of the integrated triad of sensing, processing, and actuating components required for successful implementation of smart structures technology. The effectiveness of any sensing system depends on the existence of some reliable correlation between the sensor output and the parameter being measured. In the particular case of embedded optical fibers, the output from the optical system must be related to the deformation of the composite structure in which it is embedded. In order to establish this relationship and characterize the optical strain sensing system, several objectives were defined.

The preliminary initial objective for this summer program was to assemble an optical system at AFAL similar to one in use at NASA Langley Research Center (NASA-LaRC). Composite-embedded sensors were to be tested on this system with the results compared to those obtained using conventional devices, such as strain gages. In this manner a preliminary characterization of the optical system was to be achieved. However, this objective was not met because the optical equipment did not arrive (although it had been purchased prior to the start of the summer program).

The next objective involved successfully embedding fiber-optic strain sensors in composite components. Several fabrication issues were addressed as part of this task. The results are summarized in the following section.

The final objective was to investigate the effect of embedded fiber-optic sensors on the tensile stiffness properties of the composite material. These results are described in Section IV.

III. FABRICATION ISSUES:

Successful fabrication of filament-wound advanced composite tubes with embedded fiber-optic strain sensors hinged on finding satisfactory solutions to a number of obstacles. Most of the difficulties encountered stemmed directly from the fragile nature of optical fibers. In particular, many complications arose from the need to protect the fiber-optic pigtails - a length of lead fiber is required to connect the embedded optical fibers to the particular optical processor - from severe environmental disturbances, such as handling and the flow of excess resin, during the bagging and curing processes, respectively. An additional limitation is imposed by the minimum allowable radius of curvature to insure the optical integrity of the fibers. This is particularly important when looping the fibers within the composite structure.

To further complicate an already difficult process, preliminary efforts indicated that the fiber-optic strain sensors should exit the tube in a radial direction some distance away from the end. The first tube was produced with the sensor ingress and egress sites at one end. This tube was tested at NASA-LaRC where it was discovered that clamping the end of the tube for dynamic testing resulted in an undesirable perturbation of the optical signal. In order to avoid this, subsequent tubes were wound with the sensors brought out through the surface a few inches from the end, providing a length of tube to grip during testing which contained no sensors.

This complicates the winding process by requiring it to be carefully monitored in order to prevent the fiber-optic pigtail from being wound under or broken. In addition, when winding directly over the fiber-optic sensor, extreme caution is required in order to maintain the precise alignment and to prevent kinking of the optical fibers, which could cause them to break or cause an increase in the attenuation.

Protecting the pigtails from the flow of excess resin during the curing process was accomplished by bringing the optical fibers up through the cure materials and coating these critical areas with silicone RTV sealant to provide stress relief. The fibers were then covered by a nonporous release ply to separate them from the flowing resin and to keep the silicone from adhering to the cure materials. This proved to be a satisfactory procedure for fabricating composite-embedded fiber-optic strain sensors.

During the curing process, residual stresses develop in composite structures due to a mismatch in the coefficients of thermal expansion of the various plies. These stresses may cause microbending of the optical fibers which would reduce their effectiveness as strain sensors by significantly increasing attenuation losses.

Seven tubes were manufactured using a variety of fabrication techniques in order to establish the optimal fabrication parameters. All of the tubes were filament wound on 1.5 inch diameter stainless steel mandrels. After cleaning with acetone and steel wool, the mandrels were coated with a layer of Knomark, Inc.'s Esquire high gloss transparent boot polish, followed by a layer of Miller-Stephenson MS-122 aerosol release agent. The tubes were filament wound on an En-Tec Model EN010236 five-axis computer-controlled filament winding machine with a 48-inch diameter by 180-inch long winding capability and equipped with a Helman HE-1002A tensioning system. All of the filament winding utilized two 12K tows of graphite fiber and standard epoxy resin. During winding, the tension on the fibers was maintained between two and three pounds. After winding, the tubes were covered with release ply, fiberglass bleeder/ breather, and vacuum bagging. In all cases, the non-embedded portions of the optical fibers (pigtails) were coated with Dow Corning Corp.'s Silastic 732 clear RTV adhesive/sealant for stress relief at the ingress and egress points and for protection of the exposed fibers during handling. This silicone RTV has a working range between-85 degrees and 450 degrees Fahrenheit. The tubes were cured in a Baron-Blakeslee autoclave for two hours at 350 degrees Fahrenheit under 85 psig pressure and full vacuum (15 psig). The autoclave heat-up and cool-down rate was numerically controlled not to exceed five degrees per minute. Exceptions to this fabrication procedure are noted in the specific descriptions below.

The first three tubes fabricated were nominally 54 inches long. The mandrels were coated with teflon tape prior to winding in an unsuccessful attempt to facilitate mandrel removal. After winding, the tubes were stored in the freezer over the weekend prior to curing. The cure cycle for these three tubes used only 50 psi pressure and included a one hour hold at 220 degrees Fahrenheit. After curing, a hydraulic jack was rigged up to extract the mandrels from these tubes.

The first tube was filament wound using a 0.2-inch bandwidth of expired (two year old) Fiberite G40/5245C graphite/epoxy prepreg tows. The layup was $[90/+\text{-}60/\text{optical fiber}/90]_T$, where the subscript "T" stands for "total" to distinguish this from a symmetric laminate. A twenty-foot length of G2 Corp.'s proprietary pressure-sensitive optical fiber was embedded in this tube. The two loops of optical fiber extended beyond the far end of the graphite/epoxy tube approximately two inches. Attempts at winding zero degree plies in this tube proved to be unsuccessful. Unfortunately, after curing, this tube would not release from the mandrel and had to be cut off. However, this tube did demonstrate that nonporous release cloth serves very well to separate the silicone from the curing materials.

The second and third tubes were wet wound using a 0.15-inch bandwidth of Hercules IM7 fibers and 55A epoxy resin (4 parts Shell Epon Resin 826, 1 part Celanese Specialty Resin EPI-REZ 5022, and 1 part Morton-Thiokol 9999-3493 Methylene Dranilene). The layup was $[90/+-60/\text{optical fiber}/90_2]_T$ for the second tube and $[90/+-60/\text{optical fiber}/90]_T$ for the third tube. Two independent loops of Newport's multimode fiber with a 125 micron diameter core and a 500 micron diameter jacket were embedded in the second tube and one double loop of Lightwave Technology's single mode fiber with a 125 micron diameter core and a 250 micron diameter jacket was embedded in the third tube. Both of these tubes came out perfectly free of wrinkles and with a good surface texture. However, vacuum bagging material was found to adhere to the silicone, while teflon tape does not.

Unfortunately, the second tube demonstrated that optical fibers would break if a wrinkle formed in the cure materials beneath them. Also, although there was only minimal bleed during the cure, misfortune struck again when the peel ply stuck to these two tubes, causing the fiber-optic pigtails to break off during its removal. A chromic acid digestion test was performed on the end of the second tube to dissolve the resin, thus exposing the glass and graphite fibers. The graphite fibers were trimmed away to leave the fragile fiber-optic sensor cores exposed for connection to the optical systems. This effort was successful in demonstrating that operable fiber-optic pigtails could be recovered. However, in this particular case, two of the four leads were broken off during handling too close to the tube to utilize.

Approximately four inch leads were left in-tact on the third tube. Although dynamic tests cannot be performed on this tube because of the short leads, a Helium-Neon laser light was directed through the fiber to demonstrate the continuity thereof. As part of the continuing research, an attempt will be made to fusion splice longer pigtails onto the ends of these leads.

The remaining tubes were filament wound using Fiberite IM6/934 graphite/epoxy prepreg tows and cured according to the standard cure procedures described above. The fourth and fifth tubes wound were nominally 58 inches long. The fourth tube had a layup of $[90/+-60/\text{optical fiber}/90_2]_T$ with the same optical fiber as the second tube. This tube was taken to NASA-LaRC for dynamic and optical testing. The measured lowest natural frequency of 10.2 Hz was surprisingly close to the predicted value of 10.7 Hz for a cantilevered tube (the analysis was based on thin-walled shell theory).

The fifth tube had four loops of G2 Corp.'s proprietary pressure-sensitive optical fiber embbedded in a $[90/+-45/\text{optical fiber}/90_2]_T$ layup. Three pieces of nonporous teflon were embedded in this tube at the locations shown in Figure 1. The purpose of

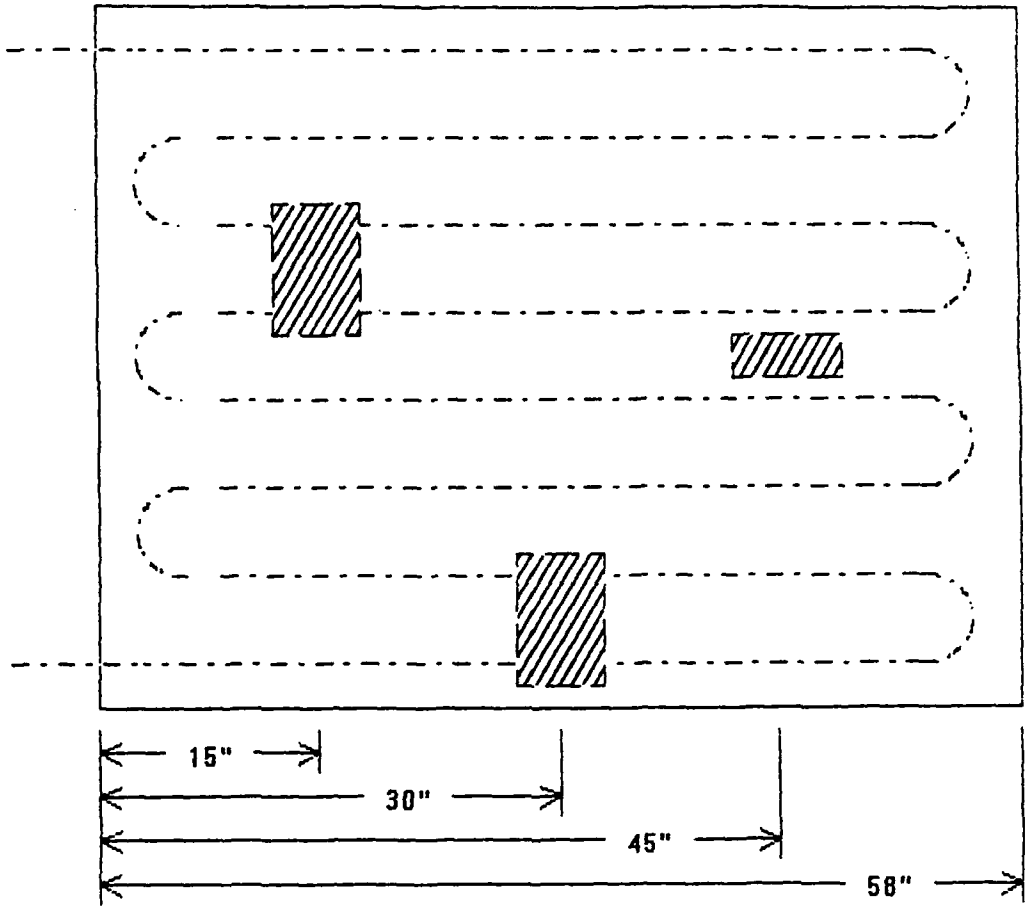


FIGURE 1. Schematic of fifth tube (unrolled) with embedded fiber-optic sensor and teflon tape (not to scale).

the embedded teflon tape was to ascertain whether an optical time domain reflectometer (OTDR) could locate delaminations in a tube. Optical time domain reflectometry monitors the intensity of backscatter from picosecond pulses of light launched into the sensor. Point disturbances (stress concentrations) cause an increase in the local backscattering. By measuring the time delay, and knowing the velocity of light in glass, the distance to the disturbance can be determined. However, this test was not successful because of high attenuation in the fiber, indicating a possible internal break. One of the fiber-optic pigtails broke near the surface, but this should not have adversely affected the OTDR technique, which needs only one connection.

One interesting aside is that this tube had more resin bleed on one end than on the other, and had fewer wrinkles on the end with less bleed. This would imply that the change in circumference accompanying resin bleed is a main cause of wrinkles.

The final two tubes manufactured (six and seven) were nominally 12 inches long and were wound with only one tow of prepreg. The sixth tube employed a bandwidth of 0.08 inches to form a layup of $[+-45/+-45/\text{optical fiber}/+-30]_T$. The seventh tube employed a bandwidth of 0.06 inches for a layup of $[+-45/\text{optical fiber}/+-30]_T$. A single loop of Lightwave Technology's single mode optical fiber with a 125 micron diameter core and a 250 micron diameter jacket was wound helically in each of these tubes, with the legs 180 degrees apart. The Mach-Zehnder interferometer was employed to demonstrate successful fiber continuity in these tubes.

The fiber-optic pigtails on the sixth tube were wrapped around the bare mandrel. Those on the seventh tube were coated with silicone and then wrapped around the bare mandrel. In the latter case, the silicone did adhere slightly to the mandrel. Although both techniques worked satisfactorily, coating the optical fibers with silicone and protecting them with release ply (as done in the earlier tubes) yielded the best overall results.

Another comparison performed on these two tubes dealt with the rotation angle of the "eye" during winding of the helical plies. The "eye" delivers the fiber onto the mandrel and, thus, controls the direction of the tension on the fiber tow during winding. For the sixth tube the eye was rotated perpendicular to the ply angle, while for the seventh tube the eye was rotated beyond the ply angle (resulting in a smaller angle than the ply angle). This latter situation improved the ability of the tow to follow the eye.

IV. STIFFNESS DEGRADATION:

Parallel research efforts focussed on determining the mechanical degradation of the composite material as a result of the optical fiber inclusion. Two flat plates were filament wound simultaneously (one on either side of a 14-inch by 14-inch flat mandrel) using Union Carbide G40 graphite fiber tows and standard 55A epoxy resin. The 12-inch by 14-inch laminated plate was wet wound on an En-Tec Tumble Winder with a 150-lb. capability. The fabricated laminates consisted of four plies all oriented longitudinally to form a $[0_2/\text{optical fiber}/0_2]_T$ laminate and a $[0_2]_S$ laminate. Thirty lengths of Owens-Corning 250 micron diameter optical fiber were embedded along the midplane of the first plate.

After curing the composite laminates at 350 degrees Fahrenheit, the ends were trimmed and the depthwise and chordwise locations of the optical fibers were measured to ascertain the extent of drift that had occurred during processing. Estimates of the depth of the optical fiber were made by viewing the end of the plate through a microscope. Many of the fibers were found to have drifted almost to the surface. The average depth of the optical fibers at one end of the plate was approximately one fiber diameter, rather than the expected depth of approximately 4.4 fiber diameters. However, it should be pointed out that these measurements were taken near the end of the plate in order to preserve the plate for static tensile testing. More was trimmed off of the other end and the average depth was found to be approximately 5 fiber diameters. Thus, the evidence is somewhat inconclusive. Nevertheless, pending further research, it is advised that embedded fiber-optic sensors be covered with a layer of composite material at some other orientation than that of the optical fibers to prevent the fibers from drifting outwardly. This rule-of-thumb was followed when making the seven tubes discussed above.

The plates were cut on a bandsaw into 22 coupons approximately one-inch wide for tensile testing. Ten of the coupons each had three embedded 250 micron diameter optical fibers. The rough-cut edges of the coupons were polished on a router jig with a diamond-coated blade. The specimens were then measured at three locations to determine the width and thickness. These values are reported in Table 1. The average thickness of all 22 specimens was found to be 0.0870 inches implying an average ply thickness of 0.022 inches, almost four times the nominal value of 0.006 inches. Fiberglass loading tabs were bonded onto the specimens and a single Micro-Measurements CEA-03-250UN-350 strain gage (gage factor of 2.06) was mounted on each specimen in the longitudinal direction.

Table 1: Specimen Thickness (t) and Width (w) Dimensions

(all dimensions in inches)

Spec. No.	t_1	t_2	t_3	t_{ave}	w_1	w_2	w_3	w_{ave}
				Plain Specimens				
1	.0933	.0865	.0897	.0898	.998	.998	.988	.995
2	.0928	.0877	.0875	.0893	1.019	1.013	1.029	1.020
3	.0866	.0946	.0873	.0895	.989	.999	1.018	1.002
4	.0891	.0869	.0823	.0861	1.023	1.030	1.031	1.028
5	.0882	.0884	.0810	.0859	1.052	1.051	1.049	1.051
6	.0862	.0877	.0822	.0854	.964	.963	.976	.968
7	.0796	.0866	.0828	.0830	1.005	1.013	1.015	1.011
8	.0883	.0851	.0805	.0846	1.037	1.035	1.030	1.034
9	.0879	.0889	.0849	.0872	.990	.988	.978	.985
10	.0829	.0848	.0848	.0842	1.053	1.054	1.053	1.053
11	.0909	.0910	.0906	.0908	1.002	1.000	.997	1.000
12	.0849	.0916	.0853	.0873	.853	.855	.852	.853
				Specimens with Embedded Fiber-Optic Sensors				
1	.0881	.0920	.0884	.0895	.952	.950	.954	.952
2	.0857	.0849	.0798	.0835	1.001	.987	.983	.990
3	.0902	.0863	.0858	.0874	.872	.885	.884	.880
4	.0844	.0852	.0859	.0852	.913	.914	.925	.917
5	.0840	.0860	.0835	.0845	.916	.900	.882	.899
6	.0836	.0848	.0837	.0840	.716	.694	.688	.699
7	.0832	.0882	.0883	.0866	.805	.805	.800	.803
8	.0876	.0885	.0870	.0877	.891	.876	.863	.877
9	.0872	.0929	.0930	.0910	.753	.757	.767	.759
10	.0940	.0918	.0936	.0931	.999	1.014	1.011	1.008

Static tensile tests were performed on an MTS 880 Axial-Torsional Material Test System with a 55-kip axial testing capability. Unfortunately, due to limitations of the special momentless grips, the specimens could not be loaded to failure. Nevertheless, it was desired to quantify any degradation of the tensile modulus of the coupons with embedded optical fibers compared to those without inclusions. The specimens were loaded under stroke control at a rate of 0.015×10^{-6} inches/minute (slower on the first three specimens). Load versus strain data was taken manually with the aid of a Measurements Group P-3500 Strain Indicator. Strain levels were recorded at load increments of 100 lb. up to a maximum load of 4800 lb., after which the load was released. It should be noted that the loading tabs on the coupons with the embedded sensors were not properly bonded on, causing many of the tabs to slip off prior to reaching the maximum load.

The data obtained in these tests is summarized in Table 2. The average tensile modulus is seen to be 12.36×10^6 psi (with a coefficient of variation of 0.37×10^6 psi) for the coupons without embedded sensors compared to an elastic tensile modulus of 12.35×10^6 psi (with a coefficient of variation of 0.43×10^6 psi) for the coupons with embedded sensors. Since this data is actually only significant to three digits, any difference is statistically insignificant, leading to the conclusion that the inclusion of longitudinally embedded fiber-optic sensors does not degrade the tensile modulus of filament-wound unidirectional graphite/epoxy materials. This conclusion is consistent with that reached previously as a result of research performed at The Pennsylvania State University on graphite/bismaleimide coupons which were hand layed up using prepreg tape. The results are reported in Reference 5.

As noted above, it was not possible to test the static tensile specimens to failure, since momentless grips were not available for testing beyond 5000 lb. However, one of the specimens was tested to failure in the hydraulic grips (albeit with a possible small bending moment applied). The failure stress for this coupon was measured at 120 ksi. Although this ultimate tensile strength is only a fraction of that expected, the failure strength is highly dependent on the fiber volume fraction, which was not measured. In fact, the fiber volume fraction is assumed to be quite low (possibly less than 20%), since the average thickness (0.087 inches) was more than three and a half times the nominal thickness (0.024 inches). This also explains why the observed experimental modulus was only a third of the nominal expected value.

Table 2: Experimental Longitudinal Elastic Moduli

Spec. No.	Elastic Modulus [Msi]
Plain Specimens	
1	12.62
2	11.86
3	11.75
4	12.06
5	12.96
6	12.96
7	12.44
8	12.32
9	12.35
10	12.38
11	12.22
Average	12.36
Specimens with Embedded Fiber-Optic Sensors	
1	11.94
2	12.28
3	11.88
4	12.81
5	13.08
6	12.84
7	12.26
8	12.60
9	11.93
10	11.86
Average	12.35

V. RECOMMENDATIONS:

Continuing research should focus on the response of the fiber-optic sensor to various types of mechanical deformations. In particular, an attempt should be made to correlate the optical signals from composite-embedded fiber-optic strain sensors in various structural configurations to the mechanical response under such loadings as tension, compression, torsion (shear), pressure, and biaxial loading, such as tension-torsion and/or tension-torsion-pressure. However, to begin with, the quasi-static tensile strain response should be calibrated, including searching for possible hysteresis.

As part of this work, several configuration parameters need to be investigated, including the response of the sensor as a function of the sensor direction relative to the loading direction and the sensor direction relative to the ply (or tow) direction. For example, strain measurements could be made by bending a cantilever beam which has optical fibers above, along, and below the neutral surface to examine tension, compression, and neutral axis response. Additional investigations should be made on beams under multi-point bending. This would lead naturally to investigations of the dynamic response, such as cantilevered vibration.

Other research should attempt to quantify the degradation of mechanical properties of the composite structures due to the fiber-optic inclusions. Reductions in the residual compressive strength and stiffness and damage tolerance (resistance to fatigue and impact damage, such as delamination and crack growth) are the most likely problems. The damage tolerance issues should be correlated with results from nondestructive evaluation techniques, such as x-ray, ultrasonic, pulse-echo, and/or c-scan.

Simultaneously, the extent of degradation of the optical response due to the embedding process should be investigated, including an examination of (1) the effects of residual stresses which result in microbending and, consequently, lead to attenuation; (2) hardening of the fiber-optic coating during the cure cycle; (3) strain transfer between the composite structure and the optical fiber; (4) signal degradation due to local stress concentrations at the points of ingress and egress, and, (5) multiple fiber interaction.

Eventually, the compatibility of the embedded fiber-optic sensor should be examined with respect to both thermoset and thermoplastic materials. Environmental testing should include exposure to relatively high and low temperatures in combination with various levels of humidity. Compatibility with automated manufacturing techniques should also be investigated, including filament winding, pultrusion, 3-dimensional

braiding, and compression molding.

Finally, of course, analytical techniques should be developed which can predict a correlation between the theoretical mechanical strain and the experimentally measured strain in the optical fiber. This knowledge should be used to establish procedures for determining the optimal fiber-optic sensor configurations in actual aerospace structures.

ACKNOWLEDGMENTS

The investigators would like to gratefully acknowledge the support of the Air Force Systems Comand, the Air Force Office of Scientific Research, Universal Energy Systems, and the Air Force Astronautics Laboratory. In particular, the authors would like to express sincere appreciation to the following AFAL employees for their expertise and assistance on so many aspects of this project: Lt. Douglas DeHart, principal investigator; Capt. Ted Doederlein, project manager; Mr. James Koury and Dr. Frank Fair, in-house consultants; and, of course, the technicians.

REFERENCES

1. Udd, E., "Fiber Optics Focus," OE Reports, Jun. 1988, p. 14.

2. Jen, C. K., Farnell, G. W., Parker, M., and Cielo, P., "A Fiber-Optic Damage Monitor," Review of Progress in Quantitative Nondestructive Evaluation, Vol. 4B, 1985, pp. 831-838.

3. Crane, R. M. and Macander, A. B., "A Fiber-Optic System for Damage Assessment of FRP Composite Structures," Naval Engineers Journal, Vol. 96, No. 6, Nov. 1984, pp. 52-56.

4. Dube, C. M., Wang, T. D., Jensen, D. W., and Koharchik, M., "Laboratory Feasibility Study of a Composite Embedded Fiber Optic Sensor for Measurement of Structural Vibrations," Dynamics Technology, Inc., SDIO 87-12 SBIR, Phase I Final Report, Feb. 1988.

5. Shelley, J., "Strength Decrement in Composite Materials due to Embedded Optical Fibers," B.S. Thesis, Department of Aerospace Engineering, The Pennsylvania State University, Apr. 29, 1988, 36 pp.

6. Uttam, D., Culshaw, B., Ward, J. D., and Carter, D., "Interferometric Optical Fiber Strain Measurement," Journal of Physics E: Scientific Instruments, Vol. 18, No. 4, Apr. 1985, pp. 290-293.

7. "Smart Space Structures," AFAL Project Directive 286400F4, Air Force Astronautics Laboratory, Jan. 1988.

1988 USAF-UES SUMMER FACULTY RESEARCH PROGRAM

GRADUATE STUDENT RESEARCH PROGRAM

Sponsored by the

AIR FORCE OFFICE OF SCIENTIFIC RESEARCH

Conducted by

Universal Energy Systems, Inc.

FINAL REPORT

Observer Design for the AFAL Grid Structure Using Low-frequency Accelerometer Data

Prepared by:	Mark A. Norris
Academic Rank:	Assistant Professor
Department:	Engineering Science and Mechanics
University:	Virginia Tech
Research Location:	USAF AFAL/VSSS Edwards AFB Edwards, CA 93523
USAF Researcher:	Dr. Alok Das

Date:	5 August 1988
Contract No:	F49620-87-R-0004

Observer Design for the AFAL Grid Structure Using Low-frequency Accelerometer Data

by

Mark A. Norris

ABSTRACT

Analytical and experimental results demonstrate the low-frequency response of accelerometers in a 1-G environment. It is concluded that for low-frequency response measurements, the dynamic effect of gravity on the accelerometer response cannot be ignored. The effect is demonstrated experimentally for pendulum motion and elastic vibration of the AFAL two-dimensional Grid structure. The results of analysis and experiment show that accelerometer nodal locations exist and predominantly occur in the lower modes of vibration. Furthermore, an observer is designed to account for the accelerometer nodal locations and the dynamic effect of gravity on the accelerometer measurements.

Acknowledgements

I take this opportunity to thank Dr. Alok Das for his technical advice and support of the research. The summer spent at the research cite was extremely valuable and interesting. My intentions are to continue the working relationship. In addition, I would like to thank Waid Schlaegel and Dr. R. C. Thompson for their technical expertise and friendship. I am also indebted to the graduate students, namely, Joel Berg, Steve Kahn and Lance Carter, for their hard work and support.

In addition, I thank the Astronautics Laboratory, the Air Force Systems Command, the Air Force Office of Scientific Research for sponsorship of this research and Universal Energy Systems who made this possible.

I. INTRODUCTION

Maneuver and vibration suppression strategies for flexible structures have received considerable attention in recent years. Numerous identification and control techniques have been proposed for active vibration suppression of large space structures (LSS) (Ref. 1-7). To test and evaluate the techniques, ground tests must be performed to determine their practicality, performance and robustness (Ref. 8).

My research interests lie in the area of identification and control of flexible structures. Moreover, my activities in this area have been supported through AFOSR and NASA since September 1982. My research goals include working with the design of structures in space, which includes the development and testing of robust identification and control algorithms suitable for flexible structures.

The Air Force Astronautics Laboratory (AFAL) has a facility particularly suited to ground-test identification and control algorithms for future flexible structures. A two-dimensional grid structure has been constructed and possesses the basic dynamic characteristics of future LSS, which includes low fundamental vibration frequencies and closely-space modes. Hence, working in this facility is of particular interest to me.

II. OBJECTIVES OF THE RESEARCH EFFORT

The ultimate goal of the research effort is to improve the identification and control methodology for flexible structures. To this end, the objectives include verifying and developing existing identification and control techniques for distributed spacecraft structures using both analytical and experimental results. Objectives of the effort included:

(1) developing an observer or estimator using accelerometer data as input which accounts for the dynamic effect of gravity as the accelerometer rotates in the 1-G environment. It was and is intended to use this observer for control purposes.

(2) account for the stiffening effect of gravity in the model for the AFAL Grid structure.

(3) examine and verify the existence of identification spillover.

(4) comparison of the Variational Modal Identification algorithm with other identification techniques.

(5) identify or update physical parameters such as modulus of elasticity, torsional stiffness, etc.

Objectives (2)-(5) were completed by Joel Berg, Steve Kahn and Lance Carter, who were summer graduates students under my supervision. Objective (1) is discussed in this report.

III. ACCELEROMETERS IN PENDULUM MOTION

We begin with the mechanical representation of a vibration measuring instrument as shown in Figure 1 (Refs. 9-11). The mass, damping, and spring stiffness of the instrument are denoted m, c,

and k, respectively. The displacement of the case, the displacement of the mass relative to the case, and the absolute respectively, so that $x(t)=y(t)+z(t)$. The relative displacement $z(t)$ is measured, which is used to infer the motion $y(t)$ of the case. From Newton's second law, the equation of motion can be written as (Ref. 9)

$$m\ddot{x}(t) + c(\dot{x}(t)-\dot{y}(t)) + k(x(t)-y(t)) = 0 \tag{1}$$

which upon eliminating $x(t)$ becomes

$$m\ddot{z}(t) + c\dot{z}(t) + kz(t) = -m\ddot{y}(t) \tag{2}$$

Note that the gravitational component of acceleration can be ignored as Eqs. (1) and (2) describe motion about the equilibrium position, where gravity is considered to be a static effect. Moreover, for harmonic motion of the case $y(t)$, the accelerometer can be designed such that (Ref. 11)

$$\omega_n^2 z \cong \omega^2 y \tag{3}$$

The accelerometer parameters, m, c and k, are designed such that $\omega \ll \omega_n$, where ω and ω_n denote the excitation frequency and the natural frequency of oscillation of the accelerometer, respectively. Hence, using Eq. (3), measuring z and knowing ω_n, the acceleration of the case $\ddot{y}=-\omega^2 y$ can be determined.

Consider the case where the accelerometer rotates in a gravitational field (Fig. 2). As will become evident, gravity can no longer be considered a static effect. Using Newton's second law, Eq. (2) now has the form

$$m\ddot{z}(t) + c\dot{z}(t) + kz(t) = -m\ddot{y}(t) - mg\sin\theta(t) \tag{4}$$

We consider the case where the accelerometer is mounted to estimate the tangential component of acceleration along a structure in pendulum motion. The tangential acceleration of the accelerometer casing is then $\ddot{y}=l\ddot{\theta}$, where l represents the radial distance from the accelerometer to the pendulum support. Using the small angle approximation $\sin\theta = y/l$, Eq. (4) becomes

$$m\ddot{z} + c\dot{z} + kz = -m\left(\ddot{y} + \frac{g}{l}y\right) \tag{5}$$

Note that in pendulum motion, the angular displacement $\theta(t)$ and the tangential acceleration are harmonic with frequency ω. It is obvious that the acceleration due to gravity is no longer a static effect for small pendulum motion of the accelerometer. Hence, in the case of pendulum motion, Eq. (3) becomes

$$\omega_n^2 z = \left(\omega^2 - \frac{g}{l}\right)y \tag{6}$$

Equation (6) indicates that the dynamic effect of gravity is to reduce the output amplitude of the accelerometer. Figure 3 displays experimental results of three piezoelectric accelerometers mounted on a rigid-bar in pendulum motion. The natural frequency of vibration of the pendulum, obtained experimentally, is $\omega = 4.9$ rad/s. The three accelerometers are placed at locations $l_1 = 0.34$ m, $l_2 = 0.41$ m, and $l_3 = 0.53$ m, respectively, along the rigid-bar. Note that the output of the accelerometer at location l_2 is nearly zero because $l_2 \cong g/\omega^2$, which designates the accelerometer nodal location for the pendulum. In addition, note the 180 degree phase difference between the output of accelerometers located at l_1 and l_3.

For structures in elastic vibration, the dynamic effect of

gravity may also disturb the output of the accelerometers. For elastic motion, however, the relationship between the translation and rotation of the accelerometer is no longer kinematic as in the case of pendulum motion. In order to determine this relationship, we resort to the equations of motion. Indeed, accelerometer nodal locations for structures in elastic motion can be found using the equations of motion governing the structures motion and they can be found for the modes of vibration individually. In the next section, we present the equations of motion for structures in elastic vibration.

IV. EQUATIONS OF MOTIONS FOR STRUCTURES

The equations of motion of a flexible structure can be written in the form of a partial differential equation given by (Ref. 12)

$$\mathcal{L}\, u(P,t) + m(P)\, \ddot{u}(P,t) = f(P,t) \tag{7}$$

where u(P,t) is the displacement of point P in the domain D, m(P) is the mass density and f(P,t) is the external force density. We consider the case in which the centrifugal forces can be ignored such that $\mathcal{L}$ is a self-adjoint positive-definite differential operator representing the system stiffness. Moreover, we assume that structural damping and gyroscopic forces are small enough to be neglected. The displacement u must satisfy prescribed boundary conditions. Associated with Eq. (7), we have the eigenvalue problem

$$\mathcal{L}\, \phi(P) = \lambda\, m(P)\, \phi(P) \tag{8}$$

The solution to Eq. (8) consists of a denumerably infinite set of real eigenfunctions $\phi_r(P)$ and associated real positive eigenvalues λ_r, which represent the mode shapes and square of the natural frequencies of oscillation, respectively. The infinite set of eigenfunctions are spatially orthogonal and can be normalized to satisfy the orthonormality conditions (Ref. 13). Using the expansion theorem (Ref. 13)

$$u(P,t) = \sum_{r=1}^{\infty} \phi_r(P)\, q_r(t) \tag{9}$$

and the orthonormality conditions, we can transform the equations of motion, Eqs. (7), into an infinite set of independent second-order ordinary differential modal equations

$$\ddot{q}_r(t) + \omega_r^2 q_r(t) = f_r(t) \tag{10}$$

where $\omega_r = \sqrt{\lambda_r}$, ω_r represent the natural frequencies of oscillation and $f_r(t)$ are modal forces given by

$$f_r(t) = \int_0 \phi_r(P)\, f(P,t)\, dD \tag{11}$$

V. NODAL LOCATIONS FOR ACCERLEROMETERS

In this section, we derive the accelerometer nodal locations for structures in elastic vibration, or nodal locations for any vibration-measuring instrument in which Eq. (4) holds. Before obtaining the nodal locations, we note that Eqs. (5) and (6) were obtained using the kinematic relation between the tangential and angular acceleration and assuming small motions of the pendulum about the static equilibrium position. For structures in elastic vibration, however, the relation between the acceleration $\ddot{y}$ and the angular acceleration $\ddot{\theta}(t)$ is no longer kinematic. To obtain

the relation, we use the equations of motion of the structure.

In linear motion, the displacement of the structure is small enough so that we can assume that $\ddot{y}$ coincides with the transverse acceleration $\ddot{u}_i = \ddot{u}(P_i, t)$ at a point P_i denoting the accelerometer location. Moreover, u represents the displacement from the static equilibrium position of the structure, so that $\theta(t)$ in Eq. (4) represents any nominal rotation about the equilibrium point as illustrated in Fig. (4) and is equal to u_i', which is the local slope at P_i with respect to the static equilibrium position. Hence, Eq. (4) becomes

$$m\ddot{z} + c\dot{z} + kz = -m\ddot{u}_i - mg\sin(\alpha_i + u_i') \tag{12}$$

where α_i is a constant denoting the angle between the vertical and the tangent to the structure in equilibrium at accelerometer location P_i. We assume that α_i can be computed using a static analysis. Using a small angle approximation, Eq. (12) becomes

$$m\ddot{w} + c\dot{w} + kw = -m\ddot{u}_i - mg(\cos\alpha_i)\, u_i' \tag{13}$$

where $w = z + mg\sin\alpha_i / k$ denotes the motion of the mass m in the accelerometer about its static equilibrium position.

The accelerometer is a vibration-measuring instrument designed such that the excitation frequency ω is much smaller than the natural frequency ω_n of the accelerometer $\omega << \omega_n$, so that inertia and damping forces in Eq. (13) may be neglected because they are quite small in comparison to the elastic spring force. Hence, Eq. (13) becomes

$$a_i = -\omega_n^2 w = \ddot{u}_i + g(\cos\alpha_i)\, u_i' \quad , \; i = 1, 2, \ldots, m \tag{14}$$

where a_i represents the output of the ith accelerometer. From Eqs. (9), (10) and (14), the accelerometer output a_i is then

$$a_i = \sum_{r=1}^{\infty} \{ [g(\cos\alpha_i)\, \phi_r'(P_i) - \omega_r^2 \phi_r(P_i)] q_r(t) + \phi_r(P_i) f_r(t) \} \tag{15}$$

where $\phi_r'(P_i)$ represents the slope of the rth mode of vibration at P_i. We consider the case of free vibration; i.e., $f_r(t)=0$ $(r=1,2,\ldots)$. At the accelerometer location P where $g\,\phi_r'(P_i) = \omega_r^2 \phi_r(P_i)$, the accelerometer output does not include the contribution to the acceleration of the rth mode. Hence, nodal accelerometer locations exist for modes of vibration that satisfy $g\,\phi_r'(P_i) = \omega_r^2 \phi_r(P)$. Examining Eq. (15), for higher natural frequencies the effect of gravity may be negligible, so that accelerometer nodal locations occur predominantly in the lower modes of vibration.

VI. OBSERVER IMPLEMENTATION

In this section, we develop an observer which uses as input accelerometer measurements. In general, the motion of a structure can be expressed as a linear combination of the lower modes of vibration simply because a large amount of energy is required to excite the higher modes. We consider a modal observer using only the lower modes of vibration.

The modal-state estimator has the form (Ref. 7)

$$\dot{\hat{\underline{v}}} = A\,\underline{v} + B\,\underline{f} + K(\underline{a} - \hat{\underline{a}}) \tag{16}$$

where $\hat{\underline{v}} = [\, \hat{q}_1\ \hat{q}_2 \ldots \hat{q}_n\ \dot{\hat{q}}_1\ \dot{\hat{q}}_2 \ldots \dot{\hat{q}}_n\,]^T$ is the state estimate vector, $\underline{f} = [\, f_1\ f_2\ \ldots\ f_n\,]^T$ is the modal force vector, $\underline{a} = [\, a_1\ a_2 \ldots a_m\,]^T$ and $\hat{\underline{a}} = [\, \hat{a}_1\ \hat{a}_2 \ldots\ \hat{a}_m\,]^T$ are the m-dimensional accelerometer

output and estimated output vectors, respectively, and A, B are plant matrices given by

$$A = \begin{bmatrix} 0 & \vdots & I \\ \cdots & \cdots & \cdots \\ -\Lambda & \vdots & 0 \end{bmatrix}, \quad B = \begin{bmatrix} 0 \\ \cdots \\ I \end{bmatrix} \tag{17}$$

Note that I is the nxn identity matrix, 0 is an nxn null matrix and Λ is an nxn diagonal matrix of eigenvalues corresponding to the lowest n modes of vibration. Furthermore, the matrix K is the observer gain matrix. If the system is treated as deterministic, Eq. (16) represents a Luenberger observer. If stochastic signals are considered, the gain matrix K may be designed to satisfy a Riccati equation in which case Eq. (16) represents a Kalman filter (Ref. 14). The associated output equation has the form

$$\hat{\underline{a}} = C\,\hat{\underline{v}} + D\,\underline{f} \tag{18}$$

where C and D are mx2n and mxn dimensional matrices, respectively, and from Eq. (15) their entries are given by

$$C_{rs} = 0\,, \quad D_{rs} = \phi_s(P_r)\,, \quad r = 1,2,\ldots,m\,;\ s = 1,2,\ldots,n$$

$$C_{rs} = q_j(\cos\alpha_r)\,\phi_s'(P_r) - \omega_s^2\,\phi_s(P_r)\,, \quad r = 1,2,\ldots,m\,;\ s = n+1, n+2,\ldots,2n \tag{19}$$

A necessary condition for observability of the modal-estimator requires that the matrix C contain only n zero columns.

VII. ANALYTICAL AND EXPERIMENTAL RESULTS

To determine the effects of gravity on the accelerometer measurements, an observer was implemented for the AFAL Grid structure (Ref. 8). The two-dimensional AFAL Grid structure is illustrated in Fig. 5. The observer was a modal-state estimator

given by Eqs. (16) and (17). The model used in the observer included the first four modes of vibration provided by a Nastran model of the Grid structure. For the experimental tests, damping was added to the first mode of vibration of the observer. The amount of damping was determined experimentally. The structure was excited using an electromagnetic shaker with frequency approximately equal to the first natural frequency of the structure, so that the response consisted mainly of the first mode of vibration. Four accelerometers a_i (i=1,2,3,4) and one shaker were placed as shown in Fig. 5, where the structure is suspended vertically so that d_i=0 (i=1,2,3,4) in Eq. (19). The output equation for the observer is given by Eq. (18).

Figure 6 presents experimental data where the structures response mainly consisted of the first mode of vibration due to the resonance excitation of the shaker. Note the phase shift between a_1 and the remaining accelerometer outputs. We use the steady-state accelerometer outputs shown in Fig. 6 as input to the observer. It was necessary to add damping in the first mode of vibration of the observer, due to the resonance excitation of the structure which is used as input to the observer through Eqs. (16) and (18). Furthermore, the damping added was experimentally observed for the first mode of vibration. The observer gains were computed using the solution of a Riccati equation with appropriate values for the noise intensities of the shaker and accelerometers, so that the observer is actually a Kalman filter.

We consider two cases. In the first, the observer was constructed by ignoring the gravitational effect on the accelerometer output using g=0 in Eq. (19). In the second case,

the dynamic effect of gravity on the accelerometer output is included. The steady-state output for the observer design ignoring gravity is shown in Fig. (7). Note that the observer predicts the accelerometer outputs to be in-phase. To predict the phase-shift in accelerometer a_1, we must include the dynamic effect of gravity on the accelerometers in the observer. The steady-state observer output including gravity is shown in Fig. 8. In this second case, the observer predicts a phase shift in accelerometer a_1, which is compatible with the experimental data. Furthermore, comparing Figs. 6 and 8, we note that the amplitudes of the accelerometer outputs predicted by the observer do not match the experimental data. This is due to the disagreement between the model and the actual structure. Namely, the damping in the actual structure has been experimentally observed to be nonlinear. Moreover, the additional dynamics of the shaker are not included in the Nastran model. Results have indicated that the shaker does not shift the natural frequencies of the structure significantly, however, it does alter the structures mode shapes.

VIII. RECOMMENDATIONS

There is a need for robust identification ond control algoritms for future flexible structures, such as large space structures (LSS), whose dynamical properties are characterized by low damping and low closely-spaced frequencies. In order to maneuver, dampen, shape or point these LSS, a reliable model and robust controller is required. To prepare for on-orbit

application, it is necessary to perform ground-tests with space ready hardware to evaluate and compare the different identification and control algorithms proposed in the literature. As shown in the preliminary results of this report, the dynamic effect of gravity must be carefully examined to successfully perform grund-tests when using accelerometers.

Identification techniques such as the Eigensystem Realization Algorithm, Moving Average techniques, the Ibrahim time domain method and the Variational Modal Identification algorithm are examples of time-domain techniques that should be compared. In many instances, hardware limitations will dictate alterations of these algoritms for on-orbit application. In addition, low-authority controllers, Independent Modal-Space Control, adaptive controllers are examples of control algorithms that can be evaluated for robustness and performance. To implement these controllers, it is necessary to estimate the state of the structure. The estimator must use as inputs for instance accelerometer and proximity sensor data, filter noise and produce an optimal estimate of the structures motion for control purposes. For ground-tests, this must be performed in a 1-G environment. Preliminary results indicate that an estimator can be implemented which uses low-frequency accelerometer data as input. It is recommended that ground-tests should be used to compare the techniques. Furthermore, it is recommended that the tests do not ignore the gravity effect on low-frequency accelerometer data.

IX. REFERENCES

1. Proceedings of the First VPI&SU/AIAA Symposium on Dynamics and Control of Large Structures, Blacksburg, Va, June 1977.

2. Proceedings of the Second VPI&SU/AIAA Symposium on Dynamics and Control of Large Structures, Blacksburg, Va, June 1979.

3. Proceedings of the Third VPI&SU/AIAA Symposium on Dynamics and Control of Large Structures, Blacksburg, Va, June 1981.

4. Proceedings of the Fourth VPI&SU/AIAA Symposium on Dynamics and Control of Large Structures, Blacksburg, Va, June 1983.

5. Proceedings of the Fifth VPI&SU/AIAA Symposium on Dynamics and Control of Large Structures, Blacksburg, Va, June 1985.

6. Proceedings of the Sixth VPI&SU/AIAA Symposium on Dynamics and Control of Large Structures, Blacksburg, Va, June 1987.

7. Balas, M. J., "Active Control of Flexible Systems," Journal of Optimization Theory and Applications, Vol. 25, No. 3, 1978, pp. 415-436.

8. Das, A., et. al., "Experiment and Parameter Estimation of Flexible Structures," Second NASA/DoD CSI Technology Conference, November 17-19, 1987.

9. Meirovitch, L. Elements of Vibration Analysis, McGraw-Hill, New York, N.Y., 1986.

10. Vierck, R. K., Vibration Analysis, Harper & Row, New

York, N.Y., 1979.

11. Doebelin, E. D., Measurement Systems, McGraw-Hill, New York, N.Y., 1966.

12. Meirovitch, L. and M. A. Norris, "Parameter Identification in Distributed Spacecraft Structures," The Journal of the Astronautical Sciences, Vol. 34, No. 4, October-December, 1986, pp. 341-353.

13. Meirovitch, L., Computational Methods in Structural Dynamics, Sijthoff & Noordhoff, The Netherlands, 1980.

14. Junkins, J. L., An Introduction to Optimal Estimation of Dynamical Systems, Sijthoff & Noordhoff, The Netherlands, 1976.

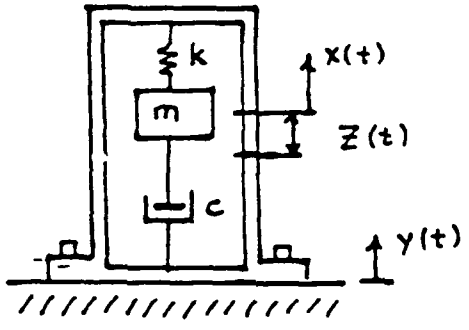


Fig. 1. Vibration Measuring Instrument

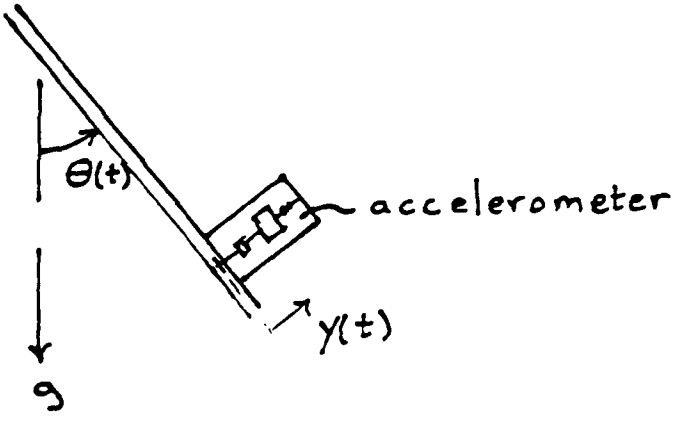


Fig. 2. Accelerometer in Pendulum Motion

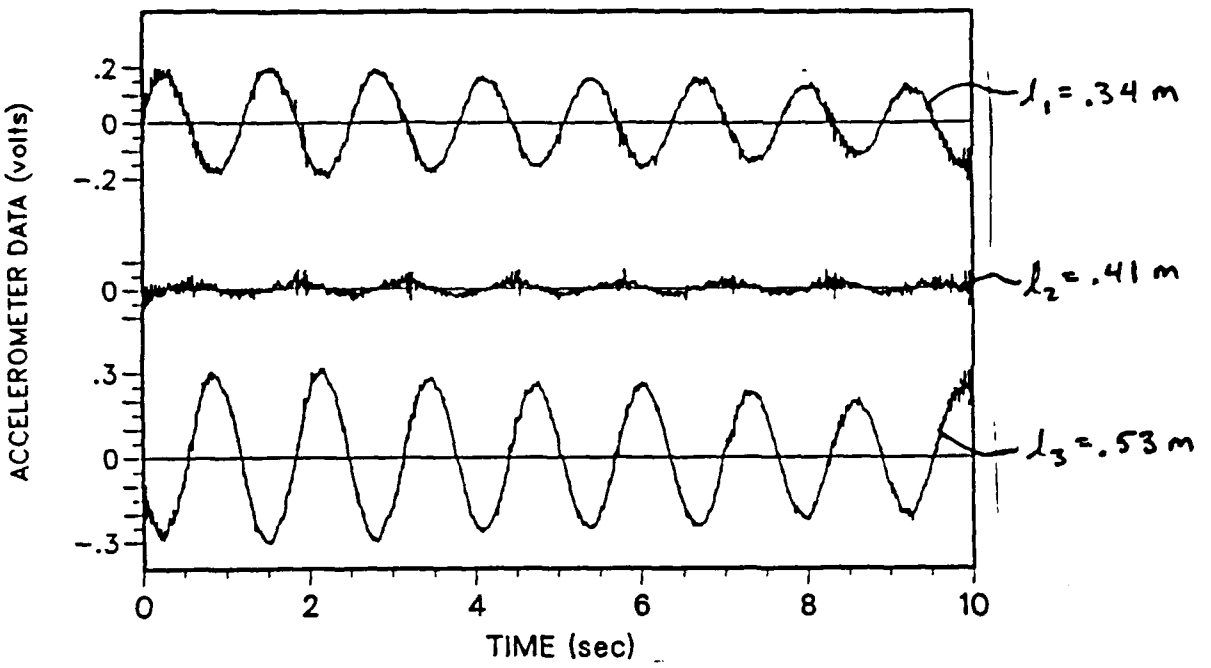


Fig. 3. Accelerometer Outputs For Pendulum Motion

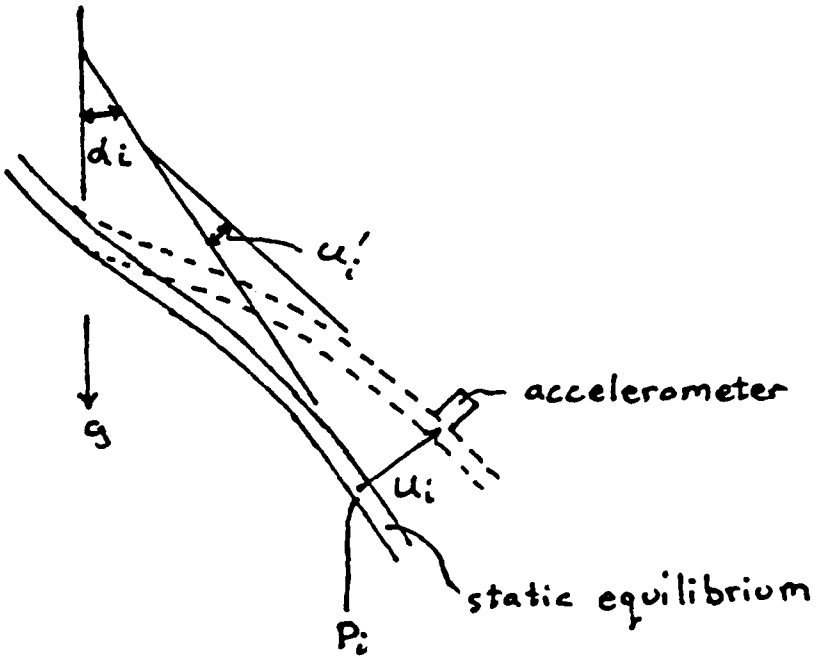


Fig. 4. Accelerometer Mounted on a Flexible Structure in 1-G.

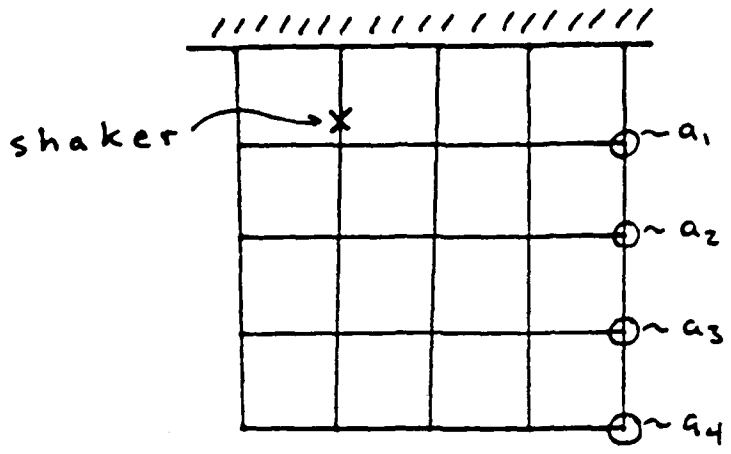


Fig. 5. AFAL Grid Illustration

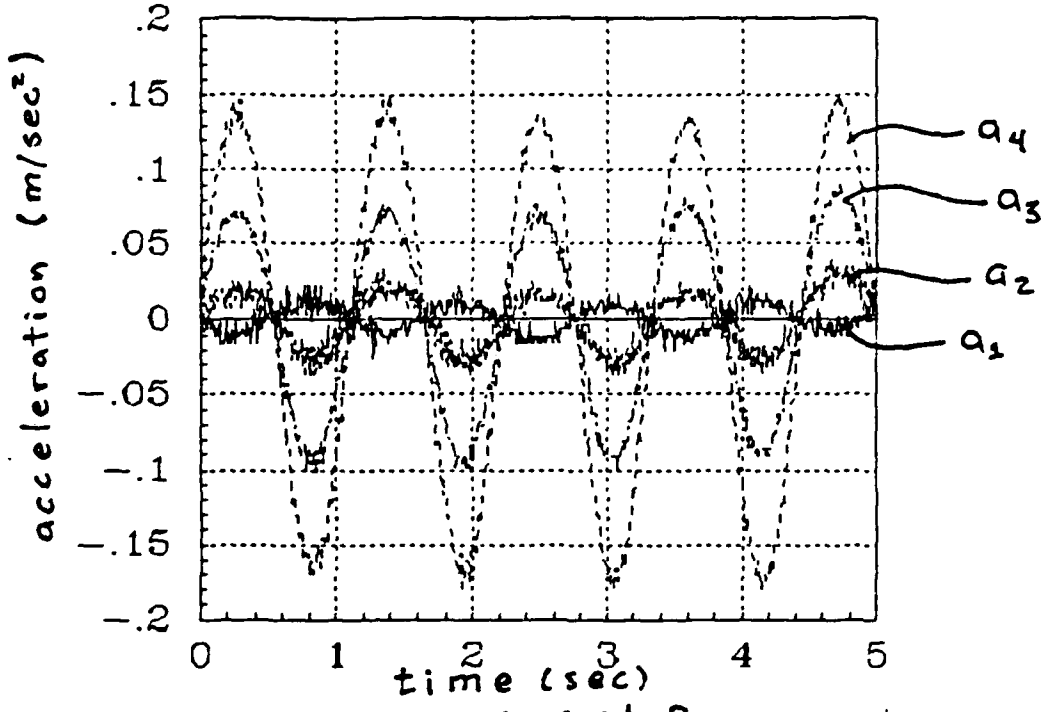


Fig.6. Experimental Grid Response to Resonance Excitation of Mode 1.

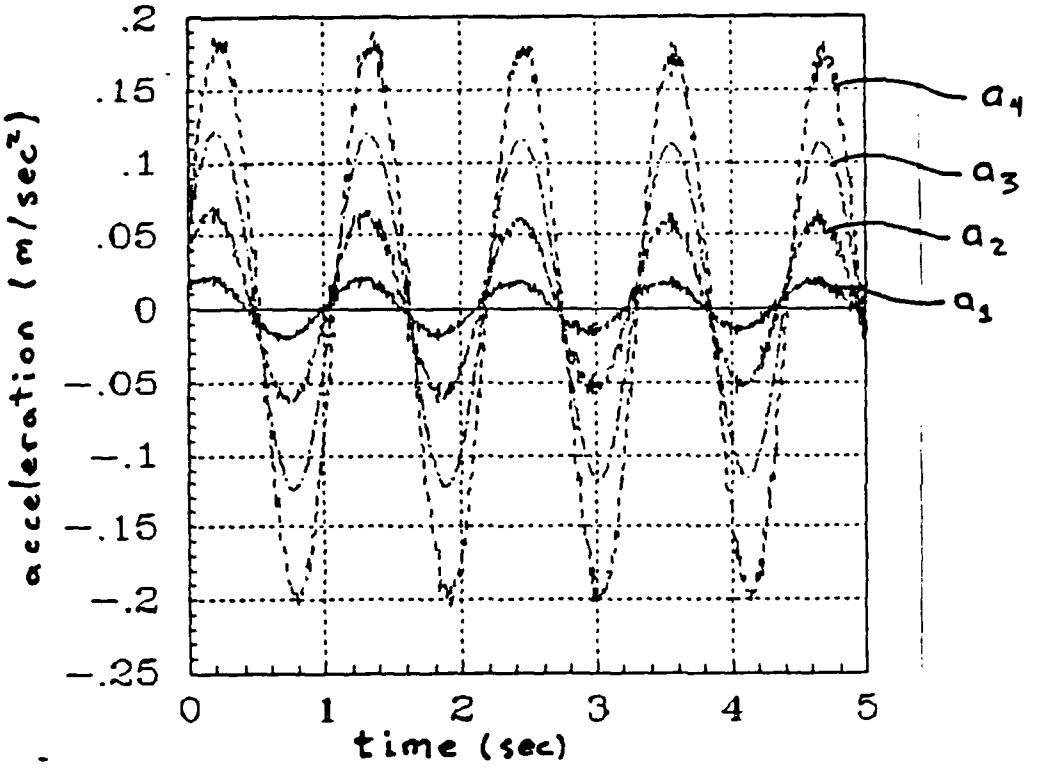


Fig. 7. Experimental Observer Response: Gravity Not Included.

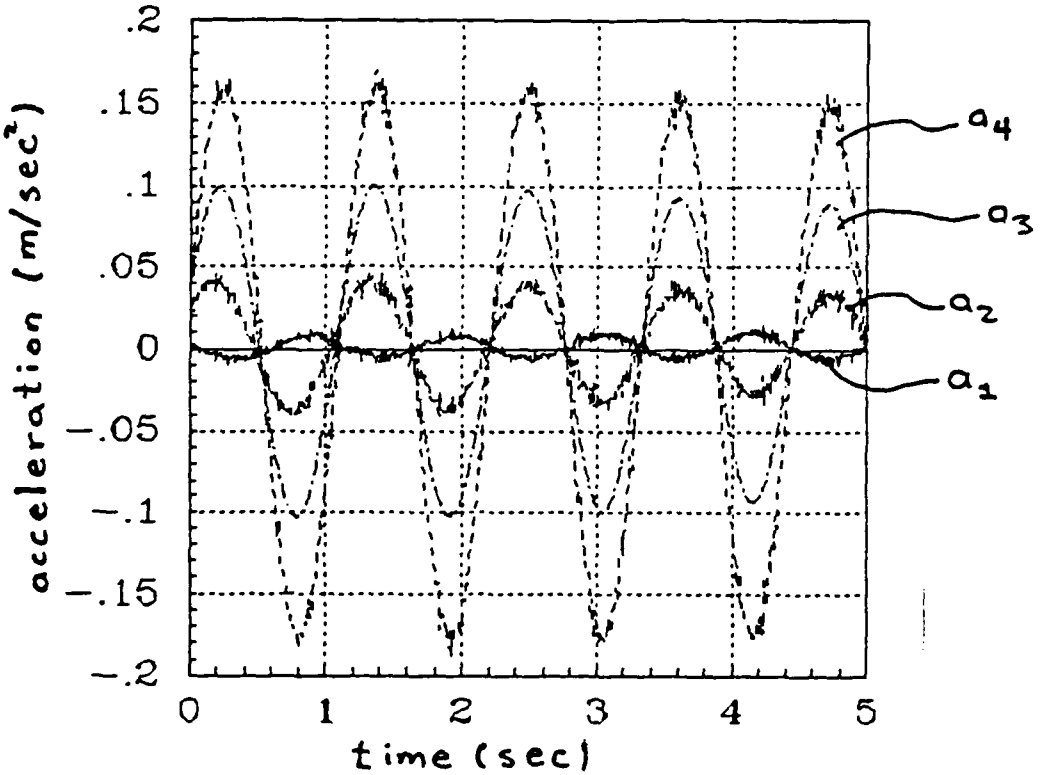


Fig. 8. Experimental Observer Response: Gravity Included.

1988 USAF-UES SUMMER FACULTY RESEARCH PROGRAM/

GRADUATE STUDENT RESEARCH PROGRAM

Sponsored by the

AIR FORCE OFFICE OF SCIENTIFIC RESEARCH

Conducted by the

Universal Energy Systems, Inc.

Final Report

PHOTOCHEMISTRY OF AZULENE SOLUTIONS AND A NOVEL PHOTOCHEMICAL NITRATION PROCESS

Prepared by:	Jodye I. Selco
Academic Rank:	Assistant Professor
Department and University:	Department of Chemistry University of Redlands
Research Location:	Air Force Astronautics Lab/LSX, Edwards Air Force Base, CA
USAF Researchers:	Dr. Patrick G. Carrick (Univ. of Dayton) Dr. Stephen L. Rodgers

Date:	30 August 1988
Contract No:	F49620-87-R-0004

PHOTOCHEMISTRY OF AZULENE SOLUTIONS AND A NOVEL PHOTOCHEMICAL NITRATION PROCESS

by

Jodye I. Selco

ABSTRACT

The solution phase photochemistry of azulene in various solvents was investigated using a variety of light sources. For the case of low power light sources, this process involves two photons of different colors and proceeds through one of the triplet states of azulene. It does not appear to be the triplet state itself that is involved in the photochemical process since they are not long lived enough to explain the secondary photon absorption. It is probably an optical isomer formed from the accessed triplet state that is involved in the chemical reaction following absorption of the secondary photon. The photochemical products formed include various products resulting from the reaction of azulene with a solvent molecule.

A novel photochemical nitration process has been investigated. This reaction involves the photodissociation of nitromethane and the subsequent attack on the solute molecule by the NO_2 radical formed during the photodissociation process. The solute used in this study was cyclohexane. Both nitrocyclohexane and dinitrocyclohexane were formed as a result of this novel photochemical process.

ACKNOWLEDGMENTS

The author would like to thank the Air Force Systems Command, Air Force Office of Scientific Research for sponsoring this research and the Air Force Astronautics Laboratory for providing me with the equipment used for this project. This summer fellowship program was administered by Universal Energy Systems, and they are gratefully acknowledged for their sponsorship. The author is also grateful for the assistance of and discussions with Dr. Stephen L. Rodgers, Dr. Partick G. Carrick and Dr. Suresh Suri at the Air Force Astronautics Laboratory.

I. INTRODUCTION

Azulene is an aromatic hydrocarbon that is a high energy isomer of naphthalene. It gains this energy in ring strain since azulene is a fused ring system containing a seven member carbon skeletal ring attached to a five member carbon ring, instead of the preferred two six-member fused ring system of naphthalene. As a result of this ring strain, more energy is gained upon combustion of azulene than of naphthalene. Higher energy compounds of azulene can be formed via the substitution of an atom or functional group for the hydrogen that is normally bound to the azulene skeleton.

When azulene is heated, it can convert to the lower energy isomer naphthalene.[1-8] Compounds of substituted azulenes are difficult to form by standard synthetic methods, because they usually involve the heating of reactants, and this is one of the methods of converting azulene to naphthalene. If these substituted azulenes can be formed as the result of a photochemical process, it can be cleaner and have higher yields than can be realized via standard synthetic methods. This photochemical process can also yield novel compounds that have not been produced so far by standard synthetic methods. Since these compounds are high energy systems, they have a high potential for fuels that yield more energy upon combustion than their lower energy counterparts.

Another form of high energy fuels that are currently being used contain a large number of nitro (NO_2) groups that are bound to carbon and/or nitrogen atoms of various unsaturated heteroatom hydrocarbon systems. The nitration of saturated hydrocarbons has long posed a problem to synthetic chemists. This reaction is difficult, messy and the

yields are low. If another method can be found that will nitrate compounds cleaner and with higher yields, more fuels can be made and tested for their effectiveness, and new fuels can be made available.

II. OBJECTIVES OF THE RESEARCH EFFORT

This research effort concentrated on photochemical methods of producing high energy content compounds. In the case of azulene, it is the azulene molecule itself that is involved in the induction of the chemical reaction. This enables reactions to occur between azulene and the solvent molecule, for all of the solvents investigated. In this manner, a great variety of substituted azulene compounds can be formed that have never been produced before. If large enough quantities of these compounds can be produced, their efficacy as fuels can be tested.

The investigation of a photochemical nitration process arose from the knowledge that nitro containing compounds usually make useful fuels and that standard nitration methods are not as efficient or effective as synthetic chemists would like. If a photochemical nitration method could be found that had higher yields of the desired compounds and resulted in solutions from which the desired compounds could be easily separated, new nitrated compounds could be formed and tested as fuels more easily than they had in the past.

III. Experimental

The azulene solutions investigated were approximately 5 x 10^{-4} M and irradiated while contained in standard 1 cm quartz cuvettes having a total volume of ~5 ml. Six different light sources were utilized for

irradiation. The excimer laser (Lambda Physik EMG 202 EMG) was filled with XeCl and had a lasing wavelength of 308 nm. When the 308 nm light was used for irradiation, a 50% reflector was used to cut down the amount of light being impinged upon the sample to avoid overheating the sample. It was also used to pump a dye laser (Lambda Physik FL 3002) that was frequency doubled to attain light of 240 nm.

Four cw lamp sources were also used to induce the observed photochemical reactions. Both a 150 W Xe lamp and a 200 W super high pressure Hg lamp (Oriel Housing #66005) were employed as well as a 20 W D_2 (Oriel #6330) lamp. The last lamp source was a Mercury Pen-Ray lamp (UVP SCT-1 with a #B213886 bulb).

All of the samples were analyzed by Gas Chromatograph-Mass Spectra (GCMS). A few of the samples were also subjected to thin layer chromatography (TLC).

In the case of the azulene samples, evidence of a photochemical occurance was indicated by a change in color that could be observed visually in the cuvette. The original azulene sample is blue; this solution turns aqua and then green when it is irradiated in the presence of a chlorinated solvent.

An EG&G optical multichannel analyzer (OMA) was also used to obtain ultra-violet and visible (UV-VIS) spectra. This instrument was also computer programmed to acquire a series of spectra as a function of real time.

An attempt was made to discern the photophysics of the azulene photochemical process. When it was discovered that the lamp sources could induce the desired reaction, it became evident that the

photophysics involved two photons of two different frequencies for the low light level sources. In these instances, a series of Schott cut-off filters and a 0.3 m monochromator (McPherson) were used to eliminate the undesired frequencies.

All of the samples used were research grade from Aldrich Chemical and were used without further purification. The solvents were all of high purity and also used without further purification.

IV. AZULENE PHOTOPHYSICS

In previous studies, a high power pulsed laser had been used to induce the photochemical reaction of azulene with various solvent molecules.[9] It had been assumed that the process being induced could only result from a single frequency multiphoton absorption in azulene. The error in this assumption was realized when an attempt was made to observe the UV-VIS absorption of the process by using the Xe lamp in conjunction with the OMA. After about 30 minutes of aligning the system and getting set up to take the absorption spectra at various times during a prolonged laser irradiation, it was observed that the reaction had been induced by the Xe lamp. This was evident by the color changes apparent in the cuvette; the solution was no longer blue, but aqua. An attempt was then made to discover the photophysics involved in the induction of the photochemical process.

By using a variety of Schott filters, it was discovered that the reaction did not proceed without light of wavelength <260 nm. When the 254 nm line of a mercury pen lamp was filtered through a 0.3 m monochromator and impinged upon the sample, no reaction was observed to

occur. When a Schott cutoff filter was used in front of a second light source, it was observed that when the two blue end lines (404 nm and 435 nm) were added to the 254 nm line a reaction could be observed. In trying to reproduce this effect, confusing results were obtained. Part of the problem in trying to reproduce this situation was that the 200 W Hg lamp was now being used as the source of the 254 nm line, but it could not be exclusively filtered out by the use of the 0.3 m monochromator. The filtered 254 nm light also included the violet line (404 nm) and the red line. This light alone also induced the observed reaction, but at a much slower rate. It was also observed that when the full output of the Hg pen lamp was impinged upon an azulene sample, the reaction could be induced to occur.

Due to the low light levels output by this source, it was concluded that the photophysics of the process must involve two photons, since no photochemistry had ever been observed in azulene with any great yield.[10,11] The one photon induction of the photochemical reaction has been investigated and found not to result in an observable reaction. The absorption of a photon in the region of 250 nm excites the S_3 state of azulene. The lifetime of the S_2 state of azulene has a lifetime of only ~2 ns,[12-15] and it is expected that the S_3 lifetime would be shorter. The lifetime of the longest lived triplet (T_1) is only 1 μs,[12] and does not seem long enough to enable the absorption of a second photon when the output powers of the light sources are taken into consideration. It is assumed that the triplet state accessed, decays into an optical isomer of azulene, maybe of the benzvalene type,[16,17] that lives long enough to absorb a second photon. No evidence of this optical isomer could be

found in the GCMS data, by UV-VIS absorption, or FTIR in the gas phase or in a matrix. The components that were identified by GCMS analysis for all experiments are listed in Table 1.

V. QUENCHING OF THE PHOTOCHEMICAL REACTION

Since the S_2 state of azulene is known to internally convert rapidly to vibrationally excited S_0,[15] it was assumed that the photochemical reaction proceeds through the triplet state. To test this hypothesis, solutions were made which contained azulene, the chlorinated solvent (CH_2Cl_2, or CCl_4) and a triplet specific quencher such as benzophenone, DABCO, 1,3,5-hexatriene, or naphthalene. These samples were irradiated with the D_2 lamp for over two hours. At the end of that time, very little color change could be observed. Although no quantitative rates could be discerned, the amount of color change observable by eye did increase with decreasing amount of added triplet quencher. When one of these samples was irradiated side-by-side with a sample which contained no triplet quencher, the rate difference was easily observable. In the unquenched sample, color changes were obvious within 5 minutes.

When these quencher containing samples were analyzed via GCMS, the major components were the azulene, the quencher (except in the case of DABCO), and small amounts of chloroazulene and dichloroazulene. A complete compilation of products are listed in Table I. In the cases of DABCO and hexatriene, evidence was found for a photochemically induced reaction involving the quencher molecule. As many as 5 different types of dimers of hexatriene were observed in the GCMS data. For DABCO, it

could be visually observed that a reaction had occured since the originally blue sample was now a violet solution that contained brown particulates.

VI. SAMPLE ANALYSIS

Since the photochemical azulene reaction results in the production of a product which is visibly colored, but whose color is different than that of the starting reactants, no other method was required to determine whether or not the reaction had taken place. One of the first separation methods used for this reaction was Thin Layer Chromatography (TLC). The only solvent found that would separate the compounds formed as the result of the photolytically induced reaction was a mixture of iso-propanol and water in a 3:1 ratio. When the silicate plates were spotted and then developed, 8 different visibly colored products could be observed. The colors of these compounds were forrest green, brown, aqua, aqua-blue, violet, orange, brown-green and yellow. No correlation between color and product identification has yet been made.

Another analysis method used was the injection of the reaction mixtures into a Hewlett-Packard GCMS which had a 25 m silicate coated capillary column. The temperature was initially 100°C and was ramped up to 200°C at the rate of 6°/min. Standard solutions of azulene in CH_2Cl_2 and azulene and naphthalene in CH_2Cl_2 were used to determine the retention times of authentic samples of these chemicals. Comparison to library mass spectra did enable the identification of some of the products, but for the most part, many of the compounds did not have authentic mass spectra in the NBS on-line library. The identity of these

samples were inferred from the starting reactants and a similarity to the corresponding naphthalene derivatives. A compilation of the products identified by this method are listed in Table I.

VII. NITRATION OF CYCLOHEXANE

A sample containing about 4.5 ml nitromethane and 0.5 ml cyclohexane was placed in a standard cuvette. The cyclohexane was not very miscible in the nitromethane, but the sample was shaken to mix these two compounds as well as possible. After shaking, most of the cyclohexane (by volume) was still sitting on top of the nitromethane. This sample was then exposed to the full output of the Hg pen lamp for two hours. Even by the end of this time no color change was observed.

This sample was analyzed by GCMS in the same manner as the azulene solutions. The three major compounds that did not travel down the column with the solvent front were cyclohexene, nitrocyclohexane and dinitrocyclohexane. No other report of such a photochemical nitration reaction of a saturated hydrocarbon could be found. The only similar report in the literature was of the nitration of an aromatic substituted benzene via the photolysis of tetranitromethane.[18]

It has been known for many years that when nitromethane is irradiated with the full output of a mercury arc lamp, it breaks into NO_2 and $CH_3\cdot$,[19] both of which are free radicals and capable of initiating radical reactions. It is presumed that this is the route by which this nitration proceeds although no direct evidence exists to support this conclusion.

VIII. CONCLUSIONS

Although a high power pulsed UV laser can induce the photochemical reaction in azulene, even a low power continuous light source such as a mercury Pen-Ray lamp can also induce this reaction to occur within 5 minutes. When the reaction results in the formation of substituted azulene, color changes are apparent within the sample.

Two photons of two different colors are required to induce the photochemical reactions observed for azulene. One of these photons needs to have a wavelength of <260 nm, and the second photon probably should have a wavelength of >260-410 nm.

This photochemical reaction can be noticeably slowed by including a triplet specific quencher in the sample solution. It is probably not the triplet state itself, but an optical isomer formed from this triplet state through which this reaction proceeds, although no direct evidence exists to support supposition.

Time resolved UV-VIS spectra were obtained for solutions of azulene in CH_2Cl_2 both with and without the triplet specific quencher naphthalene. The observed changes in the spectra indicate that in the presence of naphthalene, the reaction is greatly slowed, but that the overall spectral changes are the same whether or not naphthalene is present. The fact that naphthalene can be used as a triplet quencher in this case, indicates that it is the T_3 state of azulene that is active since it is the only one which is higher in energy than the naphthalene triplet.

The major products formed during this photochemical reaction of azulene with the solvent leads to products such as chloroazulene,

dichloroazulene, azulenecarboxaldehyde, nitroazulene (in nitromethane), cyanoazulene (in acetonitrile), as well as other products that are the result of inclusion of a solvent molecule, the oxidation of azulene or a substituted azulene and addition products such as dihydroazulene. There is also evidence that this reaction proceeds via a radical process since products such as hexachloroethane can be observed when the solvent is CCl_4.

A new nitration method has been discovered. Even a saturated hydrodarbon such as cyclohexane can be nitrated when it is dissolved in nitromethane and then irradiated with a mercury Pen-Ray lamp. Both nitrocyclohexane and dinitrocyclohexane were produced during this reaction.

IX. RECOMMENDATIONS

The frequency of the secondary photon required to induce the observed photochemical reaction induced in azulene needs to be determined. This can be done with the appropriate filters which were unavailable this summer.

A correlation needs to be made between the colors observed on the TLC plates and the compounds identified via GCMS. This will be done by using preparatory TLC plates, redissolving the compounds and reanalysis via GCMS following separation.

Quantitative studies of the quenching rates of various triplet specific quencher molecules need to be performed. This can be accomplished by studying the amounts of chloroazulene and dichloroazulene formed following the timed irradiation of standard solutions of azulene and various quenchers in a solution of a chlorinated solvent.

The novel nitration method of photochemical dissociation of nitromethane discovered this summer needs to be investigated further. Quantitative yields need to be determined. Longer irradiation times and/or more powerful mercury arc lamps need to be employed to determine whether or not a higher degree of nitration can be obtained. It does appear, however, that this method can be used to nitrate even saturated hydrocarbon based chemicals.

REFERENCES

1. E. Heilbronner, P.A. Plattner and K. Weiland, Experentia, 3, 70, (1947).

2. E. Heilbronner and K. Weiland, Helv. Chim. Acta, 30, 947, (1947).

3. L.T. Scott, J. Org. Chem., 49, 3021, (1984).

4. L.T. Scott, M.A. Kirms, A. Berg and P.E. Hansen, Tetrahed. Lett., 23, 1859, (1982).

5. U. Burger and J. Mareda, Tetrahed. Lett., 25, 177, (1984).

6. M.J.S. Dewer and K.M. Merz, J. Am. Chem. Soc., 107, 6111, (1985).

7. J. Becker, C. Wentrup, E. Katz and K. Zeller, J. Am. Chem. Soc., 102, 5110, (1980).

8. L.T. Scott, M.A. Kirms and B.L. Earl, J. Chem. Soc., Chem. Commun., 1983, 1373.

9. J. Selco, Final Report, Battelle Summer Faculty Fellowship, 1987.

10. J. Olmstead, Mol. Photochem., 1, 331, (1969).

11. M. Comtet and H.D. Mettee, Mol. Photochem., 2, 63, (1970).

12. P.M. Rentzepis, Chem. Phys. Lett., 3, 717, (1969).

13. H-J Kray and B. Nickel, Chem. Phys., 53, 235, (1980).

14. M. Orenstein, S. Kimel and S. Speiser, Chem. Phys. Lett., 58, 582, (1978).

15. Y. Hirata and E.C. Lim, J. Chem. Phys., 69, 3292, (1978).

16. K.E. Wilzbach, A.L. Harkness and L. Kaplan, J. Am. Chem. Soc., 90, 1116, (1968).

17. L. Kaplan and K.E. Wilzbach, J. Am. Chem. Soc., 90, 3291, (1968).

18. S. Sankararaman and J.K. Kochi, Recl. Trav. Chim. Pay-Bas., 105, 278, (1986).

19. J.G. Calvert and J.N. Pitts, Jr., Photochemistry, John Wiley and Sons, Inc., New York, 1966.

TABLE I

Solution Irradiated	Photoproducts
Azulene + CH_2Cl_2	Azulene Chloroazulene $C_{10}H_8CHCl$ (in ring) Dihydroazulene $C_{10}H_{11}Cl$ $C_{10}H_7CH_2Cl$ Dichloroazulene $C_{10}H_7CHO$ $C_{10}H_7N_2CO$ (?) Azoazulene (?) $C_{10}H_8N$ (?)
Azulene + $CHCl_3$	Azulenecarboxaldehyde Dichloroazulene $C_{10}H_8CO$ (not aldehyde) Chloroazulene $C_{10}H_6CO$ $C_{10}H_7CCO$ (?)
Azulene + CCl_4	Hexachloroethane C_9H_7Cl (chloroindene?) Azulene Chloroazulene Dichloroazulene $C_{10}H_6ClCOH$
Azulene + CH_3NO_2	$C_{10}H_7NO_2$ $C_{10}H_7CHO$ C_8H_{10} (?)
Azulene + CH_3CN	Dihydroazulene Azulene $C_{10}H_7COH$ $C_{10}H_7CN$
Azulene + Benzophenone + CH_2Cl_2	Azulene Benzophenone Chloroazulene
Azulene + DABCO + CH_2Cl_2	Azulene $C_{10}H_{10}CO$ Dihydroazulene DABCO $C_{10}H_8$ $C_{10}H_7CH_2Cl$ $C_{10}H_8CO$ $C_8H_{11}Cl$

Azulene + 1,3,5-Hexatriene + CCl_4	Azulene $C_9H_9CH_3$ $(Hexatriene\cdot)_2$ (4 types)
Azulene + 1,3,5-Hexatriene + CH_2Cl_2	C_8H_{10} C_8H_9COH Cyclooctatetraene $(Hexatriene\cdot)_2$ (5 types)
Cyclohexane + CH_3NO_2	Cyclohexene Nitrocyclohexane Dinitrohexane

1988 USAF-UES SUMMER FACULTY RESEARCH PROGRAM/

GRADUATE STUDENT RESEARCH PROGRAM

Sponsored by the

AIR FORCE OFFICE OF SCIENTIFIC RESEARCH

Conducted by the

Universal Energy Systems, Inc.

FINAL REPORT

INJECTION SYSTEM AND SPRAY CHARACTERISTICS

Prepared by:	Rameshwar P. Sharma, Ph.D.
Academic Rank:	Associate Professor
Department and	Mechanical Engineering
University:	Western Michigan University
Research Location:	Air Force Astronautics Laboratory AFAL/RKLA (Launch Vehicle Propulsion) Edwards AFB, CA 93523-5000
USAF Researcher:	Lt Angela B. Bartholomew
Date:	September 12, 1988
Contract No.:	F49620-87-R-0004

INJECTION SYSTEM AND SPRAY CHARACTERISTICS

BY

RAMESHWAR P. SHARMA

ABSTRACT

The atomization process in combustion applications has hundreds of publications and various theories related to liquid atomization as it applies to liquid rocket engines. A detailed literature search was conducted on atomization, spray characteristics, discharge coefficients, and various measurement techniques (for droplet velocity and size measurement). The published data are mostly empirical and only qualitatively understood with very little utility. The area of injector hydraulics is not very well understood. Very little or almost no data on atomization and mixing at high pressures are available with any reliability. This injector system and spray characteristics test project will help in establishing quantitative injector design criteria which will show the impact of injector design changes on C* performance, delta pressures, and thrust chamber compatability. This will also establish the cavitation limits and separation criteria. Most of the measurement techniques and test fixture design issues have been resolved. Many issues can only be resolved during the test setup calibration. Development of a mathematical model of this injector cold flow test setup is recommended from a future research and development point of view (for injector design, combustion, stability phenomenon and system performance) for rocket engines.

ACKNOWLEDGEMENTS

This research was sponsored by the Air Force Systems Command and The Air Force Office of Scientific Research under contract no. F49620-87-r-0004. The research was conducted at the Air Force Astronautics Laboratory(AFAL), Edwards AFB, under Universal Energy Systems Summer Faculty Research Program.

I wish to thank and appreciate the help of Lt. Angela Bartholomew, Mr. Wayne Roe, Capt. M. Walker, Mr. Bud Bocock, Mr. Tom Coultas, Mr. Don Penn, Ms. Jolene Lamb,Librarian, Dr. P. Kessel, during this study. Mr. Robert L. Wiswell provided me with support, encouragement and a truly enjoyable working atmosphere. I wish to thank Mr. Ninju Bohra, student at RPI, Ms. Carolyn Webb and Mr. Bruce Pham for their invaluable help in this study. The hospitality at AFAL will always be remembered.

I. Introduction

The atomization process in combustion applications has hundreds of publications, reviews and theories related to liquid atomization as it applies to liquid rocket engines. The published atomization data are mostly empirical and orly qualitatively understood. These are of very little utility and/or general validity. Still, very few theoretical models exist that describe the atomization process. Those that do exist, are only valid under limited or unrealistic conditions. Many of the critical parameters in the atomization process are unknown. Those that are known have not been studied enough so that they can be correctly modeled (e.g. gas densities, combustion flame motion).

The atomization and mixing performance data are required to establish injector design parameters and to have critical input data to liquid rocket engine combustor performance, stability, computer models and other methods. These performance models, such as Standardized Distributed Energy Release (SDER), Combustion Response Baseline Model, stability, etc. are forming the basis for the liquid oxygen/hydrocarbon injector methodology (under AFAL Contract F04611-85-C-0100). Advanced Rocket Injector combustor code is being developed under NASA/MSFC Contract NAS8-344928. Modeling of the liquid phase-atomization, droplet breakup and motion is currently not fully developed. The three computer programs (SDER, TPP, CICM) try to predict rocket combustion performance. In all three cases, it has been found necessary to "calibrate" the computer

model to achieve agreement with large-scale, rocket engine performance tests. Codes that are calibrated in such a manner can be relied upon to produce good results as long as they are applied to design and application conditions not different from those that they were calibrated against. However, the accuracy of the codes becomes increasingly questionable as they are applied to problems significantly different from the calibration points.

The properties of a liquid propellant that are important are the density, surface tension, and viscosity. The geometric variables of the injector that are important are orifice diameter, orifice length, orifice entrance conditions, free jet distance, impingement angle, and the number of orifices. The other parameters of importance (difficult-not understood well) are liquid velocity, velocity of combustion gases relative to the injected fluids (secondary injection) and the effects of combustion on atomization along with others.

After reviewing all the published literature, the area of injector hydraulics is not very well understood. Very little or almost no data on atomization and mixing at high pressures are available with any reliability.

II. Objectives of the Research Effort

The Air Force Astronautics Laboratory (AFAL) has started an in-house Injector Design Impact on Spray Characteristics test project for cold flow tests at high pressures and/with actual propellants. This project will help in establishing

quantitative injector design criteria which will show the impact of injector design changes on C* performance, delta pressures, and thrust chambers compatibility. This will also establish the cavitation limits and separation criteria. Figure 1 shows the schematic of the test setup.

The following objectives were set after discussing and reviewing the project with the project manager.:

1. To review the past and ongoing injector design, fabrication and testing project. This included the literature review.

2. To determine the relationship among various injector design variables and the discharge coefficient (for orifices).

3. To guide and assist in setting up the laser measuring system for spray and droplet sizes for the injection system.

III. Literature Review

The mechanism of atomization and its importance in applications has been studied and reviewed by various researchers. The mechanism for low-speed atomizing jets has been developed [1] For high-speed atomizing jets, various theories have been proposed and tested. Many of these still are in conflict and not tested. Reitz and Bracco [2] examined the validity of many of these and other proposed mechanisms for atomization with the help of various experiments. Experiments were reported with constant liquid pressures from 500 psia to 2500 psia with five different mixtures of water and glycerol into nitrogen, helium, and xenon with gas pressures up to 600 psia at room temperature. Injector nozzles with L/D ratios from 0.5 to 85 with sharp and round inlets of about 340 m diameter were used.

Castleman [3] postulated that atomization is due to aerodynamic interaction between the liquid and the gas leading to unstable wave growth on the liquid jet surface. Levich [4] analyzed this atomization model. The stability of infinitesimal waves on an axially symmetric jet surface of infinite length is considered. The flow is assumed to be incompressible. Sterling & Sleicher [5] and Taylor [6] analyzed and considered other conditions in droplet sizes and density.

Ranz [7] proposed that the droplet sizes are related to the wave lengths of the most unstable waves and further argued that the spreading angle theta of the atomizing jet is a function of densities and Reynolds & Weber numbers & wavelength.

DeJuhasz [8] proposed that the jet breakup process occurs within the nozzle itself and that liquid turbulence may play an important role. Schweitzer [9] suggested that the radial component of velocity in turbulent pipe flow could cause the immediate disruption of the jet at the nozzle exit. Holroyd [10] and Sitkei [11] proposed other mechanisms on the basis of liquid turbulence. Bergwerk [12] argued that the turbulent velocity components in the Reynolds number range of interest are not large enough to explain the atomization phenomenon. Bergwerk concluded that liquid cavitation phenomena inside the nozzle could create large amplitude pressure disturbances in the flow leading to atomization. Sadek [13] hypothesized that cavitation bubbles may influence the jet breakup process. Rupe [14] observed that high velocity laminar liquid jets could be more unstable than fully

developed turbulent jets. Rupe said that this is due to rearrangement in the cross-sectional velocity profile of the laminar jet once the constraint of the nozzle wall is removed at the nozzle exit. This redistribution of energy within the jet gives rise to radial velocity components which were thought to disrupt the jet. This effect is minimal for jets with flat exit velocity profiles which explained the greater stability that was observed for turbulent jets. Shkadov [15] investigated the effect of changes in interface tangential stresses in a boundary layer stability analysis and confirmed the existence of unstable short wavelength surface waves.

Giffen and Muraszew [16] reported that the liquid supply pressure oscillations have an effect on the outcome of the atomization process. These supply pressure oscillations are commonly found in injection systems. It has been suggested that they play an essential role in the atomization mechanism. Ferrenberg [17] at Rocketdyne, Rockwell International, investigated experimentally the injector atomization characteristics. They selected a droplet sizing interferometer (DSI), manufactured by Spectron Development Laboratories, for data collection in high pressure atomization tests.

They soon discovered that the DSI did not perform as desired with simple test data. As a result of being unable to resolve the problem of an overly dense spray, Rocketdyne decided to delete the high-pressure atomization testing and to do all

testing at atmospheric pressure.

The decision to conduct open-air tests was made although the extrapolation of the test results to the high-pressure conditions of interest would be difficult. Nearly all other atomization research programs have also been forced to conduct their tests at atmospheric conditions. No high-pressure atomization data exists for liquid rocket injectors except for limited data with coaxial injectors. Thus, a considerable need exists for high-pressure atomization data. Also, a lack of data to support extrapolation of atmospheric pressure data to high pressure remains.

For the literature review of discharge coefficients and the spray characteristics, the reader should see the AFAL Report on Injection System and Spray Characteristics.(88- No. to be assigned)

IV Test Setup

Figure 1 shows the schematic of the test setup for the cold flow injection system spray measurement. All the details of this test setup including high pressure chamber design are discussed in the project directive and design file. Basic design of the pressure chamber has been completed except a few of the issues on measurement window design, safety and measurement techniques. The pressure chamber spray measuring windows should be designed according to the following design and measurement criteria.:

Laser (Window) Measurement Design Considerations

- Quartz window surfaces should be flat within 1/4 of a wavelength at 6328A for each centimeter of the diameter.

- Window sizes:
Inlet window of 2 inch diameter with no obstructions between full diameter and spray recommended.(Minimum size 1 inch diameter).
Exit window of 4 inch diameter with no obstructions recommended. Exit window should be at least 1/2 inch larger than inlet window.
- Inlet and exit window faces should be out of parallel by 0.005 inch per inch of the diameter (closest at the top, where the top is set by the top face of the Malvern transmitter/receiver units).
- Individual windows should have parallel faces to within 15 seconds of arc.
- The bores of window housings and internal chamber surfaces should be light absorbing or at least not highly reflecting mirror finish.(e.g. sand blast)
-The alignment of transmitter/receiver must be co-axial and rigid (after adjustment).
- The transmitter/receiver must be aligned for both the windows such that the back reflection of the transmitter beam falls one centimeter above the exit aperture of the laser beam.

Measurement Considerations

- All the spray to be measured should be within the depth of field of the receiver lens (300mm for a 300mm focal length lens). Longer focal lengths will cover the 24 inch chamber easily but are not sensitive to the smaller size droplets.
- The separation of laser beam relative to the spray nozzle will determine obscuration; too close to the nozzle will give problems in the spray break-up region and too far away will bias the measurement towards the large droplets in the center of the spray.

- The data correction for high obsuration may be necessary.
- The Malvern laser is not sensitive to the velocity of droplets. Significant velocity profiled with size can bias the data toward slow moving large droplets.
- The sampling time is typically short for reasonable droplet densities where there is enough signal to noise ratio. Insufficient spray will require high gain option to smooth out the A/D bit noise. If you can see the droplet by eye, it will be all right.

One of the most important design criteria is that contamination of the measurement window should be avoided at any cost(particularly from the inside of the chamber). Many of the other testing and measurement issues were looked into and resolved. Some of these issues can only be resolved during the testing as they appear.

In baseline tests, the previously used injectors (in terms of basic design) are recommended for tests. In the beginning, the tests will have to be run to calibrate the test setup and spray measurement device. For this some of the low pressure flow tests should be conducted for which the basic flow and other discharge coefficient parameters are known to us. Once the reliability and the baseline of the test setup are established then the pressure should be raised to higher levels and the measurements should be made.

The project directive has a summary table of test run matrix and other schedules. This test matrix will have to be reviewed and modified once the limits of the test setup and measurement techniques are determined so that a complete load range is

tested without running all the test points.

V. Malvern Droplet and Particle Size Analyzer

A new method of measuring mean drop size and drop-size distribution is the Malvern Instruments Ltd., and relies upon the theories stated by Swithenbank et al [24].

The basis of diffraction methods of particle size analyzers, like the Malvern, lies in the portion of the Frensel-Kirchoff theory called the Fraunhofer diffraction theory. It describes the diffraction of the light around an opaque object. One of the limiting factors of the theory is that the area of the object illuminated must be within the same order of magnitude in size as the wavelength of light used. This is why normal, everyday objects do not have diffraction patterns around them. The pattern that results from the diffraction of a monochromatic light beam by a group of particles of a given size is a series of concentric rings with the intensity falling off with distance from the center. More importantly, the pattern of concentric rings varies with particle size. The smaller the object, the more distributed the light intensity becomes.

A key advantage of the Fraunhofer diffraction technique is that it does not require any calibration. The parameters are set by the instrument geometry and the laws of diffraction.

To extract the information from the diffraction pattern, the pattern is projected on a detector plate. The plate consists of 32 individual silicon photodiodes arranged in concentric rings. As distance from the center increases so does the sensitivity of the detectors to compensate for the diminishing

intensity of the diffraction rings. The readings from two adjacent detectors are usually combined, thereby reducing the data to 16 bands. To determine particle size information from the intensity readings, an iterative least square calculation is performed.

An initial size distribution, divided into 16 groups, is assumed either from raw data or the assumption of some particular form of distribution, e.g. Rosin Rammler. From this, a set of 16 corresponding light intensity values are calculated. The sum of the squares of the differences between these calculated values and those measured from the spray is then minimized by successively refining the assumed distribution. The logamatric of the absolute error is important in determining a faulty sample, and is known as the Log Error.

One factor that must be considered is the concentration of the sample. If the sample is too small, detection of the signal may be difficult which may result in unacceptable results due to large random errors. If the concentration is too large, systematic errors due to multiple scattering of the beam will be introduced. To protect against this problem, the Malvern incorporates two separate features. First of all, a number of samples of the spray are taken before the calculations are completed. After every spray, the intensities are stored and averaged with the other sprays. This allows the law of large numbers to come into play, thereby smoothing out any statistical fluctuations that may occur due to an irregularly

small spray. The second feature is an additional diode, located at the center of the detector plate. Any light that is not diffracted by the spray becomes focused on this detector, thereby giving a measure of the "beam obscuration". Values between 5% and 50% are ideal. The beam obscuration is also given in the table of data that is printed at the end of the testing. Recent developments in correcting the effects of multiple beam scattering in certain liquid sprays have enabled accurate measurements to be made with obscuration as high as 80%.

The equipment contained within the Malvern setup is similar to the majority of systems on the market today. The light from a low-power He-Ne laser (2mw) is expanded and collimated to a beam approximately 9mm in diameter. A background measurement of the environment is taken. Particles, whether they be dry powders, aerosols, or liquid sprays, pass through the beam and generate diffraction patterns. A Fourier transform lens focuses the pattern onto the detector plate. The intensity readings are then transferred to a personal computer for analysis. See Figure 2 for a diagram of the setup.

A correctly functioning fuel injector, when analyzed by a Malvern, will give a light distribution graph similar to the one shown in Figure 3a. Normally, there are many more small droplets than larger ones, therefore, the peak detector signal is registered by a detector in the middle to outer half. Notice that there is only one peak signal and that the intensity gradually falls off around this peak. This will become important in the detection and correction of a problem

known as beam steering. In addition notice that the log error is less than 5.0, a sign of good data. The log error, in spray analysis, is a statistical measure of the error between the ideal distribution and one that was experimentally obtained. A log error greater than 5.0 indicates that sufficient error has been introduced to make that data unacceptable. The log error for Figure 3a, is 4.10.

The Malvern Droplet and Particle Size Analyzer was designed for use in a wide range of atmospheric conditions. However, due to problems inherent to light there are situations in which alterations must be made to the equipment to insure acceptable results.

At high pressures and/or high temperatures, thermal gradients in the hot air cause random density gradients which refract the laser beam in a random high frequency pattern called "beam steering". This beam steering results in a spurious signal on the innermost detectors, with no spray present. However, the thermal gradients also affect the signal received by other channels when a spray is present, so it is not enough just to subtract out the background in an effort to correct the problem. In figure 3b, the light distribution curve has been altered to simulate the effect of beam steering.

There are two ways of knowing that the distribution in Figure 3b was unacceptable. First of all, there are two peak signals, one correct one and one due to the beam steering. Secondly, the log error is 6.30, which also signifies that the data is unacceptable.

Dodge and Cerwin [25] offer the following solution to this problem. First, determine the extent of the beam by counting how many channels were effected by the steering. Usually beam steering will only corrupt the first eight to ten channels. This is a limitation on the correction technique that must be observed if satisfactory results are to be obtained. After determining the faulty detectors, ignore the intensity readings obtained for these detectors and replace them with the ideal values, which are computed from the remaining values. As a check, generate a new light distribution curve and make sure that the new curve has only one peak signal, that the intensity falls off smoothly around the peak, and that the log error is less than 5.0. The results of this technique can be seen in Figure 3c. Notice that the curve is similar to Figure 3a in shape, and that the log error has been reduced significantly.

Another common problem with laser-diffraction methods is the high ambient light levels, especially those caused by hot gases or a combustion flame, that may affect the detectors light intensity readings. In ref. [25], Dodge and Cerwin offer a three step procedure to compensate for this problem.

VI. Recommendations

Once the test setup is complete and calibrated, from a future research point of view, the following is recommended.:

1. Development of a mathematical model to simulate the Injector Cold Flow Test Setup.
2. Development of a reliable performance model.
3. Use of other combustion models, in the future, to have a

Research and Development model for injector design and system performance for rocket engines.

VII. References

1. McCarthy, M. J., and Molloy, N. A., Chemical Eng. J.7, 1, 1974.

2. Reitz, R. D. and Bracco. F. V., "Mechanism of Atomization of a Liquid Jet," Physics Fluids, 25 (10), October, 1982.

3. Castleman, R. A., NACA Report No 440, 1932.

4. Levich, V. G., Physiochemical Hydrodynamics, Prentice Hall, NJ, 1962.

5. Sterling, A. M., and Sleicher, Jornal Fluid Mech., 68, 477, 1975.

6. Taylor, G. I. (Collected Works edited by G. K Batchelor), Cambridge, 1958.

7. Ranz, W. E., Can, J. Chem. Eng. 36, 175, 1958.

8. DeJuhasz, K.J., Trans. ASME 53, 65, 1931.

9. Schweitzer, P. H., Journal Appl Physics 8, 513, 1937.

10. Holroyd, H. B., J Franklin Inst 215, 93, 1933.

11. Sitkei, G., Acta Tech Acad Sci, Hungary 25, 87, 1959.

12. Bergwerk, W., Proc Inst Mech, England 173, 655, 1959.

13. Sadek, R., Proc. Inst. Mech. Eng. 173, 671, 1959.

14. Rupe,J. H., Jet Propulsion Laboratory Technical Report No 32, 1962, p 207.

15. Shkadov, V. Ya., Fluid Dyn. 5, 473, 1970.

16. Griffen, E.and Muraszew,A. " The Atomization of Liquid Spray ----," New York, 1970.

17. Ferrenberg, A., "Atomization and Mixing Study," Rockwell International Corp, NASA N86-23640, 1985.

18. Kuykendal, W. B., "The Effects of Injector Design Variables on Average Dropsize for Impinging Jets," AFRPL-TR-70-53, May, 1970.

19. Chew, T. J. C., "Hydraulic Flip Behavior in Typical Liquid Rocket Operating Regimes," AFRPL-TR-72-127, July, 1973.

20. George, D. J. et. al., "Holography as Applied to Jet Breakup and Analytical Method for Reducing Holographic Droplet Data," AFRPL-TR-72-72, September, 1972.

21. Dickinson, D. N., et. al., "Mass and Mixture Ratio Distribution Flow System," AFRPL TM-84-040, May, 1985.

22. Bowers, W. H. "STAR TECH Check-Out Injector," AFRPL TM-85-003, September, 1985.

23. Van Kleeck, J. A., et. al., "Tripropellant Cold Flow Investigation," Aerojet TechSystems Company, NLRDA4, Nov 1987.

24. Swithenbank,J. et. al., "A Laser Diagnostic Technique for the Measurement of Droplet and Particle Size Distribution," AIAA 14th Aerospace Sciences Meeting,AIAA paper #76-69,1976.

25. Dodge, L. G. and Cerwin, S. A., "Extending the Applicability of Diffraction-Based Drop Sizing Instruments," ASTM STP 848, 1984, pp. 72-81.

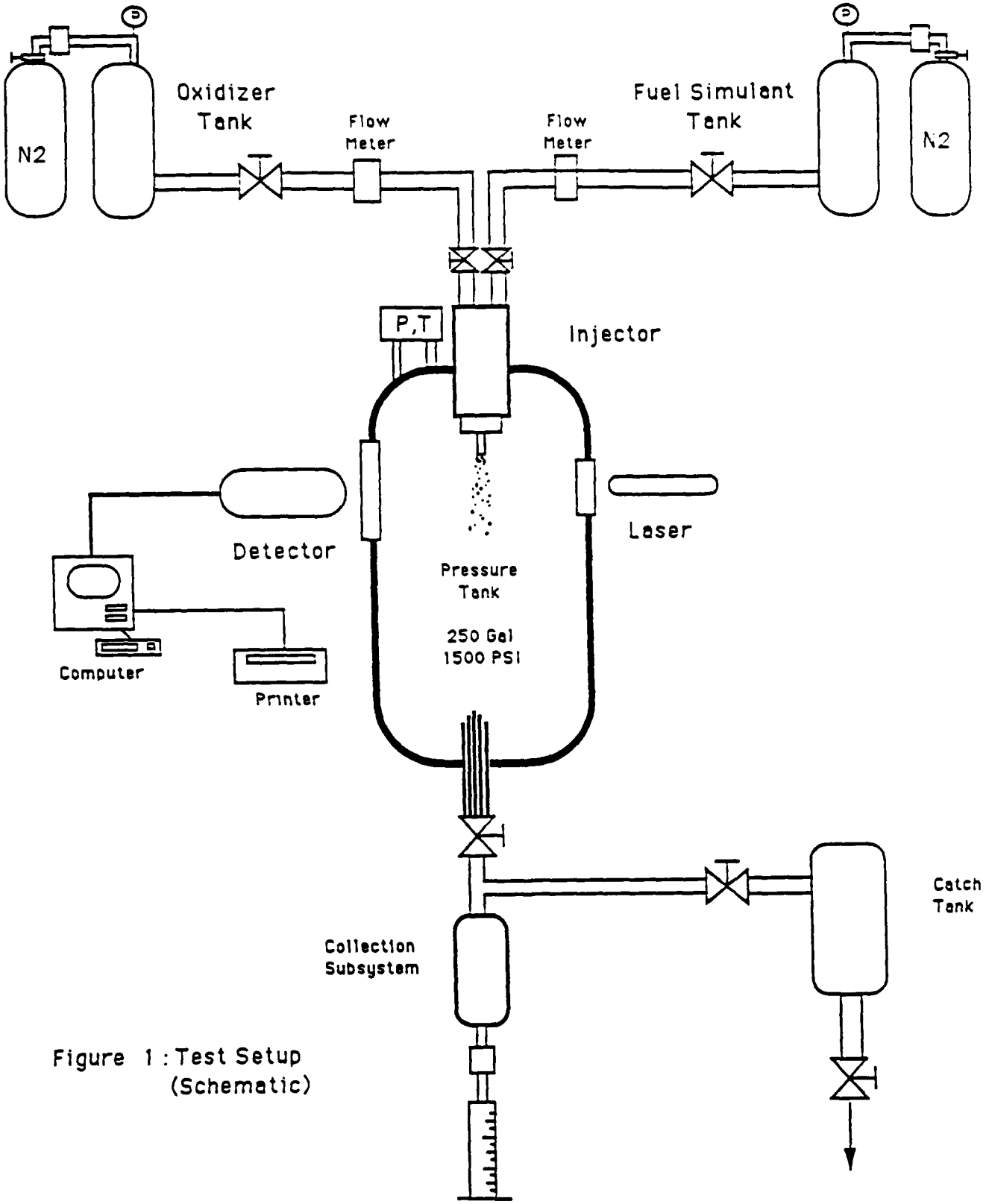


Figure 1 : Test Setup (Schematic)

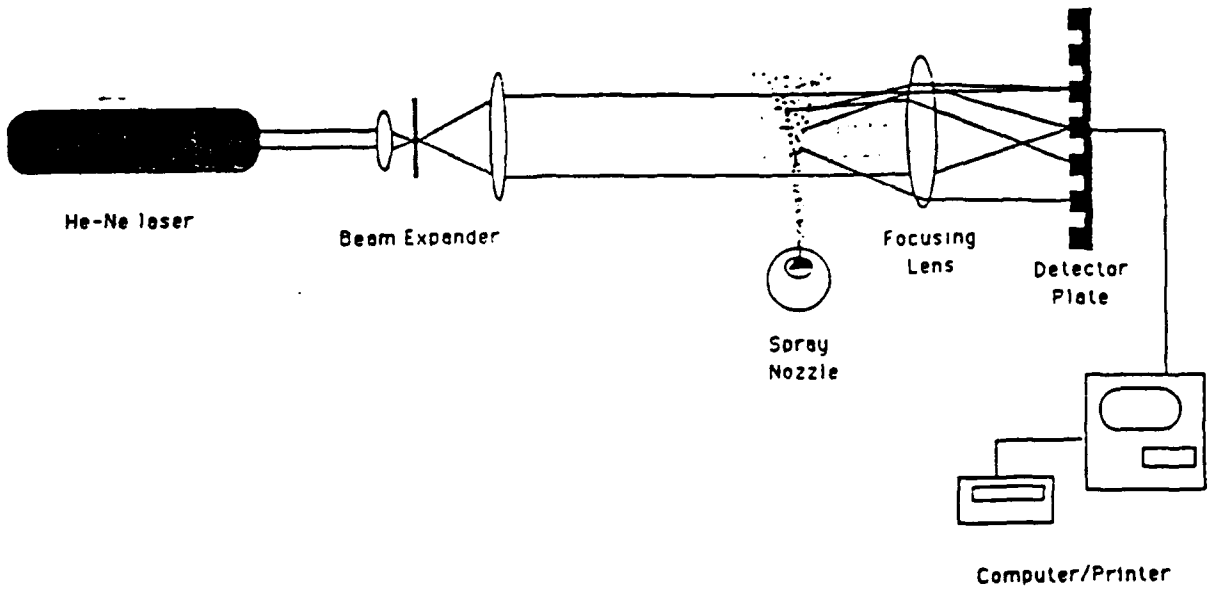


Figure 2 : The basic configuration of the Malvern Droplet and Particle Size Analyser

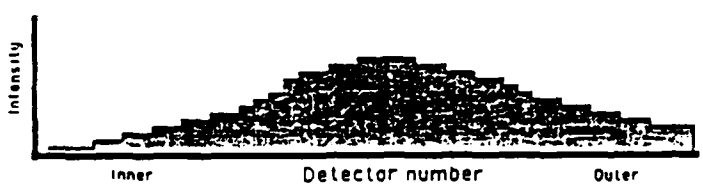


Figure 3a: Normal light scattering intensity signal on detector array, and drop size data.

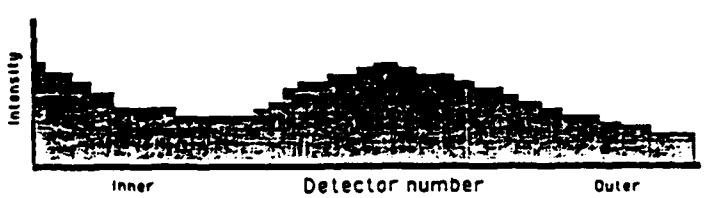


Figure 3b: Same light distribution that has been affected by beam steering

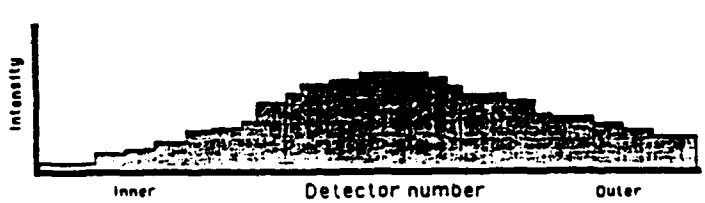


Figure 3c: New distribution after applying correction method described by Dodge and Cerwin

1988 USAF-UES SUMMER FACULTY RESEARCH PROGRAM

Sponsored by the

AIR FORCE OFFICE OF SCIENTIFIC RESEARCH

Conducted by the

Universal Energy System,Inc.

FINAL REPORT

Chemical Kinetic Mechanisms for $CH_4/NO_2/O_2$ Flames

Prepared by:	Trilochan Singh, Ph.D.
Academic Rank:	Professor
Department and	Mechanical Engineering
University:	Wayne State University, Detroit, MI
Research Location:	USAFAL/LSCC Edwards AFB, CA 93523
USAF Researcher:	David P. Weaver
Date :	August 25, 1988
Contract No :	F49620-87-R-0004

Chemical Kinetic Mechanisms for $CH_4/NO_2/O_2$ Flames

by

Trilochan Singh

ABSTRACT

The composition (37 species) profiles for a one-dimensional pre-mixed flame having $CH_4/NO_2/O_2$ ratio of .24/.56/.20 have been calculated. A chemical kinetic mechanism consisting of 160 reactions has been used for modelling the chemistry. The computed results and the experimental data of Branch et al. (4) show similar trends. The quantitative difference between the calculated composition profiles and the experimental composition profiles for CH_4, NO_2, NO, O_2, CO and CO_2 vary by a factor of 1.2 to 1.8. The computer program works over a wide range of initial reactant composition. The reasons for the differences between the computed profiles and the experimental profiles are attributed to the uncertainties in the flow rate, chemical kinetic mechanism and the rate data for various chemical reactions.

ACKNOWLEDGEMENTS

I wish to thank the Air Force Systems Command and the Air Force Office of Scientific Research for sponsorship of this research. Universal Energy System must be mentioned for their concern and help to me in all administrative and directional aspects of this program.

I also like to thank David P. Weaver, Captain J. Cor, Tim Edwards, Jeff Amfahr, Tracy Christensen , Frank Frederick, David Campbell,Larry Quinn and all other members of the Combustion Research Group at the Air Force Astronautical Laboratories for their help and co-operation in all aspects of the work.

CHEMICAL KINETICS MODELS FOR $CH_4/N_2/NO_2$ FLAMES

I. INTRODUCTION

Most solid rocket propellants are made up of complex chemical compounds of carbon, hydrogen, oxygen and nitrogen. The decomposition of these solid reactants leads to the formation of gaseous hydrocarbons and oxides of nitrogen which can react to support a flame above the surface.Current combustion models are limited in their ability to predict chemical phenomena occuring in ignition/flame spreading etc. at a level necessary to predict combustion behaviour a priori. A meeting of the JANNAF (Joint Army Navy NASA Air Force) panel entitled "Kinetic and Related Aspects of Propellant Combustion Chemistry" was held at John Hopkins University from May 2 to May 4, 1988. The scope of this panel is to focus on detailed propellant ignition and combustion chemistry and accelerate its inclusion into gun and propellant models. One of the recommendations of this meeting is that efforts should be directed to develop standarized national kinetic data base of for reactions of importance in the combustion of solid propellants and in particularly those involving nitrogen compounds.

II. OBJECTIVE

The objective of my summer 1988 (six weeks) research goal is to analyze one of the chemical kinetic models for $CH_4/NO_2/N_2/O_2$ flames. A number of mechanisms have been reported in the literature for hydrocarbon-nitrogen oxide flames (1-20).A chemical kinetic mechanism consisting of 160 reaction steps and 37 species was selected for analysis during the summer of 1988. Follow up work will be done with other chemical kinetic mechanisms.

III. LITERATURE REVIEW:

Thorne and co-workers(1) have studied low pressure (25 Torr) rich H_2-O_2-Ar flames seeded with various combinations of C_2H_2, HCN, and NO. A 9.7 cm-diameter pre-mixed flat flame burner was used for supporting the flame. Gas samples for mass spectrometric analysis were withdrawn through a quartz probe mounted above the burner. The compositon profiles of stable species such as O_2, CO, CO_2, N_2, NO etc. were obtained from mass spectrometric analysis. Relative concentrations of CN and CH are determined from LIF (Laser Induced Flourescent) signal intensity of the CN and CH transitions respectively. Thorne and co-workers(1) proposed a chemical kinetic mechanism consisting of 163 reactions. Out of this set, 11 reactions were considered as very important and 17 reactions were considered as important reactions for the conditions of their study(1).

Branch et al.(2) have reported temperature and composion profiles for stable species (CO, CO_2, H_2, NO, NO_2) in CH_2O/N_2O flames. They have proposed a set of 13 reactions , which are important for their flame conditions.

Bian, Vandoorem, and Van Tigglen (3) have reported on their experimental study of the structure of an ammonia-oxygen flame. They have proposed a set of 13 reactions mechanism to match their experimental data. The reaction $NH+O_2=NO+OH$ was found to play a significant role in the structure of their flame.

Branch and co-workers(4) have reported species (CH_4, O_2, CO, CO_2, NO, NO_2, N_2) profiles for $CH_4/NO_2/O_2$ flames at 50 torr. A set of 4 reactions have been suggested for initiation of the flame reactions.

Miller et. al. (5) have investigated the mechanism for converting HCN to NO and N_2 in low pressure (30 torr) H_2-O_2 flames doped with HCN and diluted with argon. They have suggested a 59 step reaction mechanism for the system. Of this set, 19 reactions

are considered to have significant effect on the structure of their flames.

Hepler and Smith (6) have reported on the numerical simulation of a Hydrazine/Nitrogen dioxide diffusion flame in a Burke-Schuman burner. They used a reaction set of 151 reactions for their simulation.

Glarborg and co-workers(7) have reported on the kinetic modelling of nitric oxide formation in methane combustion in well stirred reactors. They proposed a mechanism consisting of 213 reactions, out of which 10 reactions were considered as the most important reactions in NO formation from CH_4 combustion in well-stirred reactors. In addition to above, 7 reactions were considered important for their experimental conditions.

Smith and Thorne (8) have reported on the structure of two cyanogen-nitrogen dioxide flames. A set of 51 reactions was used for the flame simulation. 10 of these reactions were considered very important and 8 of these reactions were found to be important for their flame conditions.

Westbrook and co-workers (9-12) have reported on chemical kinetic models for the oxidation of higher order hydrocarbons (n-octane, iso-octane , n-butane etc.) They have proposed reaction mechanisms consisting of 465 and more reactions. Many of those reactions are not applicable for our case.

From this review it is seen that different sets of reaction mechanisms have been proposed for hydrocarbon-nitric oxide flames for various air fuel ratios. Most of the flame work has been done at low pressure. This work need to be extended to higher pressure and higher temperature regime which is more important for rocket propellant combustion. The reaction rate data for for a number of reactions used in these mechanisms have a large uncertainty. Therefore it is important that a sensitivity analysis for various

reactions be carried out over a wide range of fuel air ratios and pressure conditions and the results be compared with experimental data. This type of analysis will indicate the important/controlling reactions in the chemistry of hydrocarbons/nitric oxide flames.

The next step would be evaluation of available reaction rate data for the important reactions in the chemistry of hydrocarbon-nitrogen oxide flames. This analysis will enable us to prioritize the reactions to be included in the standarized national kinetic data base. The availability of this type of information will accelrate inclusion of these reaction mechanisms into gun and propellant models.

IV. COMPUTATIONAL MODEL:

A computer code for simulating the composition and temperature for a one-dimensional pre-mixed flat flame burner has been developed by the Sandia National Laboratory (21). This program was modified and made operational on the AFAL (Air Force Astronautical Laboratories) computing system during 1986 by Dr. Singh. The program accounts for the finite rate chemical kinetics and molecular transport. Finite difference approximations are made to discretize the governing conservation equations on a non-uniform grid from the cold boundary to the hot boundary. The Newton method is used for solving the problem. Global convergence of this algorithm is aided by invoking the time integration procedures when Newton method has convergence difficulties.

V. CHEMICAL KINETIC MECHANISM

A reaction mechanism for the combustion of $CH_4/NO_2/O_2$ flames consisting of 160 reactions and 37 species has been used for this study. The reaction set and the corresponding rate coefficients and references are shown in appendix I. The main features of the mechanisms are as follows:

Oxidation of H_2 and CO:

The oxidation of CO and H_2 play a significant part in the hydrocarbon combustion. The following reactions contain chain-branching steps that produce O, H and OH which attack the hydrocarbons.

$OH+H_2 = H_2O+H$

$H+O_2 = OH+O$

$O+H_2 = OH+H$

$OH+OH = H_2O+H$

There is considerable agreement on the rate data for these reactions (22).

CO is the primary product of hydrocarbon oxidation and is converted to CO_2 through the slow secondary reaction

$CO+OH=CO_2+H$

Formation and Consumption of CH_4:

In lean and moderately rich flames the hydrocarbon is attacked by radicals OH, O and H(22). These radicals are produced by chain branching steps of oxy-hydrocarbon reactions

$CH_4+M = CH_3+H+M$

$CH_4+H = CH_3+H_2$

$CH_4+OH = CH_3+H_2O$

$CH_4+O = CH_3+OH$

The resulting CH_3 reacts with radical species (O,OH,H) leading to the formation of CH_2O,CH_2,CH,C through reactions

$CH_3+O = CH_2O+H$

$CH_3+X = CH_2+HX$

$CH_2+X = CH+HX$

$CH+X = C+HX$

where X may be H,O,OH. The HCO radical is formed then by H atom abstraction, which decomposes leading to the yield of CO. This simple scheme is complicated by the recombination of CH_3(7) . Reactions involving CH_2, CH, C_2H_2, C_2H_3, CH_2O, HCO etc. are included in the mechanism shown in Appendix I. The rate

coefficients for a number of these reactions have a high degree of uncertainty associated with them. A number of reaction rate coefficients, for which experimental data are not available, have been estimated from the collision rate theory.

Reactions with Oxides of Nitrogen:

The presence of NO_2,N_2O and N_2 gives rise to hydrocarbon nitric oxide interactions. Thorne and co-workers (1) have suggested that the most important reactions for CH_4/NO_2 system are:

$CH_2+NO=HCNO+H$

$CH_2+NO=HCN+OH$

$H+HCNO=HCN+OH$

$CH+NO=HCN+O$

$C+NO=CN+O$

These and other possible reactions involving HCN, OH, NH, NH_2, NH_3 are shown in appendix I. The chemistry for hydrocarbon/nitric oxide is very complex and requires detailed analysis and comparison with experimental data. For the purpose of this initial short term study , the mechanism shown in appendix I has been used for simulating the composition profiles for one flame having $CH_4/NO_2/O_2$ ratio of .24/.56/.20

Computer Runs:

The computer program for the simulation of one-dimensional premixed laminar flame was run for different ratios of reactants CH_4,NO_2,N_2O,N_2 and O_2. One of the limitation of this flame program is that one has to provide reasonable initial estimates for the composition (37 species in this case) and temperature profile. The first run takes several hours to complete. The subsequent runs are started by using a restart file (for initial estimate of composition and temperature profile). Dr. Singh had completed a run for a flame having $CH_4/N_2O/N_2$ ratio of .13/.8/.07 during a previous visit to the AFAL in March 1988. The restart file from this run was used as a starting point. CH_4 mole fraction was varied from 0.13 to 0.24 in

steps of 0.01. NO_2 mole fraction was increased from 0.0 to 0.56 insteps of 0.01. N_2O mole fraction was decreased in steps of 0.01. This process was continued till the desired flame conditions having $CH_4/NO_2/O_2$ ratio of .24/.56/.20 was reached. These 60 runs took almost 4 weeks to complete. Each individual run took anywhere from 3 minutes to 3 hours. Higher incremental changes in the reactant composition from one one run to the next run did not lead to the convergence in spite of overnight runs. The flames having burning velocities of less than 35 cm/sec took longer time to converge. A number of flames having $CH_4/NO_2/N_2O/N_2$ ratio of .25/.58/.13/.04, .16/.77/.02/.05 etc. did not converge to a solution even after overnight runs. The exact reasons for non-convergence are not known and need to be investigated.

VI. RESULTS:

A sample output for a flame having $CH_4/NO_2/O_2$ ratio of .24/.56/.2 is shown in appendix II. Branch et al. (4) have reported experimental temperature and composition of stable species for this flame. The total flow rate for the system is not given in the refrence and the authors are being contacted for this information. Two flow rates of 0.04 gm/cm2-sec and 0.01 gm/cm2-sec were assumed for this study. Some of the results from appendix II are shown in Fig. 1-5.

Fig. 1 shows the comparison between the computed mole fraction for CH_4 and Branch's experimental data.(4) The agreement is not good at the flow rate of .04 gm/cm^2-sec but is slighty better at a flow rate of .01 gm/cm^2-sec. for CH_4 mole fraction. Similar trends are exhibited for CO_2, CO and NO in Fig. 2,3 and 4 respectively. Fig. 5 shows the comparison between the computed mole fraction and experimental profile for NO_2 and O_2.

A review of the Fig. 2 shows that that the computed rate for initial formation of CO_2 is slower than the corresponding experimental data . However at a distance of about 1 cm above the

burner surface the computed mole fraction of CO_2 is closer to the experimental value.

Fig. 3 shows that the agreement for CO mole fraction between the experimental data and the computed results is not good. The agreement for NO between the computed mole fraction and the experimental data of reference(4) is also not good as shown in Fig. 4.

Fig. 5 shows that the computed initial rate of disappearance for NO_2 is slower as compared to the experimental data. The computed mole fraction for NO_2 at a distance of 1 cm above the burner surface is closer to the experimental value.

The reasons for the disagreement need to be investigated. There is no time left to carry out this part of the analysis. The reasons for the difference between the experimental data and the computed results can be attributed to the uncertainties in the flow rates , the proposed mechanism and the associated rate data. A proposal for follow-up work related to this aspect will be submitted.

VII. Conclusions and Recommendations:

1. Composition profiles (37 species) for flame having $CH_4/NO_2/O_2$ ratio of .24/.56/.20 have been computed for a one-dimensional pre-mixed flame . The simulation program works over a wide range of fuel air ratio. A chemical kinetic mechanism consisting of 160 reactions and 37 species has been used for these calculations.

2. The agreement between the computed profiles of CH_4, O_2, NO_2, N_2, NO, CO, and CO_2 is not good. The qualitative trends are similar. The quantitative values differ by a factor of 1.2 to 8.

3. The reasons for the quantitative differences between the computed data and experimental data need to be investigated. These differences are attributable to the uncertainties in the flow rate, chemical kinetic mechanism and the rate data associated with the various reactions.

4. Only limited experimental data are available for hydrocarbon/nitrogen oxides flames at low pressures (30 torrs to 50 torrs). The experimental data for temperature profile and composition profiles are needed at higher pressures and higher temperature over a wider range of fuel oxidant ratios. This presents new challenges and difficulties, which need to be addressed.

5. A sensitivity analysis for various reactions (as to their contribution to the production rate of various species) need to be completed. This will help to point out the important reaction paths in the hydrocarbon-nitric oxide chemistry.

References:

1 Thorne, L.R., Branch, M.C., Chandler, D.W., and Kee, R.J., " Hydrocarbon/Nitric Oxide Interactions in Low-Pressure Flames", Twenty-first Symposium (International) on Combustion, the Combustion Institute, pp. 965-977, 1986.

2. Branch, M.C., and Sadeqi,M., "Structure of Laminar, Premixed Flames of CH2O/NO2/O2 Mixtures", 24th JANNAF Combustion Meeting, 1987.

3 Bian,j., Vandooren, J., and Van Tigglen, P.J., "Experimental Study of an Ammonia-Oxygen Flame", Twenty-first Symposium (International) on Combustion, the Combustion Institute, pp. 953-963, 1986.

4. Branch,M.C., Alfarayedhi,A. and Sadeqi,M.,"Structure of Flames Associated with Nitramine Solid Propellants",Western States Section/Combustion Institute Spring Technical Meeting, Paper No. 87-20, Provo Utah, April 1987.

5. Miller, J.A., Branch,M.C., McLean, W.J., Chandler,D.W., Smooke,M.D., and Kee,R.J., "The Conversion of HCN to NO and N2 in H2-O2-HCN-Ar Flames at Low Pressures", Twentieth Symposium (International) on Combustion, the Combustion Institute, pp 673-684, 1984.

6. Hepler,W.A., and Smith,O.I.,"Numerical Simulation of a Hydrazine/Nitrogen Oxide Diffusion Flames in Burke-Schumann Burner", Western States Section/Combustion Institute Spring Technical Meeting, Paper # WSS/CI 87-23, Provo Utah, April 1987.

7. Glarborg, P., Miller,J.A., and Kee, R.J., "Kinetic Modelling and Sensitivity Analysis of Nitrogen Oxide Formation in Well-Stirred Reactors", Combustion and Flames 65:177-202 (1986).

8. Smith, O.I., and Thorne, R.L.,"The Structure of Cyanogen-Nitrogen Dioxide Premixed Flames"'Western States Section/Combustion Institute 1986 Fall Technical Meeting ,paper # WSS/CI 86-34, Tuscon Arizona, October 1986.

9. Axelsson, E.I., Brezinsky,K., Dryer, F.L., Pitz, W.J., and Westbrook, C.K., " Chemical Kinetic Modelling of the Oxidation of Large Alkane Fuels: n-Octane and Iso-Octane", Twenty -First Symposium (International) on Combustion, The Combustion Institute, pp 783-793. , 1986

10. Wilk, R.D., Cernansky, N.P., Pitz, W.J., and Westbrook, C.K., "Propene Oxidation at Low and Intermediate Temperatures: A Detailed Chemical Kinetic Study", 1987 Spring Technical Meeting of the Western States Section of the Combustion Institute Paper and Lawrence Livermore National Laboratory Preprint UCRL- 96404, March 1987.

11. Westbrook, C.K., and Axelsson, E., "Development of a Detailed Kinetic Reaction Mechanism for the Oxidation of N-Octane and Iso-Octane ", Western States Section of the Combustion Institute, 1985 Fall Meeting and Lawerence Livermore National Laboratory report UCRL-PREPRINT 93420, October 1985.

12. Pitz, W.J., and Westbrook, C.K., " Chemical Kinetics of the High Pressure Oxidation of n-Butane and Its Relation to Engine Knock", Combustion and Flame 63:113-133 (1986)

13. Heimrl,J.M., and Coffee,T.,P. , "Transport Algorithms for Methane Flames", US Army Ballistic Research Laboratory, Technical Report ARBRL-TR-02512, July 1983.

14.Mann, D.M., and Weaver,D.P., "An Optical and Mass Spectrometric Study of the Aluminum-Oxygen Flame", Air Force Rocket Propulsion Laboratory, Edwards AFB Technical Report, AFRPL TR-84-053, August 1984.

15. Perry,R.A., and Melius,C.F., "The Rate and Mechanism of the Reaction of HCN with Oxygen Atoms Over the Temperature Range 540-900 K", Western States Section of the Combustion Institute, Paper WSS/CI- 84-37, April 1984.

16. Miller, J.A., Parrish,C., and Brown, N.J., "A Statistical-Theoretical Investigation of the Thermal Rate Coefficient and Branching Ratio for the Reaction O+HCN = Products ", 1985 Fall Meeting of the Western States Section of the Combustion Institute, Paper WSS/CI 85-33, October 1985.

17. Miller, J.A., Kee, R.J., Smooke,M.D., and Grcar,J.F., "The Computation of the Structure and Extinction Limit of Methane-Air Stagnation Point Diffusion Flame", 1984 Spring Meeting of the Western States Section of the Combustion Institute, University of Colorado, Paper WSS/Ci 84-10, April 1984.

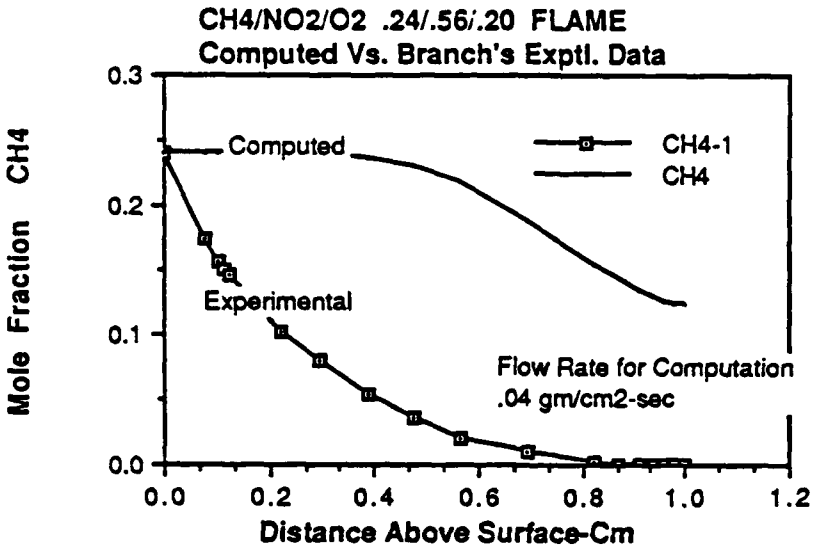
18. Pitz,W.J., Westbrook, C.K., Proscia, W.M., and Dryer, F.I.., "A Comprehensive Chemical Kinetic Reaction Mechanism for the Oxidation of n-Butane", Twentieth Symposium (International) on Combustion, The Combustion Institute, p. 831, 1985.

19. Joklik, R.G., Daily, J.W., and Pitz, W.J., "Measurements of CH Radical Concentrations in an Acetylene/Oxygen Flame and Comparison to Modelling Calculations", Twenty-first Symposium (International) on Combustion, the Combustion Institute, pp. 895-904, 1986.

20. Benson, S.W., "Combustion, a Chemical and Kinetic View", Twenty-first Symposium (International) on Combustion, the Combustion Institute, pp. 703-711, 1986.

21. Kee, R.J., Grcar, J.F., Smooke, M.D., and Miller, J.A., "A Fortan Program for Modelling Steady Laminar One-Dimensional Premixed Flames", Sandia National Laboratories Report, SANDS-8240, Dec. 1985.

22. Warnatz,J., "The Structure of Laminar Alkane-,Alkene-, and Acetylene Flames", Eighteenth Symposium (International) on Combustion, the Combustion Institute, pp 369-384, 1981


CH4/NO2/O2 .24/.56/.20 FLAME
Computed Vs. Branch's Exptl. Data
Mole Fraction CH4
0.3
0.2
0.1
0.0
Computed
CH4-1
CH4
Experimental
Flow Rate for Computation
.04 gm/cm2-sec
0.0
0.2
0.4
0.6
0.8
1.0
1.2
Distance Above Surface-Cm

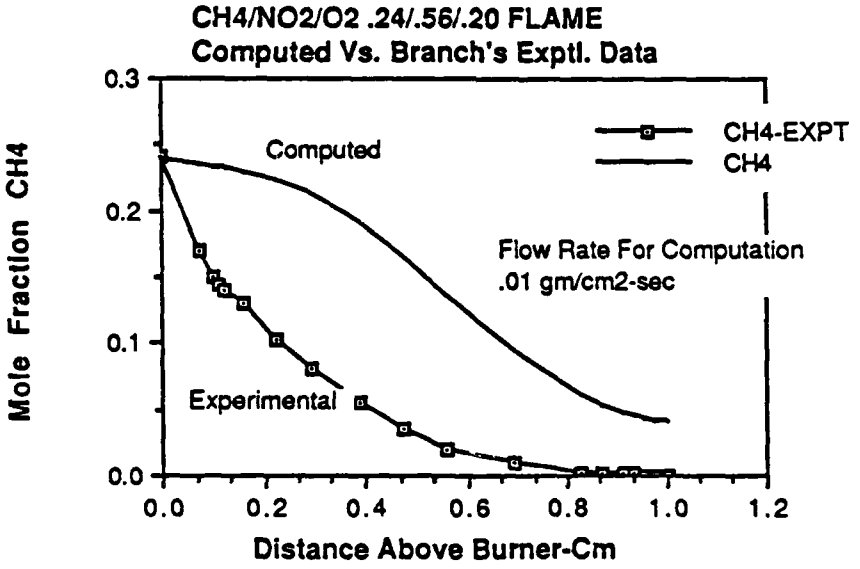
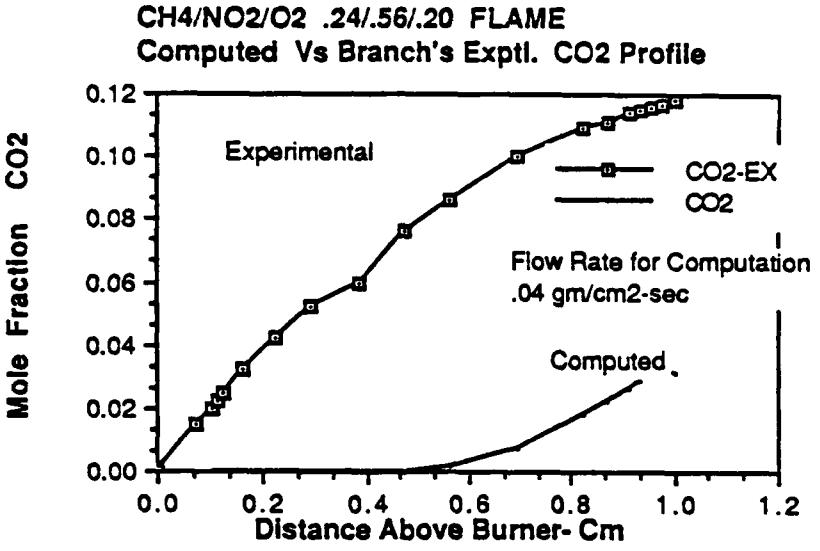

CH4/NO2/O2 .24/.56/.20 FLAME
Computed Vs. Branch's Exptl. Data
Mole Fraction CH4
0.3
0.2
0.1
0.0
Computed
CH4-EXPT
CH4
Flow Rate For Computation
.01 gm/cm2-sec
Experimental
0.0
0.2
0.4
0.6
0.8
1.0
1.2
Distance Above Burner-Cm

Figure: 1


CH4/NO2/O2 .24/.56/.20 FLAME
Computed Vs Branch's Exptl. CO2 Profile
Mole Fraction CO2
0.12
0.10
0.08
0.06
0.04
0.02
0.00
Experimental
CO2-EX
CO2
Flow Rate for Computation
.04 gm/cm2-sec
Computed
0.0
0.2
0.4
0.6
0.8
1.0
1.2
Distance Above Burner- Cm

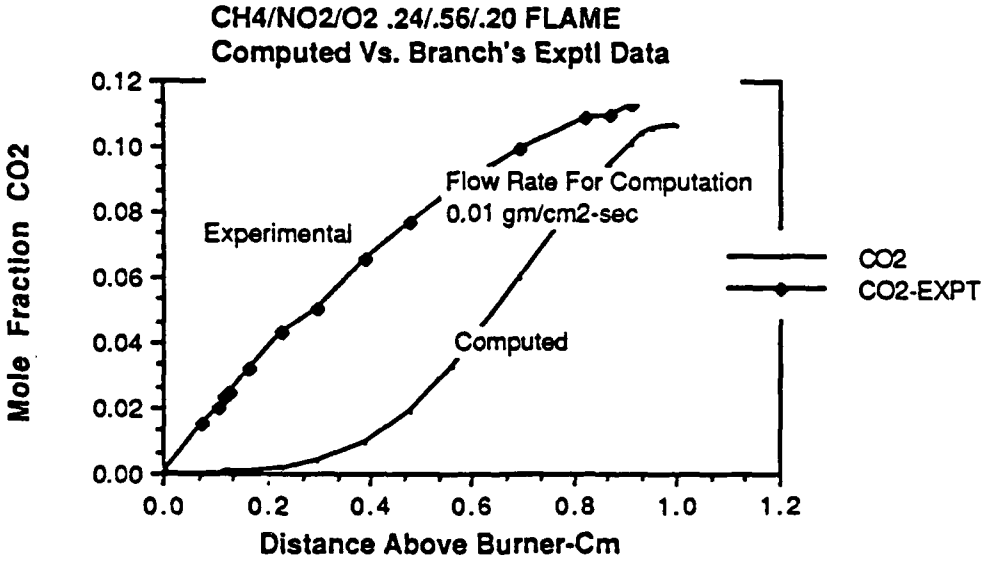
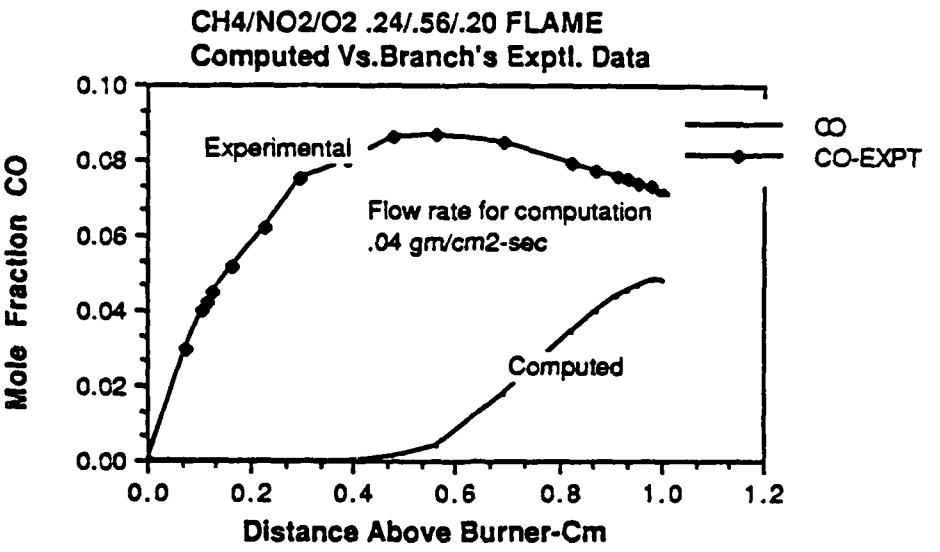

CH4/NO2/O2 .24/.56/.20 FLAME
Computed Vs. Branch's Exptl Data
Mole Fraction CO2
0.12
0.10
0.08
0.06
0.04
0.02
0.00
Flow Rate For Computation
0.01 gm/cm2-sec
Experimental
Computed
CO2
CO2-EXPT
0.0
0.2
0.4
0.6
0.8
1.0
1.2
Distance Above Burner-Cm

Figure: 2


CH4/NO2/O2 .24/.56/.20 FLAME
Computed Vs.Branch's Exptl. Data
Mole Fraction CO
0.10
0.08
0.06
0.04
0.02
0.00
Experimental
Flow rate for computation
.04 gm/cm2-sec
Computed
0.0
0.2
0.4
0.6
0.8
1.0
1.2
Distance Above Burner-Cm
CO
CO-EXPT

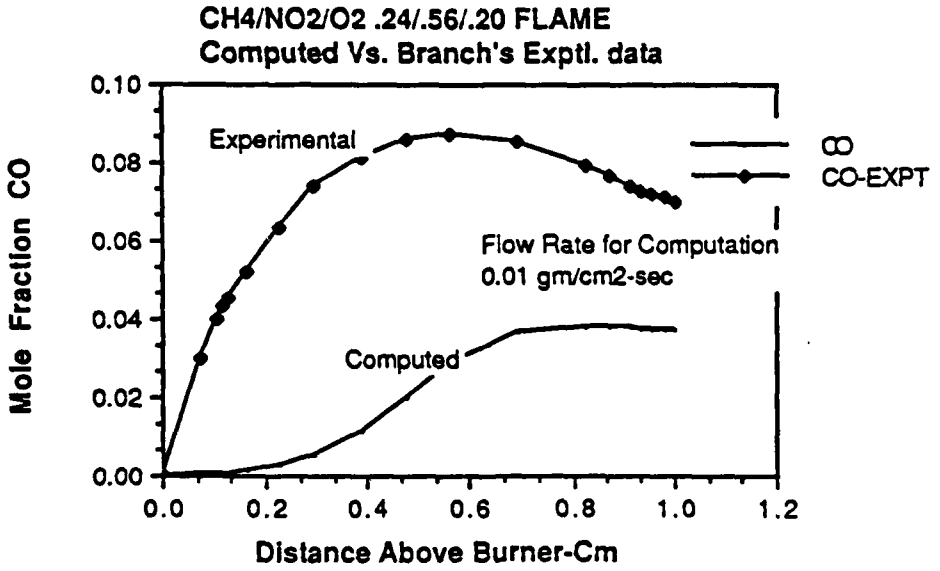
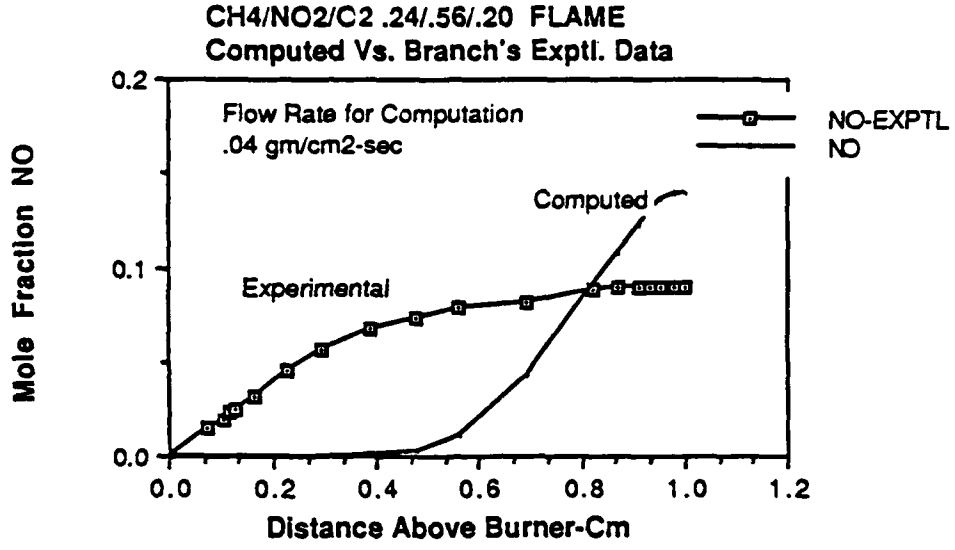

CH4/NO2/O2 .24/.56/.20 FLAME
Computed Vs. Branch's Exptl. data
Mole Fraction CO
0.10
0.08
0.06
0.04
0.02
0.00
Experimental
Flow Rate for Computation
0.01 gm/cm2-sec
Computed
0.0
0.2
0.4
0.6
0.8
1.0
1.2
Distance Above Burner-Cm
CO
CO-EXPT

Figure: 3


CH4/NO2/C2 .24/.56/.20 FLAME
Computed Vs. Branch's Exptl. Data
Flow Rate for Computation
.04 gm/cm2-sec
NO-EXPTL
NO
Computed
Experimental
Mole Fraction NO
0.2
0.1
0.0
0.0
0.2
0.4
0.6
0.8
1.0
1.2
Distance Above Burner-Cm

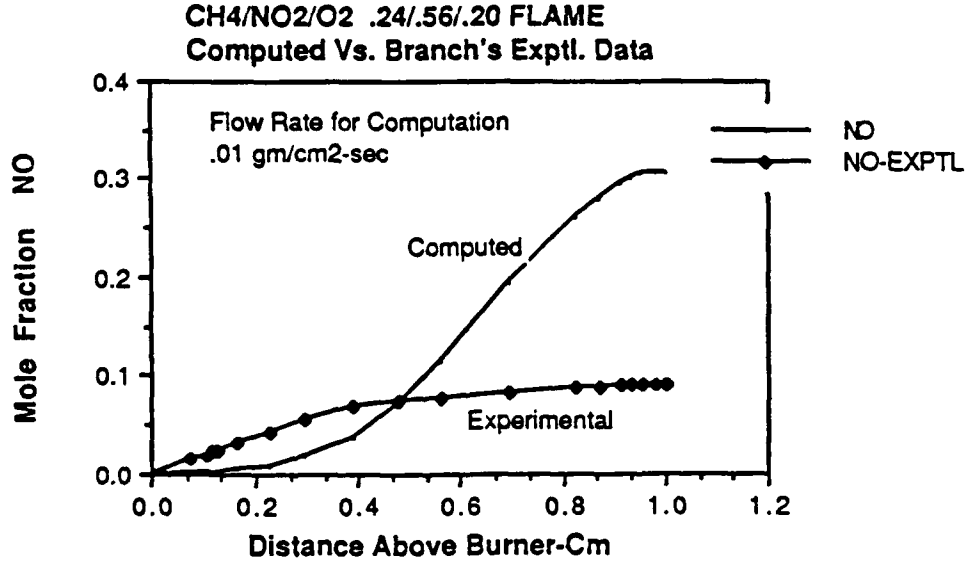
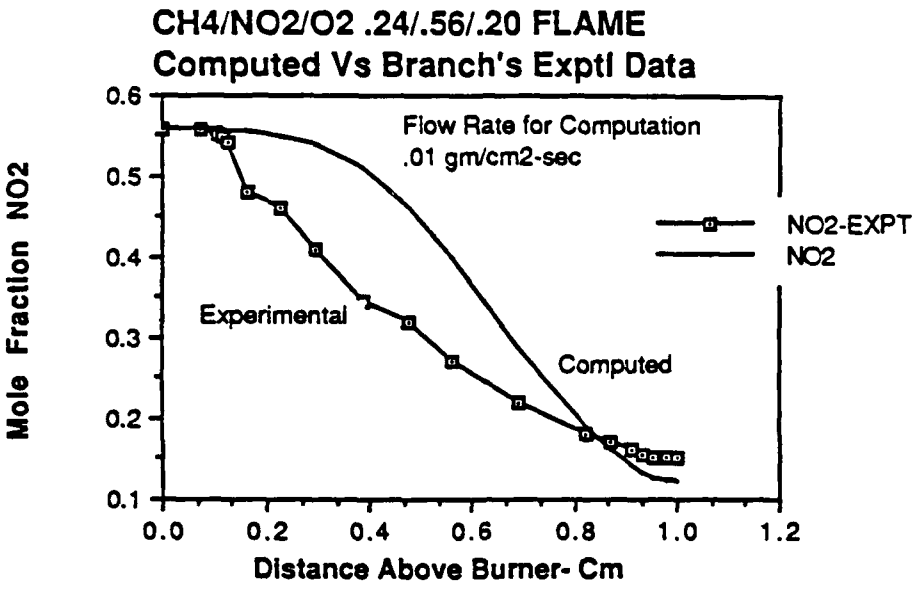

CH4/NO2/O2 .24/.56/.20 FLAME
Computed Vs. Branch's Exptl. Data
Flow Rate for Computation
.01 gm/cm2-sec
NO
NO-EXPTL
Computed
Experimental
Mole Fraction NO
0.4
0.3
0.2
0.1
0.0
0.0
0.2
0.4
0.6
0.8
1.0
1.2
Distance Above Burner-Cm

Figure: 4


CH4/NO2/O2 .24/.56/.20 FLAME
Computed Vs Branch's Exptl Data
Mole Fraction NO2
0.6
0.5
0.4
0.3
0.2
0.1
Flow Rate for Computation
.01 gm/cm2-sec
NO2-EXPT
NO2
Experimental
Computed
0.0
0.2
0.4
0.6
0.8
1.0
1.2
Distance Above Burner- Cm

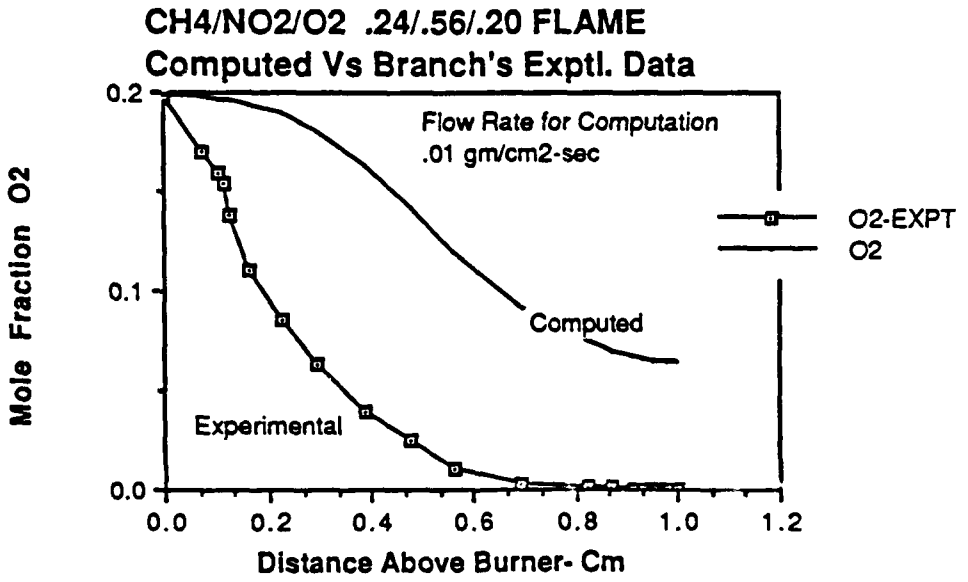

CH4/NO2/O2 .24/.56/.20 FLAME
Computed Vs Branch's Exptl. Data
Mole Fraction O2
0.2
0.1
0.0
Flow Rate for Computation
.01 gm/cm2-sec
O2-EXPT
O2
Computed
Experimental
0.0
0.2
0.4
0.6
0.8
1.0
1.2
Distance Above Burner- Cm

Figure: 5

APPENDIX MAY BE OBTAINED FROM

UNIVERSAL ENERGY SYSTEMS, INC.

OR FROM THE AUTHOR

1987 USAF-UES SUMMER FACULTY RESEARCH PROGRAM

Sponsored by the

AIR FORCE OF SCIENTIFIC RESEARCH

Conducted by the

Universal Energy Systems, Inc.

FINAL REPORT

Generic Requirements for a CAE/CAD/CAM System

Prepared by:	Albert A Heaney, PhD
Academic Rank:	Professor
Department & University:	Electrical Engineering Dept California State University - Fresno
Research Location:	ESMC/DVEP Patrick AFB FL
USAF Research:	Captain William Ramey
Date:	12 August 1988
Contract No:	F49620-87-R-0004

Generic Requirements for a CAE/CAD/CAM System

Albert A. Heaney

ABSTRACT

It is well recognized that the use of computer aided engineering, computer aided design/drafting, and computer aided manufacturing (CAE/CAD/CAM) equipment will have a significant impact on the design/manufacturing productivity of a facility particularly in the "high tech" area. For a facility that is convinced of this fact and prepared to make an investment into the purchase of such equipment, the questions that first arises is the quantity and kind of equipment to purchase. In particular, what hardware platforms, what software products, what support equipment, and what network configuration is needed? This study was aimed at developing a data base that would provide the basis for answering these questions relative to the specific CAE/CAD/CAM needs at ESMC. The study dealt with a methodology for identifying the needs of diverse groups that make up the engineering/drafting/analysis/maintenance operations at ESMC. The result of the study makes specific recommendations relative to each group that is to become part of the "network" even though some of the groups have some experience with CAD/CAM and others have no experience at all.

ACKNOWLEDGMENTS

This is to acknowledge the support of Captain Bill Ramey in his initial guidance of this research effort and his introduction to various contractor personnel.

The effort focal point, Mr Ray Laudermilch of ESMC/DVE, was very supportive particularily when it came time to provide secretarial help to type this report. I also would like to thank Peggy Norman for her typing support. In addition, I wish to thank the Air Force Systems Command, the Air Force Office of Scientific Research for sponsorship of this research and Universal Energy Systems, Inc. for the administrative aspects of the program.

I. INTRODUCTION

This study is an attempt at obtaining user requirements for a planned computer aided design environment at ESMC. The need for a CAD/CAM network has long been recognized at ESMC. It is realized that such a system will improve design methodology, establish standard formats for transferring design/manufacturing data, create visibility at all levels of the CAE/CAD/CAM process, significantly improve the design cycle time, and improve management controls. Discussions concerning network protocols, standardized interfaces, network structures, software packages and hardware platforms, etc., have been discussed at ESMC relative to a CAD/CAM network for some five years. The problem of identifying the specific needs of each "group" together with a topological network for the entire system has been controversial requiring extended discussions and considerable delay in final implementation. In the interim, technology continues to evolve making some detail decisions obsolete thus fostering further discussions. To get out of this "loop" it was proposed that a data base be established that deals with current generic needs within each of the "groups" that are to be represented and tied into the system. The generic data base is to be used to identify the number and location of the

physical sites that are to be "tied" into the system, details concerning "generic" hardware platforms, software packages, memory space, and support equipment needed at each site, and site-to-site communication paths. This information together with general system level specifications can be used as a basis for generating a CAE/CAD/CAM System Specification. The System Specification in turn is to be used to generate a Request for Proposal (RFP) so that one system level vendor will supply a fully integrated "turnkey" system and be responsible for installation, maintenance, and training. Some of the system level goals include:

Compatible with multi-vendor software

Standard interfaces on main "trunk"

Not locked into a specific hardware platform

Expandable without significant degradation (user transparent)

Technology Upgradable

Etc.

The author's research interests include the full spectrum of design methodology which includes CAE/CAD, simulation, and emulation. In addition, the author was previously involved with a local area network study for the

Rome Air Development Center (RADC). These efforts contributed to my assignment to the CAE/CAD/CAM study effort at ESMC.

II. OBJECTIVE

The primary objective of this study was to identify the specific CAE/CAD/CAM needs at ESMC by developing a generic data base from which a system level specification could be generated. The intent was to identify those groups whose level of production would be significantly augmented by the use of CAD/CAM equipment and then to identify each group's needs in the use of such equipment (as opposed to desires). The number of hardware platforms and support equipment needed at each "node", the amount of storage required at each node, file sizes to be transferred between nodes, and the number and lcoation of the nodes had to be determined. Some relationship between the level of activity in each group and the quantity of equipment needed had to be established. If the quantity is too low, the impact would be minimal. If the quantity is too high, the system would be too costly and may result in not being funded at all. Hence, the intent was to provide each group with a configuration that would have a significant impact in the way they do their

business while at the same time being conservative in the quantity of equipment provided. It is recognized that the initial impact of a CAD/CAM system on any one group may reduce the production of that group in that a number of people would have to spend a considerable amount of time being trained. Hence, there would be a "phase-in" period over which the nature of doing business would be changed. During the full transition period each group would develop experience with the system and would then be in a position to determine whether additional hardware platforms, software products or support equipment are needed, or whether any replacements/update are recommended.

One of the questions that developed during the study has to do with whether or not certain CAM equipment would reside "in-house." This issue has to do with the way management intends to do business. If, for example, PC board fabrication is to be "farmed-out", then wire routing and wire lists need not necessarily be generated. These issues (e.g., whether or not to purchase wire wrap equipment) will be considered a separate issue to be resolved by management and no purchase of fabrication equipment will be considered in this study. An important characteristic of the system network will be the "visibility" provided management relative to the status of on-going projects.

It is recommended that managers of each "group" be tasked with the responsibility of maintaining a status file which will reflect the activities of each project within the group. All files, including the status files, should be coded so as to provide access to those with a "need-to-know".

III. DATA COLLECTION STRATEGY

At the beginning of the study the author reviewed various catalogs as well as a previous study (1) of ESMC CAD/CAM needs. The previous study dealt with general benefits of a CAD/CAM system and the relationship between design technologies and correpsonding commercially available software "tools". The CAD/CAM needs specifically required at ESMC were never addressed. In order to address specific needs, the author first identified "key" people and then began to make appointments to speak to those people with the intent of identifying the CAD/CAM "needs" of each group. The number of people that needed to be interfaced with and the problem of identifying a "suitable" time to meet resulted in the conclusion that another method of collecting the needed data had to be found. The author subsequently recommended that a "survey" be drawn up, that a "charge number" be attached, and that a key

"focal point" be identified and tasked with the responsibility of transferring the survey to cognizant individuals capable of addressing the detailed questions relative to their own group's experience with and needs for a CAD/CAM system. This method of approach would quickly identify all the cognizant individuals and filter down to them simultaneously. There would be less hesitancy in filling out the survey questions in that they would be able to "charge" their time. Promptness in collecting the data was necessary in view of the fact that the author was limited to the ten-week period to do the study and write this report.

IV. THE SURVEY

The detailed survey is listed in Appendix 1. Each question was designed to identify key information needed to develop the full scope of a system level specification. The intent was not to identify specific hardware platforms or software products, but rather to identify generic requirements, thereby allowing a system level vendor maximum flexibility in performing all of the hardware/software tradeoffs and interface requirements needed for the development of one fully integrated network. This approach avoids the problem

of "tunnel vision" in which each group sees its needs from its own perspective but does not deal with the complete system.

The first two questions deal with needed generic software "tools". The tool description given are clarified by correlating them with the vendor supplied tools currently in use (Question 2). The quantity of hardware platforms and support equipment needed within each group is identified by the response to questions 3, 4, and 5. The descriptions of the activities asked for in question 4 identify the type of hardware platforms needed (e.g., PC, workstation, minicomputer). File sizes in current use and corresponding communication paths (node-to-node) are identified by questions 6 and 7. Question 8 was intended to aid those groups that desired to utilize, CAD/CAM equipment to replace some or all of the present mode of performing their function. Support was given in defining files within their present mode of doing business. Assuming that the "defined" files were digitized, a guide was provided (Question 9) for computing each of the file sizes in bytes of memory. In order to keep memory storage requriements within reasonable bounds, the survey asked each group to address only "active files". Question 8 also asked for the name of the group that originates each listed nondigitized file so

that all future node-to-node commuication paths could be identified. Also, the computation of the file sizes can be used to determine data block sizes to be transferred on the network.

V. SURVEY INPUT

The actual turnaround time between the survey being sent out and responses coming in was considerably longer than was anticipated. This fact reduced the amount of time needed to interface with each of the responders in order to clarify the result. Nevertheless, it is believed that the data received represents a reasonable estimate of the basic needs of each group relative to their present mode of doing business. Each person tasked with the responsibility of responding to the Survey was contacted in order to assure that each group's response was consistent with the original intent of each of the questions. It is the author's belief that there may be some duplication of effort among the various groups particularly in the area of drafting. Once again it is emphasized that the actual needs of each group heavily depends on the way business is carried out at PAFB. The author can only base his recommendations on the data supplied independently by each of the groups

represented. Many of the groups did not spend the time to thoroughly answer questions 8 and 9. These two questions are key to planning the data storage requirements at each node as well as node-to-node communication paths and the data block sizes that would have to be transferred between those nodes. Much of the subsequent interaction with the groups on the part of the author was aimed at estimating the missing data. In that most groups will be interacting with Drafting, it is assumed that the maximum block size that may be transferred between nodes is 440k bytes (an E-size drawing).

All groups responding to the Survey will require full CAD/CAM configurations except for Engineering Control. The Maintenance Support group is responsible for the maintenance of all of the instrumentss (e.g., antennas) at all (64) of the instrument sites. All of the maintenance procedure documents for this network are stored at the Maintenance Control Center (MCC) at PAFB. This network requires one workstation at the MCC and one monitoring (access) terminal at each of the instrument sites. The primary use of the network is to enable each Range site to quickly access detailed maintenance procedures form the MCC and thereby minimize the down-time of a particular instrument. Much of the information needed are on pages that are a mixture of

text and graphics and can be output to a printer. Some of the information are drawings and would require a plotter at the Range site. A decision would have to be made as to whether a facismile machine could replace the plotter at a particular site. For this study it will be assumed that a plotter will be required at each of the Range sites.

In computing the number of workstations required by each group the following relationships were used:

One workstation per four engineers

One workstation per three draftsman

It is believed that since a phase-in period will be required before full utilization of a CAD/CAM system will be obtained that the above figures will provide a sufficient quantity of such equipment to make a significant impact on the performance of each group. When a system becomes fully utilized it is expected that the same quantity of work could be done with fewer people. At such time experience will dictate the type and quantity that will best suit the needs of each group.

As noted in Table A1-1 of the Appendix, eight groups responded to the Survey. These groups however represent 72 physical sites when one takes into

account the 64 instrumentation sites. Software needs for each of the eight groups are shown in Table A1-2. The generic software tools that the groups indicated are needed are somewhat described by the corresponding vendor supplied software tools in current use listed in Table A1.2. These vendor supplied tools are listed only to lend clarification to the "tool needs" indicated and are not necessarily the software tools being requested. The memory size and configuration needed to store the software tools are not listed in this study but are being left to the target system vendor to compute.

Data storage memory requirements for each of the eight groups is shown in Table A1.3. These figures are based on file sizes currently in use by those groups who have limited CAD/CAM capability, (groups A and B), and on file size computations made for those groups who presently have no CAD/CAM capability. The memory media (RAM, disk, etc) and the memory configuration (central, distributed) needed to store the data is being left to the target system vendor to design. As indicated earlier, this study is intended to provide the raw data needed by a system level vendor to perform all of the tradeoffs needed to design an optimal integrated system.

VI. RECOMMENDATIONS

The hardware platforms needed by each of the eight groups represented in this study together with the needed software tools indicated in Table A1.2, the identification of the 72 nodes on the network, and the maximum data block size (440k bytes) needed to be transmitted across the network comprise the generic description of the system configuration. With the exception of the hardware platforms, the complete generic description of the system has been addressed in earlier sections of this report. Hence, this section will deal only with the recommended hardware platforms needed as an initial installation by each of the eight groups. These recommendations are shown in Table A2.1. Justification for the hardware platform recommendations are based on the following:

1. The number of workstations recommended for each group is based on the number of engineers/draftmen located within each group and the relationship described in Section V of this report.

2. It was assumed that all engineers currently have access to their own Personal Computer (PC) and therefore no additional PC purchases for engineers

are reflected in Table A2.1.

3. The support equipment recommendations are also made without regard to the kind or quantity of support equipment currently residing at each of the "nodes".

Although the specific characteristics of a workstation are to be addressed by the target system vendor, generally a workstation is characterized by very fact processing, color graphics capability, and an operating system designed to work in a distributed environment.

As a final comment the author would like to recognize that with the awarding of a new contract to CSR and the subsequent restructuring of the mode of operation, that the number and function of the several groups may be changed. However, it is felt that this change may effect the distribution of the CAD/CAM equipment, but not necessarily the type or quantity of needed equipment.

REFERENCE

Zobrist, G.W., Specification of a Computer Aided Design System, 1987 USAF-UES Summer Faculty Research Program

A P P E N D I X

SURVEY

1) In generic terms, list all the software "tools" needed in your group (e.g. Heat Transfer). On a scale of 1-to-5 how frequently are these tools used? (Scale: 1-very frequently, 5-seldom).

2) List the vendor supplied tools currently being used, if any (e.g. P-CAD).

3) Up to how many design/design modification/analysis activities that could be done with CAD/CAM equipment may be going on in your group simultaneously?

4) Describe the activities of 3) and the corresponding required support equipment (e.g. wire wrap / Printer; PCB routing / Plotter). If CAD/CAM equipment is not currently being used, estimate the kind of support equipment needed and correlate with the activities of 3).

5) Identify all the support equipment needed by your group. Justify the need. Estimate how frequently each item in your equipment list will be used (hrs/week).

6) If files in computer memory are currently being used, list the "file names" used and correlate with each of the activities listed in 4) (e.g. autoplacement).Identify the group that originates each of the listed files, even if it is your own group.

7) List the name and estimate the memory size (e.g. 5K bytes) of each of the files listed in 6) but generated within your group.

8) Relative to the activities listed in 4) for which no files in computer memory are currently being used but for which it is desired to digitize the "current files" (e.g. blueprints), it will be necessary to estimate the memory size needed to store all such "current files". The precise definition of a "file" may vary from one group to another. A file, for example, may be considered to be all documents that fall into a common reference system. For example, all drawings that make up a "subsystem" may be considered to define a "file". Based upon the reference system used within your group, list the "file names" needed for each design / design modification /analysis activity listed in 4). As a first level input, it is recommended to confine your inputs to the day-to-day operations (i.e. active files). Again, identify the group that originates each of the listed files, even if it is your own group.

9) List the name and estimate the memory size of each file listed

in 8) but generated within your own group. To aid in computing this information, the following guide is provided:

An 8.5x11 sheet of text .....8k bytes

An "A" size drawing .....27k bytes

A "B" size drawing .....55k bytes

A "C" size drawing .....110k bytes

A "D" size drawing .....220k bytes

A "E" size drawing .....440k bytes

A "J" size drawing .....1M bytes

10) Identify features of a future CAD/CAM system that you consider valuable for the activities performed in your group.

GROUP IDENTIFICATION

GROUP DESIGNATION	GROUP	CONTACT
A	Comm/Timing Systems	Jim Wright
B	Data/Command/Met Systems	T.M. Hall
C	Engineering Control	E.C. Tweedy
D	Special Projects	J.H. Sojourner
E	Metric System Engineering	R. Marquiss
F	Telemetry Systems	Tom Conroy
G	Maintenance Support	Jim Isaacson
H	Drafting	Dick Cumberland

TABLE A1-1

TABLE A1.2

Generic Software Tools Needed vs Expected Frequency of Use

Vendor Supplied Software Tools	Generic Software Tools Needed	Group Frequency of Use							
		A	B	C	D	E	F	G	H
P-CAD	Schematic Capture	2	1			1	1		1
P-CAD	PC Board Layout	3	3				3		2
P-CAD	PC Board Routing	2	3				3		2
Wiremaster	Wirelist	3	2				2		2
Slice/Spice	Circuit Simulation (analog)	3	4			3	1		
ALTERA, ORCAD	Circuit Simulation (digital)		1			3	1		
Super Compact	Microwave Circuit Simulation	2					2		
	Filter Design/Simulation	2				1			
COMM NET 2, Netwk 2	Comm Network Simulation	3							
	Control System Simulation					1	3		
COMPACT	Command, Control, Comm						3		
RF Tool Kit	RF System Analysis						2		
MSC PAL II	Finite Element Analysis					1			
	Heat Transfer					3			
CAASE	Strength of Materials					3			
	MODAL Analysis					1			
MATHCAD, TK SOLVER	Mathematical Analysis					3	3		
BASIC,PASCAL,6800 Assem.	Software Development	4							
AUTOTROL,REDLINER	Mechanical Drafting	5				1	3		1
CADKEY	Graphic Illustrations	2	1				2		4
Harvard Proj Manage,Timeline	Project Scheduling	4	2				5		
Dbase III	Database Management	1	2				1		
Overhead Express, Windows	Briefing Presentation	3	3	1	1	3	3	1	
Framework,Supercale	Spreadsheet	4	2				5		
Wordstar, Sidekick	Wordprocessing	1	1	1	1	3	1	1	3

Scale: 1- Very Frequently 5 - Seldom

REQUIRED DATA STORAGE

GROUP	TOTAL DATA STORAGE REQUIRED	# FILES
A	1.5 Megabytes	18
B	2.2 Megabytes	420
C	184 Megabytes	23,000 records
D	One Hard Disk	
E	15.0 Megabytes	Working Files
F	10.0 Megabytes	Working Files
G	800 Megabytes	50,000 Pages
H	1.1 Gigabytes	5,000 Drawings

TABLE A1.3

RECOMMENDED HARDWARE PLATFORMS FOR EACH GROUP

HARDWARE PLATFORMS	GROUP RECOMMENDATIONS							
	A	B	C	D	E	F	G	H
Workstations	16	9		1	15	10	1	10
Personal Computers			2				66	
Dot Matrix Printers	16	9	2	1	15	10	66	2
Lazer Printers	2	2			2	2	1	1
Pen Plotters (A-E sizes)	3	4		1	2	2	66*	2
Lazer Plotters (A-E sizes)								2
Scanner	1	1						2

TABLE A2.1

* Consider the use of a facimile machine at each of the 64 instrumentation sites and allow two plotters to be placed at the MCC.

1988 USAF-UES SUMMER FACULTY RESEARCH PROGRAM

GRADUATE STUDENT RESEARCH PROGRAM

Sponsored by the

AIR FORCE OFFICE OF SCIENTIFIC RESEARCH

Conducted by the

Universal Energy Systems, Inc.

FINAL REPORT

ALASKAN HF TEST DATA ANALYSIS

Prepared By:	George N. Bratton, Ed.D.
Academic Rank:	Associate Professor
Department and	Mathematics/Computer Science
University:	Austin Peay State University
Research Location:	ESD/AVP Hanscom AFB, MA 01731
USAF Researcher:	Lt Barry Kirby

Date:	August 25, 1988
Contract No:	F49620-87-R-0004

ALASKAN HF DATA ANALYSIS

by

George N. Bratton

ABSTRACT

The performance of networked high frequency communication in a disturbed environment is being tested in an attempt to document the superiority of networking as opposed to point to point HF communication. Although implementation problems have dramatically delayed the collection and analysis of sufficient data on which to base valid inference, the types of data that will be available have been recognized. A software system for providing initial (Stage 1) analysis has been developed, tested, and documented for use by Air Force personnel. Review of pre-implementation simulations indicates there may be potential problems with the particular networking protocols and field comparisons of networking protocols has been recommended.

ACKNOWLEDGEMENTS

I want to thank the Air Force Systems Command and the Air Force Office of Scientific Research for sponsoring this valuable program. The opportunities afforded to me and my colleagues would have been not available otherwise. Special mention must also be given to Universal Energy Systems, Inc. for their very efficient and simultaneously very cooperative operation of this program.

The personnel at ESD/AVP have been most helpful and kind during my appointment. Lt Col David Cook and Lt Barry Kirby, with whom I worked directly, were especially helpful. Also, without the cooperation and assistance of Dr. John Dalphin, the other SFRP fellow at ESD/AVP, the work I have done could not have been completed.

I. INTRODUCTION

The Air Force Electronic Systems Division Office, ESD/AVP, is sponsoring a project to demonstrate and evaluate high frequency (HF) network performance in the Alaskan auroral zone. Automatic adaptive HF radio equipment was installed at several Alaskan Air Force sites. Network control algorithms which choose the network node and the frequency on which to transmit a message have been designed. Data on the history of transmissions are stored on a microcomputer at each node and it returned to ESD/AVP on a monthly basis.

Tests of the network have been designed to evaluate the performance of this system in terms of link establishment, message reliability, network throughput, and network routing delays. The intent of these tests is to contrast the performance of such a network to point-to-point (non-networked) HF communication, and, hopefully, to demonstrate the superiority of networking.

During the summer of 1988 the author served as the data analyst/statistican at ESD/AVP. This research group had no member with the background to perform the necessary summary and analysis of the test data. My statistical training and experiences in providing data analysis services to inferential problems in a variety of

disciplines enabled me to join this group and to provide many of the desired services.

II. OBJECTIVES OF THE RESEARCH EFFORT

The preliminary goals of my summer research effort were to a) provide the data analysis and summary of network performance in the Alaskan test and b) based on these data develop an index that contrasts the percent connectivity of a network of k nodes to a network of fewer than k nodes.

The planned Alaskan test implementation consisted of eight nodes (automatic adaptive radio equipment) at different air bases. The scheduled implementation and operational status of the network has been hampered severely by problems with hardware failures and power interruptions. The loss of power to the microcomputers has resulted in the loss of some data that might have otherwise been included in the analyses.

The graphs in appendix A summarize the network on the air status and the overall effectiveness of communication. The proposed testing involves each active node transmitting 20 messages (a total of 160 messages per day) at regularly spaced intervals. These were automatically generated and contain a standard 1040

character message. The graphs clearly show the parsity of real data that has come from the test sites.

This parsity of data has meant that preliminary goal b) could not even be addressed. It was consequently replaced with two other goals; c) the development and document a software system which could be used by ESD/AVP personnel to produce the kinds of analyses and summaries I was currently providing and d) conduct an in-depth review of the network simulation results.

The software system was desired by ESD/AVP so that the analysis could be continued, at least at the preliminary stages, in house if my request for continued support under the Research Initiation Program was denied. Regardless of that result, any in-depth or more sophisticated analysis would not be within the realm of expertise of ESD/AVP personnel.

The review of the network simulation was important for two reasons. First of all, by reviewing this document along with other reports on the design and implementation of the test, I could gain a more detailed understanding of the HF communication network, the variables that are important in the study, and consequently, develop appropriate summary and inference tools. Secondly, since the simulation's data were used

to choose the network routing protocol for the test, I could check/verify the results of this inference.

III. RESULTS OF HF DATA ANALYSIS

The initial level of data analysis, denoted as Stage 1, focuses on three characteristics of message transmission. These are connectivity, which is the percentage of attempted transmissions that are received by the final destination, delay, which is the time in minutes from the transmission of the message by the source node until it is received by the final destination, and the number of character errors in the received transmission.

Percent connectivity has been analyzed without attempting to control for differing auroral effects or varying sun spot activity. While studying these effects might be scientifically rewarding (history shows this is a difficult task), the goal of the test program was to study network performance, at least in Stage 1, regardless of conditions which make communication difficult. This first analysis had as its goal providing a simple overview of what has happened in the test network rather than any attempts to explain why.

Percent connectivity has been computed with both

the day as the unit of measurement and the hour of the day as the unit of measurement. For each unit of measurement (daily or hourly) the total number of attempted transmissions, successful non-relayed transmissions, and successful relayed transmissions was computed. Point-to-point percent connectivity (denoted P1) is the total successful non-relayed transmissions divided by the total attempted transmissions. Network percent connectivity (denoted P2) is the total successful transmissions (non-relayed plus relayed) divided by the total attempted transmission. The contribution of networking to successful HF communication is then the quantity P2 - P1. Graphs of P1 and P2 by date are given in appendix B for the months of February, March, and June. For each date shown the contribution of the network is the difference in the height of the adjoining bars (P1 and P2). Due to inoperability problems, no data is presented for either April or May.

Viewing these graphs one sees large fluctuations in percent connectivity for both quantities P1 and P2. This may be, in large part, due to the instability in the number of messages attempted. Not only is there a large monthly fluctuation in messages attempted but there is great fluctuation on a daily basis also. For

instance, in the month of June, the values for the 10th and 11th are based on 5 and 4 attempted transmissions, respectively, whereas the vaules for the 20th and 21st are based on 37 and 29 attempted transmissions, respectively.

The number of character errors in successful transmissions can be determined since all messages are identical, consisting of 1040 blank characters. The distributions of character errors for successful transmissions in the months of February, March, and June are shown in the table below. The categories in the distribution were chosen to represent meaningful levels of message accuracy.

CHARACTER ERROR DISTRIBUTION

# OF ERRORS IN MESSAGE	FEBRUARY	MARCH	JUNE
none	66 (57.4%)	111 (69.4%)	85 (61.1%)
less than 10 (1%)	41 (35.6%)	37 (23.1%)	38 (27.3%)
less than 100 (10%)	6 (5.2%)	11 (6.9%)	13 (9.4%)
100 or more	2 (1.8%)	1 (.6%)	3 (2.2%)

Again, April and May data as well as a distribution of character errors for relayed messages are excluded because of the limited data available in each of these categories.

No Stage 1 analysis of delay times has been done for two reasons. Primarily, the routing protocol which is in operation assumes eight operational stations and all activities at any operational station may include attempts to communicate with all other seven stations. These communications may be on one of fifteen frequencies. Since no more than four stations have ever been simultaneously on the air (and more commonly, only three stations) there is much delay time in trying to send messages to or to measure link quality to stations that are not operational. Secondly, even with the operational stations, operator failure to enter the proper time when coming on the air has meant that many recorded delay times (particularly in June) are clearly spurious.

To attempt to get a more realistic picture of the actual nature of the active portion of the network some of the data in the message history was discarded prior to the Stage 1 analysis. Transmissions that were attempted to stations that were not operational on a particular date were purged from the message history prior to the percent connectivity computations. A station was, for the purpose of these analyses, deemed to be not operational on a day if it neither initiated a transmission nor received a transmission. Although this

criterion is still rather loose it helps to provide a clearer picture of the actual network activity. This purging does not, however, completely remove the effect of these non-operational stations.

To conduct the necessary hypothesis testing, to construct confidence intervals, or to attempt any other inferential activity on the data that are available would be a serious error for several reasons. The primary reason that such activities would be erroneous is that the network has not, even for a single transmission, been operational as designed. As mentioned previously, the routing protocol tries to make contact with seven other sites both in measuring link quality and in attempting to transmit messages. Discarding transmissions attempted to stations known to be non-operational from analyses only addresses a portion of the problem. These non-entities (non-operational stations) affect every possible characterization of network performance. It is impossible, if one thought it was desirable, to explain the exact nature of and to partition out the exact magnitude of these effects.

A simple, second reason to restrain from inference is sample size. The few operational days and the resulting importance of atmospheric considerations (not

being controlled by time) also makes any inferential activity inappropriate.

IV. DEVELOPMENT OF THE SOFTWARE SYSTEM

The purpose for developing a data summary and analysis system was to essentially automate most of the Stage 1 data analysis. Since the period of data collection must now (due to the problems cited earlier) extend well past my period of appointment, the research team wished to be able to obtain the same types of summary statistics and graphs in the future that I had provided.

The functional requirements of this system were no user data entry, rather all data transfer and file restructuring is done electronically, and minimal user interaction. The second requirement is necessary to insure that the system produces consistent and accurate results in the event that I cannot be the user or at least review the work.

The author and Dr. John Dalphin, ESD/AVP's other SFRP appointee, jointly concentrated their efforts on the design, implementation, documentation, testing, and finally, refinement of a customized data reduction and

summary software system. The word system is used since it is a combination of FORTRAN programs and the use of commercial software packages.

Dr. Dalphin wrote the FORTRAN programs and I wrote the macros and menus to automate the commercial software operation. This "package" provides the user with the capability to (a) download a month's message history, (b) purge the file of any "false" failed transmissions (attempted transmissions to non-operational stations), (c) summarize the participation of each node (test site) in the network, (d) compute daily percentage of throughput for both network and point to point transmissions, (e) summarize error rates and delays in transmissions, (f) search and report from the database as needed, and (g) produce appropriate tables and graphs from the data.

This system was tested in two fashions. The accuracy and file handling capability was tested by analyzing a file of simulated data (throughput, etc., known) which consisted of 3472 message records. The accuracy, appropriateness, and utility of the written instructions and documentation was tested by having an ESD/AVP staff person, with no prior exposure to this work, conduct the analysis of a month's data. Following this testing the necessary modifications were made.

VI. NETWORK SIMULATION RESULTS

A detailed presentation of the results of the system simulation is prohibited because of the space limitations in this proposal. (The simulation report is a 60 page document.) Briefly stated, the simulation used a computer model of ionopheric effects on HF communication (IONCAP) to determine the availability of network nodes for transmissions at a given time. Link Quality Assessments (LQA) were generated from this model. The networking protocols were then compared on two measures, percent messages transmitted successfully (PD) and average delay time (DT). The results of this simulation were then used to choose the protocol that is being employed in the network test in Alaska.

By reviewing in detail this simulation I became aware of several possible problems that may occur in Alaska as a result of the choice of protocol. While the modeling procedures seem to be basically sound, the results for the chosen protocol depend on the accuracy of the IONCAP model and the relevance of the parameters that are input into the model. The one parameter of concern, when contrasted with what is actually occuring in Alaska, is the length of time that is spent in group

LQA activity.

For protocols B, C, D, and E the collection of LQA measurements by all nodes is done on an hourly basis. The time required for this is time during which no messages can be transmitted by any node. In the simulation this is a user-specified parameter. Clearly, the amount of time taken in this activity has direct bearing on the DT values for these protocols. The input value in the simulation was 10.9 minutes whereas the true time is about 19 minutes in Alaska. Consequently, the network is spending about 1/3 of its time in this activity. The "best" protocol was chosen to be protocol E which even in the simulation had longer delay time than the random protocol, protocol A. (Protocol E did possess slightly higher PD, but the preference for PD over DT was never explained.) This underestimate of the true delay may have dramatic effects on the performance of the network, once it becomes fully operational. A very rough estimate is that the average delay will be increased by 15%-20%.

VI. RECOMMENDATIONS

1. No conclusions on the performance of a networked HF communication system can be drawn from the sparse data

collected thus far.

2. No conclusions on the performance of the network should be made until the network has been fully operational for a period of 90-120 days.

3. The use of the software system, developed jointly with Dr. John Dalphin, will provide accurate results, consistent with my approaches and standard statistical practices.

4. Once the network is fully operational, the use of LQA data as a basis for communication should be carefully studied. In particular, the known instability of LQA measurements may mean that the routing protocols rely on other techniques (i.e. random selection) rather than LQA. Furthermore, how accurately does LQA data predict the actual character errors?

5. If LQA is validated as claimed, then how can the collection of LQA data be optimized? That is, how often should LQA be gathered and how much of an impact on the throughput of the network does this overhead have.

6. Other promising protocols, particularly the random protocol should be tested. Results of these tests should be compared to the currently used protocol, provided that ionopheric conditions can be controlled.

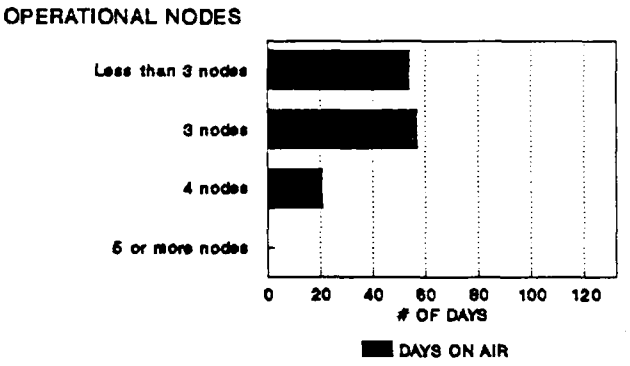
7. Geographic locations of network sites should be examined. Are there particular sites that are more or

less employed than others for the relaying of transmissions? If certain sites are "more valuable", then extraordinary measures need to be employed to insure that such sites stay operational.

I have also submitted a proposal for continued support of my research efforts under the Research Initiation Program. In that document I have explained in detail the techniques that I would employ to address these recommendations for continued research.

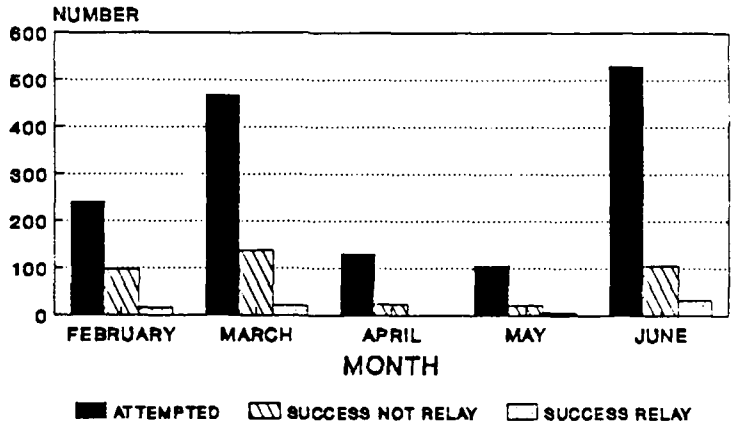
APPENDIX A

ON AIR STATUS
FEB. THRU JUNE 88*



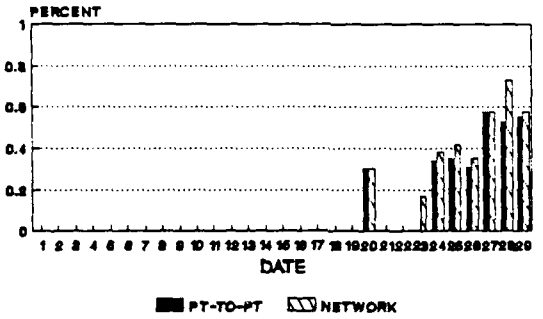
*122 TOTAL DAYS

NETWORK ACTIVITY
BY MONTH

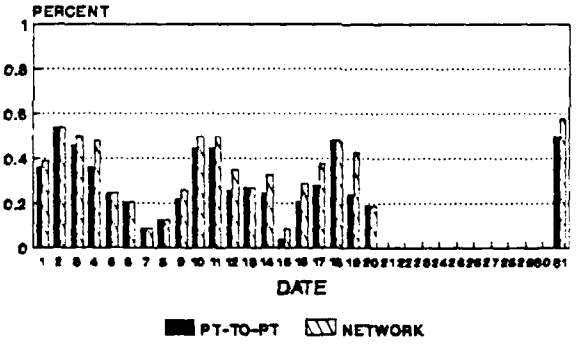


APPENDIX B

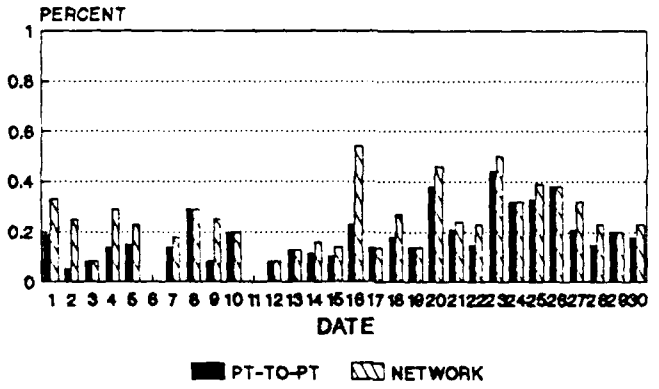
CONNECTIVITY
FEBRUARY DATA



CONNECTIVITY
MARCH DATA



CONNECTIVITY
JUNE DATA



1988 USAF-UES SUMMER FACULTY RESEARCH PROGRAM/

GRADUATE STUDENT RESEARCH PROGRAM

Sponsored by the

AIR FORCE OFFICE OF SCIENTIFIC RESEARCH

Conducted by the

Universal Energy Systems, Inc.

FINAL REPORT

STAGE 1 ANALYSIS OF ALASKAN HIGH FREQUENCY RADIO NETWORK

Prepared by:	John F. Dalphin, Ph.D.
Academic Rank:	Professor
Department and	Computer & Information Sciences
University:	Towson State University
Research Location:	USAF ESD/AVP Hanscom AFB Boston, Massachusetts 01731
USAF Researcher:	Lt. Barry A. Kirby

Date:	15 Sep 88
Contract No:	F49620-87-R-0004

STAGE 1 ANALYSIS OF ALASKAN HIGH FREQUENCY RADIO NETWORK

by

John F. Dalphin

ABSTRACT

Voice and data communications in the military currently rely primarily on microwave, satellite relay and other high technology mechanisms. These media, however, are the very ones most sensitive to EMF and other enemy intervention.

In considering other aternatives for maintaining communications in a hostile (nuclear) environment, the Air Force is testing the use of a high frequency radio network. This testing is taking place in Alaska where the aurora borealis produces deionization effects similar to those anticipated in a nuclear environment.

In the experiment high frequency radios located at Air Force sites function in a store-and-forward network structure. Each radio is controlled by a Zenith 150 computer which queues messages, selects transmission targets based on message traffic and dynamic link quality analysis (frequency selection), and maintains a history of its operation. Fixed length digital messages are transmitted and relayed; routing information, delay times and character error counts are captured in the data.

Statistical analysis of reduced data is performed and a graphical representation of the results is prouuced for briefing purposes.

Acknowledgements

The Summer Faculty Research Program experience at Hanscom Air Force Base was made possible by a combined effort involving personnel at the Air Base and those performing support at Universal Energy Systems. I appreciate the support provided by the following individuals of AVP:

LTC James D. Taylor

LTC David J. Cook

MAJ Thomas A. Bird

CAPT Jeff C. Valiton

CAPT Timothy D. Smith

1LT Barry Kirby

Mr. Peter Hughes

Others who provided support and cheerful collegial interaction are:

Mr. Edward A. Davis (ACSI)

Mr. Alan L. Cohn (ACSI)

Mr. George Sawyer (MITRE)

Mr. Jack Fletcher who acted as the Effort Focal Point for the SFRP participants at Hanscom AFB provided important coordination for the project. Likewise, those at UES were most helpful and responsive in providing SFRP direction from afar.

I. INTRODUCTION

The high frequency radio experiment in Alaska entered the operational mode early in 1988; initial test data began to be generated in February. Monthly data sets had been received since that time and were in need of reduction and analysis. MITRE Corporation personnel associated with the project had prepared some preliminary analyses based on their reduction of the data.

Hanscom AVP personnel desiring to have valid data analysis available to evaluate continuation of the experiment, sought - through the Summer Faculty Research Program individuals - expertise in computer systems and programming and data reduction and statistical analysis. To meet this need, two individuals were brought on board through the SFRP: Dr. George Bratton whose strengths lie in statistical analysis, and myself (Dr. John Dalphin) whose strengths lie in programming and analysis of systems.

My experience in computer science through programming, analysis and teaching related concepts such as data structures was an excellent supplement to Dr. Bratton's statistical analytic background. Together we functioned as an advisory team to AVP and aided them in their experimental analysis.

II. OBJECTIVES OF THE RESEARCH EFFORT

"Stage 1" Analysis of the High Frequency Network had as its objectives:

- The reduction of the large quantity of data received from the communications nodes;
- The organization of data in an efficient structure to facilitate corelation and analysis;
- The development of statistical measures of the performance of the network from the perspective of operation with or without a networking strategy (with being the implementation of the store-and-forward algorithm, without being a direct connection model);
- The production of a set of programs and a system to allow AVP personnel to perform the analysis themselves and generate statistical results with associated graphical representations;
- Generation of documentation and instructions for the system developed;
- Preliminary consideration of latter stages of the analysis for future (Stage 2 & 3) refinement of results.

III. "STAGE 1" ANALYSIS

Stage 1 Analysis is designed to investigate basic performance of the network by developing statistical measures of relayed messages versus point-to-point communication. In theory, two nodes which may not be able to communicate directly may be able to link through a third node due to atmospheric conditions.

The basic message history data are extracted from removable "hard" disks which are returned monthly from each of the Alaskan sites. MITRE Corporation personnel have been extracting the data and building a message history file. This information is the input to the system which finally generates tabular and graphical analysis of the performance.

Processing the data is performed in four steps:

- Purging the transmission records of transmissions to nodes which are not operational (FORTRAN program);
- Summarizing message history by day and by hour (two FORTRAN programs);
- Entry of results into an integrated data base/spread sheet program (ENABLE) to allow further manual manipulation as necessary;
- Preparation of graphical bar chart output (using Harvard Graphics) to represent characteristics of network operation.

A comprehensive combined operation guide and documentation was prepared by the two SFRP fellows and is used by AVP personnel each month to analyze the new data received (copy attached).

IV. RECOMMENDATIONS

The Alaskan High Frequency Network, although initiated in February 1988, appeared to be experiencing severe problems keeping a minimum number of nodes in operation at any one time. In the data available (covering February through June), rarely were more than three nodes operational at one time. Due to this limitation, more complex analyses comparing multi-node performance were not possible. This performance difficulty was a disappointment to personnel at AVP and MITRE as well as the two SFRP appointees.

Due to this difficulty, the following recommendations seem appropriate:

- Further data be gathered for analysis before attempting to reach any conclusions about the performance of the network;
- Once the network is functioning in a reliable fashion, the Link Quality Assessment algorithm be bypassed to ascertain the value contributed by this complex, time-consuming portion of the network operation. A month's data without the algorithm then can be compared with data from a month with the algorithm functioning to determine if the system overhead produces greater efficiency than achievable with a simpler approach having less overhead;
- Resources should be invested in the network to insure a minimum number of nodes remains operative for testing purposes;
- The study should be continued to test the primary hypothesis of communication improvement through networking using high frequency radio communication and computerized control.

1988 USAF-UES SUMMER FACULTY RESEARCH PROGRAM

GRADUATE STUDENT RESEARCH PROGRAM

SPONSORED BY THE

AIR FORCE OFFICE OF SCIENTIFIC RESEARCH

CONDUCTED BY THE

UNIVERSAL ENERGY SYSTEMS, INC.

FINAL REPORT

PREPARED BY: WAYNE A. CHARLIE[1], PH.D., P.E. AND STEVEN J. PIERCE[2]

ACADEMIC RANK: ASSOCIATE PROFESSOR[1] AND GRADUATE STUDENT[2]

DEPARTMENT: CIVIL ENGINEERING

UNIVERSITY: COLORADO STATE UNIVERSITY

RESEARCH LOCATION: AIR FORCE ENGINEERING AND SERVICE CENTER
HQAFESC (RDCS)
TYNDALL AIR FORCE BASE
PANAMA CITY, FLORIDA

USAF RESEARCHERS: DR. ALLEN ROSS AND STAN STRICKLAND

DATE: 15 SEPTEMBER 1988

CONTRACT NO: F49620-87-0004

High Intensity Stress Wave Propagation in Partially Saturated Sand

by

Wayne A. Charlie, Ph.D., P.E.
and
Steven J. Pierce

Abstract

We conducted high amplitude, Split Hopkinson Pressure Bar (SHPB) laboratory tests on specimens of 20-30 Ottawa and Eglin sands to evaluate the influence of saturation and capillary pressure on compressional wave velocity, stress transmission and damping. All specimens were compacted to a constant dry density and then subjected to a constant input stress. For specimens compacted at various water contents, both the wave speed and the transmitted stress ratio were found to increase as the saturation was increased from zero to approximately 30 percent and then decreased with increasing saturation. For specimens compacted dry, saturated and then desaturated utilizing the pressure-plate method, both the wave speed and the transmitted stress ratio were found to decrease with increasing saturation. Analysis of the experimental results indicates that these trends may be explained by the effect that capillary pressure has on the compaction effort required to compact the sands to a given dry density.

Acknowledgements

We wish to thank the Air Force Systems Command, the Air Force Office of Scientific Research and the Air Force Engineering and Service Center for sponsorship of this research. Universal Energy Systems, Inc. provided administrative and directional support. Dr. Allen Ross and Mr. Stan Strickland provided considerable technical support and encouragement in every phase of the research. Colonel Dale Hokanson's support of the USAF Summer Faculty/Graduate Student Research Program is greatly appreciated. Cheryl Garfield's help in obtaining housing and administrative support and Sergeant Frank Doerle's help in obtaining supplies was invaluable. We thank everyone for making our summer a fruitful, worthwhile and constructive experience.

I. Introduction

Stress wave velocity and stress transmission through soils are basic parameters required for the dynamic analysis of soil-structure response of buried structures subjected to blast loadings. During the life of a buried structure, it is probable that the field conditions will be significantly different than during construction. This is particularly true with regard to soil moisture and capillary pressure. However, there are no theoretical, empirical or numerical methods currently available for predicting large amplitude compressive stress wave velocity, stress transmission or damping in partially saturated sand as a function of saturation. Prediction of these values is currently based on the assumption that saturation and changes in saturation have little or no influence. Values are generally determined at in-situ or placed saturation and possible changes in saturation and, hence, changes in these values are ignored.

Research conducted on partially saturated soils by Bishop and Blight (1963), Fredlund and Morgenstern (1976), Hryciw and Dowding (1987), Fredlund (1986) and Wu et al. (1984) have shown that the shear strength, soil compressibility, cone penetration and low-amplitude shear wave velocity is affected by capillary stress. Ross et al. (1986) found that saturation affected wave speed and stress transmission in samples of 50-80 silica sand subjected to high amplitude compressive stress wave loading. The soil was compacted to the same dry density at various water contents. The only apparent reason for the difference was due to the water content (saturation) and capillary pressure during compaction and testing. Their research suggests that capillarity may also affect high amplitude stress wave parameters. Our research was conducted to see if soil saturation and hence capillary stress would change compressional stress wave parameters at large strain levels.

Professor Wayne Charlie's research interests have been in soil dynamics and explosive-induced compressional stress wave propagation in water saturated soil. He has conducted research for AFOSR on blast-induced liquefaction of saturated sand. He has also conducted research and has consulted in the area of strength and potential volume change of partially saturated soils. Graduate student Steven Pierce's research interests are in the area of stress wave transmission in partially saturated soil. Steve has also been involved in the AFOSR funded blast-induced liquefaction research conducted by Professor Charlie.

II. Objectives of Research

Our objective as participants in the 1988 Summer Faculty/Graduate Student Research Program was to determine if differences in wave speed, stress transmission and damping were actually due to capillary pressure. If so, our objective was to determine if it was due to the capillary pressure during soil compaction, the capillary pressure during testing, or both. Our secondary objective, which has now become our primary objective, was to develop a theoretical method to predict wave speed, stress transmission and damping as a function of capillary pressure.

Partially saturated soils are defined for our research as having continuous air and water phases. Because of capillary effects at the air-water interfaces, the porewater pressure, u_w, is less than the poreair pressure, u_a. Continuous air and water phases generally occur at water saturation levels less than approximately 85 percent (McWhorter and Sunada, 1977). If the poreair pressure is at atmospheric pressure, ($u_a = o$), the porewater pressure must be negative ($u_w < 0$). Most soil deposits located a few meters or more above the regional groundwater table are partially saturated and the air pressure is at atmospheric pressure.

Bishop et al. (1963) first suggested that the constitutive relations for partially saturated soils must include total stress, σ, poreair pressure, u_a, and porewater pressure, u_w. Bishop defined the effective stress, $\bar{\sigma}$, for partially saturated soil as:

$$\bar{\sigma} = (\sigma_n - u_a) + X(u_a - u_w) \qquad \text{Eq. 1}$$

where X is an empirical parameter representing the proportion of soil suction, ($u_a - u_w$,) that contributes to effective stress. Fredlund (1986) suggested a theoretical model for the change in volume of a partially saturated soil which does not include an empirical parameter X. Fredlund has shown that a change in the volumetric strain, ϵ, of a partially saturated soil is a function of the total stress, σ, the poreair pressure, u_a, and the porewater pressure, u_w, in the soil. This can be expressed as:

$$\epsilon = C_t \cdot d(\sigma - u_a) + C_w \cdot d(u_a - u_w) \qquad \text{Eq. 2}$$

where C_t is the compressibility of the soil structure with respect to a change in (σ-u_a), and C_w is the compressibility of the soil structure with respect to a change in ($u_a - u_w$). Because wave speed is a function of soil compressibility,

a similar relationship may exist between the wave speed and $(\sigma - u_a)$ and $(u_a - u_w)$.

III. Research Conducted

To meet our objectives, we tested two sands (20-30 Ottawa sand and Eglin sand) at various saturation levels. These sands were compacted both moist and dry and subjected to two confining stresses. The samples compacted moist were compacted at various moisture contents to give various saturation levels. This compaction method was utilized by Ross et al. (1986). The samples compacted dry were saturated after compaction and then desaturated utilizing the pressure plate apparatus. Saturation -desaturation versus capillary pressure curves for the two sands were experimentally determined by us at Colorado State University. The pressure-plate desaturating equipment utilized was developed at Colorado State University and was taken to Tyndall Air Force Base for our summer research. Our dynamic testing was conducted with the Split Hopkinson Pressure Bar Apparatus (SHPB) located at the Engineering and Service Center at Tyndall Air Force Base. Details of the SHPB are given by Ross et al. (1986).

Dr. Allen Ross and Stan Strickland supported and assisted us in our research. Dr. Ross guided us in our dynamic testing techniques and Professor Charlie supplied the expertise in partially saturated soil. Steven Pierce prepared the samples, conducted the tests and reduced and plotted the data.

IV. Research Results

Experimental results and those obtained by Ross et al. (1988) for 20-30 Ottawa and Eglin sands compacted moist to a void ratio of 0.510 are given in Figures 1 through 4. These Figures show that both the wave speed and stress transmission increase as saturation increases from 0 to approximately 30 percent and then decrease at increasing saturation levels above 30 percent.

Our experimental results for 20-30 Ottawa and Eglin sands compacted dry to a void ratio of 0.510, then saturated and desaturated by the pressure plate apparatus, are given in Figures 4 through 12. These Figures show that both wave speed and stress transmission increase with increasing confining stress, and decrease with increasing saturation.

V. Recommendations

The moisture content and hence saturation and capillary pressure during compaction and during testing are important factors to consider in predicting

The moisture content and hence saturation and capillary pressure during compaction and during testing are important factors to consider in predicting wave velocity and stress transmission in partially saturated compacted sand. We recommend that additional experimental research be conducted and that theoretical models be developed. For the experimental research, we recommend that water content (saturation), capillary pressure and compaction methods be varied and the wave speed, stress transmission, quasi-static stiffness and lateral stress variations be determined. The energy required to compact sand to a constant dry density as a function of water content should be determined to better understand how saturation influences compaction. To develop theoretical models, we recommend that the theory of effective stress developed by Bishop and Blight (1963) and expanded by Fredlund (1985) for quasi-static stiffness of partially saturated soils be incorporated to mathematically model stress wave velocity and stress transmission.

VI. References

Bishop, A. W., Blight, G. E., "Some Aspects of Effective Stress in Saturated and Partially Saturated Soils," Geotechnique, Vol. 13, No. 3, Sept., 1963, pp. 177-179.

Fredlund, D. G., "Soil Mechanics Principles that Embrace Unsaturated Soils," Proc. of the Eleventh Int. Conf. on Soil Mechanics and Foundation Eng., SSMFE, San Francisco, 1986, pp. 465-472.

Fredlund, D. G. and Morgenstern, N. R., "Constitutive Relations for Volume Change in Unsaturated Soils," Canadian Geotechnical J., Vol. 13, 1976, pp. 261-276.

Hryciw, R. D. and Dowding, C. H., "Cone Penetration of Partially Saturated Sands," Geotechnical Testing Journal, ASTM, Vol. 10, No. 3, Sept. 1987, pp. 135-141.

McWhorter, D. and Sunada, D. K., Ground-Water Hydrology and Hydraulics, Water Resources Publications, Fort Collins, Colorado, 1977.

Ross, C. A., Nash, P. T. and Friesenhahn, C. J., "Pressure Waves in Soils Using a Split-Hopkinson Pressure Bar," ESL-TR-86-29, AF Engineering and Services Center, Tyndall AFB, Florida, July 1986.

Ross, C. A., Thompson, P. Y. and Charlie, W. A., "Moisture Effects on Wave Propagation in Soils," Abstracts Seventh ASCE/EMD Speciality Conf. Virginia Polytechnic Institute and State University, Blacksburg, Virginia, May 1988.

Wu, Shiming, Gray, Donald, H., Richart, F. E., "Capillary Effects on Dynamic Modulus of Sands and Silts," J. of Geotechnical Eng., ASCE, Vol. 110, No. 9, Sept. 1984, pp. 1188-1203.

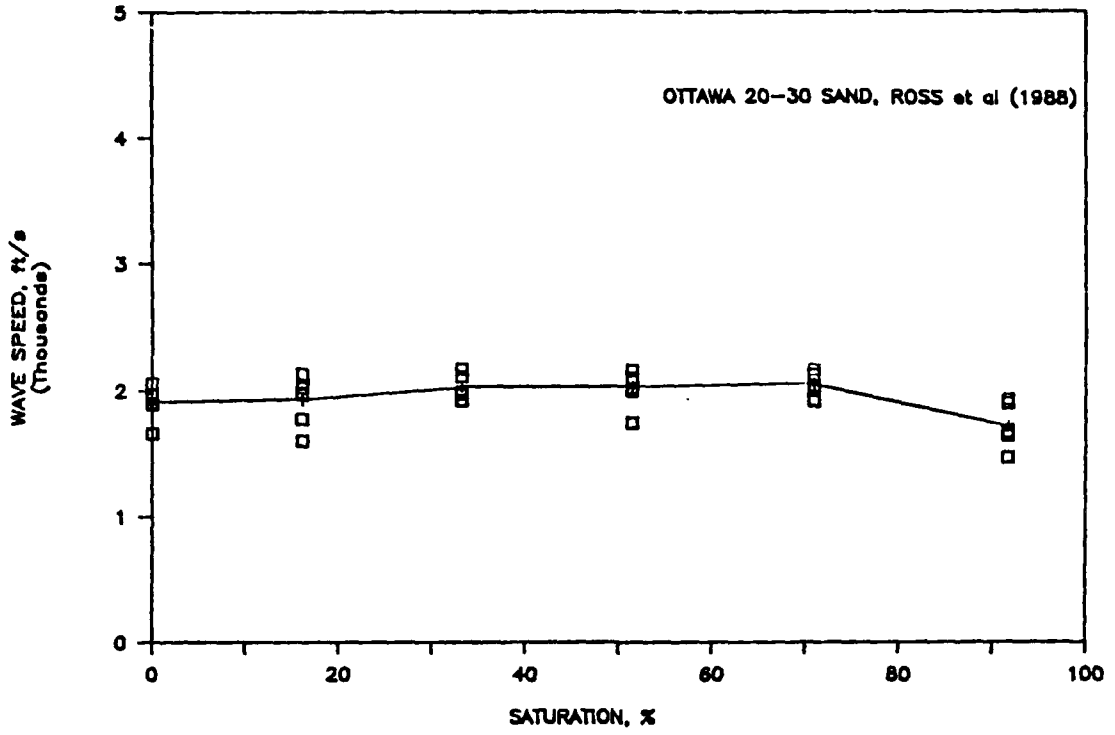


Figure 1. Wave Speed Results for 20-30 Ottawa sand compacted moist and tested with zero confining stress.

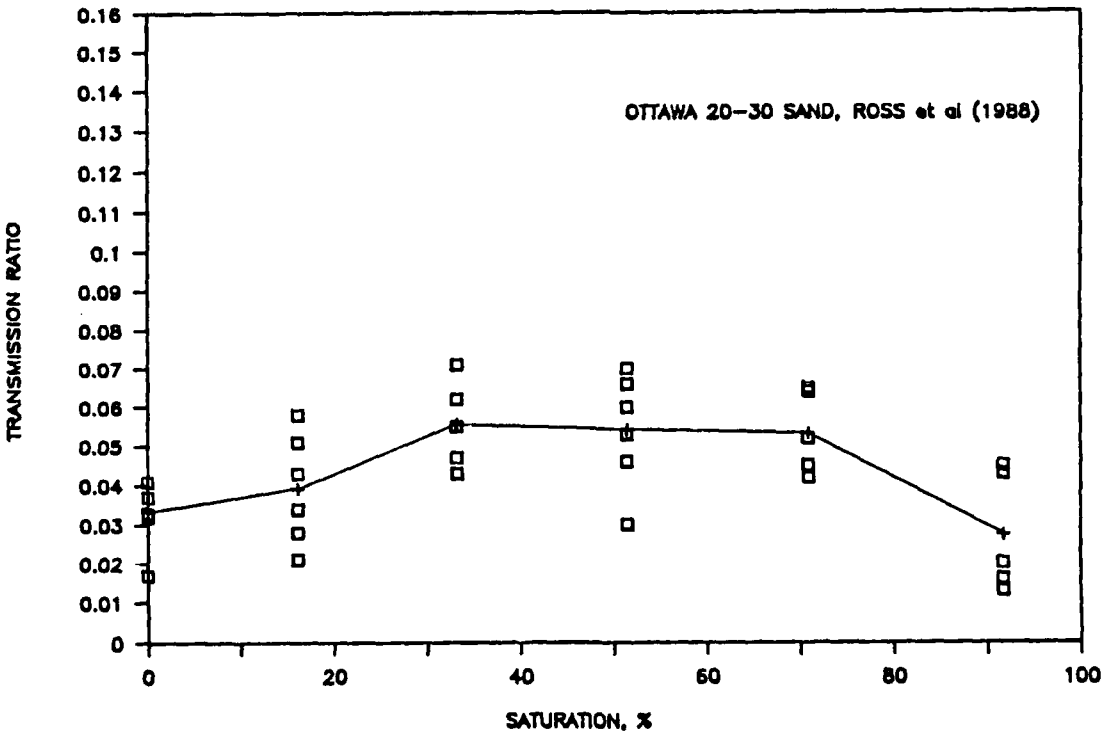


Figure 2. Transmission ratio results for 20-30 Ottawa sand compacted moist and tested with zero confining stress.

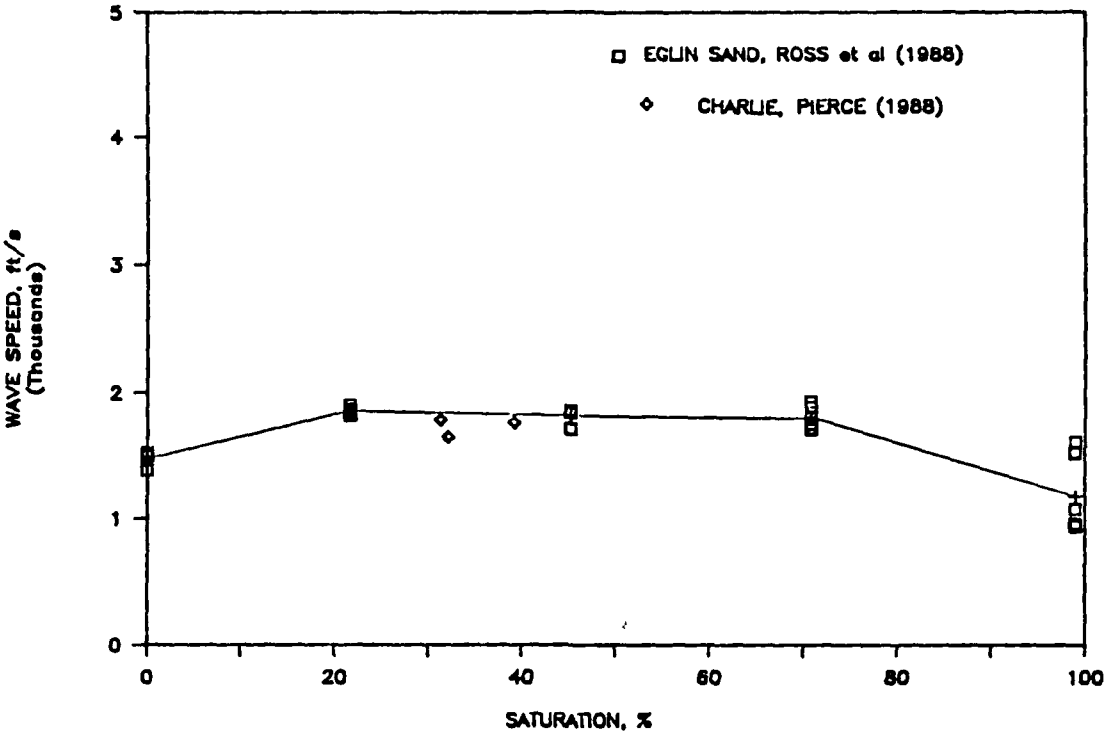


Figure 3. Wave speed results for Eglin sand compacted moist and tested with zero confining stress.

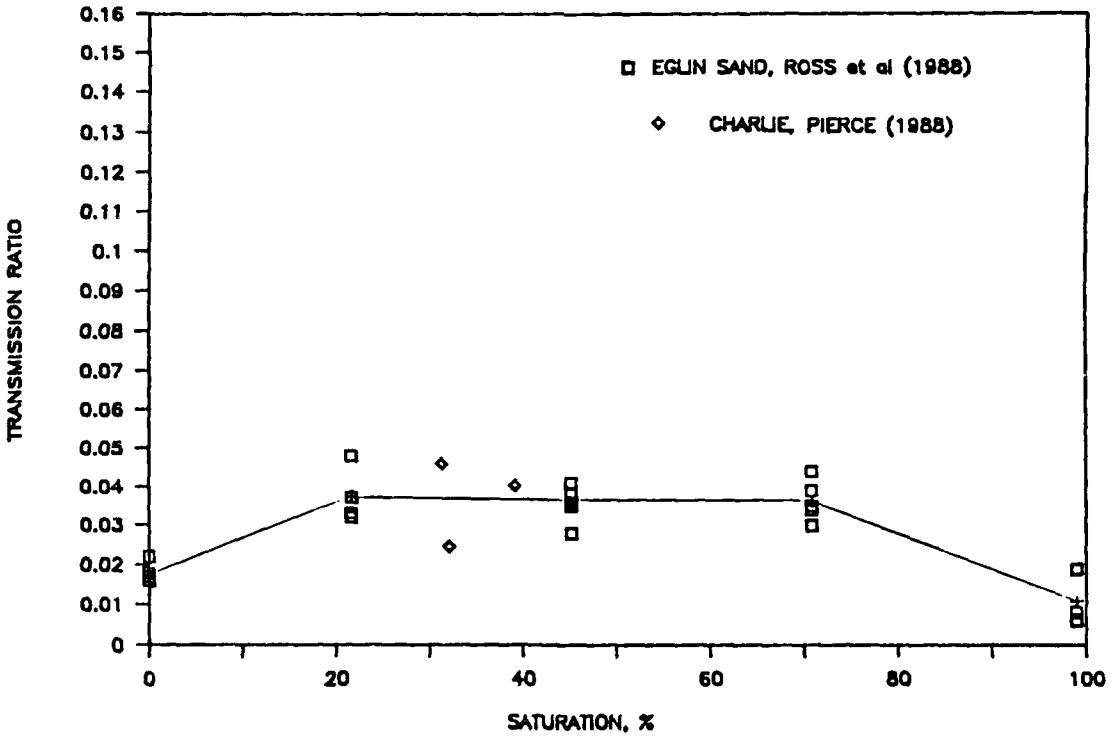


Figure 4. Transmission ratio results for Eglin sand compacted moist and tested with zero confining stress.

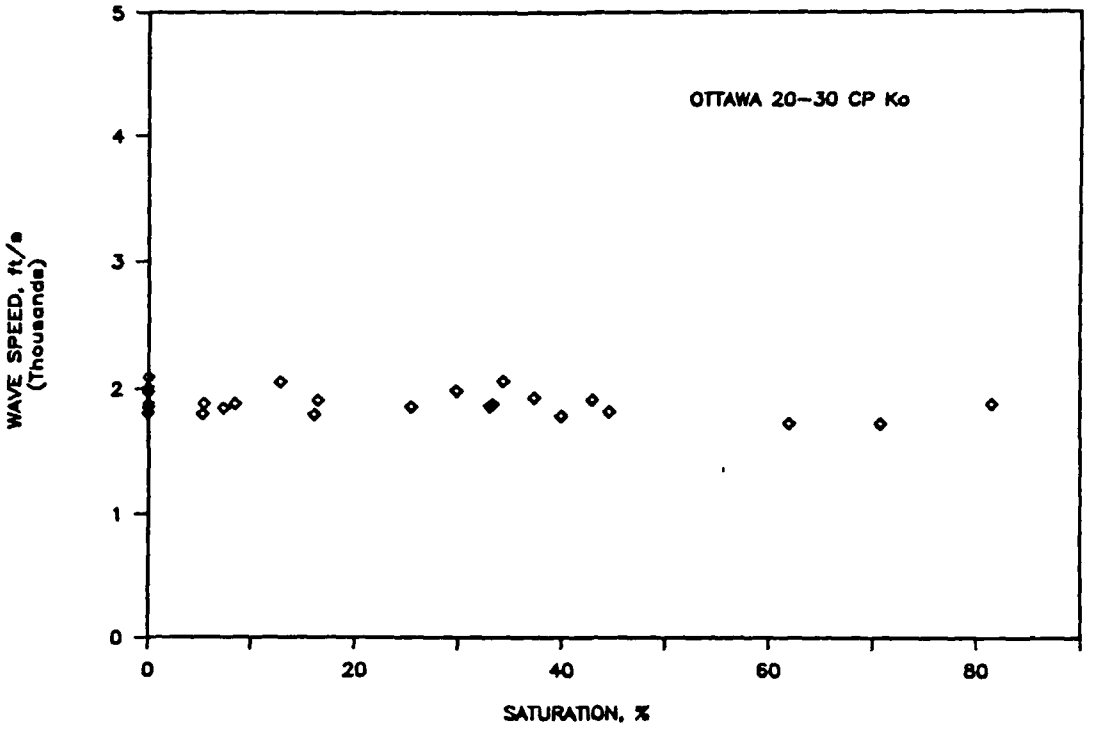


Figure 5. Wave speed results for 20-30 Ottawa sand compacted dry and tested with zero confining stress.

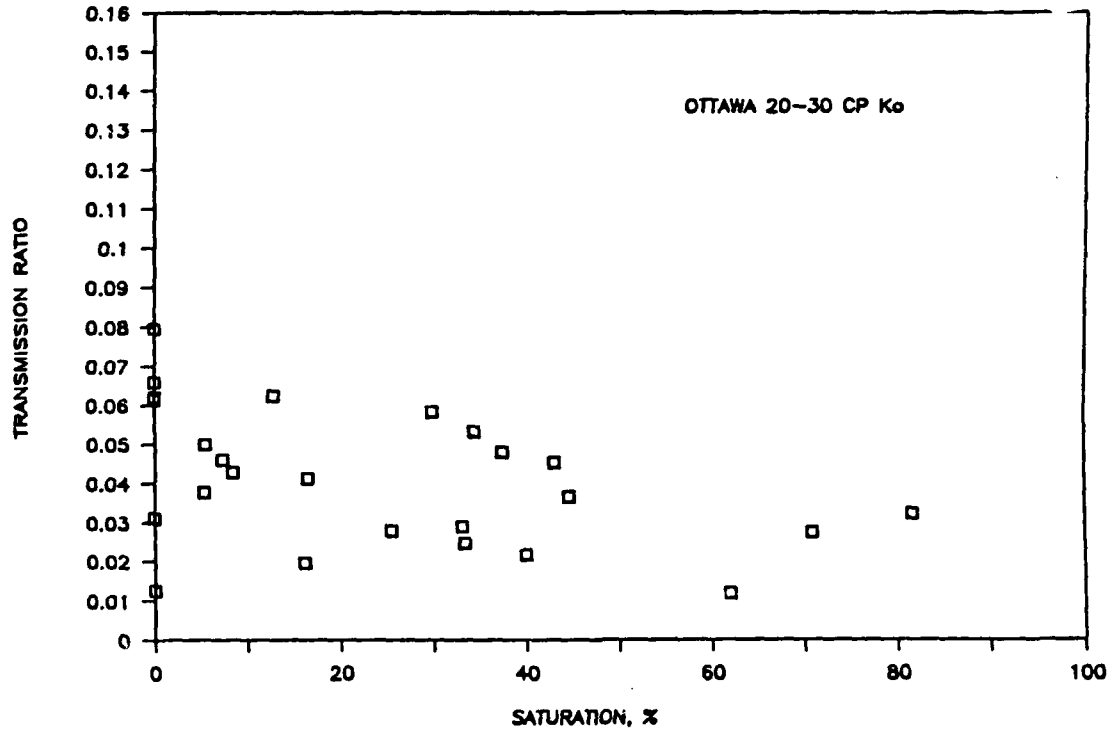


Figure 6. Transmission ratio results for 20-30 Ottawa sand compacted dry and tested with zero confining stress.

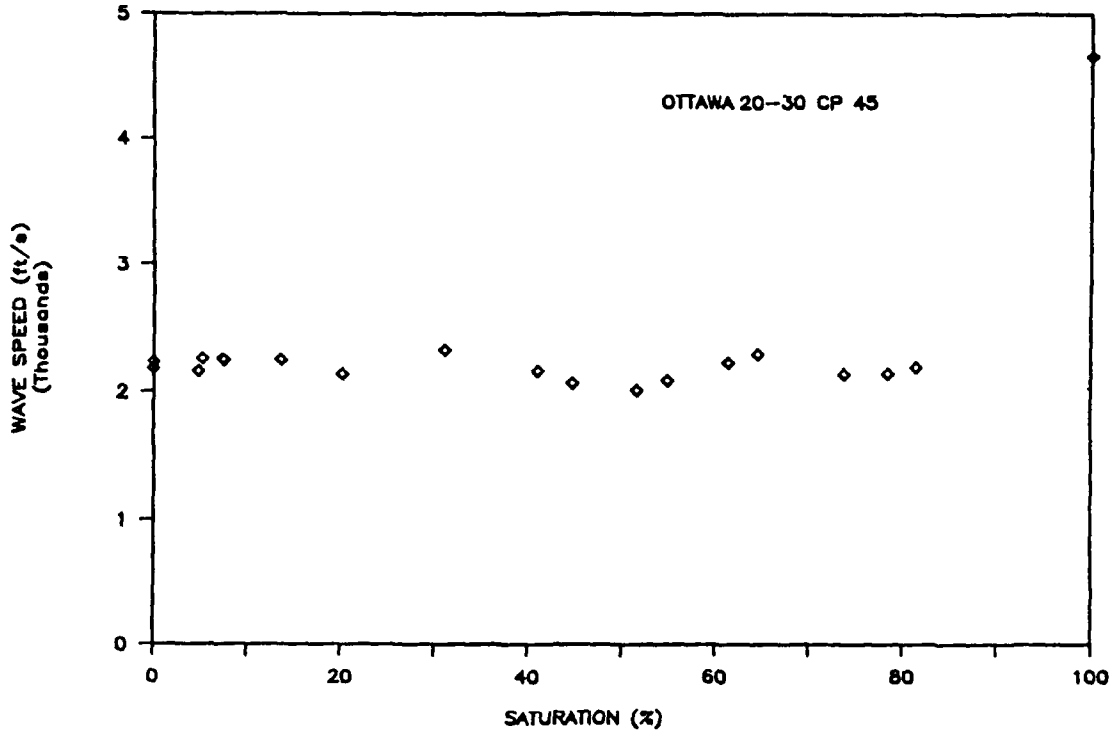


Figure 7. Wave speed results for 20-30 Ottawa sand compacted dry and tested with 45 p.s.i. confining stress.

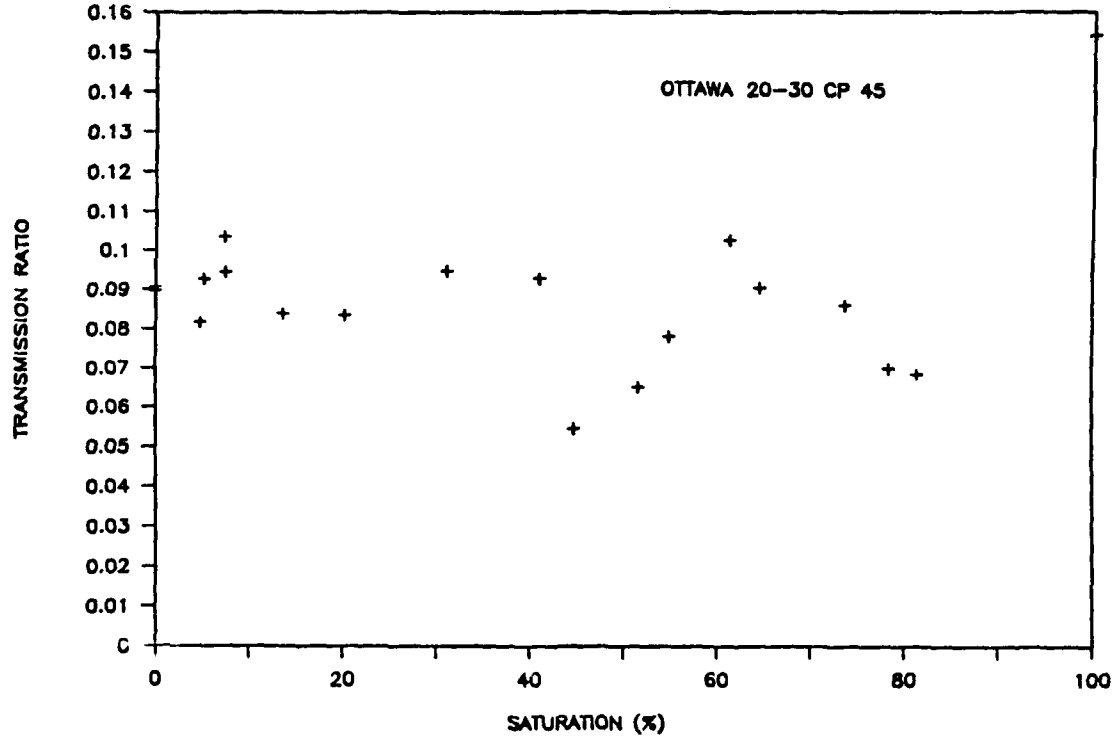


Figure 8. Transmission ratio results for 20-30 Ottawa sand compacted dry and tested with 45 p.s.i. confining stress.

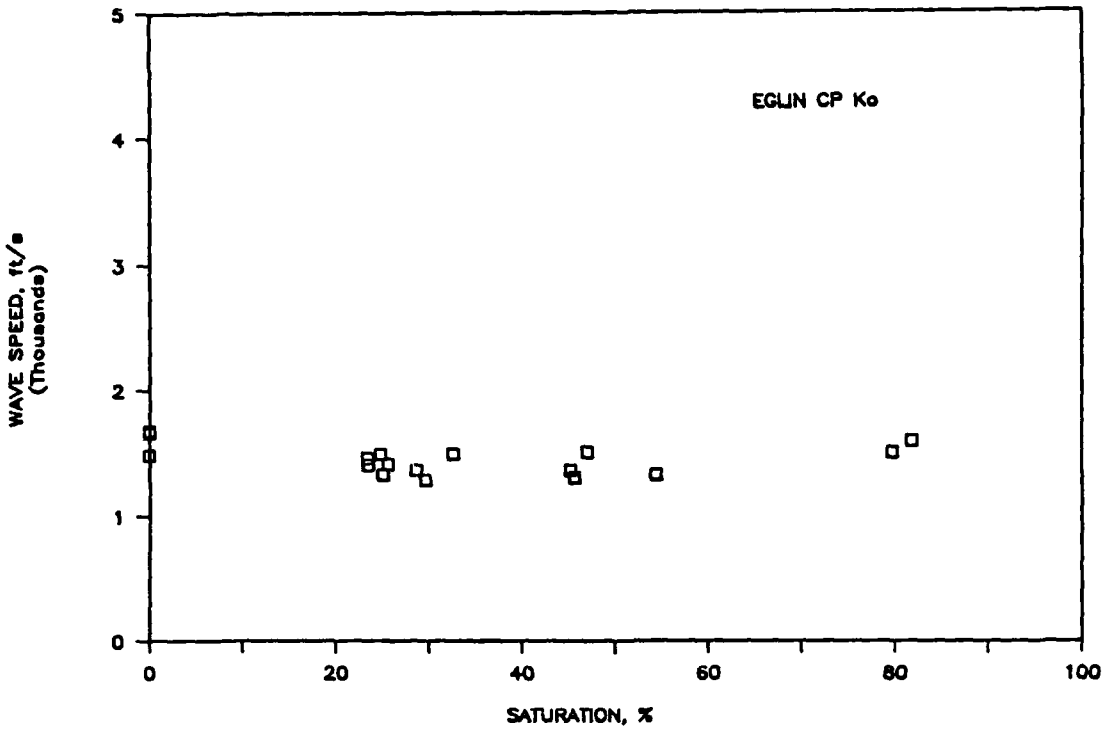


Figure 9. Wave speed results for Eglin sand compacted dry and tested with zero confining stress.

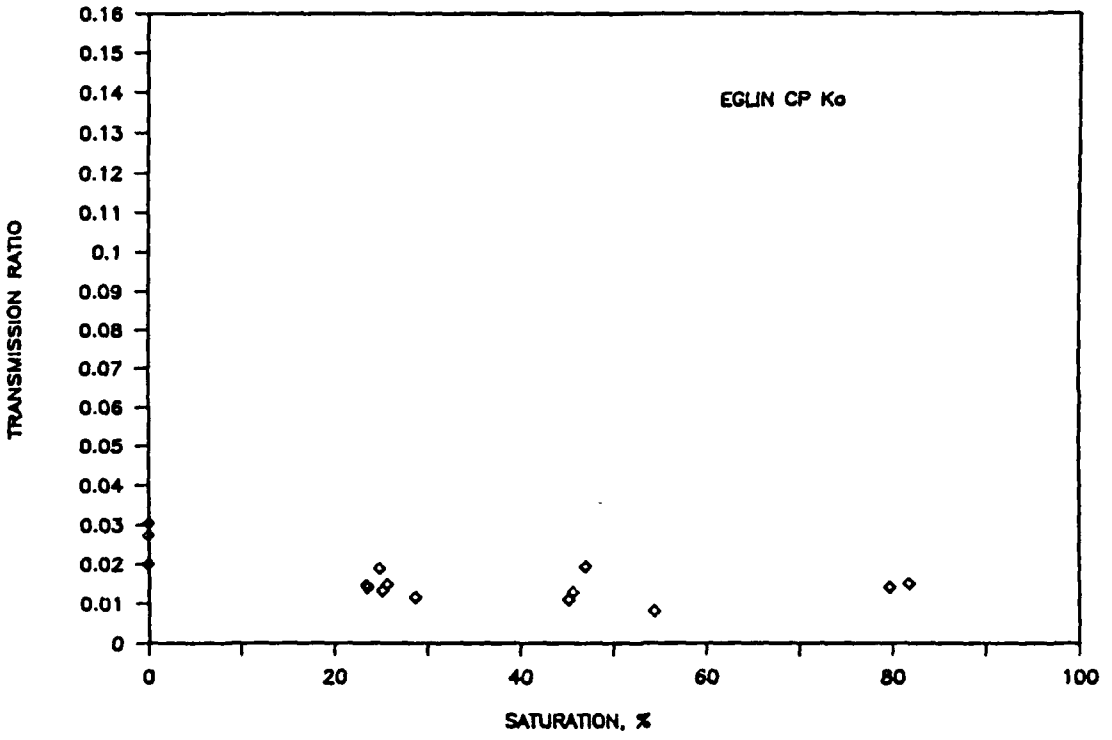


Figure 10. Transmission ratio results for Eglin sand compacted dry and tested with zero confining stress.

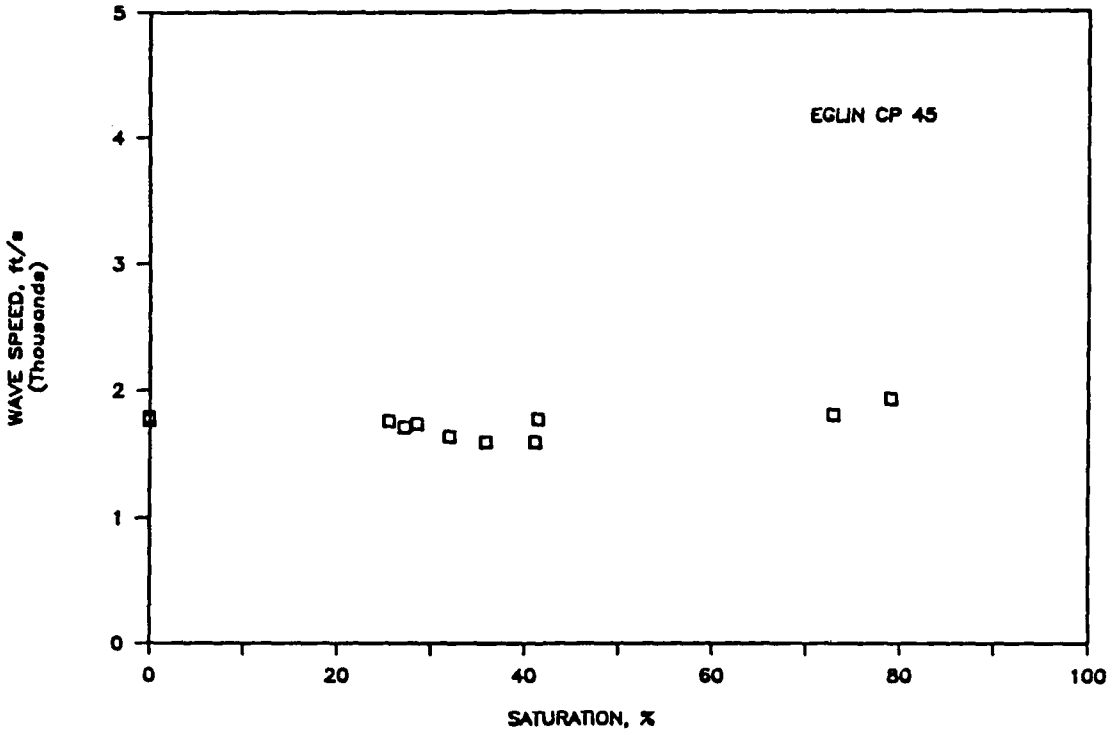


Figure 11. Wave speed results for Eglin sand compacted dry and tested with 45 p.s.i. confining stress.

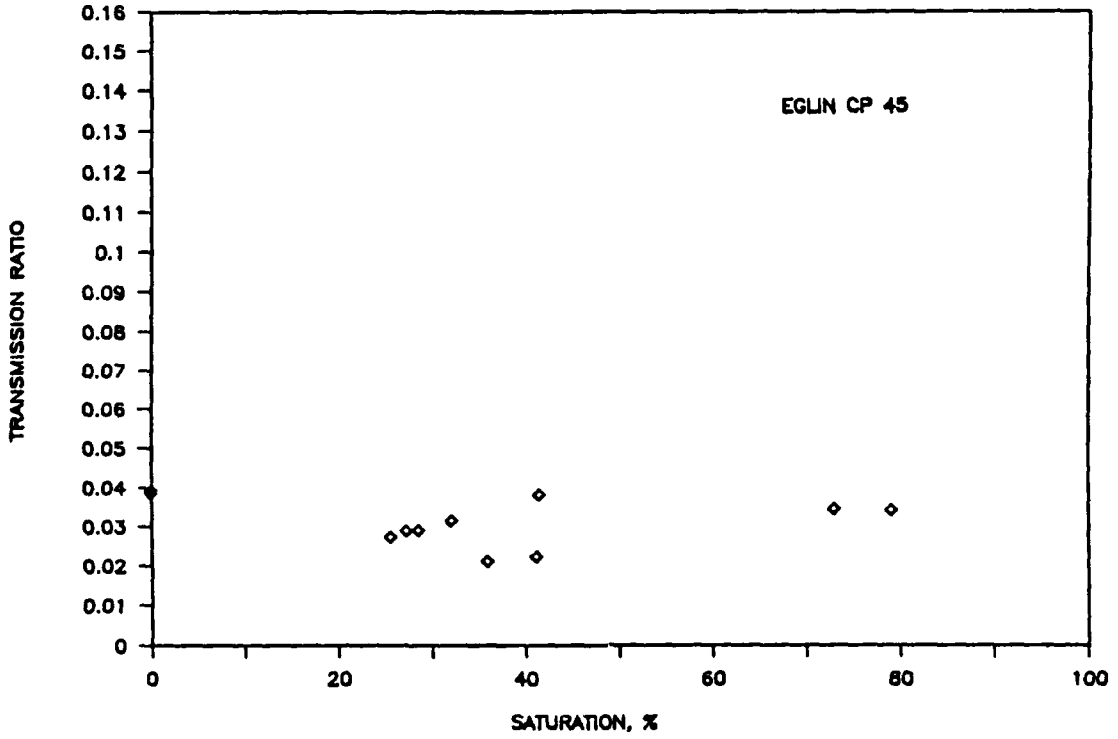


Figure 12. Transmission ratio results for Eglin sand compacted dry and tested with 45 p.s.i. confining stress.

1988 USAF-UES SUMMER FACULTY RESEARCH PROGRAM/

GRADUATE STUDENT RESEARCH PROGRAM

Sponsored by the

AIR FORCE OFFICE OF SCIENTIFIC RESEARCH

Conducted by the

Universal Energy Systems, Inc.

FINAL REPORT

INDIVIDUALIZATION OF HUMAN TISSUE BY THE SEROLOGIC IDENTIFICATION OF ERYTHROCYTE ANTIGENS

Prepared by:	David H. DeHeer, Ph.D.
Academic Rank:	Associate Professor
Department and	Department of Biology
University:	Calvin College
Research Location:	Air Force Mortuary Services
	Tyndall Air Force Base
	Panama City, FL 32403-6001
USAF Researcher:	Mr. L.H. Nester
Date:	August 10, 1988
Contract No.:	F49620-87-R-0004

INDIVIDUALIZATION OF HUMAN TISSUE BY THE SEROLOGIC IDENTIFICATION OF ERYTHROCYTE ANTIGENS

by

David H. DeHeer, Ph.D.

ABSTRACT

Air Force investigators frequently are required to identify and individualize multiple tissue fragments recovered after aircraft mishaps. Serologic techniques offer the greatest possibility for individualization because they detect genetically determined antigens present in tissue. To permit the analysis of tissue, extracts of human red blood cells and skeletal muscle were prepared in 5% ammonium hydroxide and clarified by centrifugation. The erythrocyte antigens in the extracts were identified in a sensitive hemagglutination-inhibition assay performed in 96-well microtiter plates. Both direct and indirect assays were developed using commercially available antisera. A detailed procedure manual was written and investigation specialists were trained in the application and use of the serologic techniques.

ACKNOWLEDGEMENTS

I wish to thank the Air Force Systems Command and the Air Force Office of Scientific Research for their sponsorship of this research. I also wish to thank Universal Energy Systems, Inc. for their competent administration and direction of this program.

I am grateful to Maj. Larry Bramlitt and Maj. Pat Eagan, my Focal Point Effort officers, and to Cheryl Garfield for their efficient and courteous assistance throughout the summer. I wish to thank Leonard Nester, Chief of Mortuary Services, for orienting me to the problems facing mortuary personnel. For their advice, direction, and support, I am indebted to Col. William Craig, Cam Beauchemin, Donn Durham, Bonnie St. Clair, Jeannette Laningham, Linda White and Maria Johnson. I am especially grateful to Pete Kay, Brad Bates and Gary Huey, the Identification Specialists with whom I worked closely, for their ongoing help and friendship; they provided excellent technical assistance and contributed greatly to this research effort.

I. INTRODUCTION:

Airplane crashes, especially those involving high speed tactical aircraft, frequently result in loss of life with mutilation and fragmentation of the victims. In those mishaps involving multiple victims, investigating identification specialists are faced with three major tasks: (1) identification of remains, e.g., identifying tissue and determining which is human; (2) individualization of tissue, e.g., determining the identity of the remains; and (3) reassociation of multiple tissue fragments. These tasks may be accomplished by a variety of methods, including fingerprint and footprint analyses, hair analysis, dental comparisons, anthropological studies, and serologic procedures. Each technique is useful because it has the potential for detecting genetically determined markers or characteristics that may be individual specific.

The circumstances of a particular mishap, however, may limit the number of identification techniques that can be used. For example, fingerprints and footprints may be destroyed, hair may be burned, dentition may be obliterated, or extensive fragmentation may preclude anthropological identification. Under these circumstances, serologic techniques offer the greatest potential ior individualization and reassociation because each cell and tissue in a fragment possesses unique markers that can be identified by appropriate laboratory techniques.

The most common serologic procedures are those employed for identification of erythrocyte surface antigens. Erythrocyte antigens are present on red blood cells and most are ubiquitous in human tissue (Race and Sanger, 1975; Oriol et. al., 1980); this distribution obviates the need to analyze only blood or blood cells, a tissue that is rarely recovered after aircraft mishaps. Air Force identification specialists currently use a macroscopic hemagglutination-inhibition technique to identify erythrocyte antigens in tissue fragments (Boorman et. al., 1977). The analysis is limited to detection of ABH antigens and uses tissue that has been heated prior to the preparation of an extract. Since heat may denature or otherwise destroy protein antigens, the current procedure may preclude successful analysis of some tissue fragments. Also, tissue from individuals with identical ABO types could not be individualized using present techniques.

II. OBJECTIVES OF THE RESEARCH EFFORT:

The hemagglutination-inhibition technique used by the identification specialists employs a test tube procedure that requires comparatively large quantities of reagents, tissue extracts and supplies. It is cumbersome and very time consuming especially when hundreds of fragments are recovered for analysis. The first objective was to miniaturize the assay and to simplify data collection.

The second objective was to develop a technique for the preparation of tissue extracts that does not require heat and which can be performed rapidly. In the existing protocol, each tissue sample is washed with saline, heated to boiling for 10 minutes, homogenized for 3-5 minutes, and centrifuged to pellet cellular debris and contaminants. Various dilutions of the supernatant fluid then are assayed for ABH antigens in the hemagglutination-inhibition test. This procedure is very tedious; at present one technician can prepare and test approximately 25 tissue extracts per day.

To increase the likelihood of distinguishing between tissue fragments from two or more individuals, erythrocyte antigens other than ABH must be tested. A third objective was to develop hemagglutination-inhibition procedures that would employ at least ten commercially available antisera. Since certain antisera require an indirect rather than a direct assay, routine protocols for both types of assays would be required.

A fourth objective was to train the identification specialists in the use of all procedures and to develop a detailed and extensive procedure manual together with appropriate forms for recording data.

III. RESEARCH SUMMARY

At the time of an aircraft mishap the identification specialists perform all serologic testing at a facility, usually a hospital laboratory, in close proximity to the crash site. All reagents and supplies and most equipment are acquired from the facility. So that this practice may be continued, all newly developed procedures were designed to utilize reagents and supplies likely to be found in a clinical facility. This practice does restrict the type of serologic assays that can be performed.

Both antibody titration and hemagglutination-inhibition assays were performed in 96-well "V" bottom microtiter plates (Wegman and Smithie, 1966; Davie, 1979). Direct titration assays utilized commercially available antisera of IgM class. The assay was performed by mixing 25 µl of an antibody dilution, 25 µl of diluent, and 25 µl of a 0.2%-0.3% suspension of erythrocytes of known type and specificity. Unbuffered isotonic saline containing 1% bovine serum albumin (BSA) was used as the diluent (van Oss et. al., 1978). After a 30 minute room temperature incubation, the microtiter plates were centrifuged at 1,300 x g for 3 minutes at room temperature. Finally the plates were placed at an approximate 60° angle for at least 30 minutes or until cell streaming was observed in the negative control wells. Hemagglutination was assessed by visual inspection based on the appearance of a cell

button and cell streaming. The degree of hemagglutination was scored from negative to 4+.

In a direct inhibition assay, 25 µl of the appropriate antibody dilution, determined previously in titration assays, was mixed with 25 µl of a dilution of tissue extract. The mixture was incubated at 4°C overnight (at least 15 hours). 25 µl of a 0.2%-0.3% suspension of red blood cells were added and the mixture was incubated for 30 minutes at room temperature. The microtiter plates were centrifuged and incubated at an approximate 60° angle as in the titration assays. The degree of hemagglutination was scored from negative (complete inhibition) to 4+ (no inhibition).

A considerable effort was made to devise a simple, effective technique for preparing tissue extracts. Three diluents were tested: (1) saline containing 1% BSA; (2) deionized water; and (3) 5% (v/v) ammonium hydroxide. Two methods of disrupting cell membranes also were explored: (1) homogenization with a Potter-Elvehjem tissue grinder; and (2) homogenization with a motorized high-speed Biomixer. Finally, the optimal time of homogenization and/or incubation was explored.

Erythrocytes of known type and specificity were placed in each of the three diluents and homogenized for varying times ranging from 0 to 8 minutes in 1 minute increments. The efficacy of cell disruption was assessed on the basis of pellet size after centrifugation at 1,540 x g

for 30 minutes at room temperature and on the basis of soluble hemoglobin in the supernatant. Hemoglobin concentration was determined spectrophotometrically by measuring optical density at 540 nm. The quantity of soluble erythrocyte antigen in each extract was determined in hemagglutination-inhibition assays using the appropriate antiserum.

Comparison of the effectiveness of saline and deionized water as diluents demonstrated that maximum solubilization of membrane antigen occurred after homogenization in water for 2 minutes with a Biomixer. However, five volumes of 5% ammonium hydroxide completely disrupted erythrocytes as evidenced by the absence of a cell pellet after centrifugation and by maximum hemoglobin release. Lower concentrations of ammonium hydroxide were less effective or ineffective in disrupting cell membranes. Since the 5% ammonium hydroxide solution alone caused complete hemolysis, homogenization was unnecessary.

To eliminate the possibility that ammonium hydroxide interfered with hemagglutination-inhibition assays, 25 µl of 5% ammonium hydroxide was substituted for 25 µl of tissue extract. Neither false positive agglutination of erythrocytes nor lysis of red cells was observed.

Dilution experiments demonstrated that as little as 0.5 µl of packed human erythrocytes solubilized in 5% ammonium hydroxide could be correctly typed using the hemagglutination-inhibition procedure. Assay

sensitivity was estimated to be at least 1,000-fold greater than that obtained with the previous assay and extract preparation procedures.

Since erythrocyte samples are rarely if ever recovered after an aircraft mishap, preliminary experiments were performed to determine the effectiveness of the extract and assay procedures with striated muscle, a tissue more commonly recovered after mishaps. Extracts of human skeletal muscle were prepared in 5% ammonium hydroxide without homogenization and assayed for ABO and MN antigens using the microtiter procedure. Each specimen was correctly typed.

In order to increase the number of antigens that can be identified in tissue, an indirect hemagglutination-inhibition assay was developed. This assay employed a commercially available anti-IgG antiserum which was titrated using indirect Coomb's positive erythrocytes. The indirect assay differed from the direct inhibition assay in that the erythrocytes were washed three times after the incubation step and anti-IgG was added prior to centrifugation.

In a final effort, a detailed procedure manual was written listing step-by-step instructions as well as the theoretical basis for each serologic technique. Seven forms were designed for recording data. Each identification specialist was provided with a copy of the 67-page manual and was trained in the application, use and interpretation of the serologic techniques.

IV. RECOMMENDATIONS

A. A second work bench should be installed in the Forensic Laboratory at Tyndall AFB to provide additional work space. The existing bench as well as the new one should be equipped with a center module with 3 or 4 full-length shelves and numerous electrical outlets. Rationale: (1) the existing bench space is completely utilized and more is required at the present time; (2) as new procedures and equipment are added, more bench space will be essential.

B. The identification specialists should work a minimum of two consecutive days per week in the laboratory, preferably working in pairs. Rationale: (1) nearly all of the procedures they will use are new and require practice to develop and maintain proficiency; (2) the hemagglutination-inhibition assays require an overnight incubation; they need to be set up one day and evaluated the next; and (3) other procedures are too lengthy to be performed in a single day.

C. Serologic procedures currently are performed at a facility near the the site of an aircraft mishap. However, in the future they should be accomplished in the Forensic Laboratory at Tyndall AFB. Rationale: (1) the required microtiter equipment and antisera may be unavailable in the field, particularly at small clinical

facilities; (2) the amount of work space and refrigerat r ..ce available to the identification specialists in the field will be insufficient to perform large numbers of assays in a short period of time, and (3) the equipment located in the Forensic Laboratory is not portable.

D. Additional identification techniques should be developed and implemented in the following sequence: (1) ELISA microplate assays for erythrocyte surface antigens; ELISA assays are more sensitive and less cumbersome than hemagglutination-inhibition procedures and can be automated; (2) an elution assay to replace the hemagglutination-inhibition assay; (3) electrophoretic assays for identification of polymorphic enzymes in tissue extracts; (4) DNA fingerprinting procedures. This sequence, which increases in technological complexity but also in capability for individualization, should be completed over the next 3-4 years. DNA fingerprinting, while offering the greatest potential for individualization, is technically very complex and rather expensive to perform. It should receive the lowest priority. It is noteworthy that the FBI is just beginning an intensive study of DNA fingerprinting procedures and applications. Development of this technology at the Forensic Laboratory should not begin until after the FBI has completed and published the results of its study.

E. The identification specialists should attend an annual two-week refresher course in serological procedures to be conducted at the Forensic Laboratory at Tyndall AFB. Rationale: (1) serologic procedures will need to be refined as more experience using them is acquired; (2) the identification specialists are not full time serologists - a time of intensive training and review would be beneficial.

F. D. Deheer should accompany the identification specialists to the first multiple-victim aircraft mishap that occurs after the summer visit. Rationale: (1) the new techniques have been performed in the laboratory with laboratory specimens, not actual specimens acquired in the field; (2) first-hand knowledge obtained at an actual mishap will be beneficial in modifying existing procedures and in designing additional procedures.

REFERENCES

Boorman, K.E., B.E. Dodd and P.J. Lincoln. Blood Group Serology. Theory, Techniques, Practical Applications. 5th edition, Churchill Livingstone, London, 1977.

Davie, M.J. ABO, Gm and Km Grouping of Bloodstains on Microtitre Plates. J. Forens. Sci. Soc. 1979, 19: 59-64.

Oriol, R., J.P. Cartron, J. Cartron, and C. Mulet. Biosynthesis of ABH and Lewis Antigens in Normal and Transplanted Kidneys. Transplantation, 1980, 29: 184-188.

Race, R.R. and R. Sanger. Blood Groups in Man. Blackwell Scientific Publications, Osney Mead, Oxofrd, 1975.

Van Oss, C.J., J.F. Mohn and R.K. Cunningham. Influence of Various Physicochemical Factors on Hemagglutination. Vox Sang. 1978, 34: 351-361.

Wegman, T.G. and O. Smithie. A Simple Hemagglutination System Requiring Small Amounts of Red Cells and Antibodies. Transfusion, 1966, 6: 67-73.

1988 USAF-UES SUMMER FACULTY RESEARCH PROGRAM/

GRADUATE STUDENT RESEARCH PROGRAM

Sponsored by the

AIR FORCE OFFICE OF SCIENTIFIC RESEARCH

Conducted by the

Universal Energy Systems, Inc.

FINAL REPORT

ESTIMATION OF JET FUEL CONTAMINATION IN SOILS

Prepared by:	Deanna S. Durnford, PhD.
Academic Rank:	Assistant Professor
Department and	Agricultural and Chemical Engineering
University:	Colorado State University
Research Location:	USAFESC/RDVW, Tyndall AFB, Florida
USAF Researcher:	Jack Milligan
Date:	September 1, 1988
Contract No:	F49620-87-R-0004

ESTIMATION OF JET FUEL CONTAMINATION IN SOILS

by

Deanna S. Durnford

ABSTRACT

A petroleum product used for jet fuel called JP4 has been found in well bores penetrating unconfined aquifers underlying several air force bases. Because of the widespread use of JP4 and its potential for contamination of the vadose zone, an accurate method for predicting the total quantity and distribution of this fuel in the subsurface is essential.

A methodology that can be used to estimate the quantity of JP4 in soil from well bore data was developed and illustrated during this project. The basic data required was determined and laboratory column studies were used to illustrate the procedure.

ACKNOWLEDGEMENTS

I wish to thank the Air Force Office of Scientific Research/AFSC, United States Air Force for sponsoring this research and Universal Energy Systems for their administration of the program. My experience was very rewarding, both professionally and personally, because of the opportunity to interact with both researchers and staff at Tyndall AFB. Although the people who contributed to this work and the quality of this experience are too numerous to mention by name, I would be remiss if I did not at least acknowledge the support and help of Mr. Jack Milligan. His enthusiasm and patience is sincerely appreciated.

I. INTRODUCTION:

Monitoring or observation wells are commonly used to estimate the total quantity of an immiscible hydrocarbon in the subsurface environment. After leakage or spillage of a light non-aqueous phase liquid (LNAPL), monitoring wells are installed and the thickness of the floating LNAPL in each well bore is measured. From this data, an estimate of the horizontal extent of the floating contaminant and total accumulation in the subsurface is made. However, there are interpretive problems involved in making these estimates accurately. It has been recognized for some time that the thickness of the LNAPL in the well bore is not the same as the thickness of the saturated region of LNAPL in the formation. However, to our knowledge, a well documented, verified method to predict the relationship between the "apparent" thickness in the well and "actual" thickness in the soil formation has not been developed.

The LNAPL of primary interest to the U.S. Air Force is JP4, a petroleum product used for jet fuel that has been found in well bores penetrating unconfined aquifers underlying several Air Force bases. Because of the widespread use of JP4 and consequent potential for serious groundwater and soilwater contamination, an accurate method that uses well bore data to predict the total quantity and distribution of JP4 is essential. Inaccuracies in this prediction result in overestimation or underestimation of the product to be removed from the subsurface. If the quantity of product is underestimated, clean up activities may be terminated before sufficient product is removed. Alternatively, if the total quantity of product is overestimated, costs of clean up will be overestimated since total cost is often based on the volume of product to be removed.

Estimation of the total quantity of a petroleum product in the subsurface environment involves (a) estimation of the product retained in the unsaturated zone and (b) estimation of the extent and vertical accumulation of the product in the saturated region located above the groundwater. Both of these aspects involve immiscible flow processes in the vadose zone. My academic and research background is in the area of groundwater and soilwater hydraulics, with special emphasis on processes that occur in the vadose zone. This background and area of interest is very complimentary to the background and interests of Mr. Jack Milligan, the research counterpart at the USAF Environics Laboratory, Tyndall AFB. Whereas my background tends to be theoretical, Mr. Milligan's interests are more centered on the experimental verification and application of theory. The complimentary nature of our interests is the primary reason why I was assigned to the Environics Laboratory for this program.

II. OBJECTIVES OF THE RESEARCH EFFORT:

At this time, there is no well documented, verified theory for predicting the relationship between well bore hydrocarbon thickness and actual quantity of hydrocarbon in the soil formation. The objective of this research, therefore, is to develop and show applicability of a theory to predict the "actual" thickness of JP4 in a soil formation from the "apparent" thickness of JP4 in the well bore. The theory is based on knowledge of fundamental soil properties and pertinent properties of JP4.

The procedure proposed to meet the objective stated above is:

(a) Develop an appropriate theory making realistic but initially simplistic assumptions regarding the soil formation and properties of JP4. These assumptions include soil homogeneity and uniformity, static

conditions, simplified mathematical representations of the capillary properties of the JP4-water-air system and time independent properties of JP4.

(b) Measure the properties of JP4 and the soil parameters needed to use the theory developed.

(c) Use laboratory column data collected by Jack Milligan at the USAF Environics Laboratory to demonstrate the validity of the theory.

III. SUMMARY OF RELATIONSHIP BETWEEN WELL BORE JP4 THICKNESS AND JP4 VOLUME IN THE SOIL.

If equilibrium and homogeneous conditions are assumed, the relationship between the "apparent" thickness of JP4 in an observation well and the volume of JP4 in the soil formation can be determined. The link between the two quantities is given by relating equilibrium pressures determined from the well bore data to the equilibrium volumetric quantities of water, JP4 and air in the soil that correspond to these pressures. The relationship is defined by the capillary pressure-saturation functions for the three fluids and the soil matrix.

The basic data required to determine the relationship between well bore and soil formation JP4 are:

a. ρ_w: density of the soilwater

b. ρ_o: density of the JP4

c. ρ_a: density of air (assumed zero)

d. ϕ: porosity

e. $\frac{Pc}{\rho g}(S)$ or $\frac{Pc}{\rho g}(\theta)$: capillary pressure-saturation curves for an air/organic system and for an organic/water system

After obtaining the required basic data, the capillary pressure curves are fit to an appropriate empirical equation. This allows integration of a mathematical function rather than numerical

integration of a data curve. For this report, we have used the Brooks-Corey equation (Brooks and Corey, 1964; Corey, 1977) because of its simplicity. We will also assume no hysteresis and no air entrapment. Further, we will assume that the organic occurs throughout the entire soil profile from the ground surface to the saturated water region. This assumption allows the use of an organic/air capillary pressure curve to represent the capillary relationships between the organic and air from the ground surface to the organic-water interface even when water is present in the profile.

A simplification of the equation that will be developed in the following sections can be obtained that is a first approximation of the quantity in the saturated zone of organic in the soil. This first approximation is similar to the "rule of thumb" values found in the literature (e.g. Concawe, 1979). This will be discussed in Section IV of this report.

In general, the procedure used is to first estimate the volume of both the organic and air in the soil profile after a spill by subtracting the total water in the profile from the total volume of the voids. Hence, the difference between the porosity and the water content determined from the water/organic capillary pressure curve is integrated from zero to the depth of the water-organic interface, that is, the location of the organic entry capillary pressure into the water phase. Secondly, an estimate of the total air in the profile after a spill is estimated by integrating the difference between porosity and organic content from zero to the depth of air-organic interface. Again, this level is more exactly defined as the air entry pressure. In this case, the organic/air capillary pressure curve is used. The difference of the two volumes obtained by integration is an estimate of

the volume of organic in the soil profile. The procedure is illustrated in the following section using the Brooks-Corey relationship. This equation is an empirical representation of capillary pressure as a function of saturation given by $Se = \left(\frac{Pd}{Pc}\right)^{\lambda}$ where Pd is the displacement pressure and λ is called the pore size distribution factor. Se is an effective saturation defined by $Se = \frac{s - s_r}{1 - s_r}$. It is assumed that entry and displacement pressures (as defined by Brooks and Corey) are approximately the same. For further discussion of this approximation, see Corey, 1977.

After a spill, equilibrium conditions are assumed as shown in Figure 1. If the capillarity between the organic and the water is not influenced by the presence of air, we can use the capillary pressure curve for a water/organic system to estimate the total volume of organic and air in the soil profile. Using the Brooks-Corey relationship, the volume of soil voids occupied by air and organic per unit area is:

$$V_a + V_o = \int_o^{Da^{ow}} (\phi - \theta_w^{ow})\, dz = \phi \int_o^{Da^{ow}} (1 - s_w^{ow})\, dz \qquad \text{(Eqn 3)}$$

$$= \phi \int_o^{Da^{ow}} \left[1 - \left(1 + \frac{\Delta\rho g z}{P_d{}^{ow}}\right)^{-\lambda^{ow}}\right] dz \qquad \text{(Eqn 4)}$$

since $s_w^{ow} = \left(\frac{P_c{}^{ow}}{P_d{}^{ow}}\right)^{-\lambda^{ow}}$ (the Brooks-Corey equation with Srw = 0)

and $P_c{}^{ow} = P_d{}^{ow} + \Delta\rho g z$

Integrating equation 4 gives:

$$V_a + V_o = \phi D_a{}^{ow} - \phi B \left[\frac{\left(1 + \frac{Da^{ow}}{B}\right)^{-\lambda^{ow}+1}}{-\lambda^{ow} + 1} - \frac{1}{-\lambda^{ow} + 1}\right] \qquad \text{(Eqn 5)}$$

where $B = \frac{P_d{}^{ow}}{\Delta\rho g}$

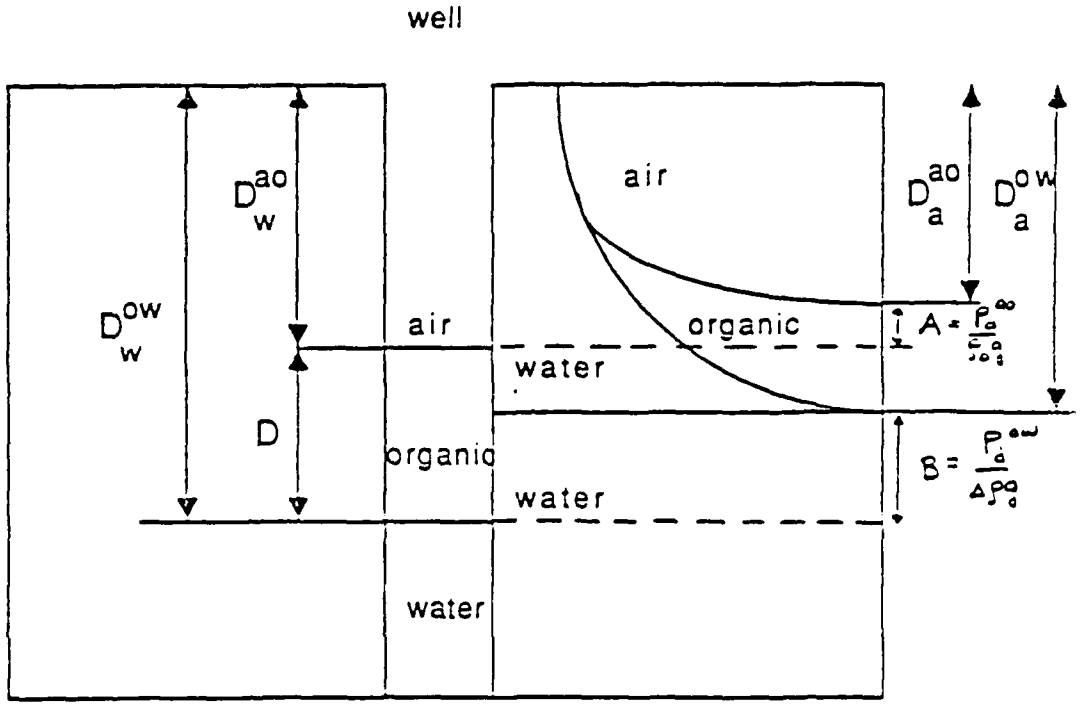


Figure 1: Notation used for equilibrium conditions.

Units on V_a and V_o are length. Therefore, the equation is the volume of air and organic per unit horizontal area. Other notation is given in the list of symbols. In addition, we have assumed that the residual water saturation (s_{wr} as defined by Brooks and Corey) is zero.

Using a similar procedure, the volume of air per unit area in the profile after a spill is estimated from the organic/air capillary pressure curves. Again, the assumption is made that the organic is in contact with air throughout the profile and the presence of water in the profile does not affect the capillarity between the organic and air. With this assumption:

$$V_a = \phi \int_o^{D_a^{ao}} (1-s_o^{ao})\, dz = \phi \int_o^{D_a^{ao}} \left[1 - \left(1 + \frac{\rho_o g z}{P_d^{ao}}\right)^{-\lambda^{ao}}\right] dz \qquad \text{(Eqn 6)}$$

where $s_o^{ao} = \left(\frac{P_c}{P_d^{ao}}\right)^{-\lambda^{ao}}$

and $P_c^{ao} = P_d^{ao} + \rho_o g z$

Integrating equation 6 gives:

$$V_a = \phi D_a^{ao} - \phi A \left[\frac{\left(1+\frac{D_a^{ao}}{A}\right)^{-\lambda^{ao}+1}}{-\lambda^{ao}+1} - \frac{1}{-\lambda^{ao}+1}\right] \qquad \text{(Eqn 7)}$$

where $A = \frac{P_d^{ao}}{\rho_o g}$

If the total change in water in the aquifer before and after the spill is zero and it is further assumed that $\lambda^{ao}=\lambda^{ow}$, then the volume of organic per unit area can be estimated by subtracting equation 7 from equation 5, so that:

$$V_o = \phi\,(D_a^{ow} - D_a^{ao}) - \frac{(A-B)}{-\lambda+1}\,\phi + \frac{A\phi}{-\lambda+1}\,(1 + \frac{D_a^{ao}}{A})^{-\lambda+1}$$

$$- \frac{B\phi}{-\lambda+1}\left(1 + \frac{D_a^{ow}}{B}\right)^{-\lambda+1} \qquad \text{(Eqn 8)}$$

Equation 8 relates the volume of organic (V_o) in the soil to the capillary pressure curve parameters as defined by the Brooks-Corey relationship (A, B and λ) and the depths to the organic water interface (D_a^{ow}) and the air organic interface (D_a^{ao}) as delineated by the location of the displacement pressures in the Brooks-Corey relationship. It still remains to relate the volume of organic to the measureable depth of organic in the well bore. Figure 1 shows that the following relationships hold:

$$D + A - B = D_a^{ow} - D_a^{ao} \qquad \text{(Eqn 9)}$$

$$D_w^{ow} - D - A = D_a^{ao} \qquad \text{(Eqn 10)}$$

$$D_w^{ao} + D - B = D_a^{ow} \qquad \text{(Eqn 11)}$$

and $$D_w^{ow} - D = D_w^{ao} \qquad \text{(Eqn 12)}$$

Substituting these into equation 8 gives:

$$V_o = \phi\,(D + A - B) + \frac{A\phi}{-\lambda+1}\left[\frac{D_w^{ao}}{A}^{-\lambda+1} - 1\right]$$

$$- \frac{B\phi}{-\lambda+1}\left[\frac{D_w^{ow}}{B}^{-\lambda+1} - 1\right] \qquad \text{(Eqn 13)}$$

The units on V_o are again length, that is, V_o is the volume of organic per unit area. If both sides of the equation are divided by porosity, the equation is in terms of an equivalent depth of organic.

IV. DEMONSTRATION OF THE RELATIONSHIPS IN SECTION III USING COLUMN DATA:

Mr. Jack Milligan, the research counterpart for this summer program at the Environics Lab, Tyndall AFB, has collected data that represents the relationship between "apparent" and "actual" thickness for a series of sands. The petroleum product, JP4, was added in increments at a point near the water table. For each increment, the "actual" thickness in the soil was determined by visually estimating the region of JP4 saturation. When visual averages are used, A and B will be marked with primes, i.e. A' and B'. Further, since the JP4 was added at the water table, the full equilibrium profile is not developed in the columns. Therefore, the last two terms in equation 13 are difficult to evaluate and no attempt was made to quantify the pore size distribution index.

IV.A BASIC DATA REQUIRED:

In addition to the column data collected by Mr. Milligan, some of the basic properties of JP4 and the capillary pressure-saturation curves for the column sands are needed. Capillary pressure curves for three column sands (median sizes of 0.5, 0.6 and 0.8mm) were determined. For the theory in section III, only the JP4/air and H20/JP4 curves are needed. The H20/air curves were measured for completeness. Data measured for JP4 is given in Table 1. The only data required for the analyses are fluid densities. However, surface tensions were also measured to provide some insight into the accuracy of the capillary pressure curves.

TABLE 1: BASIC PROPERTIES OF JP4

	Clean	Contaminated[1]
Surface Tension (dynes/cm)		
Water/air	75.5	59.0
JP4/air	25.0	27.3
Water/JP4[2]	25.0	5.3
Density (gms/cm³)		
JP4	0.745	0.769[3]

1 Obtained from well W-4, Tyndall AFB

2 Initially 38.4, stabilized at 25.0 after 16 hours

3 JP4 in lab column study of 0.8mm size sand was also measured as 0.77

IV.B DISCUSSION OF COLUMN DATA

The data for the 0.5mm sand column test will be used to discuss the trends seen in the column data. During this discussion, a value of JP4 density of 0.77 will be used.

The data is discussed in three sections. In the initial period of the tests, all JP4 added to the column either entered the well bore or was in equilibrium in the soil formation at negative pressures. The second stage begins when enough JP4 has been added so that the capillary pressure exceeds the entry pressure needed for the JP4 to enter the positive pressure zone. The third stage begins when all the water is at positive pressures and the JP4 has reached the water table.

IV.B.1. DATA SET 1: ALL JP4 IN THE FORMATION IS AT NEGATIVE PRESSURES.

Initially, the JP4 added to a column enters the well bore and then establishes an equilibrium in the soil at negative pressures, i.e. all JP4 is located above the JP4/air interface in the well bore. The JP4 will continue to be held in the formation at negative pressures until enough JP4 is added so that the capillary pressure at the location of zero pressure in the organic is equal to or greater than the organic entry pressure. Notation is shown in Figure 2.

For the 0.5 mm data used in this illustration, data set 1 includes the first 900 mls of fuel added (approximately). A capillary pressure of approximately 7.1 cm of water is needed for entry of the organic into water. An appropriate A' value of 5.5 cm of organic is also indicated from the data. Both the 5.5 cm of organic and 7.1 cm distance to the water table below the JP4/air interface in the well bore are from the column data. These numbers, however should also be predictable from the capillary pressure-saturation curves.

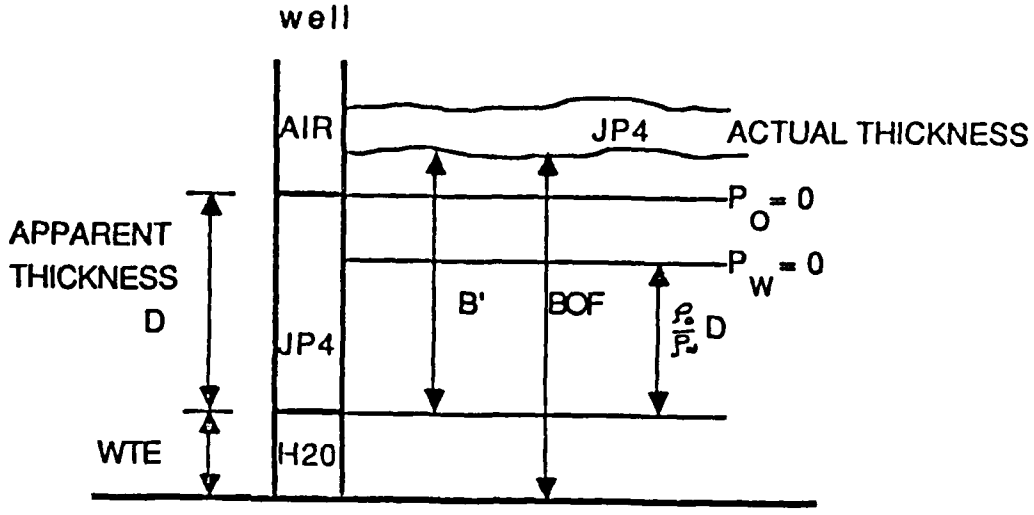


Figure 2: Notation when all JP4 is at negative pressure.

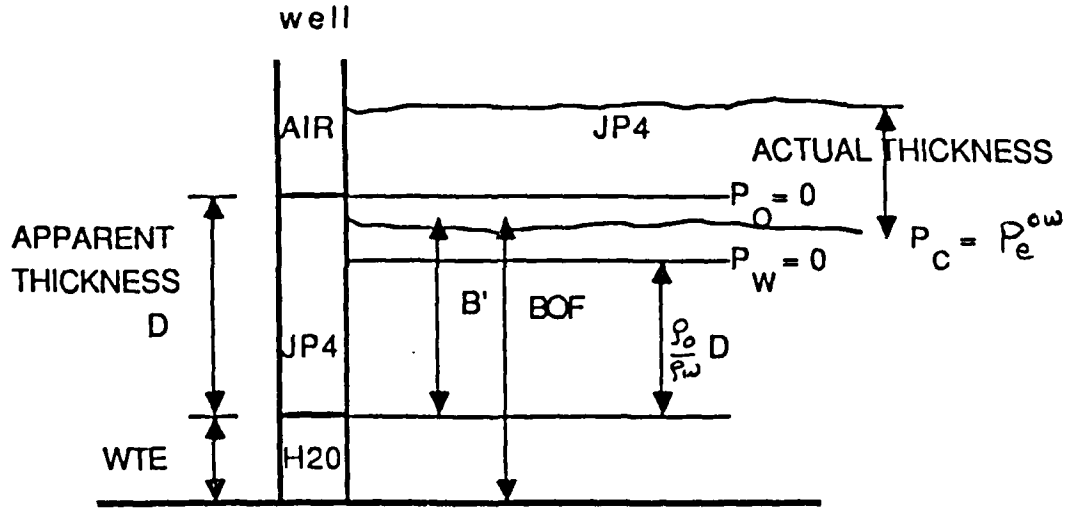


Figure 3: Notation when JP4 is at both positive and negative pressure.

The end of this data set occurs when B' = BOF-WTE = D or when the water table is $(P_e/\rho_w g)^{ow}$ cm below the oil water interface in the well. At this point, JP4 enters the positive pressure zone.

IV.B.2. DATA SET 2: JP4 AND H20 BOTH OCCUPY ZONES OF POSITIVE AND NEGATIVE PRESSURES.

After the JP4 enters the region below the organic/air interface in the well, the JP4 is at negative pressures above the interface and positive pressures below the interface. Water is at negative pressures above the water table and positive pressures below the water table. The water table can be located by multiplying ρ_o/ρ_w * D. The interface between the organic and water in the formation is always at a capillary pressure head equal to the organic entry pressure. This is illustrated in Figure 3.

The portion of the data for the 0.5 mm column that falls within this data set represents the cumulative fuel added from about 900 mls to 3100 mls. This region should demonstrate the "rule of thumb" equation given in section III that relates the actual and apparent thicknesses:

$$D + A' - B' = \text{the actual thickness} \qquad \text{(Eqn 14)}$$

where D = the apparent thickness in the well. Using the "average" visual A' and B' values of 5.5 and 30.6 obtained from the column data, the predicted and calculated values of the actual thickness are plotted in Figure 4. Note that the apparent and actual thicknesses are linearly related by equation 14 but the ratio is not a constant. In this data set, the ratio varies from 5.5 to 2.75.

The end of this data set occurs when the JP4/H20 interface in the formation is at the water table, i.e. B = 0.77 * D.

IV.B.3. DATA SET 3: ALL WATER IS AT POSITIVE PRESSURES, JP4 HAS REACHED THE WATER TABLE IN THE FORMATION.

When the interface between the JP4 and the water in the formation is at the water table, all water is at positive pressures. In an infinite aquifer, as more JP4 is added, the water would flow horizontally out of the spill region and the JP4/water interface would continue to move downward. However, since the columns are a closed system, an increase in JP4 cannot displace the water that occupies the pores. Therefore, the minimum value of B occurs when the fuel just reaches the water table or B = 0.77 * D. Additional fuel added does not relate to a physically feasible field case.

IV.B.4. SUMMARY OF ANALYSIS FOR 0.6 MM AND 0.8 MM COLUMN DATA

Data sets 1,2 and 3 were delineated for the 0.6 mm column data. Assuming that A' = 2 cm and B' = 22.5 cm, predicted and measured values of actual thickness for data set 2 are plotted on Figure 5. Note that the predicted values are slightly higher than the measured values. A better fit is obtained when A' - B' is -22, rather than -20.5. This is also plotted on Figure 5. The difference could be attributed to several factors including simply the difficulty of measuring these values to within the accuracy required.

The 0.8 mm column data is more difficult to analyze than the other data sets, partly because this data set has more scatter but increased accuracy is needed. Figure 6 plots the predicted and measured actual JP4 thickness if A' - B' is assumed to be (-13.2) cm.

V. RECOMMENDATIONS

The following are recommended for future work in this area:

1. The columns provide valuable intermediate verification of theory. Therefore, they should be continued and expanded. Some possible considerations are:

a) Design tensiometers that can measure negative organic and negative water pressures for instrumentation of the columns.

b) During data stage 1, the JP4 when initially applied, was at positive pressures and, hence, entered the well bore and then the soil. This simulates a field case where wells are in place before and during a spill. If the equilibrium location of the JP4 is in the negative pressure zone only, none of the JP4 will enter wells that are installed after a spill. Another series of column tests could be designed to simulate this second field case.

c) It would be interesting to modify the columns so that free outflow of water can occur in response to the addition of JP4.

2. An extension of the column studies to two dimensions could be accomplished using a laboratory sand tank. Instrumentation of the column is important in order to verify theory. Concepts of apparent and actual thickness can be extended directly to two dimensions. In addition, prediction of the horizontal extent of a spill if the total quantity of leakage is known (or vice versa) would be an interesting application.

References

Brooks, R.H. and A.T. Corey. 1964. Hydrology Paper No.3, "Hydraulic Properties of Porous Media" 1964. Colorado State University, Fort Collins, CO.

Concawe, 1979. "Protection of Groundwater from Oil Pollution", Den Haag.

Corey, A.T. 1977. "Mechanics Of Heterogeneous Fluids In Porous Media". Water Resources Publications, Fort Collins, CO.

List of Symbols

P_c	capillary pressure
P_d	displacement pressure
P_e	entry pressure
s	saturation
S_e	effective saturation
s_r	residual saturation
θ	volumetric water content
λ	empirical exponent used as index of pore size distribution
ρ	fluid density
ϕ	porosity

Superscripts and subscripts

o	organic
w	water
a	air

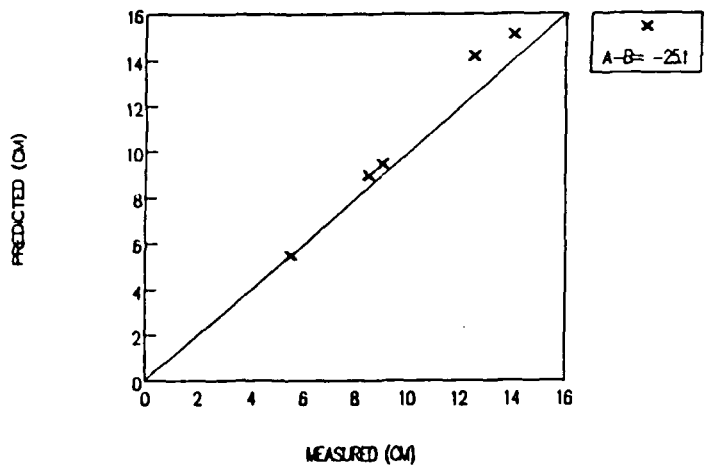


Fig 4: Measured and predicted JP4 "actual" thickness for 0.5 mm sand column.

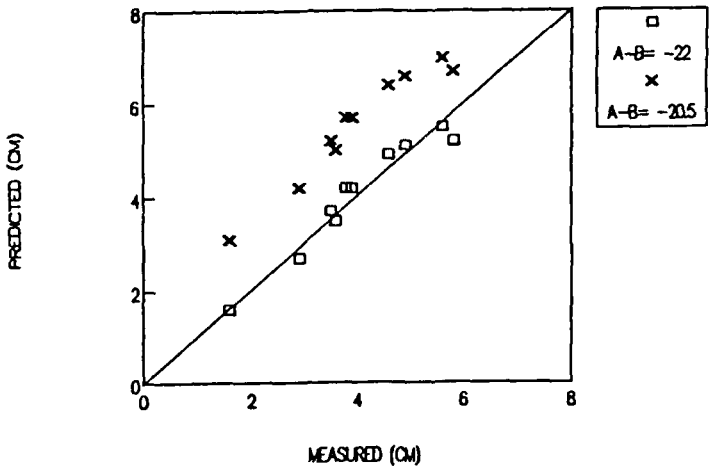


Fig 5: Measured and predicted JP4 "actual" thickness for 0.6 mm sand column.

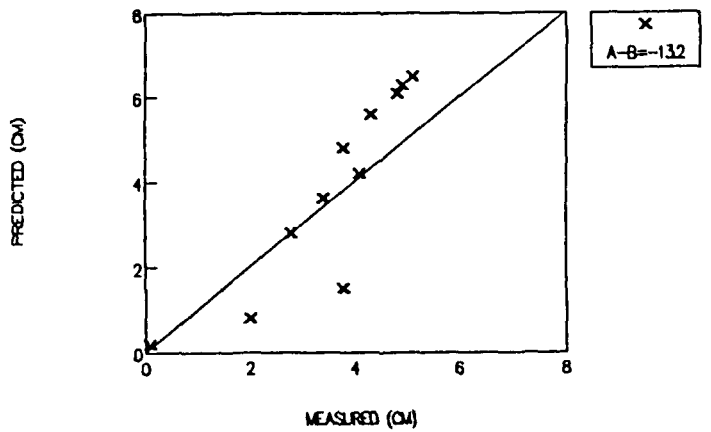


Fig 6: Measured and predicted JP4 "actual" thickness for 0.8 mm sand column.

1988 USAF-UES SUMMER FACULTY RESEARCH PROGRAM

GRADUATE STUDENT RESEARCH PROGRAM

Sponsored by the

AIR FORCE OFFICE OF SCIENTIFIC RESEARCH

Conducted by the

Universal Energy Systems, Inc.

FINAL REPORT

COGENERATION ASSESSMENT ON MILITARY BASES

Prepared by:	Dr. E. K. Greenwald, P.E.
Academic Rank:	Associate Professor
Department and	Engineering Professional Development
University:	University of Wisconsin - Madison
Research Location:	FACILITY SYSTEMS AND ANALYSIS BRANCH
	HEADQUARTERS AIR FORCE ENGINEERING
	AND SERVICE CENTER (HQAFESC-RDCS)
	TYNDALL AIR FORCE BASE, FL 32403-6001
USAF Researcher	Thomas Hardy
Date:	September 25, 1988
Contract No:	F49620-87-R-0004

COGENERATION ASSESSMENT ON MILITARY BASES

by

DR. E. K. GREENWALD, P.E.

ABSTRACT

The primary research consisted of developing a methodology for determining the technical and economic feasibility of establishing a cogeneration plant on a military base. The methods of analysis developed are preliminary in nature, designed to screen among the several cogeneration technologies available and to develop parameters so that an appropriate and promising technology can be recognized and identified for additional engineering study. If the situation looks promising, a final engineering analysis and design should be conducted by consulting engineers experienced in cogeneration technology.

There is a trend in government towards the privatization of services where applicable. Therefore, the methodology was developed under the assumption that the cogeneration project would be owned and operated by a private third-party. The pros and cons of this issue were developed as an secondary assignment.

ACKNOWLEDGEMENTS

I wish to thank the Air Force Engineering and Service Center and the Air Force Systems Command, Air Force Office of Scientific Research for sponsorship of this summer work effort. Thanks also to Universal Energy Systems for there courtesy and assistance in the administrative aspects of the program.

Ms Purcell and Ms Garfield, RDX secretaries, was most helpful with their assistance in finding where things were located and taking my telephone messages. Mr. Tom Hardy, my RDCS interface, was most helpful and the individual who originally suggested the topic of the investigation.

I. INTRODUCTION:

Many large industrial plants are incorporating cogeneration technologies into their utility systems to more efficiently utilize their fuel energy and to accrue the cost savings which such systems provide. The success of these sys ems in industry pose the following questions. Are cogeneration systems suitable for application on a military base? What are the issues of concern? How does one determine their technical and economic feasibility? Since congress has not appropriated any funds, how could they be financed? Should third-party ownership arrangements be considered?

The Facilities and Systems Analysis Brance (RDCS) of the AFESL is responsible for keeping abreast of new energy sources and new power plant technology for potential application to the air base of the future. Therefore, they have an interest and an obligation to investigate the merits of cogeneration technology and how it might apply to an Air Force Base.

I have been active in the area of energy engineering for over twelve years, originally as a private consultant, and now as a teacher and researcher in the College of Engineering. My experience and interest in the general area of energy engineering and in cogeneration technology, in particular, led to my assignment to conduct this work.

II. OBJECTIVES OF THE RESEARCH:

The intersection of four major evolving trends during the past decade has made private ownership of a military utility plant potientialy a viable idea. These trends are 1) the encouragement by government for private parties to enter into the generation of public power through the passage of the 1978 Public Utility regulator Act (PURPA), 2) the movement towards privitization of essential services which have been traditionally provided by government, 3) the rapid escalation of energy costs, and 4) the decline of our electrical reserves caused by the combination of high interest rates and the political and environmental obstacles to building new power plants.

One objective of my summer research effort, was to define and to develop the relevant issues concerning the public ownership and operation of a cogeneration plant on a military base. The stated goal was to provide information to, and provoke discussion among the policy makers who make the decisions concerning the potential for private ownership of cogeneration plants on military bases.

A second, and primary objective, was to develop an engineering methodology for evaluating the technical and economic feasibility for developing a cogeneration capability on a base. The methodology was developed to be used by base engineering personnel to make the initial feasibility assessment.

III. APPROACH

A. RELEVANT ISSUES:

The relevant issues concerning the establishment of third-party owned and operated cogeneration plants were developed and investigated in the following areas, legal, financial, the IRS and tax implications, the potential effects on the environment and pollution, the political, and the socioeconomic effects on the local community. These were then catergorized as being advantageous, or not to cogeneration.

B. METHODOLOGY FOR ASSESSMENT:

Various methodologies for assessing the technical and economical feasibility for cogeneration were investigated. The key was to establish the primary parameters which control the economic viability of a cogen project, and then, to establish numerical ranges for these parameters which work.

In addition, for economic viability, it is extremely important to have a good match between the energy outputs of the cogeneration equipment proposed and the base's real energy requirements. When these two items match, a minimum of the potential energy output is wasted. A method is developed and explained for achieving this match by matching the thermal-to-electric ratios of the equipment with the base's energy requirements. A detailed example is worked out completely for a hypothetical Air Force Base.

IV. RECOMMENDATIONS:

A: REVELANT ISSUES

1. POTENTIAL ADVANTAGES

The potential advantages of third-party owned cogeneration plants on military installations are as follows:

a. No capital from the taxpayers is needed for plant construction or operation.

b. New public utility plant construction might be deferred.

c. Reduced annual base operating cost to taxpayers.

d. A potential for increased energy security.

e. A potential for increased energy reliability.

f. An over-all conservation of fossil fuels and a reduction of the contribution to the greenhouse effect.

g. Potential to update and replace aging plant equipment.

The third-party ownership arrangement provides the financial means for building and operating the cogeneration plant without the use of any taxpayer's dollars. A review of the various methods of third-party financing suggest the Energy Service Contract as the most feasible contractual arrangement. In this arrangement, the third-party provides the people and the finances to design, build,

and operate the cogeneration facility, selling electricity and thermal energy to the government at prices below current costs. Because of the private ownership feature, various tax benefits such as accelerated depreciation are available and they can be partially passed on to the government in the form of reduced energy costs.

The electrical power cogenerated on-site will release an equal amount of power for the local utility company to redistribute to other customers. If enough cogeneration sites are developed, construction of a future public power plant might be deferred or even canceled.

The increased overall operating efficiency plus the tax benefits allow the government to purchase electricity and thermal energy at below prevailing rates throughout the lifetime of the contract. Therefore, annual utility cost to the taxpayer are reduced.

A cogeneration system located on a military base offers an incremental increase in energy security over an exposed public utility system. This increase in security is provided by being better isolated from automobile accidents and the potential of terrorist or anti-war protestor activities. In addition, the public utility is available for backup power when necessary.

Similarly, the reliability of the electrical power may be better, particularly in areas of high thunderstorm activity such as in the southeastern United States. By not having distribution tentacles spread out over a large service area, the exposure to lighting strikes is reduced.

The higher system efficiency of a cogeneration plant will consume significantly less fuel than conventional utility systems and thus assist in the drive for American energy interdependence and in the conservation of our fossil fuel supplies.

Lastly, the new cogeneration plant may replace or allow for the replacement of aging physical plant which is more prone to mechanical failure and inefficient operation. A cogeneration plant is most economically feasible when it is time to replace a boiler system.

2. POTENTIAL DISADVANTAGES

Several potential problem areas for third-party owned cogeneations plants are as follows:

a. Potential socioeconomic impact on the surrounding community.

b. The local utility may not be receptive to cogeneration projects.

c. Local environmental and pollution standards

d. Other more viable energy conservation strategies may be available.

e. Control and ownership questions.

f. Energy dependence on a private third-party.

g. Energy

The Conference Report for the 1988 Department of Defense Appropriation Bill expresses concern for the effects on the remaining customers of an utility system if a Federal customer is allowed to leave the utility system to

purchase power elsewhere.

Thus, the effect of a cogeneration project on the local utilities needs to be considered. An economically feasible and properly sized cogeneration system will not totally replace the electric utility. Only a base load will be replaced with the balance of power still being purchased from the utility. The base's fuel purchases will be significantly increased and this will have a positive effect on the local community. In some cases, where the local electric utility's reserve is low, they should welcome the load reduction. However, most generally, the local electric company will not appreciate the loss of the electric load and will protest in anyway available to them. However, under PURPA, they are required to sell to the cogenerator the supplemental, maintenance and backup power required at a fair price.

Usually a standby charge will have to be negotiated.

Every cogeneration plant will contribute to the local air and noise pollution levels somewhat. It needs to be determined, on a case by case basis, if the added pollution burden can be tolerated by the current local, state and federal standards which apply to the local community. If exotic antipollution devices are necessary to comply with the local standards, the economics of the project may be jeopardized.

The basic efficiency of the over-all base energy consumption needs to be evaluated. There may be energy conservation alternatives available which would

provide for a greater energy savings for higher financial rates of return. It makes no engineering or financial sense to maximize the efficiency of power production if the consumption is to be inefficient. What would be gained on one-hand, will be lost on the other. Therefore, before a cogeneration plant is given serious consideration, a thorough energy audit should be conducted by experienced and competent engineering personnel to determine the energy efficiency of current base operations. In the past, military bases have been notorious for their inefficient consumption of energy. Only when base engineering is satisfied that it is operating in a reasonably efficient manner, should it contemplate an on-site energy production project.

In order for the tax benefits to be fully accepted by the IRS, the third-party owner has to be the actual the owner-operator in fact. Thus, the third-party, and not base personnel, will exert complete and total operational control over the cogeneration plant. They will sell power to the base according to the terms of the working agreement. This is really not such a new concept as base personnel currently have no control over the utilities which currently are supplying their energy. Thus, assuming the original contract is properly written, there should be no problems concerning the ownership and operational control question.

There is, however, the potential for major problems if the selected third-party owner-operator is not financially strong enough or technically competent to sustain the plant's operation. The owner-operator needs to be very

carefully screened on both financial and technical grounds with adequate protections built into the contract to handle any situation that might arise.

The question of exporting power to customers other than the military base needs to be considered and covered in the working agreement. Except for special situations, the base should require all energy to be sold to the base and the plant should be sized accordingly.

The fuel source to be used by the cogeneration plant has to be determined with the important parameters being reliability and fuel cost. Whatever technology is used, it should be capable of being powered by at least two different fuel sources. For example, a low cost interpretable natural gas contract with a fuel oil backup would satisfy both requirements of low cost and backup.

3. SUMMARY

The above discussion outlines the positive and negative issues concerning the establishment of a third-party owned cogeneration system on a military base. While a particular base or situation may require additional considerations not mentioned above, the major issues have been addressed.

Nothing presented either prohibits or suggests that all military bases immediately move towards becoming cogenerators. However, once a decision is made to consider

the potential for cogeneration at a given base, a through technical and economic analysis needs to be made to appraise the feasibility. Each base's situation is unique and has to be analyzed accordingly.

B. METHODOLOGY FOR ASSESSMENT

1. PRIMARY FACTORS

The single key requirement for economic success of any cogeneration system is the productive around-the-clock use of both the electrical and thermal energies. It is no problem to productively consume the electrical energy. In the worse case, it can be sold to an electric utility. This is usually not a desirable action. However, finding a suitable andd productive, around-the-clock use for the thermal energy produced can be an engineering challenge. For this reason, the methodology developed focused on finding productive uses for the thermal energy. Space heating, chilled water air conditioning, domestic hot water and other potential thermal loads were considered as potential uses.

The primary factors for evaluating the cogeneration potential are:

a. Fuel cost ($ per mmBTU)

b. Electricity costs, utility buy/sell rates,

c. Thermal loads (#/hr of steam and pressure, psi)

d. Equipment costs ($/kw)

e. Plant utilization (hrs/year)

f. Electrical loads (megawatts)

Other secondary factors are maintenance costs, operating personnel costs, the cost of owning and financing, and utility standby fees.

Favorable ranges of these parameters are: fuel costs under $3.00 per million BTU's, a current composite* electricity cost of over $0.05/Kwh, the ratio of electricity to fuel costs (cents per Kwh divided by dollars per million BTU's) greater than 1-1/4 to 1-1/2, average steam loads greater than 25,000 lbs per hour with system pressures of less than 100 psi, installed equipment costs less than $750/kwh, plant utilization of over 6,000 hours per year and electrical loads of over five megawatts. All of these factors do not need to be favorable before a plant can be economically justified. However, the more factors which are favorable, the better the potential. If one or more factors are outside of the favorable range, then a more careful evaluation needs to be conducted before a commitment is made.

* A composite electricity cost is defined as the total electrical cost billed ($) divided by the total number of Kwh consumed.

2. METHODOLOGY

The key to establishing an economically successful cogeneration project is to have the maximum, productive utilization of both the thermal and the electrical energies produced by the plant. To achieve this state of operation, the size and type of equipment has to be selected very carefully to closely match the energy requirements of the base. The task is to size the cogeneration equipment

according to the energy consumption profiles of the base. The type of equipment chosen will depend somewhat upon the mix of thermal and electrical energy requirements. To develop the information necessary to realize this match requires that the following tasks to be performed.

a. Conduct a base-wide energy audit

b. Develop the data from the energy audit for cogeneration analysis

c. Analyze current and future utility rate schedules

d. Consider all viable conservation opportunities

e. Identify and quantify base energy flows

f. Develop a electrical energy profile for the base

g. Develop a thermal energy profile for the base

h. Assess the cogeneration potential available

i. Develop equipment options

j. Determine outputs for selected equipment

k. Consider and plan for future energy growth

l. Match the thermal and electrical load profiles

m. Perform economic analysis of chosen equipment

n. Select equipment according to the best engineering and economic design

3. ENERGY AUDIT

The detailed energy consumption information necessary to correctly size, specify, purchase, and install a cogeneration plant requires a high level engineering study

(energy audit) of the base be conducted. Better results are obtained when the audit is conducted by an qualified outside consulting engineering firm which specializes in energy engineering. The perfunctory audits which have been performed on many bases by base personnel are really not suited for the level of design and decision making needed for a cogeneration feasibility analysis.

The following is a list of items that should be completed to adequately prepare for, and conduct, an energy audit. The list was taken and modified from an University of Wisconsin short course on energy auditing. course on energy auditing. It is reproduced here to provide the reader with some comprehension of what data and information are required.

a. Graph at least 24 months of electrical consumption data. Graph both energy consumption (kwh) and demand (kw) data. Twenty-four hour demand charts are highly desirable for detailed analyses of a typical work day and also of the weekend.

b. Develop the same type set of graphs for fuel consumptions, natural gas, diesel, etc.

c. Compute unit costs for all utilities available on base:

   Steam ($/1,000 lb)

   Compressed air ($/kcf)

   Refrigeration ($/k ton-hrs)

   Electricity ($/kwh, $/kw)

   Domestic hot water ($/mmBTU)

   Chilled water ($/mmBTU)

d. Develop an annual breakdown for the electric power consumed by category:

   HVAC, Lighting ,Heating, Motors, Refrigeration, Fans, Pumps, Other

e. Develop an annual breakdown for the fuel consumption by category:

   Process steam, Domestic hot water, Space heating, Absorption air conditioning, Other

f. Develop one-line energy flow balance diagrams for all the major utilities.

g. Evaluate the electric rate schedule options available using the last 12 months of kwh and kw consumption data for cost comparison.

h. Similarly, explore natural gas and other fuel supply options, long-term contracts, interruptible schedules, etc.

i. Develop a master list of energy conservation opportunities.

   Projects completed during the previous five years.

   Projects planned for near future.

   Projects planned for the distant future.

j. Request pre-audit surveys to be conducted by outside vendors. Vendors will usually be happy to conduct these surveys. Use the

data they provide to advantage; however, be wary of any equipment purchase recommendations which may accompany the survey data.

Lighting survey (GE, Phillips, Sylvania)

Steam leaks (Furmanite, Leak Repair, etc.)

Steam Trap survey (Sarco, Yarway, etc.)

Insulation survey (Owens Corning, Manville)

Cooling Tower (Marley, Baltimore Air Coil)

Roof Ventilation (Green Heck, in-house)

Compressed air (Ingersol Rand, in-house)

V-belt Drives (in house)

Motors, 50 hp and larger (in-house)

Check for power-factor, loading, etc.

Combustion efficiency (gas company, Clever Brooks, in-house)

Power-factor survey (in-house)

Other

k. Identify all heat sinks and sources, by temperature, and by the BTU's available; identify areas for potential heat recovery.

l. Identify all low efficiency process equipment, such as older HVAC and refrigeration equipment.

m. Identify poorly operating controls and instrumentation; boilers, HVAC, process, etc.

n. Select the members for the core energy audit team wisely.

o. Select an outside engineering consultant(s).

p. Develop a detailed time and activity schedule for the energy audit, including plans for providing the necessary instrumentation for making important energy measurements.

q. Develop a five year strategic energy plan

r. Conduct the energy audit looking for energy conservation opportunities and ways to reduce energy consumption.

4. DATA REQUIRED FOR COGENERATION ANALYSIS

With the background of experience and information provided by a base-wide energy audit, the data required for a cogeneration analysis should be relatively easy to develop. If no energy audit has been conducted, then the data collection will be more difficult and it will probably be less reliable. Careful use must be made of guestimates.

Some of the data required for a thorough economic and engineering analysis of the cogeneration potential are as follows:

Electricity

Electric Consumption Profiles (Demand (kw) and Energy (kwh))

+ Daily variation, night time, weekends
+ Annual variation, seasonal effects
+ Growth expectation

Electricity Cost Analysis

+ Demand rates
+ Energy rates

- off-peak
- on-peak
- mid-peak

+ Interconnect charges
+ Supplemental charges/rates
+ Standby charge
+ Avoided cost or buyback charge
+ Inflation trend

Thermal Load Profiles

Steam, Chilled Water, Hot Water, Dry Hot Air, Other

+ Daily variations; nighttime, weekend
+ Annual variation; seasonal
+ Present cost factors
  - Cost basis (i.e. oil, gas, etc.)
  - Inflation trend
+ Growth expectations
+ Condensate return
+ Potential for heat recovery; temperature and BTU's

Fuels

+ Source, delivery point
+ Delivery pressure/Flow rate available
+ Rate schedules
+ Interruptible schedule
+ Applicable taxes
+ Heating value (HHV,LHV)

Electric/Thermal Profile Match

Site Data

+ Plant location

+ Elevation

+ Ambient temperature ranges

- Daily

- Annual

- Extremes

+ Space available

+ Proximity to thermal loads

+ Neighborhood quality

+ EPA District and local pollution restrictions

Third-Party Considerations

+ Guaranteed minimums - Take or pay

+ Aesthetics

+ Noise specifications

+ Contract duration

+ Contact termination details

- Abandonment

- Right of first refusal

- Market value

+ Utilities

- Water

- Sewer

- Communications

+ Site access

5. ENERGY PROFILES

From the information developed in the above procedures, a set of base specific energy profiles can be developed for the base. These profiles will indicate the amounts of thermal and electrical energies which can be used productively in a base loaded mode. It is then a matter of matching the technology and the equipment to these energy profiles so that both the thermal and the electrical energies are produced in the proper proportion to each other and in a base loaded mode.

6. SUMMARY

An example assessment problem is worked completely in the report titled, COGENERATION - A METHODOLOGY FOR ASSESSMENT. This report was developed as part of the summer research project and is 82 pages in length. It presents, in detail, a method for determining the preliminary assessment of the cogeneration potential of a military base. It, being too voluminous to be presented here, was presented to Mr. Thomas Hardy of RDCS-AFESL.

REFERENCES

Trane notes from a 1981 University of Wisconsin short course in Industrial Digestation, Department of Engineering Professional Development, College of Engineering

ASHRAE Handbook of Fundamentals

Equipment catalogs from various manufacturers.

Trane Company's manual "Design Considerations for Central Chilled Water Plants.

1988 USAF-UES FACULTY RESEARCH PROGRAM/

GRADUATE STUDENT RESEARCH PROGRAM

Sponsored by the

AIR FORCE OFFICE OF SCIENTIFIC RESEARCH

Conducted by the

Universal Energy Systems, Inc.

FINAL REPORT

SOIL VAPOR EXTRACTION OF VOLATILE ORGANIC CHEMICALS

Prepared by:	Dr. Neil J. Hutzler and David B. McKenzie
Academic Rank:	Associate Professor and Graduate Student
Department and University:	Civil Engineering Michigan Technological University
Research Location:	USAFESC/RDVW Tyndall AFB, FL 32403
USAF Researcher:	Dr. Tom Stauffer
Date:	August 18, 1988
Contract No:	F49620-88-C-0053

SOIL VAPOR EXTRACTION OF VOLATILE ORGANIC CHEMICALS

by

Dr. Neil J. Hutzler and
David B. McKenzie

ABSTRACT

Laboratory experiments were conducted to measure the rate of removal of volatile organic chemicals from unsaturated porous materials by vapor extraction. Columns were packed with uniform sand and a fired, porous clay and contaminated with water containing trichloroethylene, toluene, or 1,1,1-trichloroethane. Organic-free air was drawn through the column into a gas chromatograph, which was programmed for automatic sampling.

All volatile organic chemicals were effectively removed from the column by vapor extraction. TCE and toluene exhibited similar behavior because their volatility is approximately the same. 1,1,1-TCA, which has a higher air/water partitioning coefficient, was removed at a faster rate. Toluene and TCA were more slowly removed from the porous clay because of the time required for diffusion out of the particles.

The rates of vapor extraction as determined by experiments were compared to predictions made by a mathematical model of the soil column system. While the model could predict the early removal rates of the volatile compounds quite well, it did not simulate the tailing of the compounds seen in the experiments.

Acknowledgments

We want to thank the Air Force Systems Command and the Air Force Office of Scientific Research for sponsoring this research. We would also like to acknowledge Universal Energy Systems for their administrative support in all aspects of the program.

We would like to thank the Air Force Engineering and Services Center for the provision of administrative and technical services throughout the summer. Dr. Tom Stauffer was invaluable in helping set up our experimental apparatus and offering technical advice. Maj. Thomas Lubozynski ensured that we had the administrative resources needed for our work and welcomed us to participate in numerous discussions concerning Air Force research. We would like to thank Don Wickman and Mike Henley for their assistance in the laboratory, and, especially, for offering help when we required the use of the lab computer system. Lt. Mike Elliott provided technical support and advice for designing the experiments. Dr. Len Lion and Mark Brusseau were helpful in discussions which allowed us to benefit further from our research. In general, we would like to thank all personnel at the Center for making our time both enjoyable and productive.

I. INTRODUCTION

Soil vapor extraction is emerging as an effective technology for cleaning up soils contaminated with volatile chemicals such as fuels and solvents. While there is considerable evidence of the efficacy of vapor extraction (Hutzler, et al., 1988), studies are needed to define the limits of the process for removing specific compounds in various soil materials.

II. OBJECTIVES OF RESEARCH AND EXPERIMENTAL DESIGN

The primary objectives of this project were to examine the effects of soil structure and chemical volatility on the rate at which volatile compounds can be extracted from unsaturated soils and to validate a model developed by Gierke et al. (1988). Experiments were developed to measure the removal of volatile organic chemicals (VOC's) from unsaturated soil columns by vapor extraction techniques. Two soil types were used in the soil column experiments. One was Ottawa Sand, a round, homogeneous silica sand, and the other was Verilite, a fired clay with a high internal porosity. Neither soil demonstrated any adsorption under saturated conditions. The properties of each soil is shown in Table 1.

Chemicals were chosen based upon their volatility and their importance to the Air Force as groundwater contaminants. Toluene, trichloroethene (TCE), and 1,1,1-trichloroethane (TCA) were chosen to give a range of volatility. Chemical characteristics are shown in Table 2.

TABLE 1 - Soil Properties

	Ottawa Sand	Verilite
Particle diameter (cm)	0.07	0.07
Bulk Density (g/cm^3)	1.99	0.45
Solid Density (g/cm^3)	2.65	1.51
Particle Density (g/cm^3)	2.65	0.75
Total Porosity	0.33	0.70
Microporosity	--	0.50
Macroporosity	0.33	0.40

TABLE 2 - Chemical Characteristics (20^oC)

	Toluene	TCE	TCA
Density (g/ml)	.867	1.46	1.35
Mole. wt. (g/mole)	92.1	131.5	133.4
Solubility (mg/l)	515	1.1	4400
Henry's Constant	0.23	0.36	0.61
Vapor Pressure (mm)	22	60	100

The removal rates of the chemicals as measured in these experiments were then compared to the removal which would be predicted by an Air, Dispersed Flow, Diffusion-into-Aggregates Model (ADFDAM) developed by Gierke et al. (1988). This model incorporated flow and mass transfer parameters that were determined independently during the experiments.

III. MATERIALS AND METHODS

Experimental Apparatus

The apparatus used to perform the vapor extraction experiments is illustrated in Figure 1. Two soil columns were alternatively used, one which was packed with uniform sand and the other was packed with a fired, porous clay. Dimensions of these columns are shown in Table 3.

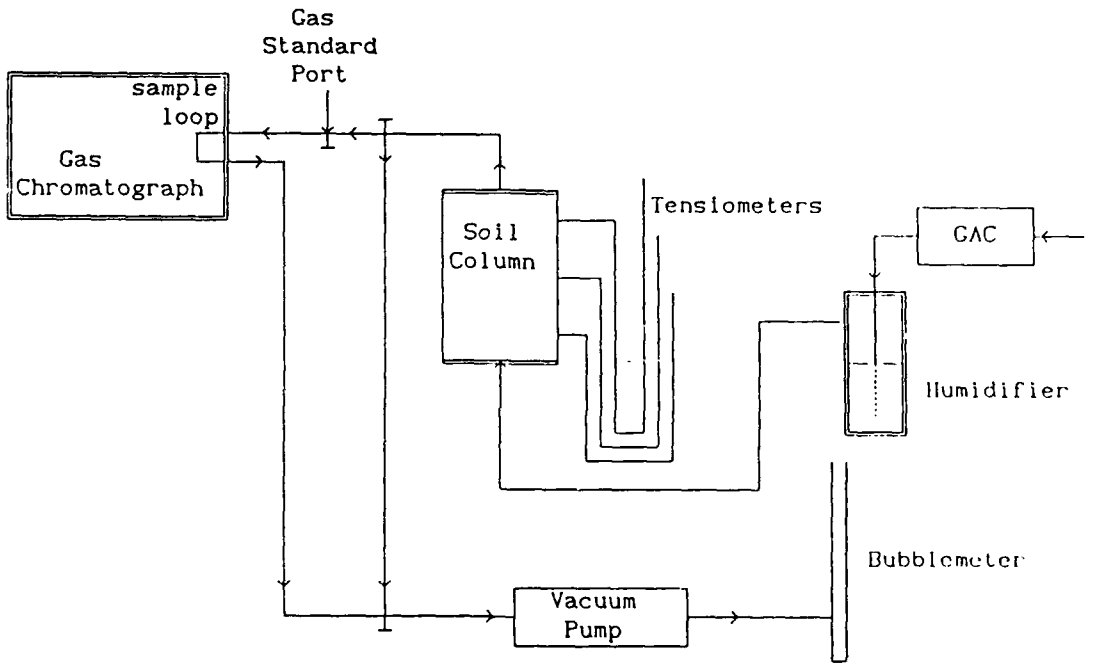


Figure 1. Soil Vapor Extraction Laboratory Apparatus.

TABLE 3 - Column Dimensions

	Uniform Sand	Porous Clay
Length (cm)	29.9	20.2
Diameter (cm)	10.8	10.8
Total Volume (ml)	2739.1	1847.8
Pore Volume (ml)	903.9	1186.4
Media Volume (ml)	1835.2	661.4

Air is drawn into the system by a vacuum pump and first flows through a granular activated carbon column to remove impurities from the lab air and to ensure that organic-free air is used in the stripping process. The air passes through a humidifier to saturate it with water vapor and eliminate any drying of the soil during the experiment. The humidifier also serves as an indicator of air flow through the entire system. Bubbling in the humidifier indicates that the system does not leak. The air is then pulled into the bottom of the soil column and is distributed by an air manifold. This manifold consists of four lengths of 1/8" stainless steel tubing with 1/16" holes drilled into them tapped into place through four air ports around the flange of the soil column. The air then flows through the length of the column and is collected at the top. The air is conducted through another 1/8" stainless steel tube, which is wrapped with heat tape to eliminate the condensation of stripped chemicals to the cold metal, and flows to a gas chromatograph (GC). The air containing the stripped chemical is directed into a 10-port valve attached to the GC. This valve is normally in the fill position. At specified times, the valve is actuated to inject the sample into the gas chromatograph. The air is drawn through the valve by the gas pump. From the pump, the air is delivered to a bubblemeter for flow measurement. Additional valving is provided to allow for injection of standards into the gas chromatograph for calibration.

Procedure

The experimental procedure consisted of a series of steps to contaminate and decontaminate the packed columns. A water solution was prepared by injecting pure chemical into a Tedlar bag filled with Milli-Q water. This solution was allowed to equilibrate for 3 days to ensure

that the chemical was completely dissolved. Aqueous solutions were prepared so as to be below the solubility limit for each chemical. A soil column would be contaminated by pumping the prepared solution up through it. This was continued until approximately 4 pore volumes of water were pumped through. Then pumping was stopped, and the column was capped and allowed to equilibrate for at least 48 hours. The column was then allowed to drain by gravity and was again capped. The air manifolds were then installed. To eliminate back-diffusion of chemical into the air lines, the air manifolds were not connected to the humidifier until the experiment was just about to be initiated.

Gas standards were prepared in Tedlar bags. These were prepared by injecting a measured mass of pure chemical into a known volume of air which was measured with a wet test meter. Prior to the start of each experiment, these standards were injected into the gas chromatograph, and a calibration curve was developed.

At the start of an experiment, the contaminated soil column was attached to the system as shown in Figure 1. The pump was started, and the line to the gas sample loop was allowed to flush for approximately 2 minutes. The gas chromatograph was then started, and sampling was initiated at programmed intervals, usually every 30 minutes. The conditions for the gas chromatograph for each chemical are summarized in Table 4.

At end of each experiment, selected gas standards were injected again to insure similarities in calibration curves from the beginning of the experiment to its termination.

TABLE 4. Gas Chromatograph Conditions

Chemical	Toluene	TCE	1,1,1-TCA
Detector	FID	ECD	FID
Oven Temp (^{o}C)	200	120	200
Detector Temp (^{oC})	200	350	200
Aux. Temp (^{o}C)	200	150	200
Retention Time (min.)	9.41	3.89	2.26
Gas Sample Loop (mL)	0.5	1.5	0.5

IV. EXPERIMENTAL RESULTS

Five experiments were performed for this study. TCE was extracted from the uniform sand column, only, while toluene and 1,1,1-TCA were removed from both sand and porous clay. The important experimental conditions for each of these five experiments are summarized in Table 5.

Figure 2 shows the reduction of relative air concentration with respect to time for the first four experiments. The rate at which chemical is removed is relatively high but rapidly drops off as the air-filled pores are evacuated. The removal rate slowly approaches zero. The effect of chemical volatility is seen by comparing the relative concentration of the air from the sand column. TCA, which has the highest air/water partitioning coefficient, is stripped from the column in the shortest time as would be expected. Little difference is noted between toluene and TCE because there is less difference in volatility. The effect of soil structure is more dramatic in this series of experiments. The time to remove toluene from the porous clay is much longer because of the additional time required for the chemical to diffuse out of the porous particle.

TABLE 5 - Experimental Conditions

Media	Chemical	Conditions
Uniform Sand (porosity = 0.33)	TCE	S = 0.33 Q = 4.6 mL/min T = 24 °C C = 0.012 mg/L
	Toluene	S = 0.38 Q = 4.0 mL/min T = 24 °C C = 15.2 mg/L
	1,1,1-TCA	S = 0.32 Q = 3.0 mL/min T = 22 °C C = 11.5 mg/L
Porous Clay (porosity = 0.64)	Toluene	S = 0.66 Q = 3.1 mL/min T = 21 °C C = 17.5 mg/L
	1,1,1-TCA	S = 0.62 Q = 3.0 mL/min T = 22 °C C = 12.5 mg/L

S = degree of saturation, Q = air flow rate, T = temperature
C = initial air concentration

The experimental data summarized in Figure 2 were used to validate a model developed by Gierke et al., (1988). The data from the first experiment where TCE was removed from Ottawa Sand are replotted in Figure 3 along with model predictions. Due to difficulties with the gas chromatograph, the experiment was terminated after 5 hours, but a gas concentration measured at 20 hours showed no detectable TCE in the extracted air. The column was loaded with a TCE contaminated solution

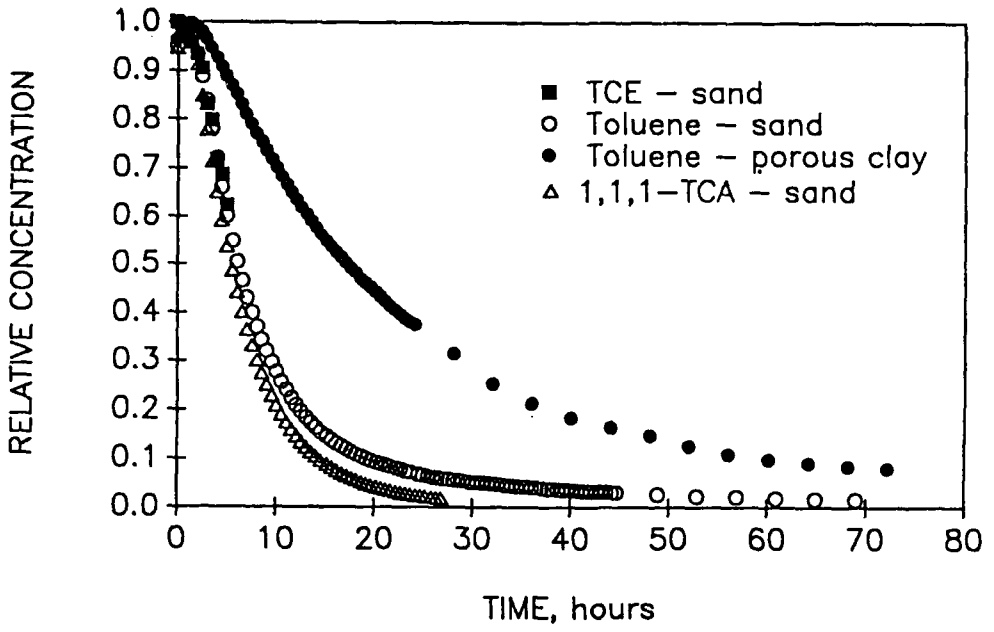


Figure 2. Stripping of volatile organic chemicals from unsaturated soil. Air velocity = 0.03 cm/s.

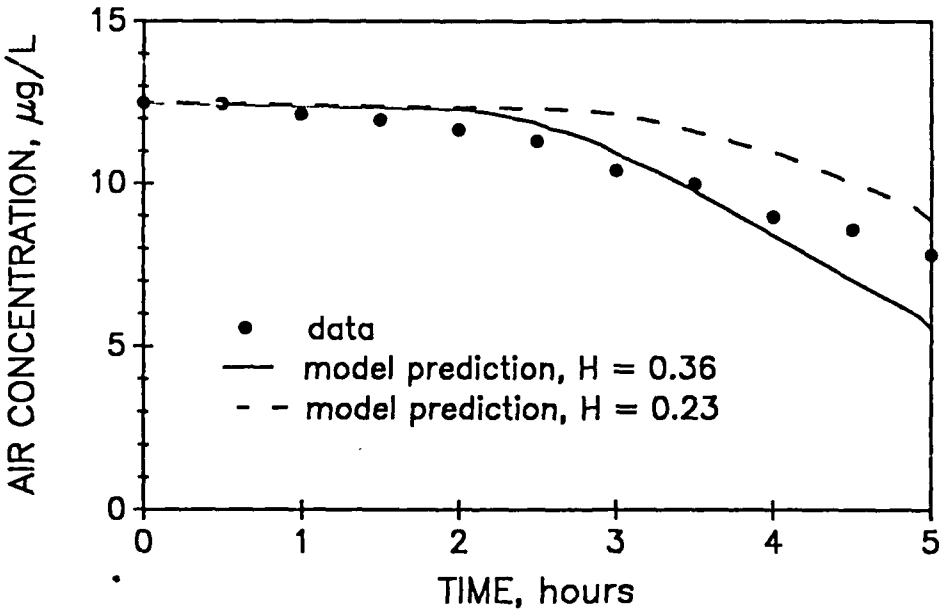


Figure 3. Stripping of TCE from uniform sand -- data and model predictions. Air Velocity = 0.038 cm/s.

with a concentration of 0.054 mg/L. The first measured gas concentration removed from the column gave a concentration of 0.0125 mg/L. These measured values give an experimentally-determined Henry's Constant of 0.23, lower than the 0.36 value determined by Howe et al.

(1986). It can be seen in Figure 3, that using either Henry's constant in the model gives a reasonable prediction of the measured data. As would be expected, the prediction based on a Henry's constant of 0.36 estimates a faster removal rate. The predictions look even better when the data are plotted as mass of chemical removed as a function of time Figure 4.

In the next experiment, toluene was extracted from Ottawa Sand. A much higher concentration of contaminating solution was pumped onto the column (67 mg/L), but the air flow rate to remove the contaminant was maintained at 4.0 mL/min or approximately the same flow rate as the first experiment. Figure 5 shows the data along with the model prediction based on a Henry's constant of 0.227 (Howe et al., 1986). The model predicts the data very well early in the experiment but begins to deviate at the lower air concentrations. This is believed to be due to the combined effects of adsorption onto the sides of the plexiglas column and a slow rate of diffusion out of a layer of water at the bottom of the column.

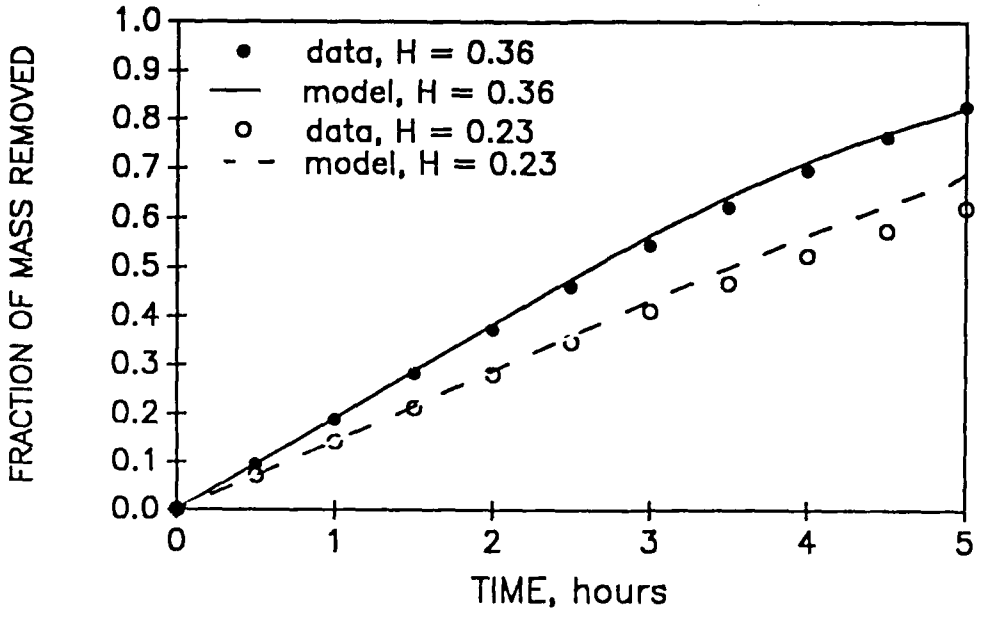


Figure 4. TCE removal from uniform sand expressed as mass removed -- data and model predictions. Air velocity = 0.038 cm/s.

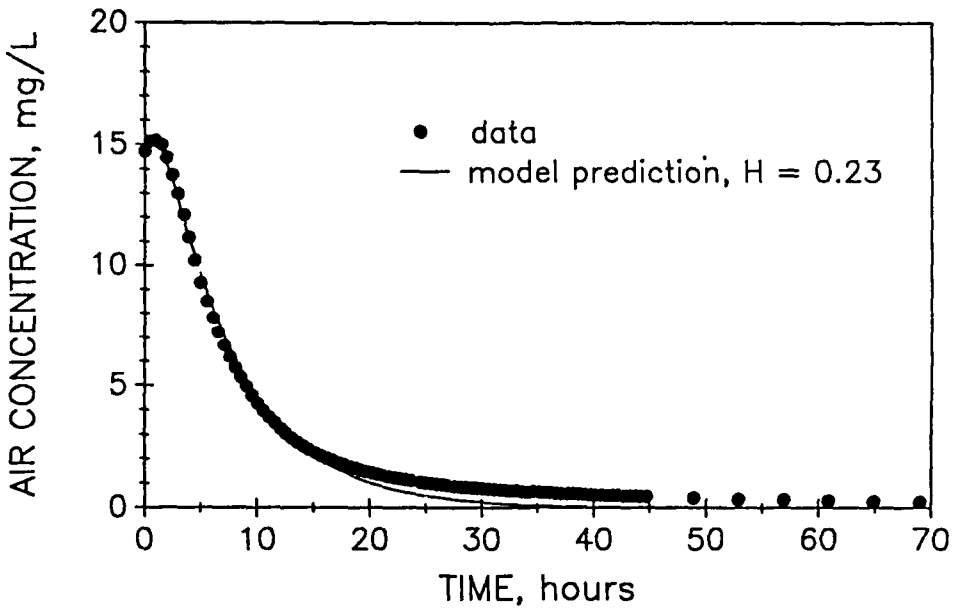


Figure 5. Stripping of toluene from uniform sand -- data and model prediction. Air velocity = 0.035 cm/s.

Toluene solution (67 mg/L) was then used to contaminate the column packed with porous clay particles. The air flow rate was slightly lower (3.1 mL/min) because of the difficulty of resetting the pump at low flows. Figure 6 shows the data and the model prediction based on a Henry's constant of 0.23. Again, the model predicts quite well during the early portion of the experiment but underestimates the chemical tailing seen toward the end of the run. After extracting for 72 hours, the pump was shut off for 24 hours and then restarted. The concentration in the exhaust air increases because toluene had slowly diffused out of the clay particles. This indicates that the removal efficiency might have been improved by the intermittent operation of the pump.

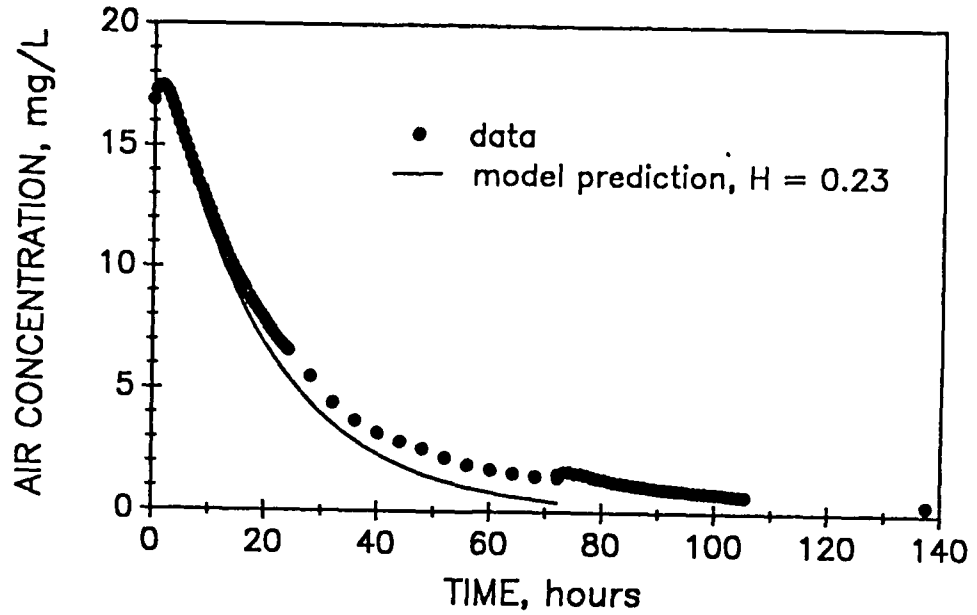


Figure 6. Stripping of toluene from porous clay -- data and model prediction. The air flow was stopped for 23 hours at 72 hours. Air velocity = 0.026 cm/s.

V. CONCLUSIONS AND RECOMMENDATIONS

A number of conclusions can be made from this work.

1. Volatile chemicals were successfully extracted from the unsaturated porous material in a reasonable length of time.

2. VOCs with a larger air/water partitioning coefficient were extracted at a faster rate than those with lower Henry's constants.

3. VOCs were extracted from the structured, porous clay at a slower rate than from the sand because of the time required for the chemical to diffuse out of the immobile water contained within the particle.

4. Flow interruption may increase the rate of removal based on pump operating time and thus decrease the operational costs of vapor extraction systems. This needs to be investigated further.

5. Adsorption onto the plexiglas column appears to have slowed the rate at which chemical could be extracted from the column. Additional studies on the effects of soil adsorption, especially at low moisture contents, are warranted.

6. Studies should be conducted to evaluate soil vapor extraction of mixtures of compounds from nonuniform soils to move the experimental conditions closer to those expected in field systems.

VI. REFERENCES

Gierke, J.S., "Modeling the Movement of Volatile Organic Chemicals Through Homogeneous, Isotropic, Unsaturated Soils With Cocurrent Air and Water Flow", MSCE Thesis, Michigan Technological University, Houghton, MI, University Microfilms, Ann Arbor, MI, 1986.

Gierke, J.S., N.J. Hutzler, and J.C. Crittenden, "Modeling the Transport of Volatile Organic Chemicals in Unsaturated Soils: Mass Transfer Mechanisms, Water Resources Research, in preparation, 1988.

Howe, G.B., M.E. Mullins, and T.N. Rogers, "Evaluation and Prediction of Henry's Law Constants and Aqueous Solubilities for Solvents and Hydrocarbon Fuel Components Volume I: Technical Discussion", USAFESC Report No. ESL-86-66, U.S. Air Force Engineering and Services Center, Tyndall AFB, FL, 86 pp., 1986.

Hutzler, N.J., and J.S. Gierke, "Validation of an Unsaturated VOC Transport Model," 1988 CSCE/ASCE National Conference on Environmental Engineering, Vancouver, B.C., Canada, July 13-15, 1988.

Hutzler, N.J., J.S. Gierke, and L.C. Krause, "Movement of Volatile Organic Chemicals in Soils," in Reactions and Movement of Organic Chemicals in Soils, B.L. Sawhney, ed., Soil Science Society of America, Madison, WI, in press, 1988a.

Hutzler, N.J., B. Murphey, and J.S. Gierke, "State of the Technology Review -- Soil Vapor Extraction Systems," prepared for U.S. EPA, Hazardous Waste Engineering Research Lab, Cincinnati, Ohio, 1988b.

1988 USAF-UES SUMMER FACULTY RESEARCH PROGRAM

GRADUATE STUDENT RESEARCH PROGRAM

Sponsored by the

AIR FORCE OFFICE OF SCIENTIFIC RESEARCH

Conducted by the

Universal Energy Systems, Inc.

FINAL REPORT

A PRELIMINARY INVESTIGATION OF NEURAL NETWORKS FOR THE AIR FORCE ENGINEERING AND SERVICES CENTER

Prepared by:	W. Pratt Mounfield, Jr. Ph.D.
Academic Rank:	Assistant Professor
Department and	Mechanical Engineering
University:	Louisiana State University
Research Location:	HQ-AFESC/RDCP Tyndall AFB, FL 32403
USAF Researcher:	Edward Alexander
Date:	5 August 88
Contract No.:	F49620-87-R-0004

A PRELIMINARY INVESTIGATION OF NEURAL NETWORKS FOR THE AIR FORCE ENGINEERING AND SERVICES CENTER

by

W. Pratt Mounfield, Jr. Ph.D.

ABSTRACT

Adaptive Neural Systems were searched in the recent literature for algorithms to solve optimization problems that may be encountered under the Rapid Runway Repair Directive. In particular, the solutions to the Traveling Salesman Problems were sought, because of the similarity to TSP and the Minimum Operating Strip Problem. The TSP problem was simulated under a continuous systems simulation program (ACSL) for ten cities using the Hopfield and Tank solution model. The TSP is an example to a N-P complete problem and a good local minimum was found based upon random initial conditions. Areas of further research were discussed, including the application of simulated annealing and Genetic Algorithms to the TSP problem.

I. INTRODUCTION

Research for the Rapid Runway Repair (RRR) task USAF-TAF SON 319-79, is currently assigned to the Air Force Engineering and Services Center (AFESC), Tyndall Air Force Base, Florida. Results of the R&D work of the last nine years include the definition and selection of a general purpose, joystick operated excavator for airstrip repair, several different methods for rapid surface repair, and a bomb damage assessment/minimum operating strip (MOS) selection software routine. There is a similarity between the MOS routines and the RRR excavator as currently envisioned by AFESC, that is both solutions will require massive amounts of computer calculations to adequately solve their respective tasks without the aid of human intervention (i.e. to function autonomously). A question that has been recently been asked is, do Adaptive Neural Systems (ANS) have anything to offer in order to reduce the cost/computation requirement of RRR tasks?

In this vein, Dr. W. Pratt Mounfield, Jr., Assistant Professor of Mechanical Engineering, Louisiana State University, received an UES/AFOSR summer faculty fellowship, sponsored by AFESC, to investigate the characteristics of Adaptive Neural Systems. Dr. Mounfield is well qualified to investigate this subject with knowledged gained from both his academic and industrial experience. He has a five year acquaintance with the RRR task, having been with the first group to visit AFESC from the University of Florida and has acted as a consultant to the BDM Corporation on the RRR excavator. Professor Mounfield has taught and practiced mathematical techniques in automatic controls, robotics, adaptive

controls, and optimal estimation (parameter estimation and filtering). He has had the insight to see that the combination of optimal estimation and ANS would offer faster and more stable solutions to problems solved by ANS, a fact borne out by the latest literature [14][18]. Dr. Mounfield is committed to continue his ANS research and bring to bear his considerable simulation and control experience to this exciting and state-of-the-art control/optimization subject.

II. OBJECTIVES OF RESEARCH EFFORT

The objectives in the summer faculty research effort were threefold: (1) to search the current literature from the AFESC library in order to determined mathematically what a Adaptive Neural Systems was, (2) to simulate a simple ANS of choice to determine the ANS dynamic equation's response during a solution of a "classical" optimization problem with a ANS, and (3) to review the RRR literature at AFESC to determine the applicability of ANS to one (or more) current RRR tasks. There is no funded ANS research at AFESC (as of August 1988) that uses or defines the response of these systems to problem solving. Therefore, an obvious extension of the three objectives is for Dr. Mounfield to help define the required mathematics and solution techniques for ANS under a UES/AFOSR mini-grant.

III. DEFINITION OF ANS

There exists a large class of optimization problems where one searches for the best solutions. However, from the engineering viewpoint, little meaning can be attached to a "best" solution because of the arbitrary weights assigned to cost functions. The

"best" solution then in the engineering sense may be a "very good" solution, where "best" exists only for a very small task.[2] Adaptive Neural System (ANS) have been advanced as a method to solve such engineering problems. Adaptive Neural Systems are not new, the first mathematical definitions are over 40 years old[9]. However, not until 1982 with the papers and presentations of J.J. Hopfield has ANS research brought fruit with solutions to optimization problems [9].

The most common structure of ANS is the neural network (NN), where there is formed a network of P.E.'s (processing elements) interconnected by information channels called interconnects [1]. There are for every P.E. multiple inputs, but only one output, and each are governed by first-order differential equations. The coefficients multiplying the inputs to each P.E. are self adjusting (adaptive) by the minimization of some particular specific problem functional.[13] In ANS there is no separate memory array for data, the interconnections for the P.E.'s are the "program" and the weights assigned to the interconnections is the "data". The results from the parallel response of the P.E.'s are not stored in some specific memory location, but the "result" consists of the overall state of the Network after it has reached some equilibrium state[10].

The neural network sparking the most recent interest in ANS is the Hopfield and Tank (H-T) network of two CAN's (crossbar associative networks). CAN's are characterized by highly interconnected symmetric networks of processing elements. The details that do matter in these CAN's are the dimensionality and

symmetry of the network, but the details of individual P.E.'s and it's strength of interconnects is not as important. Therefore, Neural Networks are very fault tolerant[11] and may be viewed as highly redundant.

Another feature of neural networks is that the time required for convergence to a nearest neighbor minimum is not dependent upon the number of minima in the entire function to minimize. The H-T network carries out O(1) time parallel searches in which the time required to search through N items is fixed and does not vary with N.[1] This behavior of the H-T network is based upon the analog implementation of the network and obviously does not hold true for the simulation of H-T networks on digital computers without parallel architecture.

Taking a clue from biological systems, a collective analog model may be formed where each "neuron" simultaneously sums the outputs of 100's or even 1000's of other neurons in order to determine its weighted output. A classical optimization problem, the Traveling Salesman Problem (TSP), may be solved by the parallel organization of a neural network. The organization of the network is highly parallel, with parallel input channels, parallel output channels, and a large degree of inter-connectivity between P.E.'s. Similar to the their biological cousins, the P.E.'s input/output relationship may be modeled as a sigmoid monotonic function, bounded between $\pm V_i$. This function may be represented as

$$V_i = g(u_i) = (1.0 + \tanh(u_i/u_o))/2.0 \quad (1)$$

The equations of motion of the analog circuit may be modeled as

$$\frac{du_i}{dt} = -\frac{u_i}{\tau} + \sum_{j=1}^{N} T_{ij}V_j + I_i \qquad (2)$$

where τ = time constant of P.E.

u_i = internal voltage of P.E.

u_o = gain, low gain forces convergence away from a continuous solution to a bi-state solution

I_i = external input to each P.E. (optional)

T_{ij} = interconnection matrix for each P.E.

When the width of the gain curve is narrow (i.e. $u_o << 1.0$), the high-gain limit and <u>stable</u> states of the network of P.E.'s are a <u>local</u> minimum of the energy function (a Lyapunov function [6])

$$E = -1/2 \sum_{i}^{N}\sum_{j}^{N} T_{ij}V_iV - \sum_{i}^{N} V_iI_i. \qquad (3)$$

The optimization of the specific TSP is based upon the choice of the connectivities (T_{ij}) and the input bias I_i. The specific TSP energy function to minimize may be formed such that the lowest energy state corresponds to the "best path" between cities. There are N^{10} solutions to this problem for N cities, with (N-1)!/2 unique solutions (not N! because of cyclic symmetry [7]), therefore the solution technique must favor stable states and short paths.

If the TSP problem is considered a symmetric matrix of N rows of P.E.'s, representing N unique cities, and N columns representing positions of particular cities in a continuous loop through N cities, the equations of motion for each P.E. may be formed as [2]

$$\frac{du_{ij}}{dt} = -u_{ij} - A\sum_{j\neq i} V_{ij} - B\sum_{k\neq i} V_{kj} - C\Big(\sum_{i}\sum_{l} V_{il} - n\Big) - D\sum_{k} d_{ik}(V_{k,i+1} + V_{k,i-1}) \qquad (4)$$

Mathematically, this function is formed to assure that only one city in a particular row, and only one in a particular column, and only N cities are "on", and the function is minimized with short distances between all cities. The function $g(u_i)$ forces the solutions to be discrete, and the states of the outputs V_{ij} may be interpreted as the position of a particular city in the tour. H-T reported that for a ten city problem their network found valid solution in 16 of 20 simulations, and 9 of the 16 were the global minimum for the tour, the other 7 were of the next best minimum tour.[2] These results are absolutely dependent upon the initial starting condition of u_{ij}, because this particular neural network solves the minimization problem in a deterministic manner from the initial conditions of a particular set of u_{ij}[2]. With the addition of simulated annealing ("slow cooling"), modeled by the addition of noise to the P.E.'s u_{ij}'s, the H-T network finds a near-global-minimum length solution to ten city TSP problem, there is no claim of global minimum solutions from every initial condition.[1]

The formulation of the TSP by H-T has been extended to other engineering problems, including the optimization problem related to computer wiring and electronic circuit design [7]. In [7] the authors discuss the application of simulated annealing to their problem and the TSP. They demonstrate that neural solutions are considerably better (400%) than random solutions to the wire routing problem. Simulated annealing has also been extended to image processing for object recognition and texture labeling [8]. H-T has also reported the solution to a data-shelving (task assignment) problem where each assistant (worker) should be

assigned to one collection of books to shelve in order to maximize the shelving rate [9].

IV. SIMULATION OF A TEN CITY TSP WITH ACSL

In the interest of understanding the complexities of neural networks, Dr. Mounfield has simulated a ten city traveling salesman problem (TSP) in FORTRAN running under the simulation language Advanced Continuous Simulation Language (ACSL). ACSL is used by Dr. Mounfield as the simulation program of choice for continuous or discrete/analog systems. Within the ACSL environment the user writes simulations of dynamic systems based upon differential and/or finite difference equations. These "equations of motion" may be linear or nonlinear, time invariant or time varying, and may include all types of scaler and vector/matrix equations that are handled as single functions. The user writes the differential equations and the required input/output functions for the system at hand in a high level language that is similar to a free format FORTRAN. The ACSL translator transforms the high level source code to FORTRAN 77, and automatically (if desired) complies and links the FORTRAN object code to the ACSL run-time libraries.

Within the ACSL run time libraries are functions to interactively change <u>any</u> parameter within the ACSL source code, plot any variable, choose from one of many integration routines, start and stop the simulation, etc. etc. User supplied subroutines may also be linked to the ACSL source code in any language adhering to the FORTRAN/C/BASIC/??? parameter passing requirement particular to the user's computer. In particular for the TSP problem for example, a function to calculate the distances between cities may be written

in FORTRAN and linked to the ACSL object code as a reusable module. For these obvious reasons, Dr. Mounfield believes that ACSL is tremendous time saver during the development of neural network algorithms. ACSL could be linked with a faster implementation of the TSP subroutines in an array processor for a factor of 100 times or more speed up of the simulated solutions.

The ACSL source code to implement a CAN is very simple, because the are only a few different functions of high order that must be called during the simulations. The P.E.'s state variables are the solutions to NxN first-order differential equations, this function is performed by one call in ACSL for the NxN array U,

$$U = INTVC(\dot{U}, U_o), \qquad (5)$$

where

U_o = NxN array of initial conditions.

$\dot{U}$ = NxN array of $\frac{du_{ij}}{dt}$

The user may specify how ACSL should integrate these equations as the solutions to the differential equations, whether using fourth-order Runge-Kutta integration, second or first order Euler integration, Gear's method, or others. The integration method may be interactively changed during run time and one can specify different methods for different portions of the dynamic equations.

The energy function to assure the valid solution of the TSP problem and to minimize the distances between the cities was written in FORTRAN 77 (see appendix). This routine could be written in ACSL, however once this module was written it can (as was) used to be linked with <u>any</u> TSP problem. Similarly, the

modules for calculating the distances between cities was written in FORTRAN 77 and linked with the ACSL module.

V. RESULTS OF SIMULATION OF TEN CITY TSP PROBLEM

The Cartesian coordinates for ten cities were randomly generated within ACSL to fall within $0 \leq P_{xy} \leq 1$, where P_{xy} are cartesian coordinates of each city. With the equations of motion as before

$$\frac{du_{ij}}{dt} = -u_{ij} - A \sum_{j \neq i} V_{ij} - B \sum_{k \neq i} V_{kj} - C\left(\sum_{i} \sum_{j} V_{ij} - n \right) \qquad (6)$$

$$-D \sum_{k} d_{ik} (V_{k,i+1} + V_{k,i-1})$$

where
$A = 500.0$
$B = 500.0$
$C = 200.0$
$D(t) = 100.0 \leq D(t) \leq 500.0$
$u_o = 0.02$

the neural network converged in four time constants or less to near minimum stable solutions. The actual time for convergence was approximately 30 seconds on a Digital Equipment Corporation VAXStation II mini-computer. The graphical solution to the ten city tour was plotted as intervals of 0.4 seconds on the VAXStation II using GKS (graphic kernel system) subroutine calls. The continuous solution to the TSP shows an interesting convergence to the final state where links are formed and broken as the dynamic system seeks a valid and minimum solution to the differential equations. In figure (1) the TSP solution is shown near the initial conditions, which were randomly chosen to fall with a mean of 0.1 for the u_{ij}'s. The initial conditions were such that at time equal to $t = 0.0^+$ there were several P.E.'s of large enough magnitude so that their output V_{ij} was equal to +1.0. Therefore,

lines were drawn between cities in the still invalid tour based upon where the outputs were active in the rows and columns of the V_{ij} array. This solution continued so that more "cities" were active in figure (2) where there are 9 cities with outputs $u_{ij} \geq 0.5$ and consequently their $V_{ij} = 1.0$. There are new lines connecting the active cities in the still invalid tour.

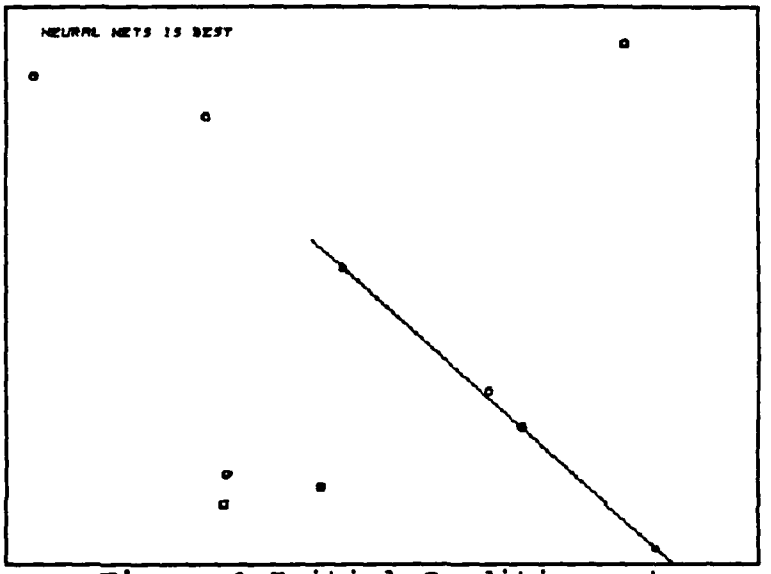


Figure 1 Initial Conditions at Time = 0.0 seconds

The simulation continues in figure (3) until all of the cities are connected, however there is crossing over of paths between cities so that a shorter total path may be possible to achieve. In the final figure (4) the minimum for these particular initial conditions has been reached in a stable configuration. The final total tour path is 3.88 units. This tour length is with the

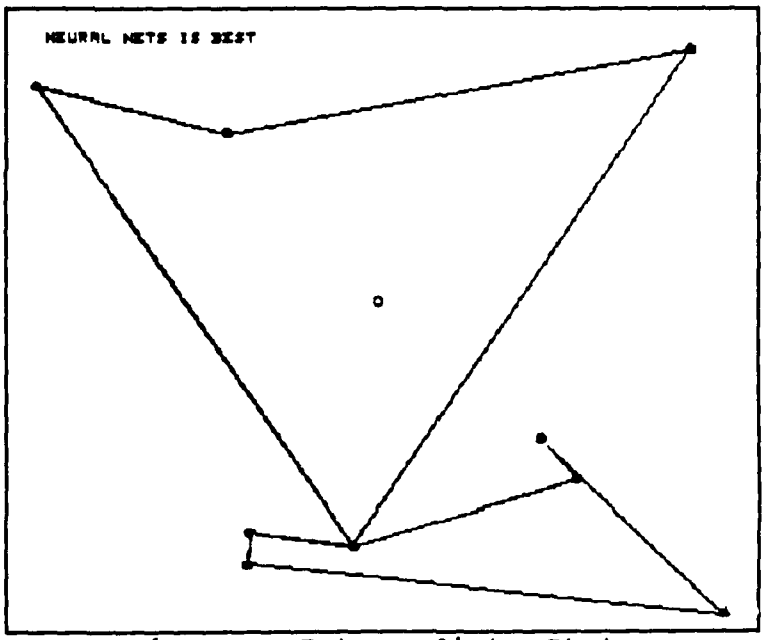


Figure 2 Intermediate State

global minimum of approximately 3.5 units. The global minimum was found by an exhaustive calculation of the (N-1)!/2 valid solutions. The solution found for these particular initial conditions are then within 10% of the global minimum, a position classified as a very good engineering solution. Simulations with different initial conditions found other valid short but not shorter paths.

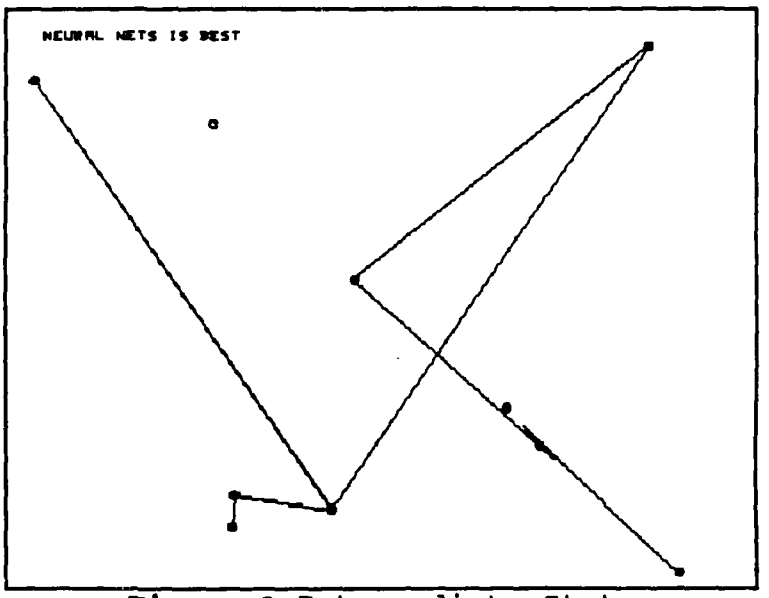


Figure 3 Intermediate State

VI. OUTSTANDING PROBLEMS IN THE LITERATURE

There are several outstanding problems in the literature regarding solutions techniques that may be applicable to the TSP. For example, the mathematics for the design and simulation for Adaptive Neural Systems is now just emerging in the literature. There are no definitive works that

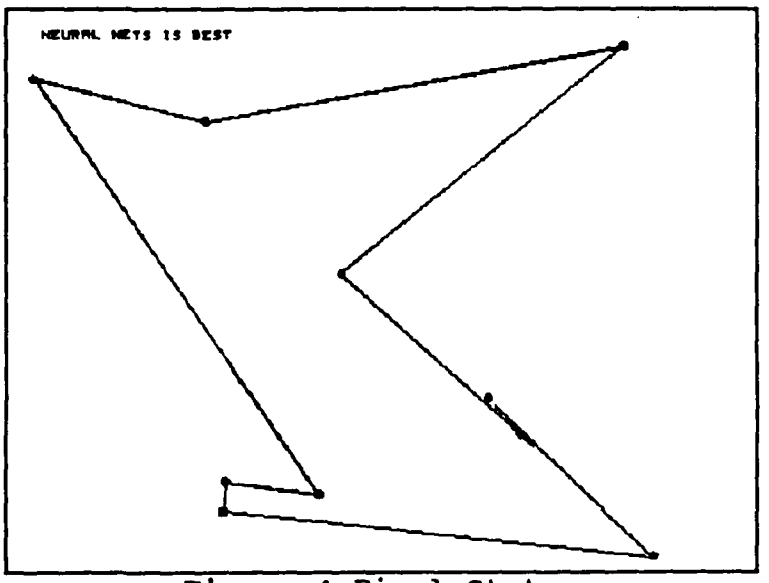


Figure 4 Final State,
Tour Distance = 3.88

provide a systems engineer with guidelines for the design of ANS's to solve a particular class of problem. There are isolated reports of design of limited systems[12], but by far "the use and application of neural networks have often been heuristic and 'opportunistic' in nature, i.e., the network has been customized to serve the needs of the task at hand"[12].

There has recently been advanced methods to increase the "learning" rate for multi-layer neural networks for signal processing based upon a least-squares minimization [14]. The multi-layer networks are believed to be suitable for image compression, text-to-speech transformation, and rule learning. It is not known how such method would apply to optimization problems such as the TSP.

Genetic Algorithms (GA's) may hold promise for applications because GA's are a relatively global search procedure based upon population genetics[15] where the interconnection weight space is searched for minima. The strengths of GA's are said to be the efficient and effective search of high dimensional problems, where there exists multi-modal, noisy and discontinuous surfaces. It is claimed that GA's place no restriction on the network architecture, so they may be applicable to many different engineering problems.

H-T's method for the solution to the TSP problem did not guarantee a globally-optimum solution, for the network computes locally optimal solutions. H-T state that "even among the extremely good solutions, the topology of the optimization surface in the solution space is very rough; may good solutions in the solution space are at least similar to the best solution, and a

complicated set of local minima exist"[16]. H-T did extend their work to include a class of problems in which a global optimum is found because no local minima exist[16]. An example to this problem is a linear programming problem where one must minimize a function subject to one (or more) inequality constraints.

VII. RECOMMENDATIONS

Therefore is my recommendation are that in order to gain acceptance within the engineering and Air Force community for Adaptive Neural Systems, there needs to be additional work on (1) the analysis of convergence rates, (2) algorithms for reaching near global minimums, and (3) guidelines for "programming" neural systems for classes of problems. In addition, (4) the least-square minimization should be investigated to extended this technique to optimization problems, perhaps in a sequential computational mode as a Kalamn Filter update equation. (5) The Genetic Algorithms (GA's) approach should be investigated for application to optimization problems because of GA's claimed efficient and effective searches of high dimensional problems. And finally, (6) the linear programming problem with ANS where one must minimize a function subject to one (or more) inequality constraints, should be researched for applicability to other optimization problems in engineering.

VIII. ACKNOWLEDGEMENTS

I wish to thank the Air Forces Systems Command, and the Air Force Office of Scientific Research for the sponsorship of the Summer Faculty Research Program. I also wish to thank Universal Energy Systems for their prompt, courteous and efficient administration of this research program. These three organizations have provided me with an opportunity for research and personal development that will I believe be of lasting importance to my career and Louisiana State University.

I extend a special thanks to the Air Force Engineering and Services Center at Tyndall AFB for sponsoring my summer research. In particular, Colonel L.D. Hokanson for his interest in the future of Adaptive Neural Systems; Dr. Daniel Stone for his support of our research in parameter estimation and optimization; Edward Alexander for the opportunity to provide him with future engineering solutions with ANS; and to Cheryl Garfield and Pat Purcell for their help and humor during these short ten weeks.

IX. APPENDIX

```
"FILE NAME: tspman10.csl"
"DATE LAST EDITED: 6/ 30 /88"
     "THIS FILE CONTAINS THE ACSL SOURCE CODE TO PERFORM "
     "THE SIMULATION OF A neural network (simple)"
     " for the traveling salesman problem for 10 cities"
INITIAL
     "DEFINE THE SIMULATION PARAMETERS"
CINTERVAL CINT = 0.4    $"SET THE COMMUNICATION INTERVAL"
NSTEPS    NSTP = 1$"SET NUM INTEGRATION STEPS per COMM INTERVAL"
MAXTERVAL MAXT = 0.02 $"SET THE MAXIMUM SIZE OF THE INTEGRATION"
CONSTANT  TSTP = 4.00$"SET THE MAXIMUM TIME FOR THE SIMULATION"
CONSTANT   ialg = 4
ARRAY da(  10,10  ) $"distance weights"
ARRAY u(  10,10  )  $"neural equation of state"
ARRAY pos( 10,2  ) $"positions of each city in cartesian corr"
ARRAY v( 10,10)     $"outputs from level one"
ARRAY ud(10,10), uo(10,10), up( 10,10)
integer tour( 10), m
m  = 10
constant a= 500, b= 500, c= 200, d= 500, offset=10 , u0=0.02
GAUSI( 555555555)
constant meanu=.0, stdu = .1, lbp=.0, ubp = 1.
do loop2 i = 1,m
   do loop3 j = 1,m
      uo( i,j) = GAUSS( meanu, stdu)
      da( i,j) =0. $v(i,j) = 0.
   loop3 ..continue
   pos( i,1) = UNIF( lbp, ubp) $pos( i,2) = UNIF( lbp, ubp)
loop2 ..continue
call distca( da, pos ,m)  $"the calculated distance between cities"
END $"OF INITIAL SECTION"
DYNAMIC
DERIVATIVE
procedural ( v = u, u0, m)
  call vtanhu( v, u, u0, m)
end
up = INTVC( ud, uo )
call xferb( u = up , 100 )
procedural  ( ud = u, v, da, a,b,c,d, m, offset)
   call xdot( ud , u, v, da, a,b,c,d, m, offset)
end
procedural ( tdsum , tour = da , v, m)
   call tourd( tdsum , tour, da, v, m)
end
TERMT(T .GT.TSTP)
END $"OF DERIVATIVE"
END $"OF DYNAMIC"
procedural (v)
print fmat2, v
fmat2.. format( 10f4.1)
end
eND $"OF PROGRAM"
```

```
 subroutine xdot( xd, x, v, dist, a,b,c,d, m, offset)
 implicit none
 parameter p=10
 integer*4 i,j,k,l,m
 real*4 a,b,c,d
 real*4 xd( m,m),x( m,m), v( m,m), msum
 real*4 dsum( p,p), csum( p,p), rsum( p,p), dist( m,m), offset
 msum = 0.0
 do i = 1,m
    do j = 1,m
       dsum( i,j) = 0.0
       csum( i,j) = 0.0
       rsum( i,j) = 0.0
       do l = 1,m
          if (l .ne. j) then
             csum( i,j) = csum( i,j) +v( i,l)
          endif
          if (l .ne. i) then
             rsum( i,j) = rsum( i,j) +v( l,j)
          endif
       enddo
       if (j .eq. m) then
          do k = 1,m
          dsum(i,j) = dsum(i,j)+ dist(i,k)*( v(k,1) +v(k,j-1))
          enddo
       elseif (j .eq. 1) then
          do k = 1,m
          dsum(i,j) = dsum(i,j)+ dist(i,k)*( v(k,j+1) +v(k,m))
          enddo
       else
          do k = 1,m
          dsum(i,j) =dsum(i,j)+dist(i,k)*(v(k,j+1)+v(k,j-1))
          enddo
       endif
       msum = msum + v( i,j)
    enddo
 enddo
 do i = 1,m
    do j = 1,m
       xd( i,j) = -x( i,j) -a* csum( i,j) -b* rsum( i,j)
&                 -c* ( msum -offset)  -d* dsum( i,j)
    enddo
 enddo
 return
 end
```

X. REFERENCES

[1] Helht-Nelson, R., "Performance Limits of Optical, Electro-Optical, and Electronic Neurocomputers", Proceedings of SPIE, International Society of Optical Engineers, Vol 634, 1987, pp. 277-306.

[2] Hopfield, J.J., and Tank, D.W., "'Neural' Computation of Decisions in Optimization Problems", Biological Cybernetics, Vol 52, 1985, pp. 141-152.

[3] Guez, A., Eibert, J.L., and Kam, M., "Neural Network Architecture for Control", IEEE Control System Magazine, April 1988., pp. 22-25.

[4] Bavarian, B., "Introduction to Neural Networks for Intelligent Control", IEEE Control System Magazine, April 1988., pp. 3-7.

[5] Kohonen, T., Self-Organization and Associative Memory, Springer-Verlag, 1984.

[6] Hopfield, J.J., Tank, D.W., "Collective Computation with Continuous Variables", NATIO ASI Series, Vol 20, Disordered Systems and Biological Organization, Springer-Verlag, 1986.

[7] Solla, S.A., "Configuration Space Analysis for Optimization Problems", ibid.

[8] Geman, D., Geman, S., "Bayesian Image Analysis", ibid.

[9] Tank, D.W., and Hopfield, J.J., "Collective Computation in Neuron Like Circuits", Scientific American, pp. 104-114.

[10] Caudill, M., "Neural Networks, Part I, II, III", AI Expert, December 1987, February 1988, June 1988.

[11] Denker, J.S., "Neural Network Models of Learning and Adaptation", Physica Vol 22D, 1986, pp. 216-232.

[12] Guez, A., Protopopescu, V., Barhen, J., "On the Stability, Storage Capacity and Design of Nonlinear Continuous Neural Networks", Oak Ridge National Laboratories, Technical Memo 10329, February 1987.

[13] Simpson, P.K., "A Survey of Artificial Neural Systems", Unisys, San Diego Systems Engineering Center, 1987.

[14] Shepanski, J.F., "Fast Learning in Artificial Neural Systems: Multi-layer Perceptron Training Using Optimal Estimation", AI West '88, Long Beach, May 4-6, 1988, pp. 509-517.

[15] Smith, T.A., and Pitney, G.A., "Calibration of Neural Networks using Genetic Algorithms, with Applications to Optimal Path Planning".

[17] Hopfield, J.J., and Tank, D.W., "Simple 'Neural' Optimization Networks: An A/D Converter, Signal Decision Circuit, and a Linear Programming Circuit", IEEE Transactions on Circuits and Systems, vol CAS-33, No. 5, May 1986, pp.533-541.

[18] Shepanski, J.F., TRW, San Diego, CA, private conversations, Summer 1988.

1988 USAF-UES SUMMER FACULTY RESEARCH PROGRAM/

GRADUATE STUDENT RESEARCH PROGRAM

Sponsored by the

AIR FORCE OFFICE OF SCIENTIFIC RESEARCH

Conducted by

Universal Energy Systems, Inc.

FINAL REPORT

Rapid Measurements of Adsorption and Desorption of Volatile Organic Compounds

Prepared by:	Richard S. Myers, Ph.D.
Academic Rank:	Professor
Department and	Physical Sciences
University:	Delta State University
Research Location:	USAFESC/RDVW
	Tyndall AFB, FL 32403-6001
USAF Researcher:	Thomas B. Stauffer

Date:	July 26, 1988
Contract No:	F49620-87-R-0004

Rapid Measurements of Adsorption and Desorption of Volatile Organic Compounds

by

Richard S. Myers

ABSTRACT

A technique for the measurement of concentration changes due to the rapid adsorption of volatile organic compounds was used to determine the speed with which these compounds are sorbed on soil and aquifer materials. The technique works well for adsorbing materials with a reasonably high organic carbon content. Results indicate a rapid initial adsorption followed by a slower approach to equilibrium. Most of the adsorption occurred within ten minutes. Desorption, however, proceeded at a much slower rate.

Acknowledgements

I wish to express my appreciation to the Air Force Systems Command, the Air Force Office of Scientific Research, and the Air Force Engineering and Services Center for sponsoring this research. I also wish to thank Universal Energy Systems for effectively and efficiently administering the Summer Faculty Research Program.

The willing contributions of many people enhanced my summer research experiences. Dr. Tom Stauffer gave support with direction and assistance. Dr. Leonard Lion, Dr. Neil Hutzler, and Mr. Mark Brusseau provided helpful discussions. Mr. Don Wickman and Ms. Kim Buggs cheerfully provided technical and laboratory assistance. I wish to thank each of them for contributing to a rich and rewarding summer.

I. INTRODUCTION

One of the major factors affecting the fate of organic contaminant materials in the soil environment is the rate at which the contaminant is sorbed on the soil particles. To better understand how organic chemicals behave in groundwater, it is necessary to understand the factors which affect the partitioning of the contaminant between the soil and water phases. A study of the kinetics of adsorption and desorption processes is of fundamental importance in understanding the transport of contaminants in the soil in general and in aquifers in particular. Knowledge of the rates of sorption will be useful in refining various partition and transport models.

There is evidence to show that while hydrophobic compounds may adsorb rapidly, the desorption is much slower. This indicates that the sorbed compound is very strongly, or perhaps irreversibly, bound to the soil particles (Ditoro and Horzempa, 1982; Karickhoff and Morris, 1985). Most evidence comes from soil-water slurry experiments where equilibration time is on the order of hours to days (Hamaker, 1972). The literature contains few reports of the changes occurring in the first few minutes of adsorption onto a natural soil (Wahid and Sethunathan, 1978 ; Wauchope and Myers, 1985; Wu and Gschwend, 1986) and none with aquifer material. These and other kinetic studies generally show a rapid initial adsorption followed by a slow approach to equilibrium (Karichkoff, 1980; Peel and Benedek, 1980).

This study examines the changes that occur in the first minutes of the sorption process as a result of rapid mixing of soil, contaminant, and water. The contaminant, or pollutant, material is a volatile,

hydrophobic, organic compound. This type of compound is of particular interest due to environmental problems associated with spills and leakages of fuels and solvents.

II. OBJECTIVES OF RESEARCH EFFORT

In order to understand how volatile organic chemicals, specifically substituted aromatics and halogenated solvents, behave in soils and aquifers, it is necessary to measure not only the rates of adsorption, but also the rates of desorption. The contaminants in this study include volatile, nonpolar organic compounds, such as those found in jet fuels and solvents. The adsorbents include a soil (muck) and aquifer material.

The first objective of this project was to develop an analytical technique which can be used for the rapid determination of the extent of adsorption and desorption of volatile organic compounds.

The second objective was to use this method to investigate the kinetics of sorption, particularly the initial stages of the sorption process.

III. MATERIALS AND METHODS

Materials. Two natural soils with contrasting properties were used for this study. Belle Glade muck, a surface soil, had a very high total organic carbon content, 18.6 %. Aquifer material from Barksdale Air Force Base, LA, had 0.105 % total organic carbon. Both materials were passed through a 1.0 mm sieve.

Three chlorinated hydrocarbons were used as contaminants. Trichloroethylene (TCE) and 1,2,4-trichlorobenzene (TCB) were purchased from Fisher Scientific, and 1,2-dichlorobenzene (DCB) was purchased from

Fluka. All were used without further purification. Their Henry's Law constants of 0.06 to 0.4 (mol/mL air)/(mol/mL water) indicated that the measured concentration in the gas phase would be proportional to the concentration in the liquid phase. Deionized, distilled water was used for the preparation of slurries.

Experimental Apparatus. Kinetic measurements were made using a modification of the apparatus described by Wu and Gschwend (1986). A one liter reaction flask with two necks, containing approximately 0.95 L slurry, was continuously stirred with a magnetic stirrer. During the first two hours and at selected periods of analysis, air was pumped through the slurry at a rate of 20 mL/s by a stainless steel bellows pump (model MB-21, Metal Bellows Co., Newton, MA) and recycled in an all glass and stainless steel closed loop. For analysis a small portion of the flow (30 mL/min) was passed through a closed, parallel loop containing the photoionization detector of a gas chromatograph (Series 2000, Perkin Elmer Corp., Norwalk, CT). The signal from the photoionization detector, measuring concentration in the gas phase, was recorded on a strip chart recorder. The system was maintained at 24.0 $\pm$ 0.5 °C, except that the photoionization detector was maintained at 150 °C. In order to check its baseline response and to zero it, the detector was occasionally switched to a similar loop containing only water-saturated air. The system could be used up to three days without the loss of contaminant due to leaks or decomposition by the photoionization detector.

Procedure for Adsorption Kinetics. With the system initially containing only water and air, the detector was adjusted to a zero baseline. A small amount of the contaminant was introduced with a microliter syringe and allowed to dissolve.

The solid adsorbent was mixed with a measured amount of water for at least a day to establish a natural state of wetting. To begin the adsorption process the solid suspension was poured into the reaction flask through the side neck. In every case the masses of water, soil, and contaminant were known. It was previously determined that opening the side neck momentarily did not result in a measurable loss of contaminant. With air circulating in the system, the concentration of the contaminant in the gas phase was measured continuously for the first two hours and then at intervals for 24 to 48 hours.

Desorption Kinetics. The same experimental apparatus was used for desorption kinetics. Into the reaction flask were placed 475 mL water, 10 g wetted soil, and 32 mg dichlorobenzene contaminant. The system was stirred for 24 hours, at which time another 475 mL water was added. With air circulating in the closed system, the concentration in the gas phase was measured for five hours and again at 24 hours.

Purge-induced Desorption. At the conclusion of an adsorption kinetics experiment the system was rearranged to produce an open system in which water-saturated air was pumped through the reaction flask. A portion of that air was sent to the detector and then vented. As air was pumped through the flask, the contaminant was stripped from the aqueous phase, which induced desorption from the solid surfaces to the water. The desorption was usually complete within four to five hours. The rate of desorption is dependent upon the air flow rate. With the present system it was not possible to reduce the air flow to the point where meaningful desorption data could be obtained. However, it was demonstrated that this technique could be used to investigate purge-induced desorption kinetics. That is left to a future project.

IV. RESULTS AND DISCUSSION

The experimental systems which gave meaningful results for adsorption kinetic results are described in Table 1.

Table 1. Experimental Systems for Adsorption Kinetics

Expt. no.	Figure	Sorbate	C_o, ppm	C_e/C_o	Sorbent	Solid conc., g/L	K_p, mL/g	K_{oc}
1	1,3	DCB	39	0.23	muck	107	31	170
2	1,3	DCB	39	0.79	muck	12	22	120
3	1	DCD	19	0.75	muck	12	28	150
4	1,3	DCB	1.4	0.67	muck	11	46	250
5	1,3	DCB	1.4	0.72	muck	5	73	390
6	2	TCB	1.5	0.28	muck	11	240	1300
7	2	TCE	0.78	0.66	muck	43	12	65
8	2	TCE	0.78	0.39	muck	100	15	81
9	5	TCE	1.5	0.968	aquifer	64	0.52	500
10	5	DCB	1.3	0.947	aquifer	61	0.91	870
11	5	DCB	1.3	0.972	aquifer	11	2.7	2600
12		DCB	6.8	0.949	aquifer	11	5.1	4900
13	5	DCB	14	0.911	aquifer	11	9.3	8900

Additional adsorption experiments were attempted using montmorillonite clay as the adsorbent; however, the amount adsorbed was so small that the kinetics could not be measured with this apparatus.

The partition coefficients, K_p and K_{oc}, were determined at by the concentrations at the end of the kinetics experiment. They are defined by

$$K_p = \frac{x / m}{C_e} \qquad K_{oc} = \frac{K_p}{F_{oc}}$$

where x/m is the amount of contaminant $\underline{x}$ (in ug) adsorbed by a mass $\underline{m}$ of

soil (in g) at equilibrium with the solution of concentration C_e (in ug contaminant/mL solution). F_{oc} is the fraction by mass of the organic carbon in the soil. The use of K_{oc} "corrects" the value of K_p, assuming organic carbon to be the actual adsorbent. Often similar values of K_{oc} are obtained for a given soil and contaminant (Hamaker and Thompson, 1972). In this study the values of K_p and K_{oc} for a particular compound and soil show some degree of variation because the system may not have been at equilibrium when the kinetics experimental run was stopped. In order to work with as many systems as possible in a limited amount of time, most kinetic runs were discontinued at the end of one or two days. This was consistent the overall goals of the project to investigate the initial minutes and hours of adsorption.

The degree of adsorption of the contaminants by muck for the first hour is shown in Figure 1. The 1,2,4-trichlorobenzene data are represented in Figure 2 (Left) , and trichloroethylene in Figure 2 (Right). In every case it appears that there is a fast initial adsorption followed by a slower approach to equilibrium.

A typical example of the approach to equilibrium over a period of one day is shown for 1,2-dichlorobenzene in Figure 3. In order to compress the time axis the relative concentration can be plotted as a function of the common logarithm of time. Some of the 1,2-dichlorobenzene data are shown in Figure 3 (Right). A comparison of the relative decrease in adsorption for the three chlorinated hydrocarbons is shown in Figure 4. In general compounds with a greater hydrophobicity and larger molecular weight have a slower uptake during adsorption.

The extent of adsorption (the value of K_p) is much smaller for adsorption onto the Barksdale aquifer material, which has a much lower

amount of organic carbon. These data are shown in Figure 5. In both cases, though, the data follow the same pattern as previously seen. There is a fast initial adsorption, followed by a slower approach to equilibrium. However, in the case of trichloroethylene the initial rate of adsorption onto aquifer material is somewhat slower than that for adsorption onto muck.

The desorption of dichlorobenzene from muck after a 24-hour adsorption period is represented in Figure 6. The rate of desorption appears to be much slower than the rate of adsorption. This indicates that the dichlorobenzene is adsorbed very strongly onto the soil particles, perhaps even to the point that some of it may be irreversibly bound to the soil. As Figure 7 indicates, the desorption process progresses at a slower rate than adsorption. After 100 minutes (log = 2) the adsorption is very nearly complete, but the only about one-fourth of the dichlorobenzene has desorbed.

V. RECOMMENDATIONS

a. The rates of sorption should be considered when developing and refining models for the transport and partition of contaminants in surface waters and in aquifers. In some cases it appears that the rates of sorption may be fast compared to the flow of water in aquifer systems. But this may not apply to contaminants that have been in contact with soil for long periods of time.

b. This project has caused questions to arise which should be addressed in further research.

1. How well do present models of sorption(one-box, two-box, and diffusion) fit the sorption data generated in this project?

2. How can the sensitivity of this technique be improved so

that sorption on aquifer materials can be easily investigated?

3. What is the theoretical basis for adsorption onto materials with very low organic carbon content? What are the characteristics of adsorption sites? Are they uniformly distributed?

4. How can this apparatus be modified to study purge-induced desorption kinetics?

REFERENCES

Ditoro, D.M. and Horzempa, L.M. 1982. Reversible and resistant components of PCB adsorption - desorption: Isotherms. Environ. Sci. Technol. 16, p. 594-602.

Hamaker, J.W. 1972. The interpretation of soil leaching experiments. p. 115-133. In R. Haque and V.H. Freed (ed.) Environmental dynamics of pesticides. Plenum Press, New York.

Hamaker, J.W. and Thompson, J.M. 1972. Adsorption. p. 49-143. In C.A. Goring and Hamaker, J.W. (ed.) Organic chemicals in the soil environment. Mercel Dekker, Inc., New York.

Karickhoff, S.W. 1980. Sorption kinetics of hydrophobic pollutants in natural sediments. In R.A. Baker (ed.) Contaminants and Sediments, vol. II, Ann Arbor Science Publishers, Ann Arbor, MI, p. 193-205.

Karickoff, S.W. and Morris, K.R. 1985. Sorption dynamics of hydrophobic pollutants in sediment suspensions, Environ. Toxicology and Chem. 4, p. 469-479.

Peel, R.G. and Benedek, A. 1980. Attainment of equilibrium in activated carbon isotherm studies, Environ. Sci. Technol., 14 p. 66-71.

Wahid, P.A. and Sethunathan, N. 1978. A simple method to study pesticide sorption in soils at short time intervals, Soil Sci., 126, p. 56-58.

Wauchope, R.D. and Myers, R.S. 1985. Adsorption-desorption kinetics of atrazine and linuron in freshwater-sediment aqueous slurries, J. Environ. Qual., 14 p. 132-136.

Wu, S.C. and Gschwend, P.M. 1986. Sorption kinetics of hydrophobic organic compounds to natural sediments and soils, Environ. Sci. Technol., 20 p. 717-725.

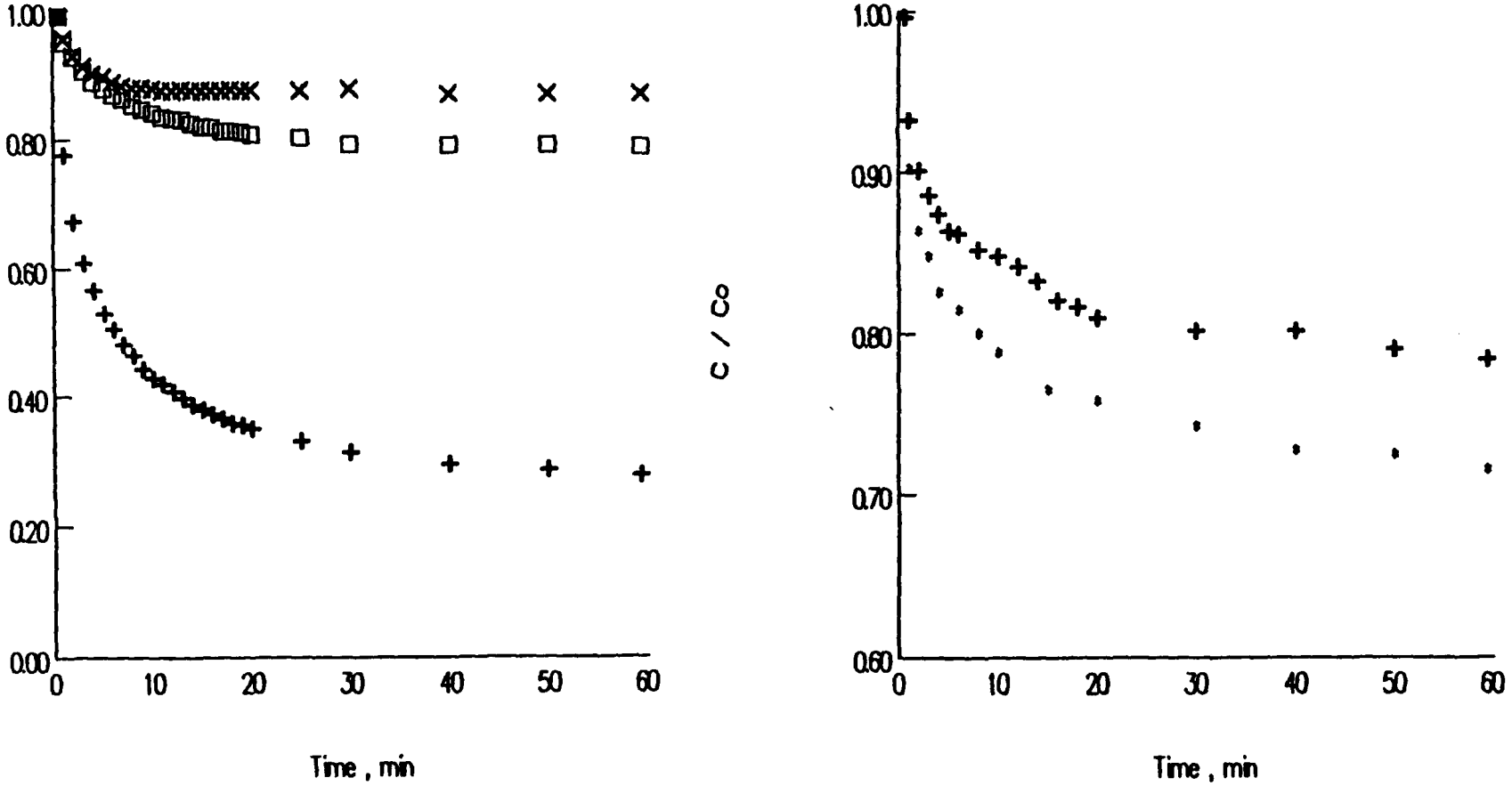


Figure 1. Experimental results for the first hour of adsorption of 1,2-dichlorobenzene by muck. (Left) □, 39 ppm DCB, 12 g muck/L; +, 39 ppm DCB, 107 g muck/L; x, 19 ppm DCB, 12 g muck/L. (Right) *, 1.4 ppm DCB, 11 g muck/L; +, 1.4 ppm DCB, 5 g muck/L.

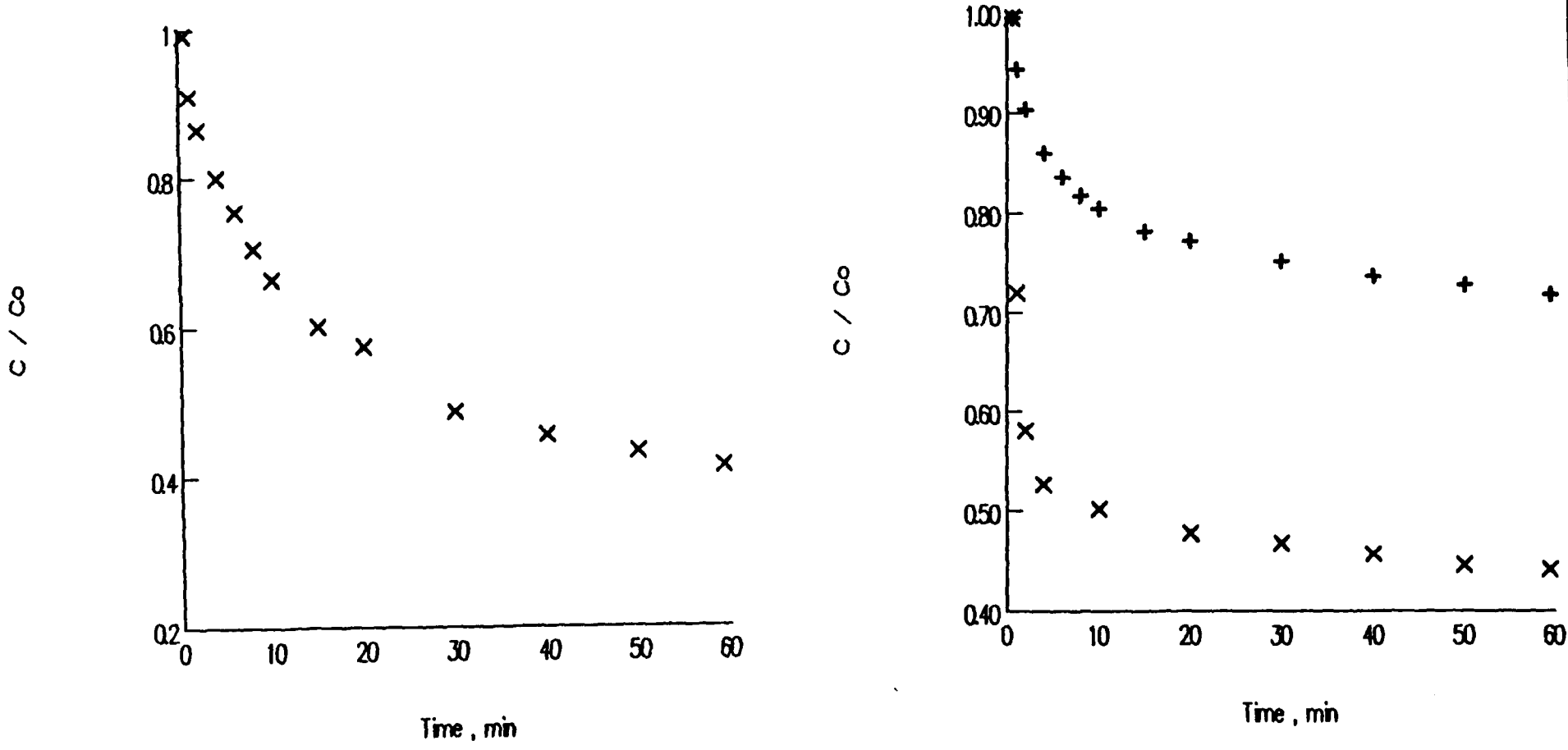
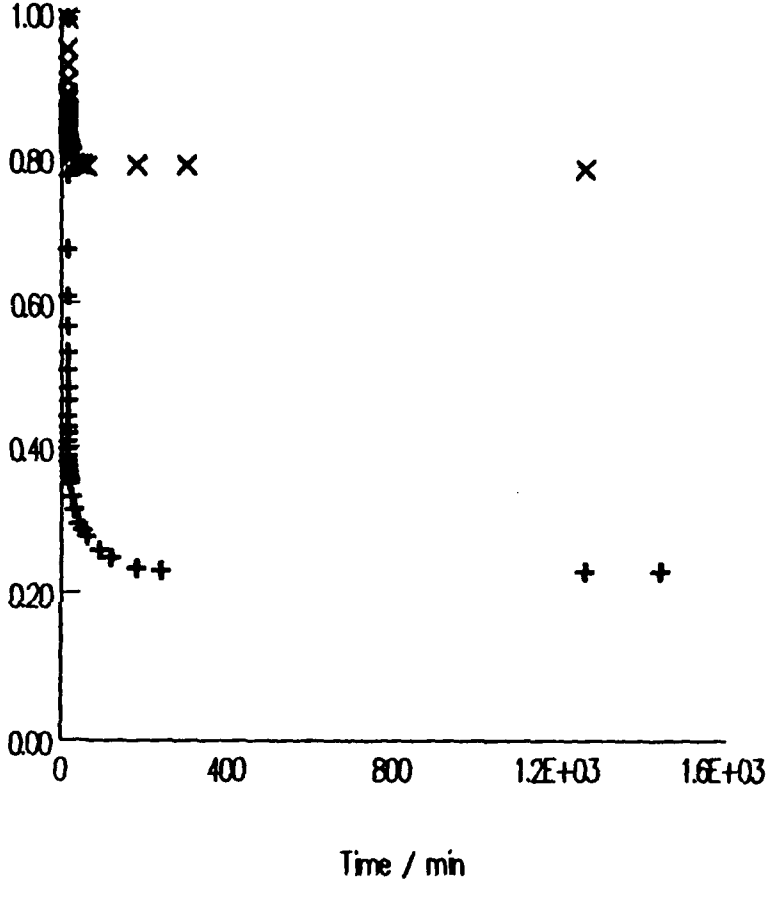


Figure 2. Experimental results for the first hour of adsorption. (Left) 1,2,4-trichlorobenzene by muck. C_o = 1.5 ppm TCB, 11 g muck/L. (Right) trichloroethylene by muck. + , 0.78 ppm TCE, 43 g muck/L; x , 0.78 ppm TCE, 100 g muck/L.



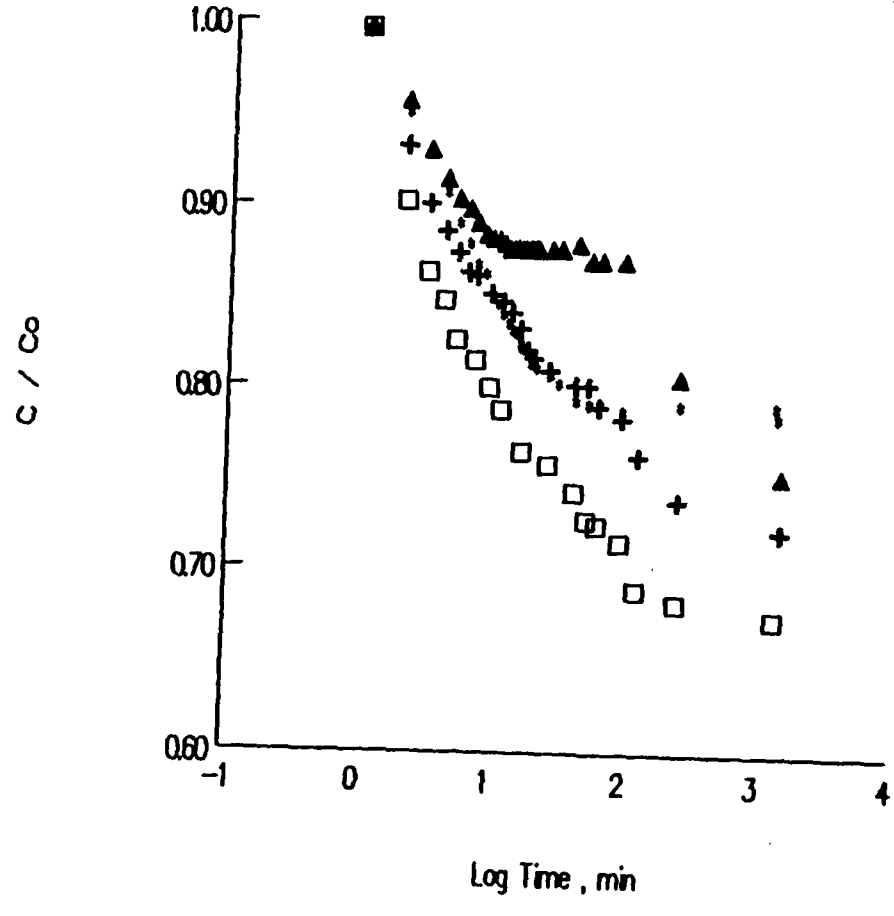


Figure 3. Relative concentration of 1,2-dichlorobenzene during one day of adsorption. C_o = 39 ppm DCB; + 107 g muck/L; x, 12 g muck/L. (Right) Relative adsorption of 1,2-dichlorobenzene by muck over a one day period. *, 39 ppm DCB, 12 g muck/L; ▲, 19 ppm DCB, 12 g muck/L; □, 1.4 ppm DCB, 11 g muck/L; +, 1.4 ppm DCB, 5 g muck/L.

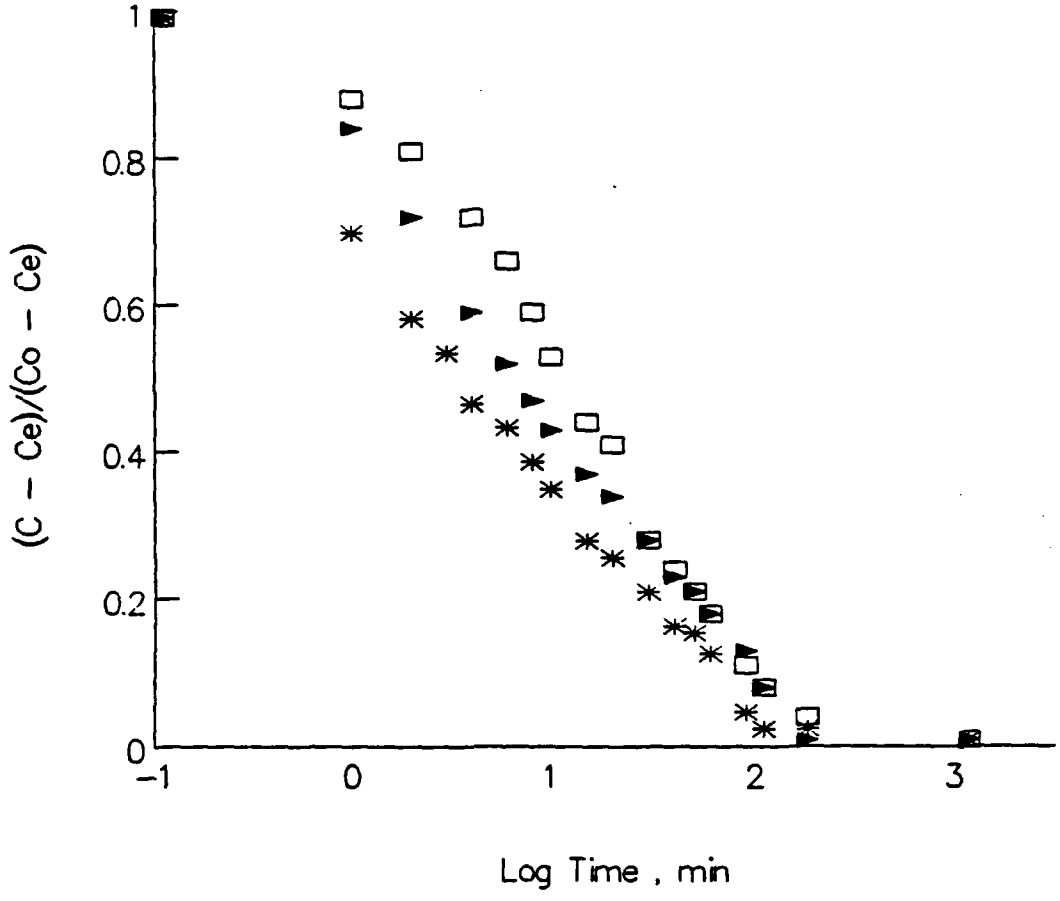
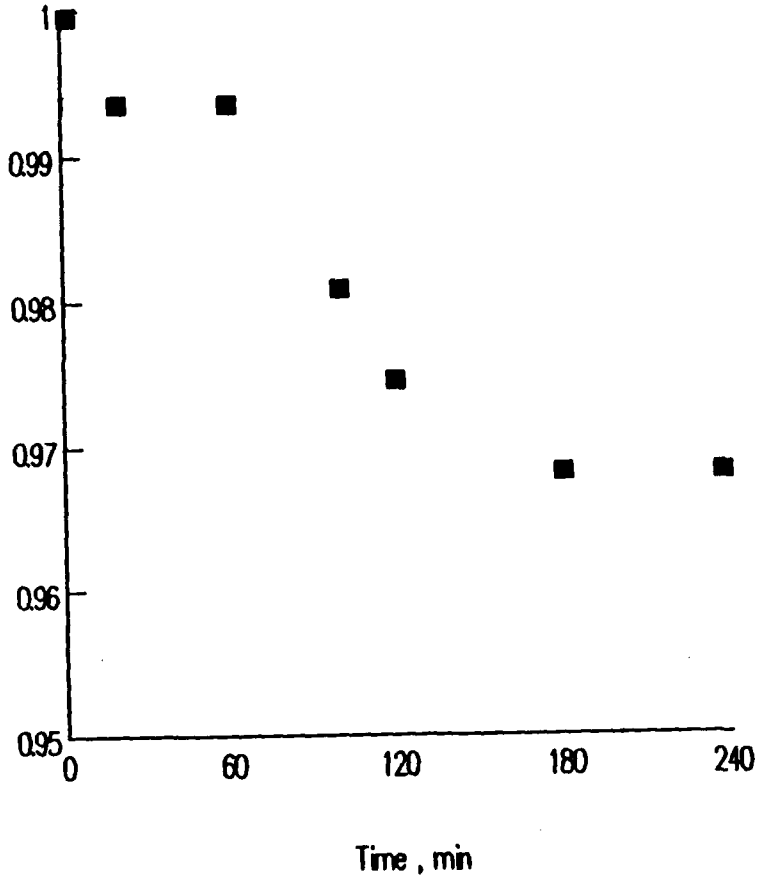


Figure 4. Comparison of the experimental results for the chlorinated hydrocarbons adsorbed onto muck. *, Dichlorobenzene; □, trichlorobenzene; ▲, trichloroethylene.



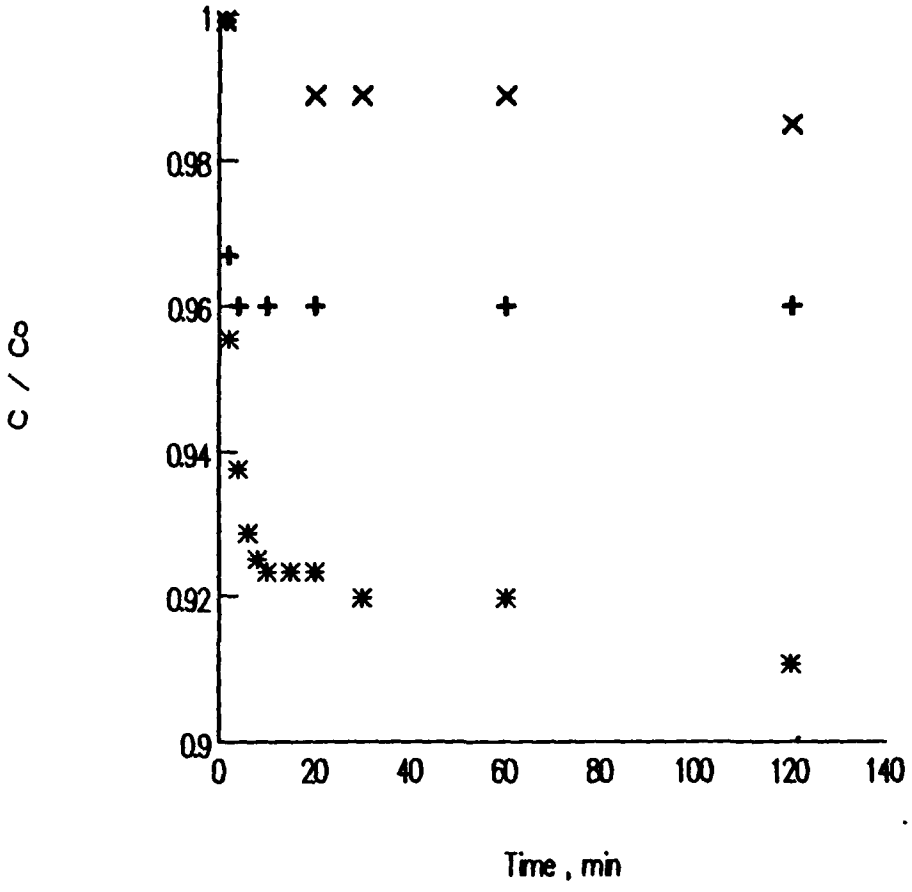


Figure 5. Adsorption by aquifer material. (Left) 1.5 ppm trichloroethylene on 64 g solid/L. (Right) Dichlorobenzene; *, 14 ppm DCB, 11 g solid/L; x, 1.3 ppm DCB, 11 g solid/L; +, 1.3 ppm DCB, 61 g solid/L.

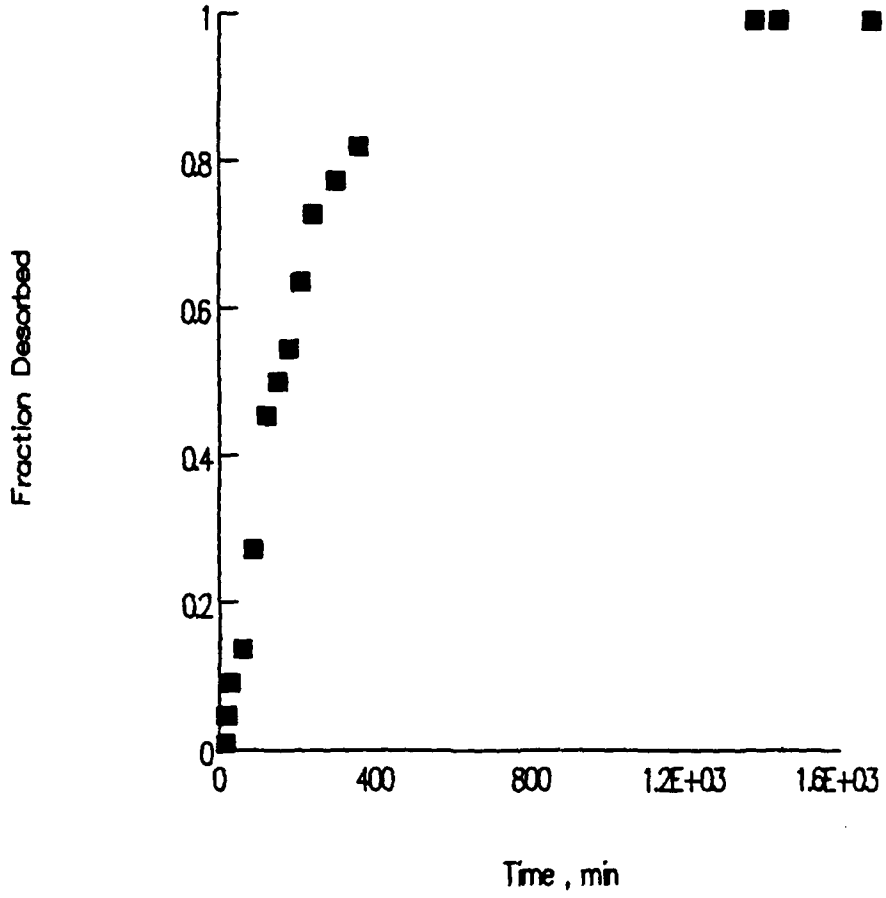


Figure 6. Desorption of Dichlorobenzene from muck after 24-hour adsorption. Total DCB = 34 mg/L. Total soil = 11 g/L.

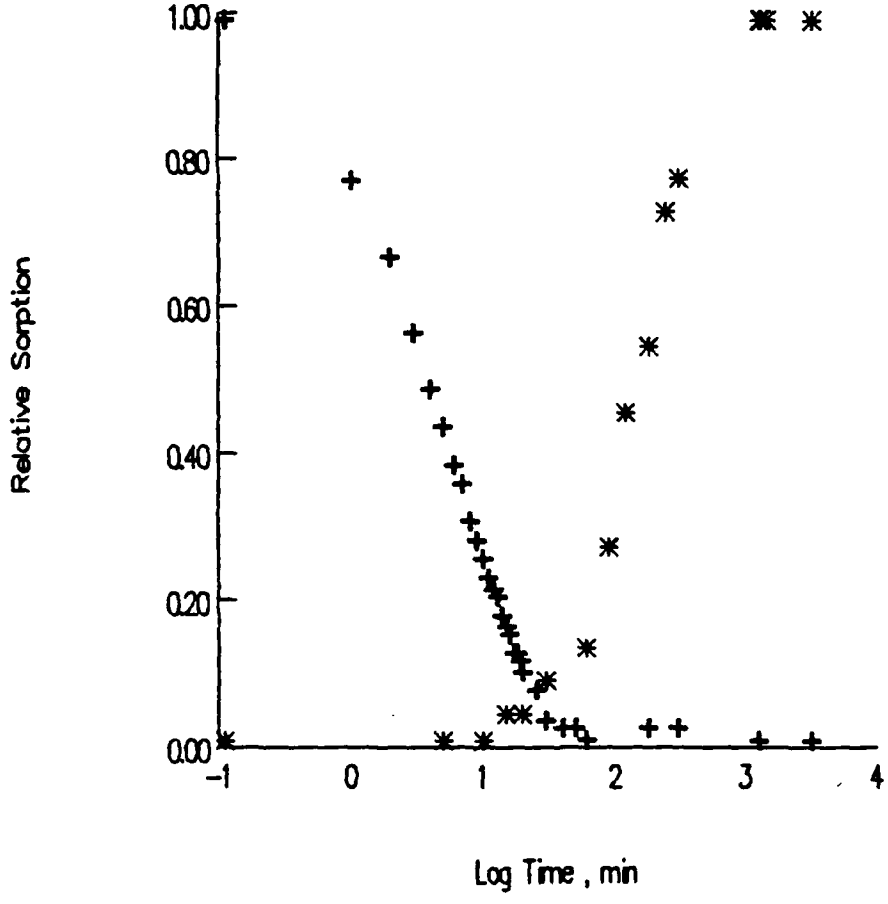


Figure 7. Comparison of rates of adsorption (+) and desorption (*) in systems with 32 mg DCB and 11 g/L muck.

1988 USAF-UES SUMMER FACULTY RESEARCH PROGRAM

Sponsored by the

AIR FORCE OFFICE OF SCIENTIFIC RESEARCH

Conducted by the

UNIVERSAL ENERGY SYSTEMS, INC.

FINAL REPORT

PREFABRICATED HYPAR STRUCTURAL SYSTEM COST COMPARISON WITH BOX AND ARCH STRUCTURES

Prepared by:	Ramalingam Radhakrishnan, PH.D., P.E.
Academic Rank:	Assistant Professor
Department and University:	Department of Civil Engineering Prairie View A & M University
Research Location:	USAF Tyndall AFB/RDCS Panama City, Florida 32403
USAF Researcher:	Lt Randy Burkett

Date:	29 July 1988
Contract No.:	F 49620-87-R-0004

PREFABRICATED HYPAR STRUCTURAL SYSTEM
COST COMPARISON WITH BOX AND ARCH STRUCTURES

by

Ramalingam Radhakrishnan

ABSTRACT

The USAF is interested in the evaluation and selection of an economical shelter system that can protect equipment and personnel from conventional weapons. Details of the three types of protective structures are given. The Hypar protective structure system uses prefabricated hyperbolic paraboloid shells which could be erected in a short notice at preferred locations on a foundation slab. An equivalent rectangular box and arch (barrel vault) are conventional type structures which require cast-in-place construction. Design of structural elements, structural details, construction time, unit price of materials and labor for the three structures are presented. Cost comparison of Hypar, Box, and Arch structures and recommendations for selection are provided.

Acknowledgements

The author wishes to thank the Air Force systems command and the Air Force Office of Scientific Research for sponsorship of this Summer Faculty Research Program, and Universal Energy Systems for all their help.

The author expresses sincere thanks and great appreciation to Lt Randy Burkett for the support, encouragement and a truly enjoyable atmosphere. The author is grateful to Mr Stan Strickland, Division Head, RDCS, for the support and encouragement.

The author conveys special thanks to Major Bramlitt and Mrs Cheryl Garfield for all the help provided during the program. The author is immensely thankful to Ms Tami White for typing this report.

The author acknowledges with great appreciation the support of his home institution and the encouragement of Dr Wayne D. Perry (Dean), Dr R. N. S. Rao (Associate Dean), and Dr K. M. A. Rahman (Chairman, Department of Civil Engineering) of the college of Engineering at Prairie View A & M University, Prairie View, Texas.

I. INTRODUCTION:

The HYPAR Protective Structure System consists of prefabricated hyperbolic paraboloid shells. These concrete shells are 5" in thickness with an energy absorbing 1" thick asphalt/glass coating on the outside and a thin polyester fabric protection on the inside. The Hypar shell panels are fabricated in two sizes: 1. Base Hypar and 2. Apex Hypar. Seven panels of Base Hypar and eight panels of Apex Hypar are required to produce one octagonal Hypar unit. The prefabricated shell panels can be easily transported and erected quickly on a foundation slab of 40'-2" x 40'-2" size at any preferred location.

A Hypar structure erected such that it is below ground level with atleast 2 feet of soil berm cover will provide protection from high impulse blast loadings of conventional weapons.

Tests conducted in the past on full-scale models of Hypar structure, box structure and arch structure proved clearly that any one of the three structures can be designed and constructed to meet the threat criteria and provide protection to personnel and equipment. The real challenge is to select one of the three protective structures to meet the needs at the lowest construction cost.

II. OBJECTIVES OF THE RESEARCH EFFORT:

The primary goal of this study was to determine the cost savings of selecting a Hypar unit compared to a Box or Barrel Vault (arch) structure. Specifically, the objectives were as follows:

1. Establish the total cost of materials, prefabrication of panels and erection of a Hypar unit in the field.

2. Design an equivalent rectangular box structure. Compute the total cost of cast-in-place construction of a box structure in the field.

3. Design an equivalent barrel vault structure (arch) and calculate the total cost of cast-in-place construction of the arch structure in the field.

4. Compare the cost and present advantages for selection.

III. Design Criteria:

No. of units: 1 unit

Soil: Sandy soil

Depth of Berm: 2 feet deep soil above top edge of structure

Wave Speed: 1000 fps

Subsurface Explosion Weight (W): 520 lb TNT

Distance of blast (R): 10 ft from the structure

Height of blast (H): 5 ft above the floor slab.

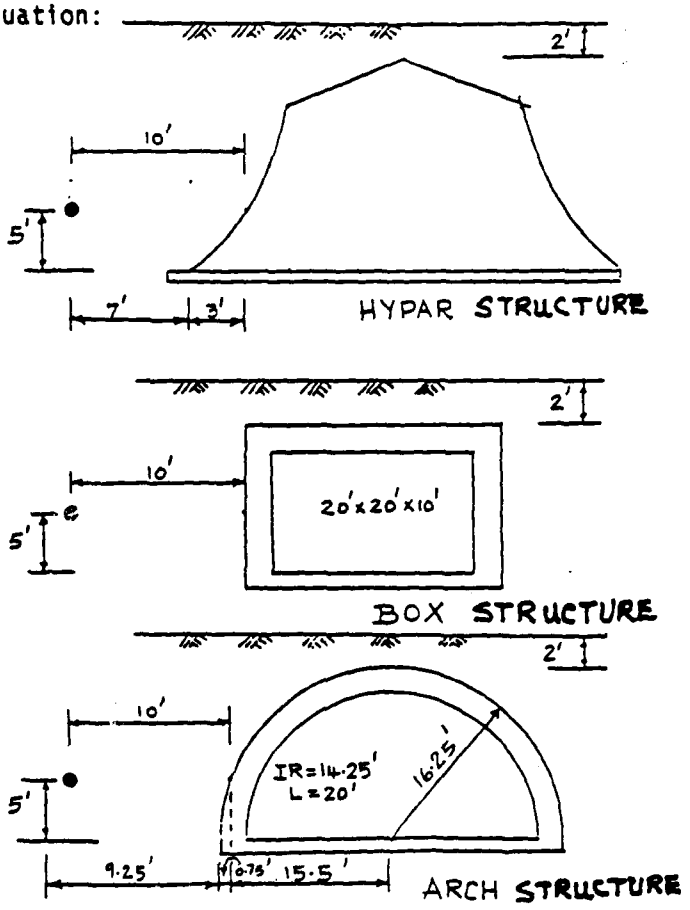
Structural Requirement: No breaching.

Loading: Drake/Little blast Model.

Reflected Pressure: $Pr = \frac{1,331,900}{R^{2.75}}$, psi

Structural Materials: CONCRETE Compressive Strength = 5,000 Psi
REINFORCING STEEL Yield Stress = 60,000 Psi

Structures for Evaluation:



IV. COST DATA:

For the purpose of this study, cost information was taken from the 1988 Dodge unit Cost Data (Ref. 7). Cost data reflects current construction practices nationally. The unit costs used represent average prices. Prices are those which would be incurred by a general contractor who subcontracted for all items of work. Costs include the subcontractor's overhead and profit. The general contractor's overhead and mark up are not included in any of the prices.

V. HYPAR STRUCTURE:

The plan, elevation and structural details are shown in the following page. The construction of a hypar unit requires the following:

1. Foundation Slab: Concrete slab of 9 3/4 inches in thickness with reinforcing steel bars of #3 size at 4" centers should be constructed at the preferred location where the hypar unit is to be built. Construction of the foundation slab involves the preparation of ground, building form, positioning the reinforcing steel, placing and curing concrete so that the foundation slab will be ready for erection of hypar panels. An important item of work during this phase is setting the anchors in correct locations before placing concrete. Anchors should be prepositioned such that the bolt holes in the legs of the hypar panel will match so that proper fit during the installation of the hypar panels will be possible.

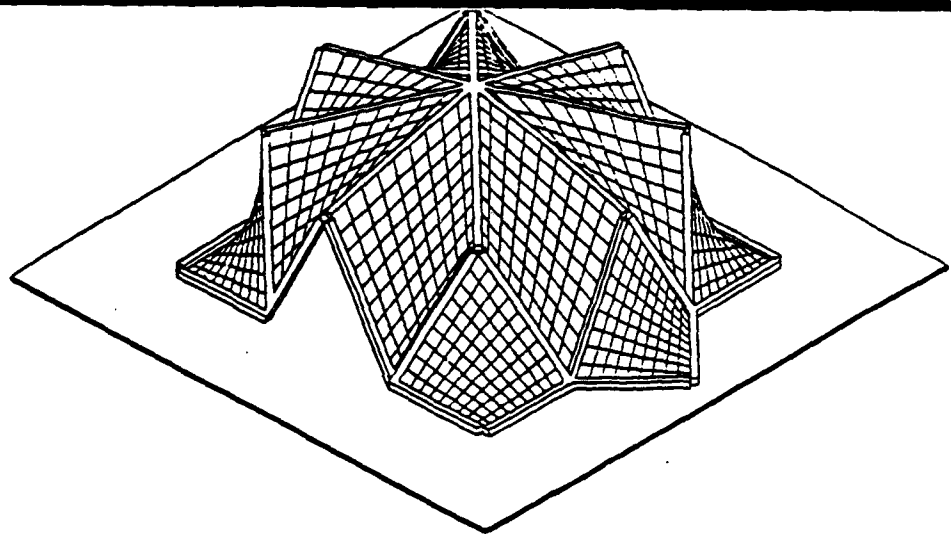
2. Hypar Panels are doubly curved shells, but they are ruled surfaces. Therefore, form for the shape of the hyperbolic paraboloid is not difficult to make. Hypar panels will be cast in precast concrete fabrication plants. It is assumed that 100 units of the shelter will be built as a minimum.

   a) Base Hypar Panels

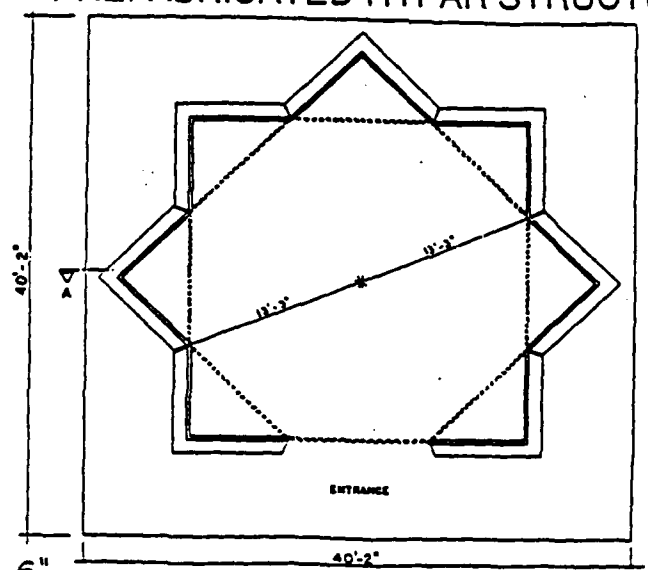
   To facilitate casting the 700 panels required for building 100 units, 10 molds will be prepared for use as form for the fabrication of the base hypar panels.
   Cost of Mold = 80(SF) x $16 per SF = $1,280
   Form Cost for Base Hypar = $1,280 x $\frac{10}{700}$ x 7 = $128 per unit

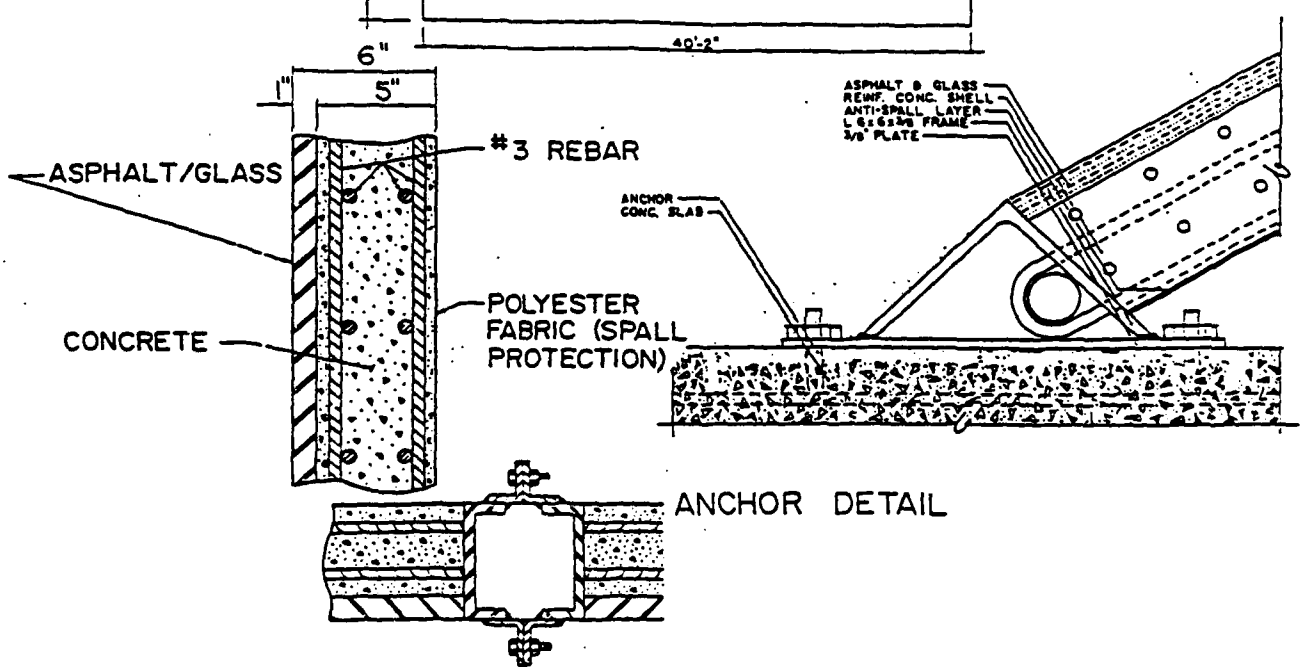
   b) Apex Hypar Panels

   To build 100 units, 800 panels will be required and 10 molds will be prepared for use as form for the fabrication of the Apex hypar panels.
   Cost of Mold = 117 (SF) $16 per SF = $1,872
   Form Cost for Apex Hypar = 1,872 x $\frac{10}{800}$ x 8 = $187 per unit



PREFABRICATED HYPAR STRUCTURE





3. Installation of Hypar:

Hypar panels will be shipped after fabrication from precast plants and stored at bases or in the field. They could be assembled very quickly once the foundation slab is ready for installation.

If the foundation slab is to be built, then 28 days will be required for conrete to attain full strength. Installation of panels is expected to take 4 days. Therefore, a unit could be made available for use in approximately 30 days.

If the foundation slab is prebuilt at preferred locations or an existing pad of equivalent thickness and strength could be used, a unit could be made available for use in 4 days.

Equipment:		Personnel:	
	1 Cherry Picker		2 Drivers
	1 Fork Lift		2 Operators
			2 Laborers
		Total =	6

Time

Positioning Panels	1 day
Assembling & Bolting Base and Apex Panels	1 day
Drilling Holes for Expansion Anchors	1 day
Fixing Base panel legs to Foundation	1 day
Total	4 days

Cost of Instal. = 6 x 8 x 4 x $30 = $5,760

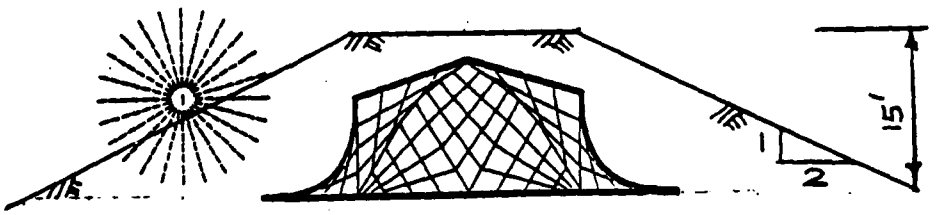
4. Earth Cover (Soil Berm):

Top Surface Area = 25' x 25'

Bottom Area of side (25' + 15' x 2 x 2) = 85' x 85'
Volume of Soil = 58,875 - 4500 = 54,375 CF = 2,014 CY

Cut & Fill or Piling Earth

Cost (For 150' Haul) = $1.78/CY
An operating Engineer could pile earth of 250 CY/day
Using 2 Operating Engineers, 4 days would be required to complete this work. Total Cost to provide soil cover = $3600.00



EARTH COVER

HYPAR STRUCTURE SYSTEM

QUANTITY OF CONSTRUCTION MATERIALS PER UNIT

DESCRIPTION	DETAILS	QUANTITY
1. Foundation		
Concrete Slab:	Cast in place concrete	
Size: 40'-2"x40'-2"x9.75"	40.17x40.17x9.75/12=1310 CF	49 CY
Reinforcing Steel:	480x40'x0.376 = 7219 lb	3.6 Tons
#3 @ 4", one layer		
Both ways, Each face		
Form:	40.16x4x9.75/12= 131 SFCA	131 SF
Curing Surface:	40'x40'	1600 SF
Anchor Bolts:	8 NOS outside, 4 NOS inside	
1" dia x 18" long	per leg = 12x2x7	168 NOS
2. Base Hypar (For 7 Panels)		
Concrete:	Panel prefabricated in plant	
Size: 8.0'x12.5' Edges	Area=64.3x1.25 (curve)	
5" Thick Concrete	80 x 5/12 x 7 = 233 CF	9 CY
Reinforcing Steel:		
33 NOS #3 bars	33x4x0.5(7.75+12.25)x0.376x7	
Both ways, Each face	= 3474.2	1.74 T
Form (special):	Assumption: 100 units to be	
Mold preparation time 32 hrs	built; 10 molds to be made	
Mat+Labor cost = 80x$16	and each put to 70 reuses	
= $1280 per mold	1280 x 10 x 7/700	$128.00
Edge Beams:		
C 6x10.5	10.5x12.5'x2x7	1838 lb
L 3x2x5/16	5.0x12.5'x2x2x7	1750 lb
L 6x6x3/8	14.9x8.0'x2x7	1668 lb
PL 18x3/8	23.0x8.0'x2x7	2576 lb
Fillet weld 1/4" Thick:		
Apex side	12.5'x4x2x7	700 ft
Base side	8.0'x2x7	112 ft
3. Apex Hypar (For 8 Panels)		
Concrete:	Panel Prefabricated in plant	
Size: 12.5'x13'.0 Edges	Area=93.6x1.25 (curve)	
5" Thick concrete	117 x 5/12 x 8 = 390 CF	15 CY
Reinforcing Steel:		
33 NOS #3 bars	33x4x13x0.376x8	
Both ways, Each face	= 5161.7 lb	2.6 T
Form (special):	Assumption: 100 units to be	
Mold preparation time 32 hrs	built; 10 molds to be made and	
Mat+Labor cost = 117 x $16	each put to 80 reuses	
= $1870 per mold	1870 x 10 x 8/800	$187
Edge Beams:		
C 6x10.5	10.5x13'x4x8	4368 lb
L 3x2x5/16	5.0x13'x2x4x8	4160 lb
Fillet weld 1/4" Thick:	13'x4x2x8	832 Ft
Connection Bolts:		
Base to Apex 12 NOS 3/4" dia	12x2x2x7	336
Apex to Apex 12 NOS 3/4" dia	12x2x8	192

COST OF HYPAR STRUCTURAL SYSTEM

Description	UNIT	MAT	LABOR	EQU	ML&E	TOTAL
1. Foundation slab						
Concrete 49 cy (Cast-in-place)	CY	57.00	-	-	57.00	2800
Reinforcing Steel Quant: 3.6 Tons (Erected in place)	TON	500.00	250.00	5.00	755.00	2720
Form in place Quant: 131 SFCA	SF	1.25	-	4.24	5.49	720
Conc. Placing Quant: 49 CY	CY	2.34	-	0.16	2.50	130
Conc. Curing Quant: 1600 SF	SF	-	0.10	-	0.10	160
Anchor Bolts: 1" dia x 18 Quant: 168 NOS	Ea	2.44	-	-	2.44	410
setting anchor bolts Quant: 168 NOS	Ea	10.90	4.25	-	15.15	2550
2. BASE HYPAR (prefab): (7 Panels)						
Concrete: 9 CY	CY	55.00	-	-	55.00	500
Reinforcing Steel Quant: 1.74 Tons	Ton	500.00	100.00	-	600.00	1050
FORM: Cost of Mold	-	-	-	-	-	130
Concrete Placing	Panel	100.00	-	-	100.00	700
Concrete Curing	Panel	-	50.00	-	50.00	350
Edge Beams: C.6 x 10.5 Quant: 1838 lb	lb	0.60	-	-	0.60	1110
L 3 x 2 x 5/16 Quant: 1750 lb	lb	0.60	-	-	0.60	1050
L 6 x 6 x 3/8 Quant: 1668 lb	lb	0.60	-	-	0.60	1000
Pl 18 x 3/8" Quant: 2576 lb	lb	0.60	-	-	0.60	1550
Fillet weld 1/4" Tk Apex Side 700 Ft	Ft	3.00	-	-	3.00	2100
Base side 112 Ft	Ft	3.00	-	-	3.00	340
3. APEX HYPAR (Prefab): (8 Panels)						
Concrete: 15 CY	CY	55.00	-	-	55.00	830
Reinf Steel Quant: 2.6 Tons	Ton	500.00	100.00	-	600.00	1560
FORM: Cost of Mold	-	-	-	-	-	190
Placing Concrete	Panel	100.00	-	-	100.00	800
Curing Concrete	Panel	-	50.00	-	50.00	400
Edge Beams: C 6 x 10.5 Quant: 4368 lb	lb	0.60	-	-	0.60	2630
L 3 x 2 x 5/16 Quant: 4160 lb	lb	0.60	-	-	0.60	2500
Weld Fillet 1/4" Tk Quant: 832 ft	Ft	3.00	-	-	3.00	2500

Description	UNIT	MAT	LABOR	EQU	ML&E	TOTAL
4. Connection Bolts:						
Fasteners						
Base to Apex						
3/4" dia. 336 NOS	Ea	0.70	-	-	0.70	240
Apex to Apex						
3/4" dia. 192 NOS	Ea	0.70	-	-	0.70	140
5. Asphalt Membrane -		-	-	-	-	1520
6. Spall Protection Coat		-	-	-	-	1750
					TOTAL	$40,180

VI. Box Structure:

Dimensions: Inside 20' x 20' x 10', Outside 25' x 25' x 13.5'

1. Wall: Two-way slab; 10' x 20'; all edges fixed.

BOX STRUCTURE SIDE WALL (Trial Design)

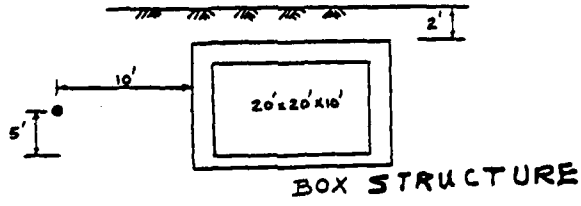
TRIAL	D(IN)	d(IN)	q_y (Psi)	T (ms)	t_d/T	F	q_m (Psi)
1	14	12	194.4	14.1	0.43	5	972.0
2	20	18	437.4	9.4	0.64	3.5	1093.5
3	26	24	777.6	7.0	0.86	2.8	2177.3
4	28	26	912.6	6.5	0.92	2.6	2372.8
5	30	28	1058.4	6.0	1.0	2.5	2646.0

Final Design

Thickness of slab = 30"; d = 28"
$f'_{dc} = 1.25\ f_c = 6.25$ ksi; $f_{dy} = 1.2\ f_y = 72.0$ Ksi
Design Pressure = P_r = 2368.5 psi for R = 10 ft
Static Yield Resistance of Slab (Tk 30" with 1% Reinf Steel)
q_y = 1,058.4 Psi
Natural Period of Slab = 6.05 milli sec;
Duration of pressure = 6 ms
t_d/T = 6.0/6.06 = 1.0; Ductility Factor = 20
Dynamic Yield Resistance of Slab = 2.5 q_y = 2,646.0 Psi
Area of Reinf. Steel = 0.01 x 12 x 28 = 3.36 in^2/ft
Use #7 bars at 4", Two Layers, Both ways, Each Face.

2. Roof: Two-way Slab; 20' x 20'; all edges fixed
Average Design Pressure = 348.0 Psi
Provide 30" thick slab with 1% Reinf. Steel considering the possibility that the roof slab may receive direct hit.

3. Foundation: Two-way slab; 20' x 20'; all edges fixed
Average Design Pressure = 343.7 Psi
concrete cracking may be allowed. Try 12" Thick slab; d = 10" with 0.5% Reinf. Steel; q_y = 54 psi, q_m = 1080 psi.
Use 12" Slab with #4 bars at 4" Both ways, Each Face.



BOX STRUCTURE

COST OF RECTANGULAR BOX STRUCTURE

Description	UNIT	MAT	LABOR	EQU	ML&E	TOTAL
1. Foundation Slab						
Concrete 24 CY	CY	57.00	-	-	57.00	1368
Reinforcing Steel:						
Quant: 2.5 Tons	Ton	500.00	250.00	5.00	755.00	1888
Form in place:						
Quant: 100 SFCA	SF	1.25	4.24	-	5.49	549
Placing Conc.:						
Quant: 24 CY	CY	-	2.34	0.16	2.50	60
Curing Conc.:						
Quant: 625 SF	SF	-	0.10	-	0.10	63
Dowels, steel	-	-	-	-	-	200
2. Walls						
Concrete 84 CY	CY	57.00	-	-	57.00	4788
Reinforcing Steel: #7 @ 4 "O.C						
Quant: 27.00 Tons	Ton	500.00	250.00	5.00	755.00	20385
Form in place:						
Quant: 1800 SFCA	SF	1.48	4.06	-	5.54	9980
Placing conc:						
Quant: 84 CY	CY	2.34	0.16	-	2.50	210
Curing Conc.:						
Quant: 1800 SF	SF	-	0.05	-	0.05	90
Finishing Walls:						
Quant: 1800 SF	SF	-	0.10	-	0.10	180
3. Roof Slab						
Concrete 58 CY	CY	57.00	-	-	57.00	3306
Reinforcing Steel:						
Quant: 14.7 Tons	Ton	500.00	250.00	5.00	755.00	11099
Form:						
Quant: 650 SFCA	SF	1.85	3.32	-	5.17	3361
Placing concrete:						
Quant: 58 CY	CY	-	3.34	0.16	3.50	210
Curing Concrete:						
Quant: 625 SF	SF	-	0.10	-	0.10	63
Finishing Slab:						
Quant: 650 SF	SF	-	0.10	-	0.10	65
					TOTAL	$57,858

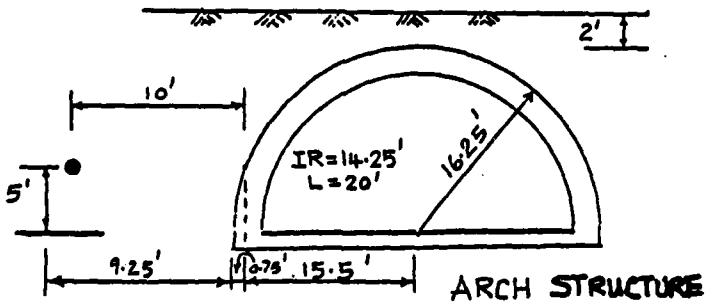
VII. ARCH STRUCTURE:

Dimensions: Inside Radius = 14.25'; length = 20';
outside Radius= 16.25', length = 24'

1. Arch: Thickness of Arch = 24", with 0.5% Reinf. Steel
   Design Pressure = 843.2 Psi
   q_{yc} = 693.7 Psi; T = 8.5 ms; T_d = 6 ms; ductility = 3.0
   q_m = 971.2 Psi; Asc = 0.005 x 12 x 24 = 1.44 m^2
   Asl = 0.002 x 12 x 24 = 0.6 m^2
   Use 24" thick arch with circumf. bars #7@4", Longit. Bars #4@4"
2. End Walls: Provide 24" Thick Concrete wall
   #7 Bars@4", Two layers, Bothways, Each Face
3. Foundation Slab: Provide 12" Thick Slab #4 Bars@ 4",
   Bothways, Each Face

COST OF ARCH (BARREL VAULT) STRUCTURE

Description	UNIT	MAT	LABOR	EQU	ML&E	TOTAL
1. Foundation Slab						
Concrete 29 Cy	CY	57.00	-	-	57.00	1653
Reinforcing Steel:						
Quant: 3.3 Tons	Tons	500.00	250.00	5.00	755.00	2492
Form in place:						
Quant: 117 SF	SF	1.25	4.24	-	5.49	643
Placing concrete:						
Quant: 29 Cy	CY	-	2.34	0.16	2.50	73
Curing concrete:						
Quant: 780 SF	SF	-	0.10	-	-	78
Dowels, Steel	-	-	-	-	-	200
2. End walls						
Concrete: 48 CY	CY	57.00	-	-	57.00	2736
Reinforcing Steel:						
Quant: 15 Tons	Ton	500.00	250.00	5.00	755.00	11325
Form in place						
Quant: 1470 SF	SF	1.48	4.06	-	5.54	8144
Placing concrete						
Quant: 48 CY	CY	-	2.34	0.16	2.50	120
Curing Concrete						
Quant: 1470 SF	SF	-	0.05	-	0.05	74
Finishing 1470 SF	SF	-	0.10	-	0.10	147
3. ARCH						
Concrete: 86 CY	CY	57.00	-	-	57.00	4902
Reinforcing Steel						
Quant: 8.2 Tons	Ton	500.00	250.00	5.00	755.00	6191
Form (Curved)						
Quant: 2130 SF	SF	1.85	3.32	-	5.17	11012
Placing concrete:						
Quant: 172 CY	CY	-	3.34	0.16	3.50	602
Curing Concrete:						
Quant: 2130 SF	SF	-	0.10	-	0.10	213
Finishing Conc.:						
Quant: 2130 SF	SF	-	0.10	-	0.10	213
				TOTAL		$50,818



ARCH STRUCTURE

VIII. Summary of the Results

HYPAR STRUCTURE OPTION #1

Description	Quantity	M&L Cost	Total
1. Foundation Slab			
Concrete 9 3/4" Tk	49 CY	$ 57.00/cy	2,800
Reinf. Steel #3@4"	3.6 T	$755.00/T	2,720
Form	131 SF	$ 5.49/SF	720
Placing Concrete	49 CY	$ 2.50/CY	130
Curing Concrete	1600 SF	$ 0.10/CY	160
Anchor Bolts	168 NOS	$ 2.44/Ea	410
Setting Bolts	168 NOS	$ 15.15/Ea	2,550
2. Base Hypar (7 Panels)			
Concrete 5 " Thick	9 CY	$ 55.00	500
Reinforcing Steel	1.74 T	$600.00	1,050
Form	-	-	130
Placing Concrete	7 Panels	$100.00	700
Curing Concrete	7 Panels	$ 50.00	350
Edge Beams	7832 Lb	$ 0.60	4,700
Welding	812 Ft	$ 3.00	2,440
3. Apex Hypar (8 Panels)			
Concrete 5" Thick	15 CY	$ 55.00	830
Reinforcing Steel	2.6 T	$600.00	1,560
Form	-	-	190
Placing	8 Panels	$100.00	800
Curing	8 Panels	$ 50.00	400
Edge Beams	8528 Lb	$ 0.60	5,130
Welding	832 Ft	$ 3.00	2,500
Connection Bolts	528 NOS	$ 0.70	380
Asphalt Membrane	-	-	1,520
Spall Protection Coat	-	-	1,750
	Total		$34,420
Installation (Optional)			
6(P) x 8 Hrs x 4 days = 192 Hrs		$30/hr	5,760
		Total	$40,180

HYPAR STRUCTURE OPTION #2

Description	Quantity	M&L Cost	Total
1. Foundation Slab			
Using the existing or prebuilt pad and connecting the base panels to pad with expansion anchors 3/4" dia. 8" long.			
Anchor Bolts	168 NOS	$ 3.67/Ea	620
Drilling Bolts	168 NOS	$ 10.78/Ea	1,820
2. Base Hypar (7 Panels)			
Concrete 5 " Thick	9 CY	$ 55.00	500
Reinforcing Steel	1.74 T	$600.00	1,050
Form	-	-	130
Placing Concrete	7 Panels	$100.00	700
Curing Concrete	7 Panels	$ 50.00	350
Edge Beams	7832 Lb	$ 0.60	4,700
Welding	812 Ft	$ 3.00	2,440
3. Apex Hypar (8 Panels)			
Concrete 5" Thick	15 CY	$ 55.00	830
Reinforcing Steel	2.6 T	$600.00	1,560
Form	-	-	190
Placing	8 Panels	$100.00	800
Curing	8 Panels	$ 50.00	400
Edge Beams	8528 Lb	$ 0.60	5,130
Welding	832 Ft	$ 3.00	2,500
Connection Bolts	528 NOS	$ 0.70	380
Asphalt Membrane	-	-	1,520
Spall Protection Coat	-	-	1,750
	Total		$27,370
Installation (Optional) 6(P) x 8 Hrs x 4 days = 192 Hrs $30/hr			5,760
		Total	$33,130

COST OF BOX STRUCTURE

Description	Quantity	M&L Cost	Total
1. Foundation Slab			
Concrete (12" Thick)	24 CY	$ 57.00	1,368
Reinf. Steel (#4@4" One Layer)	2.5 T	$755.00	1,888
Form	100 SF	$ 5.49	549
Placing Concrete	24 CY	$ 2.50	60
Curing Concrete	625 SF	$ 0.10	63
Dowels, Steel	-	-	200
2. Walls			
Concrete (30" Thick)	84 CY	$ 57.00	4,788
Reinf. Steel #7@4" (Two Layers)	27 T	$755.00	20,385
Form in place	1800 SF	$ 5.54	9,980
Placing Concrete	84 CY	$ 2.50	210
Curing Concrete	1800 SF	$ 0.05	90
Finishing Walls	1800 SF	$ 0.10	180
3. Roof Slab			
Concrete (30" Thick)	58 CY	$ 57.00	3,306
Reinf. Steel (#7@4" Two Layers)	14.7 T	$755.00	11,099
Form	650 SF	$ 5.17	3,361
Placing Concrete	58 CY	$ 3.50	203
Curing Concrete	625 SF	$ 0.10	63
Finishing	650 SF	$ 0.10	65
		Total	**$57,858**

COST OF ARCH STRUCTURE

Description	Quantity	M&L Cost	Total
1. Foundation Slab			
Concrete (12" Thick)	29 CY	$ 57.00	1,653
Reinf. Steel (#4@4" One Layer)	3.3 T	$755.00	2,492
Form	117 SF	$ 5.49	643
Placing Concrete	29 CY	$ 2.50	73
Curing	780 SF	$ 0.10	78
Dowels, Steel	-	-	200
2. End Walls			
Concrete (24" Thick)	48 CY	$ 57.00	2,736
Reinf. Steel (#7@4" Two Layer)	15 T	$755.00	11,325
Form	1470 SF	$ 5.54	8,144
Placing Concrete	48 CY	$ 2.50	120
Curing Concrete	1470 SF	$ 0.05	74
Finishing	1470 SF	$ 0.10	147
3. Arch			
Concrete (24" Thick)	86 CY	$ 57.00	4,902
Reinf. Steel (#7 cir #4 long @4")	8.2 T	$755.00	6,191
Form	2130 SF	$ 5.17	11,012
Placing Concrete (Curv)	2x86 CY	$ 3.50	602
Curing Concrete	2130 SF	$ 0.10	213
Finishing	2130 SF	$ 0.10	213
		TOTAL	$50,818

ESTIMATE OF CONSTUCTION TIME

Description of Work	(Number of Days)						
Structure	Hypar			Box		Arch	
Option	(A)	(B)	(C)	(A)	(B)	(A)	(B)
Foundation Slab:	Need	Need	Exist	Need	Need	Need	Need
Preparation	5	5	0	5	5	5	5
Concrete Placing	1	1	0	1	1	1	1
Curing (*)	28	14	0	28	7	28	7
Wall (& Arch):							
Preparation				7	7	7	7
Concrete Placing				2	2	2	2
Concrete Curing				28	7	28	28
Roof:							
Preparation				7	7	-	-
Concrete Placing				1	1	-	-
Concrete Curing				28	14	-	-
Installation of Panels	4	4	4	-	-	-	-
Earth Cover	4	4	4	4	4	4	4
Total	42	28	8	111	55	75	54
Average Time	-	30	8	-	60	-	54

*Curing time may be reduced using superplasticizers.

Comparison Table for Evaluation

Description	Unit	Hypar		Box	Arch
Options		#1	#2		
1. Floor Area	SF	665	665	400	570
2. Inside Volume	CF	4000	4000	4000	4000
3. Concrete	CY	73	24	166	163
4. Reinf. Steel	T	8	4.3	44.2	26.5
5. Form Cost	$	1040	320	13890	19799
6. Cost	$	34420	27370	57858	50818
7. Instal. Cost	$	5760	5760	-	-
8. Total Cost	$	40180	33130	57858	50818
9. Constr. Time	Days	30	8	60	54

IX. Conclusions:

1. In Hypar structure, flexure is not the major mode of load resistance. Instead, membrane action of shell is effective in resisting the load. Since, bending is the mode of resistance in other conventional structures, quantity of concrete and reinforcing steel increases the total cost considerably for box and arch structures. By choosing the hypar Structure System, the greatest economy in the use of materials is achieved due to reduced shell thickness and quantity of reinforcing steel.

2. Prefabrication of the panels in precast plant reduces construction time in the field.

3. Comparatively, long time required for form work, placing and curing of concrete elements in the field for a box or an arch structure can be avoided.

4. Hypar Panels may be stored in bases for installation when needed.

5. If the foundation slab is prebuilt or an equivalent pavement is available at preferred locations, the hypar panels can be installed quickly using expansion anchors.

6. No special skill is required for the installation of hypar panels. Military personnel could install without training.

7. In the case of box or arch structure, spall protection coat could not be easily provided.

8. Total cost of construction of a Hypar unit is considerably less compared to a box or an arch structure.

9. It is expected that the transportation of panels from precast plants to the site up to 50 miles would not cost anything extra. Beyond 50 miles, additional transportation expenses must be considered.

10. Total cost shown in the tables does not include cost for ground preparation and cost for earth cover. These are common for all the three structures and therefore not included.

11. Cost evaluation shown is for construction in U.S. For the General Contractor's overhead and profit, an additional amount equal to 10% of the total cost should be added.

12. Cost adjustments are necessary for construction in other countries. In such cases, the total cost should be multiplied by the area cost factor. Extreme area cost factors are: 0.98 in Germany and 1.41 in Azores.

Recommendation

Three structures were evaluated for selection. Minimizing the total cost of construction is an important criterion in selecting the Structure to provide protection from the high impulse blast loadings. Considering the total cost and construction time, the hypar structure system is the most economical and is recommended for selection.

Suggestions for Future Research

1. The weight of base hypar panel is 6580 lb and that of apex hypar panel is 9353 lb. The above includes the weight of concrete, reinforcing steel, edge beam channels and angles and tensile membrane. The total weight of a hypar super structure unit is about 60 Tons. This is prohibitively high for transporting the panels to the site by air. In order to reduce the weight of hypar panels and thus improve the air transportability of the hypar system, the use of high strength materials and composites should be explored.

2. If the anchor side edge beams of the base hypars can be made rigid, the foundation slab may not be required. This would enable anchoring the hypar unit to the soil directly. If this could be done, time delay in building the foundation slab and waiting for 28 days to allow the concrete to reach its full strength could be eliminated. So, the design of the support edges of base hypars as a rigid frame may be investigated.

3. The contribution of the cost of edge beams and the cost of welding the connection angles to the edge beams is high and is a major component of the total cost of hypar system. Study leading to the economic redesign of the connections would be beneficial.

X. REFERENCES:

1. Moriarty, T.F., Von Buelow, P., Development and Testing of an Underground Protective Shelter Constructed of Hyperbolic Paraboloid Shell Elements, ESL-TR-86-37, Engineering and Services Laboratory, Air Force Engineering and Services Center, Tyndall Air Force Base, FL 32403, Dec 85.

2. Kiger, S.A., Albritton, Gayle E., Response of Buried Hardened Box Structures To Effects of Localized Explosions, WES - TR SL-80-1, Mar 80.

3. Kiger, S.A., Albritton, Gayle E., Response of Buried Hardened Arch Structure To The Effects of Localized Explosions, WES - TR SL-79-13, Dec. 79.

4. Fundamentals of Protective Design for Conventional Weapons (1984), U.S. Army Engineer Waterways Experiment Station, Vicksburg, Miss.

5. Protective Construction Nuclear Blast Resistant Design TR-20 (Vol. 4) March 1985, Federal Emergency Management Agency.

6. Design of Structures to Resist Nuclear Weapons Effects, ASCE-Manuals and Reports on Engineering Practice - No 42, 1985.

7. 1988 Dodge Unit Cost Data, McGraw-Hill Information Systems Company.

8. Building Construction Cost Data 1987, Means, R. S. Means Company.

9. The Building Estimator's Reference Book, Editor: Mclurg, Frank. Walker Company, 1973.

10. Glenn M. Hardie, Construction Estimating Techniques, Prentice-Hall, Inc., 1987.